



**HAL**  
open science

# Cosmological solutions of string theory

Paul Marconnet

► **To cite this version:**

Paul Marconnet. Cosmological solutions of string theory. Mathematical Physics [math-ph]. Université Claude Bernard - Lyon I, 2023. English. NNT : 2023LYO10179 . tel-04607596

**HAL Id: tel-04607596**

**<https://theses.hal.science/tel-04607596>**

Submitted on 10 Jun 2024

**HAL** is a multi-disciplinary open access archive for the deposit and dissemination of scientific research documents, whether they are published or not. The documents may come from teaching and research institutions in France or abroad, or from public or private research centers.

L'archive ouverte pluridisciplinaire **HAL**, est destinée au dépôt et à la diffusion de documents scientifiques de niveau recherche, publiés ou non, émanant des établissements d'enseignement et de recherche français ou étrangers, des laboratoires publics ou privés.

**THÈSE de DOCTORAT DE  
L'UNIVERSITÉ CLAUDE BERNARD LYON 1**

**École Doctorale N° 52  
PHAST : Physique et Astrophysique**

**Discipline : Physique Théorique**

Soutenue publiquement le 26/09/2023, par :

**Paul MARCONNET**

---

**Solutions cosmologiques de  
la théorie des cordes**

---

Devant le jury composé de :

<b>GRAÑA Mariana, Directrice de Recherche, CEA Saclay</b>	<b>Rapporteure</b>
<b>VALENZUELA Irene, Chercheuse, CERN et IFT Madrid</b>	<b>Rapporteure</b>
<b>ANDRIOT David, Directeur de Recherche, LAPTh Annecy</b>	<b>Examineur</b>
<b>HOHENEGGER Stefan, Maître de Conférences, Université Lyon 1</b>	<b>Examineur</b>
<b>PETRINI Michela, Professeure des Universités, Université Sorbonne</b>	<b>Examinatrice</b>
<b>SAMTLEBEN Henning, Professeur des Universités, ENS de Lyon</b>	<b>Président</b>
<b>VAN RIET Thomas, Professeur Associé, KU Leuven</b>	<b>Examineur</b>
<b>TSIMPIS Dimitrios, Professeur des Universités, Université Lyon 1</b>	<b>Directeur de thèse</b>



# Abstract

Accounting for the accelerated expansion of the universe during the current dark energy era or the early phase of inflation within the framework of string theory is an open and notoriously difficult problem. This thesis presents new perspectives on some aspects of this long-standing challenge.

The first part explores flux compactifications of ten-dimensional type II supergravities on group manifolds with orientifolds and  $D$ -branes. We classify the possible solutions allowed by this framework, and look for maximally symmetric backgrounds, with a particular emphasis on de Sitter solutions. We then develop the tools required to analyze the stability of the effective scalar potential, the scale separation, the flux quantization, the compactness of the internal manifold as well as the perturbative regime of the solutions.

The second part is devoted to the study of time-dependent flux compactifications of ten-dimensional type IIA supergravity on various classes of six-dimensional manifolds (Calabi-Yau, Einstein, Einstein-Kähler), in order to construct cosmological backgrounds where the four-dimensional spacetime is Friedmann-Lemaître-Robertson-Walker. The cosmologies we present are universal in that they do not depend on the detailed features of the compactification manifold. Once the equations of motion are rewritten as an appropriate dynamical system, the existence of solutions featuring a phase of accelerated expansion is made manifest. The fixed points of this dynamical system, as well as the trajectories on the boundary of the phase space, correspond to analytic solutions which we determine explicitly. Furthermore, some of the resulting cosmologies exhibit eternal or semi-eternal acceleration, whereas others allow for a parametric control on the number of e-foldings. We also obtain several cosmologies featuring an infinite number of cycles of alternating periods of accelerated and decelerated expansions.

The third and last part of the thesis focuses on the effects of warped compactifications on the spectrum of gravitational waves. When non-smearred  $O_p/D_p$  sources are included in the higher-dimensional theory, the warp factor has non-trivial effects on the Kaluza-Klein tower of gravitational waves. We study the profile of the warp factor when moving away from a source, and develop a method to determine the gravitational wave spectrum which overcomes the difficulties due to the region where the warp factor becomes negative.



# Résumé

Rendre compte de l'expansion accélérée de l'univers durant la phase actuelle d'énergie noire ou pendant l'inflation dans le cadre de la théorie des cordes est notoirement difficile. Cette thèse de doctorat présente de nouvelles perspectives sur certains des aspects de ce problème.

La première partie de la thèse explore les compactifications avec flux des supergravités de type II à dix dimensions sur des variétés de groupe avec orientifolds et  $D$ -branes. Nous classifions les solutions permises par ce cadre, et cherchons des vides maximale-ment symétriques, en se concentrant plus particulièrement sur les solutions de de Sitter. Nous développons ensuite les outils nécessaires pour analyser la stabilité du potentiel scalaire effectif, la séparation d'échelles, la quantification des flux, la compacité de la variété interne ainsi que le régime perturbatif des solutions.

La deuxième partie est consacrée à l'étude des compactifications avec flux dépendant du temps de la supergravité de type IIA à dix dimensions sur différentes classes de variétés à six dimensions (Calabi-Yau, Einstein, Einstein-Kähler), afin de construire des solutions cosmologiques où l'espace-temps à quatre dimensions est de type Friedmann-Lemaître-Robertson-Walker. Les cosmologies que nous présentons sont universelles en ce sens qu'elles ne dépendent pas des caractéristiques détaillées de la variété interne. Une fois les équations du mouvement réécrites sous la forme d'un système dynamique approprié, l'existence de solutions présentant une phase d'expansion accélérée est rendue manifeste. Les points fixes de ce système dynamique ainsi que les trajectoires sur le bord de l'espace des phases correspondent à des solutions analytiques que nous déterminons explicitement. En outre, certaines des cosmologies résultantes présentent une accélération éternelle ou semi-éternelle, alors que d'autres permettent un contrôle paramétrique du nombre de  $e$ -folds. Nous obtenons également plusieurs cosmologies présentant un nombre infini de périodes alternées d'expansions accélérées et décélérées.

La troisième et dernière partie de la thèse se concentre sur les effets des compactifications "déformées" sur le spectre d'ondes gravitationnelles. Lorsque des sources  $O_p/D_p$  non-moyennées sont incluses dans la théorie à dimensions supplémentaires, le facteur de déformation a des effets non triviaux sur la tour de Kaluza-Klein d'ondes gravitationnelles. Nous étudions le profil du facteur de déformation lorsque l'on s'éloigne d'une source, et nous développons une méthode pour déterminer le spectre d'ondes gravitationnelles, en surpassant les difficultés dues à la région où le facteur de déformation devient négatif.



# Remerciements

Mener à terme une thèse de doctorat est rarement une épreuve aisée, mais la tâche peut s'avérer bien plus légère dès lors qu'on a la chance d'être encadré et entouré par les bonnes personnes. C'est à elles que j'aimerais adresser ici mes sincères remerciements.

Je commencerai naturellement par remercier mon directeur de thèse, Dimitrios Tsimpis. Merci, pour m'avoir accompagné le long de ce chemin sinueux, pour m'avoir guidé et soutenu, pour avoir été à l'écoute et disponible comme tu l'as été. J'ai appris tellement de choses auprès de toi, depuis les bancs de l'amphithéâtre il y a maintenant plus de six ans, jusqu'à aujourd'hui à travers des discussions toujours aussi passionnantes. Je suis conscient de la chance que j'ai eue d'avoir réalisé ma thèse aux côtés d'un directeur aussi bienveillant et d'une si grande qualité scientifique.

Viennent ensuite mes remerciements à David Andriot, mon co-directeur informel et mentor. C'est avec toi que les choses sérieuses ont commencé il y a quatre ans à Vienne, où j'ai eu l'opportunité de m'aventurer dans la recherche scientifique. Merci, pour ta confiance dès nos premiers échanges, pour m'avoir mis sur les rails sans attendre et m'avoir propulsé rapidement dans le vif du sujet. Ton soutien m'a été d'une immense valeur, particulièrement dans les moments compliqués, et je ne saurais te remercier assez pour tout ce que tu as fait pour moi, tant sur le plan scientifique que sur le plan humain.

Je profite de l'évocation de cette période viennoise pour remercier chaleureusement toutes les personnes qui ont rendu mes séjours là-bas si formidables. Merci en premier lieu à Timm Wrase pour avoir rendu ma venue possible, et pour notre collaboration tant sur place qu'à distance. Je n'aurais pas de mots assez justes pour rendre honneur à tous les moments partagés avec cette belle équipe, Céline, Niccolò, Laura, Romain. Des baignades dans le Danube jusqu'au sommet des pistes de skis autrichiennes, en faisant un crochet obligatoire par *Burgasse* après un verre de *Sturm* ("ça va mal..."), les retours en city-bike au coeur de la nuit, les cours de valse pour tenter de se fondre dans la masse aux bals viennois... Merci infiniment pour tous ces souvenirs que je garderai précieusement.

Je prends quelques lignes pour exprimer ma gratitude aux professeurs de l'École Normale Supérieure de Lyon qui m'ont transmis leur passion et donné l'envie de me lancer dans cette voie à travers leurs cours magistraux : Dimitrios bien sûr, mais aussi François Gieres, Stefan Hohenegger, Marc Magro, Henning Samtleben. Merci pour ces années d'études si riches, et pour avoir provoqué le déclic.



---

Un merci supplémentaire à Henning et Stefan pour avoir accepté de faire partie de mon jury de soutenance, aux côtés de Mariana Graña, Michela Petrini, Irene Valenzuela, Thomas Van Riet, David et Dimitrios. Je vous suis à tous grandement reconnaissant du temps accordé, mais aussi des retours pertinents pendant et après la soutenance. Je remercie tout particulièrement Irene et Mariana pour leur relecture du manuscrit et leurs commentaires sur ce dernier.

Le quotidien à l'IP2I n'aurait pas été si agréable sans toutes ces personnes dont j'ai eu la chance d'être entouré, des collègues avec qui j'ai commencé par partager un bureau et qui sont désormais de chers amis. Merci Alfred, pour ta sympathie et ta bonne humeur, ton soutien dans cette dernière ligne droite non sans rebondissements, ton aide pour la préparation et le déroulement de cette soutenance, tes charmantes photos sur ce fameux voyage retour... Baptiste, merci pour tout, des discussions passionnées devant un tableau aux nombreux concerts auxquels on a pu assister ensemble, des bricolages de cette machine à café aux parties d'échecs acharnées, tous ces moments que, j'espère, on continuera de partager. Un immense merci également à Antoine pour ton écoute et ton soutien, particulièrement au cours de cette année 2021 qui a été de loin la plus difficile à surmonter. Merci enfin à mes compagnons d'infortune qui ont complété successivement cette fine équipe, Fabio, Ginevra, Sharam, Wanda.

Je termine cette série de remerciements par ceux destinés à mes parents. Le vent dont on rêve quand on est à vélo, qui reste dans le dos malgré les changements de cap – et il y en a eus – qui souffle d'une force inépuisable, qui rend aisée n'importe quelle ascension. Les passions et les projets se sont succédé et vous avez toujours été là, avec le même soutien indéfectible, sans jamais chercher à me dissuader ou me convaincre de rester sur la voie toute tracée. Peu importe les revirements, vous avez gardé intacts cet enthousiasme et cette curiosité qui ont fait de vous, pour Lucas et moi, de si chers parents.

# List of publications

The present thesis is elaborated from the following publications:

- [1] D. Andriot, P. Marconnet, and T. Wrase, *New de Sitter solutions of 10d type IIB supergravity*, *JHEP* **08** (2020) 076, [[arXiv:2005.12930](#)].
- [2] D. Andriot, P. Marconnet, and T. Wrase, *Intricacies of classical de Sitter string backgrounds*, *Phys. Lett. B* **812** (2021) 136015, [[arXiv:2006.01848](#)].
- [3] D. Andriot, P. Marconnet, and D. Tsimpis, *Warp factor and the gravitational wave spectrum*, *JCAP* **07** (2021) 040, [[arXiv:2103.09240](#)].
- [4] D. Andriot, L. Horer, and P. Marconnet, *Charting the landscape of (anti-) de Sitter and Minkowski solutions of 10d supergravities*, *JHEP* **06** (2022) 131, [[arXiv:2201.04152](#)].
- [5] D. Andriot, L. Horer, and P. Marconnet, *Exploring the landscape of (anti-) de Sitter and Minkowski solutions: group manifolds, stability and scale separation*, *JHEP* **08** (2022) 109, [[arXiv:2204.05327](#)]. [Erratum: *JHEP* 09, 184 (2022)].
- [6] D. Andriot, P. Marconnet, M. Rajaguru, and T. Wrase, *Automated consistent truncations and stability of flux compactifications*, *JHEP* **12** (2022) 026, [[arXiv:2209.08015](#)].
- [7] P. Marconnet and D. Tsimpis, *Universal accelerating cosmologies from 10d supergravity*, *JHEP* **01** (2023) 033, [[arXiv:2210.10813](#)].



# Contents

Introduction	1
<b>I Classical de Sitter backgrounds</b>	<b>13</b>
<b>1 General set-up and ansatz</b>	<b>15</b>
1.1 Context and motivations . . . . .	15
1.2 The ansatz . . . . .	16
1.3 The equations . . . . .	18
1.3.1 IIA supergravity . . . . .	18
1.3.2 IIB supergravity . . . . .	19
<b>2 Charting the Landscape</b>	<b>21</b>
2.1 Classification of possible solutions . . . . .	21
2.1.1 Source configurations and fields for a single dimensionality $p$ . . . . .	23
2.1.2 Source configurations and fields for multiple dimensionalities . . . . .	30
2.1.3 T-duality and supersymmetry . . . . .	34
2.2 The solutions . . . . .	37
2.2.1 Procedure to find solutions . . . . .	37
2.2.2 Numerical code . . . . .	39
2.2.3 (Anti-) de Sitter no-go theorems . . . . .	41
2.2.4 Results: known and found solutions . . . . .	43
2.3 De Sitter, intersecting sources and 4d $\mathcal{N} = 1$ supersymmetry . . . . .	46
<b>3 Exploring the Landscape</b>	<b>49</b>
3.1 Algebra identification and compactness . . . . .	49
3.1.1 Elements of algebra . . . . .	49
3.1.2 Examples of algebras . . . . .	51
3.1.3 Method and tools for the identification . . . . .	54
3.1.4 Results . . . . .	58
3.2 Stability . . . . .	60
3.2.1 Scalar fields and potential . . . . .	60
3.2.2 Field space metric and redundancy . . . . .	62
3.2.3 Numerical tool MaxSymSolSpec (MSSSp) . . . . .	66

## Contents

---

3.2.4	Results: stability of the solutions and (swampland) conjectures . . .	66
3.3	Scale separation . . . . .	72
3.3.1	General comments on mass gap and scale separation . . . . .	72
3.3.2	No-go theorems for anti-de Sitter on Ricci flat or nilmanifolds . . .	74
<b>4</b>	<b>Consistent truncations and stability</b>	<b>77</b>
4.1	Context and motivations . . . . .	77
4.2	Dimensional reduction on group manifolds . . . . .	78
4.2.1	Truncation ansatz . . . . .	78
4.2.2	Dimensional reduction . . . . .	81
4.3	The code MSSV . . . . .	86
4.4	Consistent truncations . . . . .	88
4.5	Stability analysis . . . . .	89
4.5.1	Flat directions . . . . .	90
4.5.2	De Sitter solutions . . . . .	91
4.5.3	Minkowski solutions . . . . .	95
4.5.4	Anti-de Sitter solutions . . . . .	97
4.6	Summary and outlook . . . . .	98
<b>5</b>	<b>Intricacies of classical de Sitter backgrounds</b>	<b>101</b>
5.1	Motivations . . . . .	101
5.2	6d geometry of solution 14 . . . . .	103
5.2.1	Foreword on the change of basis . . . . .	103
5.2.2	Lattice, orientifolds . . . . .	103
5.2.3	Harmonic forms . . . . .	104
5.2.4	Flux quantization . . . . .	106
5.3	Checking requirements for a classical solution . . . . .	106
5.4	Solution 15 . . . . .	108
5.5	Scale separation for de Sitter . . . . .	110
5.6	A word on smeared sources . . . . .	113
5.7	Outlook . . . . .	114
<b>II</b>	<b>Time-dependent compactifications</b>	<b>115</b>
<b>6</b>	<b>Bird's eye view on time-dependent compactifications</b>	<b>117</b>
6.1	Context and state of the art . . . . .	117
6.2	Summary of the results . . . . .	118
<b>7</b>	<b>The framework</b>	<b>129</b>
7.1	General set-up . . . . .	129
7.2	1d consistent truncation . . . . .	131
7.3	Cosmological 4d consistent truncation . . . . .	133

<b>8</b>	<b>Cosmological solutions</b>	<b>135</b>
8.1	Analytic solutions . . . . .	135
8.1.1	Minimal (zero-flux) solution . . . . .	136
8.1.2	Single-flux solutions . . . . .	137
8.2	Two-flux solutions: dynamical system analysis . . . . .	140
8.2.1	Case study I: $\lambda, k$ . . . . .	145
8.2.2	Case study II: $k, m$ . . . . .	151
8.2.3	Case study III: $\lambda, m$ . . . . .	153
8.2.4	Case study IV: $\varphi, \chi$ . . . . .	155
8.3	Outlook . . . . .	156
<b>III Warp factor and the gravitational wave spectrum</b>		<b>159</b>
<b>9</b>	<b>Kaluza–Klein gravitational waves in a warped toroidal background</b>	<b>161</b>
9.1	Context and motivations . . . . .	161
9.2	The general set-up . . . . .	165
9.2.1	The toroidal $p$ -brane background and its warp factor . . . . .	165
9.2.2	Aparté: moving away from a source . . . . .	167
9.2.3	Gravitational waves and their spectrum . . . . .	171
<b>10</b>	<b>The spectrum</b>	<b>173</b>
10.1	Issues and method to determine the spectrum . . . . .	173
10.1.1	Negative region and tachyons . . . . .	173
10.1.2	Restricting the domain and reformulating the eigenmode equation . . . . .	174
10.1.3	Numerical method to determine the spectrum . . . . .	177
10.2	Spectrum . . . . .	181
10.3	Summary and outlook . . . . .	186
<b>IV Appendices</b>		<b>189</b>
<b>A</b>	<b>Details on the determination of the gravitational wave spectrum</b>	<b>191</b>
A.1	Tachyon in a non-compact case . . . . .	191
A.1.1	Orientifold source and negative region . . . . .	191
A.1.2	$D_p$ -brane source . . . . .	193
A.2	Numerical details . . . . .	194
A.2.1	Making use of the symmetries . . . . .	194
A.2.2	Bijjective map . . . . .	194
A.3	Tachyonic spectrum . . . . .	195
<b>B</b>	<b>Cosmological solutions</b>	<b>199</b>
B.1	Analytic solutions . . . . .	200
B.1.1	Compactification on Calabi-Yau manifolds . . . . .	200
B.1.2	Compactification on Einstein manifolds . . . . .	214
B.1.3	Compactification on Einstein-Kähler manifolds . . . . .	223
B.2	Two-flux dynamical systems . . . . .	225

## Contents

---

B.2.1	Compactification on Calabi-Yau manifolds . . . . .	226
B.2.2	Compactification on Einstein manifolds . . . . .	229
B.2.3	Compactification on Einstein-Kähler manifolds . . . . .	233
<b>C</b>	<b>Minkowski and (anti-) de Sitter solutions</b>	<b>237</b>
C.1	De Sitter solutions . . . . .	237
C.2	Minkowski solutions . . . . .	266
C.3	Anti-de Sitter solutions . . . . .	270

# Introduction

All traditional societies and religions have had their stories of the universe. Inquiries into its nature, structure, its origin, evolution and fate are long-standing ones. While being amongst the oldest, it is only recently that these could be addressed in a proper scientific context. Even a century ago, we did not know why the sky is dark at night nor why stars shine as they do, we ignored that there are other galaxies than ours, we had no clue about what the universe actually contains, and perhaps most of all, we did not understand the universe as an entity on its own.

Recent advances in both theoretical and observational cosmology in the past three decades have brought to us a complete new perspective on all these questions. Precise measurements of temperature fluctuations in the cosmic microwave background (CMB) [8–13] – a snapshot of the universe when it was just 380 000 years old – observations of type Ia supernovae [14, 15], as well as galaxy surveys mapping the distribution of large-scale structures [16] have established the so-called  $\Lambda$ CDM standard model of cosmology. It describes a universe filled with only 5% ordinary atoms, 27% dark matter and 68% dark energy [11], accounted for by a cosmological constant  $\Lambda$ . The latter drives the current accelerated expansion of the universe, but it is fair to say that we do not know much about its nature. There is now strong evidence that large-scale structures such as galaxies were seeded by primordial density inhomogeneities, caused themselves by quantum fluctuations [17–22], which were subsequently stretched to cosmic size during an era of very rapid expansion called *inflation* [23–25]. Understanding the microphysical mechanisms underlying the accelerated expansion of the universe during the current phase of dark energy or during inflation remains an open problem for modern physics, and is the central topic of the present thesis.

## • Inflation and dark energy

Observations of the CMB and galaxy surveys tell us that on large scales, our universe is nearly isotropic. Further assuming that we humans on Earth are no privileged observers – assumption sometimes referred to as the Copernican principle – this also implies that the universe is homogeneous, which is well described by the so-called Friedmann-Lemaître-Robertson-Walker (FLRW) metric,

$$ds^2 = -dt^2 + a(t)^2 d\Omega_k^2, \quad (1)$$

where the *scale factor*  $a(t)$  characterizes how the size of spatial slices evolves in time, and  $d\Omega_k^2$  is the spatial metric of either Euclidean space, the three-sphere (in which case



we talk of a closed universe) or of hyperbolic space (open universe).

These observational facts actually constitute a puzzle within standard Big Bang cosmology, which goes under the name of the *horizon problem*. The latter can be summarized as follows: let us think of the CMB as a precise temperature map of a large patch of the universe at the time of recombination, when it was much smaller and much hotter. This patch turns out to be so large that it is made of many (over 40000) causally disconnected regions, in the sense that the time elapsed since the Big Bang did not suffice to bring them into causal contact, and these could never exchange any information. In particular, these disconnected regions could not exchange photons in order to be at thermal equilibrium with each other. However, this equilibrium is precisely what we witness in the CMB: we do observe that the temperature is the same everywhere, to a level of one part in  $10^5$ . Calling this a coincidence would be highly implausible, and one has to come up with a mechanism to explain the correlations of temperatures in the CMB.

One solution to the horizon problem (and in fact to many other issues of the standard Big Bang cosmology) is provided by the paradigm of *inflation* [23–25]. It postulates that the universe underwent a period of rapid – close to exponential – expansion before being populated by the matter we know. If this era of accelerated expansion lasted long enough, it allows us to extend the duration between the Big Bang singularity and the time of recombination when the CMB was released, so that all past light cones ending on the corresponding space slice can now intersect before the singularity. In other words, this allows all points of the CMB patch to have been in causal contact in the past, and thus would remedy the horizon problem.

For such a period of accelerated expansion to occur, one needs to violate the so-called *Strong Energy Condition* (SEC), which can be written in some coordinates as

$$R_{00} = T_{00} + g^{ij}T_{ij} \geq 0. \quad (2)$$

It has to be violated because  $R_{00} = -\frac{3\ddot{a}}{a}$  has to be negative if one imposes  $\ddot{a} \geq 0$ , where dots stand for derivatives with respect to time  $t$ . The simplest way to realize this is to consider a homogeneous scalar field  $\varphi(t)$  called the *inflaton* [24, 25], which is minimally coupled to gravity,<sup>1</sup>

$$S = \int d^4x \sqrt{|g|} \left( \frac{R}{2} - \frac{1}{2} g_{\mu\nu} \partial^\mu \varphi \partial^\nu \varphi - V(\varphi) \right), \quad (3)$$

and has a positive potential energy. In this case, Eq. (2) becomes

$$R_{00} = 2(\dot{\varphi}^2 - V(\varphi)), \quad (4)$$

from which we read that there is acceleration whenever the potential energy of the inflaton gets bigger than twice its kinetic energy. In the limit where  $V(\varphi) \gg \dot{\varphi}^2$ , the scalar field sector behaves as an effective cosmological constant  $\Lambda \sim V$ , and the spacetime is approximately de Sitter space, with corresponding exponential scale factor  $a(t) \sim e^{\sqrt{\Lambda}t}$ . Thus, dark energy may also be modelled with a scalar potential, provided that the system stays at a roughly constant value of the potential energy. This can be the case if the

---

<sup>1</sup>In this section, the Planck mass is set to 1 for simplicity.

potential admits a positive, meta-stable minimum which is called a *de Sitter vacuum*, or a region of almost flat runaway (that is considered in quintessence models). Constructing de Sitter vacua from a fundamental perspective will be precisely the subject of the first part of this thesis.

The classical dynamics of Eq. (3) is given by the Friedmann equation and the Klein-Gordon equation for  $\varphi$ ,

$$3H^2 = \frac{1}{2}\dot{\varphi}^2 + V \quad \text{and} \quad \ddot{\varphi} + 3H\dot{\varphi} = V', \quad (5)$$

where  $V' = \partial_\phi V$  and we defined the Hubble parameter  $H = \frac{\dot{a}}{a}$ . One can combine these equations into

$$\varepsilon \equiv -\frac{\dot{H}}{H^2} = \frac{\frac{1}{2}\dot{\varphi}^2}{H^2} = \frac{\frac{3}{2}\dot{\varphi}^2}{\frac{1}{2}\dot{\varphi}^2 + V}, \quad (6)$$

and the condition for acceleration translates into  $\varepsilon < 1$ . Now, to have a sufficiently long period of inflation to solve the horizon problem (and other constraints), one needs to prolong the situation where the potential energy dominates over the kinetic energy. This can be done with a fairly flat potential  $V$  on which the physical system is slowly rolling down. This way, the conditions for extended slow-roll inflation can be expressed as conditions on the shape of the potential [26],

$$\epsilon_V \equiv \frac{1}{2} \left( \frac{V'}{V} \right)^2 \ll 1 \quad \text{and} \quad |\eta_V| \equiv \frac{|V''|}{V} \ll 1. \quad (7)$$

These are called the potential slow-roll parameters.

One can then engineer different types of potential – providing or not an explanation of why they should have such a shape – and derive the dynamics of the cosmology they give rise to.

- **Ultraviolet sensitivity of inflation and the need for quantum gravity**

Scenarios such as (3) are toy-models as long as they remain decoupled from the rest of physics, and they lack ultraviolet (UV) completions. One way to address these deficiencies would be to work in the paradigm of effective field theories (EFT). Before diving into it, let us say a few words about what we call EFT.

Physical processes and phenomena occur over a large range of length scales. Luckily, most of the time one can study the physics of such phenomena only at the relevant scale and do not have to resolve the small-scale details of a more complete and more fundamental theory. For instance, one can thankfully describe fluid dynamics without having to report the motion and interactions of the atoms that constitute water molecules. The fluid-mechanical paradigm will be sufficient to describe phenomena up to a certain length (or energy) scale, beyond which the theory will stop being relevant and should be replaced by something else. This reasoning is particularly useful when the full theory is not known or not computable, in which case one can parametrize our ignorance of the unknown physics by a collection of so-called *irrelevant* interactions, which decouple and are suppressed when we consider processes at a low energy with respect to the cut-off scale where the effective theory breaks down.

Nonetheless, there exist situations where the high energy degrees of freedom do not decouple, and the low-energy theory is strongly affected by the irrelevant interactions:

we call this phenomenon *UV sensibility*. It turns out that inflation falls into this class, as we will explain below.

The previous claim goes under the name of *eta problem(s)* [27]. It mainly concerns slow-roll inflation but variations thereof also arise in most non-slow-roll models (see [28] for a discussion on this matter). One first observation is the following: the maximal cut-off  $\Lambda_c$  of inflation as an EFT is obviously the Planck mass  $M_p$  beyond which quantum gravitational effects are guaranteed to become relevant. On the other hand, in order for the EFT to remain valid during the freeze-out of cosmological perturbations, the cut-off has to be larger than the Hubble scale  $H$ , so

$$H < \Lambda_c < M_p. \quad (8)$$

Now, it is well-known that quantum corrections tend to push the mass of scalar fields up to the cut-off of the EFT,

$$\Delta m^2 \sim \Lambda_c^2. \quad (9)$$

For inflation, the mass of the inflaton is directly related to the second slow-roll parameter  $\eta \sim V''$  in (7). But since consistency of the EFT requires  $\Lambda_c > H$ , the eta parameter receives order-one corrections

$$\Delta\eta \sim \frac{\Lambda_c^2}{H^2} > 1, \quad (10)$$

which spoils the delicate flatness of the potential needed for sustained inflation. Enforcing a small physical  $\eta$  would then require to fine-tune the bare parameter and we run into naturalness issues (note that symmetry considerations can improve the protection of  $\eta$  against large corrections but cannot solve the problem entirely).

Another issue arises when considering order-six interactions in the tower of non-renormalizable operators of the EFT, of the form

$$\Delta V = cV(\varphi)\frac{\varphi^2}{\Lambda_c^2}, \quad (11)$$

where  $c$  is a  $\mathcal{O}(1)$  constant and  $V$  represents the renormalizable terms in the potential. In a theory with a single scalar field, it is difficult to justify the absence of couplings of the form (11). Provided that the cut-off  $\Lambda_c$  is larger than the vacuum expectation value (VEV) of the inflaton, the operator will only give a small contribution to the potential,  $\Delta V \ll V$ . However, such a correction reflects on  $\eta$  – because of its dependency on  $V$  – as

$$\Delta\eta = \frac{M_p^2}{V}\partial_\phi^2(\Delta V) \approx 2c\left(\frac{M_p}{\Lambda_c}\right)^2 > 1, \quad (12)$$

where we have restored the Planck mass. Thus, even if the operator (11) is Planck-suppressed, it cannot be ignored in discussions of the inflationary dynamics. A similar argument can be done for more general non-renormalizable interactions, which can yield comparable or larger effects.

The upshot of the above argument is that inflationary theories have the special feature that some irrelevant operators of the EFT play a crucial role at low energy, not only for precision observables, but even for the zeroth-order dynamics. This UV sensitivity begs for a treatment of inflation in a UV-complete theory of quantum gravity.

• String theory

Up to date, the most developed framework for quantum gravity is *string theory*, whose starting point is to replace the point-particles of quantum field theory by finite size objects, including one-dimensional vibrating strings. There exist five string theories, which are related to one another by dualities, and they all have 10 dimensions of spacetime. In this thesis, we will be concerned with the low-energy limit of these theories, which are 10d *supergravity* theories. The latter can be thought of as supersymmetric extensions of General Relativity, or alternatively as field theories with local supersymmetry. Of interest to us, these supergravities admit gravitational backgrounds where the 10d spacetime is split as a product of an extended 4d spacetime with a 6d compact space

$$\mathcal{M}_{10} = \mathcal{M}_4 \times \mathcal{M}_6 . \tag{13}$$

At length scales much larger than the characteristic size of  $\mathcal{M}_6$ , the EFT around the background is a 4d quantum field theory coupled to gravity whose spectrum depends itself on the geometry of the extra dimensions. Deriving the precise features of the lower-dimensional effective theory requires to perform a Kaluza-Klein *compactification* [29, 30]. In particular, compactifying the 10d fields down to 4d will give rise to a certain number of scalar fields – the so-called *moduli* – which are associated to the size and shape of the extra dimensions (we will come back to this point below). We will be particularly interested in backgrounds where the 4d spacetime  $\mathcal{M}_4$  is *maximally symmetric* – meaning that it is either anti-de Sitter, Minkowski, or de Sitter space – coming from compactifications of 10d supergravities.

Let us recall the big picture. We want to account for the observed accelerated expansion of our universe (dark energy and/or inflation) within the framework of string theory using its supergravity low-energy limit which is well-understood. The aim is thus to construct solutions of 10d supergravity where the 4d spacetime is de Sitter, or more generally FLRW (1). The problem however, is that it turns out to be a formidable task to do so. Let us give a flavour of why it is the case. Recall that in order to achieve accelerated expansion, one needs to violate the SEC (2) and we saw that it could be done with scalar fields with positive potential energy. Thus, one could think that all we need is a certain compactification for which the 4d EFT has a positive scalar potential and there should be regions of the field space where one can violate the SEC, or even (meta-stable) minima of the potential at positive values, if we search hard enough among all the possible vacua of string theory.

However, there is a twofold problem: (i) all 10d pure supergravities have their energy-momentum tensors satisfying the SEC, and (ii) the SEC is hereditary, in the sense that if it holds for the higher-dimensional theory, it will remain valid for any compactification thereof. This claim constitutes a well-known no-go theorem first discovered by Gibbons [31, 32] and later refined by Maldacena and Nuñez [33]. It can be stated as follows: *cosmic acceleration is forbidden in models descending from pure 2-derivative 10d supergravity with time-independent compactifications on non-singular manifolds without boundaries*. Thus, if one ever wishes to model accelerated expansion with 10d supergravity, one has to circumvent at some point the no-go theorem, typically by relaxing one or several of its assumptions. We shall review extensively in the next section the various routes one can follow in order to do so.

In any case, one still has to construct a positive scalar potential with the various

ingredients provided by string theory. These include *fluxes*  $F_p$  – which are higher-dimensional generalizations of the electromagnetic flux – they contribute positively to the potential as [34]

$$V_{\text{fluxes}} \sim \sum_p \frac{1}{2p!} \int_{\mathcal{M}_6} \sqrt{|g_6|} e^{c_p \phi} |F_p|^2, \quad (14)$$

where  $c_p$  are constant coefficients and  $\phi$  is the dilaton, a scalar field predicted in the massless spectrum of closed strings. One can also make use of the curvature of the compact manifold gathering the extra dimensions,

$$V_{\text{curvature}} \sim - \int_{\mathcal{M}_6} \sqrt{|g_6|} \mathcal{R}_6, \quad (15)$$

so that negatively curved (hyperbolic) spaces help in building positive potentials. One can also resort to so-called *orientifolds* sources which are exotic objects with negative tension: they enter the potential as

$$V_{\text{sources}} \sim -\text{tension} \int_{\Sigma_n} \sqrt{|g_n|}, \quad (16)$$

where  $g_n$  is the determinant of the 10d metric pulled-back on the hypersurface  $\Sigma_n$  wrapped by the orientifold. The resulting scalar potential is the sum of all the contributions mentioned above.

- **De Sitter constructions in string theory**

Let us present a bird’s eye view of the existing attempts to constructing de Sitter space from string theory, together with their respective issues. We follow closely [34] and [35], and refer to these reviews for additional details and a more complete list of references.

- **Classical constructions.** These will be the central topic of this thesis, and constitute perhaps the most natural way to build de Sitter vacua. By classical we mean the tree-level of perturbative string theory, that is 10d supergravity at the two-derivative level, with fluxes and  $O_p/D_p$  sources. For concreteness, we focus here on type II supergravities, whose bosonic sector can be decomposed as

$$S = S_{\text{bulk}} + S_{\text{sources}}, \text{ with } S_{\text{bulk}} = S_0 + S_{\text{CS}}, \quad S_{\text{sources}} = S_{\text{DBI}} + S_{\text{WZ}}. \quad (17)$$

We follow Appendix A of [36] for notations and conventions and refer to it for more technical details. The fields in the bulk action are the 10d metric  $g_{MN}$  (with  $M, N = 0, \dots, 9$ ), the dilaton  $\phi$  and the Kalb-Ramond two-form  $b$ . One considers in addition Ramond-Ramond (RR)  $p$ -form gauge fields  $C_p$  with  $p = 1, 3$  in type IIA and  $p = 0, 2, 4$  in type IIB. The corresponding fluxes (field-strengths) are

$$\begin{aligned} \text{IIA: } & H = db, \quad F_0, \quad F_2 = dC_1 + bF_0, \quad F_4 = dC_3 - H \wedge C_1 + \frac{1}{2} b \wedge bF_0, \\ \text{IIB: } & H = db, \quad F_1 = dC_0, \quad F_3 = dC_2 - H \wedge C_0, \quad F_5 = dC_4 - H \wedge C_2. \end{aligned} \quad (18)$$

The  $S_0$  action then reads

$$S_0 = \frac{1}{2\kappa_{10}^2} \int d^{10}x \sqrt{|g_{10}|} \left( e^{-2\phi} \left( \mathcal{R}_{10} + 4|\text{d}\phi|^2 - \frac{1}{2}|H|^2 \right) - \frac{1}{2} \sum_p |F_p|^2 \right), \quad (19)$$

where  $2\kappa_{10}^2 = (2\pi)^7(\alpha')^4$  and  $\alpha'$  is the square of the string length  $l_s$ . Here,  $\mathcal{R}_{10}$  is the 10d Ricci scalar and  $|g_{10}|$  the absolute value of the 10d metric's determinant. The Chern-Simons  $S_{CS}$  terms will not be relevant for the present discussion, so let us now turn to the sources contributions. The dynamics of  $D$ -branes and orientifolds is captured by the Dirac-Born-Infeld (DBI) action  $S_{DBI}$  and the Wess-Zumino (WZ) term  $S_{WZ}$ , whose expression are respectively given by

$$\begin{aligned} S_{DBI} &= -c_p T_p \int_{\Sigma_{p+1}} d^{p+1}\xi e^{-\phi} \sqrt{|\iota [g_{10} - b] + \mathcal{F}|}, \\ S_{WZ} &= -c_p \mu_p \int_{\Sigma_{p+1}} \sum_q \iota [C_q] \wedge e^{-\iota[b] + \mathcal{F}}, \end{aligned} \tag{20}$$

where  $\Sigma_{p+1}$  is the world-volume wrapped by the source and  $\iota[\cdot]$  the pull-back to it.  $\mathcal{F}$  denotes here the field strength of the world-volume gauge field. The tension  $T_p$  can be determined from amplitude computations (e.g. the exchange of a closed string between two  $D$ -branes) and is given by  $T_p^2 = \frac{\pi}{\kappa_{10}^2} (4\pi^2 \alpha')^{3-p}$ . The constant coefficient  $c_p$  is equal to 1 for a  $D$ -brane, and equal to  $-2^{p-5}$  for an  $O_p$ -plane. We thus see that orientifolds carry negative tension, which makes them crucial in circumventing de Sitter no-go theorems.

Finding de Sitter solutions in this corner of the moduli space typically amounts to coming up with a particular ansatz (e.g. for the internal geometry and the fluxes) and then solve the 10d equations of motion (e.o.m.), including the Einstein equations for the 10d metric, the e.o.m. for the dilaton and the fluxes, as well as the Bianchi identities for the latter – sometimes referred to as tadpole cancellation conditions. We shall go back to these in details in Chapter 1. The 10d solution corresponds to a critical point of the scalar potential of the 4d effective theory which is obtained after compactification. One then has to address the stability of this critical point to make sure that the solution is free from tachyons. Up to date however, not a single de Sitter solution without tachyons has been constructed within this set-up. It remains an open problem to understand this obstruction or to come up with counter-examples. This is one of the main subject of the present thesis, and will be discussed extensively in the subsequent chapters.

- **Non-geometric fluxes.** These objects arise when one considers a T-duality chain starting from an NSNS 3-form flux  $H$ . To be concrete, let us consider here a compactification on  $T^6$  with such an NSNS 3-form flux  $H_{abc}$  on some 3-cycle. Under a first T-duality – say in direction  $a$  – the  $H$  flux is mapped to so-called geometric fluxes  $f^a{}_{bc}$  associated with a twist in the torus topology (these correspond to the structure constants for compactifications on group manifolds, which we will consider extensively in Part I of the thesis). One can perform another T-duality along direction  $b$ , which leads to a “dual torus” that is locally geometric but cannot be described globally in terms of a fixed geometry [37]. The non-geometric fluxes resulting from T-duality are commonly denoted  $Q^{ab}{}_c$ . The T-duality chain can be pushed one step further, giving rise to other non-geometric fluxes denoted  $R^{abc}$ . In summary,

$$H_{abc} \xleftrightarrow{T_a} f^a{}_{bc} \xleftrightarrow{T_b} Q^{ab}{}_c \xleftrightarrow{T_c} R^{abc}. \tag{21}$$

These non-geometric fluxes do not have a 10d origin which can be traced back in actions such as (19), so vacua found within these constructions are qualitatively different from the above category. The thing of interest is that the  $Q$ - and  $R$ -fluxes yield contributions in the 4d potential that scale differently in the scalar fields than the geometric fluxes or the other contributions coming from sources or internal curvature. For instance, the  $Q$ - and  $R$ -fluxes give rise to terms in the potential which scale respectively linearly and cubically in the 6d volume modulus  $\rho$ , and these terms are particularly useful to offset other contributions, and enlarge the parameter space. Within this framework, it turns out to be possible to build meta-stable de Sitter vacua, although they remain scarce [38–40].

However, not having a duality frame in which fluxes can be geometric implies that the resulting 4d supergravity should describe both string momentum and winding modes – which are otherwise traded via T-duality – and thus, that some of the extra-dimensions must be close to the self-dual radius (and cannot be made large) for the two types of modes to be relevant at low energy. This is problematic to have good control over the solution since one can no more ignore higher derivative corrections to the effective action. Hence, although non-geometric fluxes may constitute interesting ingredients in dS model building and should be considered in full generality, it is hard to expect constructing trustable dS vacua without addressing the issue of control over derivative corrections.

- **Quantum corrections.** The vast majority of de Sitter constructions considered in the recent literature consist of classical compactifications with fluxes and orientifolds sources as described in the first paragraph, together with “quantum corrections”. These include higher-derivative corrections (higher order in  $\alpha'$ ), string-loop corrections (higher order in  $g_s$  the string coupling constant), non-perturbative effects, etc. These corrections are typically used to stabilize the Kähler moduli. There are two main constructions going along these lines: the first one is KKLT [41] (named after the authors Kachru, Kallosh, Linde and Trivedi), the other one being the so-called Large Volume Scenario (LVS) [42].

In the former case, one starts from type IIB string theory compactified on a Calabi-Yau three-fold ( $CY_3$ ). The latter is a 6d Ricci-flat manifold equipped with a globally defined and nowhere vanishing holomorphic three-form. In addition, it possesses a unique covariantly constant spinor, used to construct a unique two-form dubbed the Kähler form. When the 10d theory is compactified on the  $CY_3$  in order to extract the effective 4d theory, the holomorphic and the Kähler forms are integrated over two- and three-cycles of the manifold and respectively give rise to complex structure moduli and Kähler moduli, which correspond to massless scalar fields in the 4d theory. The Kähler moduli characterize the size and volume of the internal manifold, whereas the complex structure moduli account for its shape. A basic example would be a two-torus  $T^2$  (which is a  $CY_1$ ) of edges  $l_1$  and  $l_2$ : the volume  $l_1 l_2$  is the Kähler modulus, while the ratio  $l_1/l_2$  defining its shape corresponds to the complex structure modulus.

One then considers a GKP-like warped compactification (again named after the authors Giddings, Kachru and Polchinski) [43], that features RR fluxes and orientifolds. These admit *imaginary self-dual* Minkowski solutions which have the important



property of having all complex structure moduli and the dilaton stabilized.

In order to generate a potential for the remaining unstabilized Kähler moduli, the KKLT construction makes use of non-perturbative corrections coming from gaugino condensation and  $D_3$ -branes instantons. After taking these corrections into account, the resulting scalar potential admits a stable supersymmetric minimum at a negative value, that is, an AdS vacuum. Furthermore, the latter can be parametrically scale-separated, meaning that it can truly be perceived as four-dimensional at low energy, which is a crucial feature for phenomenology.

The last step towards a dS vacuum consists in adding anti- $D_3$  branes ( $\bar{D}_3$ ): these break the supersymmetry – which is needed to have de Sitter space – and contributes positively to the scalar potential in order to uplift the minimum to a positive value. The  $\bar{D}_3$  are placed (or rather attracted) at the tip of a so-called Klebanov-Strassler (KS) throat [44] smoothly glued to the  $CY_3$ . This allows to fine-tune the energy contribution of the  $\bar{D}_3$  which is necessary to yield a meta-stable dS vacuum without spoiling its stability.

The LVS shares a similar starting point but takes a different route when it comes to stabilizing the Kähler moduli for the Minkowski solution. It incorporates the leading perturbative  $\alpha'$  correction to the Kähler potential, which can be tuned against the non-perturbative corrections so to provide a non-supersymmetric AdS vacuum with exponentially large volume, thus putting the solution in a regime where further corrections are in better control [42]. One may then do a similar antibrane uplift as in KKLT to end up with a dS vacuum.

Nonetheless, both these scenarios are at the center of vivid debates about the validity of each step involved in the construction. It is beyond the scope of this introduction to go through all the criticisms in details, but let us just mention a few arguments. Already at the level of the GKP compactification: the construction requires a small but non-zero constant contribution from the fluxes to the superpotential, which is often denoted  $W_0$  in the literature. The corresponding flux configurations breaks supersymmetry and one should at this stage (even before adding the non-perturbative corrections mentioned above) consider perturbative string loop and higher derivative corrections. However, these are not fully known and it is not clear whether they are small enough to be counteracted by the non-perturbative ones [45]. Another related problem is that it is not clear whether it is possible to achieve a parametrically small  $W_0$  since it would be in tension with the recently proposed tadpole conjectures [46], although some great progress has been made in that direction [47–50]. There are also numerous objections regarding control on the non-perturbative terms added for stabilizing the Kähler moduli [51, 52]. Lastly, the antibrane uplift to dS is far from being fully understood: it is argued that the backreaction of antibranes may cause brane-flux instabilities (for LVS, the situation might be even more dramatic as it was argued recently that uplift scenarios in this case were out of control due to derivative corrections [53]). We refer to [35] and references therein for a thorough discussion on these arguments and how they may be circumvented.

- **Other constructions.** There exist other scenarios for constructing de Sitter space, which are somewhat less studied in the literature but are worth mentioning briefly.



These include brane-world scenarios with non-compact extra-dimensions [54–56], or constructions within non-critical string theory [57–59]. The idea in the latter setting is the following: for non-critical string theories of dimension  $D$ , the effective action receives an extra contribution proportional to  $D - D_c$  where  $D_c$  is the critical dimension. If one considers  $D > D_c$ , then the extra positive contribution to the effective potential may help in finding de Sitter vacua. However, as pointed out by the authors of these works themselves, it is complicated to understand whether there is any perturbative control over these solutions.

- **Outline of the thesis**

Let us get give a brief outline of the thesis, which is divided into 3 parts.

The first one is devoted to the study of classical de Sitter backgrounds. In Chapter 1, we describe the precise setting, ansatz and ingredients that we use. The framework is 10d type II supergravity with fluxes and  $O_p/D_p$  sources compactified on so-called group manifolds. We discuss their geometry, and provide the equations to be solved in order to construct maximally symmetric backgrounds. Indeed, although the main focus is on de Sitter, we also consider Minkowski and anti-de Sitter backgrounds in the analysis.

In Chapter 2, we give a complete classification of the possible solutions allowed in such a framework. It turns out that there is only a finite number of distinct  $O_p/D_p$  source configurations, which are constrained by tadpole cancellation conditions. In each configuration, we work out the precision orientifold projection and the associated field content to be plugged in the equations. We study the supersymmetry of these configurations and how some of them are related by T-duality. This procedure allows us to divide the solution space – that we refer here to as the *Landscape* of (anti-) de Sitter and Minkowski solutions of 10d type II supergravities – into smaller regions with different properties. This turns out to be useful in order to organize the search for new solutions but also to understand the absence of de Sitter solutions in certain regions. Indeed, in some of them, it becomes possible to prove no-go theorems against the existence of de Sitter vacua. We then present the procedure we follow to solve the equations and look numerically for new solutions.

Chapter 3 is then devoted to the exploration of this Landscape, and we study in more details the properties of the backgrounds living in the different regions. We develop tools to characterize the internal geometry of each solution: this requires to properly identify the underlying group manifold, and decide whether it is or can be made compact by taking an appropriate quotient by a discrete subgroup. We also develop some formalism to generically analyze the stability of the 4d scalar potential, and make some comments about the scale separation of the backgrounds. All the (anti-) de Sitter and Minkowski solutions, as well as their properties, are provided in Appendix C.

We proceed in Chapter 4 by taking further the stability analysis through the prism of consistent truncations. We present very general tools to study the perturbative stability of classical flux compactifications, and apply them on our database of (anti-) de Sitter and Minkowski solutions.

We end this first part in Chapter 5, where we discuss more subtle intricacies of de Sitter string backgrounds including flux quantization, control on large volume and small string coupling constant  $g_s$ , scale separation, and the apparent tension which occurs

when one tries to satisfy all these requirements at the same time.

In the second part of the thesis, we turn to time-dependent compactifications of 10d type IIA supergravity, taking an alternative route towards accelerated expansion (among the options which circumvent the no-go theorems discussed above). We begin in Chapter 6 by giving a bird’s eye view on time-dependent compactifications: we provide some context and a state of the art on the existing literature. We then give a summary of the results found in the two subsequent chapters.

Chapter 7 presents the framework that we use here for the compactification. We explain our ansatz, provide the equations of motion and discuss how these can be derived from a 4d and 1d consistent truncations. The set-up we use is “universal” in the sense that the solutions do not depend on the detailed features of the compactification manifold, but only on the properties which are common to all the manifolds belonging to that class (whether they are Calabi-Yau manifolds, Einstein manifolds, Einstein-Kähler manifolds, etc.).

We then present in Chapter 8 the solutions that we obtain within this framework. The complexity depends on the number of fluxes that we turn on. Up to one flux, the equations can be solved analytically. When two-fluxes are considered, the solutions are not analytical anymore but one can perform a dynamical system analysis that reveals a very rich behaviour. In this picture, the existence of solutions featuring a phase of accelerated expansion is made manifest. The fixed points of this dynamical system, as well as the trajectories on the boundary of the phase space, correspond to the analytic solutions mentioned above. Furthermore, some of the resulting cosmologies exhibit eternal or semi-eternal acceleration, whereas others allow for a parametric control on the number of e-foldings. At future infinity, one can achieve both large volume and weak string coupling. We also obtain several cosmologies featuring an infinite number of cycles of alternating periods of accelerated and decelerated expansions. All the solutions, as well as further computational details are provided in Appendix B.

The third and last part of the thesis focuses on the effect of compactifications similar to the ones considered above on the spectrum of gravitational waves. When one includes (non-smearred)  $O_p/D_p$  sources in the higher-dimensional theory, the warp factor is in general non-constant, and has non-trivial effects on the Kaluza-Klein tower of gravitational waves coming from extra-dimensions. In Chapter 9 we explain the general set-up used for this analysis. We present the warped background over which Kaluza-Klein gravitational waves are studied and the key equations defining their spectrum. There, we also discuss the profile of the warp factor when moving away from a source, which is more generally a question of interest in de Sitter constructions as well.

Finally, Chapter 10 describes the method we use to determine the gravitational wave spectrum and in particular to overcome difficulties due to the region where warp factor becomes negative near the sources, responsible for tachyonic modes. We then present the results that we obtain, and compare them to unwarped extra dimensions. More details about the determination of the spectrum are given in Appendix A.



CLASSICAL DE SITTER PART I  
BACKGROUNDS



# 1 General set-up and ansatz

## 1.1 Context and motivations

As emphasized in the introduction, string theory backgrounds with maximally symmetric spacetimes have always been of prime importance. To start with, a 4-dimensional (4d) de Sitter spacetime is relevant for the connection to cosmology, since it can describe in good approximation our universe in an early inflation phase, or in the far future. A 4d Minkowski spacetime is relevant for particle physics models that may be derived from string theory, or to describe our nearby universe. Last but not least, 4d anti-de Sitter spacetimes are typically considered in a holographic context, but they also appear in various phenomenology related topics, for instance in certain constructions of de Sitter solutions [41, 42] or in the matter of scale separation, revived recently in the swampland program [52, 60]. In addition, the general belief that non-supersymmetric solutions are unstable is shared in various forms for all maximally symmetric spacetimes: see for instance [61–65] for de Sitter, [66, 67] for Minkowski and [68] for anti-de Sitter. The importance of such solutions, and the common properties they may share, motivates us here to classify them, within a certain (standard) ansatz. In turn, the classification helps us finding new types of solutions, as well as new existence no-go theorems, and noticing few general properties.

We focus here on solutions of 10d type IIA/B supergravities with  $D_p$ -branes and orientifold  $O_p$ -planes, as candidates for classical string backgrounds. Checking whether the supergravity solutions actually meet the string effective theory requirements, allowing them to be in the classical string regime, is not always trivial: see e.g. [2] for de Sitter and [69] for anti-de Sitter. This will be the subject of Chapter 5. We further restrict ourselves to a historically standard ansatz, namely one where the extra dimensions are gathered as a group manifold, defined below. In addition, fluxes living there are constant, as well as the  $O_p/D_p$  contributions to the equations: this last point corresponds to having  $O_p/D_p$  sources smeared, or more precisely, considering an integrated version of the solution rather than a localized one. More details on this ansatz is provided in Section 1.2 and in [70]. One interest of this ansatz is that it allows, through a consistent truncation, for an equivalent description as a 4d gauged supergravity, also sometimes used to find those solutions. A further reason to restrict to classical solutions with such an ansatz is the relative simplicity of the setting, of potential interest to further phenomenological applications, while still providing a variety of interesting examples: de Sitter solutions,

(non-) supersymmetric Minkowski ones with fluxes, (non-) supersymmetric (non-) scale separated anti-de Sitter ones, and so on.

## 1.2 The ansatz

As stated above, we are interested in classical solutions of 10d type II supergravities on a 4d maximally symmetric spacetime, i.e. de Sitter, Minkowski or anti-de Sitter, times a 6d compact group manifold  $\mathcal{M}$ , with  $D$ -branes and orientifold planes as sources. The 10d metric reads

$$ds_{10}^2 = g_{\mu\nu} dx^\mu dx^\nu + g_{mn} dy^m dy^n, \quad (1.1)$$

where  $g_{\mu\nu}$  denotes the metric of the 4d extended spacetime and  $g_{mn}$  is the metric for the internal space  $\mathcal{M}$ . We do not include a warp factor, so the sources can be viewed as “smeared”, or rather, some equations can be considered integrated. We come back in Section 5.6 to the question of a localized version of our solutions. The reason for our ansatz is that we will consider intersecting sources, for which a localized description is notoriously difficult to obtain. For the same reason, we take a constant dilaton  $e^\phi = g_s$ . The 6d metric is expressed in a flat basis in terms of 1-forms  $e^a$  as follows

$$ds_6^2 = g_{mn} dy^m dy^n = \delta_{ab} e^a e^b, \quad e^a = e^a{}_m dy^m, \quad de^a = -\frac{1}{2} f^a{}_{bc} e^b \wedge e^c, \quad (1.2)$$

where the last equation is the Maurer-Cartan equation. It defines  $f^a{}_{bc}$  which will here be taken constant, and thus correspond to structure constants of a Lie algebra. This algebra underlies the group manifold  $\mathcal{M}$ . Compactness of the latter requires  $f^a{}_{ac} = 0$  (with sum), a condition to be used from now on. In the following, we will additionally restrict ourselves to work in a basis of  $\{e^a\}$  such that  $f^a{}_{ac} = 0$  *without sum*. This choice of basis is preferred to prove the existence of lattices and thus compactness [71]. The  $f^a{}_{bc}$  can be related in full generality to spin connection coefficients (see e.g. Appendix A of [72]), so the 6d Ricci tensor in the flat basis can be expressed as

$$2 \mathcal{R}_{cd} = -f^b{}_{ac} f^a{}_{bd} - \delta^{bg} \delta_{ah} f^h{}_{gc} f^a{}_{bd} + \frac{1}{2} \delta^{ah} \delta^{bj} \delta_{ci} \delta_{dg} f^i{}_{aj} f^g{}_{hb}, \quad (1.3)$$

where we specified to a compact group manifold.

We allow for  $D_p$ -branes and  $O_p$  orientifold planes, collectively named sources;  $p$  is their dimensionality, sometimes also called size. For a maximally symmetric spacetime, the sources must be along the 3 space extended dimensions, therefore restricting the dimensionality to  $p \geq 3$ . In addition, supergravity fluxes can be purely internal (along the 6d) or spanning the whole 4d, leaving us to use only the 6d  $k$ -forms  $F_{k=0,\dots,6}$  for RR fluxes and the 6d 3-form  $H$  for the NSNS one. As part of the ansatz, motivated in [70], the fluxes components in the 6d orthonormal coframe are constant.

For each source, we then split the 1-forms into the two sets  $\{e^{a_{\parallel}}\}$  and  $\{e^{a_{\perp}}\}$ , taken globally distinct. Every flat index can then be specified as being parallel or transverse to a given source. For instance, for any internal  $q$ -form  $F_q$ , we denote by a label  $(n)$  its number of legs along a source, with  $0 \leq n \leq 2$ , meaning

$$F_q = \frac{1}{q!} F_{q a_{1\perp} \dots a_{q\perp}}^{(0)} e^{a_{1\perp}} \wedge \dots \wedge e^{a_{q\perp}} + \frac{1}{(q-1)!} F_{q a_{1\parallel} a_{2\perp} \dots a_{q\perp}}^{(1)} e^{a_{1\parallel}} \wedge e^{a_{2\perp}} \wedge \dots \wedge e^{a_{q\perp}} + \dots, \quad (1.4)$$

and each  $F_q^{(n)}{}_{a_1\dots a_q}$  is here a constant number. Each source defines naturally parallel and transverse volume forms,  $\text{vol}_{\parallel}$  and  $\text{vol}_{\perp}$ , in terms of the  $\{e^{a_{\parallel}}\}$  and  $\{e^{a_{\perp}}\}$ . Few more useful conventions on our forms include

$$\begin{aligned} \epsilon_{1\dots 6} &= 1, \quad \text{vol}_{\parallel} \wedge \text{vol}_{\perp} = \text{vol}_6 = d^6 y \sqrt{|g_6|} = e^1 \wedge \dots \wedge e^6, \\ *_6(e^{a_1} \wedge \dots \wedge e^{a_q}) &= \frac{1}{(6-q)!} \delta^{a_1 b_1} \dots \delta^{a_q b_q} \epsilon_{b_1 \dots b_q c_{q+1} \dots c_6} e^{c_{q+1}} \wedge \dots \wedge e^{c_6}, \quad *_6^2 A_q = (-1)^q A_q, \\ A_q \wedge *_6 A_q &= \text{vol}_6 |A_q|^2, \quad |A_q|^2 = A_q{}_{a_1 \dots a_q} A_q{}_{b_1 \dots b_q} \delta^{a_1 b_1} \dots \delta^{a_q b_q} / q!. \end{aligned} \quad (1.5)$$

An important distinction to make is whether sources  $O_p/D_p$  (with single  $p$ ) are parallel or intersecting. All sources that are along the same directions are said to be parallel and are part of one set  $I$ . We denote by  $N$  the number of sets: if  $N = 1$ , sources are said to be parallel, if  $N > 1$  they are intersecting. To stress the importance of this distinction, let us mention a few de Sitter examples. It turns out that de Sitter solutions with parallel sources are expected not to exist (conjecture 1 in [70]), while having intersecting ones was shown to help in [73] to get a positive cosmological constant. De Sitter solutions satisfying the above ansatz with  $N > 1$  were obtained in IIA for  $p = 6$ , in particular in [74], and in IIB for  $p = 5$  in [1].

We will also consider in the next chapter the case of sources with multiple dimensionalities  $p$ . For example, one such de Sitter solution is known, with  $p = 5, 7$  in [75]. This situation requires a few more notations, and we follow the formalism introduced in Section 6 of [73]. The sources energy momentum tensor (EMT) is defined via

$$\frac{1}{\sqrt{|g_{10}|}} \sum_{\text{sources}} \frac{\delta S_{\text{DBI}}}{\delta g^{MN}} = -\frac{e^{-\phi}}{4\kappa_{10}^2} T_{MN}, \quad (1.6)$$

where  $S_{\text{DBI}}$  was given in (20). Its trace  $g^{MN} T_{MN}$  is denoted  $T_{10}$ , and the total contribution of sources for each dimensionality  $p$  is written  $T_{10}^{(p)}$  so that one can decompose

$$T_{10} = \sum_p T_{10}^{(p)} = \sum_p \sum_I T_{10}^{(p)I}, \quad (1.7)$$

with a split into all sets  $I$  for a given  $p$ , introducing a  $T_{10}^{(p)I}$ . Each of the  $T_{10}^{(p)I}$  is proportional to  $N_{s,p}^I = N_{O_p}^I - N_{D_p}^I$  (see (4.12) below for more details), the number of sources in the set  $I$ , given by the difference of the number of  $O_p$  and  $D_p$ . With this notation, the 6d EMT can be written as

$$T_{ab} = \sum_p \sum_I \delta_a^{a_{\parallel I}} \delta_b^{b_{\parallel I}} \delta_{a_{\parallel I} b_{\parallel I}} \frac{T_{10}^{(p)I}}{p+1}. \quad (1.8)$$

To make this clearer, let us give an example. For the source configuration considered in [1] which consists of 3 sets of sources:  $O_5/D_5$  in sets  $I = 1, 2$  that wrap directions (1, 2) and (3, 4) respectively, and one set  $I = 3$  which contains  $D_5$  branes only along (5, 6), one ends up with the following 6d EMT,

$$T_{ab} = \text{diag} \left( \frac{T_{10}^{(5)1}}{p+1}, \frac{T_{10}^{(5)1}}{p+1}, \frac{T_{10}^{(5)2}}{p+1}, \frac{T_{10}^{(5)2}}{p+1}, \frac{T_{10}^{(5)3}}{p+1}, \frac{T_{10}^{(5)3}}{p+1} \right), \quad (1.9)$$



with  $p = 5$ . The case of single dimensionality  $p$  is recovered by dropping the unnecessary upper  $(p)$ ; we will do so in the following. In addition, we have the 4d trace  $g^{\mu\nu}T_{\mu\nu} = 4 \sum_p T_{10}^{(p)}/(p+1)$ .

## 1.3 The equations

We give in this section the type II supergravities equations of motion (e.o.m.) and Bianchi identities (BI), in our framework with sources of multiple dimensionalities,  $3 \leq p \leq 8$ . These equations encompass in particular the case of single dimensionality sources, obtained by setting to zero the appropriate source variables. By combining a few equations as in [73], one obtains the following useful expression of  $\mathcal{R}_4$ ,

$$\mathcal{R}_4 = g_s \sum_p \frac{T_{10}^{(p)}}{p+1} - g_s^2 \sum_{q=0}^6 |F_q|^2 . \quad (1.10)$$

### 1.3.1 IIA supergravity

- the fluxes e.o.m.

$$d(*_6 H) - g_s^2 (F_0 \wedge *_6 F_2 + F_2 \wedge *_6 F_4 + F_4 \wedge *_6 F_6) = 0 , \quad (1.11)$$

$$d(*_6 F_2) + H \wedge *_6 F_4 = 0 , \quad (1.12)$$

$$d(*_6 F_4) + H \wedge *_6 F_6 = 0 , \quad (1.13)$$

- the fluxes BI

$$dH = 0 , \quad (1.14)$$

$$dF_0 = - \sum_I \frac{T_{10}^{(8)I}}{9} \text{vol}_{\perp(8)I} , \quad (1.15)$$

$$dF_2 - H \wedge F_0 = \sum_I \frac{T_{10}^{(6)I}}{7} \text{vol}_{\perp(6)I} , \quad (1.16)$$

$$dF_4 - H \wedge F_2 = - \sum_I \frac{T_{10}^{(4)I}}{5} \text{vol}_{\perp(4)I} , \quad (1.17)$$

- the dilaton e.o.m.

$$2\mathcal{R}_4 + 2\mathcal{R}_6 + g_s \sum_p \frac{T_{10}^{(p)}}{p+1} - |H|^2 = 0 , \quad (1.18)$$

- the 4d Einstein equation (equivalent to its trace)

$$4\mathcal{R}_4 = g_s \sum_p \frac{7-p}{p+1} T_{10}^{(p)} - 2|H|^2 + g_s^2 (|F_0|^2 - |F_2|^2 - 3|F_4|^2 - 5|F_6|^2) , \quad (1.19)$$

- the 6d (trace-reversed) Einstein equation

$$\begin{aligned} \mathcal{R}_{ab} = & \frac{g_s^2}{2} \left( F_2{}_{ac} F_2{}^b{}^c + \frac{1}{3!} F_4{}_{acde} F_4{}^b{}^{cde} \right) + \frac{1}{4} H_{acd} H_b{}^{cd} \\ & + \frac{g_s}{2} T_{ab} + \frac{\delta_{ab}}{16} \left( -g_s T_{10} - 2|H|^2 + g_s^2 (|F_0|^2 - |F_2|^2 - 3|F_4|^2 + 3|F_6|^2) \right) , \end{aligned} \quad (1.20)$$

$$\text{with } T_{ab} = \sum_p \sum_I \delta_a^{a||I} \delta_b^{b||I} \delta_{a||I} \delta_{b||I} \frac{T_{10}^{(p)I}}{p+1} , \quad (1.21)$$

- the Jacobi identity (or Riemann BI)

$$f^a{}_{e[b} f^e{}_{cd]} = 0 . \quad (1.22)$$

### 1.3.2 IIB supergravity

- the fluxes e.o.m.

$$d(*_6 H) - g_s^2 (F_1 \wedge *_6 F_3 + F_3 \wedge *_6 F_5) = 0 , \quad (1.23)$$

$$d(*_6 F_1) + H \wedge *_6 F_3 = 0 , \quad (1.24)$$

$$d(*_6 F_3) + H \wedge *_6 F_5 = 0 , \quad (1.25)$$

$$d(*_6 F_5) = 0 , \quad (1.26)$$

- the fluxes BI

$$dH = 0 , \quad (1.27)$$

$$dF_1 = - \sum_I \frac{T_{10}^{(7)I}}{8} \text{vol}_{\perp(7)I} , \quad (1.28)$$

$$dF_3 - H \wedge F_1 = \sum_I \frac{T_{10}^{(5)I}}{6} \text{vol}_{\perp(5)I} , \quad (1.29)$$

$$dF_5 - H \wedge F_3 = - \sum_I \frac{T_{10}^{(3)I}}{4} \text{vol}_{\perp(3)I} , \quad (1.30)$$

- the dilaton e.o.m.

$$2\mathcal{R}_4 + 2\mathcal{R}_6 + g_s \sum_p \frac{T_{10}^{(p)}}{p+1} - |H|^2 = 0 , \quad (1.31)$$

- the 4d Einstein equation (equivalent to its trace)

$$4\mathcal{R}_4 = g_s \sum_p \frac{7-p}{p+1} T_{10}^{(p)} - 2|H|^2 - g_s^2 (2|F_3|^2 + 4|F_5|^2) , \quad (1.32)$$

## Chapter 1. General set-up and ansatz

---

- the 6d (trace-reversed) Einstein equation

$$\begin{aligned} \mathcal{R}_{ab} = & \frac{g_s^2}{2} \left( F_{1\ a} F_{1\ b} + \frac{1}{2!} F_{3\ acd} F_{3\ b}{}^{cd} + \frac{1}{2 \cdot 4!} F_{5\ acdef} F_{5\ b}{}^{cdef} - \frac{1}{2} *_{6} F_{5\ a} *_{6} F_{5\ b} \right) \\ & + \frac{1}{4} H_{acd} H_b{}^{cd} + \frac{g_s}{2} T_{ab} + \frac{\delta_{ab}}{16} (-g_s T_{10} - 2|H|^2 - 2g_s^2 |F_3|^2) , \end{aligned} \quad (1.33)$$

$$\text{with } T_{ab} = \sum_p \sum_I \delta_a{}^{a_{||I}} \delta_b{}^{b_{||I}} \delta_{a_{||I} b_{||I}} \frac{T_{10}^{(p)I}}{p+1} , \quad (1.34)$$

- the Jacobi identity (or Riemann BI)

$$f^a{}_{e[b} f^e{}_{cd]} = 0 . \quad (1.35)$$

Let us stress that the only variables entering the equations are the constants

$$f^a{}_{bc}, H_{abc}, g_s F_{q a_1 \dots a_q}, g_s T_{10}^I , \quad (1.36)$$

and that the equations to solve are quadratic polynomials in these variables. The exact number of (scalar) equations and (scalar) variables will depend on the explicit orientifold projection, which is discussed in the next chapter.

## 2 Charting the Landscape

In this chapter, we chart the space of solutions – which we will refer to as the *Landscape* of (anti-) de Sitter and Minkowski solutions (within this ansatz) – into smaller regions, according to the possible source configurations. Indeed, not everything is allowed when it comes to placing the  $D$ -branes and orientifold planes: as we will explain in the following, it can be understood as being constrained by the structure of the Bianchi identities for the RR fluxes. Only a restricted number of configurations turn out to be possible and inequivalent and we classify those. This will allow a systematic and organised exploration of the solutions space, that will be the subject of Chapter 3.

### 2.1 Classification of possible solutions

In IIA, we can a priori have  $p = 4, 6, 8$  sources, and in IIB,  $p = 3, 5, 7, 9$ . Our ansatz presented in the previous chapter is however more restrictive. As we will see, sources are here visible only if their transverse volume appears in the right-hand side of the sourced RR Bianchi identity. This first implies that we cannot have  $p = 9$  sources, since we do not consider hypothetical  $F_{-1}$  fluxes. In addition, since we consider constant fluxes, we get that  $dF_0 = 0$ , so we cannot admit  $p = 8$  source. This leaves us in IIA with  $p = 4, 6$ , and  $p = 3, 5, 7$  in IIB; we will also see that  $p = 3$  sources cannot really contribute here. Given the above ansatz for solutions on a 4d maximally symmetric spacetime with orientifolds, we now present a systematic approach that will allow us to determine all possible source configurations, as well as the allowed fields or variables among (1.36).

1. We first consider an orientifold  $O_p$ -plane, and place it along the first  $p - 3$  internal dimensions, in the set  $I = 1$ .
2. An  $O_p$  imposes a projection. Because of our ansatz where variables are constant, the projection sets to zero many flux components and structure constants [70]. We then give the explicit list of remaining variables.
3. We finally look at each sourced RR Bianchi identity

$$dF_{8-p} - H \wedge F_{6-p} = \varepsilon_p \sum_I \frac{T_{10}^{(p)I}}{p+1} \text{vol}_{\perp(p)I}, \quad \varepsilon_p = (-1)^{p+1} (-1)^{\lfloor \frac{9-p}{2} \rfloor}, \quad (2.1)$$

where the right-hand side indicates the various  $p$ -sources which are present, through the total contribution  $T_{10}^{(p)I}$  in each set  $I$ , together with the transverse volume form  $\text{vol}_{\perp(p)I}$  to this set. Using the Maurer-Cartan equation  $de^a = -\frac{1}{2}f^a{}_{bc}e^b \wedge e^c$ , we compute the various components on the left-hand side using the list of variables remaining after the projection. Each potentially non-zero component can be interpreted as giving rise to a  $\text{vol}_{\perp(p)I}$  in the right-hand side, with a non-zero  $T_{10}^{(p)I}$ . On the contrary, there cannot be any source (in our ansatz) whose transverse directions do not appear in the left-hand side.<sup>1</sup> We identify this way the possible placements of source sets, i.e. the allowed source configurations, and they will turn out to be very constrained.

4. We then start over by adding another  $O_p$  in a different set, studying the resulting projection, the allowed variables and remaining sources. In case this leads to a contradiction, we take it back and conclude that other sets  $J$  can at best contain  $D_p$ -branes, implying in our conventions  $T_{10}^{(p)J} \leq 0$ .

We will proceed in the following with this systematic approach, first considering a single dimensionality  $p$  and then allowing for multiple ones. This will result in identifying all possible source configurations and the associated sets of variables. This provides a natural classification of the possible solutions, and we will distinguish the various possibilities into so-called solution classes.

Anticipating on our results, we now present these classes and the symbols to denote them. Given our ansatz, a solution class is defined by the number and dimensionalities of  $O_p$ . This defines the allowed variables under the corresponding projections. The symbol to be used is  $s$  for single dimensionality of  $O_p$  and  $D_p$ , and  $m$  for multiple dimensionalities. To this, we add a subscript carrying the  $p$ 's of the  $O_p$ : for instance  $m_{5577}$  stands for 2  $O_5$  and 2  $O_7$ . In the case where different choices of  $O_p$  lead to the same set of allowed variables and sources (up to the nature of the latter, i.e.  $D_p$  or  $O_p$ ), then the class is defined by the maximum number of  $O_p$ . This will become clear in the following, but for example, it will be the case for  $s_{6666}$  instead of  $s_{666}$ , or  $m_{5577}$  instead of  $m_{577}$ . Finally, note that a solution is sometimes searched within a certain class, but once found, it ends up having many variables and sources set to zero, in such a way that it can belong to another class with more  $O_p$ : in that case, the convention is to place it in the latter.

The classes defined as above amount to consider some sets of source directions as “equivalent”. This means that directions are equivalent up to a relabeling, not considering the orientation. For instance, given an  $O_p$  along directions 123, choosing another set along 145 or 245 is equivalent since one can consider  $1 \leftrightarrow 2$ , which does not change the placement of the first  $O_p$ , ignoring orientation. However, when it comes to a concrete solution, doing a relabeling (or more generally a change of basis) that does not preserve source volume forms, in particular their orientation, typically does not lead to a solution. Indeed, changing the orientation of a source can be compensated by changing the sign of the corresponding  $T_{10}^{(p)I}$ , which however does not solve the equations anymore. Because of this, solution classes could be split into subclasses: the variables and source directions of

---

<sup>1</sup>Proceeding this way, we neglect the possibility of having sources in a set  $I$  such that  $T_{10}^{(p)I} = 0$ , i.e. where  $O_p$  and  $D_p$  contributions perfectly cancel each other. We view this here as going beyond our ansatz. See in particular [76] for a discussion of such Minkowski solutions.

each subclasses can be mapped into each other by some transformation, e.g. a relabeling, but actual solutions do not survive this transformation. We will have an example of this for  $m_{5577}$ , and will then introduce the subclass  $m_{5577}^*$ .

We now turn to the systematic determination of the solution classes, and will provide summaries of those in Sections 2.1.1 and 2.1.2.

### 2.1.1 Source configurations and fields for a single dimensionality $p$

#### • $O_3$ -plane

The case of  $p = 3$  sources is special, because they are transverse to all 6d dimensions, and are thus only points in  $\mathcal{M}$ . A first consequence is that no structure constant  $f^a{}_{bc}$  survives the orientifold projection. In addition, given our ansatz, only the following flux components remain after an  $O_3$  projection

$$O_3 : F_3^{(0)}, H^{(0)}, \quad (2.2)$$

or in other words

$$s_3 : F_3{}_{abc}, H_{abc}, \quad a, b, c = 1, \dots, 6. \quad (2.3)$$

Considering an  $O_3$ , the left-hand side of the Bianchi identity for  $F_5$  boils down to  $-H \wedge F_3$ , which can be non-zero with the above components, and proportional to the 6d volume form. We can then have  $p = 3$  sources. In short we get

$$s_3 : 1 O_3 \text{ (at a point)} \Rightarrow p = 3 \text{ sources at points}. \quad (2.4)$$

#### • $O_4$ -plane

The orientifold projection of an  $O_4$  restricts the structure constants and fluxes to be [77]

$$O_4 : f^{a||b_{\perp}c_{\perp}}, f^{a_{\perp}b_{\perp}c_{||}}, F_2^{(0)}, F_4^{(1)}, H^{(0)}. \quad (2.5)$$

The other possible type of structure constants,  $f^{a||b_{||}c_{||}}$ , is vanishing due to the antisymmetry of  $b, c$ , since there is only one direction parallel to the  $O_4$ . We also recall that we restrict ourselves for simplicity to a basis where  $f^a{}_{ac} = 0$  without sum. We now place an  $O_4$  in the set  $I = 1$  along the internal direction 1. We deduce the following list of remaining variables after one  $O_4$  projection

$$\begin{aligned} s_4 : F_2 : & F_2{}_{23}, F_2{}_{24}, F_2{}_{25}, F_2{}_{26}, F_2{}_{34}, F_2{}_{35}, F_2{}_{36}, F_2{}_{45}, \\ & F_2{}_{46}, F_2{}_{56}, \\ F_4 : & F_4{}_{1234}, F_4{}_{1235}, F_4{}_{1236}, F_4{}_{1245}, F_4{}_{1246}, F_4{}_{1256}, F_4{}_{1345}, \\ & F_4{}_{1346}, F_4{}_{1356}, F_4{}_{1456}, \\ H : & H_{234}, H_{235}, H_{236}, H_{245}, H_{246}, H_{256}, H_{345}, H_{346}, \\ & H_{356}, H_{456}, \\ f^{a||1b_{\perp}c_{\perp}} : & f^1{}_{23}, f^1{}_{24}, f^1{}_{25}, f^1{}_{26}, f^1{}_{34}, f^1{}_{35}, f^1{}_{36}, f^1{}_{45}, f^1{}_{46}, f^1{}_{56}, \\ f^{a_{\perp}1b_{\perp}c_{||}} : & f^2{}_{31}, f^2{}_{41}, f^2{}_{51}, f^2{}_{61}, f^3{}_{21}, f^3{}_{41}, f^3{}_{51}, f^3{}_{61}, f^4{}_{21}, f^4{}_{31}, \\ & f^4{}_{51}, f^4{}_{61}, f^5{}_{21}, f^5{}_{31}, f^5{}_{41}, f^5{}_{61}, f^6{}_{21}, f^6{}_{31}, f^6{}_{41}, f^6{}_{51}. \end{aligned} \quad (2.6)$$

## Chapter 2. Charting the Landscape

---

There are 30 fluxes and 30 structure constants. From this list, it is straightforward to compute the components of  $dF_4$  and  $H \wedge F_2$ . It is easy to verify that  $e^1$  never appears in these 5-forms. This means the components are purely along directions 23456, i.e.  $\text{vol}_{\perp 1}$ , in other words

$$s_4 : \quad 1 \ O_4 \text{ (along direction 1)} \Rightarrow p = 4 \text{ sources along direction 1} . \quad (2.7)$$

We conclude that imposing one  $O_4$  projection with our ansatz allows to have only  $N = 1$  set of sources: the one with the  $O_4$ . In other words, with an  $O_4$ ,  $p = 4$  sources can only be parallel!

### • $O_5$ -plane

We turn to  $p = 5$  and proceed as above. We recall the choice of working in a basis where  $f^a_{ac} = 0$  without sum. One  $O_5$  projection then leaves us with

$$O_5 : \quad f^{a\parallel b_{\perp}c_{\perp}}, f^{a_{\perp}b_{\perp}c_{\parallel}}, F_1^{(0)}, F_3^{(1)}, F_5^{(2)}, H^{(0)}, H^{(2)} . \quad (2.8)$$

Having the  $O_5$  in a set  $I = 1$  along directions 12, one is left with the following variables

$$\begin{aligned} s_5 : \quad F_1 : & F_{1\ 3}, F_{1\ 4}, F_{1\ 5}, F_{1\ 6}, \\ F_3 : & F_{3\ 134}, F_{3\ 135}, F_{3\ 136}, F_{3\ 145}, F_{3\ 146}, F_{3\ 156}, F_{3\ 234}, F_{3\ 235}, \\ & F_{3\ 236}, F_{3\ 245}, F_{3\ 246}, F_{3\ 256}, \\ F_5 : & F_{5\ 12345}, F_{5\ 12346}, F_{5\ 12356}, F_{5\ 12456}, \\ H : & H_{123}, H_{124}, H_{125}, H_{126}, H_{345}, H_{346}, H_{356}, H_{456}, \quad (2.9) \\ f^{a\parallel 1 b_{\perp 1} c_{\perp 1}} : & f^1_{34}, f^1_{35}, f^1_{36}, f^1_{45}, f^1_{46}, f^1_{56}, f^2_{34}, f^2_{35}, f^2_{36}, \\ & f^2_{45}, f^2_{46}, f^2_{56}, \\ f^{a_{\perp 1} b_{\perp 1} c_{\parallel 1}} : & f^3_{14}, f^3_{15}, f^3_{16}, f^3_{24}, f^3_{25}, f^3_{26}, f^4_{13}, f^4_{15}, f^4_{16}, \\ & f^4_{23}, f^4_{25}, f^4_{26}, f^5_{13}, f^5_{14}, f^5_{16}, f^5_{23}, f^5_{24}, f^5_{26}, \\ & f^6_{13}, f^6_{14}, f^6_{15}, f^6_{23}, f^6_{24}, f^6_{25}, \end{aligned}$$

namely 28 flux components and 36 structure constants. From there one computes  $dF_3$ ,  $H \wedge F_1$ , and deduces the possible non-zero components. It is straightforward to deduce that source sets can be along the following directions

$$\begin{aligned} s_5 : \quad 1 \ O_5 \text{ (along directions 12)} \Rightarrow p = 5 \text{ sources along directions } 12, 34, 35, 36, \\ \hspace{20em} (2.10) \\ \hspace{20em} 45, 46, 56 . \end{aligned}$$

So contrary to  $p = 4$ , we can have here intersecting sources. The source directions in (2.10) are, apart from 12, all equivalent. We then place a second  $O_5$  in a second set  $I = 2$

## 2.1 Classification of possible solutions

---

along 34, and determine the remaining variables to be

$$\begin{aligned}
s_{55} : \quad & F_1 : F_{1\ 5}, \quad F_{1\ 6}, \\
& F_3 : F_{3\ 315}, \quad F_{3\ 316}, \quad F_{3\ 325}, \quad F_{3\ 326}, \quad F_{3\ 415}, \quad F_{3\ 416}, \quad F_{3\ 425}, \quad F_{3\ 426}, \\
& F_5 : F_{5\ 34125}, \quad F_{5\ 34126}, \\
& H : H_{125}, \quad H_{126}, \quad H_{345}, \quad H_{346}, \\
f^{a\parallel 2} b_{\perp 2} c_{\perp 2} : & f^3_{15}, \quad f^3_{16}, \quad f^3_{25}, \quad f^3_{26}, \quad f^4_{15}, \quad f^4_{16}, \quad f^4_{25}, \quad f^4_{26}, \\
f^{a\perp 2} b_{\perp 2} c_{\parallel 2} : & f^1_{53}, \quad f^1_{63}, \quad f^1_{54}, \quad f^1_{64}, \quad f^2_{53}, \quad f^2_{63}, \quad f^2_{54}, \quad f^2_{64}, \\
& f^5_{13}, \quad f^5_{23}, \quad f^5_{14}, \quad f^5_{24}, \quad f^6_{13}, \quad f^6_{23}, \quad f^6_{14}, \quad f^6_{24},
\end{aligned} \tag{2.11}$$

namely 16 fluxes and 24 structure constants. We then compute the Bianchi identity components, and verify that sources can be along

$$s_{55} : \quad 2 O_5 \text{ (along directions 12, 34)} \Rightarrow p = 5 \text{ sources along directions 12, 34, 56} . \tag{2.12}$$

We finally consider a third  $O_5$  in  $I = 3$  along 56. In this case, the structure constants are not constrained further, but only the  $F_3$  flux remains, i.e. the variables are

$$\begin{aligned}
s_{555} : \quad & F_3 : F_{3\ 135}, \quad F_{3\ 136}, \quad F_{3\ 145}, \quad F_{3\ 146}, \quad F_{3\ 235}, \quad F_{3\ 236}, \quad F_{3\ 245}, \quad F_{3\ 246}, \\
f^{a\parallel 2} b_{\perp 2} c_{\perp 2} : & f^3_{15}, \quad f^3_{16}, \quad f^3_{25}, \quad f^3_{26}, \quad f^4_{15}, \quad f^4_{16}, \quad f^4_{25}, \quad f^4_{26}, \\
f^{a\perp 2} b_{\perp 2} c_{\parallel 2} : & f^1_{53}, \quad f^1_{63}, \quad f^1_{54}, \quad f^1_{64}, \quad f^2_{53}, \quad f^2_{63}, \quad f^2_{54}, \quad f^2_{64}, \\
& f^5_{13}, \quad f^5_{23}, \quad f^5_{14}, \quad f^5_{24}, \quad f^6_{13}, \quad f^6_{23}, \quad f^6_{14}, \quad f^6_{24},
\end{aligned} \tag{2.13}$$

for a total of 8 flux components and 24 structure constants. We compute the Bianchi identity components, and those remain as above

$$s_{555} : \quad 3 O_5 \text{ (along directions 12, 34, 56)} \Rightarrow p = 5 \text{ sources along directions 12, 34, 56} . \tag{2.14}$$

### • $O_6$ -plane

We proceed as above. One  $O_6$  projection allows for the following variables

$$O_6 : \quad f^{a\parallel} b_{\perp} c_{\perp}, \quad f^{a\perp} b_{\perp} c_{\parallel}, \quad f^{a\parallel} b_{\parallel} c_{\parallel}, \quad F_0^{(0)}, F_2^{(1)}, F_4^{(2)}, F_6^{(3)}, H^{(0)}, H^{(2)} . \tag{2.15}$$



## Chapter 2. Charting the Landscape

---

Placing the  $O_6$  in the first set  $I = 1$  along 123, we are left with the following variables

$$\begin{aligned}
s_6 : \quad & F_0 : F_0, \\
& F_2 : F_{2\ 14}, F_{2\ 15}, F_{2\ 16}, F_{2\ 24}, F_{2\ 25}, F_{2\ 26}, F_{2\ 34}, F_{2\ 35}, F_{2\ 36}, \\
& F_4 : F_{4\ 1245}, F_{4\ 1246}, F_{4\ 1256}, F_{4\ 1345}, F_{4\ 1346}, F_{4\ 1356}, F_{4\ 2345}, \\
& \quad F_{4\ 2346}, F_{4\ 2356}, \\
& F_6 : F_{6\ 123456}, \\
& H : H_{124}, H_{125}, H_{126}, H_{134}, H_{135}, H_{136}, H_{234}, H_{235}, \\
& \quad H_{236}, H_{456}, \tag{2.16} \\
f^{a_{\parallel 1} b_{\perp 1} c_{\perp 1}} : & f^1_{45}, f^1_{46}, f^1_{56}, f^2_{45}, f^2_{46}, f^2_{56}, f^3_{45}, f^3_{46}, f^3_{56}, \\
f^{a_{\perp 1} b_{\perp 1} c_{\parallel 1}} : & f^4_{51}, f^4_{61}, f^5_{41}, f^5_{61}, f^6_{41}, f^6_{51}, f^4_{52}, f^4_{62}, f^5_{42}, f^5_{62}, \\
& f^6_{42}, f^6_{52}, f^4_{53}, f^4_{63}, f^5_{43}, f^5_{63}, f^6_{43}, f^6_{53}, \\
f^{a_{\parallel 1} b_{\parallel 1} c_{\parallel 1}} : & f^1_{23}, f^2_{31}, f^3_{12},
\end{aligned}$$

namely 30 fluxes and 30 structure constants (as for  $p = 4$ ). From those we compute  $dF_2$ ,  $H \wedge F_0$ , and deduce that the directions of possible sources

$$\begin{aligned}
s_6 : \quad & 1\ O_6 \text{ (along directions 123)} \Rightarrow p = 6 \text{ sources along directions } 123, 145, 146, \\
& \tag{2.17} \\
& \quad 156, 245, 246, 256, 345, 346, 356.
\end{aligned}$$

This means that we can have intersecting sources. Given directions 123, the other possible sets in (2.17) are all equivalent. We place a second  $O_6$  in set  $I = 2$  along 145, and we are left with the following variables

$$\begin{aligned}
s_{66} : \quad & F_0 : F_0, \\
& F_2 : F_{2\ 16}, F_{2\ 24}, F_{2\ 25}, F_{2\ 34}, F_{2\ 35}, \\
& F_4 : F_{4\ 1246}, F_{4\ 1256}, F_{4\ 1346}, F_{4\ 1356}, F_{4\ 2345}, \\
& F_6 : F_{6\ 123456}, \\
& H : H_{124}, H_{125}, H_{134}, H_{135}, H_{236}, H_{456}, \tag{2.18} \\
f^{a_{\parallel 1} b_{\perp 1} c_{\perp 1}} : & f^1_{45}, f^2_{46}, f^2_{56}, f^3_{46}, f^3_{56}, \\
f^{a_{\perp 1} b_{\perp 1} c_{\parallel 1}} : & f^4_{51}, f^5_{41}, f^4_{62}, f^5_{62}, f^6_{42}, f^6_{52}, f^4_{63}, f^5_{63}, f^6_{43}, f^6_{53}, \\
f^{a_{\parallel 1} b_{\parallel 1} c_{\parallel 1}} : & f^1_{23}, f^2_{31}, f^3_{12},
\end{aligned}$$

namely 18 fluxes and 18 structure constants. We proceed as above and obtain the following sources

$$\begin{aligned}
s_{66} : \quad & 2\ O_6 \text{ (along directions 123, 145)} \Rightarrow p = 6 \text{ sources along directions } 123, 145, \\
& \tag{2.19} \\
& \quad 246, 256, 346, 356.
\end{aligned}$$

## 2.1 Classification of possible solutions

Given 123 and 145, the other directions in (2.19) are equivalent. We place a third  $O_6$  in set  $I = 3$  along 256, and we are left with

$$\begin{aligned}
 s_{6666} : \quad F_q : \quad & F_0, \quad F_{2\ 16}, \quad F_{2\ 24}, \quad F_{2\ 35}, \quad F_{4\ 1246}, \quad F_{4\ 1356}, \quad F_{4\ 2345}, \quad F_6\ 123456, \\
 H : \quad & H_{125}, \quad H_{134}, \quad H_{236}, \quad H_{456}, \\
 f^{a\parallel 1}{}_{bc} : \quad & f^1_{45}, \quad f^2_{56}, \quad f^3_{46}, \quad f^1_{23}, \quad f^2_{31}, \quad f^3_{12}, \\
 f^{a\perp 1}{}_{b\perp 1}{}_{c\parallel 1} : \quad & f^4_{51}, \quad f^4_{63}, \quad f^5_{41}, \quad f^5_{62}, \quad f^6_{52}, \quad f^6_{43},
 \end{aligned} \tag{2.20}$$

namely 12 fluxes and 12 structure constants. Proceeding as above we obtain

$$\begin{aligned}
 s_{6666} : \quad 3\ O_6 \text{ (along directions 123, 145, 256)} \Rightarrow p = 6 \text{ sources along directions} \\
 \hspace{20em} \tag{2.21} \\
 \hspace{20em} 123, 145, 256, 346 .
 \end{aligned}$$

Placing an  $O_6$  along the last set of directions 346 preserves exactly the same variables and sources. This was already noticed in [74]: the fourth orientifold involution comes for free. This is why we name the above class  $s_{6666}$ .

### • $O_7$ -plane

We finally consider  $p = 7$ . The components allowed under an  $O_7$  projection are

$$O_7 : \quad f^{a\parallel}{}_{b\perp c\perp}, \quad f^{a\perp}{}_{b\perp c\parallel}, \quad f^{a\parallel}{}_{b\parallel c\parallel}, \quad F_1^{(1)}, \quad F_3^{(2)}, \quad F_5^{(3)}, \quad H^{(2)}. \tag{2.22}$$

We start with one  $O_7$  along 1234 and get after projection the following list of variables

$$\begin{aligned}
 s_7 : \quad F_1 : \quad & F_{1\ 1}, \quad F_{1\ 2}, \quad F_{1\ 3}, \quad F_{1\ 4}, \\
 F_3 : \quad & F_{3\ 125}, \quad F_{3\ 126}, \quad F_{3\ 135}, \quad F_{3\ 136}, \quad F_{3\ 145}, \quad F_{3\ 146}, \\
 & F_{3\ 235}, \quad F_{3\ 236}, \quad F_{3\ 245}, \quad F_{3\ 246}, \quad F_{3\ 345}, \quad F_{3\ 346}, \\
 F_5 : \quad & F_5\ 12356, \quad F_5\ 12456, \quad F_5\ 13456, \quad F_5\ 23456, \\
 H : \quad & H_{125}, \quad H_{126}, \quad H_{135}, \quad H_{136}, \quad H_{145}, \quad H_{146}, \\
 & H_{235}, \quad H_{236}, \quad H_{245}, \quad H_{246}, \quad H_{345}, \quad H_{346}, \\
 f^{a\parallel 1}{}_{b\perp 1}{}_{c\perp 1} : \quad & f^1_{56}, \quad f^2_{56}, \quad f^3_{56}, \quad f^4_{56}, \\
 f^{a\perp 1}{}_{b\perp 1}{}_{c\parallel 1} : \quad & f^5_{16}, \quad f^5_{26}, \quad f^5_{36}, \quad f^5_{46}, \quad f^6_{15}, \quad f^6_{25}, \quad f^6_{35}, \quad f^6_{45}, \\
 f^{a\parallel 1}{}_{b\parallel 1}{}_{c\parallel 1} : \quad & f^1_{23}, \quad f^1_{24}, \quad f^1_{34}, \quad f^2_{13}, \quad f^2_{14}, \quad f^2_{34}, \\
 & f^3_{12}, \quad f^3_{14}, \quad f^3_{24}, \quad f^4_{12}, \quad f^4_{13}, \quad f^4_{23}.
 \end{aligned} \tag{2.23}$$

There are here 32 flux components and 24 structure constants. We obtain the following possible sources

$$\begin{aligned}
 s_7 : \quad 1\ O_7 \text{ (along 1234)} \Rightarrow p = 7 \text{ sources along } 1234, 3456, 2456, 2356, \\
 \hspace{20em} \tag{2.24} \\
 \hspace{20em} 1456, 1356, 1256 .
 \end{aligned}$$

## Chapter 2. Charting the Landscape

From (2.24), we add a second  $O_7$  in the set  $I = 2$  along 1256 and obtain the following variables

$$\begin{aligned}
 s_{77} : \quad & F_1 : F_{1\ 1}, F_{1\ 2}, \\
 & F_3 : F_{3\ 135}, F_{3\ 136}, F_{3\ 145}, F_{3\ 146}, \\
 & \quad F_{3\ 235}, F_{3\ 236}, F_{3\ 245}, F_{3\ 246}, \\
 & F_5 : F_{5\ 13456}, F_{5\ 23456}, \\
 & H : H_{135}, H_{136}, H_{145}, H_{146}, H_{235}, H_{236}, H_{245}, H_{246}, \quad (2.25) \\
 f^{a\parallel_1 b_{\perp_1} c_{\perp_1}} : & f^1_{56}, f^2_{56}, \\
 f^{a_{\perp_1} b_{\perp_1} c_{\parallel_1}} : & f^5_{16}, f^5_{26}, f^6_{15}, f^6_{25}, \\
 f^{a\parallel_1 b_{\parallel_1} c_{\parallel_1}} : & f^1_{34}, f^2_{34}, f^3_{14}, f^3_{24}, f^4_{13}, f^4_{23}.
 \end{aligned}$$

The Bianchi identity allows for the following source configurations

$$s_{77} : 2 O_7 \text{ (along 1234 and 1256)} \Rightarrow p = 7 \text{ sources along 1234, 1256} . \quad (2.26)$$

### • Summary

Our ansatz with at least one  $O_p$  and a single dimensionality  $p$  allows for only few possible source configurations and associated field content (variables). This information allows to classify possible solutions into classes. We summarize these results in Table 2.1.

Solution class	Number of sets with $O_p$	$O_p$ sets directions	Possible $D_p$ sets directions	Field content
$s_3$	1 $O_3$	pt		(2.3)
$s_4$	1 $O_4$	1		(2.6)
$s_5$	1 $O_5$	12	34, 35, 36, 45, 46, 56	(2.9)
$s_{55}$	2 $O_5$	12, 34	56	(2.11)
$s_{555}$	3 $O_5$	12, 34, 56		(2.13)
$s_6$	1 $O_6$	123	145, 146, 156, 245, 246, 256, 345, 346, 356	(2.16)
$s_{66}$	2 $O_6$	123, 145	246, 256, 346, 356	(2.18)
$s_{6666}$	3 or 4 $O_6$	123, 145, 256, (346)	(346)	(2.20)
$s_7$	1 $O_7$	1234	3456, 2456, 2356, 1456, 1356, 1256	(2.23)
$s_{77}$	2 $O_7$	1234, 1256		(2.25)

Table 2.1: Source configurations allowed in our ansatz for a single dimensionality  $p$ , with at least one  $O_p$ . To each of those corresponds a list of variables or field content (structure constants, fluxes) allowed by the orientifold projection. Together, these pieces of information define a solution class.

### • Comments on de Sitter solutions

The results obtained offer a new light on various observations and constraints regarding de Sitter solutions, and we pause here to comment on those. The question of finding

de Sitter solutions with our ansatz and a single dimensionality  $p$  has been studied in great details and is highly constrained [70, 77, 78]. A first result is that only  $p = 4, 5$  or  $6$  would allow for solutions, the other  $p$ 's leading to no-go theorems. In addition, we mentioned already that de Sitter solutions with parallel sources are conjectured not to exist [70], while solutions have been found with intersecting sources for  $p = 5$  or  $6$ . The details of the intersection was shown in [73] to play a role: let us add a word on this point. Of particular interest was the case of ‘‘homogeneous overlap’’, where each single set  $I$  overlaps the other sets in the same manner, i.e. the number of common directions is the same with each other set and denoted  $N_o$ . Different situations are named ‘‘inhomogeneous overlap’’. In general, one has  $0 \leq N_o \leq p - 3$ , where  $N_o = p - 3$  means that sources are parallel. It was noticed in [73] that the choice of homogeneous overlap with  $N_o = p - 5$  for  $p = 5, 6$  would simplify the equations of motion and make these two cases very analogous. As it turns out, the de Sitter solutions obtained for  $p = 5, 6$  both verified  $N_o = p - 5$ . Contrary to the other  $p$ 's, the case of  $p = 4$  could only be loosely constrained in [73].<sup>2</sup> An obvious difference with  $p = 5, 6$  is that  $O_4/D_4$  only wrap one internal dimension, so they cannot overlap;<sup>3</sup> few more differences were pointed out in [73].

As we now explain, the results obtained here clarify the previous observations:

- $p = 4$ : we obtain that the only possible source configuration is a single set of parallel sources. This emphasizes the difference with  $p = 5, 6$ , and makes it very unlikely to find any de Sitter solution (with our ansatz) for  $p = 4$ .
- $p = 5, 6$  and homogeneous overlap: when looking at all possible source configurations, we discover to our surprise that the only possible cases of homogeneous overlap correspond to those already studied and obey  $N_o = p - 5$ .<sup>4</sup> What appeared previously as an interesting choice turns out to be the only possibility. This possibility also has a relation to supersymmetry, as we will see in Section 2.1.3.

In more details, the source configurations are those of classes  $s_{6666}$ ,  $s_{55}$  or  $s_{555}$ ; de Sitter solutions, however, cannot be found in the latter [1], but were found in the two former. The same homogeneous overlap can also be achieved in the other classes  $s_5$ ,  $s_6$  and  $s_{66}$ , by turning off some of the sets with  $D_p$ .

- $p = 5, 6$  and inhomogeneous overlap: such source configurations can appear in classes  $s_5$ ,  $s_6$  and  $s_{66}$ . Only those may then provide new and different examples of de Sitter solutions.

---

<sup>2</sup>We note that our ansatz, in particular the specification to group manifolds, was not implemented in [73]. One constraint put forward in that paper for  $p = 4$  is (4.3): this requirement turns out to be automatically satisfied when specializing to our ansatz, since then  $F_6 = 0$ ,  $\mathcal{R}_{||I} = 0$ ,  $\mathcal{R}_{||I}^{\perp I} \leq 0$ , as shown there in section 4.3. Another constraint, (4.5), remains less trivial.

<sup>3</sup>We do not consider here sources placed at angles, but only orthogonal ones. It could be that the former is however contained in the latter by projection.

<sup>4</sup>Although of no interest for de Sitter, the case  $p = 7$  also exhibits a single possibility of homogeneous overlap, that is, the source configuration of  $s_{77}$  (possibly extended with an extra source in  $s_7$ ), which also obeys  $N_o = p - 5$ .

### 2.1.2 Source configurations and fields for multiple dimensionalities

We proceed systematically to determine the solution classes in the case of multiple dimensionalities, as done previously for a single dimensionality.

- IIA systematics

Given our ansatz, one can have in type IIA supergravity  $p = 4, 6$  sources. We first consider one  $O_6$  along directions 123: the variables allowed by the projection are given in (2.16). From those we compute the components of the Bianchi identity sourcing the  $p = 4$  sources, namely the terms  $dF_4$  and  $H \wedge F_2$ , while the analysis for  $p = 6$  sources is already made in (2.17). We obtain the following possible sources

$$m_6 : \quad 1 O_6 \text{ (along directions 123)} \Rightarrow p = 4 \text{ sources along directions 4, 5, 6,} \quad (2.27)$$

$$p = 6 \text{ sources along directions 123, 145, 146, 156, 245,} \\ 246, 256, 345, 346, 356 .$$

From this point we have two options: adding an  $O_6$  or an  $O_4$ . If we add an  $O_6$ , the list of remaining variables is given in (2.18), and now the Bianchi identities give

$$m_{66} : \quad 2 O_6 \text{ (along directions 123, 145)} \Rightarrow p = 4 \text{ sources along direction 6,} \quad (2.28)$$

$$p = 6 \text{ sources along directions 123, 145, 246,} \\ 256, 346, 356 .$$

From (2.28), we can add an  $O_4$  along 6, which up to relabeling, is considered below in (2.32). The other option is to add a third  $O_6$ . However, in that case the remaining variables are given in (2.20), and the  $F_4$  Bianchi identity does not allow for any  $p = 4$  source; this is thus not a multiple dimensionalities configuration.

If from (2.27) we rather add an  $O_4$  along 4 (all directions being equivalent), the list of remaining variables is

$$m_{46} : \quad F_2 : F_{2 \ 15}, F_{2 \ 16}, F_{2 \ 25}, F_{2 \ 26}, F_{2 \ 35}, F_{2 \ 36},$$

$$F_4 : F_{4 \ 1245}, F_{4 \ 1246}, F_{4 \ 1345}, F_{4 \ 1346}, F_{4 \ 2345}, F_{4 \ 2346},$$

$$H : H_{125}, H_{126}, H_{135}, H_{136}, H_{235}, H_{236}, \quad (2.29)$$

$$f^{a \parallel 1 b \perp 1 c \perp 1} : f^1_{45}, f^1_{46}, f^2_{45}, f^2_{46}, f^3_{45}, f^3_{46},$$

$$f^{a \perp 1 b \perp 1 c \parallel 1} : f^4_{51}, f^4_{61}, f^5_{41}, f^6_{41}, f^4_{52}, f^4_{62}, f^5_{42}, f^6_{42}, f^4_{53},$$

$$f^4_{63}, f^5_{43}, f^6_{43},$$

namely 18 flux components and 18 structure constants, and the Bianchi identities for  $p = 4$  and  $p = 6$  give

$$m_{46} : \quad 1 O_6 \text{ (along 123)} \text{ and } 1 O_4 \text{ (along 4)} \Rightarrow p = 4 \text{ sources along 4,} \quad (2.30)$$

$$p = 6 \text{ sources along 123, 156, 256, 356 .}$$

Directions being equivalent, we can add an  $O_6$  along 156. The remaining variables are

now

$$\begin{aligned}
m_{466} : \quad & F_2 : F_{2\ 25}, F_{2\ 26}, F_{2\ 35}, F_{2\ 36}, \\
& F_4 : F_{4\ 1245}, F_{4\ 1246}, F_{4\ 1345}, F_{4\ 1346}, \\
& H : H_{125}, H_{126}, H_{135}, H_{136}, \\
& f^{a||_1 b_{\perp_1} c_{\perp_1}} : f^2_{45}, f^2_{46}, f^3_{45}, f^3_{46}, \\
& f^{a\perp_1 b_{\perp_1} c_{||_1}} : f^4_{52}, f^4_{62}, f^5_{42}, f^6_{42}, f^4_{53}, f^4_{63}, f^5_{43}, f^6_{43},
\end{aligned} \tag{2.31}$$

namely 12 flux components and 12 structure constants, and the Bianchi identities give

$$\begin{aligned}
m_{466} : \quad & 2\ O_6 \text{ (along 123, 156) and } 1\ O_4 \text{ (along 4)} \Rightarrow p = 4 \text{ sources along 4,} \\
& p = 6 \text{ sources along 123, 156.}
\end{aligned} \tag{2.32}$$

We cannot add any more source.

Finally, if we rather start by considering one  $O_4$  along 4, the list of allowed variables is given up to relabeling in (2.6). The result of the Bianchi identity of  $F_4$  is given in (2.7), while the  $F_2$  leads us to the following sources

$$\begin{aligned}
m_4 : \quad & 1\ O_4 \text{ (along directions 4)} \Rightarrow p = 4 \text{ sources along direction 4,} \\
& p = 6 \text{ sources along directions 123, 125, 126, 135, 136,} \\
& 156, 235, 236, 256, 356.
\end{aligned} \tag{2.33}$$

From there, we can add an  $O_6$  along 123, bringing us back to the case (2.30). Overall, this gives 5 possible solution classes.

### • IIB systematics

We turn to type IIB supergravity, where our ansatz allows for  $p = 3, 5, 7$  sources. We first consider one  $O_5$  along directions 12. The list of allowed variables is given in (2.9), and  $p = 5$  sources are given in (2.10). The  $F_5$  Bianchi identity does not allow for any  $p = 3$  source. The Bianchi identity for  $F_1$  leads us to the following

$$\begin{aligned}
m_5 : \quad & 1\ O_5 \text{ (along directions 12)} \Rightarrow p = 5 \text{ sources along directions 12, 34, 35, 36,} \\
& 45, 46, 56, \\
& p = 7 \text{ sources along directions 2456, 2356, 2346, 2345,} \\
& 1456, 1356, 1346, 1345.
\end{aligned} \tag{2.34}$$

From there, we can either add one  $O_5$  or one  $O_7$ . Another  $O_5$  can be placed without loss of generality along 34. The remaining variables are given in (2.11) and from the Bianchi identities, we deduce

$$\begin{aligned}
m_{55} : \quad & 2\ O_5 \text{ (along directions 12, 34)} \Rightarrow p = 5 \text{ sources along directions 12, 34, 56,} \\
& p = 7 \text{ sources along directions 2456, 2356, 1456, 1356.}
\end{aligned} \tag{2.35}$$

From (2.35), we can add an  $O_7$ , which will be considered below in (2.39). We rather add a third  $O_5$  along 56. The remaining variables are given in (2.13), and the allowed  $p = 5$

## Chapter 2. Charting the Landscape

---

sources are the same. However, the  $F_1$  Bianchi identity does not allow for any  $p = 7$  source, which brings us back to a single dimensionality case.

If from (2.34) we rather add an  $O_7$  along 2456 (all directions being equivalent) the list of remaining variables is

$$\begin{aligned}
 m_{57} : \quad & F_1 : F_{1\ 4}, \quad F_{1\ 5}, \quad F_{1\ 6}, \\
 & F_3 : F_{3\ 145}, \quad F_{3\ 146}, \quad F_{3\ 156}, \quad F_{3\ 234}, \quad F_{3\ 235}, \quad F_{3\ 236}, \\
 & F_5 : F_{5\ 12345}, \quad F_{5\ 12346}, \quad F_{5\ 12356}, \\
 & H : H_{124}, \quad H_{125}, \quad H_{126}, \quad H_{345}, \quad H_{346}, \quad H_{356}, \\
 & f^{a\parallel_1 b_{\perp_1} c_{\perp_1}} : f^1_{34}, \quad f^1_{35}, \quad f^1_{36}, \\
 & f^{a_{\perp_1} b_{\perp_1} c_{\parallel_1}} : f^3_{14}, \quad f^3_{15}, \quad f^3_{16}, \quad f^4_{13}, \quad f^5_{13}, \quad f^6_{13}, \\
 & f^{a\parallel_2 b_{\parallel_2} c_{\parallel_2}} : f^2_{45}, \quad f^2_{46}, \quad f^2_{56}, \quad f^4_{25}, \quad f^4_{26}, \quad f^5_{24}, \quad f^5_{26}, \quad f^6_{24}, \quad f^6_{25}.
 \end{aligned} \tag{2.36}$$

There are 18 flux components and 18 structure constants, and the Bianchi identities allow the following sources

$$m_{57} : \quad 1 O_5 \text{ (along 12)} \text{ and } 1 O_7 \text{ (along 2456)} \Rightarrow p = 5 \text{ sources along } 12, 34, 35, 36, \tag{2.37}$$

$$p = 7 \text{ sources along } 2456, 1356, 1346, 1345 .$$

From there we add an  $O_5$  along 34 (all directions being equivalent), and obtain the following list of variables

$$\begin{aligned}
 m_{5577} : \quad & F_1 : F_{1\ 5}, \quad F_{1\ 6}, \\
 & F_3 : F_{3\ 145}, \quad F_{3\ 146}, \quad F_{3\ 235}, \quad F_{3\ 236}, \\
 & F_5 : F_{5\ 12345}, \quad F_{5\ 12346}, \\
 & H : H_{125}, \quad H_{126}, \quad H_{345}, \quad H_{346}, \\
 & f^{a\parallel_1 b_{\perp_1} c_{\perp_1}} : f^1_{35}, \quad f^1_{36}, \\
 & f^{a_{\perp_1} b_{\perp_1} c_{\parallel_1}} : f^3_{15}, \quad f^3_{16}, \quad f^5_{13}, \quad f^6_{13}, \\
 & f^{a\parallel_2 b_{\parallel_2} c_{\parallel_2}} : f^2_{45}, \quad f^2_{46}, \quad f^4_{25}, \quad f^4_{26}, \quad f^5_{24}, \quad f^6_{24}.
 \end{aligned} \tag{2.38}$$

This gives 12 flux components and 12 structure constants, and Bianchi identities give

$$m_{5577} : \quad 2 O_5 \text{ (along 12, 34)} \text{ and } 1 O_7 \text{ (along 2456)} \Rightarrow p = 5 \text{ sources along } 12, 34, \tag{2.39}$$

$$p = 7 \text{ sources along } 2456, 1356 .$$

The last thing we can add from here is an  $O_7$  along 1356. Doing so, one obtains the exact same list of variables as in (2.38), so in that sense, the last  $O_7$  ‘‘comes for free’’. This explains why the solution class was already called  $m_{5577}$ . The Bianchi identities give the same sources as above, and one cannot add any more source. From (2.37), we could also have added an  $O_7$  along 1356. In this case, one ends up again with the same variables as in (2.38). The Bianchi identities therefore give the same sources, namely

$$m_{5577} : \quad 1 O_5 \text{ (along 12)} \text{ and } 2 O_7 \text{ (along 2456, 1356)} \Rightarrow p = 5 \text{ sources along } 12, 34, \tag{2.40}$$

$$p = 7 \text{ sources along } 2456, 1356 .$$

## 2.1 Classification of possible solutions

Solution class	Number of sets with $O_p$	$O_p$ sets directions	Possible $D_p$ sets directions	Field content
$m_4$	1 $O_4$	4	123, 125, 126, 135, 136, 156, 235, 236, 256, 356	(2.6)
$m_{46}$	1 $O_6$ , 1 $O_4$	123, 4	156, 256, 356	(2.29)
$m_{466}$	2 $O_6$ , 1 $O_4$	123, 156, 4		(2.31)
$m_6$	1 $O_6$	123	4,5,6 145, 146, 156, 245, 246, 256, 345, 346, 356	(2.16)
$m_{66}$	2 $O_6$	123, 145	6, 246, 256, 346, 356	(2.18)

Table 2.2: Source configurations in type IIA supergravity allowed by our ansatz for multiple dimensionalities with at least one  $O_p$ , together with the associated list of allowed variables or field content. These two pieces of information form together a solution class.

From there, we can only add an  $O_5$  along 34 to reach the case discussed above. It is obvious that this extra  $O_5$  also “comes for free”.

Starting now with one  $O_7$  along 1234, the list of variables is given in (2.23) and the corresponding  $p = 7$  sources in (2.24). Possible sources are as follows

$$\begin{aligned}
 m_7 : \quad & 1 \ O_7 \text{ (along 1234)} \Rightarrow p = 3 \text{ sources at points,} \\
 & p = 5 \text{ sources along } 15, 16, 25, 26, 35, 36, 45, 46, \quad (2.41) \\
 & p = 7 \text{ sources along } 1234, 3456, 2456, 2356, 1456, 1356, 1256 .
 \end{aligned}$$

From there, we can add an  $O_5$ , bringing us back to (2.37). We rather add a second  $O_7$  along 1256 and obtain the variables given in (2.25). The Bianchi identities allow for the following sources

$$\begin{aligned}
 m_{77} : \quad & 2 \ O_7 \text{ (along 1234 and 1256)} \Rightarrow p = 3 \text{ sources at points,} \\
 & p = 5 \text{ sources along } 46, 45, 36, 35, \quad (2.42) \\
 & p = 7 \text{ sources along } 1234, 1256 .
 \end{aligned}$$

From there, we can add an  $O_5$ , bringing us back to (2.40). We will also see below that the addition of an  $O_3$  from (2.41) and (2.42) is not possible with multiple dimensionalities.

We finally consider from the start an  $O_3$ . The allowed variables are given in (2.3). Having  $p = 3$  sources is then possible as indicated in (2.4). However, the Bianchi identities of  $F_1$  and  $F_3$  do not allow for any  $p = 7$  nor  $p = 5$  source, bringing us to a single dimensionality case. Overall, we find 6 distinct solution classes (not counting the “free”  $O_7$  or  $O_5$ ).

### • Summary

We summarize in Tables 2.2 and 2.3 the source configurations with multiple dimensionalities and associated field content (allowed variables) obtained in Section 2.1.2 and 2.1.2. This information defines the solution classes.



Solution class	Number of sets with $O_p$	$O_p$ sets directions	Possible $D_p$ sets directions	Field content
$m_5$	1 $O_5$	12	34, 35, 36, 45, 46, 56 2456, 2356, 2346, 2345, 1456, 1356, 1346, 1345	(2.9)
$m_{55}$	2 $O_5$	12, 34	56 2456, 2356, 1456, 1356	(2.11)
$m_{57}$	1 $O_5$ , 1 $O_7$	12, 2456	34, 35, 36 1356, 1346, 1345	(2.36)
$m_{5577}$	1 (or 2) $O_5$ , 1 (or 2) $O_7$	12, (34), 2456, (1356)	(34), (1356)	(2.38)
$m_7$	1 $O_7$	1234	15, 16, 25, 26, 35, 36, 45, 46 pt, 3456, 2456, 2356, 1456, 1356, 1256	(2.23)
$m_{77}$	2 $O_7$	1234, 1256	pt, 35, 36, 45, 46	(2.25)

Table 2.3: Source configurations in type IIB supergravity allowed by our ansatz for multiple dimensionalities with at least one  $O_p$ , together with the associated list of allowed variables or field content. These two pieces of information form together a solution class. The  $p = 3$  sources are located at a point, denoted pt. The cases of 1  $O_5$ , 2  $O_7$ , or 2  $O_5$ , 1  $O_7$ , or 2  $O_5$ , 2  $O_7$  form just one class: they all give the same allowed variables and the same four sources (up to their  $O_p/D_p$  nature).

### 2.1.3 T-duality and supersymmetry

Having identified all solution classes within our ansatz with at least one  $O_p$ , a few comments are in order regarding T-duality relations and the unbroken supersymmetries.

- **T-duality**

Some source configurations are T-dual to others. For example, the configuration of  $m_{46}$  with 3 sets, i.e. 1  $O_4$  along 4, 1  $O_6$  along 123 and 1  $D_6$  along 156 of (2.30) is T-dual to the configuration of  $s_{55}$  of (2.12). This can be seen by performing a T-duality along direction 1 and relabeling  $2 \leftrightarrow 4$ . Turning the  $D_p$ -branes into  $O_p$ -planes, we get that the sources of  $m_{466}$  in (2.32) are T-dual to those of  $s_{555}$  in (2.14). Similarly, the configuration of  $m_{5577}$ , i.e. 2  $O_5$  along 12, 34 and 2  $O_7$  along 1356, 2456, mentioned below (2.39), is T-dual to the configuration of  $s_{6666}$  with 4  $O_6$  given below (2.21). One should perform the T-duality along 6, followed by a relabeling  $1 \leftrightarrow 2$ ,  $3 \leftrightarrow 6$ . Finally, T-dual source configurations with 2 sets are displayed in Figure 2.1.

One may then wonder whether beyond the source configurations, the solution classes as a whole are actually T-dual. This would mean that the allowed variables or fields are transformed into each other by T-duality. This is however not the case, as one can verify using the standard T-duality rules on flux indices [37]. This point was made in [75] regarding the de Sitter solution with  $O_5 \& O_7$  (belonging to  $m_{5577}$ ): T-duality on the fields leads to non-geometric  $Q$ -fluxes, which are not allowed in our settings. So the solutions cannot be concluded to be T-dual. Anticipating on our solutions, the same will be true

here. In type IIB, we also find de Sitter solutions in  $m_{5577}$ . All of them have either a  $f^2_{46}$  or a  $f^4_{26}$  non-zero. T-duality then gives  $f^a_{b6} \rightarrow Q_b^{a6}$ , i.e. generates a non-geometric  $Q$ -flux, so our solutions are not T-dual to geometric ones and are truly new. Similarly in IIA, our de Sitter solutions in  $m_{46}$  admit  $f^4_{15}, f^4_{16}$  non-zero. The T-duality rule is  $f^a_{1c} \rightarrow -Q_c^{a1}$ , so again, a non-geometric  $Q$ -flux would be generated from our solutions, so they are not T-dual to known geometric ones and are truly new.<sup>5</sup> Even though the complete solution classes are not T-dual, the source configurations still are, and this will be useful for the supersymmetry analysis that we now turn to.

### • Unbroken supersymmetries

We have considered various configurations of static branes and orientifolds. It would be interesting to determine whether those preserve some supersymmetry (i.e. are “mutually BPS”), first to have a chance to obtain a 4d supersymmetric effective theory, but also to avoid possible (open string) instabilities. One set of parallel branes breaks half of type II supersymmetries. Two orthogonal sets break a further half, i.e. a quarter, if and only if their total number of Neumann-Dirichlet (ND) boundary conditions,  $\mathcal{N}_{ND}$ , is a multiple of 4:  $\mathcal{N}_{ND} = 4i > 0$  for some positive integer  $i$ . In other words, the total number of directions belonging to one set and not to the other, which is always an even number, should be a multiple of 4. If this does not hold, supersymmetry is broken.

Given we work in the orthonormal (co)frame, our sets are orthogonal, it is then straightforward to perform the supersymmetry check. Our configurations are along the 3 external space dimensions, and have for each set  $p - 3$  internal dimensions; only the latter can be ND. Let us first consider configurations of single dimensionality  $p \geq 4$ . For  $p = 4$ , two different sets only have  $\mathcal{N}_{ND} = 1 + 1 = 2$  so intersecting  $p = 4$  sources break supersymmetry. For  $p \geq 5$ , let us denote  $N_o \geq 0$  the number of common internal directions of two orthogonal sets. Two conditions need to be obeyed:

$$4i = 2(p - 3 - N_o) , \quad 2(p - 3 - N_o) + N_o \leq 6 . \quad (2.43)$$

The first one is the condition for unbroken supersymmetry; the second one is the requirement that the total of internal dimensions of the two sets is smaller than 6. We deduce that  $1 \leq i \leq \frac{3}{2}$ , and conclude that we must have  $i = 1$ , i.e.  $N_o = p - 5$ , to preserve supersymmetry. Since there is no other possible value for  $N_o$ , this means that this value of  $N_o$  must hold for all pairs of sets, in other words there is an homogenous overlap. As discussed in Section 2.1.1, the value  $N_o = p - 5$  is precisely the one for which solutions with homogeneous overlap can be found here, as initially advocated from equations of motion for de Sitter solutions in [73]. This result also implies that configurations with inhomogeneous overlap break supersymmetry.

We extend the analysis to source configurations with multiple dimensionalities. We apply the rule  $\mathcal{N}_{ND} = 4i > 0$  to pairs of sources in such configurations, allowing us to determine those that leave some unbroken supersymmetry. A remaining question is the

---

<sup>5</sup>It is conceivable that the problematic structure constants  $f^a_{1c}$  disappear via a rotation among e.g. directions 1 and 2, applied to the Maurer-Cartan equations. However, such a rotation may in turn transform a single set of  $D_6$  along 156 into two sets along 156 and 256. As a consequence, the rewritten solution, assuming it is still a solution, would have a source configuration which is not T-dual anymore to the one in  $s_{55}$ , when performing T-duality along the new, rotated, directions. This is another way to view the obstruction.

## Chapter 2. Charting the Landscape

amount of supersymmetry that is left unbroken. Each pair of orthogonal sets verifying  $\mathcal{N}_{ND} = 4i > 0$  preserves a quarter of the initial amount. It is well-known that adding a third source as we do with  $D_5/O_5$  (along 12, 34, 56) or  $D_6/O_6$  (along 123, 145, 256) breaks supersymmetry by a further half. For  $D_6/O_6$  one can add the fourth source along 346 for free. In those two cases, one then preserves  $\mathcal{N} = 1$  in 4d. Thanks to the T-duality relation of these source configurations to those with  $O_4/O_6$  and  $O_5/O_7$  (see Section 2.1.3), we deduce the number of preserved supersymmetries for configurations with multiple dimensionalities. The results are summarized in Table 2.4.

Solution class	Sources directions allowing for unbroken SUSY	4d $\mathcal{N}$ of preserved SUSY
$s_3$	pt	4
$s_4$	1	4
$s_5$	12, (34, 56)	4,(2,1)
$s_{55}$	12, 34, (56)	2,(1)
$s_{555}$	12, 34, 56	1
$s_6$	123, (145, 256, 346)	4,(2,1)
$s_{66}$	123, 145, (256, 346)	2,(1)
$s_{6666}$	123, 145, 256, (346)	1
$s_7$	1234, (1256, 3456)	4,(2,1)
$s_{77}$	1234, 1256	2
$m_4$	4, 123, (156)	2,(1)
$m_{46}$	4, 123, (156)	2,(1)
$m_{466}$	4, 123, 156	1
$m_6$	4, 123, (156)	2,(1)
$m_{66}$	6, 123, 145	1
$m_5$	12, 2456, (34, 1356)	2,(1)
$m_{55}$	12, 34, 2456, (1356)	1
$m_{57}$	12, 2456, (34, 1356)	2,(1)
$m_{5577}$	12, 34, 2456, (1356)	1
	12, 2456, 1356, (34)	1
$m_7$	pt, 1234, (1256, 3456)	4,(2,1)
	15, 1234, (26, 3456)	2,(1)
$m_{77}$	pt, 1234, 1256	2
	35, 1234, 1256, (46)	1

Table 2.4: Internal directions of the source sets that allow for unbroken supersymmetry, for each solution class previously identified. The corresponding number  $\mathcal{N}$  of preserved supersymmetries in 4d is given. The sets in parentheses are optional in the class, to which the amount  $\mathcal{N}$  in parentheses corresponds. Some classes allow for different supersymmetry-preserving configurations, then specified on distinct rows.

We see through Table 2.4 that among all possible solution classes, it is eventually only few redundant source configurations that appear and preserve supersymmetry.

## 2.2 The solutions

We classified in Section 2.1 the possible solutions with our ansatz into a list of solution classes, summarized in Section 2.1.1 and 2.1.2. In this section, we look for new solutions in those classes, most of our efforts being dedicated to de Sitter ones.

### 2.2.1 Procedure to find solutions

To find a solution with a 4d maximally symmetric spacetime within our ansatz, one has to solve the equations listed in Section 1.3, together with the constraints

$$\mathcal{R}_4 \text{ sign}, \quad T_{10}^{J=D_p \text{ only}} \leq 0, \quad (2.44)$$

where the sign constraint on the 4d curvature is e.g.  $\mathcal{R}_4 > 0$  for de Sitter, and the second constraint is about possible source sets without  $O_p$ . This is done numerically as further detailed in Section 2.2.2.

Prior to this, one should start by choosing a solution class among those listed in Table 2.1, 2.2 and 2.3. This determines the source configuration as well as the allowed variables to be considered non-zero in the equations; considering that list of variables amounts to ensure that the orientifold projection is satisfied. Given the source configuration, the labeling of the sets can be fixed, and the transverse volume forms as well as the internal energy momentum tensor can be determined; those quantities are needed in the equations to solve. We provide in the following two examples of single dimensionality (and a priori inhomogeneous overlap), but the procedure extends to cases of multiple dimensionalities.

- **Category  $s_5$ :**

We label the source sets as in Table 2.5.

Set $I$	Sources	Space dimensions								
		4d	1	2	3	4	5	6		
1	$O_5, (D_5)$	⊗	⊗	⊗	⊗	⊗				
2	$(D_5)$	⊗	⊗	⊗			⊗	⊗		
3	$(D_5)$	⊗	⊗	⊗			⊗		⊗	
4	$(D_5)$	⊗	⊗	⊗			⊗			⊗
5	$(D_5)$	⊗	⊗	⊗				⊗	⊗	
6	$(D_5)$	⊗	⊗	⊗				⊗		⊗
7	$(D_5)$	⊗	⊗	⊗					⊗	⊗

Table 2.5:  $O_5/D_5$  source configuration in the class  $s_5$ . Sources in parentheses are not mandatory.

This leads us to the following volume forms

$$\begin{aligned}
 I = 1 : \quad & \text{vol}_{\parallel_1} = e^1 \wedge e^2, \quad \text{vol}_{\perp_1} = e^3 \wedge e^4 \wedge e^5 \wedge e^6, \\
 I = 2 : \quad & \text{vol}_{\parallel_2} = e^3 \wedge e^4, \quad \text{vol}_{\perp_2} = e^1 \wedge e^2 \wedge e^5 \wedge e^6, \\
 I = 3 : \quad & \text{vol}_{\parallel_3} = e^3 \wedge e^5, \quad \text{vol}_{\perp_3} = -e^1 \wedge e^2 \wedge e^4 \wedge e^6, \\
 I = 4 : \quad & \text{vol}_{\parallel_4} = e^3 \wedge e^6, \quad \text{vol}_{\perp_4} = e^1 \wedge e^2 \wedge e^4 \wedge e^5, \\
 I = 5 : \quad & \text{vol}_{\parallel_5} = e^4 \wedge e^5, \quad \text{vol}_{\perp_5} = e^1 \wedge e^2 \wedge e^3 \wedge e^6, \\
 I = 6 : \quad & \text{vol}_{\parallel_6} = e^4 \wedge e^6, \quad \text{vol}_{\perp_6} = -e^1 \wedge e^2 \wedge e^3 \wedge e^5, \\
 I = 7 : \quad & \text{vol}_{\parallel_7} = e^5 \wedge e^6, \quad \text{vol}_{\perp_7} = e^1 \wedge e^2 \wedge e^3 \wedge e^4,
 \end{aligned} \tag{2.45}$$

where the  $-1$  in  $\text{vol}_{\perp_I}$  are due to the 6d orientation. The source energy momentum tensor is given by

$$T_{ab} = \text{diag} \left( \frac{T_{10}^1}{6}, \frac{T_{10}^1}{6}, \frac{T_{10}^2 + T_{10}^3 + T_{10}^4}{6}, \frac{T_{10}^2 + T_{10}^5 + T_{10}^6}{6}, \right. \tag{2.46}$$

$$\left. \frac{T_{10}^3 + T_{10}^5 + T_{10}^7}{6}, \frac{T_{10}^4 + T_{10}^6 + T_{10}^7}{6} \right).$$

The list of variables is given in (2.9). The equations to solve are given in Section 1.3, setting  $T_{10}^{(3)I} = T_{10}^{(7)I} = 0$ , thus giving  $T_{10} = T_{10}^{(5)}$ .<sup>6</sup> As in [1], simplifications occur in the equations. Because of the  $O_5$  projection and the fluxes being constant, the e.o.m. for  $F_1$  and the BI for  $F_5$  are trivially satisfied: these six-forms vanish identically. In addition, following the reasoning of Section 3.2 of [70], the off-diagonal  $a_{\parallel_I} b_{\perp_I}$  Einstein equations for a set  $I$  with an  $O_5$  projection are trivially satisfied. With such a projection for  $I = 1$ , we are left with the Einstein equations along the blocks 12 and 3456, i.e. 13 equations.

- **Category  $s_{66}$ :**

Similarly, we label the source sets as in Table 2.6.

Set $I$	Sources	Space dimensions								
		4d	1	2	3	4	5	6		
1	$O_6, (D_6)$	⊗	⊗	⊗	⊗	⊗	⊗			
2	$O_6, (D_6)$	⊗	⊗	⊗	⊗			⊗	⊗	
3	$(D_6)$	⊗	⊗	⊗		⊗		⊗		⊗
4	$(D_6)$	⊗	⊗	⊗		⊗			⊗	⊗
5	$(D_6)$	⊗	⊗	⊗			⊗	⊗		⊗
6	$(D_6)$	⊗	⊗	⊗			⊗		⊗	⊗

Table 2.6:  $O_6/D_6$  source configuration in the class  $s_{66}$ . Sources in parentheses are not mandatory.

<sup>6</sup>These equations are formally the same as in [1], up to the volume forms and the  $T_{ab}$ . One should pay attention to the typo in that paper: the missing sign  $\varepsilon_5$ . We corrected this here.

This leads us to the following volume forms

$$\begin{aligned}
 I = 1 : \quad \text{vol}_{\parallel_1} &= e^1 \wedge e^2 \wedge e^3, \quad \text{vol}_{\perp_1} = e^4 \wedge e^5 \wedge e^6, \\
 I = 2 : \quad \text{vol}_{\parallel_2} &= e^1 \wedge e^4 \wedge e^5, \quad \text{vol}_{\perp_2} = e^2 \wedge e^3 \wedge e^6, \\
 I = 3 : \quad \text{vol}_{\parallel_3} &= e^2 \wedge e^4 \wedge e^6, \quad \text{vol}_{\perp_3} = e^1 \wedge e^3 \wedge e^5, \\
 I = 4 : \quad \text{vol}_{\parallel_4} &= e^2 \wedge e^5 \wedge e^6, \quad \text{vol}_{\perp_4} = -e^1 \wedge e^3 \wedge e^4, \\
 I = 5 : \quad \text{vol}_{\parallel_5} &= e^3 \wedge e^4 \wedge e^6, \quad \text{vol}_{\perp_5} = -e^1 \wedge e^2 \wedge e^5, \\
 I = 6 : \quad \text{vol}_{\parallel_6} &= e^3 \wedge e^5 \wedge e^6, \quad \text{vol}_{\perp_6} = e^1 \wedge e^2 \wedge e^4.
 \end{aligned} \tag{2.47}$$

The source energy momentum tensor is given by

$$T_{ab} = \text{diag} \left( \frac{T_{10}^1 + T_{10}^2}{7}, \frac{T_{10}^1 + T_{10}^3 + T_{10}^4}{7}, \frac{T_{10}^1 + T_{10}^5 + T_{10}^6}{7}, \right. \\
 \left. \frac{T_{10}^2 + T_{10}^3 + T_{10}^5}{7}, \frac{T_{10}^2 + T_{10}^4 + T_{10}^6}{7}, \frac{T_{10}^3 + T_{10}^4 + T_{10}^5 + T_{10}^6}{7} \right).$$

The list of variables is given in (2.18). The equations to solve are those of Section 1.3, setting  $T_{10}^{(4)I} = T_{10}^{(8)I} = 0$ , thus giving  $T_{10} = T_{10}^{(6)}$ . Regarding simplifications in our setting, let us mention that the  $F_0$  BI is automatically satisfied given our ansatz. As for  $p = 5$ , all off-diagonal  $a_{\parallel_I b_{\perp_I}}$  Einstein equations for a set  $I$  with an  $O_6$  projection are trivially satisfied. Here the projection is for  $I = 1, 2$ , leaving the Einstein equations along 11, 66, and the blocks 23 and 45, giving 8 equations.

Last but not least, once a solution to the equations of Section 1.3 and the constraints (2.44) is found, a remaining task is to verify that the group manifold  $\mathcal{M}$ , for which structure constants have been found, is compact. We will come back to this matter in greater detail in the next chapter.

Let us add that the equations to solve enjoy an overall scaling symmetry, associated to a parameter denoted  $\lambda$  in Section 5.5 where further details are given. To help in the search for solutions, this freedom is sometimes fixed at first, by giving a value to one of the variables, e.g.  $g_s T_{10}^1 = 10$ . One should keep in mind that all variable values can later be rescaled at will, in the absence of possible further constraints, such as requiring the supergravity solution to be a classical string background. This is true in particular for the values of the curvatures  $|\mathcal{R}_4|$  and  $|\mathcal{R}_6|$ , that can for instance be lowered.

### 2.2.2 Numerical code

The numerical code `MaxSymSolSearch` (MSSS) used to find new solutions follows the one used and described in [1], with several extensions and improvements; we refer to that paper for more technical details. As explained in Section 2.2.1, the first step is to choose a solution class. This amounts to indicate to the code the sets of sources, their directions, and the sets in which there are  $O_p$ . From this information, the code deduces the theory to use (IIA or IIB supergravity), and the list of allowed variables under the orientifold projection. As shown in Section 2.2.1, the code also works out the volume forms and the energy momentum tensor components. From there, the code obtains all equations to solve, listed in Section 1.3: the equations of motion (e.o.m.) for the fluxes, their

Bianchi identities, the Einstein equations, the dilaton e.o.m., and the Jacobi identities on the structure constants. These equations are derived in components, i.e. as scalar, quadratic and algebraic equations. As indicated in Section 2.2.1, simplifications can occur depending on the class, because some equations are trivially satisfied. The remaining number  $N_{\text{eq}}$  of non-trivial equations varies according to the class,<sup>7</sup> as well as the number of variables.

At this stage, the code is ready to solve the equations, i.e. look for a solution. Prior to this, one can indicate at this point further specifications on the solution ansatz. This typically amounts to set to zero, or to some other value, some of the variables, either to help the code or to look for more specific solutions within a class. Two kinds of ansätze are often used. The first one consists in leaving almost all allowed variables free, and letting the program look for solutions. This has the potential drawback to leave too much freedom, potentially diluting too much solutions, if any, in the parameter space, such that the program may not find them. The second ansatz consists in starting close to another class for which we know there exist solutions. This means setting many of the extra (compared to the other class) variables to zero, leaving free only few of them. This may have the drawback of being too restrictive, and then missing possible solutions in the starting class. Finally, a more refined approach can be taken to choose an ansatz, for instance setting progressively one by one some variables to zero, to simplify step by step a solution.

Once the ansatz is further specified, the code tries to solve the set of  $N_{\text{eq}}$  equations. To that end, we make use of minimisation techniques and proceed as follows. Every equation is written in the form  $E_i = 0$ ,  $i = 1, \dots, N_{\text{eq}}$ , and we consider the following quantity

$$S = \sum_{i=1}^{N_{\text{eq}}} (E_i)^2, \quad \text{such that} \quad (S = 0) \iff (E_i = 0 \quad \forall i = 1, \dots, N_{\text{eq}}). \quad (2.48)$$

We then use algorithms implemented in `Wolfram Mathematica` to minimise  $S$  to zero. As indicated in Section 2.2.1, we add at this point the constraints (2.44). In particular, we ask for the condition  $\mathcal{R}_4 > \epsilon$ ,  $-\tilde{\epsilon} < \mathcal{R}_4 < \tilde{\epsilon}$  or  $\mathcal{R}_4 < -\epsilon$  (for instance  $\epsilon = 10^{-3}$ ,  $\tilde{\epsilon} = 10^{-7}$ ) depending on whether we look for de Sitter, Minkowski or anti-de Sitter solutions. A solution is considered valid if one reaches the standard precision  $S \sim 10^{-30} \ll \epsilon, \tilde{\epsilon}$  [1], with in addition for a Minkowski solution  $\mathcal{R}_4 \sim 10^{-15} \sim \sqrt{S}$ . This usually requires to do a two-step minimisation: we first run a `NMinimize` that yields a first solution  $s_1$ . One then refines it by running a `FindMinimum`, where one uses  $s_1$  as a starting point. This last step can sometimes be iterated. Further final validity checks of the solution include the evaluation of the maximum  $|E_i|$ , which should be of order  $10^{-15}$ .

For a given ansatz (solution class and further specifications of variables), if we obtain the desired precision after the previous steps, we conclude that we have found a solution, otherwise we only claim that we were not able to find any solution in this set-up (this corresponds to the question mark in Table 2.7). This last situation does not necessarily mean that such solutions do not exist, as e.g. in the case of a no-go theorem. It can also simply underline the computational complexity.

---

<sup>7</sup>We note a typo in [1] on this matter: the number of non-trivial equations for  $s_{55}$  is  $N_{\text{eq}} = 56$ .

### 2.2.3 (Anti-) de Sitter no-go theorems

Prior to looking for new solutions, it is useful to be aware of existence no-go theorems for some solution classes. In turn, a failure in finding new solutions may signal a previously unnoticed no-go theorem. Let us say a few words on these no-go theorems, and find new ones for both de Sitter or anti-de Sitter solutions.

Most of the de Sitter no-go theorems were established for sources of single dimensionality  $p$  (see e.g. [70, 77, 78]). The case of multiple dimensionalities was poorly studied. For the latter, a few no-go theorems were still obtained, beyond group manifolds, in Section 6 of [73]. In particular,  $p = 3\&7$  was excluded for de Sitter solutions. Some constraints were also established in IIA, but we note from (2.27) that the overlap of  $p = 4$  and  $p = 6$  considered in [73] cannot happen in our ansatz. We will still make use of some of the equations of [73] in the following.

It has been noticed with single dimensionality that having intersecting sources instead of only parallel ones helps to get de Sitter solutions. One may then expect that having multiple dimensionalities can also help. We illustrate this idea in Section 2.2.3, before finding a new no-go theorem when adding too many orientifolds in Section 2.2.3. Finally, this last situation will lead as well to existence no-go theorems for anti-de Sitter, discussed in Section 2.2.3.

- **Warm-up:  $p = 4\&6$**

De Sitter no-go theorems for single dimensionality sources do not generalize easily to the case of multiple dimensionalities. We know that for  $p = 6$  alone, one needs for de Sitter  $F_0 \neq 0$  and  $\mathcal{R}_6 < 0$ . How do those statements get modified with  $p = 4$  on top? This is a priori an important question when looking for solutions with  $p = 4\&6$ , because an  $O_4$  imposes  $F_0 = 0$  in our ansatz. Let us reproduce here these no-go theorems while extending to multiple dimensionalities with  $p = 4\&6$ . We follow the reasoning of [36] to derive the initial no-go theorems.

We first need preliminary equations. In Section 6 of [73] are given the dilaton e.o.m., the ten-dimensional Einstein trace and the four-dimensional one. Combining those, one reaches there (6.7) given by

$$\mathcal{R}_4 + 2\mathcal{R}_{10} - |H|^2 + g_s^2 \sum_{q=0}^6 |F_q|^2 = 0 . \quad (2.49)$$

Introducing a parameter  $p_0 \geq 3$ , another combination leads to (6.10) given by

$$(p_0 - 3)\mathcal{R}_4 = -2|H|^2 + g_s^2 \sum_{q=0}^6 (8 - p_0 - q)|F_q|^2 + g_s \left( \sum_p \frac{p_0 + 1}{p + 1} T_{10}^{(p)} - T_{10} \right) . \quad (2.50)$$

Now, equating (2.49) and (2.50) for  $p_0 = 6$  yields

$$\begin{aligned} \frac{9}{2}\mathcal{R}_4 &= -3|H|^2 + 3g_s^2 (|F_0|^2 - |F_4|^2 - 2|F_6|^2) + \frac{3}{5}g_s T_{10}^{(4)} \\ &= -2\mathcal{R}_6 - g_s^2 (|F_2|^2 + 2|F_4|^2 + 3|F_6|^2) + \frac{g_s}{5} T_{10}^{(4)} . \end{aligned} \quad (2.51)$$

We recover for  $T_{10}^{(4)} = 0$  the requirements  $F_0 \neq 0$  and  $\mathcal{R}_6 < 0$ . However, with  $T_{10}^{(4)} > 0$  as can be the case with  $O_4$ , these requirements do not hold anymore.



Similarly, equating (2.49) and three times (2.50) for  $p_0 = 4$ , we get

$$\begin{aligned} \frac{7}{2}\mathcal{R}_4 &= -7|H|^2 + 7g_s^2 (2|F_0|^2 + |F_2|^2 - |F_6|^2) - g_s T_{10}^{(6)} \\ &= -2\mathcal{R}_6 + g_s^2 (|F_0|^2 - |F_4|^2 - 2|F_6|^2) - \frac{g_s}{7} T_{10}^{(6)} . \end{aligned} \quad (2.52)$$

With an  $O_4$  setting  $F_0 = 0$  and with  $T_{10}^{(6)} = 0$ , we recover the known de Sitter requirements  $F_2 \neq 0$  and  $\mathcal{R}_6 < 0$  for  $p = 4$ . Now with  $T_{10}^{(6)} < 0$ , i.e. with  $D_6$  and possibly a few  $O_6$ , we can again waive these requirements. We conclude that allowing for multiple dimensionalities gives more freedom, i.e. relaxes some of the de Sitter no-go theorems for single dimensionality.

- **A new de Sitter no-go theorem for  $m_{466}$**

Adding too many orientifolds in different sets may however lead to new no-go theorems, because one projects out many fields. It was already noticed to be the case for 3  $O_5$ , i.e. the class  $s_{555}$ , that project out  $F_1$  thus forbidding de Sitter solutions [1]. As mentioned in Section 2.1.3, the source configuration in class  $m_{466}$  is T-dual to the previous one, so one would as well expect a no-go theorem against de Sitter solutions in  $m_{466}$ . We found one and prove it in the following.

Inserting the 4d Einstein equation (1.19) in the 6d one (1.20), one obtains

$$\begin{aligned} \mathcal{R}_{ab} &= \frac{g_s^2}{2} \left( F_{2\ ac} F_{2\ b\ c} + \frac{1}{3!} F_{4\ acde} F_{4\ b\ cde} \right) + \frac{1}{4} H_{acd} H_b\ cd \\ &+ \frac{g_s}{2} \left( T_{ab} - \delta_{ab} \sum_p \frac{T_{10}^{(p)}}{p+1} \right) + \frac{\delta_{ab}}{4} (\mathcal{R}_4 + 2g_s^2 |F_6|^2) , \end{aligned} \quad (2.53)$$

which was used in [70] to get constraints on the Ricci tensor components. We are now interested in the case of 2  $O_6$  along 123 and 156, and an  $O_4$  along 4, i.e. class  $m_{466}$  with variables (2.31) and sources (2.32). In that case the sources along 1 are all the  $p = 6$  ones, so one has

$$T_{11} = \sum_I \frac{T_{10}^{(6)I}}{7} = \frac{T_{10}^{(6)}}{7} . \quad (2.54)$$

Most interestingly, these three orientifolds impose so much projection that no  $f^a_{bc}$  with an index along 1 is left. This implies that  $\mathcal{R}_{11} = 0$ . From (2.53), we deduce, using further the remaining flux components in (2.31)

$$g_s \frac{T_{10}^{(4)}}{5} = \frac{1}{2} \mathcal{R}_4 + |H|^2 + g_s^2 |F_4|^2 + g_s^2 |F_6|^2 . \quad (2.55)$$

The fact there is no  $F_2$  contribution is due to  $F_2$  having no component along 1: this, together with the absence of  $F_0$ , is the T-dual statement of having no  $F_1$  in IIB with 3  $O_5$ , and this will allow us to conclude on the no-go. We now compare (2.55) to (2.51) (where we recall that  $F_0 = 0$  with  $O_4$ ). It is expected that the coefficients differ given the former is one equation and the latter is a trace. We deduce

$$\mathcal{R}_4 + g_s^2 |F_6|^2 = 0 \Rightarrow \mathcal{R}_4 \leq 0 . \quad (2.56)$$

This is a no-go theorem against de Sitter solutions. It would be interesting to derive a 4d version of it, for which one would need the tools developed for no-go theorem 9 of [78]. This would allow us to compute the constant  $c$  that characterises the obstruction and compare it to the swampland de Sitter conjectures [78–81].

• **Anti-de Sitter no-go theorems for  $s_{555}$  and  $m_{466}$**

Anti-de Sitter solutions are rarely constrained by no-go theorems, since they typically are favored by the equations of motion (see e.g. [82]). When having however too many orientifolds, we will see as above that anti-de Sitter solutions are not possible. We start with  $s_{555}$ , the class with 3  $O_5$ . Combining equations of motion in the case of intersecting sources with single dimensionality  $p$  (with our ansatz on the warp factor and the dilaton), we obtained (3.5) in [73] that we repeat here

$$(p - 3)\mathcal{R}_4 = -2|H|^2 + g_s^2 \left( (7 - p)|F_1|^2 + (5 - p)|F_3|^2 + (3 - p)|F_5|^2 \right) . \quad (2.57)$$

It is easy to deduce the no-go theorem for de Sitter mentioned above, for  $p = 5$  and  $F_1 = 0$  as in  $s_{555}$ . Looking closer at the allowed variables (2.13) in that class, we actually realise that  $H = F_1 = F_5 = 0$ . This implies

$$\mathcal{R}_4 = 0 , \quad (2.58)$$

which in particular gives a no-go theorem for anti-de Sitter solutions as well.

As motivated in Section 2.2.3, it is expected to get a similar no-go theorem for the T-dual source configuration, i.e. 2  $O_6$  and 1  $O_4$  as in the class  $m_{466}$ . The equations derived in Section 2.2.3 are independent of the sign of  $\mathcal{R}_4$ , so we consider the last equation, namely (2.56). Again, a closer look at the variables (2.31) allowed in  $m_{466}$  makes us realise that  $F_6 = 0$ . This implies once again (2.58) for  $m_{466}$ , and a no-go theorem for anti-de Sitter. These no-go theorems make Minkowski solutions in those 2 classes very special.

### 2.2.4 Results: known and found solutions

We present in Table 2.7 the known and found solutions in our ansatz, classified in solution classes. To find new ones, we have proceeded as indicated in Section 2.2.1. We looked for de Sitter solutions in each solution class, while we only searched for Minkowski and anti-de Sitter solutions in some of them. The new solutions were not tailored in any specific way in this analysis. They rather serve as a proof of concept for their existence in certain classes, whenever no solution was previously known in the given class.

We label the solutions with the class name, the sign of the cosmological constant, and the number of the solution in its class: for instance  $m_{46}^+1$  is the de Sitter solution number 1 in the class  $m_{46}$ . For  $s_{55}$ , we start counting the de Sitter solutions at 28, since 1-27 refer to the solutions found in [1, 65]; for all other classes we start at 1.

Let us first comment on de Sitter solutions. To start with, we found new solutions in classes where solutions were already known:  $s_{55}$  [1, 65],  $s_{6666}$  [74, 89–92] and  $m_{5577}$  [75]. Only one solution was known in  $m_{5577}$  and we found here several. In addition, those fall in the two subclasses,  $m_{5577}$  and  $m_{5577}^*$ . We recall that these solutions have source configurations which are T-dual to those of  $s_{6666}$ , but the solutions are not, because of the field content (see Section 2.1.3). Secondly, we found new solutions in the new class

Solution class	dS sol.	Mink. sol.	AdS sol.
$s_3$	×	[43]	
$s_4$	?	[82]	
$s_5$	?	[82]	
$s_{55}$	[1, 65], <b>28</b>	[1, 83]	<b>1-4</b>
$s_{555}$	×	<b>1-4</b>	×
$s_6$	?	[82]	
$s_{66}$	<b>1</b>	[83]	
$s_{6666}$	[74], <b>1-4</b>	[84, 85]	[84, 86, 87]
$s_7$	×	[82]	
$s_{77}$	×		
$m_4$	?		
$m_{46}$	<b>1-10</b>	<b>1-2</b>	<b>1-5</b>
$m_{466}$	×	<b>1-6</b>	×
$m_6$	?		
$m_{66}$	?		
$m_5$	?		
$m_{55}$	<b>1-4</b>		
$m_{57}$	?		
$m_{5577}$	[75], <b>1-12</b> , <b>1*</b>		[87, 88]
$m_7$	?		
$m_{77}$	?		

Table 2.7: Solutions on a 4d maximally symmetric spacetime with orientifold that accommodate our ansatz. A reference or a number indicates that solutions have been found. A reference means that an example can be found in the corresponding paper; more references are provided in the main text. A number labels a new solution that has been found in this work; without a reference, it means the solution is the first in its class up to our knowledge. We recall that when a solution is found in a class, it does not mean that all possible sources in the class are turned on. A cross ( $\times$ ) indicates a no-go theorem against finding a solution in a given class. A question mark means that we have searched for solutions without finding any, potentially hinting at a no-go theorem, or at computational complexity. An empty box means that we have not searched for a solution, and are not aware of corresponding solutions in the literature.

$m_{46}$  where no solution was known before. Some of these solutions have, in terms of sets, 1  $O_4$  along 4, 1  $O_6$  along 123 and 1  $D_6$  along 156. This source configuration is T-dual to that of  $s_{55}$ , so finding solutions there may not be surprising; however because of the field content, the solutions are again not T-dual to geometric ones and are thus truly new (see Section 2.1.3). These seemingly T-dual solutions in  $m_{46}$ ,  $s_{55}$ ,  $s_{6666}$  and  $m_{5577}$ , all have source configurations that preserve supersymmetry, as discussed in Section 2.1.3. It is also the case for the new solution found in the new class  $s_{66}$ , which essentially differs from those in  $s_{6666}$  because of the field content. Finally, we find new solutions, which have source configurations that break supersymmetry. It is the case of the other solutions found in  $m_{46}$ , with 2 additional  $D_6$  along 256 and 356, as well as the new solutions found in the new class  $m_{55}$ , which have at least three sets of  $D_p$ -branes.

We turn to Minkowski solutions, for which a few references already appear in Table 2.7. A list of known Minkowski solutions on group manifolds (found using supersymmetry conditions) with parallel sources (i.e. only one set) is given in Section 2.4 of [76]; all but one of them fit the ansatz of [82]. That ansatz includes some group manifolds, but also goes beyond them. Regarding intersecting sources, a list of known Minkowski solutions on group manifolds is given in Section 5 of [73]; a new one,  $s_{55}^0 1$ , was found in [1]. All those had only 2 sets of sources. To those one should add the solutions in the class  $s_{6666}$  indicated in Table 2.7. Here, we found new Minkowski solutions in new classes with 3 sets of sources: 4 in  $s_{555}$  and 6 in  $m_{466}$ . These two classes are very special because of the no-go theorems against de Sitter and anti-de Sitter solutions, discussed in Section 2.2.3 and 2.2.3. We also find 2 new Minkowski solutions in the new class  $m_{46}$ .

We finally consider anti-de Sitter solutions. Beyond references given in Table 2.7, we can mention the recent works [69, 85] that have solutions in  $s_{6666}$ . We find here new solutions in new classes: 5 in  $m_{46}$  (with 3 sets of sources), and 4 in  $s_{55}$  (with 2 sets of sources). For the latter, we do not find solutions with 3 sets, i.e. with a last set having  $D_5$ . This may hint at a (surprising) no-go theorem or at computational complexity.

For Minkowski and anti-de Sitter solutions, similar points on T-duality relations and on the supersymmetry preserved by the source configurations can be made, as for de Sitter solutions. It would also be interesting to know whether these new Minkowski and anti-de Sitter solutions preserve (bulk) supersymmetry, given their fluxes and geometry. We do not investigate this question here, but it could in principle be done following the material reviewed in [93].

For all solutions, a remaining important point is to identify the 6d group manifold and verify its compactness. This requires tools that will be developed and presented in Chapter 3. Identifying the manifold, in particular the underlying algebra, is not straightforward because in each solution, the structure constants are obtained in an arbitrary basis, suited to the placement of the sources, with metric  $\delta_{ab}$ . Through an appropriate change of basis, the structure constants can be brought to a form where the algebra can be recognised. From there one can discuss whether the group manifold can be compact.

We provide in Appendix C the complete list of solutions. Let us recall, as indicated at the end of Section 2.2.1, that an overall rescaling is available to modify together the value of all variables in these solutions;  $|\mathcal{R}_4|$  and  $|\mathcal{R}_6|$  can in particular be lowered.

## 2.3 De Sitter, intersecting sources and 4d $\mathcal{N} = 1$ supersymmetry

In [70], 3 conjectures on classical de Sitter solutions have been formulated. Since that paper, no proof nor counterexample to these conjectures have been found, in spite of progress in this field. These conjectures are believed to hold true at least for the ansatz presented in [70] and used in the present thesis, if not beyond it. Of particular interest here is conjecture 1, claiming that there exists no classical de Sitter solution with parallel sources, i.e. a single set of sources. We propose here a fourth conjecture, that somehow extends conjecture 1.

**Conjecture 4.** *There is no classical de Sitter solution with 2 intersecting source sets.*

We believe again that this is true within our solution ansatz, and maybe beyond it, hence the general formulation of the conjecture.

A first argument in favor of conjecture 4 is that among all de Sitter solutions known and found listed in Table 2.7, none of them has less than 3 source sets ( $I = 1, 2, 3$ ). We also ran specific searches for de Sitter solutions with only 2 sets in several classes, but did not find any. Let us emphasize that the claim of conjecture 4 is made possible here for the first time thanks to the classification of solutions, that provides an overview of the possibilities. The T-duality relations described below also make manifest the role played by our classification to support this conjecture.

A second argument comes from T-duality. As discussed in Section 2.1.3, some source configurations are T-dual to each other. If we restrict ourselves to exactly 2 source sets, we have the following T-duality chains between source configurations of classes, displayed on Figure 2.1,

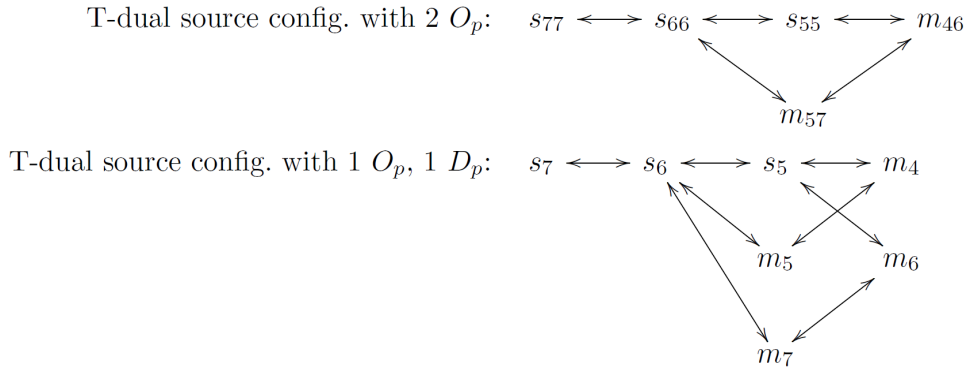


Figure 2.1: T-duality chains between the various classes of solutions.

where by definition,  $m_4$  with 2 source sets means 1  $O_4$  and 1  $D_6$ , etc. The different arrows on one class correspond to different possible choices of directions along which to perform the T-duality. The placement of source sets and T-duality directions is not detailed here, but should be clear when looking at the information of each class. Interestingly, we cover with these two T-duality chains (which only differ by the nature

## 2.3 De Sitter, intersecting sources and 4d $\mathcal{N} = 1$ supersymmetry

of the sources) all classes that can admit exactly 2 sets; in particular, no class is left isolated. The argument in favor of conjecture 4 is now the following: we know of no-go theorems on de Sitter solutions in  $s_7$  and  $s_{77}$  with (at least) 2 sets [73]. The T-duality relation to the configurations of the other classes suggests no-go theorems there as well. As discussed in Section 2.1.3, a complete T-duality relation of the classes is not strictly speaking realised, because few fields in one class can prevent a solution to be T-dual to another one, even if the source configurations are. This remains a strong hint in favor of an obstruction on de Sitter for all classes in these T-duality chains, which are all classes allowing for exactly 2 source sets. This supports conjecture 4. We tried to prove such a no-go theorem for  $s_{66}$ , inspired by the T-duality relation to  $s_{77}$ , but failed. The proof may again be difficult to achieve, as for the case of a single set in conjecture 1. Having it would still be very interesting, and further deriving through a 4d version the corresponding value of  $c$  in de Sitter swampland conjectures [78–81].

An interesting consequence of conjecture 4 is the result in a 4d effective theory. The “effectiveness” refers here to a certain truncation, and for the following implication to hold, we need a truncation that preserves the contribution of sources (source sets should not be erased through the truncation). This includes at least consistent truncations as we will see. If classical de Sitter solutions require at least 3 intersecting source sets, this implies, as discussed in Section 2.1.3, that supersymmetry is reduced at least by  $2^3$ , and since the truncation considered preserves the sources, we conclude

**Conjecture 4. implies** *A 4d effective theory of a classical string compactification, admitting a de Sitter critical point, can at most be  $\mathcal{N} = 1$  supersymmetric.*

As mentioned in Section 2.2.4, we know examples of de Sitter solutions admitting source configurations that break completely supersymmetry, so a non-supersymmetric 4d theory is a priori also possible (coming then probably with instabilities).

Our solution ansatz actually allows for a consistent truncation giving a 4d gauged supergravity (see Section 2.3 of [70]). This means that any solution in the latter will be one in our 10d theory. But there exists many 4d gauged supergravities, defined in particular by their turned-on gaugings, most of them having no higher dimensional origin as a classical compactification. It has been already noticed that finding de Sitter solutions in 4d gauged supergravities with extended supersymmetries ( $\mathcal{N} > 1$ ) seems difficult precisely when requiring a classical compactification origin. This observation is exactly in agreement with conjecture 4 and its implication. (Meta-) stable de Sitter solutions in 4d gauged supergravities with *extended* supersymmetries typically require Fayet-Iliopoulos terms (whose higher dimensional origin is in general unclear), non-compact gaugings (which would correspond to non-compact extra dimensions) [94–99] or non-geometric fluxes [100] (whose stringy origin is not in a standard classical compactification); some of the latter examples are even disputed in [101]. More examples and arguments were provided recently in [99, 102], beyond the (meta-) stable case. Further references can be found in Footnote 7 of [65]. These observations on 4d gauged supergravities are consistent with our claims, thanks to the consistent truncation allowed by our solution ansatz.

## Chapter 2. Charting the Landscape

---

The constraint phrased in conjecture 4 on classical de Sitter solutions and resulting 4d effective theories is interesting for phenomenology. The configurations of intersecting sources considered here typically allow to build particle physics models (see [73] or the recent works [103, 104]). Having at most  $\mathcal{N} = 1$  in 4d *naturally* allows for chirality in those models, as wished for phenomenology. Looking for classical de Sitter solutions thus provides unexpectedly several required ingredients to build, *together with cosmology*, viable particle physics models.

## 3 Exploring the Landscape

In the previous chapter, we decomposed in several classes what we called so far the Landscape of classical Minkowski and (A)dS solutions of type II supergravities. This classification was done according to the  $O_p/D_p$  sources content. We now turn to exploring each of these regions. One first thing to determine is the existence of dS solutions in a given class: this is of course not automatic and in some cases the non-existence can be made precise with no-go theorems which we prove here. In other regions, (A)dS solutions can be found: we then proceed by characterising their properties, including the study of the internal space's geometry (and whether it can be made compact), the stability of the potential at the critical point, and the possible scale separation. The discussion of these properties will be completed in Chapter 5 where we analyse the flux quantization and whether the supergravity solutions are actually weakly coupled while still having a large internal volume.

### 3.1 Algebra identification and compactness

In this section, we focus on the identification of Lie algebras  $\mathfrak{g}$  underlying the 6d group manifolds  $\mathcal{M}$  in the solutions found, and the compactness of  $\mathcal{M}$ . We first recall in Section 3.1.1 a few useful elements of algebras. We illustrate those in various examples in Section 3.1.2. We then present in Section 3.1.3 the method used for this identification, as well as the (partly numerical) tools developed. We finally present our results in Section 3.1.4, namely the identification of all 6d algebras appearing in the solutions found in [1, 4, 65], and what can be said on the compactness of the corresponding group manifold  $\mathcal{M}$ .

#### 3.1.1 Elements of algebra

We consider a real 6d Lie algebra  $\mathfrak{g}$ . In a given basis, it is expressed by the commutation relations of the 6 vectors  $\{E_a\}$ ,  $a = 1, \dots, 6$ , in terms of the structure constants  $f^a_{bc}$

$$\mathfrak{g} : [E_b, E_c] = f^a_{bc} E_a, \quad (3.1)$$

and the structure constants are bound to verify the Jacobi identities. Real 6d Lie algebras are classified. Levi's decomposition indicates that any Lie algebra  $\mathfrak{g}$  is the semi-direct sum of a semi-simple algebra  $\mathfrak{s}$  and a solvable ideal  $\mathfrak{r}$  called the radical of  $\mathfrak{g}$

$$\mathfrak{g} = \mathfrak{s} \ltimes \mathfrak{r}. \quad (3.2)$$



We will distinguish two cases:

- $\mathfrak{g} = \mathfrak{r}$  is solvable (to be defined below).
- $\mathfrak{g}$  is not solvable. This last case can be further divided in three situations:  $\mathfrak{g} = \mathfrak{s}$  is semi-simple,  $\mathfrak{g} = \mathfrak{s} \oplus \mathfrak{r}$  is a *direct* sum, or  $\mathfrak{g} = \mathfrak{s} \ltimes \mathfrak{r}$  is a (non-trivial) *semi-direct* sum. This division will however not be crucial to us since we will only consider few algebras that are not solvable.

We now introduce a few elements to define solvability, and a particular case, nilpotency, of a Lie algebra; a mathematical review on solvable algebras and the corresponding solvmanifolds can be found in [71]. We first recall that an ideal  $\mathfrak{i}$  of an algebra  $\mathfrak{g}$  is a subalgebra that verifies  $[\mathfrak{g}, \mathfrak{i}] \subseteq \mathfrak{i}$ . Any Lie algebra  $\mathfrak{g}$  possesses three series of ideals: the derived series, the lower central series, and the upper central series. We will only need the first two: the lower central series  $\{\mathfrak{g}^{(k)}\}_{k \in \mathbb{N}}$  is defined recursively as follows

$$\mathfrak{g}^{(k)} = [\mathfrak{g}^{(k-1)}, \mathfrak{g}], \quad \mathfrak{g}^{(0)} = \mathfrak{g}, \quad (3.3)$$

while the derived series  $\{\mathfrak{g}^{(k)}\}_{k \in \mathbb{N}}$  is defined as

$$\mathfrak{g}^{(k)} = [\mathfrak{g}^{(k-1)}, \mathfrak{g}^{(k-1)}], \quad \mathfrak{g}^{(0)} = \mathfrak{g}. \quad (3.4)$$

The sets of successive dimensions of ideals in the lower central and derived series are respectively denoted CS and DS. These two sets of integers are readily computable from the list of structure constants, and are often different from one Lie algebra to another one. They are basis independent: they will then be useful for the identification of algebras. And indeed, a first use can be seen through the following definitions. An algebra is solvable iff  $\exists k$  s.t.  $\mathfrak{g}^{(k)} = 0$ ; in other words, its DS ends with 0. An algebra is nilpotent iff  $\exists k$  s.t.  $\mathfrak{g}^{(k)} = 0$ ; in other words, its CS reaches 0. The latter is a particular case of the former.

Another useful definition is that of the nilradical  $\mathfrak{n}$  of a solvable Lie algebra  $\mathfrak{g}$ :  $\mathfrak{n}$  is the maximal nilpotent ideal of  $\mathfrak{g}$ . It is unique, and solvable algebras are classified according to their nilradical. Determining it is thus an important step towards identifying a solvable algebra.

A necessary condition for compactness of the group manifold is the unimodularity (also known as unipotence) of the Lie algebra: this is defined as

$$\forall b, \quad \sum_a f^a_{ab} = 0. \quad (3.5)$$

The ansatz used to find solutions required a stronger condition, namely  $f^a_{ab} = 0$  without sum on  $a$ . This is motivated by an appropriate choice of basis [4, 71]. The list of (isomorphism classes of) indecomposable unimodular real solvable Lie algebras up to dimension 6 is given in [105]; there are 100 6-dimensional ones. The list of unimodular real non-solvable 6d Lie algebras is given in [74] and below in Table 3.1: there are only 16 of them. We will also make use of the classification given in [106], which does not restrict to unimodular algebras, but gives the CS and DS values for all algebras.

A last element which will be useful is the Killing form. It is a symmetric bilinear form on the algebra  $\mathfrak{g}$

$$B(x, y) = \text{Tr}(\text{ad}(x) \cdot \text{ad}(y)) , \quad x, y \in \mathfrak{g} \quad \iff \quad B_{ab} = f^c_{da} f^d_{cb} . \quad (3.6)$$

This (0,2)-tensor, equivalently represented by a (symmetric) matrix, has interesting properties. To start with, one has

- $\mathfrak{g}$  is semi-simple iff  $B$  has a non-zero determinant,
- $\mathfrak{g}$  is solvable iff  $B(\mathfrak{g}, [\mathfrak{g}, \mathfrak{g}]) = 0$ ,
- If  $\mathfrak{g}$  is nilpotent then  $B$  is identically zero.

In addition, the signature of  $B$  is invariant under a real change of basis. This will be of interest to us for the identification of algebras: we will be interested in the number of positive and negative eigenvalues of  $B$ . Finally, if  $B$  only has negative eigenvalues (implying that it is semi-simple) then  $\mathfrak{g}$  is compact.

A solvable algebra  $\mathfrak{g}$  gives rise to a compact group manifold  $\mathcal{M}$  whenever a lattice can be found. Let us consider a discrete subgroup  $\Gamma$  of the group  $G$  associated to  $\mathfrak{g}$ . This  $\Gamma$  is a lattice if the quotient  $G/\Gamma$  is compact. This quotient is then precisely the group manifold  $\mathcal{M}$ , and it is called a solvmanifold. A particular case is a nilmanifold, the quotient of a nilpotent group by a lattice. Given an indecomposable solvable algebra, whether or not a lattice can be found is not always settled. As a consequence, we cannot always conclude on the compactness of  $\mathcal{M}$  once the algebra is identified. We refer to [71, 107] for more details on this matter of compactness.

Beyond the elements presented above, many more exist, with associated methods to help identifying Lie algebras given in terms of their structure constants. We can mention, among others, the upper central series and their dimensions (US), the number of generalized Casimir invariants, decomposability properties, etc. We refer the interested reader to [106]. The above will be enough for our purposes.

#### 3.1.2 Examples of algebras

Let us illustrate the previous definitions with a few examples. We start with low dimensional real unimodular Lie algebras. In 1 or 2 dimensions, there are only  $\mathfrak{u}(1)$  and  $2\mathfrak{u}(1)$ . In 3 dimensions, there are six of them. We give them below in terms of their non-zero structure constants in some basis; the directions numbering, 123 or 456, is chosen for convenience

$$\begin{aligned}
 3\mathfrak{u}(1) : & \quad (f^a_{bc} = 0) \quad (\text{nilpotent}) & (3.7) \\
 \text{Heis}_3 : & \quad f^4_{56} = 1 \quad (\text{nilpotent}) \\
 \mathfrak{g}_{3.5}^0 = \mathfrak{iso}(2) : & \quad f^4_{56} = 1, f^5_{46} = -1 \quad (\text{solvable}) \\
 \mathfrak{g}_{3.4}^{-1} = \mathfrak{iso}(1, 1) : & \quad f^4_{56} = 1, f^5_{46} = 1 \Leftrightarrow f^4_{46} = 1, f^5_{56} = -1 \quad (\text{solvable}) \\
 \mathfrak{so}(3) = \mathfrak{su}(2) : & \quad f^1_{23} = 1, f^2_{31} = 1, f^3_{12} = 1 \quad (\text{simple}) \\
 \mathfrak{so}(2, 1) = \mathfrak{sl}(2, \mathbb{R}) : & \quad f^1_{23} = 1, f^2_{31} = 1, f^3_{12} = -1 \quad (\text{simple})
 \end{aligned}$$

Of those, only  $\mathfrak{so}(2, 1)$  does not lead to a compact group manifold. Others are either compact, or admit lattices giving compact group manifolds.

### Chapter 3. Exploring the Landscape

	Algebra	$\mathcal{M}$ compactness	CS	DS	Eigenvalues
Semi-simple	$\mathfrak{so}(3, 1)$	×	6	6	3+, 3-
	$\mathfrak{so}(3) \oplus \mathfrak{so}(3)$	✓	6	6	6-
	$\mathfrak{so}(3) \oplus \mathfrak{so}(2, 1)$	×	6	6	2+, 4-
	$\mathfrak{so}(2, 1) \oplus \mathfrak{so}(2, 1)$	×	6	6	4+, 2-
Direct sum simple $\oplus$ solvable	$\mathfrak{so}(3) \oplus 3\mathfrak{u}(1)$	✓	6, 3	6, 3	3-
	$\mathfrak{so}(3) \oplus \text{Heis}_3$	✓	6, 4, 3	6, 4, 3	3-
	$\mathfrak{so}(3) \oplus \mathfrak{g}_{3,5}^0$	✓	6, 5	6, 5, 3	4-
	$\mathfrak{so}(3) \oplus \mathfrak{g}_{3,4}^{-1}$	✓	6, 5	6, 5, 3	1+, 3-
	$\mathfrak{so}(2, 1) \oplus 3\mathfrak{u}(1)$	×	6, 3	6, 3	2+, 1-
	$\mathfrak{so}(2, 1) \oplus \text{Heis}_3$	×	6, 4, 3	6, 4, 3	2+, 1-
	$\mathfrak{so}(2, 1) \oplus \mathfrak{g}_{3,5}^0$	×	6, 5	6, 5, 3	2+, 2-
	$\mathfrak{so}(2, 1) \oplus \mathfrak{g}_{3,4}^{-1}$	×	6, 5	6, 5, 3	3+, 1-
Semi-direct sum simple $\ni$ solvable	$\mathfrak{so}(3) \ni 3\mathfrak{u}(1)$	✓	6	6	3-
	$\mathfrak{so}(2, 1) \ni 3\mathfrak{u}(1)$	×	6	6	2+, 1-
	$\mathfrak{so}(2, 1) \ni 2\mathfrak{u}(1) \oplus \mathfrak{u}(1)$	×	6, 5	6, 5	2+, 1-
	$\mathfrak{so}(2, 1) \ni \text{Heis}_3$	×	6	6	2+, 1-

Table 3.1: All 6-dimensional real unimodular Lie algebras, that are not solvable. The compactness is that of an associated group manifold  $\mathcal{M}$ , possibly thanks to a lattice. CS denotes the successive dimensions of the ideals in the lower central series, and DS those of the derived series. Eigenvalues with  $p+$ ,  $m-$  denotes that the Killing form admits  $p$  positive eigenvalues and  $m$  negative ones, the remaining  $6 - p - m$  eigenvalues being 0.

In 4, 5 or 6 dimensions, the only (semi)-simple real unimodular Lie algebra that is indecomposable, is the following 6-dimensional one

$$\begin{aligned} \mathfrak{so}(3, 1) : \quad & f^1_{23} = 1, \quad f^2_{31} = 1, \quad f^3_{12} = 1, \quad f^1_{56} = -1, \quad f^5_{61} = 1, \quad f^6_{15} = 1 \quad (3.8) \\ & f^2_{46} = 1, \quad f^4_{62} = -1, \quad f^6_{24} = -1, \quad f^3_{45} = -1, \quad f^4_{53} = 1, \quad f^5_{34} = 1. \end{aligned}$$

This algebra is not compact. From these ingredients, one can build all 6-dimensional real unimodular Lie algebras, that are not solvable. Following [74, 106] (and notations of [107]), we list them here in Table 3.1, and determine some of their properties. We provide below few more comments on them, before turning to solvable algebras in 4, 5 or 6 dimensions.

For completeness, we give as follows the structure constants for the semi-direct sum

### 3.1 Algebra identification and compactness

Algebra	$\mathcal{M}$ compactness	CS	DS	Eigenvalues
$3\mathfrak{u}(1) \oplus 3\mathfrak{u}(1)$	✓	6,0	6,0	0
$\text{Heis}_3 \oplus 3\mathfrak{u}(1)$	✓	6,1,0	6,1,0	0
$\mathfrak{g}_{3,5}^0 \oplus 3\mathfrak{u}(1)$	✓	6,2	6,2,0	1-
$\mathfrak{g}_{3,4}^{-1} \oplus 3\mathfrak{u}(1)$	✓	6,2	6,2,0	1+
$\text{Heis}_3 \oplus \text{Heis}_3$	✓	6,2,0	6,2,0	0
$\mathfrak{g}_{3,5}^0 \oplus \text{Heis}_3$	✓	6,3,2	6,3,0	1-
$\mathfrak{g}_{3,4}^{-1} \oplus \text{Heis}_3$	✓	6,3,2	6,3,0	1+
$\mathfrak{g}_{3,5}^0 \oplus \mathfrak{g}_{3,5}^0$	✓	6,4	6,4,0	2-
$\mathfrak{g}_{3,4}^{-1} \oplus \mathfrak{g}_{3,5}^0$	✓	6,4	6,4,0	1+,1-
$\mathfrak{g}_{3,4}^{-1} \oplus \mathfrak{g}_{3,4}^{-1}$	✓	6,4	6,4,0	2+

Table 3.2: 6-dimensional real unimodular solvable Lie algebras, that are decomposable and do not contain a 4d or 5d indecomposable subalgebra; rather they are a direct sum of 3-dimensional subalgebras. We also give some properties: the compactness of an associated group manifold  $\mathcal{M}$  (thanks to a lattice), the CS and DS, and the number of positive and negative eigenvalues of the Killing form.

algebras appearing in Table 3.1

$$\begin{aligned} \mathfrak{so}(3) \ni 3\mathfrak{u}(1) : \quad & f^1_{23} = 1, f^2_{31} = 1, f^3_{12} = 1, f^4_{35} = -1, f^5_{34} = 1, \\ & f^4_{26} = 1, f^6_{24} = -1, f^5_{16} = -1, f^6_{15} = 1 \end{aligned} \quad (3.9)$$

$$\begin{aligned} \mathfrak{so}(2,1) \ni 3\mathfrak{u}(1) : \quad & f^1_{23} = -1, f^2_{31} = -1, f^3_{12} = 1, f^4_{15} = -1, f^5_{14} = -1, \\ & f^4_{26} = 1, f^6_{24} = 1, f^5_{36} = -1, f^6_{35} = 1 \end{aligned} \quad (3.10)$$

$$\begin{aligned} \mathfrak{so}(2,1) \ni 2\mathfrak{u}(1) \oplus \mathfrak{u}(1) : \quad & f^1_{12} = 2, f^2_{13} = -1, f^3_{23} = 2, f^4_{24} = 1, f^5_{25} = -1, \\ & f^5_{14} = 1, f^4_{35} = 1 \end{aligned} \quad (3.11)$$

$$\begin{aligned} \mathfrak{so}(2,1) \ni \text{Heis}_3 : \quad & f^1_{12} = 2, f^2_{13} = -1, f^3_{23} = 2, f^5_{25} = 1, f^6_{26} = -1, \\ & f^6_{15} = 1, f^5_{36} = 1, f^4_{56} = 1. \end{aligned}$$

For the last two, there could be no basis where  $f^a_{ac} = 0$  without sum on  $a$ .

Let us comment on the compactness of  $\mathcal{M}$  indicated in Table 3.1. Most of the time, its non-compactness is due to  $\mathfrak{so}(2,1)$ . The semi-direct sum  $\mathfrak{b} \ni \mathfrak{f}$  can be interpreted geometrically as leading for  $\mathcal{M}$  to a fibration, where the fiber comes from  $\mathfrak{f}$  and is over a base generated by  $\mathfrak{b}$ . Indeed, when one moves in  $\mathfrak{b}$ , there is a change on the elements of  $\mathfrak{f}$ . In addition, if the base in a fiber bundle is non-compact, the manifold is non-compact as well. We conclude that  $\mathfrak{so}(2,1) \ni \mathfrak{f}$  are non-compact.

There are many more real unimodular solvable Lie algebras, in 4, 5 or 6 dimensions. Let us first focus on 6d decomposable ones. Those are a direct sum of lower dimensional real unimodular solvable algebras. If one of those is a 4d or 5d indecomposable one, then the rest can only be  $2\mathfrak{u}(1)$  or  $\mathfrak{u}(1)$ . Otherwise, either the 6d algebra is  $6\mathfrak{u}(1)$  or it contains a 3d indecomposable real unimodular solvable algebra: we list the 6d algebras built in this way in Table 3.2, together with some properties.

Algebra	$\mathcal{M}$ compactness	CS	DS	Eigenvalue
$\mathfrak{g}_{6.83}^{0,l}$ ( $l \neq 0$ )	?	6,5	6,5,1,0	$4l^2$
$\mathfrak{g}_{6.84}$	?	6,4,3	6,4,1,0	2
$\mathfrak{g}_{6.88}^{0,\mu_0,\nu_0}$ ( $ \mu_0  +  \nu_0  \neq 0$ )	$\mu_0\nu_0 \neq 0$	6,5	6,5,1,0	$4(\mu_0^2 - \nu_0^2)$
$\mathfrak{g}_{6.89}^{0,\nu_0,s}$ ( $ s  +  \nu_0  \neq 0$ )	$\nu_0 \neq 0$	$s\nu_0 \neq 0$ : 6,5 $s\nu_0 = 0$ : 6,3	$s\nu_0 \neq 0$ : 6,5,1,0 $s\nu_0 = 0$ : 6,3,1,0	$2(s^2 - \nu_0^2)$
$\mathfrak{g}_{6.90}^{0,\nu_0}$	$\nu_0 \neq 0$	$\nu_0 \neq 0$ : 6,5 $\nu_0 = 0$ : 6,3	$\nu_0 \neq 0$ : 6,5,1,0 $\nu_0 = 0$ : 6,3,1,0	$2(1 - \nu_0^2)$
$\mathfrak{g}_{6.91}$	?	6,5	6,5,1,0	
$\mathfrak{g}_{6.92}^{0,\mu_0,\nu_0}$ ( $\mu_0\nu_0 \neq 0$ )	✓	6,5	6,5,1,0	$-4\mu_0\nu_0$
$\mathfrak{g}_{6.92}^0$	✓	6,5	6,5,1,0	-4
$\mathfrak{g}_{6.93}^{0,\nu_0}$	$ \nu_0  > \frac{1}{2}$	$\nu_0 \neq 0$ : 6,5 $\nu_0 = 0$ : 6,3	$\nu_0 \neq 0$ : 6,5,1,0 $\nu_0 = 0$ : 6,3,1,0	$2(1 - 2\nu_0^2)$

Table 3.3: 6-dimensional real unimodular (indecomposable) solvable Lie algebras with nilradical  $\mathfrak{g}_{5.4}$ , from Tables 28 and 29 of [107], and their properties. The compactness of an associated group manifold  $\mathcal{M}$ , when settled, is read from the last remarks of Section 8.3 and 8.4 in [107]; the conditions indicated here on parameters are sufficient, we do not know if they are necessary. We also give the CS and DS. The Killing form for these algebras admits at most one non-zero eigenvalue, that we indicate explicitly.

Finally, real 6d unimodular solvable Lie algebras that are indecomposable are classified according to their nilradical as e.g. in [107], into so-called “isomorphism classes”: for any such algebra, one can find an isomorphism or change of basis that maps it to one (and only one) of these classes. Let us give one example: those whose nilradical is  $\mathfrak{g}_{5.4}$ . These algebras are listed in Tables 28 and 29 of [107]. We have worked out some of their properties as before, and summarize them in Table 3.3. Let us also mention a typo in  $\mathfrak{g}_{6.83}^{0,l}$ , whose correct structure constants are provided in the following for completeness

$$\mathfrak{g}_{6.83}^{0,l} : \quad f^1_{24} = f^1_{35} = 1, \quad f^2_{26} = f^3_{36} = -f^4_{46} = -f^5_{56} = l, \quad f^3_{26} = -f^4_{56} = 1. \quad (3.12)$$

### 3.1.3 Method and tools for the identification

- **General method**

A 6d Lie algebra obtained in one of our solutions is given in terms of its structure constants  $f^a_{bc}$  in an arbitrary basis of vectors  $\{E_a\}$ . It must correspond to one (and only one) of the algebras appearing in the tables of [106, 107]. Those are however given a priori in a different basis  $\{E'_a\}$ , typically with a minimal amount of non-zero structure constants  $f^a_{bc}'$ . This is the reason why the identification of our algebras is challenging.

The two algebras are isomorphic if and only if there exists a change of basis  $M$  such that

$$E'_a = E_b (M^{-1})^b{}_a \Leftrightarrow e^{a'} = M^a{}_b e^b, \quad \det M \neq 0, \quad (3.13)$$

where we also indicate the transformation of 1-forms  $\{e^a\}$ . The two sets of structure constants are equivalently related in the following way

$$f^a{}_{de} = (M^{-1})^a{}_k M^b{}_d M^c{}_e f^{kbc'}. \quad (3.14)$$

The relations (3.14) amount to a high number of non-linear equations (depending on  $M$ ), and it would be computationally too involved to try to solve them for every tabulated algebra. Rather, the method will consist in making use of the (basis) invariants and ideals defined in Section 3.1.1 to reduce as much as possible the number of candidate algebras among the tabulated ones. Only then, and if there is more than one candidate algebra, we will find an explicit change of basis verifying (3.14).

In more detail, to identify a 6d Lie algebra obtained in one solution in terms of its structure constants, we proceed as follows:

- We start by computing its CS, DS and the eigenvalues of its Killing form. The DS tells us if it is solvable or not. If it is not, it must be one of the 16 listed in Table 3.1. As can be seen there, the properties of the algebras allow to discriminate among all of them except for two. In this last case, we need an explicit change of basis to conclude. Apart from the latter, the procedure described so far has been automatized into the numerical tool `AlgId`, that we present below.
- In case the 6d algebra is solvable, we identify its nilradical. This is easily done using the definition given in Section 3.1.1 and comparing to tables of nilpotent algebras. If necessary, one can compute as well the CS, DS of the nilradical to help in this comparison. If the CS indicates that the 6d algebra is nilpotent, then the nilradical is the algebra itself. Let us now consider that we face a solvable non-nilpotent algebra. In case it is indecomposable, one uses the nilradical to find a table of candidate algebras in [106, 107]. For all these candidate algebras, the CS, DS and eigenvalues can again be computed and compared: see for instance Table 3.3. Once one is left with only few candidate algebras, an explicit change of basis needs to be found towards one of them. A dedicated numerical tool, `AlgIso`, is presented below, providing a numerical matrix  $M$  verifying (3.14). Another option is to find an analytical change of basis; we will give a few examples below.
- A last possibility is that the 6d (real unimodular) non-nilpotent solvable algebra is decomposable. In that case, the tables of 6d indecomposable algebras are not useful and one has to devise what are the possibilities, according to the nilradical. One particular case is that of a decomposition into two 3d solvable algebras: such algebras are listed in Table 3.2, and their comparison is automatized in the tool `AlgId`.

We summarize our procedure in Figure 3.1.

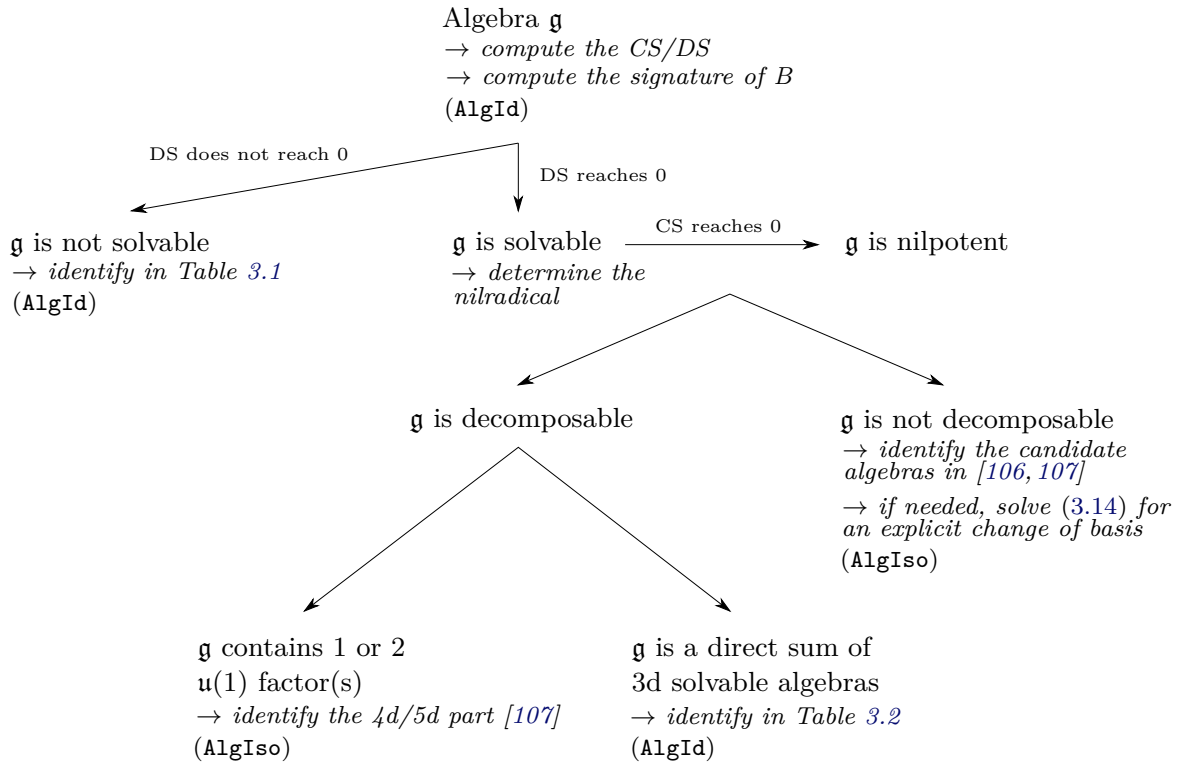


Figure 3.1: Summary of the procedure used for the identification of 6d unimodular Lie algebras.

• Numerical tools AlgId and AlgIso

We present in the following the numerical tools AlgId and AlgIso that we developed to help us identifying the algebras of our solutions. These tools are however built for a broader use.

The main input of the code AlgId is a set of structure constants of a Lie algebra, as well as its dimension. The first part of the code computes the CS, DS, the Killing form eigenvalues, and its signature. In a second part, these results are compared to a data base of 6d algebras, namely the 16 of Table 3.1 and the 9 of Table 3.2 (without  $6\mathfrak{u}(1)$ ), and the code indicates any match. These outputs should help identifying the initial algebra.

This code is meant to work not only for structure constants taking integer or round values, as e.g. in classification tables, but also when having numerical values as those obtained in our solutions. Because of the latter, a precision parameter  $\epsilon$  needs to be specified, and the code then interprets as vanishing, or sets to zero, various key quantities smaller than  $\epsilon$ : this avoids problems related to “numerical zeros” which are not exactly zero. In our case, a suitable value turns out to be  $\epsilon = 10^{-10}$ .

To compute the CS and DS of an algebra  $\mathfrak{g}$  with vectors  $\{E_a\}$ , the code proceeds as follows. The CS and DS are the set of dimensions of the series of ideals  $\mathfrak{g}_{(k)}$  and  $\mathfrak{g}^{(k)}$ . Each of these ideals is obtained by brackets between elements of subalgebras of  $\mathfrak{g}$ . The idea of the code is to compute all these brackets, and store their result. More precisely, each bracket gives a vector, which is stored as the rows of a matrix  $M_v$ , when expressed

in the initial basis  $\{E_a\}$ . Here is an example

$$\begin{aligned} [E_1, E_2] &= f^3_{12} E_3 \\ [E_1, E_3] &= f^2_{13} E_2 + f^4_{13} E_4 \\ &\vdots \end{aligned} \quad \rightarrow \quad M_v = \begin{pmatrix} 0 & 0 & f^3_{12} & 0 & \dots \\ 0 & f^2_{13} & 0 & f^4_{13} & \dots \\ & & \vdots & & \end{pmatrix}. \quad (3.15)$$

Determining the dimension of one ideal amounts to finding how many of these vectors are linearly independent. This could be done by computing the rank of the matrix  $M_v$ . But this option is not flexible enough in the case of numerical input, for instance in the case where two vectors are very similar, and should be equal up to a numerical error. What is rather done is then to complete the matrix  $M_v$  into a square one, by determining the orthogonal space to the rows of  $M_v$ , and then compute the determinant of the square matrix. If the determinant is too small, the code considers it to be zero and decides that the vectors in  $M_v$  are not independent. On the way, the vectors are normalised to 1 to allow for a fair evaluation of the determinant. This method to determine the linear independence is actually implemented every time a new vector is added to  $M_v$ : if it is found linearly independent, the dimension of the ideal is increased by one; if the vector is not independent, then it is not added to  $M_v$ . This is done recursively until one has tested all vectors obtained by all brackets defining the ideal. One obtains in this manner the dimension of the ideal, and builds this way the CS and DS of the algebra considered.

The rest of `AlgId` is straightforward, so let us now present `AlgIso`. That code aims at finding an isomorphism between two algebras that are specified as input. If one of the algebra depends on parameters, as e.g. some of the tabulated ones, these parameters are automatically turned into variables and the code also searches for appropriate values. To find an isomorphism between the two algebras, the method amounts to solving the equations (3.14), where the variables are the matrix elements of  $M$ , the change of basis. To solve these equations, we proceed via a two-step minimisation of a loss function, built from the equations to solve. More details on this procedure can be found e.g. in [4], where this approach was used to find supergravity solutions. If a solution to the equations is found, then the isomorphism  $M$  and possible values of algebra parameters are provided.

- **Analytical changes of basis**

While most non-nilpotent solvable algebras are identified, following the method described in Section 3.1.3, thanks to a final numerical change of basis, a few can still be determined by an analytical one. We present some examples below. For the latter, Table 3.1 is enough for the identification. The analytical change of basis in that case can still serve further purposes, such as a classicality study [2].

- **Solutions  $s_{6666}^+ \mathfrak{3}, 4$**

We start with solutions  $s_{6666}^+ \mathfrak{3}, 4$  which have the following non-zero structure constants

$$s_{6666}^+ \mathfrak{3}, 4 : \quad f^1_{45}, f^5_{14}, f^3_{46}, f^6_{34}, f^2_{13}, f^2_{56}. \quad (3.16)$$

From this set, one identifies the nilradical to be  $\mathfrak{g}_{5,4}$ , with directions and non-zero structure constants

$$\mathfrak{n} = \{1, 2, 3, 5, 6\}, \quad f^2_{13}, f^2_{56}. \quad (3.17)$$



## Chapter 3. Exploring the Landscape

These algebras are thus among those of Table 3.3. To completely identify them, we determine in the following an analytical isomorphism. A first step is a relabeling on the set (3.16)

$$1 \rightarrow 2, 2 \rightarrow 1, 3 \rightarrow 4, 4 \rightarrow 6, 5 \rightarrow 3, 6 \rightarrow 5 : \quad f^2_{63}, f^3_{26}, f^4_{65}, f^5_{46}, f^1_{24}, f^1_{35}. \quad (3.18)$$

This small set of structure constants obeys a few relations, thanks to the Jacobi identities

$$f^1_{e[3f^e_{46}]} = 0 \Leftrightarrow \frac{f^1_{53}}{f^1_{24}} = \frac{f^2_{36}}{f^5_{46}}, \quad (3.19)$$

$$f^1_{e[2f^e_{56}]} = 0 \Leftrightarrow \frac{f^1_{53}}{f^1_{24}} = \frac{f^4_{56}}{f^3_{26}}. \quad (3.20)$$

We then perform the following rescaling

$$e^{a \neq 1', 4'} = e^a, \quad e^{1'} = \frac{1}{f^1_{35}} e^1, \quad e^{4'} = \frac{f^1_{24}}{f^1_{53}} e^4, \quad (3.21)$$

leading, thanks to the above relations, to the new structure constants

$$f^2_{36}' = -f^5_{46}' = f^2_{36}, \quad f^3_{26}' = -f^4_{56}' = f^3_{26}, \quad f^1_{35}' = f^1_{24}' = 1. \quad (3.22)$$

We introduce the parameters  $\mu_0 = -f^2_{36}$  and  $\nu_0 = f^3_{26}$ . Given that  $\mu_0 \neq \nu_0$  in our solutions, we identify the algebra to be  $\mathfrak{g}_{6,92}^{0, \mu_0, \nu_0}$ , for both solutions.

### • Solution $m_{5577}^{+*} 1$

For this solution, we have the following set of non-vanishing structure constants:

$$m_{5577}^{+*} 1 : \quad f^6_{23} = f^6_{14}, \quad f^2_{35} = f^1_{45}, \quad f^4_{15} = f^3_{25}. \quad (3.23)$$

The nilradical is identified to be  $\mathfrak{g}_{5,4}$  with

$$\mathfrak{n} = \{1, 2, 3, 4, 6\}, \quad \text{and} \quad f^6_{23} = f^6_{14}, \quad (3.24)$$

so the algebra can be found in Table 3.3. One can perform the following relabeling of directions

$$1 \rightarrow 2, 2 \rightarrow 3, 3 \rightarrow 5, 4 \rightarrow 4, 5 \rightarrow 6, 6 \rightarrow 1 : \quad f^1_{35} = f^1_{24}, \quad f^3_{56} = f^2_{46}, \quad f^4_{26} = f^5_{36}. \quad (3.25)$$

We have in addition the following signs:  $f^3_{56} > 0, f^5_{36} < 0$ . We then perform the following rescaling on forms

$$e^{1'} = \frac{1}{f^1_{35} \sqrt{-f^3_{56} f^5_{36}}} e^1, \quad e^{2,3'} = \frac{1}{\sqrt{f^3_{56}}} e^{2,3}, \quad e^{4,5'} = \frac{1}{\sqrt{-f^5_{36}}} e^{4,5}, \quad e^{6'} = \sqrt{-f^3_{56} f^5_{36}} e^6. \quad (3.26)$$

The new normalization allows to directly identify the algebra to be  $\mathfrak{g}_{6,92}^0$ .

### 3.1.4 Results

Using the method and tools described in Section 3.1.3, we have identified all algebras of the solutions found in [4], as well as the algebras of the previously found solutions  $s_{55}^0 1$  and  $s_{55}^+ 1 - 28$  [1, 65]. This allows in particular to discuss the compactness of the group manifolds, using the material of Section 3.1.2 or further results in [107]. We summarize our findings as follows.

### 3.1 Algebra identification and compactness

- De Sitter solutions

algebra	$\mathfrak{so}(3) \oplus \mathfrak{so}(3)$	$\mathfrak{so}(3) \oplus 3\mathfrak{u}(1)$	$\mathfrak{so}(3) \oplus \text{Heis}_3$	$\mathfrak{so}(3) \oplus \mathfrak{g}_{3,4}^{-1}$	$\mathfrak{g}_{3,5}^0 \oplus \mathfrak{g}_{3,5}^0$
solutions	$s_{6666}^+ 1$	$m_{46}^+ 10$	$s_{55}^+ 20, 21$	$s_{55}^+ 19$	$s_{55}^+ 14$
compactness	✓	✓	✓	✓	✓
algebra	$\mathfrak{g}_{3,4}^{-1} \oplus \mathfrak{g}_{3,4}^{-1}$	$\mathfrak{g}_{3,4}^{-1} \oplus \mathfrak{g}_{3,5}^0$	$\mathfrak{g}_{6,76}^{-1}$	$\mathfrak{g}_{6,92}^{0,\mu_0,\nu_0}$	$\mathfrak{g}_{6,92}^0$
solutions	$s_{55}^+ 15$	$s_{55}^+ 22 - 27$	$s_{55}^+ 16, 17$	$s_{6666}^+ 3, 4, m_{5577}^+ 3 - 6$	$m_{5577}^{+*} 1$
compactness	✓	✓	✓	✓	✓

Table 3.4: Algebras identified in de Sitter solutions, leading to compact group manifolds.

algebra	$\mathfrak{so}(3, 1)$	$\mathfrak{so}(2, 1) \oplus \mathfrak{so}(2, 1)$	$\mathfrak{so}(3) \oplus \mathfrak{so}(2, 1)$	$\mathfrak{so}(2, 1) \oplus 3\mathfrak{u}(1)$
solutions	$m_{55}^+ 1, s_{6666}^+ 2$	$m_{55}^+ 2 - 4, m_{5577}^+ 2, 7, 12$	$m_{5577}^+ 1$	$m_{46}^+ 1 - 9$
compactness	×	×	×	×
algebra	$\mathfrak{so}(2, 1) \oplus \text{Heis}_3$	$\mathfrak{so}(2, 1) \oplus \mathfrak{g}_{3,5}^0$	$\mathfrak{so}(2, 1) \oplus \mathfrak{g}_{3,4}^{-1}$	
solutions	$s_{55}^+ 18$	$s_{55}^+ 12, m_{5577}^+ 9, 10$	$s_{55}^+ 1 - 11, 13, 28, m_{5577}^+ 8, 11$	
compactness	×	×	×	

Table 3.5: Algebras identified in de Sitter solutions, leading to non-compact group manifolds.

Finally, the solution  $s_{66}^+ 1$  was identified to be on  $\mathfrak{g}_{6,88}^{0,\mu_0,0} = \mathfrak{g}_{6,88}^{0,1,0}$ , but we do not know whether this algebra can provide compact group manifolds.

- Minkowski solutions

algebra	$\text{Heis}_3 \oplus \text{Heis}_3$	$\mathfrak{g}_{6,88}^{0,\mu_0,\nu_0}$	$\mathfrak{g}_{6,89}^{0,\nu_0,s}$	$\mathfrak{g}_{5,14}^0 \oplus \mathfrak{u}(1)$	$\mathfrak{so}(3) \oplus \mathfrak{so}(2, 1)$	$\mathfrak{so}(2, 1) \oplus 3\mathfrak{u}(1)$
solutions	$s_{55}^0 1$	$s_{555}^0 4$	$s_{555}^0 2, 3$	$m_{466}^0 4$	$s_{555}^0 1$	$m_{46}^0 1$
compactness	✓	✓	✓	✓	×	×

Table 3.6: Algebras identified in Minkowski solutions, leading to compact (✓) or non-compact (×) group manifolds.

Several other Minkowski solutions were found with algebras that may or may not provide compact group manifolds: we refer in the following to related propositions in [107] that could help in settling this matter, in case there is a particular interest in a specific solution. This is the situation encountered for solutions  $m_{46}^0 2$  and  $m_{466}^0 3, 5$  with algebra  $\mathfrak{g}_{5,17}^{0,0,r} \oplus \mathfrak{u}(1)$  (Prop. 7.2.13),  $m_{466}^0 1, 2$  with  $\mathfrak{g}_{5,13}^{-1,0,r} \oplus \mathfrak{u}(1)$  (Prop. 7.2.6), and  $m_{466}^0 6$  with  $\mathfrak{g}_{5,7}^{p,-p,-1} \oplus \mathfrak{u}(1)$  (Prop. 7.2.1).

• Anti-de Sitter solutions

algebra	$\mathfrak{so}(3) \oplus \mathfrak{3u}(1)$	$\mathfrak{so}(3) \oplus \mathfrak{g}_{3.5}^0$	$\mathfrak{g}_{3.5}^0 \oplus \mathfrak{g}_{3.5}^0$	$\mathfrak{g}_{6.10}^{0,0}$
solutions	$m_{46}^-$ 1, 2	$s_{55}^-$ 1	$s_{55}^-$ 2, 3, 4	$m_{46}^-$ 4, 5
compactness	✓	✓	✓	✓

Table 3.7: Algebras identified in anti-de Sitter solutions, leading to compact group manifolds.

Finally, solution  $m_{46}^-$  3 was found on the algebra  $\mathfrak{g}_{6.34}^{0,0,0}$ , and we do not know if the latter can provide a compact manifold.

## 3.2 Stability

In this section, we present the key elements of the 4d effective action

$$\mathcal{S} = \int d^4x \sqrt{|g_4|} \left( \frac{M_p^2}{2} \mathcal{R}_4 - \frac{1}{2} g_{ij} \partial_\mu \phi^i \partial^\mu \phi^j - V \right), \quad (3.27)$$

obtained after dimensional reduction and consistent truncation of our 10d solutions, allowing us to determine their stability. We first discuss in Section 3.2.1 the scalar fields considered and the scalar potential  $V$ , then in Section 3.2.2 the field space metric  $g_{ij}$  and the problem of field redundancy. We present in Section 3.2.3 the numerical tool that we have developed for these computations, and we finally discuss in Section 3.2.4 the stability of our solutions, inferred from these considerations, and compare it to various conjectures.

### 3.2.1 Scalar fields and potential

As explained above, we consider a restricted set of 4d scalar fields  $(\rho, \tau, \sigma_I)$ , where  $I = 1, \dots, N$  runs over the sets of (parallel) sources. The 6d volume  $\rho$  and 4d dilaton  $\tau$  were introduced together with their potential in [38]. The  $\sigma_I$ , related to internal volumes wrapped by the sources, can be defined independently: they were introduced and motivated in [108, 109]. The generic scalar potential depending on  $\sigma_I$  was obtained in [77] for  $N = 1$ , and in [70] for  $N > 1$ , with a single source dimensionality  $p$ ; here we will extend it to multiple dimensionalities.

All these scalar fields are obtained as specific fluctuations around the background 6d metric and dilaton. To obtain the 4d scalar potential, one should introduce these fluctuations in the 10d action. A first result is the following potential  $V$  depending on  $\rho, \tau$

$$\frac{2}{M_p^2} V = -\tau^{-2} \left( \rho^{-1} \mathcal{R}_6 - \frac{1}{2} \rho^{-3} |H|^2 \right) - g_s \tau^{-3} \sum_{p,I} \rho^{\frac{p-6}{2}} \frac{T_{10}^{(p)I}}{p+1} + \frac{1}{2} g_s^2 \tau^{-4} \sum_{q=0}^6 \rho^{3-q} |F_q|^2, \quad (3.28)$$

while  $\mathcal{R}_6, H, F_q, T_{10}^{(p)I}$  should still be fluctuated with respect to the  $\sigma_I$ ; we will do so in the following. Let us emphasize that in this potential, the terms in  $F_5$  or  $F_6$  are not obtained in the same way as the others, because of the contribution of corresponding 4d components; we refer the interested reader to the appendix of [78], which completes the derivation of the potential. It is shown there that eventually, these terms can be recast in the same form as the other  $F_q$ , including the fluctuation to come with respect to  $\sigma_I$ , so we treat here all fluxes together.

Each  $\sigma_I$  is defined with respect to a given set  $I$  of parallel sources. For this reason, while fluctuations with respect to  $\sigma_I$  were generically described in the aforementioned papers, the resulting potential (and kinetic terms described in Section 3.2.2) is dependent on each specific source configuration. We need here these results for each solution class of [4], because we have found solutions on a compact manifold for almost all of them (see Section 3.1.4), justifying the study of a corresponding 4d theory. In addition, the formulas of [70] need a slight generalization to the case of multiple dimensionalities, as we encounter in some solution classes. For these reasons, we present here once again the definition of these fields and corresponding fluctuations, introducing however new notations and tools allowing a more systematic treatment for any solution class. This will be used in the numerical tool `MaxSymSolSpec` (`MSSSp`) that we have developed, to provide the potential for any source configuration.

For each set  $I$  of  $p$ -sources, with certain parallel and transverse directions, one defines as follows a 4d scalar fluctuation  $\sigma_I$  on the 6d vielbeins

$$e^{a_{\parallel I} m} \rightarrow \sigma_I^{\frac{A_I}{2}} e^{a_{\parallel I} m}, \quad e^{a_{\perp I} m} \rightarrow \sigma_I^{\frac{B_I}{2}} e^{a_{\perp I} m}, \quad A_I = p - 9, \quad B_I = p - 3. \quad (3.29)$$

The exponents  $A_I$  and  $B_I$  are chosen in such a way that the determinant  $|g_6|$  is left invariant under this fluctuation. This should be done for all sets  $I$  of sources (with possibly different  $p$ ). Overall, each 6d vielbein  $e^a_m$  gets multiplied by a product of powers of  $\sigma_I$  that we denote  $\pi_a$ , as follows

$$e^a_m \rightarrow \pi_a e^a_m \text{ (no sum)}, \quad \text{where } \pi_a = \prod_I \sigma_I^{\frac{P_I(a)}{2}}, \quad P_I(a_{\parallel I}) = A_I, \quad P_I(a_{\perp I}) = B_I. \quad (3.30)$$

Introducing these  $\pi_a$  is a convenient novelty. From there, one gets the fluctuations of each quantity entering the potential (3.28) by going to the orthonormal coframe and following the vielbein dependence:

$$H_{abc} \rightarrow (\pi_a \pi_b \pi_c)^{-1} H_{abc}, \quad F_{q a_1 \dots a_q} \rightarrow (\pi_{a_1} \dots \pi_{a_q})^{-1} F_{q a_1 \dots a_q}, \quad f^a_{bc} \rightarrow \pi_a (\pi_b \pi_c)^{-1} f^a_{bc} \quad (3.31)$$

The dependence in  $\mathcal{R}_6$  is then obtained using the standard formula

$$-2 \mathcal{R}_6 = \delta^{ce} f^b_{ac} f^a_{be} + \frac{1}{2} \delta^{eb} \delta^{fc} \delta_{ga} f^g_{ef} f^a_{bc}, \quad (3.32)$$

while the square of fluxes in the potential give rise to the sum of the squares of fluctuated components. Finally, the fluctuation of the source term  $T_{10}^{(p)I}$  corresponds to that of the internal volume form  $\text{vol}_{||I}$ : we get for each set  $I$

$$T_{10}^{(p)I} \rightarrow T_{10}^{(p)I} \prod_{a=a_{||I}} \pi_a . \quad (3.33)$$

One deduces from these fluctuations and (3.28) the complete potential  $V(\rho, \tau, \sigma_I)$ , for each source configuration.

As an example, the complete potential for the solution class  $s_{55}$  was given in [65]. Let us give here the potential for the class  $m_{46}$  with only 1  $D_6$ : interestingly, it admits sources of multiple dimensionalities. The sets are  $I = 1$  with an  $O_4$  along 4 and contribution  $T_{10}^{(4)}$ ,  $I = 2$  with an  $O_6$  along 123 and  $T_{10}^{(6)1}$ ,  $I = 3$  with  $D_6$  along 156 and  $T_{10}^{(6)2}$ . The potential is then given by

$$\begin{aligned} \frac{2}{M_p^2} V(\rho, \tau, \sigma_1, \sigma_2, \sigma_3) = & -\tau^{-2} \rho^{-1} \mathcal{R}_6(\sigma_1, \sigma_2, \sigma_3) \\ & + \frac{1}{2} \tau^{-2} \rho^{-3} \sigma_1^{-3} \sigma_2^3 \left( \sigma_3^{-3} |H^{(1)3}|^2 + \sigma_3^3 |H^{(2)3}|^2 \right) \\ & - g_s \tau^{-3} \left( \rho^{-1} \sigma_1^{-\frac{5}{2}} \sigma_2^{\frac{3}{2}} \sigma_3^{\frac{3}{2}} \frac{T_{10}^{(4)}}{5} + \sigma_1^{\frac{3}{2}} \sigma_2^{-\frac{9}{2}} \sigma_3^{\frac{3}{2}} \frac{T_{10}^{(6)1}}{7} + \sigma_1^{\frac{3}{2}} \sigma_2^{\frac{3}{2}} \sigma_3^{-\frac{9}{2}} \frac{T_{10}^{(6)2}}{7} \right) \\ & + \frac{1}{2} g_s^2 \tau^{-4} \left( \rho \sigma_1^{-2} \left( |F_2^{(1)3}|^2 + \sigma_3^6 |F_2^{(2)3}|^2 \right) + \rho^{-1} \sigma_1^2 \left( \sigma_3^{-6} |F_4^{(1)3}|^2 + |F_4^{(2)3}|^2 \right) \right) , \end{aligned} \quad (3.34)$$

where we recall the flux notation  $H^{(n)I=3}$ , of components having  $n$  indices along the set  $I = 3$ . We refer to the result given by **MSSSp** for the precise expression of  $\mathcal{R}_6(\sigma_1, \sigma_2, \sigma_3)$  as a sum of powers of  $\sigma_I$  times structure constants.

Let us finally recall that in our conventions, the background (i.e. our solutions) is recovered at  $\rho = \tau = \sigma_I = 1$ . Since we have a consistent truncation, this corresponds in 4d to a critical point  $\partial_{\phi^i} V = 0$ , while at this point one also has  $\frac{2}{M_p^2} V = \frac{1}{2} \mathcal{R}_4$ . This is checked on each of our solutions.

### 3.2.2 Field space metric and redundancy

Following Appendix D of [1], the kinetic terms appearing in (3.27) are given by

$$\frac{1}{M_p^2} g_{ij} \partial_\mu \phi^i \partial^\mu \phi^j = 2\tau^{-2} (\partial\tau)^2 + \frac{3}{2} \rho^{-2} (\partial\rho)^2 - \frac{1}{4} \partial_\mu (m_{ab}) \partial^\mu ((m^{-1})^{ab}) , \quad (3.35)$$

where  $m_{ab}$  is the diagonal 6d metric in orthonormal coframe fluctuated with  $\sigma_I$ ; it has determinant 1. Using the convenient notation introduced in (3.30), we obtain

$$m_{ab} = \pi_a^2 \delta_{ab} \quad (\text{without sum}) . \quad (3.36)$$

By  $(m^{-1})^{ab}$  we denote in (3.35) the coefficients of the inverse of  $m$ . It is then straightforward to obtain the kinetic terms. In particular, the expression for  $m_{ab}$  leads to many cross terms  $\partial_\mu \sigma_I \partial^\mu \sigma_J$ , i.e. non-diagonal elements of the field space metric  $g_{ij}$ .

An issue is however that the fields  $\sigma_I$  are sometimes redundant. This can be understood as follows: each  $\sigma_I$  is a metric fluctuation, in correspondence with an internal volume wrapped by a source set. The independence of the  $\sigma_I$  can be seen as the independence of these volumes: for instance if one has  $O_5$  along 12, 34 and  $D_7$  along 1234, the volumes are not independent and there would be a redundancy in the  $\sigma_I$ . This depends entirely on the source configuration, and for each of them, we need to specify a set of independent  $\sigma_I$ .

The problem of the redundancy is equivalently seen through the field space metric  $g_{ij}$ : it has vanishing determinant if there are redundant fields. Indeed, redundant fields can be removed by a field redefinition. But removing some  $\sigma_J$  would lead to vanishing field metric coefficients along the  $\partial^\mu \sigma_J$ , hence a vanishing determinant. A set of independent fields must then be identified before computing the metric. A concrete way to determine redundant fields is to find a field redefinition that removes one or more  $\sigma_J$  fields completely from the  $\pi_a$  defined in (3.30) (or equivalently sets these fields to 1). Since the  $\pi_a$  are the building blocks for the potential and the field space metric (see (3.36)), fields  $\sigma_J$  removed from the  $\pi_a$  will not appear anywhere and were certainly redundant.

A field redefinition to remove fields  $\{\sigma_X\}$  from  $\pi_a$  and keep  $\{\sigma_M\}$  can be designed as follows; it is not the most general, but it will be enough for our purposes

$$\sigma_M \rightarrow \sigma_M \prod_X \sigma_X^{s_{XM}}, \quad \sigma_X \rightarrow \sigma_X . \quad (3.37)$$

One verifies that  $\sigma_X$  are removed from all  $\pi_a$  if and only if one finds exponents  $s_{XM}$  satisfying

$$\forall a, X, \quad P_X(a) + \sum_M s_{XM} P_M(a) = 0 . \quad (3.38)$$

Let us consider a first particular solution:  $s_{XM} = 1$ , and there is a single field to remove, the last one, i.e.  $X = N$ . The field redefinition (3.37) becomes

$$\sigma_{I \neq N} \rightarrow \sigma_{I \neq N} \sigma_N, \quad \sigma_N \rightarrow \sigma_N . \quad (3.39)$$

This field redefinition was used already successfully in  $s_{6666}$  [70, 108] and  $s_{55}$  [1]. One verifies indeed that the condition (3.38) holds, with  $\sum_I P_I(a) = 2(A + B)$  for  $p = 6$  and  $\sum_I P_I(a) = 2B + A$  for  $p = 5$ , and both vanish. We verify that the same holds for  $m_{5577}$  and  $m_{5577}^*$ , allowing there again to remove the last field, curing the redundancy.

Other cases require different solutions to (3.38) to remove differently redundant fields, for instance when  $\exists a$  s.t.  $\sum_I P_I(a) \neq 0$ . This happens for  $m_{46}$  with  $O_4$  along 4,  $O_6$  along 123, and  $D_6$  along 156, 256, 356; these five sets defining  $\sigma_{1, \dots, 5}$  respectively. The field space metric determinant vanishes for five  $\sigma_I$ , but not for four. We find the appropriate field redefinition (3.37) to take the form

$$\sigma_1 \rightarrow \sigma_1 \sigma_5^3, \quad \sigma_2 \rightarrow \sigma_2 \sigma_5^2, \quad \sigma_{3,4} \rightarrow \sigma_{3,4} \sigma_5, \quad \sigma_5 \rightarrow \sigma_5, \quad (3.40)$$

removing  $\sigma_5$  from the  $\pi_a$ .

Another case is that of  $m_{55}$  with 7 sets in the following order:  $O_5$  along 12, 34,  $D_5$  along 56,  $D_7$  along 2456, 2356, 1456, 1356. Solutions have been found with all or some of these sets turned on. We consider the corresponding 7 fields  $\sigma_I$ . Solving (3.38), we find the following general field redefinition

$$\sigma_{1,2} \rightarrow \sigma_{1,2} \sigma_3 \sigma_5 \sigma_7, \quad \sigma_4 \rightarrow \sigma_4 \sigma_7, \quad \sigma_6 \rightarrow \sigma_6 \sigma_5, \quad \sigma_{3,5,7} \rightarrow \sigma_{3,5,7}. \quad (3.41)$$

### Chapter 3. Exploring the Landscape

---

It allows to remove  $\sigma_{3,5,7}$  from the  $\pi_a$ , in the case where all sources are present. In the case where  $T_{10}^3 = 0$ , one can still use (3.41), setting  $\sigma_3 = 1$  and removing  $\sigma_{5,7}$ . Similarly, for  $T_{10}^3 = T_{10}^5 = 0$ , one can use (3.41) setting  $\sigma_{3,5} = 1$  and removing  $\sigma_7$ . All these cases amount in the end to setting  $\sigma_{3,5,7}$  to 1.<sup>1</sup>

Once we know which fields  $\sigma_I$  are redundant and should be removed (or equivalently set to 1), we are left with a set of independent fields, and correspondingly a non-degenerate field space metric. Let us give this data in one example, with the source sets considered and ordered, the corresponding independent scalar fields, and the field space metric expressed in that field basis:

**m<sub>46</sub>** (1  $D_6$ ):  $O_4$  (4),  $O_6$  (123),  $D_6$  (156), or **m<sub>466</sub>**:  $O_4$  (4),  $O_6$  (123, 156).  
Fields:  $(\rho, \tau, \sigma_1, \sigma_2, \sigma_3)$

$$g_{ij} = M_p^2 \begin{pmatrix} \frac{3}{2\rho^2} & 0 & 0 & 0 & 0 \\ 0 & \frac{2}{\tau^2} & 0 & 0 & 0 \\ 0 & 0 & \frac{15}{2\sigma_1^2} & -\frac{9}{2\sigma_1\sigma_2} & -\frac{9}{2\sigma_1\sigma_3} \\ 0 & 0 & -\frac{9}{2\sigma_1\sigma_2} & \frac{27}{2\sigma_2^2} & -\frac{9}{2\sigma_2\sigma_3} \\ 0 & 0 & -\frac{9}{2\sigma_1\sigma_3} & -\frac{9}{2\sigma_2\sigma_3} & \frac{27}{2\sigma_3^2} \end{pmatrix}. \quad (3.42)$$

We give here for completeness the corresponding data for each case encountered in our solutions.

**s<sub>55</sub>**:  $O_5$  (12, 34),  $D_5$  (56), or **s<sub>555</sub>**:  $O_5$  (12,34,56). Fields:  $(\rho, \tau, \sigma_1, \sigma_2)$

$$g_{ij} = M_p^2 \begin{pmatrix} \frac{3}{2\rho^2} & 0 & 0 & 0 \\ 0 & \frac{2}{\tau^2} & 0 & 0 \\ 0 & 0 & \frac{12}{\sigma_1^2} & -\frac{6}{\sigma_1\sigma_2} \\ 0 & 0 & -\frac{6}{\sigma_1\sigma_2} & \frac{12}{\sigma_2^2} \end{pmatrix}. \quad (3.43)$$

**s<sub>66</sub>**:  $O_6$  (123, 145),  $D_6$  (256, 346), or **s<sub>6666</sub>**:  $O_6$  (123, 145, 256, 346). Fields:

---

<sup>1</sup>In the case where  $T_{10}^3 = T_{10}^5 = T_{10}^6 = 0$ , one can use (3.41), setting  $\sigma_{3,5,6} = 1$  and removing  $\sigma_7$ : this redefinition matches the more standard one (3.39). We however do not encounter this case in our solutions.

$(\rho, \tau, \sigma_1, \sigma_2, \sigma_3)$

$$g_{ij} = M_p^2 \begin{pmatrix} \frac{3}{2\rho^2} & 0 & 0 & 0 & 0 \\ 0 & \frac{2}{\tau^2} & 0 & 0 & 0 \\ 0 & 0 & \frac{27}{2\sigma_1^2} & -\frac{9}{2\sigma_1\sigma_2} & -\frac{9}{2\sigma_1\sigma_3} \\ 0 & 0 & -\frac{9}{2\sigma_1\sigma_2} & \frac{27}{2\sigma_2^2} & -\frac{9}{2\sigma_2\sigma_3} \\ 0 & 0 & -\frac{9}{2\sigma_1\sigma_3} & -\frac{9}{2\sigma_2\sigma_3} & \frac{27}{2\sigma_3^2} \end{pmatrix}. \quad (3.44)$$

$\mathbf{m}_{46}$  (3  $D_6$ ):  $O_4$  (4),  $O_6$  (123),  $D_6$  (156, 256, 356). Fields:  $(\rho, \tau, \sigma_1, \sigma_2, \sigma_3, \sigma_4)$

$$g_{ij} = M_p^2 \begin{pmatrix} \frac{3}{2\rho^2} & 0 & 0 & 0 & 0 & 0 \\ 0 & \frac{2}{\tau^2} & 0 & 0 & 0 & 0 \\ 0 & 0 & \frac{15}{2\sigma_1^2} & -\frac{9}{2\sigma_1\sigma_2} & -\frac{9}{2\sigma_1\sigma_3} & -\frac{9}{2\sigma_1\sigma_4} \\ 0 & 0 & -\frac{9}{2\sigma_1\sigma_2} & \frac{27}{2\sigma_2^2} & -\frac{9}{2\sigma_2\sigma_3} & -\frac{9}{2\sigma_2\sigma_4} \\ 0 & 0 & -\frac{9}{2\sigma_1\sigma_3} & -\frac{9}{2\sigma_2\sigma_3} & \frac{27}{2\sigma_3^2} & \frac{9}{2\sigma_3\sigma_4} \\ 0 & 0 & -\frac{9}{2\sigma_1\sigma_4} & -\frac{9}{2\sigma_2\sigma_4} & \frac{9}{2\sigma_3\sigma_4} & \frac{27}{2\sigma_4^2} \end{pmatrix}. \quad (3.45)$$

$\mathbf{m}_{55}$ :  $O_5$  (12, 34),  $D_5$  (56),  $D_7$  (2456, 2356, 1456, 1356), or  $O_5$  (12, 34),  $D_7$  (2456, 2356, 1456, 1356), or  $O_5$  (12, 34),  $D_7$  (2456, 1456, 1356). Fields:  $(\rho, \tau, \sigma_1, \sigma_2, \sigma_4, \sigma_6)$

$$g_{ij} = M_p^2 \begin{pmatrix} \frac{3}{2\rho^2} & 0 & 0 & 0 & 0 & 0 \\ 0 & \frac{2}{\tau^2} & 0 & 0 & 0 & 0 \\ 0 & 0 & \frac{12}{\sigma_1^2} & -\frac{6}{\sigma_1\sigma_2} & -\frac{3}{\sigma_1\sigma_4} & -\frac{3}{\sigma_1\sigma_6} \\ 0 & 0 & -\frac{6}{\sigma_1\sigma_2} & \frac{12}{\sigma_2^2} & -\frac{3}{\sigma_2\sigma_4} & -\frac{3}{\sigma_2\sigma_6} \\ 0 & 0 & -\frac{3}{\sigma_1\sigma_4} & -\frac{3}{\sigma_2\sigma_4} & \frac{12}{\sigma_4^2} & \frac{3}{\sigma_4\sigma_6} \\ 0 & 0 & -\frac{3}{\sigma_1\sigma_6} & -\frac{3}{\sigma_2\sigma_6} & \frac{3}{\sigma_4\sigma_6} & \frac{12}{\sigma_6^2} \end{pmatrix}. \quad (3.46)$$

$\mathbf{m}_{5577}$ :  $O_5$  (12, 34),  $O_7$  (1356, 2456), or  $\mathbf{m}_{5577}^*$ :  $O_5$  (12, 34),  $O_7$  (1456, 2356).



Fields:  $(\rho, \tau, \sigma_1, \sigma_2, \sigma_3)$

$$g_{ij} = M_p^2 \begin{pmatrix} \frac{3}{2\rho^2} & 0 & 0 & 0 & 0 \\ 0 & \frac{2}{\tau^2} & 0 & 0 & 0 \\ 0 & 0 & \frac{12}{\sigma_1^2} & -\frac{6}{\sigma_1\sigma_2} & -\frac{3}{\sigma_1\sigma_3} \\ 0 & 0 & -\frac{6}{\sigma_1\sigma_2} & \frac{12}{\sigma_2^2} & -\frac{3}{\sigma_2\sigma_3} \\ 0 & 0 & -\frac{3}{\sigma_1\sigma_3} & -\frac{3}{\sigma_2\sigma_3} & \frac{12}{\sigma_3^2} \end{pmatrix}. \quad (3.47)$$

### 3.2.3 Numerical tool MaxSymSolSpec (MSSSp)

The computation of the scalar potential and the field space metric, as described in Section 3.2.1 and 3.2.2, has been automatized in the numerical tool `MaxSymSolSpec` (MSSSp) that we have developed. The code first takes as input the list of source sets. From this data, the fields  $(\rho, \tau, \sigma_I)$  can be defined. A first task is to determine a set of independent fields, and remove the redundant ones. The user can specify a complete list of redundant fields, based for instance on Section 3.2.2. Otherwise, the code determines such a list by itself. To that end, the field space metric is computed and its rank is checked, row after row, allowing to identify redundant fields. Once a set of independent fields is identified, a proper field space metric is computed, as well as the scalar potential  $V$ . The latter is obtained by considering the fluctuations  $\pi_a$  as described in Section 3.2.1.

With a set of independent fields, the corresponding field space metric and the scalar potential, the code can compute the mass spectrum, following definitions of Section 3.2.4. This is done for a 10d supergravity solution provided as an input. The code verifies that it is a critical point of the potential. It then computes the parameter  $\eta_V$ , the masses<sup>2</sup> and their associated field space eigenvectors. Note that the mass matrix  $M$  transforms covariantly under (field space) diffeomorphisms, i.e. field redefinitions. So its eigenvalues, namely the mass spectrum, and in particular the value of  $\eta_V$ , are unchanged when choosing a different (diffeomorphic) set of independent fields.

### 3.2.4 Results: stability of the solutions and (swampland) conjectures

Having determined the scalar potential and the field space metric of the 4d effective theory (3.27), for a set of independent scalar fields  $(\rho, \tau, \sigma_I)$ , we can compute the corresponding mass spectrum for each solution of [4]. It is given by the eigenvalues (masses<sup>2</sup>) of the mass matrix, with coefficients  $M^i_j = g^{ik} \nabla_{\phi^k} \partial_{\phi^j} V$ , at the critical point  $\rho = \tau = \sigma_I = 1$ . The connection term due to  $\nabla$  vanishes at an extremum, since it is proportional to a first derivative of the potential. Therefore, one only needs to compute the eigenvalues of  $g^{-1}$  times the Hessian of the potential  $V$ , at this point. All these computations are performed using MSSSp.

From the mass spectrum, one reads the stability of the solution (at least due to this set of scalar fields). For de Sitter and anti-de Sitter solutions where  $V \neq 0$ , this is better

captured by the parameter  $\eta_V$  that we recall here

$$\eta_V = M_p^2 \frac{\min \nabla \partial V}{V}, \quad (3.48)$$

where the numerator stands for the minimal eigenvalue among the masses<sup>2</sup>. The  $\eta_V$  is computed at the critical point. Note that we use the same definition for de Sitter and anti-de Sitter extrema, although the sign of  $V$  changes.

Let us finally recall from [1] that the minimal eigenvalue of a mass matrix can only get lowered if one adds more fields. Therefore, if an instability is detected within our set of fields, it will not be cured with more fields, and we can conclude on a unstable solution. We now study the stability of each solution of [4] according to the sign of the cosmological constant.

• De Sitter

The values of  $\eta_V$  for each de Sitter solution of [4] are given in Table 3.8 and 3.9.

class	$s_{66}^+$	$s_{6666}^+$				$m_{46}^+$			
solution	1	1	2	3	4	1	2	3	4
$-\eta_V$	3.6170	18.445	2.6435	2.3772	3.6231	3.6764	3.7145	2.2769	2.8266

class	$m_{46}^+$					
solution	5	6	7	8	9	10
$-\eta_V$	0.36462	3.0124	2.0672	2.3554	2.6418	1.2539

Table 3.8: Values of  $-\eta_V$  obtained with the set of independent fields considered for each de Sitter solution in type IIA.

class	$s_{55}^+$	$m_{55}^+$				$m_{5577}^+$			
solution	28	1	2	3	4	1	2	3	4
$-\eta_V$	3.2374	2.5435	2.6059	2.7126	3.3574	4.7535	3.5034	3.2722	3.1779

class	$m_{5577}^+$									$m_{5577}^{*+}$
solution	5	6	7	8	9	10	11	12		1
$-\eta_V$	4.7957	4.9129	3.4210	3.5611	2.9333	2.9003	3.4806	2.8966		5.0483

Table 3.9: Values of  $-\eta_V$  obtained with the set of independent fields considered for each de Sitter solution in type IIB.

A first observation is that  $\eta_V < 0$  for all de Sitter solutions, in agreement with Conjecture 2 of [70]. This means that the solutions are unstable, and that a tachyon can be found among the fields  $(\rho, \tau, \sigma_I)$  considered, in agreement with the proposal made in [108]. While always successfully tested (see however [65] for a counter-example on a non-compact manifold), the check of this proposal is here extensive, since many different solution classes have been considered, including some (e.g.  $m_{46}^+$ ) where de Sitter solutions

are found for the first time. We finally point out that for each solution, there is one and only one tachyonic mass in the spectrum.

A second observation is that most values are of order -1, in agreement with the refined de Sitter conjecture [62, 63]. This is not surprising from the perspective of [65], where it is argued that less generic stability behaviours need to be searched in specific corners of the parameter space, and here, we have not performed such dedicated searches. Our aim was rather to get (generic) solutions in many different classes.

Two exceptions are nevertheless worth being mentioned. The first one is  $m_{46}^+5$ , which admits a comparatively low value  $|\eta_V| = 0.36462$ . As indicated in Table 3.5, the group manifold is however non-compact. The second one is  $s_{6666}^+1$ , which admits a comparatively high value  $|\eta_V| = 18.445$ . There, the group manifold is compact, see Table 3.4. However, such a high instability is phenomenologically uninteresting.

Last but not least, let us add a word on the solution  $s_{55}^+19$  found in [65]. Back then, its algebra was not identified. Thanks to the work of Section 3.1, we now know this algebra, and as indicated in Table 3.4, the group manifold is compact. This is interesting, because this solution admits the lowest  $|\eta_V|$  value known for a solution on a compact manifold:  $\eta_V = -0.12141$ . This emphasizes the need for dedicated searches when it comes to stability of de Sitter solutions.

- **Minkowski, and a new conjecture**

For Minkowski solutions, we do not compute  $\eta_V$  but look directly at the mass spectrum, provided in Appendix C. Interestingly, we observe the *systematic presence of a massless mode*, in all solutions, the other masses being non-tachyonic. In solutions  $m_{46}^02$  and  $m_{466}^01 - 6$ , there are even two massless modes. The systematic presence of such a 4d massless scalar field in classical, or at least 10d supergravity, Minkowski solutions is commonly believed to be true. Examples are ubiquitous in the literature, a first one being Calabi-Yau compactifications (with  $h^{1,1} \geq 1$ ). There, the presence of flat directions is related to the more general no-scale property of the potential [110, 111], which can in some models remove the dependence on some fields in the scalar potential. Less common examples include M-theory compactifications [112], compactifications to 6d [113], or maximal supergravity in 4d [114], all having Minkowski solutions with massless scalar fields, some being flat directions. The systematic presence of a massless scalar field was even proven in compactifications to 4d  $\mathcal{N} = 1$  supergravity, coming from supersymmetric Minkowski solutions of 10d type IIA supergravity with certain  $O_6/D_6$  [115, 116] (see also [40]). This idea goes along with that of a systematic tachyon in de Sitter solutions.<sup>2</sup> Following this line of thoughts and our observation, we propose here the following conjecture:

---

<sup>2</sup>Relations between the tachyon in a de Sitter solution and the sgoldstino in a (no-scale) Minkowski solution, the latter being the limit of the former, have been discussed in [108, 109, 117–119]. At first sight, we do not know whether our conjecture matches such a sgoldstino interpretation, but it would be interesting to investigate this further.

**Massless Minkowski Conjecture:** (3.49)

*10d supergravity solutions compactified to 4d Minkowski always admit a 4d massless scalar, among the fields  $(\rho, \tau, \sigma_I)$ .*

The fact the massless mode should be among  $(\rho, \tau, \sigma_I)$ , and the claim not depending on supersymmetry (of the solution or of the 4d theory), are important additions with respect to previous related statements. The conjectured massless scalar field is also not necessarily a flat direction. These points make the conjecture more interesting, connecting directly to the proposal of [108] stating a systematic de Sitter tachyon among the same fields. In addition, the complete set  $(\rho, \tau, \sigma_I)$  is necessary: the massless mode is indeed not among  $(\rho, \tau)$  alone in  $s_{55}^0$  1,  $m_{46}^0$  1,2,  $m_{466}^0$  1-6, as can be tested with MSSSp; it is however in  $s_{555}^0$  1-4, probably because of the more limited supergravity contributions. Note that in heterotic string at order  $\alpha'^0$ , the field  $\tau$  is massless in a Minkowski solution so the conjecture is valid, while fields  $\sigma_I$  cannot be defined. Let us finally mention the recent apparent counter-example [120], where Minkowski solutions are found with all moduli stabilized. Those are however obtained on mirrors of rigid Calabi-Yau manifolds, which are better described as Landau-Ginzburg models, having  $h^{1,1} = 0$ . As indicated there, since these models have no Kähler moduli, they do not have a proper 10d target space geometric description, and circumvent our conjecture by being not describable in 10d supergravity.<sup>3</sup>

An option would be to restrict the conjecture to solutions with 4d effective theories preserving at most  $\mathcal{N} = 1$  supersymmetry. Such a weaker statement could then be related to the Conjecture 4 of [4], requiring at most  $\mathcal{N} = 1$  in the 4d effective theory for de Sitter solutions: the massless mode of Minkowski may then, once again, be related to the tachyon of de Sitter, both observed to be among  $(\rho, \tau, \sigma_I)$ . Nevertheless, preserving more supersymmetry typically corresponds to having less supergravity ingredients, leading to a simpler scalar potential, that would be less likely to generate a mass. So we stick to the above version of the conjecture. In addition, there exist examples of Minkowski solutions leading to a 4d theory with  $\mathcal{N} \geq 2$  and having a massless scalar, starting with solution  $s_{55}^0$  1.

The conjecture applies in particular to classical Minkowski string backgrounds (see however below about corrections), and can as such get a swampland interpretation. Of course, it agrees with the anti-de Sitter distance conjecture [60], which provides in the asymptotics of field space a Minkowski solution with a massless mode coming from a tower. The conjecture (3.49) is however stronger as it is not strictly about the asymptotics, and the massless mode is rather to be found among the light modes of the 4d theory (see a related discussion in Section 3.3.1). A swampland-type corollary statement would then be the following:

<sup>3</sup>Similarly, without Kähler moduli, one cannot define internal volumes related to our  $\rho$  and  $\sigma_I$ , and maybe not even the 4d dilaton  $\tau$  which needs  $\rho$ . From this perspective, that example may even be viewed as being in agreement with the conjecture.

**Massless Minkowski Conjecture (swampland corollary):** (3.50)

*In a quantum gravity 4d effective theory with a scalar potential  $V(\phi^i)$ , if a critical point ( $\partial_{\phi^j} V = 0$ ) can be found in a region of field space corresponding to a classical and perturbative quantum gravity regime, and if this critical point is Minkowski ( $V = 0$ ), then the mass matrix admits a vanishing eigenvalue.*

In addition, the conjecture (3.49) specifies among which fields the massless mode can be found. Note that a vanishing mass matrix eigenvalue is equivalent to a degenerate Hessian of  $V$ . The above leads us to propose the following strong version of the conjecture:

**Strong version:** (3.51)

*If the above Minkowski critical point is realized, then there is no 4d tachyon, meaning*

$$0 = \min \nabla \partial V = \frac{V}{M_p^2} = \frac{|\nabla V|}{M_p} .$$

*In other words, the inequalities of the refined de Sitter conjectures of [62–64] are saturated.*

The strong version adds the information that the massless mode is the minimal eigenvalue of the mass matrix, meaning that there is no tachyon. This is indeed what we observe in our solutions.

There are two reasons to be careful about these swampland versions (3.50) and (3.51). First, a quantum gravity effective theory would a priori contain many corrections going beyond the classical and perturbative regime. Even though they would be small in such a regime, there is no reason here (e.g. without supersymmetry) for them to vanish. Any such non-vanishing correction could alter the claim of a vanishing mass. One should then be careful with the interpretation of the “classical and perturbative regime”: whether this means a truncation of corrections (10d supergravity interpretation) or whether these are small, could change the statement. Second, we know that any additional scalar field with respect to our set  $(\rho, \tau, \sigma_I)$  can a priori lower the value of  $\min \nabla \partial V$  (see below (4.19)). From this perspective, there is no reason for having no tachyon. In the literature, tachyons are however not observed in Minkowski compactifications (we do not consider here open string moduli, and e.g.  $D_p$ -brane instabilities). So the strong version remains plausible. This conjecture deserves in any case more investigation, and we hope to come back to it in future work.

Contrary to other swampland conjectures related to stability, the conjecture (3.49) does not depend on whether the solution is supersymmetric or not. Let us add here a word on this last question. The solutions found in [4] were obtained by solving the equations

of motion and Bianchi identities. Conditions for supersymmetry, as e.g. phrased in the language of generalized complex geometry with  $SU(3) \times SU(3)$  structures [83, 93], were not considered. Therefore, we see no reason for our solutions to be supersymmetric. For Minkowski solutions, a quick test goes as follows. Supersymmetric Minkowski solutions with  $O_3$  typically need to have their  $H$ - and  $F_3$ -flux related through the ISD condition:  $*_6 H = \epsilon g_s F_3$  [43], where for simplicity we do not specify the sign  $\epsilon$  and we fix  $e^\phi = g_s$ . The class of Minkowski solutions with  $O_p/D_p$  found in [82] generalises this relation to  $*_\perp H^{(0)} = \epsilon g_s F_{6-p}^{(0)}$ . The latter can be read in the smeared limit from the supersymmetry conditions as a particular solution, using the calibration condition  $\iota^*[8 \text{Im}\Phi_2] = \text{vol}_\perp$ . Then, a hint for supersymmetry in a Minkowski solution is that appropriate components of  $H$  and  $g_s F_{6-p}$  take the same value. It is not the case in any of our solutions, except when both vanish. We conclude again that our solutions are unlikely to be supersymmetric.

• **Anti-de Sitter**

The values of  $\eta_V$  for each anti-de Sitter solution of [4] are given in Table 3.10. We note already that all values satisfy  $\eta_V \gtrsim -1$ , in agreement with the conjecture of [52] (see also Footnote 4).

class solution	$s_{55}^-$				$m_{46}^-$				
	1	2	3	4	1	2	3	4	5
$\eta_V$	0.7785	-4	-3.8495	-2.4901	1.2531	1.5483	1.5537	1.3004	1.2548

Table 3.10: Values of  $\eta_V$  obtained with the set of fields considered for each anti-de Sitter solution.

The stability of anti-de Sitter solutions is more delicate. Let us first recall useful formulas valid for a 4d anti-de Sitter spacetime, extremum of a potential

$$\frac{\mathcal{R}_4}{4} = -\frac{3}{l^2} = \Lambda = \frac{V}{M_p^2}, \quad (3.52)$$

where  $l$  is the so-called anti-de Sitter radius, appearing in the standard metric as follows  $ds^2 = \frac{l^2}{z^2}(dz^2 + dx_\mu dx^\mu)$ . Perturbative stability then requires for any scalar of mass  $m$  to verify the Breitenlohner-Freedman (BF) bound, expressed in 4d as

$$m^2 > -\frac{9}{4l^2} \quad \Rightarrow \quad \eta_V < \frac{3}{4}, \quad (3.53)$$

from which we deduced an upper bound on  $\eta_V$  in an anti-de Sitter solution. From this criterion, we see that all solutions with positive  $\eta_V$  in Table 3.10 are perturbatively unstable.

Of interest are then the three anti-de Sitter solutions found with a negative  $\eta_V$  (on compact group manifolds): not only those are perturbatively stable (at least within these fields), but their mass spectrum only has positive masses<sup>2</sup>. This perturbative stability may challenge to some extent the swampland conjecture on non-supersymmetric anti-de Sitter solutions [68], in case these solutions are non-supersymmetric. The latter is not straightforward to determine, and the quick test proposed for Minkowski solutions at the

end of Section 3.2.4 would not work for anti-de Sitter solutions, because of an extra term in the supersymmetry conditions, depending on the cosmological constant [93]. However, as argued for Minkowski solutions, we still believe that our anti-de Sitter solutions are unlikely to be supersymmetric, making the above perturbative stability interesting.

Finally, we notice also the surprising values taken by  $\eta_V$  in these perturbatively stable solutions. Of particular interest is  $s_{55}^-2$  which gets  $\eta_V = -4.0000$  and  $s_{55}^-4$  with  $\eta_V \approx -2.5$ . The reason for such specific values might come from the particular field content of these solutions. Such choices for a solution ansatz may be of interest, and deserve more investigation. We will come back to these peculiar values in Section 3.3.1.

## 3.3 Scale separation

In this section we discuss the possibility of having scale separation in new anti-de Sitter solutions, found in previously unexplored solution classes  $s_{55}^-$  and  $m_{46}^-$  [4]. We also comment on a corresponding mass gap in Minkowski solutions. We first provide a general discussion and few observations in Section 3.3.1. We then prove in Section 3.3.2 no-go theorems for anti-de Sitter solutions in  $s_{55}^-$  and  $m_{46}^-$  on nilmanifolds (including the torus) or manifolds with a Ricci flat metric, both argued in the Introduction to be relevant for scale separation.

### 3.3.1 General comments on mass gap and scale separation

As recalled in the Introduction, scale separation is a gap between the first non-zero mass of a tower of states (here taken as the Kaluza–Klein tower) and a 4d effective theory typical energy scale; such a gap then allows for an appropriate cut-off scale that truncates the tower. For anti-de Sitter, the 4d scale considered is given by the cosmological constant, while for Minkowski, it is set by the mass of light modes. To determine whether there is a scale separation with the first massive Kaluza–Klein state, one should access the latter scale. Beyond the torus, e.g. on group manifolds, this is not an easy task: it typically requires to determine the eigenvalues of the Laplacian operator, as done e.g. in [121, 122] for nilmanifolds. In particular, the first non-zero eigenvalue, of interest here, is not necessarily related to  $\mathcal{R}_6$ , the internal scalar curvature which sets another scale.

Beyond the Laplacian eigenvalues, another contribution to the mass of 4d modes is (the second derivative of) the scalar potential. In this analysis, we only access the latter, and deduce from this potential our mass spectrum, displayed in Appendix C. In addition, we only consider scalar fields with a dependence on 4d coordinates, i.e. our truncation could be viewed as limited to the zero-modes of Kaluza–Klein towers. Their vanishing masses then get corrected by the scalar potential contribution: such fields are typically thought of as light modes. This interpretation is at least valid on a Ricci flat 6d manifold; a more careful analysis might be necessary here on group manifolds. Still, from this point of view, the mass spectrum we have at hand should not allow us to identify any scale separation. In our perturbatively stable anti-de Sitter solutions,  $s_{55}^-2-4$ , this seems consistent with the fact we do not observe important hierarchies between the masses<sup>2</sup> and  $\mathcal{R}_4$ . In particular,  $|\eta_V|$  is of order 1 (see Table 3.10).<sup>4</sup>

<sup>4</sup>This agrees with the anti-de Sitter conjecture of [52] which compares the mass of light modes to the cosmological constant, analogously to the criterion on  $\eta_V$  of the refined de Sitter conjecture [63]. The former differs from considering the mass scale of a tower, and the discussion on scale separation of [60].



Despite the fact that we may not access the right scales to discuss scale separation, we will provide in the following two hints, that would conclude on the absence of scale separation in the new anti-de Sitter solutions found in the classes  $s_{55}^-$  and  $m_{46}^-$ . A first hint is about integer values of conformal dimensions that we discuss below, a second one is given by no-go theorems for anti-de Sitter solutions discussed in Section 3.3.2. Prior to this, we will also say a word on Minkowski solutions.

As mentioned in the Introduction, so-called DGKT anti-de Sitter solutions, that we interpret as being part of  $s_{6666}^-$ , exhibit scale separation. Through the standard holographic correspondence, the light mode spectrum of these solutions with masses  $m^2$  corresponds to dual CFT operators with conformal dimensions  $\Delta$ , via the relation

$$\Delta(\Delta - 3) = m^2 l^2 \Leftrightarrow \Delta_{\pm} = \frac{3}{2} \pm \frac{1}{2} \sqrt{9 + 4m^2 l^2}, \quad (3.54)$$

where  $l$  is the anti-de Sitter radius defined in (3.52). As first discussed in [123, 124] and computed more generally in [125], supersymmetric DGKT solutions satisfy the surprising property that the  $\Delta$  take integer values. As pointed out in [126], it is also the case of some non-supersymmetric solutions, but not of all of them.

One may wonder whether this specificity of integer conformal dimensions is related to having scale separation, at least for some solutions of this class. If this would hold, one could simply test the light mode spectrum of other solutions: getting integers would at least be a hint of scale separation. For  $\Delta$  being an integer, one gets, using (3.52) at an anti-de Sitter extremum, the following first possible values

$$-M_p^2 \frac{m^2}{V} = -\frac{2}{3}, 0, \frac{4}{3}, \frac{10}{3}, 6, \frac{28}{3}, \frac{40}{3}, 18, \frac{70}{3}, \frac{88}{3}, \dots \quad (3.55)$$

We can then compare these numbers to our anti-de Sitter solutions found in new classes: none of them has a spectrum giving values close to the above. One could argue that we are considering a limited set of scalar fields, and adding more fields could alter our values, but we believe the modification would not be important. Let us also emphasize that some of the solutions were noticed in Section 3.2.4 to have integer or half integer values of  $\eta_V$ . These seemingly special values however do not match any entry of the list (3.55). Following this line of thoughts, one may conclude on the absence of scale separation in these new anti-de Sitter solutions.

Before presenting another argument, let us say a word on the new Minkowski solutions found in [4]. We already mentioned in Section 3.2.4 the apparent systematic presence of a massless mode, from which we draw the Massless Minkowski Conjecture (3.49). We note in addition for some solutions, namely  $s_{555}^0 1$ ,  $m_{46}^0 1$  and  $m_{466}^0 2, 3, 5$ , the presence of a gap in the mass spectrum: see Appendix C. The most important is in  $m_{46}^0 1$ : a ratio between two consecutive masses<sup>2</sup> is 7390.9. While such a gap is important, it remains hard, as discussed above, to conclude anything with respect to the first massive mode of a tower. But these examples deserve more investigation, such as the study of the Laplacian spectrum. We note however that according to Table 3.6 and the discussion below, none of these gapped solutions were shown to be on a compact manifold, while compactness remains crucial in this discussion, e.g. with respect to the Kaluza–Klein towers.



## 3.3.2 No-go theorems for anti-de Sitter on Ricci flat or nilmanifolds

As motivated in the Introduction, scale separation in anti-de Sitter solutions on group manifolds could be limited to those on nilmanifolds, including the torus, or manifolds with a Ricci flat metric. It is the case for the solutions found in the solution classes  $s_{6666}^-$  [69, 84–86, 127] and  $m_{5577}^-$  [69, 87, 88]. In [4], two new solution classes with anti-de Sitter solutions on group manifolds were discovered,  $s_{55}^-$  and  $m_{46}^-$ , sharing the same T-duality relation as the former two classes. We prove however in this section that anti-de Sitter solutions cannot be found in these classes on nilmanifolds, or manifolds with a Ricci flat metric, giving a hint against scale separation in these classes. We also compare this situation to that of the first two classes.

We start with the solution class  $s_{55}$  with  $O_5$  along 12, 34 and  $D_5$  along 56. We first consider the 6d (trace-reversed) Einstein equation combined with the 4d Einstein equation [4, (B.23) & (B.24)]. We take the trace of the former along 56. Using the field content of that solution class [4, (2.14)], we obtain

$$2 \sum_{a,b=5,6} \delta^{ab} \mathcal{R}_{ab} = \mathcal{R}_4 + |H|^2 + g_s^2 (|F_1|^2 + |F_3|^2 + |F_5|^2) + \frac{g_s}{3} (T_{10}^3 - T_{10}) , \quad (3.56)$$

where  $T_{10}^3 \equiv T_{10}^{(5)3} \leq 0$  because it corresponds to the contributions of  $D_5$  along 56. Using further Einstein traces and the dilaton e.o.m., namely [4, (B.1) & (B.22)], to eliminate some fluxes, we get

$$2 \sum_{a,b=5,6} \delta^{ab} \mathcal{R}_{ab} - 2\mathcal{R}_6 = 2\mathcal{R}_4 + \frac{g_s}{3} T_{10}^3 . \quad (3.57)$$

One has

$$2 \sum_{a,b=5,6} \delta^{ab} \mathcal{R}_{ab} - 2\mathcal{R}_6 = -2 \sum_{a,b=1}^4 \delta^{ab} \mathcal{R}_{ab} . \quad (3.58)$$

The field content of  $s_{55}$  indicates that all structure constants have one index which is 5 or 6. Therefore, using the Ricci tensor on a group manifold

$$2 \mathcal{R}_{cd} = -f_{ac}^b f_{bd}^a - \delta^{bg} \delta_{ah} f_{gc}^h f_{bd}^a + \frac{1}{2} \delta^{ah} \delta^{bj} \delta_{ci} \delta_{dg} f_{aj}^i f_{hb}^g , \quad (3.59)$$

we obtain

$$\begin{aligned} 2 \sum_{a,b=5,6} \delta^{ab} \mathcal{R}_{ab} - 2\mathcal{R}_6 &= \sum_{a,b=1}^6 \sum_{c,d=1}^4 \left( \delta^{cd} f_{ac}^b f_{bd}^a + (f_{bd}^a)^2 - \frac{1}{2} (f_{ab}^d)^2 \right) \\ &= \sum_{a,b=1}^6 \sum_{c,d=1}^4 \delta^{cd} f_{ac}^b f_{bd}^a + \sum_{a=5,6} \sum_{b,d=1}^4 (f_{bd}^a)^2 . \end{aligned} \quad (3.60)$$

The first term in (3.60) is a partial trace of the Killing form. The Killing form identically vanishes for nilmanifolds. In addition, a manifold with Ricci flat metric, i.e.  $\mathcal{R}_{ab} = 0$ , has (3.60) vanishing. We deduce

$$\text{Nilmanifold or Ricci flat in } s_{55} : \quad 2 \sum_{a,b=5,6} \delta^{ab} \mathcal{R}_{ab} - 2\mathcal{R}_6 \geq 0 . \quad (3.61)$$

For an anti-de Sitter solution in  $s_{55}^-$ , the right-hand side of (3.57) is however negative. This leads to a *no-go theorem on anti-de Sitter solutions in the class  $s_{55}$  on nilmanifolds (including the torus) or manifolds with Ricci flat metric*. Interestingly, as can be seen in Table 3.7, solutions  $s_{55}^-$  2-4 of [4] were found on the algebra  $\mathfrak{g}_{3.5}^0 \oplus \mathfrak{g}_{3.5}^0$ , which can lead to a solvmanifold with a Ricci flat metric (see e.g. [76]). Of course, it is not the case for these solutions, which have  $\mathcal{R}_6 < 0$ .

We turn to the solution class  $m_{46}$ . It has  $O_4$  along 4,  $O_6$  along 123, and possible  $D_6$  along 156, 256, 356. The contributions of the latter are denoted  $T_{10}^{(6)2}$ ,  $T_{10}^{(6)3}$ ,  $T_{10}^{(6)4}$  and are negative. We proceed as above, taking the trace along 56, to first get

$$2 \sum_{a,b=5,6} \delta^{ab} \mathcal{R}_{ab} = \mathcal{R}_4 + |H|^2 + g_s^2 (|F_2|^2 + |F_4|^2) + 2g_s \left( \frac{1}{7} (T_{10}^{(6)2} + T_{10}^{(6)3} + T_{10}^{(6)4}) - \sum_p \frac{T_{10}^{(p)}}{p+1} \right),$$

using that  $F_0 = F_6 = 0$  in this solution class, and then

$$2 \sum_{a,b=5,6} \delta^{ab} \mathcal{R}_{ab} - 2\mathcal{R}_6 = 2\mathcal{R}_4 + \frac{2}{7} g_s \left( T_{10}^{(6)2} + T_{10}^{(6)3} + T_{10}^{(6)4} \right). \quad (3.62)$$

The field content of  $m_{46}$  indicates that structure constants always have one index which is 5 or 6. We conclude as above

$$\text{Nilmanifold or Ricci flat in } m_{46} : \quad 2 \sum_{a,b=5,6} \delta^{ab} \mathcal{R}_{ab} - 2\mathcal{R}_6 \geq 0, \quad (3.63)$$

and deduce from (3.62) a *no-go theorem on anti-de Sitter solutions in the class  $m_{46}$  on nilmanifolds (including a torus), or manifolds with a Ricci flat metric*.<sup>5</sup>

These no-go theorems are certainly consistent with our searches for solutions in  $s_{55}^-$  and  $m_{46}^-$ . Whether or not they prevent from getting scale separation is not established, but as argued in the Introduction, this is possibly a relevant criterion. Let us finally compare to the situation in the other classes. Proceeding similarly for  $m_{5577}$  with  $O_5$  along 12, 34 and  $O_7$  along 2456, 1356, we obtain the following equality

$$2 \sum_{a,b=5,6} \delta^{ab} \mathcal{R}_{ab} - 2\mathcal{R}_6 = 2\mathcal{R}_4 + \frac{g_s}{4} T_{10}^{(7)}. \quad (3.65)$$

For the same reason as above, the left-hand side has to be positive or zero on nilmanifolds (including a torus) and manifolds with a Ricci flat metric. To avoid a no-go theorem for an anti-de Sitter solution in  $m_{5577}^-$  on such a manifold, we deduce the requirement  $T_{10}^{(7)} = T_{10}^{(7)1} + T_{10}^{(7)2} > 0$ . This means that the positive contribution of  $O_7$  in those should not be dominated by that of possible  $D_7$ , negative. Getting such a requirement is interesting, but we also identify an important difference with  $s_{55}^-$  and  $m_{46}^-$ : the absence

<sup>5</sup>As a side remark, one deduces the following constraints for Minkowski solutions

$$\text{Minkowski solutions in } s_{55} \text{ on a nilmanifold : } f^{5,6}_{bd} = 0, \quad T_{10}^3 = 0, \quad (3.64)$$

$$\text{Mink. sol. in } m_{46} \text{ on a nilmanifold : } f^{5,6}_{bd} = 0, \quad T_{10}^{(6)2} = T_{10}^{(6)3} = T_{10}^{(6)4} = 0,$$

leading to the conclusion that only two sets of sources can be present in either of those classes. This is consistent with our solutions in  $s_{55}^0$  and  $m_{46}^0$ , and those already known.

### Chapter 3. Exploring the Landscape

---

of directions with only  $D_p$ -branes. This difference is even stronger with  $s_{6666}$  where we have difficulties identifying relevant directions over which to trace as above: doing so brings further contributions to the equations, leading to looser requirements, not worth being indicated here. *The presence or absence of directions with only  $D_p$ -branes is related this way to the possibility of getting anti-de Sitter solutions on Ricci flat or nilmanifolds, which in turn could be related to scale separation.* These relations deserve more investigation.

# 4 Consistent truncations and stability

In this chapter, we re-examine the stability of our solutions through the prism of consistent truncations. We present numerical tools to analyse the perturbative stability of classical flux compactifications, and apply them on our database of (A)dS and Minkowski solutions.

## 4.1 Context and motivations

As in any dimensional reduction, a fundamental aspect is the truncation: the 10d fields, developed on an infinite basis of 6d modes, need to be truncated to a finite set, whose physics will be described by the 4d theory. There exist different choices of inequivalent truncations. Phenomenologically, the most relevant one is a low energy truncation: one truncates to the lightest modes. In practice, this is difficult to realise since it requires to first determine the complete mass spectrum, in order to identify the lightest modes. What is however often considered is the truncation to massless scalar fields, a.k.a. moduli, which are simpler to determine. Another common truncation is called a consistent truncation: the corresponding 4d theory describing the resulting finite set of modes is such that any of its 4d solutions also solves the 10d equations of motion. In practice, this corresponds to a finite set of modes which are, in some sense, independent or decoupled from those truncated. This set of modes may however contain both light and heavy modes, while other light modes may have been truncated. In this work, we will perform consistent truncations: as we will recall, finding an instability within this set of modes is sufficient to conclude on the instability of the 10d solution. Although phenomenologically debatable, this truncation will then be enough for our purposes. We implement it, as well as the corresponding dimensional reduction and resulting 4d theory, in an automated fashion in the code `MSSV`.

Proving that a truncation is consistent is challenging. It first requires to find an appropriate truncation ansatz, and then verify that all 4d equations are captured by 10d equations. As we will review in Section 4.2.1, it remains expected that the truncation of the 10d fields to left-invariant fluctuations on group manifolds is a consistent truncation, even in presence of (smeared)  $O_p/D_p$  sources. The resulting theory is expected to be a 4d gauged supergravity. But this has typically been verified in a case by case analysis, for various compactifications and source configurations. In this chapter, thanks to a detailed comparison between the 10d equations given by the code `MSSS` [4] and the 4d equations

provided by the new code `MSSV`, we prove that the truncation to left-invariant scalar fields on group manifolds is consistent for all 21 solution classes in type IIA/B described in Chapter 2, corresponding to various  $O_p/D_p$  source configurations. We actually get more: we show a perfect matching between 10d and (combinations of) 4d equations of motion, with the same amount of equations on both sides. This means that there is actually no extra degree of freedom in the 10d ansatz (even though there are more constraints to satisfy in 10d). This matching ensures that the 10d solutions of [1, 4, 65] are critical points of our 4d scalar potential. This will allow us to study their stability using the 4d theory, and corresponding tools in `MSSV`.

The chapter is organised as follows. We first discuss in Section 4.2.1 consistent truncations and truncations to left-invariant modes on group manifolds, before specifying our truncation ansatz, and recalling the orientifold projections. We then detail in Section 4.2.2 the dimensional reduction, starting from 10d type II supergravities and compactifying towards a 4d maximally symmetric spacetime, ending up with a 4d theory of the form (3.27). We give in particular the scalar potential including the axions in equations (4.14) and (4.15). We also discuss the computation of the scalar fields kinetic terms. We can then motivate and define the mass matrix and the  $\eta_V$  parameter, to be used in stability studies. The truncation, dimensional reduction and stability analysis are then implemented in the code `MSSV`, presented in Section 4.3. A first use of this code is then the verification in Section 4.4 that we have a consistent truncation of our 10d starting point. This is achieved thanks to a comparison of 10d and 4d equations of motion, as explained previously. Note that both codes, `MSSS` and `MSSV`, have compatible conventions. This could allow to use them further together, for instance `MSSS` for the search of solutions and `MSSV` to study the stability. We turn in Section 4.5 to analysing the stability of the previously mentioned solution database. We start by determining and discussing in Section 4.5.1 the generic flat directions in each of the 21 solution classes. Those appear as massless modes in the spectrum of 10d solutions. We then study the spectrum and stability of de Sitter solutions in Section 4.5.2, Minkowski solutions in Section 4.5.3 and anti-de Sitter solutions in Section 4.5.4. We comment on the results and compare them to corresponding swampland conjectures. Finally, we give a summary in Section 4.6 and provide an outlook.

## 4.2 Dimensional reduction on group manifolds

We first present in Section 4.2.1 the truncation of 10d fields, commonly followed when compactifying on 6d group manifolds. We then use it in Section 4.2.2 to perform the dimensional reduction from 10d to 4d, with a focus on scalar fields and their scalar potential  $V$ . This reduction is implemented in the code `MSSV` described in Section 4.3, and further used in Section 4.5 to study the 4d stability of 10d compactifications.

### 4.2.1 Truncation ansatz

We present here the truncation ansatz of the 10d fields to be used to derive our 4d theory. For phenomenology, one would like to truncate to the 4d light fields, eventually providing a 4d low energy effective theory. Unfortunately, for non-Ricci flat manifolds, it is generically not known what the lightest fields are (see however recent progress in [128, 129]). A

different truncation is then usually considered on other manifolds, e.g. those with an  $SU(3) \times SU(3)$  structure: that truncation has been argued to correspond to a consistent truncation [122, 130–139]. The finite set of 4d fields kept by such a truncation contains a priori both light and heavy fields, but this set is characterised by a certain independence with respect to other fields. This has the advantage to guarantee that a solution to the 4d equations of motion is also a solution to the 10d ones, which can be useful when looking for new solutions.

Here we restrict ourselves to 6d manifolds being group manifolds (see reviews in [5, 71, 74]). Those often carry an  $SU(3) \times SU(3)$  structure. They admit a basis of 1-forms  $\{e^a\}$ ,  $a = 1, \dots, 6$ , that are left-invariant under the group action. The same holds for wedge products of  $e^a$ , with constant prefactors. Under a few assumptions, it was shown in [139] that for compactifications on group manifolds, expanding all 10d fields in a basis of forms that are left-invariant under the group action gives rise to a consistent truncation. The resulting 4d theory is then a gauged supergravity [140, 141]. This was proven in the absence of orientifold projections and localized sources. As detailed below, we will consider here  $D$ -branes and orientifolds but restrict ourselves to smeared sources. In that case, it is still expected that the 4d theory, a gauged supergravity, is a consistent truncation and this has been explicitly checked either formally [100, 142–144] or in several examples [74, 75, 88]. In Section 4.4, we will verify in detail that all compactifications considered here give rise to a 4d theory that is a consistent truncation.

Since the left-invariant fields, to be considered here in our truncation, are not guaranteed to be the lightest fields in the theory, we will only obtain an upper bound on the smallest masses. However, for some simple group manifolds, namely nilmanifolds, recent progress in the understanding of the lightest modes [121, 122] indicate that the consistent truncation actually contains the lightest fields in the theory. However, as pointed out in [61], it is also possible that for other group manifolds, the left-invariant fields have masses that are larger than the Kaluza–Klein scale. We refer to [122, Sec. 5] and [5] for further related discussions.

As mentioned above, the forms that are left-invariant under the group action are wedge products of the  $e^a$  with constant prefactors. The 4d scalar fields are obtained by expanding the 10d fields in terms of left-invariant forms. In this case the prefactors, i.e. the 4d scalar fields, are still functions of the 4d spacetime coordinates  $x^\mu$  but they are constant as functions of the internal group manifold coordinates  $y^m$ . For example, the 10d dilaton gives rise in this truncation to a single real scalar  $\phi_{10d}(x^\mu, y^m) \rightarrow \phi_{4d}(x^\mu) \cdot 1$ , where 1 is the left-invariant 0-form on the internal group manifold. Another example are the axions, such as  $B_2 = \frac{1}{2} b_{ab}(x^\mu) e^a \wedge e^b + \dots$  where the  $b_{ab}(x^\mu) = -b_{ba}(x^\mu)$  are a set of 4d scalar fields that arise from the truncation and reduction of the field  $B_2$ . There will be additional terms in the expansion of  $B_2$  that will give rise to the internal  $H_3$ -flux via

$$\begin{aligned} H_3 = dB_2 &= dx^\nu \wedge \partial_\nu B_2 + e^a \wedge \partial_a B_2 \\ &= \frac{1}{2} \partial_\nu b_{ab}(x^\mu) dx^\nu \wedge e^a \wedge e^b - \frac{1}{2} b_{ab}(x^\mu) f^a{}_{cf} e^b \wedge e^c \wedge e^f + \frac{1}{3!} h_{abc} e^a \wedge e^b \wedge e^c, \end{aligned} \quad (4.1)$$

where  $e^a = e^a{}_m(y) dy^m$  and  $\partial_a = e^m{}_a(y) \partial_m$ . Here,  $h_{abc}$  is fully antisymmetric and denotes the constant flux number threading internal 3-cycles, that should be quantized in string theory provided  $e^a \wedge e^b \wedge e^c$  is a harmonic form. The same type of flux quanta will

## Chapter 4. Consistent truncations and stability

appear as constant prefactors for RR fluxes. In the above expansion we have neglected potential 4d 1-forms that would arise via  $B_2 \supset A_{\mu,a} dx^\mu \wedge e^a$  since we are only interested in scalar fields and we will neglect potential gauge fields in the models discussed below. We have also neglected a 4d 2-form that arises from  $B_2 \supset \frac{1}{2} b_{\mu\nu} dx^\mu \wedge dx^\nu$  since it is projected out by orientifold projections in our settings, as discussed in the next paragraph. However, for the 10d RR forms  $C_p$  there can be such 2-forms in 4d and they will have to be dualized into scalar fields using the 4d Hodge star.

Finally, for the 10d metric we assume a block diagonal unwarped form, consistently with the smeared sources we consider as well as the dilaton being independent of  $y^m$

$$ds^2 = G_{MN} dx^M dx^N = G_{\mu\nu} dx^\mu dx^\nu + G_{ab} e^a e^b. \quad (4.2)$$

The background 4d metric is that of a maximally symmetric spacetime: we restrict indeed to compactifications to 4d de Sitter, Minkowski or anti-de Sitter. This restricts the possible 4d background fluxes and the allowed sources. The background 6d metric should be  $\delta_{ab}$ ; the left-invariant components  $G_{ab}$  can be viewed as fluctuations around the former. Those are the 4d scalar fields generalizing the usual Kähler and complex structure moduli beyond Calabi-Yau compactifications.

Let us present an example of the set of 4d scalar fields resulting from this truncation performed together with the orientifold projections. We consider the solution class  $s_{55}$ : this type IIB setting includes  $O_5$  (and possible  $D_5$ ) along internal directions 12,  $O_5$  ( $D_5$ ) along 34 and possible  $D_5$  along 56. As a result, the list of 4d real fields, that are all functions of  $x^\mu$ , is given by

$$\begin{aligned} s_{55} : \quad & G_{11}, G_{12}, G_{22}, G_{33}, G_{34}, G_{44}, G_{55}, G_{56}, G_{66}, \\ & C_{2\ 12}, C_{2\ 34}, C_{2\ 56}, C_{4\ 1356}, C_{4\ 1456}, C_{4\ 2356}, C_{4\ 2456}, C_{6\ 123456}, \\ & b_{13}, b_{14}, b_{23}, b_{24}, \phi. \end{aligned} \quad (4.3)$$

These fields are worked out automatically in the code `MSSV` presented in Section 4.3. The number of fields for each solution class to be considered is listed in Table 4.1, while we give for completeness in Table 4.2 the number of the fields for the other 13 solution classes.

Class	$s_{55}$	$s_{555}$	$s_{66}$	$s_{6666}$	$m_{46}$	$m_{466}$	$m_{55}$	$m_{5577}$
# of fields	22	14	22	14	22	14	22	14

Table 4.1: The number of scalar fields for each solution class where new solutions have been found in [4].

In Table 4.1, the matching of the number of fields in different solution classes is remarkable. It may be understood by T-duality, as we now explain. The 10d theories are known to be generally T-dual to each other, and so should be the generic development in left-invariant fields. What matters then are the configurations of orientifolds which project out certain fields. The classes with 22 scalar fields have 2 sets with  $O_p$ -planes, and those sets are T-dual to each other when going from one class to the other, as

displayed on Figure 2.1 (provided the right background isometries are there). Since the orientifold projections are crucial in fixing the number of scalar fields, it makes sense to get the same number of fields. Similarly, in the classes with 14 scalar fields, the sets with  $O_p$  are T-dual to each other when going from one class to the other. There are two ways to see this. First, one can consider only 3 sets with  $O_p$  there, since the fourth one in  $s_{6666}$  and  $m_{5577}$  is shown to bring no further projection [4]. Alternatively, one can add without constraint an  $O_9$  to  $s_{555}$  and an  $O_8$  to  $m_{466}$  (transverse to direction 1 in conventions used here), making the resulting configurations of  $O_p$  planes T-dual to each other among the 4 classes with 14 scalars. Note that we restrict here to geometric setups: this means we allow in the NSNS sector for the  $H_3$ -flux and the metric fluxes  $f^a_{bc}$  but no non-geometric fluxes. Since the metric fluxes can become non-geometric fluxes under T-duality, each of the different classes above can give rise to different 4d theories and deserves to be studied in its own right. Non-T-dual de Sitter solutions were in particular found in several of them. This observation does not change the number of fields.

Class	$s_3$	$s_4$	$s_5$	$s_6$	$s_7$	$s_{77}$	$m_4$	$m_6$	$m_{66}$	$m_5$	$m_{57}$	$m_7$	$m_{77}$
# of fields	38	38	38	38	38	22	38	38	22	38	22	38	22

Table 4.2: The number of scalar fields for each of the remaining 13 solution classes of [4], given for completeness.

#### 4.2.2 Dimensional reduction

Having presented the truncation ansatz of our 10d fields, we are now ready to perform the dimensional reduction to 4d, eventually obtaining the corresponding 4d theory. As a starting point, the 10d actions for type IIA and type IIB supergravity are given in equations (12.1.24) and (12.1.26) in [145] and read explicitly

$$\begin{aligned}
 S^{\text{IIA/B}} &= S_{\text{NS}} + S_{\text{R}} + S_{\text{CS}}, \\
 S_{\text{NS}} &= \frac{1}{2\kappa_{10}^2} \int d^{10}x \sqrt{-G} e^{-2\phi} \left( R_{10} + 4\partial_\mu \phi \partial^\mu \phi - \frac{1}{2} |H_3|^2 \right), \quad (4.4)
 \end{aligned}$$

with, in type IIA<sup>1</sup>

$$\begin{aligned}
 S_{\text{R}} &= -\frac{1}{4\kappa_{10}^2} \int d^{10}x \sqrt{-G} \left( F_0^2 + |F_2 + F_0 B_2|^2 + \left| F_4 + C_1 \wedge H_3 + \frac{1}{2} F_0 B_2 \wedge B_2 \right|^2 \right), \\
 S_{\text{CS}} &= -\frac{1}{4\kappa_{10}^2} \int B_2 \wedge \left( F_4 + \frac{1}{2} F_0 B_2 \wedge B_2 \right) \wedge \left( F_4 + \frac{1}{2} F_0 B_2 \wedge B_2 \right), \quad (4.5)
 \end{aligned}$$

and in type IIB

$$\begin{aligned}
 S_{\text{R}} &= -\frac{1}{4\kappa_{10}^2} \int d^{10}x \sqrt{-G} \left( |F_1|^2 + |F_3 - C_0 H_3|^2 \right. \\
 &\quad \left. + \frac{1}{2} \left| F_5 - \frac{1}{2} C_2 \wedge H_3 + \frac{1}{2} B_2 \wedge F_3 + \frac{1}{2} F_1 \wedge B_2 \wedge B_2 \right|^2 \right),
 \end{aligned}$$

<sup>1</sup>We have changed the sign of the  $C_1 \wedge H_3$  term to match the convention in for example [146, App. C]. This sign change is standard in the type IIA flux compactification literature and without it the 10d solutions would not solve the 4d equations of motions so it is clearly required.



$$S_{\text{CS}} = -\frac{1}{4\kappa_{10}^2} \int C_4 \wedge H_3 \wedge F_3. \quad (4.6)$$

While most of the above 10d actions is standard textbook material, there have been arguments presented for additional terms. For example, T-duality maps the  $F_0 B_2 \wedge B_2$  term in type IIA into  $F_1 \wedge B_2 \wedge B_2$  which we included as additional term in the  $|F_5 + \dots|^2$  expression in  $S_{\text{R}}$  above [147]. This term is important and has been argued for using T-duality in the context of axion monodromy inflation in [148]. We are here interested in critical points at which axions like  $B_2$  vanish. Thus, for us this term only affects our results in the mass spectrum if appropriate  $F_1$  and  $F_5$  fluxes are present. This only happens in the anti-de Sitter solution  $s_{55}^-1$ . Likewise, there should be extra terms in the Chern-Simon's action  $S_{\text{CS}}$  as for example discussed for type IIA in [146, App. C]. We will take those terms into account below, when defining the  $F_6$  flux that is dual to a spacetime filling  $F_4$  flux.

We will expand all fields as described above and integrate over the internal six dimensions. We also rescale the 4d metric  $G_{\mu\nu}$ , of determinant  $G_4$  and curvature  $\bar{R}_4$ , towards  $g_{\mu\nu}$  of determinant  $g$  and curvature  $R_4$ , as follows:  $G_{\mu\nu} = \frac{e^{2\phi}}{\text{vol}_6} g_{\mu\nu}$ . The dimensionless internal volume of the group manifold is given by  $\text{vol}_6 = (2\pi\sqrt{\alpha'})^{-6} \int d^6y \sqrt{G_6}$ , where we recall the string length definition  $l_s = \sqrt{\alpha'}$ . This leads to the 4d Einstein frame

$$\begin{aligned} \int d^{10}x \sqrt{-G} e^{-2\phi} R_{10} &= (2\pi\sqrt{\alpha'})^6 \int d^4x \sqrt{-G_4} \text{vol}_6 e^{-2\phi} \bar{R}_4 + \dots \\ &= (2\pi\sqrt{\alpha'})^6 \int d^4x \sqrt{-g} R_4 + \dots \end{aligned} \quad (4.7)$$

Using that  $2\kappa_{10}^2 = (2\pi)^7 (\alpha')^4$  we can identify  $M_p = (\pi\alpha')^{-\frac{1}{2}}$ .<sup>2</sup> With this we obtain the 4d action in terms of the real 4d scalar fields  $\varphi^i$  and the 4d Einstein frame metric  $g_{\mu\nu}$

$$S_{4d} = \int d^4x \sqrt{-g} \left( \frac{M_p^2}{2} R_4 - \frac{1}{2} K_{ij} \partial_\mu \varphi^i \partial^\mu \varphi^j - V(\varphi^i) \right). \quad (4.8)$$

Since we are only interested in the 4d scalar potential  $V$ , we neglected in  $S_{4d}$  the 4d vector fields and 3-form fields. We also dualized 4d 2-forms  $b_2^i = \frac{1}{2} b_{2\mu\nu}^i dx^\mu \wedge dx^\nu$  into scalar fields using  $d\varphi^i = \star_4 db_2^i$ .

Lastly, we want to include  $D_p$ -brane sources and  $O_p$ -planes that fill the space in 4d and wrap internal  $(p-3)$ -dimensional spaces  $\Sigma_{p-3}$  in the group manifold. Thus, we need necessarily  $p \geq 3$  in order to have a maximally symmetric 4d spacetime. We will work in a smeared limit in which we do not keep track of the position of the localized sources in the internal space but we rather ‘‘smear’’ them over the internal space. We do not include the worldvolume fields for the  $D_p$ -branes, so that the source contributions to the 10d action are given by

$$S_{O_p/D_p} = -T_{O_p/D_p} \int \left( d^4x d^{p-3}y \sqrt{|G+B_2|} e^{-\phi} - e^{-B_2} \sum_q C_q \right) \Big|_{M^{3,1} \times \Sigma_{p-3}} \wedge j(\tilde{\Sigma}_{9-p}), \quad (4.9)$$

<sup>2</sup>Note that different conventions would lead to  $M_p$  depending on the vev of the internal volume and that of the dilaton (or the string coupling), the fields being then only fluctuations: see e.g. [149, (4.3)] in arbitrary dimensions. Here, the fields  $\phi$  and  $\text{vol}_6$  are not fluctuations but contain the full values.

## 4.2 Dimensional reduction on group manifolds

where  $|G + B_2|$  denotes the absolute value of the determinant of the tensor  $G + B_2$ , here further pulled back to the worldvolume. The  $(9 - p)$ -form  $j(\tilde{\Sigma}_{9-p})$  can be understood as the constant unit volume form on the  $(9 - p)$ -dimensional space  $\tilde{\Sigma}_{9-p}$  that is dual on the internal manifold to  $\Sigma_{p-3}$ : it satisfies  $\int_{\tilde{\Sigma}_{9-p}} j(\tilde{\Sigma}_{9-p}) = 1$ . We also indicated that the fields need to be pulled back to the source worldvolume which is given by  $M^{3,1} \times \Sigma_{p-3}$ . Note that the pullback of  $B_2$  to the worldvolume of the  $D_p$ -branes and  $O_p$ -planes vanishes for all solution classes to be considered, namely those of Table 4.1, except for  $m_{55}$  and  $s_{66}$ .<sup>3</sup> The tension of  $N_{O_p}$   $O_p$ -planes is  $T_{O_p} = -2^{p-5} N_{O_p} (2\pi)^{-p} \alpha'^{-\frac{p+1}{2}}$ , and for  $N_{D_p}$   $D_p$ -branes one has  $T_{D_p} = N_{D_p} (2\pi)^{-p} \alpha'^{-\frac{p+1}{2}}$ . Note that one can in principle add an arbitrary number of  $D_p$ -branes but the number of  $O_p$ -planes is fixed by the number of fixed points of the corresponding  $O_p$ -plane involution. The second term in the above action  $S_{O_p/D_p}$  does not contribute to the 4d scalar potential, but is relevant for the (sourced) Bianchi identities and the tadpole cancellation conditions that need to be imposed in addition to the 4d equations of motion. These extra conditions can for instance be found in [36, (2.7)] in our conventions.

The first term in the action above does contribute to the scalar potential and can be rewritten as

$$\begin{aligned} S_{O_p/D_p} &= -T_{O_p/D_p} \int d^4x d^{p-3}y \sqrt{|G + B_2|} e^{-\phi} \Big|_{M^{3,1} \times \Sigma_{p-3}} \wedge j(\tilde{\Sigma}_{9-p}) \\ &= -T_{O_p/D_p} (2\pi\sqrt{\alpha'})^{p-3} \int d^4x \sqrt{-g} e^{3\phi} \frac{vol B_{p-3}}{(vol_6)^2}, \end{aligned} \quad (4.10)$$

where we introduce the following notations

$$\begin{aligned} vol B_{p-3} &= (2\pi\sqrt{\alpha'})^{3-p} \int d^{p-3}y \sqrt{|G_6 + B_2|} \Big|_{\Sigma_{p-3}}, \\ vol_{p-3} &= (2\pi\sqrt{\alpha'})^{3-p} \int d^{p-3}y \sqrt{|G_6|} \Big|_{\Sigma_{p-3}}, \end{aligned} \quad (4.11)$$

with  $G_6$  standing for the internal components of the 10d metric, and  $vol_{p-3}$  denotes the dimensionless volume of the internal space  $\Sigma_{p-3}$  wrapped by the source. For a given dimensionality  $p$ , the sources can wrap different internal  $(p - 3)$ -dimensional spaces  $\Sigma_{p-3}^I$ ,  $I = 1, 2, \dots$ . We recall the notion of a set  $I$  of sources being along the same dimensions, and we introduce the corresponding numbers of  $N_{O_p}^I$   $O_p$ -planes and  $N_{D_p}^I$   $D_p$ -branes wrapping the same  $\Sigma_{p-3}^I$ . We then follow the conventions of [36, 70, 73] and use the notation  $T_{10}^{(p)I}$ ,<sup>4</sup>

<sup>3</sup>Since  $B_2$  is odd under the orientifold involution its pullback to an  $O_p$ -plane worldvolume is zero. However, for some  $D_p$ -branes the pullback of  $B_2$  to the worldvolume is non-zero in our solution classes  $m_{55}$  and  $s_{66}$ . Their contribution to the scalar potential is however quadratic, so they do not contribute to the gradient of the potential, but only to the mass matrix. On the 10d side, contributions from the source action to the 10d  $B$ -field equation of motion have appeared in [150, (5.3)], but we ignored them in [4] where we looked for new 10d solutions; it is a priori unclear to us whether there would be such contributions for the various solution classes. Since however the contributions in  $m_{55}$  and  $s_{66}$  do not alter the gradient of the potential, the 10d  $B$ -field equation of motion is unlikely to change. In any case, our solutions then remain critical points of the potential, and the truncation is consistent with our 10d  $B$ -field equation.

<sup>4</sup>Strictly speaking,  $T_{10}^{(p)I}$  has been defined beyond the smeared case, but for  $B_2|_{\Sigma_{p-3}} = 0$ ; we naturally extend here the definition. Note that the on-shell value of this quantity is not modified, since at our critical points, axion vevs vanish.

## Chapter 4. Consistent truncations and stability

defined in the smeared case via the following equation

$$\begin{aligned} \frac{M_p^2 T_{10}^{(p)I}}{2^{p+1}} &= \frac{1}{(2\pi)^p \alpha'^{\frac{p+1}{2}}} (2\pi\sqrt{\alpha'})^{p-3} (2^{p-5} N_{O_p}^I - N_{D_p}^I) \text{vol} B_{p-3}^I \\ &= \frac{1}{(2\pi)^3 (\alpha')^2} (2^{p-5} N_{O_p}^I - N_{D_p}^I) \text{vol} B_{p-3}^I. \end{aligned} \quad (4.12)$$

Let us also recall that we defined

$$T_{10}^{(p)} = \sum_I T_{10}^{(p)I}. \quad (4.13)$$

Combining all the contributions above, the scalar potential is then given by

$$\begin{aligned} V^{\text{IIA}}(\varphi^i) &= \frac{M_p^2 e^{2\phi}}{2 \text{vol}_6} \left( -R_6 + \frac{1}{2} |H_3|_{\text{int}}^2 + \frac{e^{2\phi}}{2} \left[ F_0^2 + |F_2 + F_0 B_2|_{\text{int}}^2 \right. \right. \\ &\quad \left. \left. + \left| F_4 + C_1 \wedge H_3 + \frac{1}{2} F_0 B_2 \wedge B_2 \right|_{\text{int}}^2 \right. \right. \\ &\quad \left. \left. + \left| F_6 + C_3 \wedge H_3 + \frac{1}{2} F_2 \wedge B_2 \wedge B_2 + \frac{1}{6} F_0 B_2 \wedge B_2 \wedge B_2 \right|_{\text{int}}^2 \right] \right. \\ &\quad \left. - \sum_{p=4,6,8} \frac{T_{10}^{(p)}}{p+1} \frac{e^\phi}{\text{vol}_6} \right), \end{aligned} \quad (4.14)$$

in type IIA and by

$$\begin{aligned} V^{\text{IIB}}(\varphi^i) &= \frac{M_p^2 e^{2\phi}}{2 \text{vol}_6} \left( -R_6 + \frac{1}{2} |H_3|_{\text{int}}^2 + \frac{e^{2\phi}}{2} \left[ |F_1|_{\text{int}}^2 + |F_3 - C_0 \wedge H_3|_{\text{int}}^2 \right. \right. \\ &\quad \left. \left. + \left| F_5 - \frac{1}{2} C_2 \wedge H_3 + \frac{1}{2} B_2 \wedge F_3 + \frac{1}{2} F_1 \wedge B_2 \wedge B_2 \right|_{\text{int}}^2 \right] \right. \\ &\quad \left. - \sum_{p=3,5,7,9} \frac{T_{10}^{(p)}}{p+1} \frac{e^\phi}{\text{vol}_6} \right), \end{aligned} \quad (4.15)$$

in type IIB.<sup>5</sup> We used  $|\cdot|_{\text{int}}$  to denote the contractions of the form only with respect to the internal metric  $G_{ab}$  on the group manifold. For type IIA we have dualized a spacetime filling  $F_4$  flux into an internal  $F_6$  flux [86, 146] and for type IIB we have used the self-duality of  $F_5$  to write a spacetime filling flux as a completely internal flux, which effectively removed the factor of  $1/2$ ; see also [78, App. A] and [149] on spacetime filling fluxes.

<sup>5</sup>We generically include  $p = 9$  sources in  $V^{\text{IIB}}$ . However, a tadpole constraint on them would require to cancel the  $O_9$ -plane charge with that of  $D_9$ -branes, meaning here  $T_{10}^{(9)} = 0$ . Such sources would then not contribute to the potential, except indirectly through the  $O_9$ -projection. Because of  $T_{10}^{(9)} = 0$ ,  $p = 9$  sources have anyway not been considered in [4, 5], i.e. in the solutions to be discussed in Section 4.5.

## 4.2 Dimensional reduction on group manifolds

Let us recall that if one restricts to algebras for which  $\sum_a f^a{}_{ab} = 0$ , the Ricci scalar for 6d group manifold is explicitly given

$$R_6 = -\frac{1}{2}f^a{}_{bc}f^b{}_{ae}G^{ce} - \frac{1}{4}f^a{}_{bc}f^e{}_{fg}G_{ae}G^{bf}G^{cg}. \quad (4.16)$$

This provides its contribution to the scalar potential.

Let us now say a word on the kinetic terms and the field space metric  $K_{ij}$ . Its computation is automatized in MSSV. The kinetic terms for the axions arise from the squares of the field strengths. For example, for  $F_{p+1}$  one finds following (4.1)

$$\begin{aligned} S_{\text{kin}, F_p} &= -\frac{1}{4\kappa_{10}^2} \int d^{10}x \sqrt{-G} |F_{p+1}|^2 \\ &\supset -\frac{1}{4\kappa_{10}^2} \int d^{10}x \sqrt{-G} \frac{1}{p!} \partial_\mu C_{p \ a_1 a_2 \dots a_p} G^{\mu\nu} G^{a_1 b_1} G^{a_2 b_2} \dots G^{a_p b_p} \partial_\nu C_{p \ b_1 b_2 \dots b_p} \\ &= -\frac{M_p^2}{4} \int d^4x \sqrt{-g} \frac{e^{2\phi}}{p!} \partial_\mu C_{p \ a_1 a_2 \dots a_p} g^{\mu\nu} G^{a_1 b_1} G^{a_2 b_2} \dots G^{a_p b_p} \partial_\nu C_{p \ b_1 b_2 \dots b_p}. \end{aligned} \quad (4.17)$$

Given our definition of the field space metric (or kinetic matrix)  $K_{ij}$  above in equation (4.8), we see that the entries corresponding to the  $C_p$  axions would be  $M_p^2/2$  multiplied by  $e^{2\phi}$  and a combination of components of the inverse internal metric. In particular, at the special point where we set all diagonal metric entries as well as  $e^{2\phi}$  to one and the off-diagonal ones to zero, all the  $C_p$  axions as well as all  $B_2$  axions will give rise to a diagonal  $K_{ij}$  submatrix with entries  $M_p^2/2$ .

In order to find the kinetic terms for the dilaton and the scalars  $G_{ab}(x^\mu)$  arising from the internal metric one has to calculate the Ricci scalar  $R_{10}$ . After doing the rescaling to 4d Einstein frame and after doing appropriate integrations by parts of second derivative terms, one can subtract the background  $R_4$  and  $R_6$  and then add the  $4\partial_\mu\phi\partial^\mu\phi$  term from equation (4.4) to get the final kinetic terms. An illustration of this procedure on few fields can be found in [1, App. D].

Neglecting flux quantization, as well as quantization of  $N_{O_p/D_p}^I$  and that of the structure constants [2], the type II supergravity actions have a large symmetry group that allows one to rescale and shift the fluxes. This enables us to move any given point in field space to the point where all axionic scalar fields and all off-diagonal metric entries are equal to zero and all diagonal metric entries and the dilaton  $e^\phi$  are equal to one. Since the classical scalar potential has a complicated dependence on the fields but is quadratic in the fluxes and linear in the sources, it is much easier to solve the equations of motions and find critical points at a fixed point in field space in terms of the flux parameters. One can then use the rescaling and shifts of the fluxes to move the critical point. If one can find in this way a point in field space at large volume, large complex structure and weak string coupling, where also the necessary quantization is obeyed, then one can trust the corresponding solution as a classical string background.

Given that most corrections to the classical flux potential are not known, it is not exactly clear where the trustworthy large volume and weak coupling regime begins. We therefore do not focus on this point but are rather interested in the mass spectrum for a given critical point. While the actual masses of the fields can change under the above

rescalings (see e.g. the  $\lambda$ -rescaling discussed in Section 5.5), the  $\eta_V$  parameter defined in (4.19) below cannot. This also means that the number of tachyons cannot change under this rescaling. This will be important and sufficient for our analysis below that we can hence carry out at any point in field space.

From the field space metric  $K_{ij}$  defined in (4.8) and discussed around (4.17), one obtains the mass matrix

$$M^i_k = K^{ij} \nabla_j \partial_k V, \quad (4.18)$$

where  $\nabla_j v_k = \partial_j v_k - \Gamma^l_{jk} v_l$  is the covariant derivative on  $v_k$  and  $\Gamma^l_{jk}$  denotes the Christoffel symbol associated with  $K_{ij}$ . The eigenvalues of  $M$  are the masses<sup>2</sup>. Considering its minimal eigenvalue, denoted by “min”, one defines for  $V \neq 0$  the parameter

$$\eta_V = M_p^2 \frac{\min(K^{ij} \nabla_j \partial_k V)}{V}. \quad (4.19)$$

As explained above, the sign and value of  $\eta_V$  are not sensitive to rescalings of the fields, so it will be a useful parameter in the following, when studying the stability of solutions in the context of the swampland program.

The fields  $\{\varphi^i\}$  to be considered can always be brought to a canonical basis  $\{\hat{\varphi}^i\}$ , where the field space metric  $K_{ij}$  becomes  $\delta_{ij}$ , i.e. the kinetic terms become diagonal and normalized. This change of basis is given by the field space diffeomorphism  $P^i_j = \frac{\partial \hat{\varphi}^i}{\partial \varphi^j}$ . In terms of matrices, one has  $(K_{ij}) = P^T \delta P$ , where  $\delta$  is simply the identity matrix; we refer to [65, (2.2)] for more detail. The fields one-forms (or here their coefficients) are obviously related by  $\partial_\mu \hat{\varphi}^i = P^i_j \partial_\mu \varphi^j$ . One can then consider the mass matrix  $\hat{M}$  in the canonical basis, of coefficients  $\hat{M}^i_k = \delta^{ij} \nabla_j \partial_k V$ . One can verify that  $\hat{M} = P M P^{-1} = \delta^{-1} P^{-T} \nabla \partial V P^{-1}$ , where the matrix  $\nabla \partial V$  computes the Hessian of  $V$  in the non-canonical field basis. We will use these formulas to get our spectrum data. Indeed, the code `MSSV` first computes the matrix  $P$  using the relation  $(K_{ij}) = P^T \delta P$ , and introducing an orthonormal matrix  $O$  and a diagonal one  $D$ , such that  $P = D^{-1} O$ . Then, the mass matrix is computed with  $\hat{M} = \delta^{-1} P^{-T} \nabla \partial V P^{-1}$ . From there, its eigenvalues and eigenvectors are determined. Expressing the eigenvectors in the non-canonical basis (to understand their field directions) then amounts to using the relation  $\partial_\mu \hat{\varphi}^i = P^i_j \partial_\mu \varphi^j$ , or in short in the code,  $\hat{\varphi} = P \varphi$ . We will obtain in this way the spectrum data, and use it to analyse the stability of solutions in Section 4.5.

### 4.3 The code `MSSV`

In this section, we briefly present how the code `MSSV` works, and provide a few useful commands. `MSSV` stands for Maximally Symmetric spacetime Solutions  $V$ , where  $V$  refers to the complete scalar potential  $V$  obtained via the dimensional reduction described above. The code has been developed with `Wolfram Mathematica 13`. `MSSV` takes as input the source configuration corresponding to a certain solution class, meaning the number of  $O_p$ -planes, of  $D_p$ -branes, and the directions along which they are placed. This is also referred to as the “model”, since this data determines the 4d theory and its field content. Once executed, the code begins by using the user’s input to find the left-invariant scalar fields and the background fluxes after the orientifold projections. The code then computes, following Section 4.2, the 4d kinetic terms and scalar potential for these fields

and fluxes and packages them as per equation (4.8). The code also determines those of the scalar fields that are generic flat directions, as discussed in Section 4.5.1. In the code we have set  $M_p = 1$ .

The next required input is that of a concrete 10d solution obtained from the code MSSV and listed in the accompanying database [4]. This amounts to assigning values to all the fluxes appearing in the variable `fluxes`. Through the command `AnalyseSol`, after performing a few checks on the 10d solution, the code is then able to extract the mass spectrum and the  $\eta_V$  value (see equations (4.18) and (4.19)). It also provides the mass matrix eigenvectors for the tachyonic and massless modes. In the case of multiple massless modes, the corresponding eigenspace is degenerate and the code chooses a random basis in field space that spans it.

Note that the computation of the mass spectrum by the code assumes to be at a critical point, where  $\partial_{\varphi^i} V = 0$ , axions (including off-diagonal metric components) vanish, and diagonal metric components as well as  $e^\phi$  are set to one. While it would be easy to change this and allow computations at generic points in field space, we find that generically the code would become very slow. In addition, all models analysed below do correspond to critical points.

We now list a few useful commands; more are provided in the code.

- `RunModel` – Initializes the model, then prints out the left-invariant scalar fields and background fluxes for the chosen source configuration along with any generic flat directions, i.e. left-invariant scalar fields that generically do not appear in  $V$ .
- `AnalyseSol` – Computes and prints out information regarding the mass spectrum, including masses of the fields, number of massless fields and their field directions, number of tachyons and their field directions, etc. This is computed for a given solution that satisfies  $\partial_{\varphi^i} V = 0$  at the critical point defined in the variable `extremum`.
- `fields` – Returns the left-invariant scalar fields for the chosen model.
- `fluxes` – Returns the set of  $F_p$ ,  $H_3$ , and metric fluxes for the chosen source configuration. Recall that we set  $f^a{}_{ab} = 0$  without the summation over  $a$ .
- `VGen` – Returns the scalar potential as a function of the left-invariant scalar fields at a generic point in field space.
- `V` – Returns the scalar potential as a function of the flux parameters defined in the variable `fluxes` and evaluated at the critical point defined in the variable `extremum`.

The two most useful commands are `RunModel` and `AnalyseModel`, which must be evaluated before calling on the other commands. Finally, let us mention that the notebook allows to analyse different source configurations as well as several solutions, without having to quit or restart it. Indeed, the main part of the code is run once and for all, and one can then just call commands, or redefine the input. This allows in particular the user to evaluate once a whole notebook where many solutions have been entered to be analysed.

## 4.4 Consistent truncations

In this section, we verify explicitly that the 4d theory obtained by the truncation and dimensional reduction described in Section 4.2 is a consistent truncation of our 10d starting point. We recall that (smeared)  $O_p/D_p$  sources are present in our compactification. We verify the consistent truncation for all 21 solution classes.

To prove the consistent truncation, it suffices to show that the 4d and 10d actions yield the same equations of motion (eoms). On the 4d side, the eoms for the scalar fields  $\varphi^i$  at an extremum, denoted by “ext”, read

$$\left. \frac{\partial}{\partial \varphi^i} V \right|_{\text{ext}} = 0. \quad (4.20)$$

Note that we restrict ourselves here to solutions without kinetic energy. The (trace of the) Einstein equation reads, for a maximally symmetric spacetime,

$$R_4 - 4V_{\text{ext}} = 0, \quad (4.21)$$

and we use in this section  $M_p = 1$ .

On the 10d side, the equations of motion are the flux eoms, denoted schematically  $F_i = 0$ , the 6d Einstein equations  $E^{ab} = 0$ , the 4d Einstein equation  $E_4 = 0$ , and the dilaton eom  $D = 0$ . These can be found e.g. in [4]. For instance, we define

$$E_4 = R_4 - \sum_p \frac{T_{10}^{(p)}}{p+1} + \sum_{q=0}^6 |F_q|^2, \quad D = 2R_4 + 2R_6 + \sum_p \frac{T_{10}^{(p)}}{p+1} - |H_3|^2. \quad (4.22)$$

Note that in [4], the authors considered the trace-reversed 6d Einstein equations, and considered linear combinations of eoms to obtain  $E_4$ , thus one expects that the matching with equations (4.20) and (4.21) should only hold up to taking linear combinations. Let us add that the metric used in [4] is  $\delta_{ab}$ , allowing to raise 6d Einstein equation indices towards  $E^{ab}$ .

For each class of solutions, we determine in components the 10d eoms using the code MSSS [4]. We remove from those the equations trivially satisfied. In 4d, we compute the components of the generic gradient at the extremum,  $\left. \partial_{\varphi^i} V \right|_{\text{ext}}$ , with the help of MSSV. At this stage, one can already check that the number of 6d Einstein equations matches with the number of scalar fields arising from the internal metric, and that the number of 10d flux eoms matches with the number of axions appearing in the potential (that is, without counting the fields associated to generic flat directions). From these two lists of equations, one can then verify the matching, which goes as follows.

For the fluxes, one has (after the appropriate labelling)

$$F_i = 2 \left. \frac{\partial}{\partial a^i} V \right|_{\text{ext}}, \quad (4.23)$$

where  $a^i$  denotes the  $i$ -th axion. The non-diagonal 6d Einstein equations  $E^{ab}$  correspond to the variations with respect to the non-diagonal metric scalar fields  $G_{ab}$  simply via

$$E^{ab} = \left. \frac{\partial}{\partial G_{ab}} V \right|_{\text{ext}}, \quad a \neq b. \quad (4.24)$$



The diagonal ones are related by

$$2E^{aa} + \delta^{aa} E^{bc} \delta_{bc} = 4 \left. \frac{\partial}{\partial G_{aa}} V \right|_{\text{ext}}, \quad (4.25)$$

where the above 6d trace accommodates the fact that  $E^{ab}$  correspond here to the trace-reversed equations. Finally, the dilaton and the 4d Einstein equation combine as follows

$$2E_4 - D = 2 \left. \frac{\partial}{\partial \phi} V \right|_{\text{ext}}, \quad -E_4 + D = R_4 - 4V_{\text{ext}}. \quad (4.26)$$

It is remarkable that the same matching of equations works for all solution classes considered, thus proving in each case the consistent truncation. Although this is not surprising, given all other working examples in the literature recalled in Section 4.2.1, this remains a non-trivial check. It was made possible thanks to the two codes `MSSS` and `MSSV` that generate all equations to be considered for all solution classes, using the same conventions. Finally, let us recall from [4] that finding 10d solutions would require in addition to solve the flux Bianchi identities (including the tadpole conditions) and the Jacobi identities on the  $f^a{}_{bc}$ , to guarantee having a group manifold.

## 4.5 Stability analysis

Stability of solutions with maximally symmetric spacetimes is at the heart of several swampland conjectures, as recalled in the Introduction; it also plays an important role for phenomenological models. In this section, we use the 4d theory discussed in Section 4.2 and the corresponding code `MSSV` described in Section 4.3 to study the stability of the de Sitter, Minkowski and anti-de Sitter solutions found in [1, 4, 65]. The solutions database can be found in two files provided with [4]. These solutions were found with the code `MSSS` [4] which is compatible with the present code `MSSV`. The conventions of [36, 73] followed in [4] are the same as in the present thesis, and we verify in particular that these solutions are critical points of the scalar potential  $V$  obtained here, satisfying  $\nabla V = 0$  as well as  $V = \frac{M_p^2}{4} R_4$ . This is actually formally ensured thanks to the analysis described in Section 4.4 regarding consistent truncations. The stability of these solutions has already been analysed using `MSSSp` in [5], considering only the 4–6 scalar fields  $(\rho, \tau, \sigma_I)$  corresponding to some dilaton and diagonal metric fluctuations. Thanks to the above dimensional reduction, embedded in the code `MSSV`, we now have a complete set of scalar fields, a corresponding scalar potential as well as kinetic terms. This allows us here to provide a more complete analysis of the perturbative stability of these solutions. The latter will essentially be discussed in terms of the parameter  $\eta_V$  defined in (4.19), or the spectrum of masses<sup>2</sup>, which are the eigenvalues of the mass matrix (4.18). Both are evaluated at the critical point of the potential, corresponding to the solution, where the axions and off-diagonal metric components vanish, while the diagonal ones and the exponential of the dilaton are equal to one. Note that thanks to the lemma in [1, Sec. 3.3], we know that adding more scalar fields, thus increasing the size of the mass matrix, can only lower its minimal eigenvalue. As a physics consequence, solutions are expected to be more unstable here than they were found to be in [5]. We also recall from Section 4.2.1 that the 4d theory used here is unlikely to be a low energy effective theory, but is rather a consistent truncation. Therefore, we analyse the stability using modes that are



not necessarily the lightest, but form an independent set with respect to other, truncated modes. Since the masses<sup>2</sup> obtained this way give upper bounds, our conclusions on instabilities should be sufficient.

We first discuss in Section 4.5.1 the appearance of flat directions in the various solution classes defined in Chapter 2. We then turn successively to the stability of de Sitter, Minkowski and anti-de Sitter solutions, in the respective sections 4.5.2, 4.5.3 and 4.5.4.

### 4.5.1 Flat directions

Compared to the partial stability analysis of [5], a new phenomenon is here the presence of massless modes in the spectrum of all de Sitter, Minkowski or anti-de Sitter solutions in certain solution classes. This should be distinguished from the massless mode discussed in the Massless Minkowski Conjecture [5], systematically observed to be present for Minkowski solutions among the fields  $(\rho, \tau, \sigma_I)$ , but not in de Sitter or anti-de Sitter solutions.

Massless modes observed in solution classes for any cosmological constant can naturally be interpreted as being flat directions. Indeed, specifying a solution class fixes the orientifolds, it thus determines a set of scalar fields and their generic potential, independently of the cosmological constant. We verify this interpretation by explicitly identifying scalar fields that do not appear in the generic potential of their solution class. We list those in Table 4.3 for the solution classes to be considered in the subsequent stability analysis, and in Table 4.4 for the remaining 13 classes of solutions.

Class	$s_{55}$	$s_{555}$	$s_{66}$	$s_{6666}$	$m_{46}$	$m_{466}$	$m_{55}$	$m_{5577}$
Flat dir. field	$C_6$ (1)	$C_6$ (1)	$C_5$ (1)	$\emptyset$	$C_5$ (3)	$C_5$ (1)	$C_6$ (1)	$\emptyset$

Table 4.3: We consider all solution classes of [4] for which the stability of a solution will be analysed in Section 4.5. For each of them, the dimensional reduction described in Section 4.2.2 provides a finite set of fields  $\{\varphi^i\}$  and a scalar potential  $V$ . We list in this table the fields  $\varphi^i$  such that  $\partial_{\varphi^i} V = 0$  generically: this means  $\varphi^i$  is a flat direction. While we actually provide in the table a  $p$ -form, the number in parentheses corresponds to the amount of its components remaining after the orientifold projections, thus to the number of scalar fields being generic flat directions in the solution class.

The flat directions identified in Table 4.3 correspond to some RR axions. So they can indeed be distinguished from the Minkowski massless mode conjectured to be among  $(\rho, \tau, \sigma_I)$ . It is easy to understand why these axions do not appear in their scalar potential. In type IIB,  $C_6$  could only enter the potential (4.15) through an  $F_7$ -flux (the dual of a 4d  $F_3$ -flux): it would appear through a term proportional to a geometric flux coming from  $dC_6$ . This 6d 7-form is however obviously vanishing. Therefore  $C_6$  only appears in kinetic terms as a fluctuation, and is then a flat direction.  $F_3$  and thus  $C_6$  are however odd under an  $O_7$  involution, so  $C_6$  has to be projected out by an  $O_7$ , as in  $m_{5577}$ . On the contrary, in type IIA,  $C_5$  can appear in the potential (4.14) through  $F_6$ , the dual of a spacetime-filling  $F_4$ . A potential term for  $C_5$  would appear through  $dC_5$ , a maximal 6d form proportional to  $\sum_a f^a{}_{ab}$ . We however require the latter sum to vanish (implemented in our ansatz)

due to the 6d compactness. So (all components of)  $C_5$  are also flat directions.  $C_5$  is odd under an  $O_6$ -plane involution: one then verifies that four  $O_6$ -planes as placed in  $s_{6666}$  project out all  $C_5$  scalar fields. The absence of these flat directions in  $s_{6666}$  and  $m_{5577}$ , as indicated in Table 4.3, is consistent with the observation in the next subsections that the only solutions without massless mode belong to these two classes.

Class	$s_3$	$s_7, m_7$	$s_4, m_4$	$s_5, m_5$	$s_6, m_6$	$s_{77}, m_{77}$	$m_{66}$	$m_{57}$
Flat dir. field	$C_4$ (15)	$\emptyset$	$C_5$ (5)	$C_6$ (1)	$C_5$ (3)	$C_4$ 3456	$C_5$ (1)	$\emptyset$

Table 4.4: Analogous table to Table 4.3, indicating flat directions for the other 13 classes of [4], for completeness. For  $s_{77}$  and  $m_{77}$ , with  $O_7$  placed along internal directions 1234 and 1256, only one of the three  $C_4$  components is a flat direction.

To those generic flat directions in solution classes, one may add more flat directions appearing when setting to zero (generically, or even in a solution) some contribution to the scalar potential, e.g. a background flux. Let us consider as an example  $C_4$ , which only appears in the potential (4.15) through  $F_5$ , i.e. as  $dC_4$  proportional to  $f^a{}_{[bc}C_{4def]a}$ . In  $s_{55}$ , as indicated in (4.3), the following  $C_4$  components are possible:  $C_4$  1356,  $C_4$  1456,  $C_4$  2356,  $C_4$  2456. The allowed structure constants (by  $O_5$  projections) that could contribute to the potential of  $C_4$  are then  $f^a{}_{bc}$  with  $a = 5, 6, bc = 13, 14, 23, 24$ . As a consequence, if one considers as a “subclass” of  $s_{55}$  the one with these 8  $f^a{}_{bc}$  vanishing, then one gets “generically” in this subclass the 4 axions of  $C_4$  being flat directions. The Minkowski solution  $s_{55}^0 1$  can be viewed as part of such a subclass, since these 8 structure constants vanish in this solution.

This analysis of flat directions will help us understanding some of the massless modes appearing in the following. To conclude, let us add a remark: RR axions enjoy a continuous shift symmetry in supergravity that is broken in string theory to a discrete shift symmetry. This makes their moduli space compact and one in principle does not have to stabilize them for phenomenology. Unless one breaks this symmetry by appropriate fluxes one expects that these axions will remain flat directions at the perturbative level. Non-perturbative effects are however generically leading to a sinusoidal potential for these axions (see for example [151, Sec. 2]). The size of these effects is model dependent and we will not study it here.

#### 4.5.2 De Sitter solutions

We compute for each de Sitter solution the mass spectrum with MSSV. We report in Table 4.5, 4.6 and 4.7 the values of the  $\eta_V$  parameter, comparing them to the values obtained with the restricted set of fields  $(\rho, \tau, \sigma_I)$ . We also give the number of massless modes and the number of tachyons. Those can be compared to the total number of fields in each class (Table 4.1) and the number of generic flat directions (Table 4.3).

## Chapter 4. Consistent truncations and stability

class	$s_{66}^+$	$s_{6666}^+$				$m_{46}^+$			
solution	1	1	2	3	4	1	2	3	4
$-\eta_V$ [5]	3.6170	18.445	2.6435	2.3772	3.6231	3.6764	3.7145	2.2769	2.8266
$-\eta_V$	3.7405	20.836	2.8604	4.7167	3.8438	4.0177	4.0679	3.6681	3.6321
$m^2 \leq 0$	$1^-, 4^0$	$1^-, 0^0$	$2^-, 0^0$	$1^-, 1^0$	$1^-, 1^0$	$2^-, 4^0$	$1^-, 4^0$	$2^-, 4^0$	$2^-, 4^0$

class	$m_{46}^+$					
solution	5	6	7	8	9	10
$-\eta_V$ [5]	0.36462	3.0124	2.0672	2.3554	2.6418	1.2539
$-\eta_V$	5.1535	3.7518	3.5399	5.9109	3.8699	8.1124
$m^2 \leq 0$	$2^-, 4^0$	$1^-, 4^0$	$2^-, 4^0$	$2^-, 4^0$	$2^-, 4^0$	$1^-, 4^0$

Table 4.5: Spectrum information for each de Sitter solution in type IIA. We first provide the value of  $-\eta_V$  for the fields  $(\rho, \tau, \sigma_I)$  obtained in [5], then the one obtained here with the complete set of scalar fields of the above dimensional reduction. By  $i^-, j^0$ , we also indicate the number  $j$  of massless modes and  $i$  of tachyons.

class	$s_{55}^+$								
solution	1	2	3	4	5	6	7	8	9
$-\eta_V$ [1]	2.8544	2.7030	2.9334	2.8966	2.9703	2.9146	2.5101	2.7790	2.2494
$-\eta_V$	3.9131	3.8971	3.9214	3.9370	3.9022	3.9063	3.8974	3.8532	3.9062
$m^2 \leq 0$	$1^-, 4^0$	$2^-, 4^0$	$1^-, 4^0$	$1^-, 4^0$	$1^-, 4^0$	$1^-, 4^0$	$2^-, 4^0$	$1^-, 4^0$	$2^-, 4^0$

class	$s_{55}^+$								
solution	10	11	12	13	14	15	16	17	18
$-\eta_V$ [1, 65]	2.0908	2.9354	2.7548	2.9518	1.7067	2.9336	2.8404	2.8748	-3.7926
$-\eta_V$	2.7609	3.9209	3.5411	3.5950	4.0847	4.2994	3.7656	3.7224	17.5906
$m^2 \leq 0$	$2^-, 4^0$	$1^-, 4^0$	$2^-, 4^0$	$1^-, 4^0$	$1^-, 4^0$	$1^-, 4^0$	$1^-, 4^0$	$1^-, 4^0$	$2^-, 4^0$

class	$s_{55}^+$								
solution	19	20	21	22	23	24	25	26	27
$-\eta_V$ [65]	0.12141	1.3624	1.7813	1.0525	1.2253	0.95955	0.90691	1.0438	1.1172
$-\eta_V$	2.5948	6.4415	4.3007	2.4940	4.0269	2.7322	3.0085	3.9184	3.9970
$m^2 \leq 0$	$2^-, 4^0$	$1^-, 4^0$	$1^-, 4^0$	$2^-, 4^0$	$2^-, 4^0$	$2^-, 4^0$	$2^-, 4^0$	$2^-, 4^0$	$2^-, 4^0$

Table 4.6: Spectrum information for each de Sitter solution in type IIB. We first provide the value of  $-\eta_V$  for the fields  $(\rho, \tau, \sigma_I)$  obtained in [1, 65], then the one obtained here with the complete set of scalar fields of the above dimensional reduction. By  $i^-, j^0$ , we also indicate the number  $j$  of massless modes and  $i$  of tachyons.

Let us start our comments by mentioning that all de Sitter solutions are perturbatively unstable, i.e. tachyonic, in agreement with Conjecture 2 of [70]. It is even true for the special solution  $s_{55}^+ 18$ : this solution was the only known perturbatively stable dS solution without a tachyon in the fields  $(\rho, \tau, \sigma_I)$  and we have now proven that it is actually

## 4.5 Stability analysis

class	$s_{55}^+$	$m_{55}^+$				$m_{5577}^+$			
solution	28	1	2	3	4	1	2	3	4
$-\eta_V$ [5]	3.2374	2.5435	2.6059	2.7126	3.3574	4.7535	3.5034	3.2722	3.1779
$-\eta_V$	3.7586	3.4316	3.4460	3.4221	3.8729	32.725	3.7931	3.8289	3.7733
$m^2 \leq 0$	$2^-, 4^0$	$2^-, 3^0$	$1^-, 3^0$	$2^-, 3^0$	$1^-, 3^0$	$2^-, 0^0$	$2^-, 0^0$	$1^-, 1^0$	$1^-, 1^0$

class	$m_{5577}^+$									$m_{5577}^{*+}$
solution	5	6	7	8	9	10	11	12	1	
$-\eta_V$ [5]	4.7957	4.9129	3.4210	3.5611	2.9333	2.9003	3.4806	2.8966	5.0483	
$-\eta_V$	5.0140	5.1358	3.7551	3.9213	3.7903	3.8044	3.9849	3.4820	5.2673	
$m^2 \leq 0$	$1^-, 1^0$	$1^-, 1^0$	$2^-, 0^0$	$1^-, 0^0$	$2^-, 0^0$	$2^-, 0^0$	$1^-, 0^0$	$2^-, 0^0$	$1^-, 1^0$	

Table 4.7: Spectrum information for each de Sitter solution in type IIB. We first provide the value of  $-\eta_V$  for the fields  $(\rho, \tau, \sigma_I)$  obtained in [5], then the one obtained here with the complete set of scalar fields of the above dimensional reduction. By  $i^-, j^0$ , we also indicate the number  $j$  of massless modes and  $i$  of tachyons.

unstable.<sup>6</sup> This stability does not survive the inclusion of the other scalar fields here. It becomes even strongly unstable, going from  $\eta_V \approx 3.8$  to  $\eta_V \approx -17.6$ . All other solutions are also very unstable with  $\eta_V < -1$ , most of them however with  $|\eta_V| \sim \mathcal{O}(1)$ . This situation is in agreement with the refined de Sitter conjecture of [62, 63]. Such values of  $\eta_V$  are in particular observed for solutions  $s_{55}^+ 19, 24, 25$ , and  $m_{46}^+ 5$ . Those four solutions all had  $|\eta_V| < 1$  with the restricted set of fields, giving hope that dedicated searches as in [65] could provide viable solutions for a slow-roll cosmological scenario; they now all verify  $\eta_V \lesssim -1$ . Still, we also observe that for most solutions, the value of  $\eta_V$  is not drastically modified when considering all the fields as here. There are a few notable exceptions to the latter, the most impressive change being observed for  $m_{5577}^+ 1$  going from  $\eta_V \approx -4.75$  to  $\eta_V \approx -32.7$ . We note that this solution is on a non-compact group manifold [5]. The solution  $s_{6666}^+ 1$ , which also has a very low value,  $\eta_V \approx -20.8$ , but does not go through a drastic change, is on a compact manifold. To summarize, all de Sitter solutions are now perturbatively unstable with  $\eta_V \leq -1$ , i.e. exhibit strong instabilities.

Another important aspect of the instabilities are the field directions of the tachyons. As conjectured in [108], the restricted set of fields  $(\rho, \tau, \sigma_I)$  always contains one tachyon, a claim verified in all solutions (except  $s_{55}^+ 18$  as mentioned above). Note that the tachyonic direction among these few fields varies, as studied in [65]. Interestingly, we observe here that some solutions have more than one tachyon, meaning that a new one appears, due to the new fields considered. Analysing the directions of the mass matrix eigenvectors, we can determine the fields responsible for the tachyons. Most of the time, a first tachyon (if not the only one) is essentially due to the dilaton and diagonal metric components: it is interpreted as the one previously seen, predominantly along  $(\rho, \tau, \sigma_I)$ . If there is a second tachyon, then the first one typically has the most negative mass squared and is

<sup>6</sup>As argued in [65], this uncommon stability could be related to the fact that the 6d group manifold is in that case non-compact.

often easily distinguished from the other one, predominantly along RR and NSNS axions. This becomes striking in solutions  $m_{5577}^+$  9, 10, which have one quasi-massless tachyon predominantly along  $C_4$ , the other tachyon being the previously known one.

The distinction between tachyons becomes less clear for solutions  $s_{55}^+$  18 – 27: there the two  $m^2 < 0$  have similar values, and important contributions of diagonal metric components can be found in both tachyonic directions. This different behaviour of the spectrum may not come as a surprise, since these solutions were all found looking precisely for very specific tachyons [65]. The same phenomenon ( $m^2$  values become close, relevant diagonal metric and dilaton contributions in both tachyons) occurs for solutions  $m_{46}^+$  3 – 5, 7 – 9,  $m_{55}^+$  3 and  $m_{5577}^+$  12. Finally we note that  $s_{6666}^+$  2 and  $m_{5577}^+$  1, 2, 7 exhibit the same mixed contributions in the tachyons, with however two fairly separate negative  $m^2$ .

It would be interesting to relate these differences in the spectrum to specific features of the solutions. Even though this would deserve more study, we note already that almost all solutions which have more than one tachyon are on non-compact manifolds [5]. The only exceptions are  $s_{55}^+$  19, 22 – 27 which were however found with non-generic, dedicated searches. This observation should be related to the discussion of massless scalar fields, that we now turn to.

Last but not least, we observe the appearance of massless modes; none had been observed before within  $(\rho, \tau, \sigma_I)$ . Massless modes have been discussed already in Section 4.5.1 on flat directions. As indicated in Table 4.3, solution classes  $s_{55}$  and  $m_{55}$  admit (the only component of)  $C_6$  as a flat direction. We recover it here as systematically contributing to the massless modes eigenvectors. The other contributions to these eigenvectors in type IIB classes are (some of) the  $C_4$  components. For the solutions  $s_{55}^+$ , there are always 4 massless modes: one is due to  $C_6$  and the others to combinations of 3 of the 4  $C_4$  components. We see a priori no reason to choose some component of  $C_4$  and not the others. Nevertheless, in  $s_{55}^+$  12 – 17, 22 – 28, only  $C_4$  1356,  $C_4$  1456,  $C_4$  2456 appear in massless modes, while  $C_4$  2356 appears in tachyons. Similarly, in  $s_{55}^+$  10, 11,  $C_4$  1456,  $C_4$  2356,  $C_4$  2456 appear in massless modes and  $C_4$  1356 in tachyons. This is a surprising asymmetry. More generally, we suspect that combinations of 3  $C_4$  components are (non-generic) flat directions of  $s_{55}^+$  as discussed in Section 4.5.1, maybe because of  $F_5 = 0$  in all solutions considered. Another surprising observation is the presence of only 3 massless modes in  $m_{55}^+$  solutions, while the same fields are present to start with as in  $s_{55}^+$ . Again, those are due to  $C_6$  and combinations of  $C_4$  components. The reduction from 4 to 3 massless modes going from  $s_{55}^+$  to  $m_{55}^+$  could be due to a different (non-closed)  $F_1$ -flux in the latter, because of the presence of  $D_7$ -branes. Finally, in  $m_{5577}$ ,  $C_6$  is projected out and only 2 components of  $C_4$  remain. The massless mode observed there in some solutions is a combination of these 2  $C_4$  components, but it is also worth noting that some solutions  $m_{5577}^+$  do not have any massless mode. It would be interesting to understand why, and more generally, determine combinations of  $C_4$  components being flat directions in (subclasses of) type IIB.

Turning to type IIA, we observe the “T-dual” behaviour, as already discussed for the number of fields in each class around Table 4.1:  $s_{66}^+$  and  $m_{46}^+$  have 4 massless modes as  $s_{55}^+$ , while  $s_{6666}^+$  solutions have 1 or no massless mode, as  $m_{5577}^+$ . The class  $s_{66}$  allows for 1  $C_5$  component which is a flat direction; the other massless modes are due here to a

combination of  $C_3$  components (6 are allowed). In  $m_{46}$ ,  $C_5$  has 3 components, all flat directions. The remaining massless mode is a combination of 1, 2 or 3 components of  $C_3$  among the 4 allowed. Finally in  $s_{6666}$ ,  $C_5$  is projected out and  $C_3$  has 4 components. The massless mode observed for some solutions is a combination of 2  $C_3$  components. As for type IIB, it would be interesting to prove that combinations of  $C_3$  can in type IIA subclasses be flat directions.

After this stability analysis, one may wonder whether there is a de Sitter solution which is more promising, phenomenologically, than others. If we stick to basic requirements of compactness of the 6d manifold and the absence of massless mode, we note a surprising (and disappointing) correlation. All solutions of  $m_{5577}^+$  with one massless mode are precisely those on a compact manifold, while those without massless mode are on non-compact ones. Similarly, the 4  $m_{55}^+$  solutions with only three massless modes (instead of the four of  $s_{55}^+$ ) are on non-compact manifolds. Regarding type IIA,  $s_{6666}^+$  3, 4 which have one massless mode are as well on a compact manifold, while  $s_{6666}^+$  2 which has none is on a non-compact one. The only exception would be  $s_{6666}^+$  1, having no massless mode on a compact manifold. This seems to come however at the cost of a very strong instability:  $\eta_V \approx -20.8$ . Finding phenomenologically appealing de Sitter solutions would thus require more efforts. Let us nevertheless give a word of caution on these phenomenological interpretations, because of the distinction between low-energy and consistent truncation mentioned in Section 4.2.1: for this warning we refer to the discussion at the end of Section 4.5.3 on Minkowski solutions. Let us also recall that massless axions could phenomenologically be less problematic, and corrections to our perturbative study may make them massive: see the discussion at the end of Section 4.5.1.

### 4.5.3 Minkowski solutions

The mass spectrum of each Minkowski solution is computed with `MSSV`. We report in Table 4.8 the number of massless modes and tachyons, comparing them to the number of them within the restricted set of fields  $(\rho, \tau, \sigma_I)$ . The total number of fields in each class can be found in Table 4.1 and that of generic flat directions in Table 4.3.

class	$s_{55}^0$	$s_{555}^0$				$m_{46}^0$		$m_{466}^0$	
solution	1	1	2	3	4	1	2	1	2
$m^2 \leq 0$ [5]	$0^-, 1^0$	$0^-, 1^0$	$0^-, 1^0$	$0^-, 1^0$	$0^-, 1^0$	$0^-, 1^0$	$0^-, 2^0$	$0^-, 2^0$	$0^-, 2^0$
$m^2 \leq 0$	$0^-, 7^0$	$2^-, 2^0$	$0^-, 3^0$	$0^-, 3^0$	$0^-, 3^0$	$1^-, 6^0$	$1^-, 7^0$	$0^-, 3^0$	$0^-, 3^0$

class	$m_{466}^0$			
solution	3	4	5	6
$m^2 \leq 0$ [5]	$0^-, 2^0$	$0^-, 2^0$	$0^-, 2^0$	$0^-, 2^0$
$m^2 \leq 0$	$1^-, 3^0$	$1^-, 3^0$	$0^-, 3^0$	$0^-, 3^0$

Table 4.8: Spectrum information for each Minkowski solution in type IIA/B. We indicate by  $i^-, j^0$  the number  $j$  of massless modes and  $i$  of tachyons, first for the fields  $(\rho, \tau, \sigma_I)$  as obtained in [5], and then for the complete set of scalar fields considered here.

In [5] the Massless Minkowski Conjecture was proposed: it postulates the systematic presence of a massless scalar field among  $(\rho, \tau, \sigma_I)$ . This was verified for all the solutions we consider here. While including new fields, we observe here the appearance of more massless modes. A first explanation for those are the flat directions due to RR axions, indicated in Table 4.3. This interpretation is perfectly verified for  $m_{466}^0$  solutions: while they had 2 massless modes among  $(\rho, \tau, \sigma_I)$ , we observe here a third one, with field directions in the 3 eigenvectors being purely among the diagonal metric, the dilaton, and  $C_5$  (the flat direction). Let us recall that massless modes form a degenerate eigenspace, so the exact field directions of each eigenvector is not a relevant information, the eigenvectors are provided in random combinations. In  $m_{46}^+$ , eigenvectors are along diagonal metric components and the dilaton as in previous massless modes, together with the 3  $C_5$  components (flat directions) and some of  $B_2, C_3$  and off-diagonal metric components. In type IIB, the same holds for  $s_{55}^0 1$  with contributions to massless modes from diagonal metric components, the dilaton and  $C_6$  (the flat direction), as well as  $C_2$  and  $C_4$ . In these last two examples, it would be interesting, as for de Sitter solutions, to understand why extra axions contribute to massless modes. For  $s_{55}^0 1$ , the interpretation is again clear, with the same previously known contributions and that of  $C_6$ , the flat direction. Finally,  $s_{55}^0 2 - 4$  provide an interesting novelty: all three massless modes are along  $C_6$ , the diagonal metric components and the dilaton. This means that there is one additional massless mode along diagonal metric components and the dilaton, not seen previously with  $(\rho, \tau, \sigma_I)$ : we verify this by noticing that the eigenvectors distinguish  $g_{55}$  and  $g_{66}$ , while those are not distinguished with  $(\rho, \tau, \sigma_I)$  and a set of  $O_5/D_5$  along directions 56. The presence of this extra massless mode makes sense, given that the T-dual source configuration in  $m_{466}^0$  has 2 massless modes among  $(\rho, \tau, \sigma_I)$ . This extra mode seems to become tachyonic for  $s_{55}^0 1$ , a discussion we now turn to.

A surprise in the spectrum of Minkowski solutions are indeed tachyonic directions. In addition to diagonal metric and dilaton contributions, the eigenvectors are along off-diagonal metric and  $C_2$  components in  $s_{55}^0 1$ , off-diagonal metric and  $C_3$  components in  $m_{46}^0 1, 2$ , and off-diagonal metric components in  $m_{466}^0 3, 4$ . We do not have a clear understanding of their appearance. Let us note however that  $s_{55}^0 1$  and  $m_{46}^0 1$  have non-compact 6d manifolds, and the compactness has not been established for  $m_{46}^0 2$  and  $m_{466}^0 3$  [5]; this may allow to discard these solutions. The solution  $m_{466}^0 4$  seems however to be on a compact group manifold; maybe the detailed lattice ensuring this compactness should still be investigated.

More generally, we conclude that the Massless Minkowski Conjecture is still verified. However, its strong version [5] is in tension with the present results: indeed, it states the absence of 4d tachyonic directions in Minkowski solutions. Nevertheless, one should be careful with the interpretation of this strong version of the conjecture. The latter might indeed be applied more strictly to low-energy effective theories of quantum gravity, while the present consistent truncation is probably not such an effective theory. If a low-energy truncation would keep less modes, the resulting spectrum would be different. In particular, it could avoid the phenomenon of “space invaders”, where including a priori more massive modes leads to having smaller (or even tachyonic) masses. If this is avoided, the strong version of the Massless Minkowski Conjecture may still hold.

The strong version also refers to other swampland conjectures, and as such could be



more sensitive to the connection to string theory. We then note that the validity of the solution  $m_{466}^0$  as a classical string background has not been tested; this requirement combined with that of the existence of a lattice ensuring the 6d compactness can be challenging [2]. It could then turn out that the present work does not provide any counter-example to that conjecture; we hope to come back to these matters in future work.

#### 4.5.4 Anti-de Sitter solutions

We compute for each anti-de Sitter solution the mass spectrum with MSSV. We report in Table 4.9 on the values of the  $\eta_V$  parameter, comparing them to the value obtained with the restricted set of fields  $(\rho, \tau, \sigma_I)$ . We also give the number of massless modes and that of tachyons, obtained with  $(\rho, \tau, \sigma_I)$  and obtained here. The total number of fields in each class can be found in Table 4.1 and the number of generic flat directions in Table 4.3.

class solution	$s_{55}^-$				$m_{46}^-$				
	1	2	3	4	1	2	3	4	5
$\eta_V$ [5]	0.77850	-4	-3.8495	-2.4901	1.2531	1.5483	1.5537	1.3004	1.2548
$\eta_V$	1.1436	2.5632	2.1117	2.7870	1.9213	1.9873	2.0293	1.8554	2.1590
$m^2$ [5]	$1^{\text{BF}}, 0^0$	$0^{\text{BF}}, 0^0$	$0^{\text{BF}}, 0^0$	$0^{\text{BF}}, 0^0$	$1^{\text{BF}}, 0^0$	$1^{\text{BF}}, 0^0$	$1^{\text{BF}}, 0^0$	$1^{\text{BF}}, 0^0$	$1^{\text{BF}}, 0^0$
$m^2$	$1^{\text{BF}}, 5^0$	$1^{\text{BF}}, 6^0$	$1^{\text{BF}}, 6^0$	$1^{\text{BF}}, 6^0$	$2^{\text{BF}}, 4^0$	$1^{\text{BF}}, 4^0$	$1^{\text{BF}}, 5^0$	$1^{\text{BF}}, 6^0$	$1^{\text{BF}}, 6^0$

Table 4.9: Spectrum information for each anti-de Sitter solution in type IIA/B. We first provide the value of  $\eta_V$  (note the definition and sign convention in (4.19)) for the fields  $(\rho, \tau, \sigma_I)$  obtained in [5], then the one obtained here with the complete set of scalar fields of the above dimensional reduction. By  $i^{\text{BF}}, j^0$ , we also indicate the number  $j$  of massless modes and  $i$  of tachyons (those with  $m^2$  below the BF bound).

Let us first recall that for anti-de Sitter solutions, a 4d perturbatively stable scalar field has a mass  $m$  verifying the Breitenlohner-Freedman (BF) bound

$$m^2 > -\frac{9}{4l^2} \quad \Rightarrow \quad \eta_V < \frac{3}{4}, \quad (4.27)$$

with the anti-de Sitter radius  $l$  (see e.g. [5, Sec. 3.4.3]). Most solutions were already found unstable within the fields  $(\rho, \tau, \sigma_I)$ , as can be seen in Table 4.9. For these unstable solutions, the addition of fields only makes  $\eta_V$  slightly larger, i.e. the solution more unstable. Looking at the eigenvectors for their tachyonic mode, we do not easily identify the previous tachyon. Diagonal metric components and dilaton always contribute to it, with however  $C_2$  for  $s_{55}^-1$ ,  $B_2$  for  $m_{46}^-2, 3$ , or off-diagonal metric components for  $m_{46}^-5$ .<sup>7</sup> One of these solutions,  $m_{46}^-1$ , gets in addition a second tachyon. Both tachyons there get also very mixed contributions from the various fields.

Three other solutions,  $s_{55}^-2 - 4$ , were found to be perturbatively stable within the fields  $(\rho, \tau, \sigma_I)$ . These solutions admitted in addition, among these fields, only positive

<sup>7</sup>We note also for some of these solutions the appearance of other negative  $m^2$ , however not tachyonic. Their eigenvectors also get mixed contributions.



$m^2$ . Here, the addition of the new fields generates one tachyon for each of these solutions (and one additional negative  $m^2$  for  $s_{55}^-4$ ). There again, the eigenvectors get very mixed contributions. We conclude that all anti-de Sitter solutions are here found to be unstable (with tachyons partly along axions). Since masses squared below the BF bound are forbidden in supersymmetric anti-de Sitter solutions, we conclude that all the anti-de Sitter solutions above are non-supersymmetric, confirming this suspicion of [5]. The tachyons we found provide perturbative instabilities in agreement with the swampland conjecture of [68].

Another phenomenon when adding the new fields is the appearance of massless modes. In type IIB, the generic flat direction is  $C_6$ . In addition, massless modes are along  $B_2, C_2, C_4$  for  $s_{55}^-1$  and  $B_2, C_4$  for  $s_{55}^-2 - 4$ . In type IIA, the generic flat directions are the 3 components of  $C_5$ . In addition, massless modes are along  $C_3$  for  $m_{46}^-1, 2$ ,  $B_2, C_3$  for  $m_{46}^-3$ ,  $B_2, C_1, C_3$  for  $m_{46}^-4, 5$ . As for de Sitter and Minkowski solutions, it would be interesting to see whether these axionic massless modes are actually flat directions of solution subclasses.

## 4.6 Summary and outlook

In this chapter, we derived a 4d theory for compactifications of 10d type II string theory on 6d group manifolds. In particular, we obtained a scalar potential  $V$  and the kinetic terms. Our setting includes NSNS- and RR-fluxes as well as (smeared)  $O_p$ -planes and  $D_p$ -branes, and the metric fluxes associated to the group manifold. Once implemented numerically in the code `MSSV`, we used this scalar potential to prove that we actually perform a consistent truncation. We finally analysed the stability of 10d solutions with 4d maximally symmetric spacetimes.

We first described in Section 4.2.1 our truncation of the 10d fields, which consists in keeping the left-invariant scalar fields on the group manifold. As discussed there, those are not guaranteed to be the lightest fields (for generic group manifolds) but they are providing a consistent truncation before orientifolding [139]. It is expected that the same still holds after including orientifold planes, as shown in various examples. In Section 4.4, we proved explicitly that our truncation is consistent for all 21 solution classes of [4]; let us recall that these compactifications include orientifolds. To reach this result, we compared the 10d equations of motion provided by the code `MSSS` [4] and the 4d equations given by `MSSV`. Even though a consistent truncation may differ from a low energy truncation, it is sufficient for our purposes when studying the stability of solutions.

Based on this truncation, we derived in Section 4.2.2 a corresponding 4d theory starting with 10d type II supergravities with  $O_p/D_p$  sources. We got in particular the scalar potentials in equations (4.14) and (4.15), and computed the scalar kinetic terms. Those allowed to define the mass matrix in equation (4.18), that provided us with the 4d mass spectrum. This derivation is automated in the code `MSSV`, a Mathematica notebook presented in Section 4.3. This code further computes the mass spectrum for a given solution and related quantities characterising stability. This code was then used in Section 4.5.1 to identify generic flat directions in the various solution classes, that would appear as massless modes in the spectrum.

We finally turned in Section 4.5.2, 4.5.3 and 4.5.4 to the stability analysis of 10d solutions with 4d de Sitter, Minkowski or anti-de Sitter spacetimes, respectively. These solutions were obtained in [1, 4, 65], forming a convenient database. Their stability had only been analysed partially on a restricted set of fields denoted  $(\rho, \tau, \sigma_I)$  in [5], and we commented here on the comparison to the stability properties now observed when including all the left-invariant fields. A first result is that all de Sitter and anti-de Sitter solutions at hand are found unstable, despite several candidates found stable within the restricted set of fields. This is in agreement with various conjectures, as discussed in those sections. We also discussed at length the field directions of the tachyons: it is often possible to identify a previously observed tachyon among the fields  $(\rho, \tau, \sigma_I)$ , while the new fields, e.g. RR and NSNS axions, contribute to a different one. But in some instances, the contributions of the various fields are more mixed.

We also commented on the numerous massless modes that we observed: some correspond to the generic flat directions, but further contributions from other axions are often noticed. Those may signal further flat directions due to peculiarities of the solutions considered, e.g. some vanishing flux, that could be viewed as a solution subclass. For Minkowski solutions more specifically, we verified that the Massless Minkowski Conjecture [5] holds, but we also note that checking its strong version is more subtle, and we discussed it. In particular, requiring the compactness of the 6d manifold together with our supergravity solutions being in a classical string regime may not be achieved; this would remove potential counter-examples to this strong version.

In general, correlations are observed between the number of tachyons, of massless modes, or the value of the  $\eta_V$  parameter, and whether or not the 6d manifold is compact. (Non)-compactness is one feature of the solutions considered which could explain the differences observed; it would be interesting to identify others.

Several questions as well as opportunities are raised after this work, having now the code `MSSV` available; some ideas were already mentioned in the introduction. To start with, one may consider verifying that the truncation to left-invariant modes on group manifolds is a consistent truncation, in full generality. By this we mean allowing for any possible  $D_p$  source configuration without orientifold. Indeed, within our ansatz, compactifications with orientifolds have all been classified in [4], and we checked those here already. In turn, this restricts to anti-de Sitter solutions, according to Maldacena-Nuñez no-go theorem [33]: only those do not require orientifolds. While the same procedure could be followed combining the codes `MSSS` and `MSSV`, and we expect this to work, the challenge could be on the amount of equations and variables to consider, larger in absence of orientifold projection.

We suggested in the introduction to combine the search for 10d solutions performed with `MSSS` and the stability analysis done with `MSSV`. One could even consider using `MSSV` alone, i.e. the 4d scalar potential, to find new solutions. Their 10d origin would however require to satisfy further constraints, namely the flux Bianchi identities (or tadpole cancellation conditions) and the Jacobi identities on the geometric fluxes. This may still be a useful approach to find interesting critical points of the 4d potential, using new techniques such as gradient descent algorithms. This could be combined with requirements on stability or tachyonic directions, as e.g. in [65].

Last but not least, it would be interesting to rewrite the 4d theory obtained here

as a 4d (gauged) supergravity. This has been achieved in a variety of examples (see Section 4.2.1). We mentioned there in particular the approach using  $SU(3) \times SU(3)$  structures, allowing to reach a 4d  $\mathcal{N} = 2$  supergravity, or  $\mathcal{N} = 1$  with an orientifold projection. While this formalism is very appealing, it seems unfortunately not to apply to some of our solution classes, where we reach  $\mathcal{N} = 1$  via the specific placement of a  $D_p$ -brane (and not an  $O_p$ -plane). It is for instance the case for the 28 de Sitter solutions of  $s_{55}^+$ , where the source configuration ( $O_5$  along directions 12, 34,  $D_5$  along 56) preserves  $\mathcal{N} = 1$  supersymmetry in 4d. Formulating the corresponding 4d theory as an  $\mathcal{N} = 1$  supergravity seems then challenging, but we hope to come back to this question in future work.

# 5 Intricacies of classical de Sitter backgrounds

Within the swampland program, conjectures were proposed asserting that any theory of quantum gravity, like string theory, and its 4d low energy effective theories, cannot admit solutions with a (quasi) de Sitter space-time [79], at least in some limit [63, 80] that could correspond to a classical perturbative regime. In this chapter, we revisit this situation and claims in great detail on interesting examples. We focus on some of the 10d supergravity solutions admitting a 4d de Sitter space-time presented above, and we test to a rare extent all requirements for them to be a classical string background. Even though the solutions do not pass all tests, this detailed analysis should provide useful tools for such studies, as well as a better understanding of the mechanisms behind this apparent obstruction.

## 5.1 Motivations

Finding classical de Sitter solutions of string theory is usually done in two steps. First, one typically looks for solutions of 10d type II supergravities with a 4d de Sitter space-time and a compact 6d manifold  $\mathcal{M}$ . Such solutions with intersecting  $D_p$ -branes and orientifold  $O_p$ -planes were found on  $\mathcal{M}$  being a group manifold in [1, 74, 75, 89–92]. The second step is to verify that these supergravity solutions are classical string backgrounds, by satisfying a list of requirements, including a small string coupling  $g_s$  and a large 6d volume in units of the string length  $l_s$ . Studies on this topic were so far rather negative [70, 92, 152–154] despite possible loopholes, leading to the situation that no stringy classical de Sitter solution has been found, in line with the swampland conjectures. In ref. [1], we have obtained new de Sitter solutions of 10d type IIB supergravity with intersecting  $O_5/D_5$  sources, thus fulfilling the above first step. In the following sections, we provide a detailed 10d analysis of the second step, on two of these new solutions.

Group manifolds are characterised by an underlying Lie algebra with structure constants  $f^a{}_{bc}$ . The latter can be related to the spin connection coefficients of the 6d metric, as can be seen e.g. in the Maurer-Cartan equations  $de^a = -\frac{1}{2}f^a{}_{bc}e^b \wedge e^c$ . The  $f^a{}_{bc}$  then enter our 10d equations as variables. When looking for solutions in [1], we allowed for a maximal freedom in the  $f^a{}_{bc}$ , in a basis of one-forms  $e^a$  where the metric was  $\delta_{ab}$ . This simplified the search of solutions, but had the drawback of making the identification of the algebra and group manifold cumbersome. We typically got many non-zero structure constants, while Lie algebra representatives in classification tables

only have a few. Algebras of some solutions could still be identified, with an isomorphism to our sets of  $f^a{}_{bc}$ . We could then verify the existence of a lattice, a discrete action on the 6d group manifold that provides its compactness. Algebras and lattices are particularly simple for the de Sitter solutions 14 and 15 of [1], providing us, up to a change of basis, with a complete knowledge of their 6d geometry; we thus focus in the following on these two solutions. The details of these solutions can be found in Appendix B.1; these correspond to solutions  $s_{55}^+14$ ,  $s_{55}^+15$ , but in this chapter we keep the notation of [1] for consistency and simplicity since we merely consider solutions of the same class  $s_{55}^+$ .

To ensure that a 10d supergravity solution is a classical string background, we identify in practice five requirements to be met: a small  $g_s$ , large 6d radii  $r^{a=1,\dots,6}$  in units of  $l_s$ , quantization of fluxes, a fixed number of orientifolds  $N_{O_5}^I$ , and lattice quantization conditions. We believe these requirements are sufficient; whether they are necessary is discussed at the end of Section 5.7. The last three requirements need the detailed 6d geometry, so they were only partially checked on the solutions in [1]. We now complete the study for solutions 14 and 15. We summarize the requirements as follows

$$\begin{aligned} g_s \ll 1, \quad r^a \gg 1, \quad N_{q a_1 \dots a_q} \in \mathbb{Z}, \\ N_s^I \in \mathbb{Z}, \quad N_s^I \leq N_{O_5}^I, \quad N_a \text{ quantized}, \end{aligned} \quad (5.1)$$

where for simplicity, we will choose a hierarchy factor of 10, i.e.  $0 < g_s \leq 10^{-1}, r^a \geq 10$ . The index  $I = 1, 2, 3$  refers to the sets of internal dimensions ( $ab$ ) wrapped by the  $O_5/D_5$  sources:  $I = 1$  along (12),  $I = 2$  along (34),  $I = 3$  along (56). The number of sources along each set is defined as  $N_s^I = N_{O_5}^I - N_{D_5}^I$ . It enters the source contributions  $T_{10}^I$  to the equations of motion and Bianchi identities. Our solutions have non-zero fluxes  $F_1, F_3, H$ , giving the flux integers  $N_{q a_1 \dots a_q}$  along some of their components. Finally, the  $N_a$  are numbers entering the  $f^a{}_{bc}$ , quantized because of the lattice. The relations to the supergravity solution data (in the left-hand side below) go as follows

$$\begin{aligned} g_s F_{q a_1 \dots a_q} &= \frac{g_s \lambda N_{q a_1 \dots a_q}}{r^{a_1} \dots r^{a_q}}, \\ g_s T_{10}^I &= \frac{6 g_s \lambda^2 N_s^I}{r^{a_1 \perp I} \dots r^{a_{4 \perp I}}}, \quad f^a{}_{bc} = \frac{r^a \lambda N_a}{r^b r^c}, \end{aligned} \quad (5.2)$$

without sum on the indices, and the indices  $a_{\perp I}$  denote the directions transverse to the set  $I$ . The three types of supergravity variables (fluxes, source contributions, structure constants) are here expressed in units of  $2\pi l_s$ . The radii  $r^a$  are introduced through a normalisation convention of the one-forms  $e^a$  that we will come back to. The parameter  $\lambda > 0$  is an overall rescaling parameter of the solution that we are free to introduce. We refer to Section 4 of [1] for more details.

In the following, we test solutions 14 and 15, expressed in the appropriate basis, upon the requirements (5.1). To that end, we provide in Section 5.2 the material needed by first discussing the 6d geometry of the group manifold for solution 14. We give a basis of globally defined one-forms, determine lattice quantization conditions, and discuss the number of orientifolds. We determine the needed harmonic forms and related flux components. We then test in Section 5.3 the solution 14 upon the different constraints (5.1). As announced, it does not succeed in satisfying all of them, but we give explicitly various values obtained, allowing to evaluate how far the solution is from a classical string

background. The same procedure is followed in Section 5.4 for solution 15, for which the results are worse. We finally relate the problem of classical de Sitter solutions to that of scale separation in Section 5.5. We argue there that one should at best expect a bounded region in parameter space for both problems. We end with an outlook in Section 5.7.

## 5.2 6d geometry of solution 14

In this section, we present in detail the geometry of the 6d group manifold for our de Sitter solution 14. We also obtain the material needed to test, in the next section, the requirements (5.1) that would allow this solution to be a classical string background.

### 5.2.1 Foreword on the change of basis

As explained in the introduction, solutions 14 and 15 of [1] were found in a basis of one-forms associated to a 6d metric  $\delta_{ab}$ ,  $a = 1, \dots, 6$ , giving respectively 8 or 7 non-zero structure constants. As detailed in Section 2.3 and Appendix C of [1], a change of basis can be performed to new one-forms  $e^a = e^a_m dy^m$ , associated to a new “metric” denoted  $g_{ab}$

$$ds_6^2 = g_{mn} dy^m dy^n = g_{ab} e^a e^b . \quad (5.3)$$

The coordinates  $y^{m=1, \dots, 6}$  parameterize circles:  $y^m \in [0, 2\pi[$  and we require the identifications  $y^m \sim y^m + 2\pi$ . As we will see, the radii  $r^a > 0$  are inside the  $e^a_m$ . The metric  $g_{ab}$  has the interesting properties of being block diagonal along the pairs of  $a$ -indices (12), (34), (56), along which are the sources, and the determinant of these blocks is equal to 1. For both solutions, the new basis gives only 4 structure constants. The corresponding algebras are then easy to identify: solution 14 is on  $\mathfrak{g}_{3.5}^0 \oplus \mathfrak{g}_{3.5}^0$ , and solution 15 is on  $\mathfrak{g}_{3.4}^{-1} \oplus \mathfrak{g}_{3.4}^{-1}$ , using notations of [105]. Both admit lattices, allowing the group manifolds to be compact. We come back to those in detail below. The new one-forms were denoted with a prime in [1], and the solution data (flux components, structure constants, etc.) was given explicitly in Appendix A of [1] under the names solution 14' and 15'. We refer to Section 2.3 and Appendices A and C for more details on these solutions; in the rest of this chapter, we work in the new basis and drop the prime. We now focus on solution 14, while solution 15 is treated in Section 5.4.

### 5.2.2 Lattice, orientifolds

For solution 14, the 4 structure constants are given by

$$\begin{aligned} f^2_{35} &= -0.28930 , & f^3_{25} &= 0.013433 , \\ f^1_{64} &= -0.67154 , & f^6_{14} &= 0.41310 . \end{aligned} \quad (5.4)$$

This corresponds to two copies of the three-dimensional solvable algebra  $\mathfrak{g}_{3.5}^0$ . We rewrite them in terms of real positive numbers  $N_{1,2,3,6} > 0$  and the radii  $r^a$ , as in the following Maurer-Cartan equations

$$\begin{aligned} de^2 &= \frac{N_2 r^2}{r^3 r^5} e^3 \wedge e^5 , & de^3 &= -\frac{N_3 r^3}{r^2 r^5} e^2 \wedge e^5 , & de^5 &= 0 , \\ de^1 &= \frac{N_1 r^1}{r^4 r^6} e^6 \wedge e^4 , & de^6 &= -\frac{N_6 r^6}{r^1 r^4} e^1 \wedge e^4 , & de^4 &= 0 . \end{aligned} \quad (5.5)$$

## Chapter 5. Intricacies of classical de Sitter backgrounds

Let us focus on one of the two copies. As discussed below, an expression for globally defined one-forms is given by

$$\begin{aligned} e^2 &= r^2 \left( \frac{N_2}{N_3} \right)^{\frac{1}{4}} \left( \cos(\sqrt{N_2 N_3} y^5) dy^2 - \sin(\sqrt{N_2 N_3} y^5) dy^3 \right) , \\ e^3 &= r^3 \left( \frac{N_3}{N_2} \right)^{\frac{1}{4}} \left( \sin(\sqrt{N_2 N_3} y^5) dy^2 + \cos(\sqrt{N_2 N_3} y^5) dy^3 \right) , \\ e^5 &= r^5 dy^5 . \end{aligned} \tag{5.6}$$

Their normalisation is such that  $e^2 \wedge e^3 = r^2 r^3 dy^2 \wedge dy^3$ . The forms  $e^{2,3}$  can be written in terms of the rotation matrix

$$A(y^5) = \begin{pmatrix} \cos(\sqrt{N_2 N_3} y^5) & -\sin(\sqrt{N_2 N_3} y^5) \\ \sin(\sqrt{N_2 N_3} y^5) & \cos(\sqrt{N_2 N_3} y^5) \end{pmatrix} , \tag{5.7}$$

which plays an important role. One verifies that the one-forms  $e^a$  are globally defined, meaning invariant under  $y^5 \sim y^5 + 2\pi$ , thanks to a coordinate identification

$$(y)_{y^5+2\pi} = A(-2\pi) (y)_{y^5} , \tag{5.8}$$

where the 2-vector  $(y)$  stands for  $y^2, y^3$ . Such an identification is admissible if the entries of  $A(-2\pi)$  are integer (more generally, one may also allow for shifts of coordinates by multiples of  $2\pi$ ). This gives the lattice quantization conditions, and ensures at the same time that we have globally defined one-forms. We refer to [71] for more details. So here, a first possibility is to have  $\sqrt{N_2 N_3} \in \mathbb{N}^*$ . In that case, the coordinates are simply mapped to themselves, i.e. they are globally defined: one is back topologically to a torus  $T^6$ , with a non-Ricci flat metric. A second possibility is  $\sqrt{N_2 N_3} \in \mathbb{N} + \frac{1}{2}$ , where the rotation gluing acts as a  $\mathbb{Z}_2$  on the coordinates. Another possibility is  $\sqrt{N_2 N_3} \in \mathbb{N} + \frac{1}{4}$  that mixes  $y^2$  and  $y^3$ . These different lattices give rise to different topologies. We refer to [155] or [76] (sections 2.3 and 5) for more details on these geometries. Further discussions and Betti numbers can also be found in [155], as well as two more lattices involving constant shifts of coordinates, not included here. Ricci flat versions were recently considered in [66, 67].

In the case of a torus, with  $\sqrt{N_2 N_3} \in \mathbb{N}^*$ , each coordinate is that of a circle without further identifications. Our orientifold involution conditions can then be mapped to conditions on coordinates:  $\sigma(e^2) = e^2, \sigma(e^{3,5}) = -e^{3,5}$  are equivalent to  $\sigma(y^2) = y^2, \sigma(y^{3,5}) = -y^{3,5}$ , as can be seen through the forms (5.6). This involution action on coordinates is the standard one on circles, so the counting of fixed points is the usual one, i.e. 2 per transverse circle. This gives  $N_{O_5}^I = 2^4 = 16$ . In the following, having this lattice in mind, we will impose the bound  $N_s^I \leq 16$ . For the other, more complicated lattices, this bound could be lowered, but smaller values for  $N_s^I$  will as well be obtained.

### 5.2.3 Harmonic forms

With the above basis  $\{e^a\}$  of globally defined one-forms, we can now determine the harmonic 1- and 3-forms with constant coefficients <sup>1</sup>: those will be needed for flux

<sup>1</sup>Further harmonic forms can be obtained in the  $\{e^a\}$  basis with globally defined functions as coefficients, such as  $\cos(\sqrt{N_2 N_3} y^5)$ , etc.; we will not need those.

quantization. To that end, we look for all closed and co-closed 1- and 3-forms<sup>2</sup>. This is complicated due to the Hodge star, involving here the inverse metric (5.3) which has off-diagonal components  $g^{ab}$ . As a warm-up, let us consider the metric to be  $\delta_{ab}$ . In that case, one obtains  $e^4, e^5$  and  $e^1 \wedge e^4 \wedge e^6, e^1 \wedge e^5 \wedge e^6, e^2 \wedge e^3 \wedge e^4, e^2 \wedge e^3 \wedge e^5$ . These forms are representative of cohomology equivalence classes. Changing the metric to  $g_{ab}$  should not change these classes, since the latter are topological, so we should get the same number of forms. In addition, the representatives may only differ by an exact piece. This is what we obtain by an explicit computation: the 1-forms remain  $e^4, e^5$ , while the harmonic 3-forms with constant coefficients are now

$$\begin{aligned} \omega_1 &= e^1 \wedge e^4 \wedge e^6 + d o_1, \quad \omega_2 = e^2 \wedge e^3 \wedge e^5 + d o_2 \\ \omega_3 &= e^1 \wedge e^5 \wedge e^6 + d o_3, \quad \omega_4 = e^2 \wedge e^3 \wedge e^4 + d o_4, \end{aligned} \quad (5.9)$$

with the following exact pieces

$$\begin{aligned} o_1 &= \alpha f^1_{46} \left( e^1 \wedge e^2 + \frac{f^1_{46}}{f^3_{25}} g^{56} e^3 \wedge e^4 \right) \\ &\quad - \frac{\alpha f^1_{46} f^2_{35} g^{34} + g^{56}}{f^6_{14}} e^5 \wedge e^6 \\ o_2 &= \alpha f^2_{35} \left( -e^1 \wedge e^2 + \frac{f^2_{35}}{f^6_{14}} g^{34} e^5 \wedge e^6 \right) \\ &\quad - \frac{\alpha f^2_{35} f^1_{46} g^{56} + g^{34}}{f^3_{25}} e^3 \wedge e^4 \\ o_3 &= \frac{g^{12} f^3_{25}}{(f^6_{14})^2 + (f^3_{25})^2 (1 + (g^{12})^2)} e^3 \wedge e^6 \\ o_4 &= \frac{g^{12} f^6_{14}}{(f^6_{14})^2 + (f^3_{25})^2 (1 + (g^{12})^2)} e^3 \wedge e^6 \\ \text{where } \alpha &= \frac{g^{12}}{(f^2_{35})^2 + (f^1_{46})^2 (1 + (g^{12})^2)}. \end{aligned} \quad (5.10)$$

We verify that those are non-zero only because of the (inverse) metric off-diagonal components.

To perform the quantization, we will need to normalise these harmonic forms. Using the duality to the homology, and changing representatives of a same (co)homology class, we have the following equalities

$$\begin{aligned} \int_{\Sigma_3} \omega_1 &= \int_{\tilde{\Sigma}_3} e^1 \wedge e^4 \wedge e^6 = r^1 r^4 r^6 \int \int \int_0^{2\pi} dy^1 \wedge dy^4 \wedge dy^6 \\ &= (2\pi)^3 r^1 r^4 r^6, \end{aligned} \quad (5.11)$$

and the same holds for all four  $\omega_i$ . Indeed, the  $e^a \wedge e^b \wedge e^c$  involved are precisely those that give  $dy^m \wedge dy^n \wedge dy^p$  times an appropriate (constant) normalisation. This is consistent

<sup>2</sup>For a lattice that does not give a torus, some of the closed and co-closed forms may turn out not to be harmonic, because they are actually not globally defined; we refer to [155] on that point. This subtlety would only remove some flux components to quantize, i.e. lead to less constraints, so we do not consider this point any further.



with the formulas used so far for flux quantization, given that the only flux components that need to be quantized are those along harmonic forms. We have just verified here that these forms can be integrated, and the result is in agreement with the normalisation ansatz used so far, that relates the radii  $r^a$  to the integral of  $e^a$ . The formula (5.2) for the quantized flux can thus be consistently used on the harmonic components.

### 5.2.4 Flux quantization

Fluxes should be quantized if and only if they are harmonic forms. This condition comes from having a flux  $F = dA$ , where  $A$  is locally but not globally defined, i.e.  $F$  is closed but not exact, in other words harmonic. It is then the transition function or patching of the gauge potential  $A$  that gives the quantization condition. Let us consider the equations solved by the fluxes in our solutions

$$\begin{aligned} dF_1 &= 0, \quad d *_6 F_1 = 0, \quad dF_3 \neq 0, \quad d *_6 F_3 = 0, \\ dH &= 0, \quad d *_6 H \neq 0. \end{aligned} \quad (5.12)$$

$F_1$  is thus harmonic, while  $F_3$  and  $H$  are not but may contain pieces which are. Only the harmonic parts of these fluxes should be quantized. Doing such a proper flux quantization requires a good knowledge of the geometry, and in particular of the harmonic forms. The lack of such a knowledge for most solutions of [1] led us to quantize all flux components, as also done in the literature, but this is overconstraining. Here, using the harmonic 1- and 3-forms identified above for solution 14, we are able to express our fluxes within the general Hodge decomposition

$$F_q = F_{q \text{ harmo}} + dA + *_6 dB, \quad (5.13)$$

where  $F_{q \text{ harmo}}, A, B$  are globally defined forms. We obtain more explicitly for solution 14

$$\begin{aligned} H &= d(b_{13} e^1 \wedge e^3 + b_{24} e^2 \wedge e^4), \quad F_1 = F_{15} e^5, \\ F_3 &= F_{3\omega_1} \omega_1 + F_{3\omega_2} \omega_2 \\ &\quad + g_s^{-1} *_6 d(a_{12} e^1 \wedge e^2 + a_{34} e^3 \wedge e^4 + a_{56} e^5 \wedge e^6), \end{aligned} \quad (5.14)$$

where  $g_s$  is introduced for notation convenience, and

$$\begin{aligned} b_{13} &= -0.34083, \quad b_{24} = 0.99383, \quad g_s F_{15} = -0.27398, \\ g_s F_{3\omega_1} &= 0.12430, \quad g_s F_{3\omega_2} = 0.012539, \\ a_{12} &= 0.82025, \quad a_{34} = -2.0877, \quad a_{56} = -0.55448. \end{aligned} \quad (5.15)$$

We deduce that only three flux components need to be quantized:  $F_{15}, F_{3\omega_1}, F_{3\omega_2}$ . To that end, we use the normalisation (5.11) for the harmonic forms, which justifies the use of the initial formulas (5.2).

## 5.3 Checking requirements for a classical solution

With all the material obtained in the previous section, we are now ready to test solution 14 against the requirements (5.1). Given the supergravity solution data, namely

### 5.3 Checking requirements for a classical solution

the left-hand sides of (5.2), we need to find 8 real parameters  $(g_s, r^a, \lambda)$  and 8 integers  $(N_{15}, N_{3\omega_1}, N_{3\omega_2}, N_s^I, N_2N_3, N_1N_6)$ , that satisfy the constraints (5.1). The source contributions are given by

$$g_s T_{10}^1 = 10, \quad g_s T_{10}^2 = -0.088507, \quad g_s T_{10}^3 = -0.77652. \quad (5.16)$$

Solution 14 has the particularity of having  $T_{10}^2 < 0$ : this implies that among the  $N_s^I$ , an upper bound should only be imposed for  $I = 1$ . We recall from [1] that  $O_5$  may still be present in the set  $I = 2$ .

For a better comparison to the results of [1], we start by testing our solution without imposing the lattice conditions. We then get the following solution to the other constraints

$$\text{No lattice condition:} \quad (5.17)$$

$$\begin{aligned} r^1 &= 86.658, \quad r^2 = 272.28, \quad r^3 = 10.834, \quad r^4 = 18.142, \\ r^5 &= 198.25, \quad r^6 = 10.562, \quad \lambda = 789.30, \quad g_s = 0.068818, \\ N_{15} &= -1, \quad N_{3\omega_1} = 38, \quad N_{3\omega_2} = 135, \\ N_s^1 &= 16, \quad N_s^2 = -17, \quad N_s^3 = -14, \\ N_2 &= 0.0028913, \quad N_3 = 0.084801 = (0.015659)^2/N_2, \\ N_1 &= 0.0018814, \quad N_6 = 0.077905 = (0.012107)^2/N_1, \end{aligned}$$

where we give the highest products  $N_1N_6$  and  $N_2N_3$  obtained. Those remain far from  $1^2$ , but are less far from the other lattice allowing for  $(1/4)^2$ . We also obtain a solution to these constraints with  $N_s^1 = 14$ ,  $N_2N_3 = 1$  and  $N_1N_6 \approx 10^{-8}$ . Solutions with lower  $N_s^1$ , down to  $N_s^1 = 1$  can also be found. On the contrary, imposing lattice conditions (and the other requirements) without the bound on  $N_s^1$  leads us at best to  $N_s^1 = 50960$ , namely

$$\text{No orientifold bound:} \quad (5.18)$$

$$\begin{aligned} r^1 &= 57.907, \quad r^2 = 162.65, \quad r^3 = 10.014, \quad r^4 = 354.99, \\ r^5 &= 2999.3, \quad r^6 = 10.014, \quad \lambda = 186.97, \quad g_s = 0.099885, \\ N_{15} &= -44, \quad N_{3\omega_1} = 1370, \quad N_{3\omega_2} = 3280, \\ N_s^1 &= 50960, \quad N_s^2 = -1195, \quad N_s^3 = -1241, \\ N_2 &= 0.28572, \quad N_3 = 3.5000 = 1^2/N_2, \\ N_1 &= 0.22048, \quad N_6 = 4.5356 = 1^2/N_1. \end{aligned}$$

As expected, we can lower this  $N_s^1$  when rather verifying the other lattice quantization conditions

$$N_2 = 0.20794, \quad N_3 = 1.2023 = \left(\frac{1}{2}\right)^2/N_2, \quad (5.19)$$

$$N_1 = 0.10602, \quad N_6 = 2.3581 = \left(\frac{1}{2}\right)^2/N_1,$$

$$\text{and } N_s^1 = 13000,$$

$$N_2 = 0.56756, \quad N_3 = 0.11012 = \left(\frac{1}{4}\right)^2/N_2, \quad (5.20)$$

$$N_1 = 0.18581, \quad N_6 = 0.33636 = \left(\frac{1}{4}\right)^2/N_1,$$

$$\text{and } N_s^1 = 3219,$$

and the other quantities verifying their constraints. These values of  $N_s^1$  remain far too high.

Lattice conditions and the bound on  $N_s^I$  have however to be respected in any case for the compactification to make sense, and we should rather test the string regime through the values of  $g_s$  and the radii. Imposing all requirements but those on the radii, we find the solution

$$\begin{aligned}
 &\text{No large radius condition:} & (5.21) \\
 &r^1 = 7.4234, \quad r^2 = 4.0198, \quad r^3 = 0.24159, \quad r^4 = 1.9131, \\
 &r^5 = 16.164, \quad r^6 = 0.11150, \quad \lambda = 1.0076, \quad g_s = 0.097666, \\
 &N_{15} = -45, \quad N_{3\omega_1} = 2, \quad N_{3\omega_2} = 2, \\
 &N_s^1 = 14, \quad N_s^2 = -8, \quad N_s^3 = -18, \\
 &N_2 = 0.27890, \quad N_3 = 3.5855 = 1^2/N_2, \\
 &N_1 = 0.019150, \quad N_6 = 52.218 = 1^2/N_1.
 \end{aligned}$$

Two radii are substringy, i.e. smaller than 1. We can also bring all of them to be greater than 1, except  $r^6$  which gets lowered to 0.025984. We get as well  $r^{1,2,4,5} > 10$  at the cost of having  $r^3 = 0.032184$  and  $r^6 = 0.93577$ . Using the lattice with  $(1/4)^2$  does not change this situation. If rather we require large radii but relax the bound on  $g_s$ , we do not find any solution to the constraints (5.1). Note that a similar analysis and result has been obtained for a known de Sitter solution of type IIA supergravity in Section 6 of [74]. As there, we conclude that our de Sitter supergravity solution 14 cannot be made a classical string background.

## 5.4 Solution 15

The 4 structure constants of solution 15 are given by

$$\begin{aligned}
 f^2_{35} &= -0.60208, \quad f^3_{25} = -0.058853, \\
 f^4_{61} &= -0.10206, \quad f^6_{41} = -0.015345,
 \end{aligned} \tag{5.22}$$

giving two copies of the solvable algebra  $\mathfrak{g}_{3,4}^{-1}$ . We focus here on one. We rewrite it as

$$de^2 = \frac{N_2 r^2}{r^3 r^5} e^3 \wedge e^5, \quad de^3 = \frac{N_3 r^3}{r^2 r^5} e^2 \wedge e^5, \quad de^5 = 0, \tag{5.23}$$

with real positive numbers  $N_{2,3} > 0$ . Globally defined one-forms can be written as in (5.6) where one replaces the rotation matrix (5.7) by the following “weighted hyperbolic rotation matrix”

$$\begin{pmatrix} \cosh(\sqrt{N_2 N_3} y^5) & -\left(\frac{N_3}{N_2}\right)^{\frac{1}{2}} \sinh(\sqrt{N_2 N_3} y^5) \\ -\left(\frac{N_2}{N_3}\right)^{\frac{1}{2}} \sinh(\sqrt{N_2 N_3} y^5) & \cosh(\sqrt{N_2 N_3} y^5) \end{pmatrix}.$$

This gives the normalisation  $e^2 \wedge e^3 = r^2 r^3 dy^2 \wedge dy^3$ <sup>3</sup>. The above matrix evaluated at  $-2\pi$  provides again the lattice quantization conditions, by requiring the entries to be

<sup>3</sup>Slightly different expressions of the one-forms would allow for the same normalisation. In particular another one more analogous to (5.6) is possible, but it would not lead to an appropriate lattice quantization.

integers. We obtain [71]

$$\cosh(\sqrt{N_2 N_3} 2\pi) = n_1, \quad n_1^2 - n_2 n_3 = 1, \quad \frac{N_3}{N_2} = \frac{n_3}{n_2}, \quad (5.24)$$

for  $n_{1,2,3} \in \mathbb{N}^*$ . Note that  $n_2 = n_3$  is not a solution to these conditions, hence the need of the “weight” in the hyperbolic rotation.

The harmonic 3-forms with constant coefficients in  $\{e^a\}$  basis are formally the same as (5.9) and (5.10), up to the relabeling  $1 \leftrightarrow 4$ ,  $2 \leftrightarrow 3$ , and setting  $g^{56} = 0$ ; this is how we define  $\omega_{1,2}$  here below. This can be understood by looking at the algebras and the metrics. Similarly, the harmonic 1-forms are now  $e^1, e^5$ . We then obtain for this solution the following Hodge decomposition of the fluxes

$$\begin{aligned} H &= d(b_{24} e^2 \wedge e^4), \quad F_1 = F_{15} e^5, \\ F_3 &= F_{3\omega_1} \omega_1 + F_{3\omega_2} \omega_2 \\ &\quad + g_s^{-1} *_6 d(a_{12} e^1 \wedge e^2 + a_{34} e^3 \wedge e^4 + a_{56} e^5 \wedge e^6), \end{aligned} \quad (5.25)$$

where

$$\begin{aligned} b_{24} &= 0.0018085, \quad g_s F_{15} = 0.13944, \\ g_s F_{3\omega_1} &= 0.0014004, \quad g_s F_{3\omega_2} = 0.00013677, \\ a_{12} &= 1.0117, \quad a_{34} = 0.048104, \quad a_{56} = -0.15985. \end{aligned} \quad (5.26)$$

This gives again only three flux components to quantize. For completeness, we finally give the source contributions

$$g_s T_{10}^1 = 10, \quad g_s T_{10}^2 = 0.49663, \quad g_s T_{10}^3 = -0.10585. \quad (5.27)$$

We now test this solution as done above for solution 14. Without imposing the lattice conditions we obtain a first solution to the other requirements (5.1)

$$\begin{aligned} \text{No lattice condition:} & \quad (5.28) \\ r^1 &= 108.00, \quad r^2 = 47.861, \quad r^3 = 21.302, \quad r^4 = 12.912, \\ r^5 &= 25.270, \quad r^6 = 10.826, \quad \lambda = 2372.7, \quad g_s = 0.0014851, \\ N_{15} &= 1, \quad N_{3\omega_1} = 6, \quad N_{3\omega_2} = 1, \\ N_s^1 &= 15, \quad N_s^2 = 14, \quad N_s^3 = -3, \\ N_2 &= 0.0028540, \quad N_3 = 0.0014083, \\ N_4 &= 0.0038956, \quad N_6 = 0.00083305. \end{aligned}$$

We find other solutions down to  $N_s^1 = N_s^2 = 1$ . On the contrary, imposing the lattice quantization conditions is more difficult. Imposing no bound on the number of sources  $N_s^{1,2}$ , we can satisfy the other constraints if we trade the integer conditions for numbers greater than 1. We then get a solution with  $N_s^1 \approx 755.40$ ,  $N_s^2 \approx 1746.1$ , which remains too high. Finally, imposing only the lattice conditions, the bound on  $N_s^I$  and the flux quantization, to test the string regime on  $g_s$  and  $r^a$ , we could not find any solution. These results are worse than for solution 14. The de Sitter supergravity solution 15 cannot be made a classical string background.

## 5.5 Scale separation for de Sitter

In this section, we discuss the matter of scale separation, and its relation to the requirements for a string classical regime. Consider a 10d (anti-)de Sitter solution with 4d cosmological constant  $\Lambda$ , and a tower of Kaluza–Klein states of mass scale  $m_{KK}$  coming from the compactification on the 6d manifold. Having a 4d low energy effective theory, involving a finite number of degrees of freedom, is only possible if one truncates the tower of states by the 4d energy cutoff. This requires what is called scale separation, namely

$$\sqrt{|\Lambda|} \ll m_{KK} . \quad (5.29)$$

It means that the typical 4d energy scale can be decoupled from the 6d one. In view of phenomenology, it is important to know whether scale separation can be achieved.

In many anti-de Sitter solutions, scale separation can actually not be reached: see e.g. [156–160] for recent papers on this point, and [87, 88, 161, 162] and references therein for older related works. This has led to recent swampland conjectures [52, 60] forbidding scale separation (see also [78, 163, 164]). Interestingly, one classical counter-example exists, the so-called DGKT anti-de Sitter solution [86] (extended recently in [85, 165, 166]). The latter belongs to the general  $\mathcal{N} = 1$  SU(3)-structure AdS<sub>4</sub> class [167], as first shown in [168]. A criticism of this solution is the problem of “smeared” sources, and we refer to [1] for more references and discussion on this point. This example remains interesting here for two reasons. First, its framework is very analogous to ours: it is a classical 10d supergravity solution, on a torus, and its intersecting sources configuration is analogous to ours. Another similarity is the presence of flux integers not constrained through the tadpole or Bianchi identity: here these are the harmonic components of  $F_3$ , giving the  $N_{3\omega_i}$ . Secondly, the DGKT solution admits a parametric control (with asymptotic limit) on the scale separation, which is the same that governs the validity of the solution as a classical string background: the more classical (small  $g_s$ , large volume, etc.), the better the scale separation. This provides an example of a relation between these two important problems.

For de Sitter solutions, a similar relation was sketched in [70]. First, it was first shown there that a classical de Sitter solution requires a small 6d curvature scale  $|\mathcal{R}_6|$  compared to that of the average internal length  $2\pi r$ :  $|\mathcal{R}_6| \times (2\pi r)^2 \ll 1$ . This is a priori possible on some manifolds thanks to internal hierarchies and/or fine-tunings. In addition, such a hierarchy in a de Sitter solution was shown to automatically imply scale separation, in the sense of

$$\mathcal{R}_4 \ll \frac{1}{(2\pi r)^2} . \quad (5.30)$$

Let us test here scale separation with the de Sitter solution 14 in the case where we ignore lattice conditions (5.17): all other requirements for a classical solution are then satisfied. With these values and the  $\lambda$ -rescaling, we first compute (in units of  $2\pi l_s$ )

$$(\mathcal{R}_4 = 3.6370 \cdot 10^{-8}) < (1/(2\pi r)^2 = 1.1873 \cdot 10^{-5}) , \quad (5.31)$$

where  $r = (\prod r^a)^{\frac{1}{6}}$ . For completeness and illustration, we compute for this set of values

the square of the Planck mass in units of  $2\pi l_s$

$$\begin{aligned} (2\pi l_s)^2 \times M_p^2 &= \frac{(2\pi l_s)^2}{\kappa_{10}^2} \int_6 d^6 y \sqrt{|g_6|} g_s^{-2} = \frac{4\pi}{g_s^2} \prod_{a=1}^6 \frac{r^a}{l_s} \\ &= 2.5767 \cdot 10^{13} = (5.0761 \cdot 10^6)^2 . \end{aligned} \quad (5.32)$$

The scale separation condition (5.30) is verified, since we consider here hierarchies of order 10 per length. This result is however only preliminary, since the largest radius  $r^2$  gives a smaller value, as well as the 6d curvature

$$1/(2\pi r^2)^2 = 3.4167 \cdot 10^{-7} , \quad |\mathcal{R}_6| = 1.2162 \cdot 10^{-6} . \quad (5.33)$$

A tower of modes associated to the radius  $r^2$  would then be difficult to separate or truncate<sup>4</sup>. The internal hierarchy  $|\mathcal{R}_6| \times (2\pi r)^2 \ll 1$  is also not verified, due to the unsatisfied lattice conditions. The lack of complete classicality (in the sense of satisfying requirements (5.1)) seems here again related to difficulties in having scale separation.

Even though classical de Sitter solutions may admit scale separation, we do not expect the same parametric control as in DGKT. As expressed in [1], classical de Sitter solutions may not exist at parametric control in an asymptotic limit, but they could still be present in a bounded region of parameter space. In such a “grey zone”, parameters are large/small enough to accommodate a classical regime as in the requirements (5.1), but they remain bounded by these same constraints and cannot be taken asymptotically. At best, one may then have scale separation in this bounded region, controlled by a bounded parameter. In the following, we illustrate this idea with a simple transformation that allows us to move in parameter space. We use a scaling parameter  $\gamma > 1$  to act as follows on the entries in the right-hand sides of (5.2)

$$r^a \rightarrow \gamma^{x_a} r^a , \quad g_s \rightarrow \gamma^g g_s , \quad N_K \rightarrow \gamma^{n_K} N_K , \quad \lambda \rightarrow \lambda , \quad (5.34)$$

and we do not consider any quantized  $H$ -flux nor  $F_5$  above because there are none in solutions 14 and 15. The powers  $x_a, g, n_K$  and their signs are not fixed. However, we relate them in such a way that the left-hand sides of (5.2) remain invariant. Taking for simplicity  $\forall a, x_a = x$ , we get

$$n_{q=1,3} = qx - g , \quad n_s^I = 4x - g , \quad n_a = x . \quad (5.35)$$

By not affecting the quantities in the left-hand sides of (5.2), we are guaranteed to still have a solution to the 10d equations.  $\mathcal{R}_4$  is also invariant under this simple transformation. The 6d radii are however changed, so the ratio of the cosmological constant to a Kaluza–Klein mass goes as the latter, and the scale separation is improved with smaller  $r^a$ , i.e.  $x < 0$ . This specific  $\gamma$ -scaling then does not help in getting classical solutions, which rather require large radii. Such a situation where two requirements go in different parametric directions is common for classical de Sitter solutions, due to the many bounds to satisfy. This leads to the bounded region in parameter space, as we illustrate in table 5.1 with the different possible signs of  $x, g$ , corresponding to various parametric directions.

<sup>4</sup>The Kaluza–Klein spectrum on a group manifold can actually be more involved than a simple inverse radius dependence: see e.g. [122] and references therein for explicit spectra.

We see from table 5.1 that in any direction of the  $\gamma$ -scaling, a parameter bound is met. Some cases in this table were also observed in the explicit example in section III. The simple  $\gamma$ -scaling was considered here for the purpose of illustration. Other transformations may do better on some of the requirements, e.g. for the lattice conditions or the scale separation. Specificities of given solutions may also help. Nevertheless, it remains unlikely that an asymptotic limit would be opened in some parametric direction.

Another transformation worth being mentioned is the following  $\beta$ -scaling: it results in having  $f^a{}_{bc}$ ,  $g_s F_{q=1,3,5}$ ,  $H$  rescaled by  $1/\beta$  and  $g_s T_{10}^I$  by  $1/\beta^2$ , with  $\beta > 1$ . This mimicks the overall  $\lambda$ -rescaling introduced in [1] and leaves 10d equations invariant, thus guaranteeing a solution. It can be generated as follows, with  $\beta^{\frac{2}{3}} \in \mathbb{N}^*$

$$\begin{aligned} r^a &\rightarrow \beta^{\frac{1}{3}} r^a, \quad g_s \rightarrow \beta^{-\frac{2}{3}} g_s, \quad \lambda \rightarrow \lambda, \quad N_s^I \rightarrow N_s^I, \\ N_{1a} &\rightarrow N_{1a}, \quad N_{3abc} \rightarrow \beta^{\frac{2}{3}} N_{3abc}, \quad N_{Habc} \rightarrow N_{Habc}, \\ N_{5abcde} &\rightarrow \beta^{\frac{4}{3}} N_{5abcde}, \quad N_a \rightarrow \beta^{-\frac{2}{3}} N_a. \end{aligned} \tag{5.36}$$

Since  $\mathcal{R}_4$  scales as  $\beta^{-2}$ , the quantity  $\mathcal{R}_4 \times (2\pi r^a)^2$  scales as  $\beta^{-\frac{4}{3}}$ , meaning that the scale separation gets enhanced when the classical regime is better verified. This is an improvement with respect to the  $\gamma$ -scaling discussed above. Constraints on fluxes and sources remain satisfied, but this scaling will hit a bound due to the lattice conditions, as in the top right corner of table 5.1. Our conclusion of a bounded region for classical de Sitter is thus not altered, but this  $\beta$ -scaling could be interesting for anti-de Sitter solutions on a flat torus, if any. In particular, the exponent in the conjecture of [60] would be given by  $\alpha = \frac{1}{6}$ .

Let us also stress two differences with an anti-de Sitter solution, that are made more obvious with table 5.1. An anti-de Sitter solution would allow for all  $N_s^I \leq 0$ , in which case there is no upper bound on  $|N_s^I|$ , contrary to the above  $N_s^1 \leq N_{O_p}^1$ . In addition, in the DGKT anti-de Sitter solution, one has  $f^a{}_{bc} = 0$ , which is not possible for de Sitter solutions on group manifolds that require  $\mathcal{R}_6 < 0$ . The former thus does not face the lattice conditions. Removing these two constraints relieves bounds in parameter space.

To conclude, if a region of classical de Sitter solutions exists, we do not exclude that scale separation also takes place there. We believe however that it would be at best controlled by a bounded parameter, contrary to the DGKT solution and despite several similarities with that framework. Such a bounded region or grey zone with classical and scale separated de Sitter solutions remains to be found. As recalled in [1], an asymptotic limit for the 6d radii is not appropriate from a phenomenological point of view, since those should get bounded from above by observations. A conservative lower bound on the average mass  $1/(2\pi r)$  in (5.31) would be the LHC energy scale, namely 14 TeV. We now rewrite the formula (5.32) for the (reduced) 4d Planck mass as follows

$$\frac{l_s}{r} = \left( \frac{2\sqrt{\pi} l_p}{g_s r} \right)^{\frac{1}{4}} \geq 6.7188 \cdot 10^{-4}, \tag{5.37}$$

with the length  $2\pi l_p = 1/M_p$ . The lower bound in (5.37) is then obtained using the above LHC value and  $g_s \leq 0.1$ . From this perspective, the room for classicality is actually restricted. If one asks in addition for scale separation, and if  $\mathcal{R}_4$  should then match the scale of early universe inflation, most likely higher than the LHC scale, the range (5.37)

	$x > 0$	$x < 0$
$g < 0$	classical ✓, scale sep. ✗, fluxes, lattice ✓, sources ✗ ( $N_s^1 \leq N_{O_p}^1$ )	With $4x = g$ : classical ✗ ( $r^a$ bound), scale sep. ✓, fluxes, sources ✓, lattice ✗ (integer cond.)
$g > 0$	With $4x = g$ : classical ✗ ( $g_s$ bound), scale sep. ✗, lattice, sources ✓, fluxes ✗ (integer cond.)	classical ✗ ( $r^a, g_s$ bounds), scale sep. ✓, fluxes, sources, lattice ✗ (integer cond.)

Table 5.1: Starting with a de Sitter solution, we act with the  $\gamma$ -scaling (5.34), (5.35) on the parameters. We indicate with a ✓ or ✗ whether or not it helps in meeting the various requirements. When it does not, the limiting bound is written in parentheses. The “integer condition” bound refers to integer numbers having to be greater than 1. Since  $N_s^1$  is very constrained,  $1 \leq N_s^1 \leq N_{O_p}^1$  in a de Sitter solution, we restrict when possible to the scaling leaving this number invariant, namely  $4x = g$ .

gets even more restricted [169]. This is where having a warp factor and a varying dilaton could help with hierarchies, even though in the concrete setting of [170], the values were not drastically altered by such effect.

## 5.6 A word on smeared sources

Beyond the question of the classical regime, or the verification of compactness, the main criticism against our solutions is a standard one on intersecting sources: they are “smeared” [171–173]. Note that, contrary to  $D$ -branes, smearing  $O$ -planes is particularly prohibited, since by definition, an  $O$ -plane stands at a fixed point. It is worth noting that our solution 14 is special since it has  $T_{10}^2 < 0$ . This means that it can be interpreted as having  $O_5$ -planes only along the set  $I = 1$ , i.e. directions (12). It could then be interesting to localize first these sources, while those along orthogonal directions could remain as smeared branes.

We prefer to view our solutions as solving an integrated version of the equations, which trades functions (warp factor, dilaton) and distributions (source  $\delta$ -functions) for constants; see a discussion in [61]. The question remains whether a localized version exists; it would capture the backreaction of our  $O_p/D_p$ . This is a well-known supergravity problem [174–177]: while localized solutions exist for parallel sources, e.g. [170], they are most of the time unknown for intersecting ones (see however [178–180] in anti-de Sitter). It is also unclear whether finding a localized solution in supergravity is relevant: indeed, the backreaction of sources is a priori important only close to them, where stringy contributions should also be taken into account. In any case, it is often believed that this problem could be cured in full string theory. Interestingly, this question has reappeared recently in the context of the swampland, with the conjectures [52, 60]. The anti-de Sitter solution [86] is a counter-example to the latter. The main criticism against this solution



is again its non-localized intersecting sources. This has motivated a (partial) localization of this anti-de Sitter solution [165, 166]. It would be very interesting to study our de Sitter solutions with intersecting sources in this new light.

### 5.7 Outlook

In this chapter, we have tested whether two 10d supergravity de Sitter solutions of [1] could be promoted to classical string backgrounds. Having identified the requirements (5.1) to be met, we have derived all the necessary material to perform these checks, to a rare extent in the literature. Eventually, our solutions do not pass these tests, as they fail to satisfy simultaneously all requirements, despite partial positive results. We also discussed the relation of this problem to that of scale separation, and what one should expect on the latter for classical de Sitter solutions. We believe that the tools developed here and the explicit results obtained should be useful in future studies.

Whether supergravity solutions could be classical string backgrounds has already been partially analysed on de Sitter solutions of [1]. Solution 14 did not appear as the most favored one: four other solutions were doing better regarding the partial requirements imposed there. But for those, a complete knowledge of the 6d geometry was missing, preventing us to go further (see however the appendix here). It would be interesting to focus more on them, or more generally, to try with other solutions, possibly obtained from ours by small deformations or transformations, that could help in satisfying the requirements. A family of de Sitter solutions obtained by varying one parameter is depicted in Figure 1 of [91]. In such a family, one may eventually find a bounded region of classical solutions, as discussed in Section 5.5.

As it appears from this work, the question of whether one can obtain classical de Sitter solutions of string theory is not settled. Even though we have not found an example for now, our study highlighted how close one can get, and how involved these tests actually are. A related matter is the definition of the requirements for a classical solution: one may consider our requirements on  $g_s$  and the radii as conservative. Can one allow for slightly higher values of  $g_s$ ? What length or volume should actually be bigger than  $l_s$  on our group manifolds? Precise answers to these questions depend on the corrections to effective theories, and those are typically difficult to determine, especially away from a more standard Ricci flat compactification. If any room could be gained from this side, it would certainly be interesting.

TIME-DEPENDENT  
COMPACTIFICATIONS

PART II



# 6 Bird's eye view on time-dependent compactifications

## 6.1 Context and state of the art

As it has been emphasized in the previous chapters, obtaining realistic 4d cosmologies from the ten-dimensional supergravities that capture the low-energy limit of superstring theory has proven notoriously difficult. At the turn of the century, it was thought that accelerating cosmologies were as difficult to achieve as de Sitter space itself, being subject to a famous no-go theorem first discovered by Gibbons [31, 32] and later rediscovered by Maldacena-Nuñez [33] in a string-theory context. More precisely, a matter whose stress-energy tensor in the higher-dimensional theory implies  $R_{00} \geq 0$ , as a consequence of the Einstein equations, is said to satisfy the strong energy condition (SEC). The SEC implies that time-independent compactifications of the higher-dimensional theory can never lead to 4d cosmologies with accelerated expansion (which includes de Sitter space as a special case).<sup>1</sup>

However, as was first pointed out in [181], time-dependent compactifications evade the no-go and can lead to 4d Einstein-frame accelerated expansion for some period of time [182–187]. Such transient acceleration is in fact generic in flux compactifications, see [188] for a review, although de Sitter space is still ruled out by the SEC, if the time-independence of the 4d Newton's constant is obeyed in a conventional way [189]. If instead the time-independence of the 4d Newton's constant is obeyed in an averaged way, even de Sitter space is not ruled out by the SEC, although the so-called dominant energy condition does rule out non-singular de Sitter compactifications [190] (see also [191, 192] for a recent discussion on energy conditions).

In [189], Russo and Townsend greatly refined the no-go of [31–33]: one of their conclusions is that, even if one imposes the SEC and the time-independence of the 4d Newton's constant in a conventional way, late-time accelerating cosmologies are *not* ruled out. However, no late-time accelerating cosmologies from compactification of the ten- or eleven-dimensional supergravities arising as low-energy effective actions of string theory have ever been constructed. Indeed, the eternal accelerating cosmologies of [193, 194] are such that the acceleration of the scale factor tends to zero at future asymptotic infinity, so that there is no cosmological horizon.

---

<sup>1</sup>The no-go was also extended in [33] to the case of massive IIA supergravity, a theory which does *not* obey the SEC.

Ref. [187] reinterpreted the accelerating solutions of [181] from the point of view of a 4d theory with a scalar potential. It was found that there is always a big-bang singularity near which the scale factor behaves as a power law:  $S(T) \sim T^{\frac{1}{3}}$ , which does not lead to enough e-foldings for inflation [193, 195]. The transient acceleration of the solutions could, however, be used to describe the current cosmological epoch [186]. The general characteristics of one-field inflation with an exponential potential were studied in [196], while cosmologies from an effective theory with multiple scalar fields were studied in [197–199]. In particular, the analysis of [200] could be relevant for the swampland conjecture [79]. Cosmological solutions of gauged supergravities and F-theory have been studied in [74, 89, 90, 94, 95, 201–208].

## 6.2 Summary of the results

In the following chapters, we re-examine some of the previous statements in the context of *universal* cosmologies, obtained by compactification to 4d of 10d Type IIA supergravity (with or without Romans mass) on 6d Einstein, Einstein-Kähler, or Calabi-Yau (CY) manifolds. In this context, the term “universal” means that the ansätze that we consider do not depend on the detailed features of the manifold on which we compactify, but only on the properties which are common to all the manifolds belonging to that class. For example, our ansatz for the CY compactification exploits the existence of a holomorphic three-form and a Kähler form, but does not assume the existence of any additional harmonic forms on the manifold.

Our universal cosmologies are obtained by solving the *ten-dimensional* supergravity equations: we do *not* start from a 4d effective action. Nevertheless, it turns out that all of the resulting 10d equations of motion are obtainable from a 1d action where all fields only depend on a time coordinate. In other words, there is a 1d consistent truncation of the theory,  $S_{1d}$ . The fields in question are the dilaton  $\phi$  and two warp factors  $A, B$  (one for the internal and one for the external space), while, by virtue of our ansatz, all fluxes manifest themselves as constant coefficients in the potential of  $S_{1d}$ , cf. Table 7.1 below.

Moreover we show that a two-scalar 4d *cosmological* consistent truncation,  $S_{4d}$ , of the 10d theory to  $\phi, A$  is possible in certain special cases. In other words, every solution of cosmological Friedmann-Lemaître-Robertson-Walker (FLRW) type of  $S_{4d}$  uplifts to a solution of the ten-dimensional equations of motion. Again, the different fluxes show up as constant coefficients in the potential of  $S_{4d}$ . At least for a certain range of the parameters in the potential, we expect our  $S_{4d}$  to coincide with the universal sector of the effective 4d theory of the compactification, see [122] for a recent discussion on consistent truncations vs effective actions. Much of the literature on string-theory cosmological models uses a 4d effective action and a 4d potential. We make contact with the potential description in Section 7.3.

Whenever a single “species” of flux is turned on,<sup>2</sup> we are able to provide analytic cosmological solutions to the equations of motion. These are described in detail in Section 8.1. Whenever multiple fluxes are simultaneously turned on, one cannot give an analytic

---

<sup>2</sup>Here we use an extended notion of “flux” that also includes non-trivial curvature, but excludes the fields  $A, B, \phi$  (the warp factors and the dilaton).

solution in general, although this can still be possible for certain special values of the flux parameters. Whenever exactly two different species of flux are turned on, although an analytic solution is not possible in general, a powerful tool becomes available: as we show in Section 8.2, the equations of motion can be cast in the form of an autonomous dynamical system of three first-order equations and one constraint. The use of dynamical-system techniques in general relativity is of course not new: refs. [181, 189, 209–214] in particular are closely related to the strategy employed here. One of the novelties of the present work is to give an exhaustive analysis of universal cosmological solutions from compactification on the previously mentioned classes of manifolds.

The resulting dynamical system description is rather intuitive and captures several generic features of cosmological solutions coming from models of flux compactification. Each solution is represented by a trajectory in a three-dimensional phase space. The constraint forces the trajectories to lie in the interior of a sphere, with expanding cosmologies corresponding to trajectories in the northern hemisphere. Whenever the system of equations admits fixed points, these correspond to analytic solutions.

The boundary of the allowed phase space corresponding to expanding cosmologies, i.e. the equatorial disc and the surface of the northern hemisphere, are both invariant surfaces. This implies that trajectories that do not lie entirely on these surfaces can only approach them asymptotically. Trajectories that do lie entirely on either of these surfaces also correspond to analytic solutions (namely analytic solutions with a single species of flux turned on: indeed restricting the trajectory to either the surface of the sphere or the equatorial disc, corresponds to turning off one of the two species of flux). Moreover, the intersection of these two invariant surfaces – the equator – constitutes a circle of fixed points, and corresponds to a family of analytic solutions with all flux turned off, described in Section 8.1.1. The dynamical system generally possesses a third invariant surface, an invariant plane  $\mathcal{P}$ , whose disposition depends on the fluxes of the solution.

The analytic solutions corresponding to fixed points are all cosmologies with a power-law scale factor,  $S(T) \sim T^a$ , with  $\frac{1}{3} \leq a \leq 1$ . The fixed points at the equator correspond to power-law (scaling) cosmologies with  $a = \frac{1}{3}$ , while  $a = 1$  corresponds to either a fixed point at the origin of the sphere (whenever the dynamical system admits such a fixed point), or a fixed point in the bulk of the sphere and on the boundary of the acceleration region. In the former case the corresponding cosmology is that of a regular Milne universe, whereas in the latter case it is a Milne universe with angular defect. In addition, we find fixed points corresponding to cosmologies with  $a = \frac{3}{4}$ ,  $\frac{19}{25}$ , or  $\frac{9}{11}$ . The list of analytic solutions is given in Table 8.1.

Trajectories interpolating between two different fixed points asymptote the respective scaling solutions in the past and future infinity. Note in particular that we find no fixed points with  $a > 1$  (which would correspond to eternally accelerating scaling cosmologies).

The question of acceleration becomes particularly transparent in the dynamical system description: the acceleration period of the solution corresponds to the portion of the trajectory that lies in a certain region in phase space. This “acceleration region” is entirely fixed by the type of flux that is turned on, with the different cases summarized in Table 6.1.

This clarifies why (transient) accelerated expansion is essentially generic in flux compactifications: there is always a trajectory that passes by any given point in phase space (corresponding to some particular choice of initial conditions). By making sure that

## Chapter 6. Bird's eye view on time-dependent compactifications

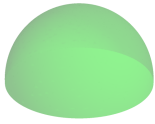

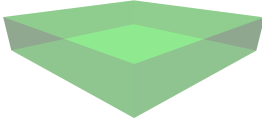
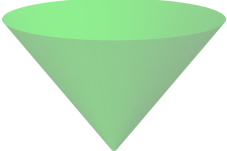
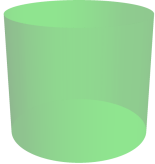
$\beta_1 \backslash \beta_2$	0	4	6
0	$\emptyset$	$\emptyset$	
4	$\emptyset$	$\emptyset$	
6			

Table 6.1: Different types of universal two-flux compactifications and their corresponding acceleration regions in the phase space. The values of  $\beta_{1,2}$  – corresponding to the two species of flux that are turned on in the solution – depend on the type of flux and its number of legs along the external-space, internal-space and time directions, cf. (8.10). The absence of an acceleration region is denoted by the empty set  $\emptyset$ .

a trajectory passes by some point in the acceleration region of the northern hemisphere, we can thus obtain a cosmological solution that will necessarily feature a period of accelerated expansion. Moreover, the only non-trivial requirement, namely the existence of an acceleration region in phase space, is not difficult to satisfy, as can be seen from Table 6.1.

In the dynamical system description, the calculation of the number of e-foldings,  $N$ , also becomes particularly transparent, since the flow parameter is simply the logarithm of the scale factor. Most instances of transient acceleration are such that the number of e-foldings is of order one,  $N \sim \mathcal{O}(1)$ , as was mentioned earlier. The exceptions that we find all correspond to dynamical systems with fixed points on the boundary of the accelerated region, and they all give rise to hyperbolic FLRW cosmologies ( $k < 0$ ). In addition, there is a flux turned on corresponding to one of the following being non-zero:  $\lambda$ ,  $m$ ,  $c_f$ ,  $c_0$ , or  $c_\varphi$ ; see Table 7.1 for the 10d origin of these coefficients.

The first of these solutions is examined in Section 8.2.1 and is obtained from compactification on a 6d Einstein manifold with negative curvature ( $\lambda < 0$ ). The second solution occurs in IIA supergravity with non-vanishing Romans mass ( $m \neq 0$ ) compactified on a Ricci-flat space, and is described in Section 8.2.2. Despite having vanishing Romans mass, the three remaining solutions ( $k < 0$  and  $c_f$ ,  $c_0$ , or  $c_\varphi \neq 0$ ) are all qualitatively very similar to the one of Section 8.2.2.

The  $k, \lambda < 0$  solution has been studied before in [193] (see also [194]) with somewhat different methods. It features a conical accelerating region, with a fixed point  $p_0$  at the origin of the cone (which coincides with the origin of the sphere), and a second fixed point  $p_1$  on the surface of the cone. Both  $p_0, p_1$  lie on the invariant plane  $\mathcal{P}$ . The invariant manifolds of  $p_0$  are the equatorial disc (in which  $p_0$  is an attractor) and the vertical  $z$ -axis (in which  $p_0$  is an unstable node). There are generic trajectories that asymptote some point on the equator at past infinity, cross into the acceleration region (the interior of the cone) at some point  $p'$ , then exit the acceleration region again at some point  $p''$ , and asymptote  $p_1$  at future infinity, see Figure 6.2.

These trajectories correspond to accelerating cosmologies with  $N \rightarrow \infty$  as  $p'' \rightarrow p_1$ . In other words, we can continuously increase the number of e-foldings and make it as large as desired, by choosing the trajectory such that the exit point from the acceleration region is sufficiently close to  $p_1$ , see Figure 6.3.

Note also the presence of semi-eternal trajectories that enter the acceleration region at some point  $p'$ , and reach the fixed point  $p_1$  at future infinity, without ever exiting the cone. The limiting case,  $p' \rightarrow p_0$ , is the unique trajectory which reaches  $p_0$  in the past and  $p_1$  at future infinity: it corresponds to eternal acceleration, with acceleration vanishing asymptotically at future infinity. In the vicinity of  $p_0$  the universe becomes de Sitter in hyperbolic slicing. This is not asymptotic de Sitter, however, as  $p_0$  is reached at finite proper time in the past. The solution can be geodesically completed beyond  $p_0$  in the past, by gluing together its mirror trajectory in the southern hemisphere.



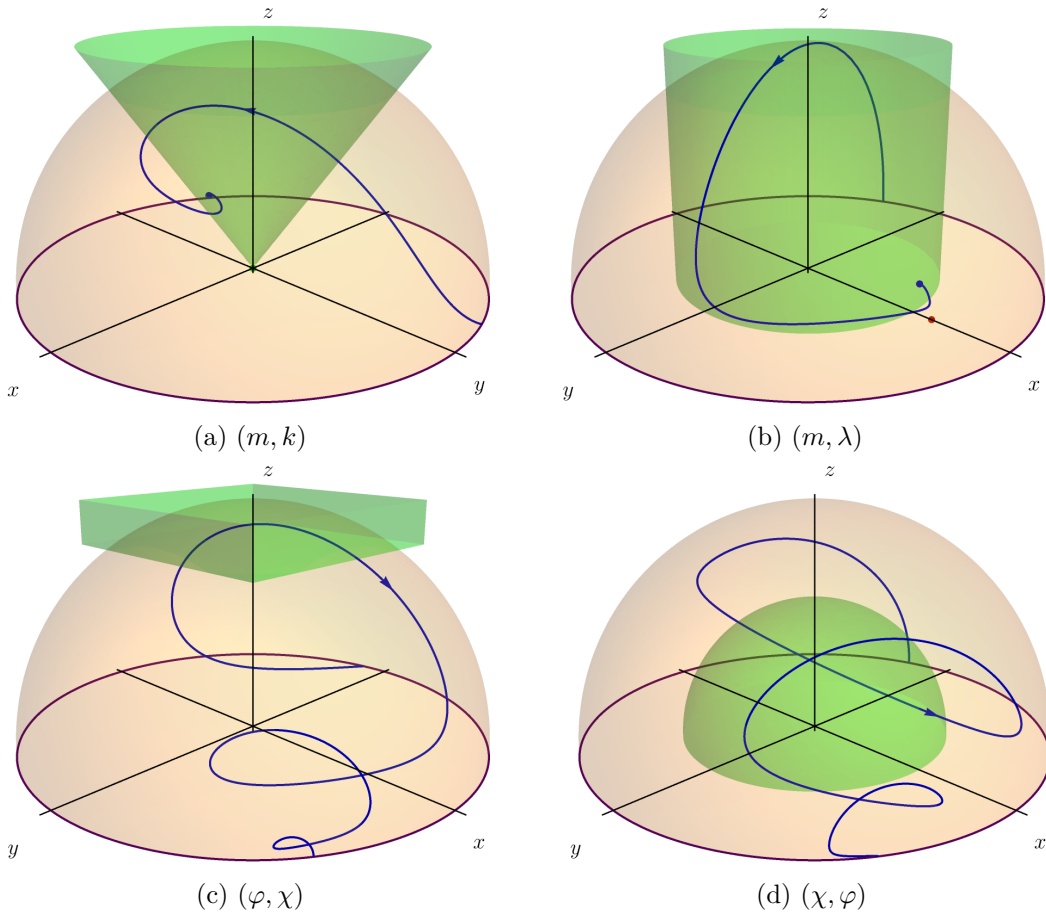


Figure 6.1: Trajectories in phase space corresponding to two-flux cosmological solutions with accelerated expansion. The corresponding dynamical systems are given in Sections 8.2.2, 8.2.3, 8.2.4. The pair of fluxes that are turned on in each case is indicated below each subfigure. The trajectories (blue lines) interpolate between a fixed point on the equator in the past infinity, corresponding to a cosmology with a power-law scale factor  $S \sim T^{\frac{1}{3}}$ , and another fixed point at future infinity. For cases 6.1c and 6.1d the second fixed point is also on the equator, and thus the solution asymptotes the same scaling cosmology in the past and future infinities. Cases 6.1a and 6.1b asymptote at future infinity a fixed point in the interior of the sphere which corresponds to a cosmology with a power-law scale factor  $S \sim T$  and  $S \sim T^{\frac{10}{25}}$  respectively. Cases 6.1c and 6.1d describe the same system, but employ different parametrizations which interchange the role of the two fluxes that are turned on. The transient accelerated expansion corresponds to the portion of the trajectory within the acceleration region depicted in green.

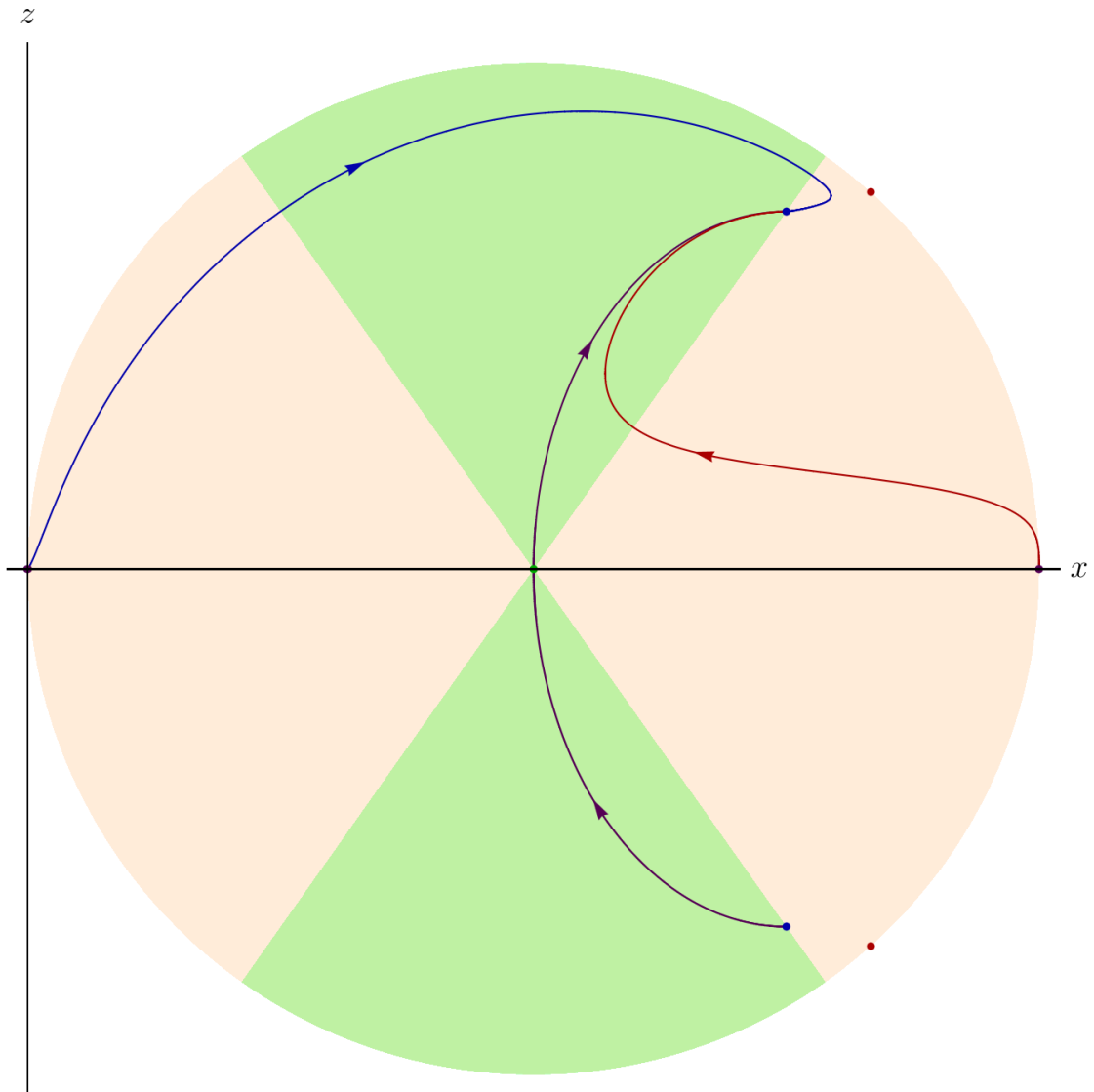


Figure 6.2: Three trajectories lying on the invariant plane  $\mathcal{P}$  of the dynamical system obtained from the compactification with  $k, \lambda \neq 0$ . The point  $p_0$  corresponding to a Milne universe is depicted in green. The point  $p_1$  (and its mirror in the southern hemisphere) is drawn in blue and corresponds to a Milne universe with angular defect. The equator fixed points coincide with a scaling cosmology with  $S \sim T^{\frac{1}{3}}$  and are illustrated in purple. The blue trajectory features transient acceleration with tunable number of e-foldings, whereas the red one corresponds to semi-eternal acceleration. Depicted in purple is the unique (fine-tuned) trajectory corresponding to eternal acceleration. The solution becomes de Sitter in the vicinity of the origin, which is reached at finite proper time. The solution can be geodesically completed in the past beyond the point at the origin, by gluing together its mirror trajectory in the southern hemisphere.

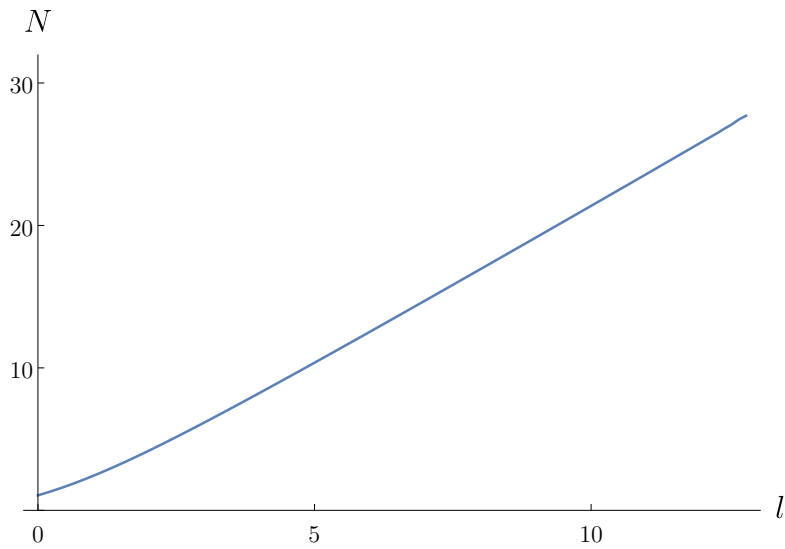


Figure 6.3: Number of e-foldings  $N$  as a function of  $l$ , which parametrizes the distance  $\Delta$  between the  $x$ -coordinates of  $p''$  and  $p_1$  for the  $(\lambda, k)$  model, viz.  $l = -\log \Delta + \text{const.}$

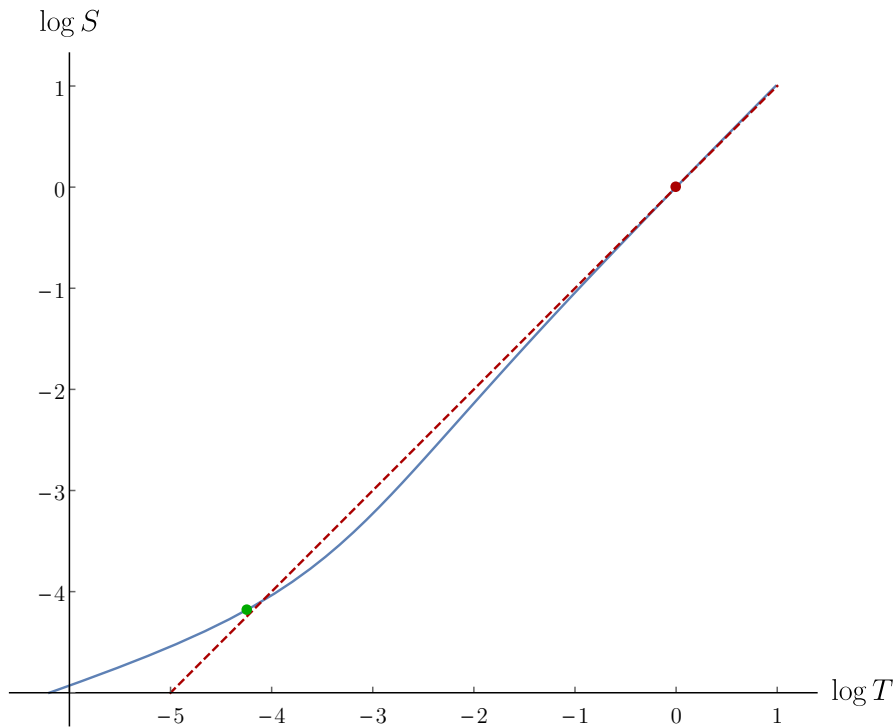


Figure 6.4: Plot log–log of the scale factor  $S$  (in blue) as a function of the cosmological time  $T$ . It corresponds to the  $(\lambda, k)$ -compactification (with  $l = 2$ ). The green dot corresponds to the beginning of inflation; the red one to its end. The red dashed line coincides with the Milne fixed point  $S \propto T$  and asymptotes the curve at future infinity.

From a given trajectory in phase space, it is then straightforward to reconstruct the scale factor  $S(T)$  as a function of the cosmological time, as depicted in Figure 6.4. This gives access to all the cosmological data (Hubble parameter  $H$ , slow-roll parameters  $\epsilon$  and  $\eta$ , the spectral tilt  $n_s$ , or the tensor-to-scalar ratio  $r$ ) needed for phenomenology.

To our knowledge, the  $k < 0$ ,  $m \neq 0$  solution has not appeared before in the literature. Like the previous solution, it features a conical accelerating region, with a fixed point  $p_0$  at the origin, and a second fixed point  $p_1$  on the surface of the cone. Both  $p_0, p_1$  lie on the invariant plane  $\mathcal{P}$ . However, unlike the previous solution, the fixed point  $p_1$  is now a stable focus on  $\mathcal{P}$ , and an attractor in the direction perpendicular to  $\mathcal{P}$ . This allows for generic trajectories that asymptote some point on the equator at past infinity, cross into the acceleration region (the interior of the cone) at some point  $p'$ , exit the acceleration region at some point  $p''$ , then enter again at some point  $p'''$ , and so on, as they spiral into  $p_1$  asymptotically at future infinity, see Figure 6.5. This asymptotic spiraling corresponds to an infinite number of periodic cycles of alternating periods of accelerated and decelerated expansion, each cycle contributing a finite number of e-foldings, so that  $N \rightarrow \infty$ .

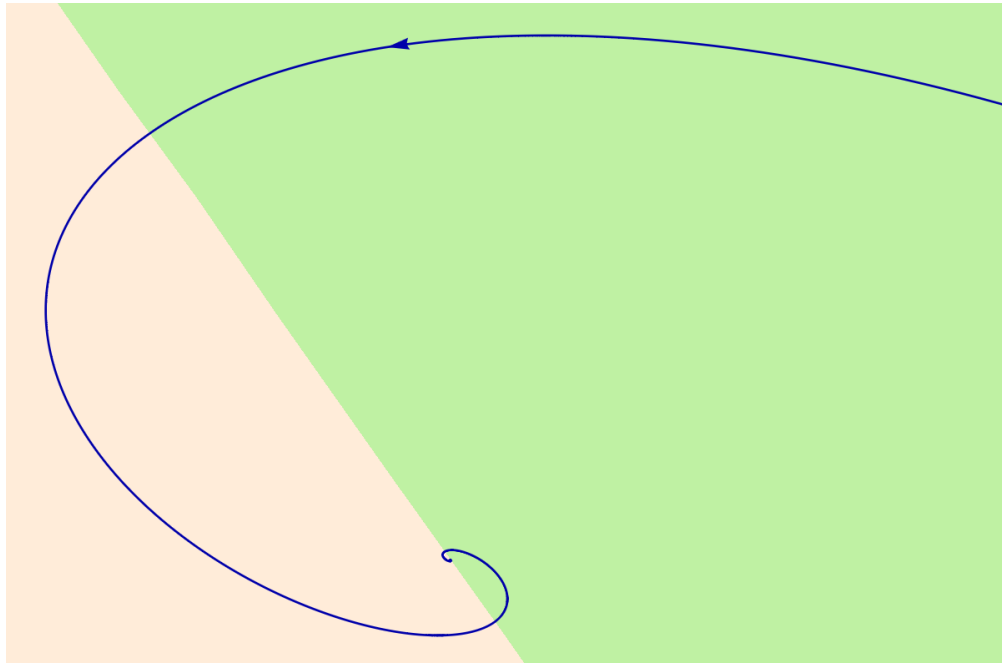


Figure 6.5: Example of a spiraling trajectory around  $p_1$  in the  $(m, k)$ -compactification.

As in the previous system, there is here a unique (fine-tuned) trajectory which reaches  $p_0$  at finite proper time in the past and asymptotes  $p_1$  at future infinity. In the vicinity of  $p_0$ , the universe becomes de Sitter in hyperbolic slicing. The solution can be geodesically completed beyond  $p_0$  in the past, by gluing together its mirror trajectory in the southern hemisphere.

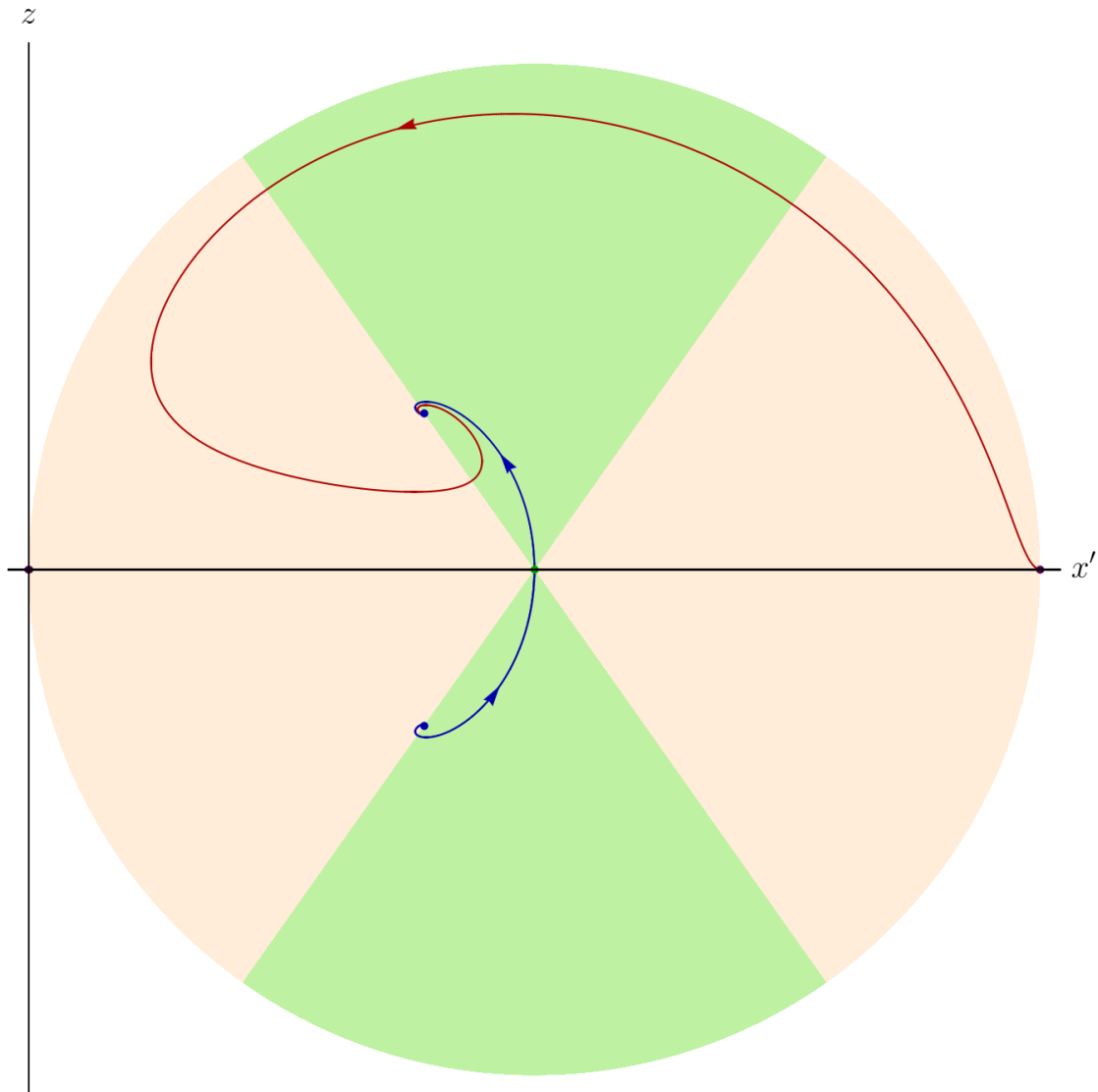


Figure 6.6: Two trajectories lying on the invariant plane  $\mathcal{P}$  of the dynamical system obtained from the compactification with  $m, k \neq 0$ . The point  $p_0$  corresponding to a Milne universe is depicted in green. The point  $p_1$  (and its mirror in the southern hemisphere) is drawn in blue and corresponds to a Milne universe with angular defect. The equator fixed points coincide with a scaling cosmology with  $S \sim T^{\frac{1}{3}}$  and are illustrated in purple. The red trajectory enters and exits the acceleration region an infinite number of times, spiraling around  $p_1$ , see Figure 6.5 for a zoom around this region. Depicted in blue is the unique (fine-tuned) trajectory: the solution becomes de Sitter in the vicinity of the origin, which is reached at finite proper time. The solution can be geodesically completed in the past beyond the point at the origin, by gluing together its mirror trajectory in the southern hemisphere.

To our knowledge, none of the remaining systems, exhibiting a parametric control on the number of e-foldings, corresponding to  $k < 0$  and non-vanishing  $c_\varphi$  (B.210),  $c_0$  (B.267) or  $c_f$  (B.284), has appeared before in the literature. These are all captured by the 4d consistent truncation (7.22) with potential given in (7.25). While they all correspond to solutions with vanishing Romans mass, they are all qualitatively very similar to the  $(m, k)$  case analyzed above: they all feature a hyperbolic FLRW universe ( $k < 0$ ) with one type of non-vanishing flux, and they all admit solutions with an infinite number of cycles of alternating periods of accelerated and decelerated expansion. In the “rollercoaster cosmology” scenario of [215] it was argued that an oscillatory behavior of this type could be relevant for inflation.



# 7 The framework

In this chapter, we begin by presenting in Section 7.1 the general set-up and the ansatz that we use, and provide a convenient packaging of the equations of motion to be solved. We make contact with the 4d cosmological quantities, such as the FLRW scale factor, the  $w$  parameter, the number of e-foldings, etc. We also discuss in Sections 7.2 and 7.3 how the system can be reduced to a 1d or 4d consistent truncation, respectively.

## 7.1 General set-up

Our ten-dimensional metric is a warped product of a four-dimensional FLRW cosmological factor and a six-dimensional compact internal space. The ansatz for the ten-dimensional metric *in 10d Einstein frame* reads

$$ds_{10}^2 = e^{2A(t)} \left( e^{2B(t)} g_{\mu\nu} dx^\mu dx^\nu + g_{mn} dy^m dy^n \right), \quad (7.1)$$

where the scalars (warp factors)  $A, B$  only depend on the conformal time coordinate, while  $y^m$  are coordinates of the internal six-dimensional space. The unwarped 4d metric is assumed to be of the form

$$g_{\mu\nu} dx^\mu dx^\nu = -dt^2 + d\Omega_k^2, \quad (7.2)$$

where  $t$  is the conformal time, and the spatial 3d part of the metric is locally isometric to a maximally-symmetric three-dimensional space of scalar curvature  $6k$ . Explicitly,

$$d\Omega_k^2 = \gamma_{ij}(\vec{x}) dx^i dx^j; \quad R_{ij}^{(3)} = 2k\gamma_{ij}, \quad (7.3)$$

with  $i, j = 1, 2, 3$ , and  $R_{ij}^{(3)}$  is the Ricci tensor of the metric  $\gamma_{ij}$ . The 3d metric is thus locally a sphere ( $k > 0$ ) or a hyperbolic space ( $k < 0$ ); the case  $k = 0$  corresponds to flat space.

The correct frame in which the predictions of our model should be compared to the cosmological data is the four-dimensional Einstein frame: this is the frame in which the effective four-dimensional Newton constant becomes time-independent. The 4d Einstein-frame metric reads

$$ds_{4E}^2 = -S^6 d\tau^2 + S^2 d\Omega_k^2, \quad (7.4)$$



where the scale factor is given by

$$S = e^{4A+B} , \quad (7.5)$$

and we have introduced of a new time variable  $\tau$  defined via

$$\frac{dt}{d\tau} = e^{8A+2B} . \quad (7.6)$$

Note that  $\tau$  is neither the conformal nor the cosmological time. It is simply the coordinate with respect to which the equations of motion are simplest to solve.

In terms of the cosmological time coordinate  $T$ ,

$$\frac{dT}{d\tau} = S^3 , \quad (7.7)$$

the metric takes the standard FLRW form,

$$ds_{4E}^2 = -dT^2 + S^2 d\Omega_k^2 . \quad (7.8)$$

Suppose we have an explicit solution of our set of equations for all fields, so that in particular we can construct the explicit expression of the scale factor. We may then always engineer a 4d perfect fluid of density and pressure  $\rho$  and  $p$  respectively, such that the scale factor in question can be seen as resulting from the 4d Einstein equations sourced by the stress-energy tensor of that fluid,

$$\begin{aligned} \left(\frac{\dot{S}}{S}\right)^2 &= \frac{8\pi G}{3}\rho - \frac{k}{S^2} \\ \left(\frac{\ddot{S}}{S}\right) &= -\frac{4\pi G}{3}(\rho + 3p) , \end{aligned} \quad (7.9)$$

where the dot refers to differentiation with respect to  $T$ . Solving the above system for  $\rho$ ,  $p$  we obtain

$$w := \frac{p}{\rho} = -\frac{1}{3} - \frac{2S\ddot{S}}{3(k + \dot{S}^2)} . \quad (7.10)$$

In particular, it follows that for  $k > -\dot{S}^2$  (and in particular for  $k = 0$ ), the condition for acceleration is equivalent to  $w < -\frac{1}{3}$ . Of course, unless  $w$  is constant, the first equality in (7.10) is simply a definition, rather than an equation of state. Nevertheless, even for non-constant  $w$ , this quantity is useful insofar as it allows us to compare to the equations of state of the different cosmological eras.

The conditions for expansion and acceleration read

$$\begin{aligned} 0 < \dot{S} &= -\frac{1}{2}d_\tau S^{-2} \\ 0 < \ddot{S} &= -\frac{1}{2}S^{-3}d_\tau^2 S^{-2} . \end{aligned} \quad (7.11)$$

The number of e-foldings,  $N$ , is defined as

$$N = \int d \ln S , \quad (7.12)$$

where the limits of the integral should be taken at the beginning and the end of the acceleration period.

## 7.2 1d consistent truncation

In all of the compactifications presented here, the internal 6d components of the Einstein equations and the dilaton equation reduce to<sup>1</sup>

$$\begin{aligned} d_\tau^2 A &= -\frac{1}{48} (\partial_A U - 4\partial_B U) \\ d_\tau^2 \phi &= -\partial_\phi U , \end{aligned} \tag{7.13}$$

where  $U$  is a function (potential) that depends on the compactification and on the flux that is turned on, given in (7.16) below. The external 4d Einstein equations reduce to the following two equations,

$$\begin{aligned} d_\tau^2 B &= \frac{1}{12} (\partial_A U - 3\partial_B U) \\ 72(d_\tau A)^2 + 6(d_\tau B)^2 + 48d_\tau A d_\tau B - \frac{1}{2}(d_\tau \phi)^2 &= U . \end{aligned} \tag{7.14}$$

The second line above is a constraint, consistently propagated by the remaining equations of motion (i.e. the  $\tau$ -derivative of this equation is automatically satisfied by virtue of the remaining equations). The important point to note here is that, as we shall see, the remaining (flux) equations of motion can be solved without imposing any additional conditions. The above equations of motion “know” about the flux content of the background which enters via  $U$  in the form of constant parameters, cf. Table 7.1. The bottom line is that we are left with three second-order equations for three unknowns (the two warp factors  $A$ ,  $B$  and the dilaton  $\phi$ ), together with a constraint, which only needs to be imposed once at some fixed initial time, and amounts to imposing an algebraic condition on the constants parameterizing the fluxes.

Moreover, equations (7.13), (7.14) can be derived from a one-dimensional action given by

$$S_{1d} = \int d\tau \left\{ \frac{1}{\mathcal{N}} \left( -72(d_\tau A)^2 - 6(d_\tau B)^2 - 48d_\tau A d_\tau B + \frac{1}{2}(d_\tau \phi)^2 \right) - \mathcal{N}U(A, B, \phi) \right\} , \tag{7.15}$$

where  $\mathcal{N}$  is a non-dynamical Lagrange multiplier which should be set to  $\mathcal{N} = 1$  at the end of the calculation; it can be thought of as originating from the lapse function. Variation of the action (7.15) with respect to  $\mathcal{N}$  imposes the constraint (second line of (7.14)), while variation with respect to the fields  $A$ ,  $B$ ,  $\phi$  is equivalent to their respective equations of motion in (7.13), (7.14). The potential  $U$  is in general a function of all three scalars  $A$ ,  $B$ ,  $\phi$ . Explicitly, it is given by

<sup>1</sup>The bosonic sector of type IIA supergravity is given in Appendix B.

$$U = \begin{cases} \frac{1}{2}c_\varphi^2 e^{-\phi/2+6A+6B} + \frac{1}{2}c_h^2 e^{-\phi+12A} + \frac{3}{2}c_\chi^2 e^{\phi+4A} + c_{\xi\xi'}^2 e^{-\phi/2+6A} - 6ke^{16A+4B} & \text{CY (B.27), (B.28)} \\ 72b_0^2 e^{-\phi+12A+6B} + \frac{3}{2}c_0^2 e^{\phi/2+10A+6B} & \text{CY (B.113), (B.114)} \\ \frac{1}{2}c_\varphi^2 e^{-\phi/2+6A+6B} + \frac{1}{2}m^2 e^{5\phi/2+18A+6B} - 6ke^{16A+4B} - 6\lambda e^{16A+6B} & \text{E (B.125), (B.126)} \\ \frac{1}{2}c_\varphi^2 e^{-\phi/2+6A+6B} + \frac{1}{2}c_h^2 e^{-\phi+12A} + \frac{3}{2}c_\chi^2 e^{\phi+4A} - 6ke^{16A+4B} - 6\lambda e^{16A+6B} & \text{EK (B.188), (B.189)} \\ \frac{3}{2}c_0^2 e^{\phi/2+10A+6B} + \frac{1}{2}m^2 e^{5\phi/2+18A+6B} - 6ke^{16A+4B} - 6\lambda e^{16A+6B} & \text{EK (B.194), (B.195)} \\ \frac{1}{2}c_\varphi^2 e^{-\phi/2+6A+6B} + \frac{3}{2}c_f^2 e^{3\phi/2+14A+6B} - 6ke^{16A+4B} - 6\lambda e^{16A+6B} & \text{EK (B.199)} . \end{cases} \quad (7.16)$$

In the above we have indicated the type of compactification in which the potentials appear (E stands for Einstein, EK for Einstein-Kähler, CY for Calabi-Yau), as well as numbers of the respective equations of motion.

Note that the potential encodes all the information about the flux (which is generically non-vanishing from the ten-dimensional point of view), as well as the external and internal curvature contributions. Indeed, this information is encoded in  $U$  via the different constants appearing in (7.16), whose 10d origin is summarized in Table 7.1.

$m$	zero-form (Romans mass)
$c_f$	internal two-form
$c_h$	external three-form
$b_0$	internal three-form
$c_\chi$	mixed three-form
$c_\varphi$	external four-form
$c_0$	internal four-form
$c_{\xi\xi'}$	mixed four-form
$k$	external curvature
$\lambda$	internal curvature

Table 7.1: List of the constant coefficients entering the potential (7.16) of the 1d consistent truncation, and their 10d origin. A form is called external (resp. internal), if all its legs are along the external (resp. internal) directions; mixed if one of its legs is along the time direction, while all remaining legs are internal.

Note also that, in terms of the potential, the derivatives of the scale factor with respect to cosmological time, cf. equations (7.11), take the form

$$\begin{aligned} S^4 \dot{S}^2 &= \frac{1}{6}U + 4(d_\tau A)^2 + \frac{1}{12}(d_\tau \phi)^2 \\ S^5 \ddot{S} &= \frac{1}{12}(\partial_B U - 4U) - 8(d_\tau A)^2 - \frac{1}{6}(d_\tau \phi)^2 . \end{aligned} \quad (7.17)$$

Moreover, the quantity

$$\frac{S\ddot{S}}{k + \dot{S}^2} = \frac{\partial_B \tilde{U} - 4\tilde{U} - 96(d_\tau A)^2 - 2(d_\tau \phi)^2}{2\tilde{U} + 48(d_\tau A)^2 + (d_\tau \phi)^2} , \quad (7.18)$$

that appears in (7.10), is written in terms of the  $k$ -independent part of the potential,

$$\tilde{U} = U + 6kS^4 . \quad (7.19)$$

In particular we see that

$$w = -1 \iff \partial_B \tilde{U} = 6\tilde{U} + 144(d_\tau A)^2 + 3(d_\tau \phi)^2 . \quad (7.20)$$

### 7.3 Cosmological 4d consistent truncation

In a subset of the cases we present here, the equations of motion (7.13), (7.14) can be written in terms of a potential  $V(A, \phi)$  which only depends on  $A$  and  $\phi$ ,

$$\begin{aligned} d_\tau^2 A &= -\frac{1}{48}e^{24A+6B}\partial_A V \\ d_\tau^2 B &= e^{24A+6B}\left(\frac{1}{2}V + \frac{1}{12}\partial_A V\right) - 2ke^{16A+4B} \\ d_\tau^2 \phi &= -e^{24A+6B}\partial_\phi V \\ -12ke^{16A+4B} + 2Ve^{24A+6B} &= 144(d_\tau A)^2 + 12(d_\tau B)^2 + 96d_\tau A d_\tau B - (d_\tau \phi)^2 . \end{aligned} \quad (7.21)$$

As can be verified, these equations can then be “integrated” into a four-dimensional action,

$$S_{4d} = \int d^4x \sqrt{g} \left( R - 24g^{\mu\nu} \partial_\mu A \partial_\nu A - \frac{1}{2}g^{\mu\nu} \partial_\mu \phi \partial_\nu \phi - V(A, \phi) \right) . \quad (7.22)$$

Indeed, in terms of the scale factor (7.5) and the cosmological time coordinate (7.7), taking suitable linear combinations thereof, equations (7.21) can be written equivalently as

$$\begin{aligned} \frac{\ddot{S}}{S} &= -\frac{1}{2}V - 8\dot{A}^2 - \frac{1}{6}\dot{\phi}^2 \\ 2\left(\frac{\dot{S}}{S}\right)^2 + \frac{2k}{S^2} &= \frac{1}{3}V + 8\dot{A}^2 + \frac{1}{6}\dot{\phi}^2 \\ \ddot{A} + \frac{3}{S}\dot{A} &= -\frac{1}{48}\partial_A V \\ \ddot{\phi} + \frac{3}{S}\dot{\phi} &= -\partial_\phi V . \end{aligned} \quad (7.23)$$

On the other hand, the 4d equations of motion resulting from (7.22) read

$$\begin{aligned} R_{\mu\nu} &= \frac{1}{2}g_{\mu\nu}V + 24\partial_\mu A \partial_\nu A + \frac{1}{2}\partial_\mu \phi \partial_\nu \phi \\ \nabla^\mu \partial_\mu A &= \frac{1}{48}\partial_A V ; \quad \nabla^\mu \partial_\mu \phi = \partial_\phi V . \end{aligned} \quad (7.24)$$

Inserting the Einstein metric (7.4) into the above, and assuming that  $A, B, \phi$  only depend on the time coordinate, results precisely in (7.23). Therefore,  $S_{4d}$  of (7.22) is a two-scalar *consistent truncation of IIA for cosmological solutions*: all cosmological solutions (i.e. all solutions with a metric of FLRW type and scalar fields that only depend on time) of  $S_{4d}$  lift to ten-dimensional solutions of IIA supergravity.

For the different compactifications admitting a consistent cosmological truncation of the form (7.22), the potential reads,

$$V = \begin{cases} 72b_0^2 e^{-\phi-12A} + \frac{3}{2}c_0^2 e^{\phi/2-14A} & \text{CY with internal 3- and 4-form fluxes} \\ \frac{1}{2}c_\varphi^2 e^{-\phi/2-18A} + \frac{1}{2}m^2 e^{5\phi/2-6A} - 6\lambda e^{-8A} & \text{E with external 4-form flux} \\ \frac{3}{2}c_0^2 e^{\phi/2-14A} + \frac{1}{2}m^2 e^{5\phi/2-6A} - 6\lambda e^{-8A} & \text{EK with internal 4-form flux} \\ \frac{1}{2}c_\varphi^2 e^{-\phi/2-18A} + \frac{3}{2}c_f^2 e^{3\phi/2-10A} - 6\lambda e^{-8A} & \text{EK with internal 2-form, external 4-form.} \end{cases} \quad (7.25)$$

Of course terms with  $k$  (the external 4d spatial curvature) cannot appear at the level of the 4d action, but rather they potentially arise as part of its solutions.

It is known [216, 217] that there exists a consistent 4d truncation in the case of the universal CY sector, i.e. a consistent truncation to the the gravity multiplet, one vectormultiplet and one hypermultiplet. Remarkably, the action  $S_{4d}$  of (7.22) is a sub-truncation thereof to the graviton and two scalars, such that all information about the flux (which is generically non-vanishing from the ten-dimensional point of view) is carried by the potential  $V$  via the constants  $m$ ,  $b_0$ ,  $c_0$ ,  $c_\varphi$ . The latter correspond respectively to non-vanishing zero-form flux (Romans mass), internal three-form flux, internal four-form flux, and external four-form flux;  $\lambda$  is the scalar curvature of the internal Einstein manifold, cf. (B.119).

Note that: (i) not all compactifications considered here admit the sub-truncation (7.22), (7.25) to gravity plus two scalars; (ii) the Einstein and Einstein-Kähler cases in (7.25) reduce to CY in the  $\lambda \rightarrow 0$  limit.

# 8 Cosmological solutions

We now present the various solutions that we found within this framework. Section 8.1 discusses the analytic solutions obtained when one type of flux is turned on. Section 8.2 explains the dynamical system techniques used here, illustrated with some notable cases in subsections 8.2.1 – 8.2.4. We then close this second part of the thesis with a discussion on possible future directions in Section 8.3. Further details of all analytical solutions and all two-flux dynamical systems studied here can be found in Appendix B.

## 8.1 Analytic solutions

In the present analysis we find three different types of analytic solutions:

- *Critical (scaling) solutions.* Their metrics are of power-law form,

$$ds^2 = -dT^2 + T^{2a}d\Omega_k^2, \quad (8.1)$$

in terms of the cosmological time  $T$ , with  $a = \frac{1}{3}, \frac{3}{4}, \frac{19}{25}, \frac{9}{11}, 1$ . They admit an interpretation as critical points in an appropriately defined phase space, as described in Section 8.2.

- *Type I solutions.* They interpolate between two asymptotically power-law metrics,

$$ds^2 \rightarrow -dT_-^2 + T_-^{\frac{2}{3}}d\Omega_k^2; \quad ds^2 \rightarrow -dT_+^2 + T_+^{\frac{2}{3}}d\Omega_k^2, \quad (8.2)$$

as  $\tau \rightarrow -\infty, \tau \rightarrow +\infty$  respectively. In terms of the dynamical system description, they correspond to trajectories interpolating between two fixed points on the equator.

The corresponding coordinate patches are parameterized by coordinates  $T_{\pm} \propto e^{b_{\pm}\tau}$ , for certain parameters  $b_{\pm}$  which depend on the particular solution. If  $b_-$  is positive,  $\tau \rightarrow -\infty$  corresponds to  $T_- \rightarrow 0$ . It follows that the solution reaches a singularity at finite proper time in the past. If  $b_-$  is negative,  $\tau \rightarrow -\infty$  corresponds to  $T_- \rightarrow \infty$ , and is therefore reached at infinite proper time in the past. An identical analysis holds for the patch parameterized by  $T_+$ , corresponding to  $\tau \rightarrow +\infty$ . All four different possibilities are realized in the analytic solutions presented here:  $\tau \rightarrow \pm\infty$  corresponding to  $T_{\pm} \rightarrow 0$ , or  $T_{\pm} \rightarrow \infty$ .

- *Type II solutions.* They interpolate between an asymptotically power-law metric,

$$ds^2 \rightarrow -dT_{\pm}^2 + T_{\pm}^{2a_{\pm}} d\Omega_k^2, \quad (8.3)$$

at either  $\tau \rightarrow -\infty$  or  $\tau \rightarrow +\infty$ , with  $a_{\pm} = \frac{1}{3}$ , and a critical solution at  $\tau = 0$  (which is reached at infinite proper time) with  $a = 1$  or  $a = \frac{3}{4}$ . In terms of the dynamical system description, they correspond to trajectories interpolating between one fixed point on the equator and an interior fixed point.

Table 8.1 below summarizes the different types of analytic solutions constructed here, the corresponding type of compactification, and the section in which the explicit details of the solution can be found.

	Critical	Type I	Type II
<b>CY</b>	$k < 0$ (B.41) $\varphi \neq 0$ and $k < 0$ (B.50) $\chi \neq 0$ and $k < 0$ (B.71) $\xi \neq 0$ and $k < 0$ (B.83) $\xi, \chi \neq 0$ and $k < 0$ (B.95) $\xi, \chi, h \neq 0$ and $k < 0$ (B.103)	$k > 0$ (B.35) $\varphi \neq 0$ (B.47) $\chi \neq 0$ (B.61), $\chi \neq 0$ and $k > 0$ (B.65) $\xi \neq 0$ (B.73), $\xi \neq 0$ and $k > 0$ (B.77) $\xi, \chi \neq 0$ and $k > 0$ (B.89) $b_0 \neq 0$ and $c_0 \neq 0$ (B.115)	$k < 0$ (B.40) $\varphi \neq 0$ and $k < 0$ (B.55) $\chi \neq 0$ and $k < 0$ (B.71) $\xi \neq 0$ and $k < 0$ (B.83) $\xi, \chi \neq 0$ and $k < 0$ (B.95) $\xi, \chi, h \neq 0$ and $k < 0$ (B.103)
<b>E</b>	$\lambda < 0$ (B.132) $\lambda < 0$ and $k < 0$ (B.143) $m \neq 0$ and $\lambda < 0$ (B.145) $m \neq 0$ and $k < 0$ (B.155) $m \neq 0, k, \lambda < 0$ (B.157) $\varphi, m \neq 0, k < 0$ (B.160) $\varphi, m \neq 0, k, \lambda < 0$ (B.163)	$\lambda > 0$ (B.130) $\lambda > 0$ and $k > 0$ (B.141) $m \neq 0$ (B.134) $\varphi \neq 0$ and $\lambda > 0$ (B.172) $\varphi \neq 0$ and $m \neq 0$ (B.148)	$\lambda < 0$ (B.131) $\lambda < 0$ and $k < 0$ (B.142) $\varphi \neq 0$ and $\lambda < 0$ (B.173) $m \neq 0$ and $k < 0$ (B.152)
<b>EK</b>	$h \neq 0$ and $\lambda < 0$ (B.190) $c_0 \neq 0$ and $k < 0$ (B.196) $c_f \neq 0$ and $k < 0$ (B.202)		

Table 8.1: List of all the analytic solutions, besides the zero-flux, flat 4d space solution of Section 8.1.1. We list the corresponding compactification manifold, the type of non-vanishing flux, together with a reference to the explicit details of the solution. Critical solutions correspond to fixed points in the dynamical-system description. All CY critical points correspond to regular Milne universes except the one with  $\varphi \neq 0$ , which is a Milne universe with angular defect. The  $\lambda < 0$  critical point corresponds to a scaling cosmology with  $a = \frac{3}{4}$ . The  $m \neq 0, \lambda < 0$  critical point corresponds to a scaling cosmology with  $a = \frac{19}{25}$ . The  $k, \lambda, m, \varphi \neq 0$  solution corresponds to AdS<sub>4</sub> in hyperbolic slicing. The  $h \neq 0, \lambda < 0$  critical point corresponds to a scaling cosmology with  $a = \frac{9}{11}$ . All the other critical points correspond to Milne universes with angular defects. Type I solutions always correspond to trajectories interpolating between two points of the equator. Type II solutions interpolate between a fixed point on the equator and an interior fixed point. For all type II CY solutions, the internal space warp factor  $e^A$  and the dilaton  $\phi$  tend to a constant at future infinity, except for the  $\varphi \neq 0$  solution for which  $e^A, e^{\phi} \rightarrow \infty$ . For all type II Einstein solutions,  $e^A \rightarrow \infty, \phi \rightarrow \text{const.}$  at asymptotic infinity, except for the  $(m, k)$  solution for which  $e^{\phi} \rightarrow 0$ .

### 8.1.1 Minimal (zero-flux) solution

The simplest solution to the form equations is given by vanishing flux. Let us consider the remaining equations of motion. The internal Einstein and dilaton equations give,

cf. (7.13),

$$A = c_A \tau + d_A ; \quad \phi = c_\phi \tau + d_\phi , \quad (8.4)$$

for some constants  $c_A, d_A, c_\phi, d_\phi$ . The external Einstein equations give, cf. (7.14),

$$B = c_B \tau + d_B ; \quad \frac{1}{12} c_\phi^2 = 12 c_A^2 + c_B^2 + 8 c_A c_B , \quad (8.5)$$

where  $c_B, d_B$  are constants. The second equation above is the constraint, which implies in particular that the ratio  $r$  defined by

$$r := \frac{c_A}{c_B} , \quad (8.6)$$

must satisfy  $r \leq -\frac{1}{2}$  or  $r \geq -\frac{1}{6}$ . The points where the constraint is saturated correspond to constant dilaton ( $c_\phi = 0$ ).

This solution thus implies a power-law form for the 4d part of the Einstein-frame metric,

$$ds_{4E}^2 = -e^{(24c_A+6c_B)\tau} d\tau^2 + e^{(8c_A+2c_B)\tau} d\vec{x}^2 , \quad (8.7)$$

where we have appropriately rescaled the  $\tau, \vec{x}$  coordinates to absorb  $d_A, d_B$ . In terms of a coordinate  $T \propto e^{(12c_A+3c_B)\tau}$  we have a power-law expansion,

$$ds_{4E}^2 = -dT^2 + T^{\frac{2}{3}} d\vec{x}^2 . \quad (8.8)$$

The time coordinate  $T$  ranges from  $T = 0$ , where we have a singularity, to  $T = \infty$ . Depending on the values of  $c_A, c_B$  and  $c_\phi$ , we can have solutions with constant dilaton such that the warp factor collapses ( $e^A \rightarrow 0$ ), or decompactifies ( $e^A \rightarrow \infty$ ) as  $T \rightarrow 0$  or  $\infty$  respectively. The opposite behavior is also possible, i.e.  $e^A \rightarrow \infty, 0$  as  $T \rightarrow 0, \infty$  respectively. We can also have solutions with constant internal space warp factor, such that either  $\phi \rightarrow \pm\infty$  or  $\phi \rightarrow \mp\infty$ , as  $T \rightarrow 0$  or  $\infty$ .

### 8.1.2 Single-flux solutions

In the case where a single type of flux is turned on, it is always possible to solve the equations analytically. Let us suppose a potential of the form

$$U = c e^{\alpha A + \beta B + \gamma \phi} , \quad (8.9)$$

for some real constants  $c, \alpha, \beta, \gamma$ , whose precise values depend on the type of flux turned on. More specifically, let  $n_t, n_s, n_i$  be the number of legs the form has along the time, 3d space, and internal directions respectively. Then, for an RR form we have

$$\alpha = 18(1-n_t) - 2(-1)^{n_t}(n_s+n_i) ; \quad \beta = 6(1-n_t) - 2(-1)^{n_t}n_s ; \quad \gamma = (-1)^{n_t} \frac{5 - (n_t + n_s + n_i)}{2} . \quad (8.10)$$

For an NS-NS three-form the constants  $\alpha, \beta$  are as above, but  $\gamma = -(-1)^{n_t}$ .

In the following, it will be useful to set

$$q := c \left[ \frac{1}{48} (\alpha - 4\beta)^2 - \frac{1}{12} \beta^2 + \gamma^2 \right] . \quad (8.11)$$



• Case  $q \neq 0$

Let us set

$$E(\tau) := \begin{cases} \ln \left[ \frac{2c_E^2}{q} \operatorname{sech}^2(c_E\tau + d_E) \right], & q > 0 \\ \ln \left[ \frac{2c_E^2}{|q|} \operatorname{csch}^2(c_E\tau + d_E) \right], & q < 0 \end{cases}, \quad (8.12)$$

where  $c_E, d_E$  are arbitrary constants. The  $A, B, \phi$ -equations of motion are then solved by

$$\begin{aligned} A &= \frac{c}{48q}(\alpha - 4\beta)E + c_A\tau + d_A \\ B &= \frac{c}{12q}(3\beta - \alpha)E + c_B\tau + d_B \\ \phi &= \frac{c\gamma}{q}E + c_\phi\tau + d_\phi, \end{aligned} \quad (8.13)$$

where  $c_A, d_A, c_B, d_B, c_\phi, d_\phi$  are arbitrary constants subject to the conditions

$$\alpha c_A + \beta c_B + \gamma c_\phi = 0; \quad \alpha d_A + \beta d_B + \gamma d_\phi = 0. \quad (8.14)$$

Moreover, the constraint (7.14) reduces to

$$\frac{1}{2}c_\phi^2 + \frac{2c}{q}c_E^2 = 72c_A^2 + 48c_Ac_B + 6c_B^2. \quad (8.15)$$

For  $\tau \rightarrow \pm\infty$ , the scale factor  $\ln S$  grows linearly in  $\tau$ . This results in a scaling solution with  $S(T) \sim T^{\frac{1}{3}}$ . For  $q > 0$ ,  $S$  goes to a constant in the  $\tau \rightarrow 0$  limit. In the case  $q < 0$  we have instead,

$$\ln S \rightarrow \delta \ln |\tau|; \quad \delta := \frac{8\beta}{(\alpha - 6\beta)(\alpha - 2\beta) + 48\gamma^2}, \quad (8.16)$$

in the  $\tau \rightarrow 0$  limit, where we took (8.15) into account. This results in a scaling solution with  $S(T) \sim T^a$ , where

$$a = \frac{\delta}{3\delta + 1}. \quad (8.17)$$

Taking (8.10) into account, we see that there are no scaling solutions with  $a > 1$  (accelerated expansion). However, there is one case which gives  $a = 1$  (scaling solution with vanishing acceleration): it involves negative external curvature and is described in Section 8.2.1.

• Case  $q = 0$

For special values of  $n_t, n_s, n_i$  it is possible to have  $q = 0$ . It can be seen that this occurs only if the flux is anisotropic in the 3d spatial dimensions. The  $A, B, \phi$ -equations of motion are then solved by

$$\begin{aligned} A &= \frac{c}{48c_E^2}(4\beta - \alpha)e^E + c_A\tau + d_A \\ B &= \frac{c}{12c_E^2}(\alpha - 3\beta)e^E + c_B\tau + d_B \\ \phi &= -\frac{c\gamma}{c_E^2}e^E + c_\phi\tau + d_\phi, \end{aligned} \quad (8.18)$$

where  $c_A, d_A, c_B, d_B, c_\phi, d_\phi$  are arbitrary constants and

$$c_E = \alpha c_A + \beta c_B + \gamma c_\phi ; \quad d_E = \alpha d_A + \beta d_B + \gamma d_\phi . \quad (8.19)$$

Moreover, the constraint (7.14) reduces to

$$c_\phi^2 = 144c_A^2 + 96c_Ac_B + 12c_B^2 . \quad (8.20)$$

The scale factor is given by

$$\ln S = (4c_A + c_B)\tau + (4d_A + d_B) + \frac{\beta c}{12c_E^2} e^{c_E\tau + d_E} . \quad (8.21)$$

The conditions for accelerated expansion read

$$c_1 + c_2 e^t > 0 ; \quad 2c_1^2 + 2c_2^2 e^{2t} + c_2(4c_1 - c_E)e^t < 0 , \quad (8.22)$$

where we have set

$$c_1 := 4c_A + c_B ; \quad c_2 := \frac{\beta c}{12c_E} ; \quad t := c_E\tau + d_E . \quad (8.23)$$

For concreteness, let us assume  $c_E > 0$ . The conditions (8.22) can then be written as

$$\tilde{c}_2 e^t > -\tilde{c}_1 ; \quad -\tilde{c}_1 + \frac{1}{4}(1 - \sqrt{1 - 8\tilde{c}_1}) < \tilde{c}_2 e^t < -\tilde{c}_1 + \frac{1}{4}(1 + \sqrt{1 - 8\tilde{c}_1}) , \quad (8.24)$$

where  $\tilde{c}_i := c_i/c_E$ ;  $i = 1, 2$ . Let us also denote  $B_\pm := -\tilde{c}_1 + \frac{1}{4}(1 \pm \sqrt{1 - 8\tilde{c}_1})$ , appearing in (8.22). Since  $B_\pm \geq 0$  for all  $\tilde{c}_1 \leq \frac{1}{8}$ , one needs  $\tilde{c}_2 > 0$  for the second condition to be satisfied, so we restrict to that case in the following. Furthermore, it holds for  $t_1 < t < t_2$  with,

$$t_1 = \ln \frac{B_-}{\tilde{c}_2} , \quad t_2 = \ln \frac{B_+}{\tilde{c}_2} . \quad (8.25)$$

If  $0 < \tilde{c}_1 < \frac{1}{8}$ : the first condition in (8.22) is always satisfied and the number of e-folds is thus given by

$$N = \tilde{c}_1(t_2 - t_1) + \tilde{c}_2(e^{t_2} - e^{t_1}) \quad (\tilde{c}_1 > 0) . \quad (8.26)$$

For the value  $\tilde{c}_1 = \frac{1}{8}$ ,  $B_- = B_+$  and there is no accelerated expansion.

If  $\tilde{c}_1 < 0$ : the first condition in (8.22) is satisfied for  $t > t_0$  with

$$t_0 = \ln -\frac{\tilde{c}_1}{\tilde{c}_2} . \quad (8.27)$$

Note that for all  $\tilde{c}_1 < 0$ ,  $t_1 < t_0 < t_2$ . In this case, the number of e-folds is given by

$$N = \tilde{c}_1(t_2 - t_0) + \tilde{c}_2(e^{t_2} - e^{t_0}) \quad (\tilde{c}_1 < 0) . \quad (8.28)$$

For  $\tilde{c}_1 \rightarrow 0$ ,  $t_1 \rightarrow -\infty$  but  $N$  is however finite and

$$\lim_{\tilde{c}_1 \rightarrow 0^-} N = \lim_{\tilde{c}_1 \rightarrow 0^+} N = \frac{1}{2} . \quad (8.29)$$

Plugging (8.25) into (8.26) and (8.28), we observe that  $N$  only depends on  $\tilde{c}_1$ , and reads explicitly

$$N(\tilde{c}_1) = \begin{cases} \frac{1}{4}(1 + \sqrt{1 - 8\tilde{c}_1}) + \tilde{c}_1 \ln \left[ 1 - \frac{1}{4\tilde{c}_1} (1 + \sqrt{1 - 8\tilde{c}_1}) \right] & \text{if } \tilde{c}_1 < 0, \\ \frac{1}{2}\sqrt{1 - 8\tilde{c}_1} + \tilde{c}_1 \ln \frac{1 + \sqrt{1 - 8\tilde{c}_1} - 4\tilde{c}_1}{1 - \sqrt{1 - 8\tilde{c}_1} - 4\tilde{c}_1} & \text{if } \tilde{c}_1 > 0. \end{cases} \quad (8.30)$$

For  $\tilde{c}_1 < 0$ ,  $N$  is monotonously increasing from 0 to  $\frac{1}{2}$ . For  $0 < \tilde{c}_1 < \frac{1}{8}$ ,  $N$  admits a maximum  $N_{\max} = 0.59980$  at  $\tilde{c}_1 = 0.038148$ , see Figure 8.1. It is the maximal number of e-folds one can obtain in such one-flux solutions.

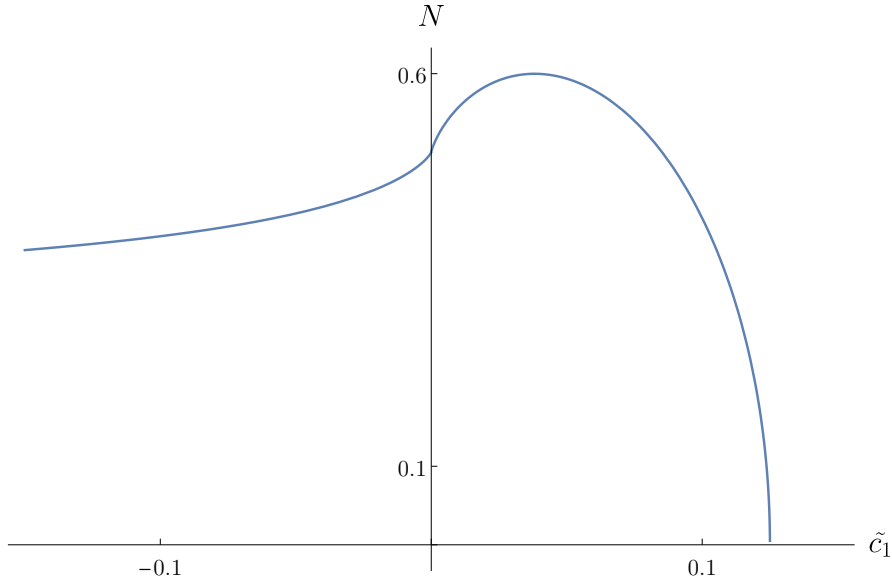


Figure 8.1: Number of e-folds  $N$  as a function of the parameter  $\tilde{c}_1$ , for one-flux compactifications.  $N$  reaches a maximum of  $N_{\max} = 0.59980$ , for  $\tilde{c}_1 = 0.038148$ .

## 8.2 Two-flux solutions: dynamical system analysis

Let us now consider the case where the potential consists of two terms,

$$U = \sum_{i=1}^2 c_i e^{E_i}; \quad E_i := \alpha_i A + \beta_i B + \gamma_i \phi, \quad (8.31)$$

where  $c_i, \alpha_i, \beta_i, \gamma_i$  are real constants. We shall assume that the potential is not everywhere non-positive, so that we can take  $c_1 > 0$ , while  $c_2$  is unconstrained.

### • The system

Let us define the following phase-space variables,

$$v = e^{-E_1/2} d_\tau A; \quad u = e^{-E_1/2} d_\tau B; \quad w = e^{-E_1/2} d_\tau \phi. \quad (8.32)$$

## 8.2 Two-flux solutions: dynamical system analysis

In terms of these, the equations of motion become an autonomous dynamical system,

$$\begin{aligned}
 d_\sigma v &= -\left(\frac{1}{8}\alpha_2 - \frac{1}{2}\beta_2\right) u^2 - \left(\alpha_2 + \frac{1}{2}\beta_1 - 4\beta_2\right) uv - \left(\frac{1}{2}\alpha_1 + \frac{3}{2}\alpha_2 - 6\beta_2\right) v^2 - \frac{1}{2}\gamma_1 vw \\
 &\quad - \left(-\frac{1}{96}\alpha_2 + \frac{1}{24}\beta_2\right) w^2 + \frac{1}{48}c_1 [\alpha_2 - \alpha_1 + 4(\beta_1 - \beta_2)] \\
 d_\sigma u &= -\frac{1}{2}(-\alpha_2 + b_1 + 3\beta_2) u^2 - \left(\frac{1}{2}\alpha_1 - 4\alpha_2 - 12\beta_2\right) uv - (-6\alpha_2 + 18\beta_2) v^2 - \frac{1}{2}\gamma_1 uw \\
 &\quad - \left(\frac{1}{24}\alpha_2 + \frac{1}{8}\beta_2\right) w^2 + \frac{1}{12}c_1 [\alpha_1 - \alpha_2 + 3(\beta_2 - \beta_1)] \\
 d_\sigma w &= -6\gamma_2 u^2 - 48\gamma_2 uv - 72\gamma_2 v^2 - \frac{1}{2}\beta_1 uw - \frac{1}{2}\alpha_1 vw - \frac{1}{2}(\gamma_1 - \gamma_2) w^2 + c_1(\gamma_2 - \gamma_1) ,
 \end{aligned} \tag{8.33}$$

where  $d\sigma := e^{E_1/2}d\tau$ , and we have used the constraint to eliminate the terms with  $c_2$  from the equations of motion. Moreover, the constraint reads

$$72v^2 + 6u^2 + 48vu - \frac{1}{2}w^2 = c_1 + c_2 e^{E_2 - E_1} . \tag{8.34}$$

To better analyse the behavior of the flow at infinity, it is useful to compactify the phase space as in [212, 214]. We introduce the new variables

$$x = \frac{2v}{4v + u} ; \quad y = \frac{w}{2\sqrt{3}(4v + u)} ; \quad z = \frac{\sqrt{c_1}}{\sqrt{6}(4v + u)} . \tag{8.35}$$

Note that in these variables the condition of expansion is equivalent to  $z > 0$ . The system (8.33) becomes

$$\begin{aligned}
 x' &= \frac{1}{4} \left( [\alpha_2 + 2\beta_2(-2 + x)](-1 + x^2 + y^2 + z^2) + [-\alpha_1 - 2\beta_1(-2 + x)]z^2 \right) \\
 y' &= \frac{1}{2} \left( (2\sqrt{3}\gamma_2 + \beta_2 y)(-1 + x^2 + y^2 + z^2) - (2\sqrt{3}\gamma_1 + \beta_1 y)z^2 \right) \\
 z' &= \frac{1}{4} z \left( \alpha_1 x + 4\sqrt{3}\gamma_1 y - 2\beta_1(-1 + 2x + z^2) + 2\beta_2(-1 + x^2 + y^2 + z^2) \right) ,
 \end{aligned} \tag{8.36}$$

where  $f' = d_\omega f$  and  $d\omega := \frac{\sqrt{c_1}}{\sqrt{6}z}d\sigma$ , while the constraint (8.34) now reads

$$c_1(1 - x^2 - y^2 - z^2) = c_2 z^2 e^{E_2 - E_1} . \tag{8.37}$$

Let us also note that

$$d\omega = \frac{\sqrt{c_1}}{\sqrt{6}z} e^{E_1/2} d\tau ; \quad dT = \frac{\sqrt{6}z}{\sqrt{c_1}} e^{12A+3B-E_1/2} d\omega , \tag{8.38}$$

as follows from the previous definitions.

### • Invariant surfaces

The equations of motion (8.36) imply

$$\begin{aligned}
 \frac{1}{2} (x^2 + y^2 + z^2)' &= \frac{1}{4} (-1 + x^2 + y^2 + z^2) \\
 &\quad \times \left( \alpha_2 x + 4\sqrt{3}\gamma_2 y - 2\beta_1 z^2 + 2\beta_2 [(-2 + x)x + y^2 + z^2] \right) ,
 \end{aligned} \tag{8.39}$$

so that the unit sphere,

$$\mathcal{S} = \{(x, y, z) \in \mathbb{R}^3 \mid x^2 + y^2 + z^2 = 1\} , \quad (8.40)$$

is an invariant surface. This implies that trajectories which include some interior (resp. exterior) point of the three-dimensional unit ball will remain there; such trajectories correspond to  $c_1, c_2$  having the same (resp. opposite) sign. Similarly, trajectories that include a point on the sphere  $\mathcal{S}$  must lie entirely on  $\mathcal{S}$ . As can be seen from the constraint (8.37), trajectories on  $\mathcal{S}$  must have  $c_2 = 0$ .

Moreover, it follows immediately from the third line in (8.36) that the plane  $z = 0$  is another invariant surface, so trajectories which include some point in the upper (resp. lower) half of the three-dimensional space  $z > 0$  (resp.  $z < 0$ ) must lie there entirely. Similarly, trajectories which include a point of the  $(x, y)$ -plane must lie entirely on that plane. The latter trajectories must have  $c_1 = 0$ , as follows from (8.37).

The intersection of the two invariant surfaces above, the unit circle  $\mathcal{C}$  in the  $z = 0$  plane, is also an invariant surface. In fact  $\mathcal{C}$  is a circle of fixed points,

$$p_{\mathcal{C}} \in \mathcal{C} := \{(x, y, z) \mid x^2 + y^2 = 1 \text{ and } z = 0\} . \quad (8.41)$$

Each point  $p_{\mathcal{C}}$  corresponds to a trajectory (solution) with  $c_1, c_2 = 0$ , i.e. the minimal solution of Section 8.1.1. In particular, the ratio  $r$  defined in (8.6) is related to the polar angle via,

$$\tan \theta = \frac{y}{x} = \pm \frac{1}{2r} \sqrt{12r^2 + 8r - 1} . \quad (8.42)$$

Another consequence of the system (8.36) is that the plane

$$\mathcal{P} := \{(x, y, z) \in \mathbb{R}^3 \mid ax + by + c = 0\} , \quad (8.43)$$

is an invariant surface, where the constants  $a, b, c$  are obtained as solutions of the system of equations<sup>1</sup>

$$\begin{aligned} (\alpha_2 - 4\beta_2)a + 4\sqrt{3}\gamma_2b - 2\beta_2c &= 0 \\ [\alpha_2 - \alpha_1 - 4(\beta_2 - \beta_1)]a + 4\sqrt{3}(\gamma_2 - \gamma_1)b - 2(\beta_2 - \beta_1)c &= 0 . \end{aligned} \quad (8.44)$$

Indeed, in this case, (8.36) implies

$$(ax + by)' = \frac{1}{2}(ax + by + c) [\beta_2(x^2 + y^2 - 1) + (\beta_2 - \beta_1)z^2] . \quad (8.45)$$

Allowed trajectories must therefore either lie entirely on  $\mathcal{P}$ , or be limited on either side of it.

As follows from (8.36), the flow equations are invariant under  $(z, \omega) \rightarrow -(z, \omega)$ , so that each trajectory in the  $z > 0$  region is paired to a “mirror” trajectory in the  $z < 0$  region. As we are ultimately interested in expanding cosmologies, we will restrict our attention to the  $z \geq 0$  region. On the other hand, taking (7.17), (8.37) into account, the condition for acceleration is written as<sup>2</sup>

---

<sup>1</sup>Solutions to this system exist, provided  $(\alpha_1\beta_2 - \alpha_2\beta_1)^2 + (\alpha_1\gamma_2 - \alpha_2\gamma_1)^2 + (\beta_1\gamma_2 - \beta_2\gamma_1)^2 \neq 0$ .

<sup>2</sup>More precisely, the left hand side of the second inequality in (8.46) is equal to  $\frac{3}{c_1} e^{-E_1} z^5 S^5 \dot{S}$ .

$$\ddot{S}(T) > 0 \iff (\beta_1 - \beta_2)z^2 - \beta_2(x^2 + y^2) + \beta_2 - 4 > 0, \quad (8.46)$$

which defines an acceleration region in the phase space. Depending on the values taken by  $\beta_1, \beta_2$ , it can be a cone, a cylinder, a ball (regular or deformed) or the region above a horizontal plane, see Table 6.1 and Figure 8.2 below.

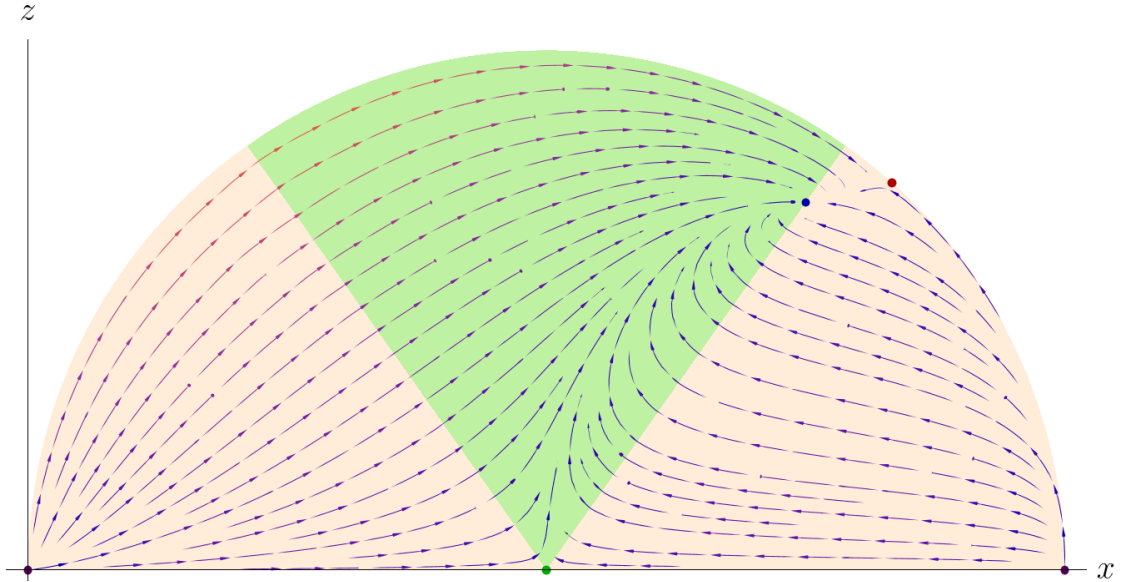


Figure 8.2: Vector field generated by the dynamical system (8.36), plotted in the invariant plane  $\mathcal{P}$ . Here, the acceleration region is a cone, depicted in green. The generic equator fixed points are illustrated in purple. This example corresponds to the case  $\lambda, k \neq 0$ , studied extensively in Section 8.2.1, and coincides with the northern hemisphere of Figure 6.2.

Note that different pairs of  $\beta_{1,2}$  lead to acceleration regions of different shape. Although the solutions are invariant under  $\beta_1 \leftrightarrow \beta_2$ , this leads to a reparametrization of the phase space of the corresponding dynamical system. Put differently, although the solutions are invariant under reflections along the diagonal of Table 6.1, the shapes of the acceleration regions are not.

Moreover, using (7.10), (7.18) and (8.37) we have

$$w = 1 - \frac{1}{3}\beta_2 + \frac{1}{3}\beta_2(x^2 + y^2) + \frac{1}{3}(\beta_2 - \beta_1)z^2. \quad (8.47)$$

Note that in the presence of external curvature (with the convention  $c_2 = -6k$ ), the above expression is to be replaced by

$$w = 1 - \frac{1}{3}\beta_1 \frac{z^2}{x^2 + y^2 + z^2}. \quad (8.48)$$

Eqs. (8.46), (8.47) are consistent with the fact that the acceleration condition is equivalent to  $w < -\frac{1}{3}$ , if  $k + \dot{S}^2 > 0$ .

## Chapter 8. Cosmological solutions

---

It is also possible to obtain an expression for the number of e-foldings  $N$  directly in terms of phase space variables. Indeed, solving (8.35) for  $v$ ,  $u$ ,  $w$ , and taking (8.32) into account, we obtain

$$d_\omega A = \frac{1}{2}x ; \quad d_\omega B = 1 - 2x ; \quad d_\omega \phi = 2\sqrt{3}y . \quad (8.49)$$

In particular this implies  $d_\omega(4A + B) = 1$ , which, taking (7.5) into account, is equivalent to

$$d \ln S = d\omega . \quad (8.50)$$

This means that the flow parameter of the system (8.36) is simply  $\omega = \ln \frac{S}{S_0}$ , so that  $S = S_0$  at  $\omega = 0$ . It follows that

$$N = \int d\omega , \quad (8.51)$$

where the limits of the integral should be taken as the points of entry and exit of the trajectory into and out of the acceleration region (8.46), respectively.

### • The scale factor

Given a solution  $(x(\omega), y(\omega), z(\omega))$  of the above dynamical system, it becomes possible to reconstruct the corresponding expression for the scale factor  $S(T)$ , which is the quantity we are ultimately interested in, in order to construct all the observables related to the cosmological model.

One can integrate (8.38) to obtain

$$T(\omega) = \sqrt{\frac{6}{c_1}} \int_{-\infty}^{\omega} d\omega' z(\omega') \exp \left[ \left(12 - \frac{\alpha_1}{2}\right) A(\omega') + \left(3 - \frac{\beta_1}{2}\right) - \frac{\gamma_1}{2} \phi(\omega') \right] , \quad (8.52)$$

where  $T = 0$  corresponds to the lower bound  $\omega \rightarrow -\infty$  and  $S = e^\omega = 0$ . Note that since we restrict to  $z > 0$ ,  $T$  is ensured to be positive. Here,  $A, B, \phi$  are completely determined by the solution (and the data of initial conditions) via (8.49), and can be computed by numerical integration. In practice, we solve the system over a finite range  $[\omega_{\min}, \omega_{\max}]$ , which gives the bounds to be used in the integrals. One can then numerically invert (8.52) to obtain  $\omega(T) = \log S$ .

Alternatively, we can compute the parametric curve  $(\log T(\omega), \omega)$  with parameter  $\omega$  which corresponds to the log–log plot  $(\log T, \log S)$ , as shown in Figure 6.4. In such a plot, the freedom in the parameter  $c_1$  can be thought as a freedom to move the curve left and right.<sup>3</sup> Furthermore, since the dynamical system is autonomous, meaning it does not depend on  $\omega$  explicitly, every shift of a solution is also a solution, viz.

$$\vec{x}(\omega) \text{ is a solution } \implies \vec{x}(\omega + \Omega) \text{ is a solution} . \quad (8.53)$$

This means that the log–log plot can also be shifted up or down at will. The only freedom left is the choice in the initial conditions  $(x_0, y_0, z_0)$ .

---

<sup>3</sup>This may also be thought as a freedom in tuning the value of  $H_0$ , the Hubble parameter at a given  $T_0$ .

## 8.2 Two-flux solutions: dynamical system analysis

From (8.52), one can express  $\dot{S}$  and  $\ddot{S}$  as functions of  $\omega$ ,

$$\begin{aligned}\dot{S} &= \frac{dS}{dT} = \left(\frac{dT}{dS}\right)^{-1} = \left(\frac{dT}{d\omega} \frac{d\omega}{dS}\right)^{-1} = \frac{dS}{d\omega} \left(\frac{dT}{d\omega}\right)^{-1} = \frac{e^\omega}{t(\omega)}, \\ \ddot{S} &= \frac{d}{dT} \dot{S} = \frac{d\omega}{dT} \frac{d}{d\omega} \dot{S} = \frac{e^\omega}{t^2} \left(1 - \frac{t'}{t}\right), \\ \ddot{S} &= \frac{e^\omega}{t^5} [t^2 + 3t'^2 - t(3t' + t'')] ,\end{aligned}\tag{8.54}$$

where  $t(\omega)$  is the integrand in (8.52), and  $t' = d_\omega t$ . From this, one may compute the Hubble parameter  $H = \dot{S}/S$  and its derivatives as functions of  $\omega$ , as well as other quantities such as the tensor-to-scalar ratio  $r$  or the scalar spectral index  $n_s$ . In principle, these could allow to further assess and restrict the viability of the models obtained in this way (beyond the mere number of e-foldings  $N$ ), but this goes beyond the scope of the present work, although it would be interesting to explore these constraints in future work.

In the following four subsections we will study in depth four dynamical systems. The first two correspond to the two open FLRW cosmologies described in Section 6.2. The one with negative internal curvature is studied in Section 8.2.1, whereas the one with non-vanishing Romans mass in Section 8.2.2. Both admit solutions with infinite or parametrically controlled number of e-foldings. The remaining two systems, studied in Sections 8.2.3 and 8.2.4, were chosen for the richness of their fixed-point structure, allowing for different interpolating solutions. All the other possible two-flux dynamical systems can be found in Appendix B.2, and are summarized in Table 8.2 below.

	$m$	$c_\varphi$	$c_\chi$	$c_{\xi\xi'}$	$c_f$	$c_h$	$b_0$	$c_0$	$k$	$\lambda$
$m$	$\emptyset$	(B.243)	$\emptyset$	$\emptyset$	$\emptyset$	$\emptyset$	$\emptyset$	(B.261)	(8.83)	(8.96)
$c_\varphi$	(B.243)	$\emptyset$	(8.111)	(B.205)	(B.278)	$\emptyset$	$\emptyset$	$\emptyset$	(B.210)	(B.237)
$c_\chi$	$\emptyset$	(8.111)	$\emptyset$	(B.216)	$\emptyset$	(B.218)	$\emptyset$	$\emptyset$	(B.220)	(B.249)
$c_{\xi\xi'}$	$\emptyset$	(B.205)	(B.216)	$\emptyset$	$\emptyset$	(B.226)	$\emptyset$	$\emptyset$	(B.223)	$\emptyset$
$c_f$	$\emptyset$	(B.278)	$\emptyset$	$\emptyset$	$\emptyset$	$\emptyset$	$\emptyset$	$\emptyset$	(B.284)	(B.290)
$c_h$	$\emptyset$	$\emptyset$	(B.218)	(B.226)	$\emptyset$	$\emptyset$	$\emptyset$	$\emptyset$	(B.228)	(B.255)
$b_0$	$\emptyset$	$\emptyset$	$\emptyset$	$\emptyset$	$\emptyset$	$\emptyset$	$\emptyset$	(B.231)	$\emptyset$	$\emptyset$
$c_0$	(B.261)	$\emptyset$	$\emptyset$	$\emptyset$	$\emptyset$	$\emptyset$	(B.231)	$\emptyset$	(B.267)	(B.273)
$k$	(8.83)	(B.210)	(B.220)	(B.223)	(B.284)	(B.228)	$\emptyset$	(B.267)	$\emptyset$	(8.55)
$\lambda$	(8.96)	(B.237)	(B.249)	$\emptyset$	(B.290)	(B.255)	$\emptyset$	(B.273)	(8.55)	$\emptyset$

Table 8.2: All possible two-flux dynamical systems. A  $\emptyset$  indicates that the corresponding pair of fluxes does not relate to a possible subcase of (7.16).

### 8.2.1 Case study I: $\lambda, k$

Let us begin with the case where  $\lambda, k \neq 0$ . From (8.36), we obtain the dynamical system

$$\begin{aligned}x' &= 2x (x^2 + y^2 - \frac{1}{2}z^2 - 1) + 2z^2 \\ y' &= 2y (x^2 + y^2 - \frac{1}{2}z^2 - 1) \\ z' &= z [1 + 2(x-1)x + 2y^2 - z^2] ,\end{aligned}\tag{8.55}$$



where we have set  $c_1 = -6\lambda$ ,  $c_2 = -6k$ ,  $(\alpha_1, \beta_1, \gamma_1) = (16, 6, 0)$ ,  $(\alpha_2, \beta_2, \gamma_2) = (16, 4, 0)$ . Moreover, we assume  $\lambda < 0$ , so that  $c_1 > 0$  as required in Section 8.2. The constraint (8.37) reduces to

$$\lambda(1 - x^2 - y^2 - z^2) = k z^2 e^{-2B} , \quad (8.56)$$

so that  $k < 0$  (resp.  $k > 0$ ) restricts to trajectories in the interior (resp. exterior) of the invariant surface  $\mathcal{S}$ , cf. (8.40). Trajectories on  $\mathcal{S}$  require  $k = 0$ , while those on the  $z = 0$  plane require  $\lambda = 0$ . The points on the equator  $\mathcal{C}$  of  $\mathcal{S}$  require  $k, \lambda = 0$ .

Besides  $\mathcal{S}$  and the invariant plane  $z = 0$ , the plane  $y = 0$  is also an invariant surface. Since eqs. (8.55) are invariant under  $y \rightarrow -y$ , we may restrict our attention to trajectories lying in the  $y, z \geq 0$  quadrant.

The condition for acceleration (8.46) reduces to

$$\ddot{S}(T) > 0 \iff z^2 > 2(x^2 + y^2) , \quad (8.57)$$

so that accelerated expansion occurs in the portion of the trajectory that lies in the upper half of the cone defined in (8.57). Moreover, from (8.47) we have

$$w = \frac{x^2 + y^2 - z^2}{x^2 + y^2 + z^2} , \quad (8.58)$$

so that  $w = -1$  whenever the trajectory passes by the  $z$ -axis. Equations (8.57), (8.58) imply that the acceleration condition is equivalent to  $w < -\frac{1}{3}$ .

• **Critical points**

For  $z > 0$  there are two critical points of the system (8.55), given by

$$p_1 = \frac{1}{2} (1, 0, \sqrt{2}) ; \quad p_2 = \frac{1}{3} (2, 0, \sqrt{5}) . \quad (8.59)$$

Both  $p_{1,2}$  lie on the invariant  $y = 0$  plane. Moreover,  $p_1$  lies on the boundary of the acceleration cone and in the interior of  $\mathcal{S}$ , while  $p_2$  lies outside the cone and on the boundary of  $\mathcal{S}$ .

On the  $z = 0$  plane, the origin  $p_0 = (0, 0, 0)$  is an isolated fixed point. In addition, we have an invariant circle of fixed points  $p_{\mathcal{C}}$ : the equator of the sphere  $\mathcal{S}$ . These points require  $k, \lambda = 0$  and correspond to the minimal solutions of Section 8.1.1.

The linearized system at  $p_1$  has eigenvalues  $-1$  (double) and  $-2$ . The corresponding eigenvectors are along the  $x$  and  $y$  directions, respectively. The linearized system at  $p_0$  has eigenvalues  $-2$  (double) and  $1$ . The corresponding eigenvectors are along the  $x, y$  and  $z$  directions, respectively.

The critical points of the dynamical system correspond to solutions that can be given analytically:  $p_1$  corresponds to the singular Milne universe given in (B.142);  $p_2$  requires  $k = 0$  (which is consistent with the fact that it lies on  $\mathcal{S}$ ) and corresponds to the critical solution with  $\lambda < 0$ , which is a decelerating power-law expansion. The origin  $p_0$  requires  $\lambda = 0$  (which is consistent with the fact that it lies on the  $z = 0$  plane) and corresponds to the regular Milne universe of (B.40).

• **The invariant surface  $\mathcal{S}$**

Restricting to trajectories on  $\mathcal{S}$ , the system (8.55) implies

$$x' = 3\left(x - \frac{2}{3}\right)(x^2 + y^2 - 1) ; \quad y' = 3y(x^2 + y^2 - 1) . \quad (8.60)$$

It follows that the projections of all trajectories on  $\mathcal{S}$  to the  $z = 0$  plane are of the form

$$a\left(x - \frac{2}{3}\right) + by = 0 ; \quad a, b \in \mathbb{R} , \quad (8.61)$$

i.e. straight lines passing by the point  $(x, y) = \left(\frac{2}{3}, 0\right)$ , which is the projection of  $p_2$  onto the  $z = 0$  plane. These trajectories correspond precisely to the solutions of (B.127), and require  $k = 0$ . More specifically, the slope of the line (8.61) is related to the constants in (B.127) via

$$\frac{a}{b} = -\frac{3\sqrt{3}c_\phi}{20c_A} . \quad (8.62)$$

• **The invariant plane  $z = 0$**

Restricting to trajectories on the  $z = 0$  plane, the system (8.55) reduces to

$$x' = 2x(x^2 + y^2 - 1) ; \quad y' = 2y(x^2 + y^2 - 1) . \quad (8.63)$$

It follows that all trajectories on the  $z = 0$  plane are of the form

$$ax + by = 0 ; \quad a, b \in \mathbb{R} , \quad (8.64)$$

i.e. straight lines passing by the point  $(x, y) = (0, 0)$ . These straight lines correspond precisely to the solutions of (B.35), and require  $\lambda = 0$ . More specifically, the slope of the line (8.64) is related to the constants in (B.35), (B.36) via

$$\frac{a}{b} = -\frac{c_\phi}{4\sqrt{3}c_A} . \quad (8.65)$$

• **The invariant plane  $y = 0$**

On the plane  $y = 0$ , the system (8.55) reduces to

$$\begin{aligned} x' &= 2x \left( x^2 - \frac{1}{2}z^2 - 1 \right) + 2z^2 \\ z' &= z \left[ 1 + 2(x - 1)x - z^2 \right] . \end{aligned} \quad (8.66)$$

All trajectories of the reduced system are attracted by the stable node  $p_1$ , except for the two trajectories on  $\mathcal{S}$  which start at the two antipodal points  $(x, y, z) = \pm(1, 0, 0) \in \mathcal{C}$ , and end on either side of the unstable node  $p_2$ .

Using a perturbative analysis, it is possible to obtain an analytic description of the trajectory connecting  $p_0$  and  $p_1$  near the critical endpoints. In the neighborhood of  $p_0$  the system (8.66) admits the solution

$$x = \frac{1}{2}c^2e^{2\omega} - \frac{3}{4}c^4e^{4\omega} + \mathcal{O}(e^{6\omega}) ; \quad z = ce^\omega - c^3e^{3\omega} + \mathcal{O}(e^{5\omega}) , \quad (8.67)$$

## Chapter 8. Cosmological solutions

---

so that the  $(x, z)$  trajectory attains  $p_0$  in the  $\omega \rightarrow -\infty$  limit, tangentially along the vertical direction ( $z$ -axis). Moreover the constraint (8.56) imposes

$$c = \sqrt{\left|\frac{\lambda}{k}\right|} e^{B_0} . \quad (8.68)$$

It can be seen from (8.58), (8.67) that  $w \rightarrow -1$  as the trajectory tends to  $p_0$ . However it would be incorrect to conclude that the solution becomes asymptotic de Sitter, since the  $p_0$  point is reached at finite cosmological time in the past. Indeed this can be seen explicitly by reconstructing the metric corresponding to the solution (8.67), (8.68): taking into account the relation between  $dT$  and  $d\omega$ , cf. (8.38), we obtain

$$dT = S^3 d\tau = \frac{1}{\sqrt{|\lambda|}} z e^{4A} d\omega . \quad (8.69)$$

Moreover from (8.49) and (8.67) we obtain the perturbative expression for  $A$  and  $z$ . Plugging into (8.69) and integrating we obtain<sup>4</sup>

$$T = \frac{1}{\sqrt{|\lambda|}} c e^{4A_0 + \omega} \left[ 1 - \frac{1}{6} c^2 e^{2\omega} + \mathcal{O}(e^{4\omega}) \right] , \quad (8.71)$$

where we imposed  $T \rightarrow 0$  as  $\omega \rightarrow -\infty$ . Taking (8.68) into account gives

$$\sqrt{|k|} T = S_0 e^\omega \left[ 1 - \frac{1}{6} c^2 e^{2\omega} + \mathcal{O}(e^{4\omega}) \right] , \quad (8.72)$$

where we have set  $S_0 := e^{4A_0 + B_0}$ , so that  $S = S_0 e^\omega$ , cf. below (8.50). Finally, inverting the perturbative series (8.72) we obtain

$$S = \sqrt{|k|} T \left[ 1 + \frac{1}{6} |\lambda| e^{-8A_0} T^2 + \mathcal{O}(T^4) \right] . \quad (8.73)$$

It then follows from (7.10) that  $w = -1 + \mathcal{O}(T^2)$ , in agreement with our previous result. Indeed up to and including terms of order  $\mathcal{O}(T^4)$  the spacetime metric becomes that of de Sitter space in hyperbolic slicing,

$$ds_{dS}^2 = -dT^2 + |k| \Lambda^2 \sinh^2 \left( \frac{T}{\Lambda} \right) d\Omega_k^2 ; \quad \Lambda := \frac{1}{\sqrt{|\lambda|}} e^{4A_0} , \quad (8.74)$$

where  $\Lambda$  is related to the scalar curvature  $R$  of de Sitter via  $\Lambda^2 = 12/R$ . This is not asymptotic de Sitter, however, as  $T = 0$  is reached at finite proper time in the past, where the space becomes a regular Milne universe. The solution can thus be geodesically completed in the past to  $T < 0$ , by gluing together its mirror trajectory in the  $z < 0$  region, cf. the comment in the paragraph preceding (8.46).

A similar analysis can be performed in the neighborhood of  $p_1$ . In that case we obtain  $S \rightarrow 2\sqrt{|k|} T$ , so that  $w \rightarrow -\frac{1}{3}$ , as the trajectory approaches  $p_1$ .

---

<sup>4</sup>We have obtained the perturbative solution to a very high order in  $e^{2\omega}$ , and we have shown that it is consistent with the closed expression,

$$2\sqrt{2|\lambda|} e^{-4A_0} T = c e^\omega + \operatorname{arcsinh}(c e^\omega) . \quad (8.70)$$

- **Comparison with the analytical solutions (B.139)**

It follows from the system (8.55) that the ellipse,

$$x = \frac{1}{2} ; \quad \frac{4}{3}y^2 + 2z^2 = 1 , \quad (8.75)$$

is an invariant submanifold. The upper vertex of the ellipse (at  $z = \frac{1}{\sqrt{2}}$ ) is the critical point  $p_1$ , while the left and right vertices (at  $y = \pm\frac{\sqrt{3}}{2}$ ) are both in  $p_C$ . The two trajectories starting at either the left or the right vertex of the ellipse and ending at the upper vertex, correspond precisely to the analytic solutions around (B.139).

- **Potential and kinetic energies**

The acceleration period can in fact be understood as a competition of the kinetic and potential energies of the system, as we would like to illustrate here.

Let us recall that, by comparing the energy-momentum tensor of a perfect fluid and that of a homogeneous scalar field  $\varphi$ , one can assign to the latter the following pressure and energy density,

$$\begin{aligned} p_\varphi &= \frac{1}{2}\dot{\varphi}^2 - V(\varphi) , \\ \rho_\varphi &= \frac{1}{2}\dot{\varphi}^2 + V(\varphi) . \end{aligned} \quad (8.76)$$

The acceleration condition  $w = p_\varphi/\rho_\varphi < -1/3$  then translates to

$$\dot{\varphi}^2 < V(\varphi) , \quad (8.77)$$

i.e. there is acceleration whenever the potential energy dominates (twice) the kinetic energy.

In our models, the 2-field 4d potential has the shape of an exponential “wall”, and the system can be thought in field space as thrown against that wall: initially the potential energy  $V$  is exponentially small and the kinetic energy  $K$  dominates. Eventually the system reaches the wall and starts climbing it,  $K$  decreases while  $V$  increases; when  $2K = V$ , acceleration begins, which starts to significantly dissipates energy (the Hubble term in the EOM of  $\varphi$  acts a friction term). When the potential energy becomes too important, the trajectory undergo a turnaround and goes back down the wall; the system starts to accelerate again and inflation stops whenever  $2K = V$ . Such a trajectory is depicted in Figure 8.3.

More quantitatively, in that case study the 4d potential is given by

$$V(A) = -6\lambda e^{-8A} . \quad (8.78)$$

To compute the kinetic energy, one first has to canonically normalize the fields,

$$A \rightarrow \tilde{A} = 4\sqrt{3}A , \quad \phi \rightarrow \phi . \quad (8.79)$$

Then, using  $g^{\tau\tau} = S(\tau)^{-3} = \exp(-13A - 3B)$ , the kinetic energy reads

$$K = \frac{1}{2}S^{-6} \left( (d_\tau \tilde{A})^2 + (d_\tau \phi)^2 \right) . \quad (8.80)$$

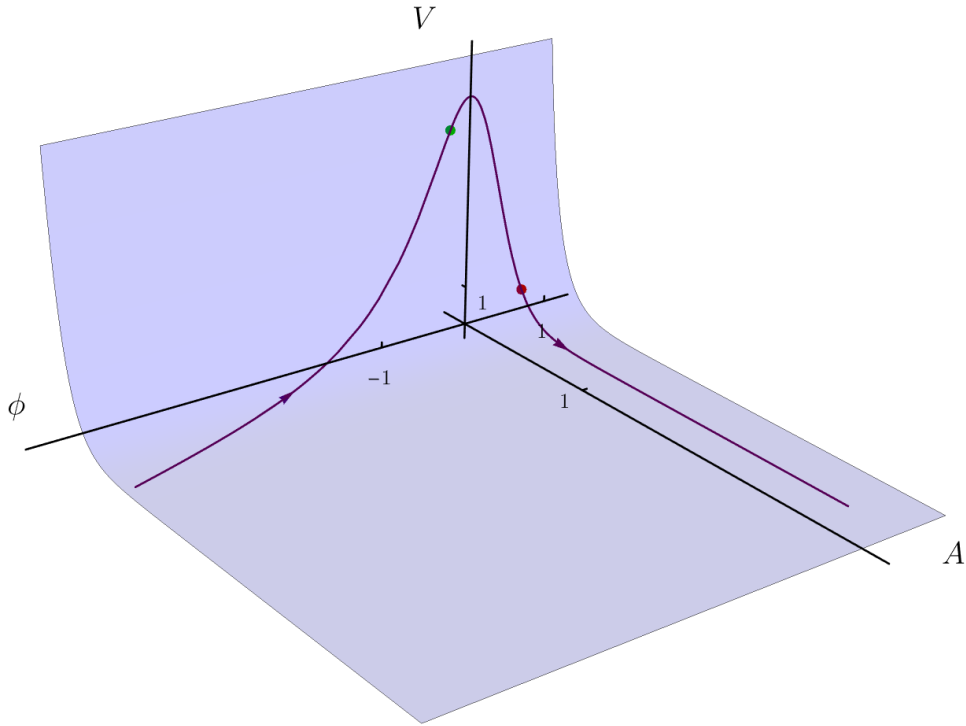


Figure 8.3: The scalar potential  $V$  plotted over the field space  $(A, \phi)$ . On it lies a typical trajectory featuring transient inflation: acceleration starts at the green dot and stops at the red dot. At these two special positions, the potential energy equals twice the kinetic energy.

We further use that  $d\omega/d\tau = \sqrt{-\lambda}/z e^{8A+3B}$ , cf. (8.38), and

$$\begin{aligned} d_\tau A &= d_\omega A \frac{d\omega}{d\tau} = \frac{\sqrt{-\lambda}}{z} \frac{1}{2} x e^{8A+3B} , \\ d_\tau \phi &= d_\omega \phi \frac{d\omega}{d\tau} = \frac{\sqrt{-\lambda}}{z} 2\sqrt{3} y e^{8A+3B} , \end{aligned} \quad (8.81)$$

to obtain

$$K = -6\lambda e^{-8A} \frac{x^2 + y^2}{z^2} = V \times \frac{x^2 + y^2}{z^2} . \quad (8.82)$$

The condition for acceleration  $\ddot{S} > 0 \Leftrightarrow V > 2K$  then precisely recovers the condition (8.86), which defines the boundaries of the acceleration region.

8.2.2 Case study II:  $k, m$ 

We now turn to the case where  $k, m \neq 0$ . Here, the system of equations reduces to

$$\begin{aligned} x' &= 2x(x^2 + y^2 - 1) + \frac{1}{2}(3 - 2x)z^2 \\ y' &= 2y(x^2 + y^2 - 1) - yz^2 - \frac{5\sqrt{3}z^2}{2} \\ z' &= \frac{1}{2}z \left( x(4x - 3) + 4y^2 + 5\sqrt{3}y - 2z^2 + 2 \right), \end{aligned} \quad (8.83)$$

while the constraint reads

$$12kz^2 e^{-2A-2B-\frac{5\phi}{2}} = m^2(x^2 + y^2 + z^2 - 1). \quad (8.84)$$

The invariant plane  $\mathcal{P}$  is given by the equation

$$5x + \sqrt{3}y = 0. \quad (8.85)$$

The acceleration condition reads

$$z^2 > 2(x^2 + y^2), \quad (8.86)$$

with

$$w = \frac{x^2 + y^2 - z^2}{x^2 + y^2 + z^2}. \quad (8.87)$$

• **Critical points**

The critical points are

$$p_C; \quad p_0; \quad p_1 = \left( \frac{1}{14}, -\frac{5}{14\sqrt{3}}, \sqrt{\frac{2}{21}} \right). \quad (8.88)$$

Both  $p_0$  and  $p_1$  lie on the boundary of the acceleration region and on the invariant plane. The point  $p_0$  requires  $m = 0$ , and corresponds to the critical solution of (B.40); the point  $p_1$  corresponds to the critical solution of (B.152).

The behavior close to the fixed point  $p_0$  is similar to that of the  $(\lambda, k)$  system analyzed in the previous section. As the trajectory approaches  $p_0$ , we have  $w \rightarrow -1$ , and the solution becomes de Sitter-like. This however is not an asymptotic de Sitter, as  $p_0$  is reached at finite proper time in the past. At  $p_0$  spacetime becomes a regular Milne universe, and the solution can be geodesically completed in the past by gluing its mirror trajectory in the  $z < 0$  region.

Close to the fixed point  $p_1$  we may linearize and solve (8.83) analytically. The solution reads, up to terms of order  $\mathcal{O}(e^{-2\omega})$ ,

$$\begin{aligned} A &= A_0 + \frac{1}{28}\omega + \frac{1}{2}ce^{-\omega}f(\omega) \\ B &= B_0 + \frac{6}{7}\omega - 2ce^{-\omega}f(\omega) \\ \phi &= \phi_0 - \frac{5}{7}\omega - 10ce^{-\omega}f(\omega), \end{aligned} \quad (8.89)$$

## Chapter 8. Cosmological solutions

---

where  $c$  is an integration constant, and we have defined

$$f(\omega) := \sqrt{17} \cos\left(\sqrt{\frac{17}{7}}\omega\right) + \sqrt{7} \sin\left(\sqrt{\frac{17}{7}}\omega\right). \quad (8.90)$$

In addition, the constraint imposes

$$k = -\frac{3}{4}m^2 e^{2A_0+2B_0+5\phi_0/2}. \quad (8.91)$$

It can be seen that, up to and including linear terms in  $\omega$ , the solution (8.89) corresponds to the critical solution of (B.152), with  $\tau \sim e^{-2\omega}$ . The acceleration can also be calculated analytically, cf. (8.46) and Footnote 2,

$$\ddot{S} = -\frac{12}{5}c e^{-2\omega} \left[ \sqrt{17} \cos\left(\sqrt{\frac{17}{7}}\omega\right) - 3\sqrt{7} \sin\left(\sqrt{\frac{17}{7}}\omega\right) \right], \quad (8.92)$$

up to terms of order  $\mathcal{O}(e^{-3\omega})$ . There is an infinite number of periodic cycles of accelerated expansion followed by decelerated expansion, each of which lasts a half period, thus contributing a number of e-foldings equal to

$$\Delta N = \sqrt{\frac{7}{17}} \pi, \quad (8.93)$$

where we have taken (8.51) into account. The scale factor can also be expressed in terms of the cosmological time,

$$S = \sqrt{\frac{7}{6}} \sqrt{|k|} T + \frac{7}{85} c S_0 \left( 19\sqrt{17} \cos\left(\sqrt{\frac{17}{7}} \ln T\right) - 17\sqrt{7} \sin\left(\sqrt{\frac{17}{7}} \ln T\right) \right) + \mathcal{O}\left(\frac{1}{T}\right), \quad (8.94)$$

where to lowest order,  $\ln T \sim \omega + \text{const}$ . The fixed point is reached as  $T \rightarrow \infty$ .

The oscillations of the system can be captured for instance by the equation of state parameter  $w$ . Since these are exponentially damped, we rather consider the following quantity,

$$W(\omega) := -\left(w(\omega) + \frac{1}{3}\right) e^\omega, \quad (8.95)$$

plotted in Figure 8.4, which is positive whenever there is acceleration, and negative otherwise.

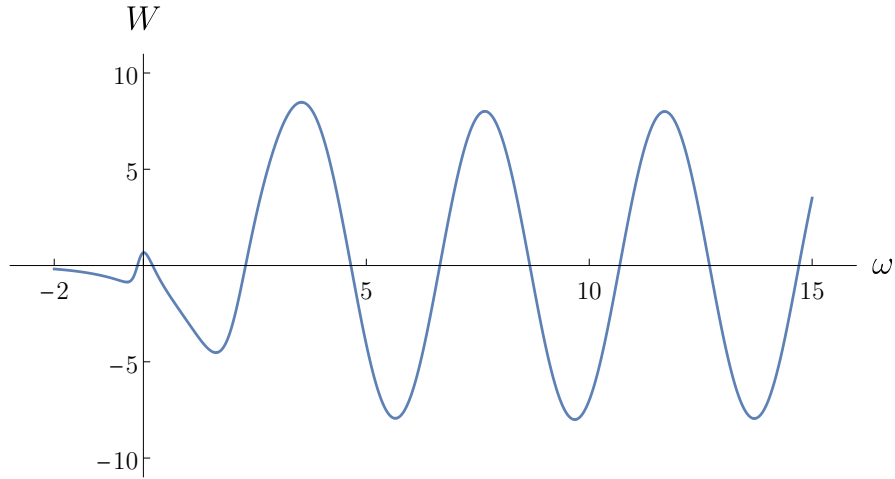


Figure 8.4: Plot of  $W$  as a function of  $\omega$ , as defined in (8.95). (Half-) periods of acceleration correspond to  $W > 0$ . As  $\omega$  increases, the duration of these accelerated periods tends to  $\sqrt{\frac{7}{17}}\pi$  in the variable  $\omega$ .

### 8.2.3 Case study III: $\lambda, m$

We proceed with the case where  $\lambda, m \neq 0$ . Here, the dynamical system is given by

$$\begin{aligned} x' &= (6x - 4)(x^2 + y^2 - 1) - z^2 \\ y' &= 6y(x^2 + y^2 - 1) - 5\sqrt{3}z^2 \\ z' &= z \left[ 6x^2 - 3x + y(5\sqrt{3} + 6y) \right], \end{aligned} \quad (8.96)$$

together with the constraint

$$1 - x^2 - y^2 - z^2 = -12 \frac{\lambda z^2}{m^2} e^{-2A - 5\phi/2}. \quad (8.97)$$

For  $\lambda < 0$ , this forces the trajectories to lie within a unit ball in three-dimensional phase space. The invariant plane is given by

$$\mathcal{P} = \left\{ (x, y, z) \in \mathbb{R}^3 \mid 15x - \sqrt{3}y = 10 \right\}. \quad (8.98)$$

The acceleration condition reads

$$x^2 + y^2 < \frac{1}{3}, \quad (8.99)$$

with,

$$w = -1 + 2(x^2 + y^2). \quad (8.100)$$

#### • Critical points

There is a unique critical point of the system (8.96) away from the  $z = 0$  plane, given by

$$p_1 = \frac{1}{38\sqrt{3}} \left( 25\sqrt{3}, -5, 8\sqrt{2} \right). \quad (8.101)$$



The critical point  $p_1$  lies on the invariant plane  $\mathcal{P}$ . The linearized system at  $p_1$  has one real and two complex conjugate eigenvalues:  $\frac{16}{19}(-4, -2 \pm i\sqrt{2})$ . The eigenvectors corresponding to the real and complex eigenvalues are orthogonal and parallel to the invariant plane  $\mathcal{P}$ , respectively. It follows that for trajectories in  $\mathcal{P}$ ,  $p_1$  is a stable focus; for trajectories orthogonal to  $\mathcal{P}$ ,  $p_1$  is a stable node.

In addition we have a circle of fixed points on the equator  $\mathcal{C}$  of the sphere  $\mathcal{S}$ ,

$$p_C \in \mathcal{C} := \{(x, y, z) \mid x^2 + y^2 = 1 ; z = 0\} , \quad (8.102)$$

and an isolated fixed point,

$$p_2 = \left(\frac{2}{3}, 0, 0\right) , \quad (8.103)$$

which lies on the  $x$ -axis. The linearized system at  $p_2$  has eigenvalues  $\frac{2}{3}(-5, -5, 1)$ . The eigenvectors corresponding to the negative eigenvalue are along the  $x$  and  $y$  directions, whereas the eigenvector corresponding to the positive eigenvalue is along the  $z$  direction. It follows that for trajectories in the  $z = 0$  plane,  $p_2$  is a stable singular node; for trajectories orthogonal to the  $z = 0$  plane,  $p_2$  is an unstable node.

The critical points of the dynamical system correspond to solutions that can be given analytically: the point  $p_1$  corresponds to the solution (B.145). The point  $p_2$  corresponds to the critical solution with  $\lambda < 0$ , and requires  $m = 0$ . The critical points  $p_C$  correspond to the minimal solution of Section 8.1.1, and require  $m, \lambda = 0$ .

• **The invariant surface  $\mathcal{S}$**

Restricting to trajectories on  $\mathcal{S}$ , the system (8.96) implies

$$x' = 6\left(x - \frac{1}{2}\right)(x^2 + y^2 - 1) ; \quad y' = 6\left(y + \frac{5}{2\sqrt{3}}\right)(x^2 + y^2 - 1) . \quad (8.104)$$

It follows that the projections of all trajectories on  $\mathcal{S}$  to the  $z = 0$  plane are of the form

$$a\left(x - \frac{1}{2}\right) + b\left(y + \frac{5}{2\sqrt{3}}\right) = 0 ; \quad a, b \in \mathbb{R} , \quad (8.105)$$

i.e. straight lines passing by the point  $(x, y) = \left(\frac{1}{2}, -\frac{5}{2\sqrt{3}}\right)$ . These trajectories correspond precisely to the solutions of (B.134), and require  $\lambda = 0$ . More specifically, the slope of the line (8.105) is related to the constants in (B.134) via

$$\frac{a}{b} = \frac{64c_A + 13c_B}{5\sqrt{3}c_B} . \quad (8.106)$$

• **The invariant plane  $z = 0$**

Restricting to trajectories on the  $z = 0$  plane, the system (8.96) reduces to

$$x' = 6\left(x - \frac{2}{3}\right)(x^2 + y^2 - 1) ; \quad y' = 6y(x^2 + y^2 - 1) . \quad (8.107)$$

It follows that all trajectories on the  $z = 0$  plane are of the form

$$a\left(x - \frac{2}{3}\right) + by = 0 ; \quad a, b \in \mathbb{R} , \quad (8.108)$$

i.e. straight lines passing by the point  $(x, y) = \left(\frac{2}{3}, 0\right)$ . These straight lines correspond precisely to the solutions of (B.127), and require  $m = 0$ . More specifically, the slope of the line (8.108) is related to the constants in (B.127) via

$$\frac{a}{b} = -\frac{3\sqrt{3} c_\phi}{20 c_A} . \quad (8.109)$$

• The invariant plane  $\mathcal{P}$

On  $\mathcal{P}$ , the system (8.96) reduces to

$$\begin{aligned} x &= \frac{2}{3} + \frac{1}{5\sqrt{3}}y \\ y' &= \frac{2}{75}y(-125 + 20\sqrt{3}y + 228y^2) - 5\sqrt{3}z^2 \\ z' &= \frac{2}{75}z(25 + 200\sqrt{3}y + 228y^2). \end{aligned} \quad (8.110)$$

All trajectories of the reduced system spiral into the stable focus  $p_1$ .

8.2.4 Case study IV:  $\varphi, \chi$

Let us finally consider the case where  $\varphi, \chi \neq 0$ . The system of equations is given by

$$\begin{aligned} x' &= x^2 - 3xz^2 + y^2 + \frac{11}{2}z^2 - 1 \\ y' &= \sqrt{3}(x^2 + y^2 + z^2 - 1) + \frac{1}{2}(\sqrt{3} - 6y)z^2 \\ z' &= -\frac{1}{2}z(9x + \sqrt{3}y + 6z^2 - 6), \end{aligned} \quad (8.111)$$

together with the constraint,

$$-3z^2c_\varphi^2e^{-2A-6B+\frac{3\phi}{2}} = c_\chi^2(x^2 + y^2 + z^2 - 1). \quad (8.112)$$

The invariant plane is defined by

$$3x - \sqrt{3}y = 4, \quad (8.113)$$

and the acceleration condition is simply given by

$$z > \sqrt{\frac{2}{3}}, \quad (8.114)$$

so that a trajectory undergoes acceleration whenever it passes above the  $z = \sqrt{\frac{2}{3}}$  plane. The equation of state parameter reads

$$w = 1 - 2z^2. \quad (8.115)$$

This system admits no fixed points, apart from those lying on the equator  $\mathcal{C}$ . Nevertheless, it is worth being discussed, in view of its connection with analytic solutions.

As argued previously, the particular case  $\varphi = 0$  and  $\chi = 0$  corresponds to one of the fixed points on  $\mathcal{C}$ , and coincide with the minimal solution (8.8). When only  $\varphi$  is turned on, the solutions are restricted to the boundary  $\mathcal{S}$  of the phase space (and their projection on the  $z = 0$  plane are straight lines); if both fluxes  $\varphi$  and  $\chi$  are turned on, trajectories live generically in the bulk and connect two fixed points of  $\mathcal{C}$ . In the former case, the trajectory that maximizes the number of e-foldings  $N$  is the one passing by the North pole: it obviously maximizes its length inside the acceleration region, but also turns out to maximize its “time” spent inside the region (which is not necessarily

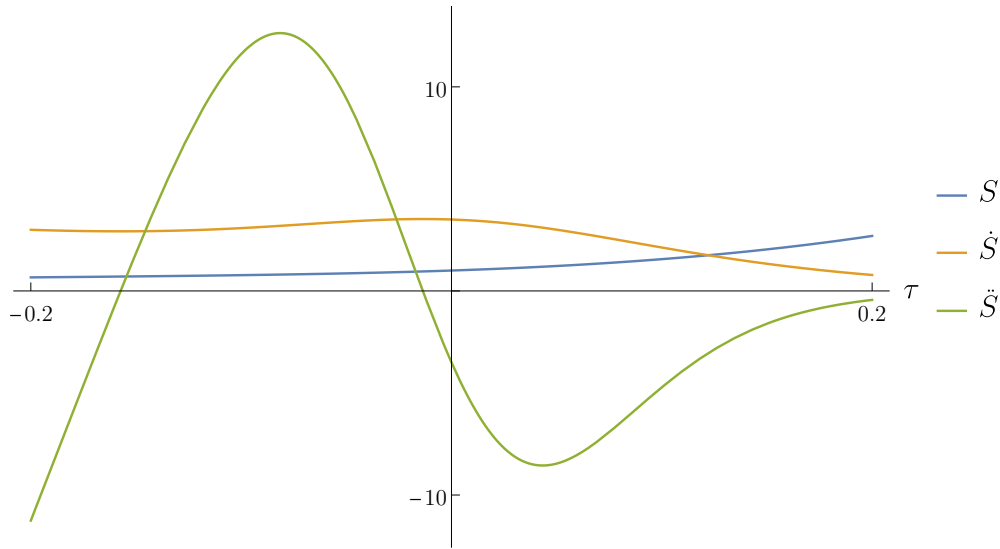


Figure 8.5: Plot of the scale factor  $S$  and its derivatives  $\dot{S}, \ddot{S}$  as functions of  $\tau$ , with parameter  $r = -\frac{9}{8}$ . This special value yields the extremal case with  $N = N_{\max} = 0.30408$ .

the same). Numerically, this maximal number of e-foldings can be determined to be  $N_{\max} = 0.30408$ .

Now, let us turn to the corresponding analytic solutions (B.43) found for  $\varphi \neq 0, \chi = 0$ . There exists a family of solutions parameterized by a real number<sup>5</sup>  $r \leq -\frac{11}{16}$ , with the following scale factor,

$$S(\tau) = e^{(4r+1)\tau} \cosh^{\frac{1}{4}}(2\sqrt{-33-48r}\tau) . \quad (8.116)$$

Having the explicit scale factor  $S$  at hand allows us to compute the derivatives  $\dot{S}, \ddot{S}$  and determine the values of  $\tau$  for which accelerated expansion starts and stop (or in other words determine the values of  $\tau$  for which one can satisfy both  $\dot{S} > 0$  and  $\ddot{S} > 0$ ), see Figure 8.5. We can then readily compute the number of e-foldings  $N(r)$  and extremize it with respect to  $r$ , see Figure 8.6. The maximal value is reached for  $r_{\max} = -\frac{9}{8}$ , which precisely gives the same  $N_{\max} = 0.30408$  as above, and is of course in line with the bound  $N_{\max} \leq 0.59980$  found in Section 8.1.2 for one-flux compactifications.

### 8.3 Outlook

It has been known for some time that transient accelerated expansion is not difficult to achieve in flux compactifications arising from string-theory effective 10d supergravities. What the present work is suggesting is that cosmologies featuring eternal or semi-eternal acceleration, or a parametric control on the number of e-foldings are also generic! The necessary ingredients in all instances thereof seem to be a negative spatial 4d curvature

<sup>5</sup>The solutions actually depend on two parameters,  $r$  and  $c_B$ , but it turns out that the number of e-foldings only depends on the former, so we can restrict to  $c_B = 1$ .

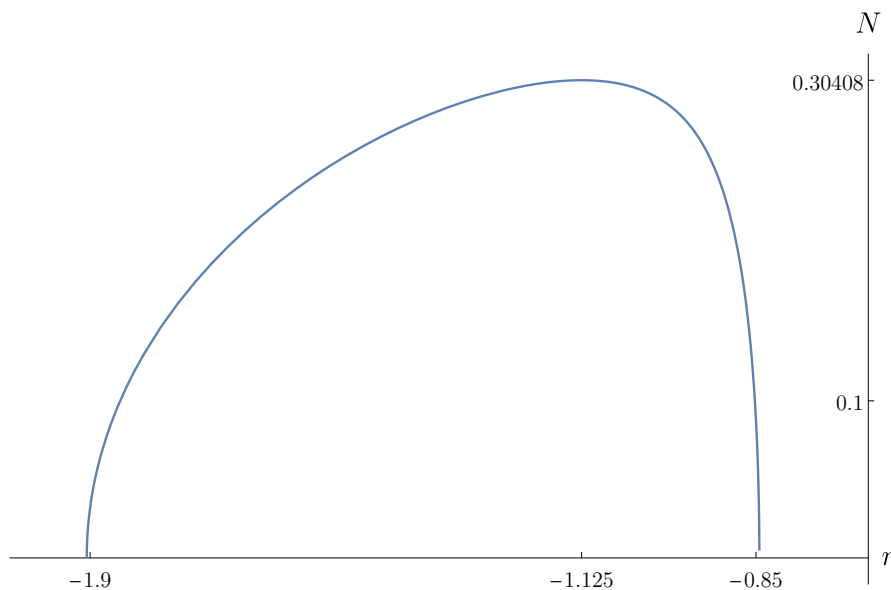


Figure 8.6: Number of e-foldings  $N$  as a function of the parameter  $r$ , for the one-flux solutions  $\varphi \neq 0$ . There is a restricted range permitting transient acceleration, and the maximal value is reached for  $r_{\max} = -\frac{9}{8}$ , giving  $N_{\max} = 0.30408$ .

(open universe), and a fixed point on the boundary of the acceleration region in the interior of the phase space.

To our knowledge, this is also the first time where examples of spiraling cosmologies with an infinite number of cycles alternating between accelerated and decelerated expansion have been shown to arise from compactification of string-theory effective 10d supergravities. This so-called “rollercoaster cosmology” has been argued to be a potentially viable alternative for inflation [215].

In all examples exhibiting a parametric control on the number of e-foldings, the acceleration vanishes asymptotically at future infinity, where spacetime approaches a Milne universe with angle defect. Moreover, these are all captured by the 4d consistent truncation (7.22) with potential given in (7.25), and require turning on one of the parameters  $\lambda$ ,  $m$ ,  $c_\varphi$ ,  $c_0$  or  $c_f$ . Smooth accelerating cosmologies, without Big Bang singularities, are also possible, and they correspond to unique fine-tuned (therefore unstable) trajectories in phase space. Instead of a singularity at  $T = 0$ , the spacetime approaches de Sitter space (in hyperbolic slicing). This, however, is not an asymptotic de Sitter, as  $T = 0$  is reached at finite proper time. These solutions can be geodesically completed to  $T < 0$  in the past, as explained previously.

As we have shown, the techniques presented here allow us to straightforwardly translate the trajectories in phase space to the explicit form of the scale factor  $S(T)$  of the corresponding FLRW solution, as a function of cosmological time. From this, the other cosmological observables can all be readily computed.

Our approach has been to work with the 10d equations of motion, not with a 4d effective potential. Nevertheless, in certain cases a graviton plus two-scalar (dilaton and warp factor) consistent truncation to a 4d theory  $S_{4d}$  is possible, such that all cosmological

solutions of  $S_{4d}$  lift to ten-dimensional solutions of IIA supergravity. This does not mean that solutions of  $S_{4d}$  uplift to 10d solutions with only dilaton and warp factor: all information about the flux (which is generically non-vanishing from the ten-dimensional point of view) enters the 4d potential of  $S_{4d}$  via certain constants.

The action  $S_{4d}$  is in fact a consistent sub-truncation of the universal CY consistent truncation of [216, 217]. Indeed, it was shown in those references that *the 4d effective theory of the universal sector of CY type II compactifications is also a consistent truncation of 10d type II supergravity*. We thus expect the consistent truncation  $S_{4d}$  of (7.22) to be part of the 4d effective action, and thus subject to e.g. the analysis and constraints presented recently in [208].

A general stability analysis of the cosmological solutions presented here would require considering (small) perturbations in the space of all 10d fields. We shall leave this important point for future work.

The dynamical system techniques as applied here, limit us to solutions with a maximum of two species of flux. It would be desirable to overcome this limitation and explore richer solutions with all possible fluxes turned on, in each universal compactification class.

Finally, setting aside the still unresolved conceptual issues associated with smeared orientifolds and  $D$ -branes, including such sources in our analysis would certainly enrich the structure of the phase space of the dynamical systems presented here, potentially leading to the appearance of fixed points corresponding to de Sitter solutions. It would be interesting to explore this possibility further.

WARP FACTOR AND THE GRAVITATIONAL WAVE SPECTRUM

PART III



# 9 Kaluza–Klein gravitational waves in a warped toroidal background

## 9.1 Context and motivations

Gravitational waves astronomy has developed in recent years at a remarkable pace. In the latest run (O3) of ground based detectors LIGO and Virgo (lately joined by KAGRA and GEO), one to two candidate events were detected every week [218, 219]. Further recent or coming observations are promising, including results by NANOGrav (and PTA) [220], while numerous exciting experiments are planned, among which the awaited eLISA. This impressive new observational window provides non-trivial tests of General Relativity [221], but it also offers the prospect of discovering new physics. Recent reviews on expectations for fundamental physics from gravitational waves can be found e.g. in [222–225]. One fascinating example would be evidence for new scalar fields, possibly axions, as described through scalar-tensor models. Such fields could for instance be present in scalar clouds around black holes, thus having various impacts on emitted gravitational waves, or even lead to scalar waves, or effects on black hole shadows [226–229]. Another interesting example are constraints or predictions that can be made with gravitational waves in string theory frameworks [230–233]. In this work, we are interested in new fundamental physics at high energy, that could leave specific signatures in gravitational waves detectable in future experiments. This is possible if the high energy events are taking place in the early universe. Indeed, the redshift due to cosmological expansion can then lower the frequency of primordial gravitational waves, allowing for an observation by e.g. eLISA. Typical high energy events in the early universe leading to the emission of such gravitational waves are related to primordial black holes [234] or (electroweak) first order phase transitions [235–238]; others can be found e.g. in [239]. Here we are interested in extra dimensions and related Kaluza–Klein towers, typically considered at high energies. Recent studies on their impact on gravitational waves include [240–242]. We focus in this chapter on the Kaluza–Klein tower of (massive) gravitational waves obtained from certain extra dimensions. We assume that events of high enough energy, possibly in the early universe, have excited the first states of this tower, and that the corresponding emitted primordial gravitational waves could be detected in future experiments. Such a possibility would provide a very distinct signature of extra dimensions. A crucial question is then that of the precise spectrum of these four-dimensional (4d) Kaluza–Klein gravitational waves.

We are interested here in a background with a warp factor. Many bottom-up



phenomenological constructions, or top-down models coming from string theory compactifications, include extended objects as branes, that typically host matter and gauge interactions. Such extended objects back-react on the geometry: this is captured in the metric by a function  $H$  called the warp factor. It is thus legitimate to consider such a warped gravitational background. Many BSM studies have used backgrounds and warp factor coming from Randall-Sundrum models [243, 244]. Motivated by a string theory origin, we rather use here the warp factor coming from  $p$ -brane solutions in supergravity compactifications (see e.g. [82]). A specificity is that the  $D_p$ -branes in that case, as well as orientifold  $O_p$ -planes to be considered, are not only back-reacting on the geometry: they also source a  $U(1)$  gauge field (or a generalization thereof). The latter is also described by the warp factor  $H$ , which is in turn the solution to a Poisson equation, i.e. a sourced Laplace equation. The warp factor to be considered in such a string or supergravity compactification context is thus not simple, since it involves Green’s functions on compact spaces, typically poorly known. We nevertheless tackled this question in [170] and provided a complete expression for such a generalized Green’s function on a torus  $\mathbb{T}^d$ , and consequently of the warp factor generated by a distribution of  $D_p/O_p$  sources: illustrations are provided in Figures 9.1 and 9.2. This allowed us to provide a first estimate of the spectrum of Kaluza–Klein gravitational waves, on a background being a warped product of Minkowski and toroidal extra dimensions. This material is reviewed and extended in section 9.2, building on [245, 246]. In the present work, we will overcome previously unnoticed difficulties and make important technical improvements, that will allow a much more complete and precise determination of this spectrum.

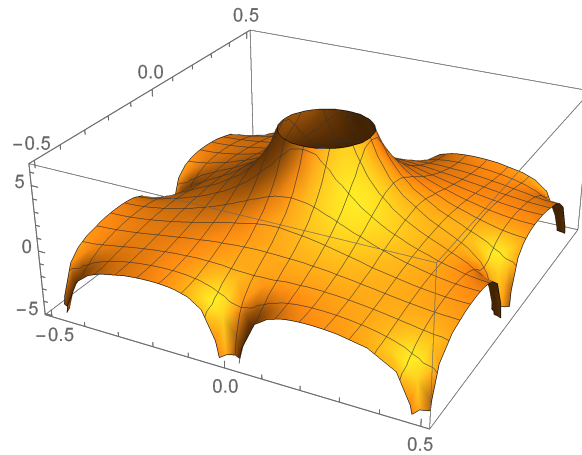


Figure 9.1: Illustration of the warp factor  $H$  on a torus  $\mathbb{T}^d$ , due to the distribution of sources detailed at the beginning of section 10.1:  $D_p$ -branes at the center and  $O_p$ -planes on the sides. Detailed specifications:  $d = 3$ ,  $p = 6$ ,  $H$  is represented up to a constant and rescaled, i.e.  $g_s^{-1}(L/l_s)(H(\boldsymbol{\sigma}) - H_0)$ , and valued on the vertical axis in terms of the coordinates  $\sigma^1, \sigma^2$  on horizontal axis, while  $\sigma^3 = 0$ .

The aim of this chapter is the determination of the Kaluza–Klein gravitational waves spectrum, but various problems encountered related to the warp factor and its sources

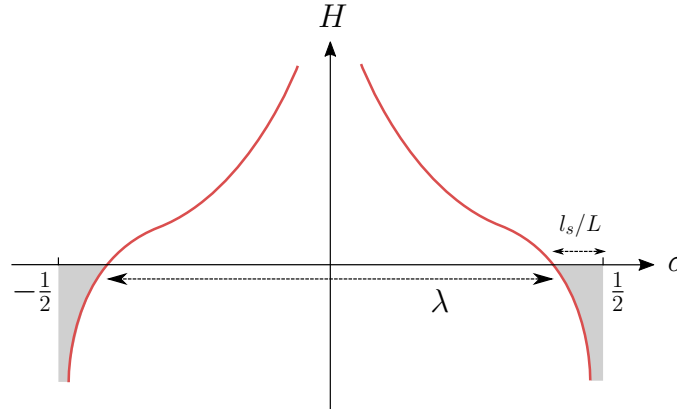


Figure 9.2: Illustration of the warp factor  $H$  along one periodic coordinate  $\sigma \in (-\frac{1}{2}, \frac{1}{2}]$ , generated by  $D_p$ -branes at  $\sigma = 0$  and  $O_p$  at  $\sigma = \frac{1}{2}$ . The average of  $H$  is adjusted such that  $H = 0$  at a string length  $\sigma = \frac{l_s}{L}$  from the  $O_p$ . This leaves a “negative region”, depicted in gray, where  $H < 0$ . To avoid this problematic region, we will conduct the analysis on a restricted domain  $\mathcal{D}$  of size  $\lambda = 1 - 2\frac{l_s}{L}$ . Detailed specifications:  $d = 2$ ,  $p = 7$ , the source distribution is given at the beginning of section 10.1,  $H$  is rescaled as  $g_s^{-1}(L/l_s)^{d-2}H$  and plotted along  $\sigma^2$ , while  $\sigma^1 = 0$ .

could be of broader interest, and find echoes in the recent string compactification literature. To start with, the warp factor has been at the center of many recent discussions, often connected to (anti-) de Sitter compactifications. The warp factor and its determination plays a crucial role in testing some swampland conjectures in specific anti-de Sitter solutions [165, 166]. Choosing for it and the dilaton non-standard boundary conditions close to  $O_p$  sources has led to debated new de Sitter solutions [247–251]; we come back to this discussion in detail in section 9.2.2. As here, though on a different background metric, the impact of the warp factor on the Kaluza–Klein spectrum appeared important in [252], as it revealed new light states that could play a critical role in the KKLT scenario [41]. Kaluza–Klein spectra, in warped compactifications to anti-de Sitter, were also computed recently in e.g. [253–256] (see also [161, 257] in relation to scale separation), even though the warp factor is then of different origin and takes a different form. Last but not least, the validity of supergravity approximations has been tested in detail in standard Minkowski compactifications with  $O_6$  in [173], building in part on [170].

More generally, this question of supergravity approximations and regime is at the heart of many of the above works, and became dramatically important for the KKLT scenario in the recent works [258, 259]. There, one considers as extra dimensions a warped compact Calabi-Yau manifold, where the warp factor is generated by various  $D_p/O_p$ . It has been pointed out [258] (see also [260]) that the negative region around an  $O_p$ , meaning where  $H < 0$  as illustrated in Figure 9.2, is likely to be large, i.e. of order of the size of the Calabi-Yau itself, in order to realise the KKLT scenario. This is problematic because within the used supergravity description, the warp factor is considered positive: see [170] or section 9.2.1 here. A first reason for requiring  $H > 0$  is that it enters the metric, and a change of sign would lead to problematic loci. The place where  $H = 0$  is thus sometimes referred to as the orientifold horizon or the singularity. A physical resolution to this problematic negative region is then hoped to come from string theory:

one argues that the classical and perturbative string regime corresponding to supergravity does not hold anymore in that region, and new stringy physics takes over. To enforce this argument in our simple setting, we use the prescription of [170] that fixes the horizon at a string length distance from the  $O_p$ , as depicted in Figure 9.2: this way, we ensure that string degrees of freedom should come in and the supergravity description breaks down. We give more details in Section 9.2.1, and compare to the compactifications of [258] and [173]. In [258], other ingredients set the size of this horizon or singularity, forcing it to be large. This implies the need of a stringy description over a large region of the Calabi-Yau. A first sketch of such a possibility has been proposed in [259]: it invokes non-perturbative stringy contributions to resolve this problematic region.

This negative region, on top of being unphysical in our supergravity description, became even more problematic to us because it would lead to tachyonic modes in the Kaluza–Klein spectrum. We argue indeed on general grounds in Section 10.1.1 and Appendix A.1 why such a negative region is likely to always generate tachyons. Due to a precision matter discussed in Appendix A.3, this phenomenon became more manifest to us when the negative region was large compared to the overall size  $L$  of the torus (e.g. for  $L/l_s < 10$ ). We thus developed tools in Section 10.1.2 to ignore that region, and solve our spectral problem on a restricted domain  $\mathcal{D}$  where  $H > 0$ , as illustrated in Figure 9.2, allowing for a spectrum without tachyonic modes. It would be interesting to see whether this problem of tachyons and the tools developed here could apply to the framework of [258, 259].

The spectrum is determined on the restricted domain  $\mathcal{D}$  where the supergravity description can be trusted. One may wonder whether the remaining region where  $H < 0$ , requiring a stringy description, could lead to important modifications of the spectrum. Capturing this extra contribution from another region actually amounts to fixing boundary conditions for each eigenmode on the restricted domain. This is a standard procedure, used for instance at the horizon of black holes. One may then reformulate the question by asking how much the spectrum is dependent on the boundary conditions imposed in  $\mathcal{D}$ . As detailed in Section 10.1.2, we consider here periodic boundary conditions on  $\mathcal{D}$ : this is actually a generic choice for any (square-integrable, piecewise-continuous) function on an interval. For this reason, we believe that the spectrum determined here is robust. It would be interesting to test the dependence on the boundary conditions more thoroughly. Leaving periodicity on  $\mathcal{D}$  would however require a different resolution method, which goes beyond the scope of the present work.

Beyond this treatment of the negative region, several important improvements are made in the numerical method used to solve the eigenmode equation, in comparison to [170]. Those are detailed in Section 10.1.3 and Appendix A.2. Various innovations allow to reach a better precision, and many more points (Fourier modes), making use in particular of the hyperoctahedral symmetries of the problem. We get this way a part of the spectrum for  $\mathbb{T}^d$  with  $d = 1, \dots, 6$ , while the analysis stopped at  $d = 3$  in [170], and many more eigenmodes for the first dimensions  $d$ . The spectrum is given in Section 10.2, and a summary of the results is provided in Section 10.3. Comparison to the older method and (tachyonic) spectrum of [170] is made in Appendix A.3.

## 9.2 The general set-up

Building on [170], we present in Section 9.2.1 the warped background over which Kaluza–Klein gravitational waves are studied, and in Section 9.2.3 the key equations defining their spectrum. We allow ourselves a digression in Section 9.2.2, where we comment on the profile of the warp factor when moving away from a source, connecting to the discussion of [248, 249] on boundary conditions.

### 9.2.1 The toroidal $p$ -brane background and its warp factor

We are interested in Kaluza–Klein gravitational waves propagating in a 4d Minkowski space-time, corresponding to a compactification on a  $D$ -dimensional toroidal  $p$ -brane background. In this subsection, we present this background, following [170]. The  $D$ -dimensional background metric is, in Einstein frame,

$$ds_E^2 = H^{-\frac{D-p-3}{D-2}} (\eta_{\mu\nu} dx^\mu dx^\nu + \delta_{ij} dx^i dx^j) + H^{\frac{p+1}{D-2}} \delta_{mn} dy^m dy^n . \quad (9.1)$$

The 4d Minkowski indices are  $\mu, \nu = 0, \dots, 3$ , while the compact toroidal indices are  $i, j = 4, \dots, p$  and  $m, n = p+1, \dots, D-1$ . The  $p$ -brane world-volume is along the first  $p+1$  dimensions, labeled with  $\mu$  and  $i$ , and it is transverse to the remaining  $D-p-1$  dimensions labeled with  $m$ . The distinction between the parallel and transverse dimensions is made thanks to the warp factor  $H$ , which has different powers along these different directions. The transverse torus  $\mathbb{T}^d$ , with  $d = D - p - 1$ , will play a crucial role in the following, because the warp factor only depends on its coordinates  $H(\mathbf{y})$ . Here and in the following, we denote  $d$ -dimensional vectors with a boldface, e.g.  $\mathbf{y}$ . We will consider a square torus, i.e. each coordinate verifies the identification  $y^m \sim y^m + 2\pi L$  with same radius  $L$ . Convenient coordinates will then be  $\sigma^m = y^m / (2\pi L) \in (-\frac{1}{2}, \frac{1}{2}]$ .

The  $p$ -brane background is a solution to an Einstein–Maxwell–dilaton type of theory. The warp factor captures the back-reaction of the  $p$ -brane, but it also gives the dilaton, and the flux or field-strength sourced electrically (or magnetically, according to conventions) by the  $p$ -brane. The latter gets translated into a Poisson equation on  $H$  over the (unwarped) compact transverse torus  $\mathbb{T}^d$ , whose solution is given by a generalized Green’s function  $G$ . In the following we will consider not only one but a distribution of such sources, each of them having a charge  $Q_i$ , and placed at a position  $\mathbf{y}_i$  in  $\mathbb{T}^d$ . More precisely, in reference to the corresponding stringy objects, the sources will be named  $D_p$ -brane or orientifold  $O_p$ -planes, with  $D$ -dimensional charge

$$Q_{D_p} = -(2\pi l_s)^{d-2} g_s , \quad Q_{O_p} = -2^{4-d} Q_{D_p} , \quad (9.2)$$

where  $l_s$  is the string length (or the fundamental length in a broader setting), and  $g_s$  a constant related to the string coupling. In such a distribution of sources, the resulting warp factor was shown in [170] to be given by

$$H = \sum_i Q_i G(\mathbf{y} - \mathbf{y}_i) + H_0 , \quad (9.3)$$

with a constant  $H_0$ . Both the generalized Green’s function  $G$  and the constant  $H_0$  are non-trivially determined, as we will now recall. We consider in the following a chargeless source configuration, i.e. with  $\sum_i Q_i = 0$ : in the absence of extra fluxes, this vanishing is

## Chapter 9. Kaluza–Klein gravitational waves in a warped toroidal background

required by compactness [170].

The generalized Green's function  $G$  on the torus  $\mathbb{T}^d$  was discussed and studied in [170], using Courant-Hilbert [261], or the comparatively recent [262] based as well on century-old mathematical references. Both  $H$  and  $G$  have to be periodic on  $\mathbb{T}^d$ , so a first naive expression as a Fourier series is

$$G(\boldsymbol{\sigma}) = -\frac{1}{(2\pi L)^{d-2}} \sum_{\mathbf{n} \in \mathbb{Z}^{d*}} \frac{e^{2\pi i \mathbf{n} \cdot \boldsymbol{\sigma}}}{4\pi^2 \mathbf{n}^2}, \quad (9.4)$$

with  $\mathbb{Z}^{d*}$  being  $\mathbb{Z}^d$  without  $\mathbf{0}$ . This sum is however not absolutely convergent for  $d \geq 2$ . An appropriate regularization is provided thanks to the following expression

$$G(\boldsymbol{\sigma}) = (2\pi L)^{2-d} \int_0^\infty dt \left( 1 - \prod_{m=1}^d \theta_3(\sigma^m | 4\pi i t) \right), \quad (9.5)$$

in terms of the theta function  $\theta_3 = \theta_{00}$ .<sup>1</sup> This expression holds up to a constant, which will not matter in  $H$  thanks to  $\sum_i Q_i = 0$ . Studying this expression in [170], we could recover analytically the expected behaviour close to the source, namely

$$\begin{aligned} d \geq 3: & \quad (2\pi L)^{d-2} G(\boldsymbol{\sigma}) \sim_{\sigma^2 \rightarrow 0} -\frac{1}{4\pi^{\frac{d}{2}}} \Gamma\left(\frac{d-2}{2}\right) \frac{1}{|\boldsymbol{\sigma}|^{d-2}}, \\ d = 2: & \quad G(\boldsymbol{\sigma}) \sim_{\sigma^2 \rightarrow 0} \frac{1}{2\pi} \ln |\boldsymbol{\sigma}|, \\ d = 1: & \quad (2\pi L)^{-1} G(\boldsymbol{\sigma}) \sim_{\sigma^2 \rightarrow 0} -\frac{1}{12} + \frac{|\boldsymbol{\sigma}|}{2}. \end{aligned} \quad (9.6)$$

The constant  $H_0$  is a crucial piece of information. One first shows that it is the average of  $H$ : for  $\sum_i Q_i = 0$ , using the periodicity in  $\sigma^m$ , one gets

$$\int_{-\frac{1}{2}}^{\frac{1}{2}} d^d \boldsymbol{\sigma} H = H_0. \quad (9.7)$$

One also verifies thanks to (9.6) that the  $d$ -dimensional integral of  $G$  is finite. In the case where  $\sum_i Q_i \neq 0$ , one could add to  $G$  a constant opposite to its  $d$ -dimensional integral, allowing to recover (9.7). We show additionally in [170] that this average of  $H$  (9.7) appears in several important places, including the 4d Planck mass, or a condition necessary to have a standard massless 4d gravitational wave. It is then required to have  $H_0 \neq 0$ . Its value actually plays an important role, as we now explain.

To avoid singularities and signature changes in the background metric (9.1), we require  $H > 0$ . As indicated with Figure 9.2, the source distribution considered however typically generates a part of the space where  $H < 0$ . This happens close to the  $O_p$ . Such sources remain necessary on a compact space because they provide charges opposite

<sup>1</sup>The convention here is

$$\theta_3(\sigma|\tau) = \sum_{n \in \mathbb{Z}} e^{2\pi i(n\sigma + \frac{n^2}{2}\tau)} = 1 + 2 \sum_{n=1}^{\infty} q^{n^2} \cos(2\pi n\sigma), \quad \text{with } q = e^{i\pi\tau}.$$

to those of the  $D_p$ . A strategy then consists in controlling the size of this “negative region” where  $H < 0$ , by allowing it to be at most of string length size away from the  $O_p$ . The reason is that below a distance  $2\pi l_s$ , new stringy physics is expected while supergravity description breaks down, so our analysis can in any case only be trusted up to this point. Fixing this distance is made possible thanks to the constant  $H_0$ , which “shifts  $H$  vertically” in Figure 9.2. The corresponding prescription of [170] was

$$H_0 = - \min_j \left\{ \sum_i Q_i G(\boldsymbol{\sigma} - \boldsymbol{\sigma}_i) \Big|_{|\boldsymbol{\sigma} - \boldsymbol{\sigma}_j| = \frac{l_s}{L}} \right\}, \quad (9.8)$$

such that  $H = 0$  at a distance  $|\mathbf{y} - \mathbf{y}^j| = 2\pi l_s$ , i.e.  $|\boldsymbol{\sigma} - \boldsymbol{\sigma}_j| = \frac{l_s}{L}$ , of any  $O_p$  labeled  $j$  or closer to it. Note that in each circle of  $\mathbb{T}^d$ , a distance of  $2\pi l_s$  at least should be allowed on each side of an  $O_p$ , to be able to have a further “positive” region described by supergravity. So circle perimeters should be larger, i.e.  $2\pi L > 2 \times 2\pi l_s$  or  $L/l_s > 2$ . Finally, in the approximation  $L \gg l_s$ , concrete values for  $H_0$  were computed from (9.8) in [170] for  $d \geq 2$ , using (9.6), namely

$$d \geq 3 : H_0 = g_s 2^{2-d} \pi^{-\frac{d}{2}} \Gamma\left(\frac{d-2}{2}\right), \quad d = 2 : H_0 = g_s \frac{2}{\pi} \ln\left(\frac{L}{l_s}\right). \quad (9.9)$$

Few comments are in order regarding the prescription (9.8). Relative to  $\eta_{\mu\nu}$ , the metric of the transverse torus is proportional to  $H4\pi^2 L^2$ .<sup>2</sup> One may then view  $\sqrt{H}$ , or at least  $\sqrt{H_0}$ , as part of the physical radius, contributing to the volume of these compact dimensions; we come back to this point in Section 9.2.3. The resulting ambiguity between  $L$  and  $\sqrt{H_0}$  was lifted in [258] by completely fixing  $L$ , and letting  $H_0$  capture volume fluctuations. On the contrary,  $H_0$  was set to 1 in [173] to match the smearing conventions, leaving the freedom to  $L$ , and verifying in that case the validity of supergravity approximations. The prescription (9.8) is yet another option. Whatever choice is made, the volume or corresponding radius, as a 4d scalar field, could be stabilized at a given value by further physical ingredients generating an appropriate potential. These are precisely physical requirements (on Euclidian instantons), necessary to realise the KKLT scenario, that fix in [258]  $H_0$  to a low value. Our compactification setting is much simpler, and although it could be interesting to study the effective 4d action using e.g. [263–266], we will leave here the volume and radius unfixed. Therefore, we do not consider any further constraint than (9.8) on  $H_0$  and  $L$ , and will analyse the outcomes for various values of  $L$ .

### 9.2.2 Aparté: moving away from a source

We make here side comments on the profile of the Green’s function and the warp factor when moving away from the sources, the related symmetries and boundary conditions. Close to a source, the generalized Green’s function on  $\mathbb{T}^d$  exhibits a spherical symmetry as can be seen in (9.6). For  $d \geq 2$ , this symmetry is however broken further away from the source: there is indeed no  $\text{SO}(d)$  symmetry among coordinates  $\sigma^m$  in the complete expression (9.5). Showing this analytically, following Appendix A of [170], and getting a

<sup>2</sup>From this observation, one could argue that a proper evaluation of a “string length distance” from an  $O_p$  for the prescription (9.8) should include the warp factor, or at least  $H_0$ . This makes the determination of  $H_0$  more complicated, and for simplicity we stick to the prescription as stated. The method developed here to determine the gravitational waves spectrum can in any case be adapted to a different value of  $H_0$ .

coordinate-dependent correction to the spherical behaviour (9.6), turns out to be difficult. The breaking of this symmetry can nevertheless be verified numerically, as displayed in Figure 9.3.

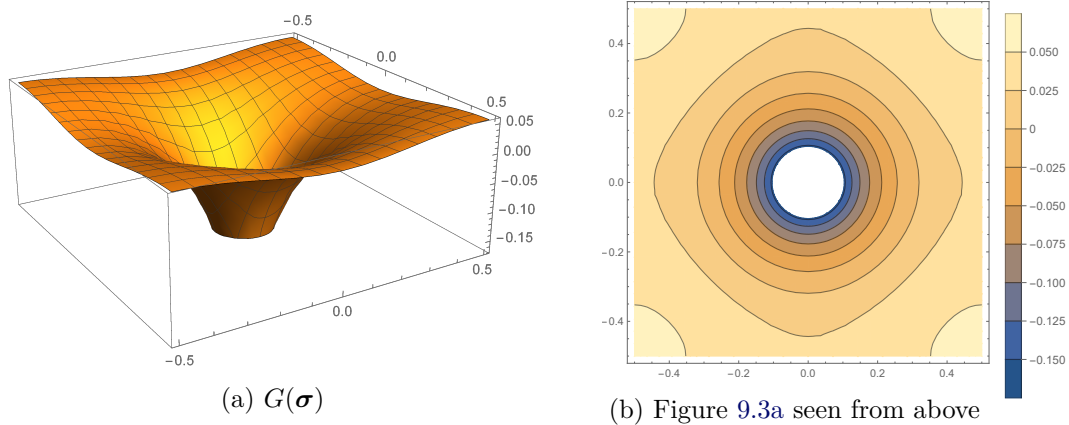


Figure 9.3: Green’s function  $G(\boldsymbol{\sigma})$  given in (9.5) for  $d = 2$ , evaluated on the vertical axis in Figure 9.3a in terms of the horizontal  $\sigma^1, \sigma^2$  coordinates. The same is displayed from above in Figure 9.3b, with horizontal cuts at fixed values of  $G(\boldsymbol{\sigma})$ . Close to the source (at  $\boldsymbol{\sigma} = \mathbf{0}$ ) we verify the spherical symmetry, but it is broken further away, where the circle turns to an approximate square.

In the warp factor  $H(\boldsymbol{\sigma})$ , the spherical symmetry around sources gets broken for an additional reason: the presence of other sources. This is made manifest in Figure 9.4. This point highlights the need to use the complete expressions of  $G$  and  $H$ , instead of only (9.6). This is important when evaluating  $H$ , to compute the constant  $H_0$  as proposed with the prescription (9.8). The computation of  $H_0$  in (9.9) rather made use of the spherical symmetry, valid there only thanks to  $l_s/L \ll 1$ .



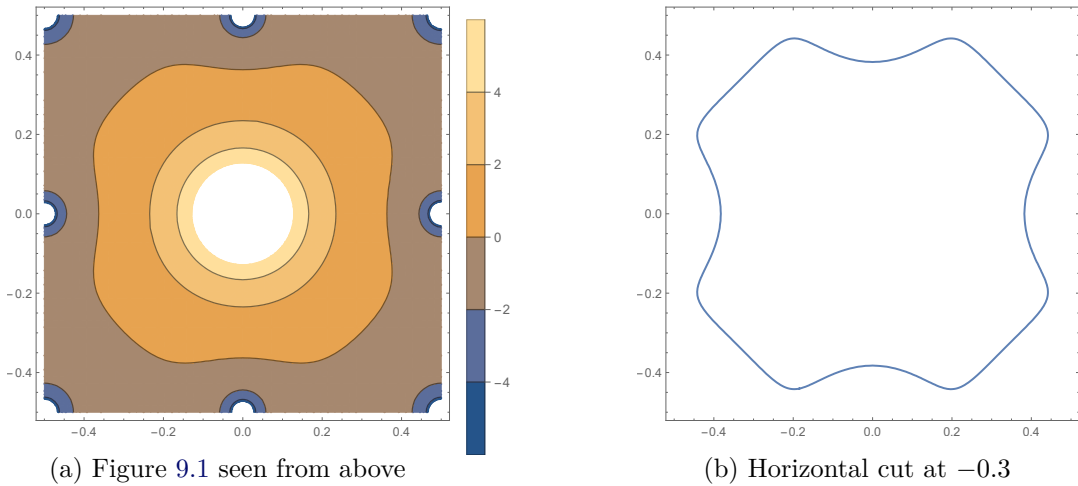


Figure 9.4: Warp factor  $H$  for  $d = 3$  displayed in Figure 9.1, viewed from above. Figure 9.4a and 9.4b show horizontal cuts at fixed values of  $H$  (several values for 9.4a, one value for 9.4b). The breaking of spherical symmetry around sources is made explicit by contours evolving from circles to angular shapes. Similar illustrations can be obtained for  $d = 2$ .

A related question has been discussed in [248, 249], following new 10d supergravity de Sitter solutions obtained in [247] with a non-standard ansatz. There, the metric exhibits several different warp factors, to describe  $O_{8_+}/O_{8_-}$  orientifolds transverse to a circle of coordinate  $y$  (i.e.  $d = 1$  here). We simplify here the discussion by restricting the setting considered there to the present ansatz. We take the  $O_{8_+}$  to correspond to a stack of  $D_8$  (with one  $O_8$ ) located at  $y = 0$ , and the  $O_{8_-}$  to be an  $O_8$  located  $y_0$ : this matches the source configuration considered here, detailed at the beginning of Section 10.1. The focus will be on the  $O_8$  at  $y_0$ . The ansatz of [249] boils down to ours if the three functions considered there,  $W$ ,  $\lambda$ ,  $\phi$ , verify the following relations to our warp factor:  $e^{-4W} = H$ ,  $e^\phi = g_s H^{-\frac{5}{4}}$ ,  $\lambda = 2W$ . Those functions are discussed there by related functions  $f_{i=1,2,3}$ . Their first derivative with respect to  $y$  verifies, in our setting,  $f'_i = W' \forall i$ .

The discussion of [249] is that of the boundary conditions to impose on the various functions close to the  $O_8$  at  $y_0$ . Two possible boundary conditions are put forward: the permissive ones and the restrictive ones. We translate them here in our setting

$$\text{Permissive : } H'|_{y \rightarrow y_0^+} = \frac{Q_{O_8}}{2}, \quad (9.10)$$

$$\text{Restrictive : } \frac{H'}{H}|_{y \rightarrow y_0^+} = \frac{Q_{O_8}}{2} \frac{1}{H}|_{y \rightarrow y_0^+}, \quad (9.11)$$

where we take  $H \geq 0$ . As we will see, it turns out that the restrictive boundary conditions require one condition more than the permissive ones, so the question is: which boundary conditions should be imposed? To see the difference, one considers the following expansion for  $H$  (and more generally for exponentials of the functions  $f_i$  in [249])

$$H(y) = a_1 |y - y_0| + a_2 |y - y_0|^2 + \mathcal{O}(|y - y_0|^3). \quad (9.12)$$



This means that  $H(y = y_0) = 0$ , which is always possible by adjusting the constant  $H_0$ , and this property actually holds in the  $d = 1$  warp factor considered in [170] (see Figure 3); in [249] this is a property of the solution considered. In addition, the expansion (9.12) is precisely about the above discussion: the profile of the warp factor when going away from the source. Indeed, the leading behaviour  $|y - y_0|$  is guaranteed by the Green's function close to the source (9.6), and the subleading terms in (9.12) are possible corrections to it. The permissive boundary conditions give one condition only, on the leading term, while the subleading terms all give vanishing contributions at  $y_0$ . On the contrary, the restrictive boundary conditions require to look at two terms in the Taylor expansion, the pole and the constant one, the remaining ones vanishing at  $y_0$ . This expansion for the restrictive boundary conditions is captured by the following in [249] (for each function  $f_i$ )

$$\text{Restrictive : } \frac{d_i^L}{|y - y_0|} + e_i^L = \frac{d_i^R}{|y - y_0|} + e_i^R \iff d_i^L = d_i^R, e_i^L = e_i^R, \quad (9.13)$$

where the superscripts  $L, R$  refer to each side of the equation, here given by (9.11). With the other boundary conditions, only one coefficient is fixed

$$\text{Permissive : } d_i^L = d_i^R. \quad (9.14)$$

The choice of boundary conditions has far reaching consequences in the context of [247–249]. Indeed, [248] considered restrictive boundary conditions and generalizations thereof, and deduced a no-go theorem against de Sitter solutions, thus potentially in contradiction with the solutions of [247]. The latter however verified only specific permissive boundary conditions, while violating the restrictive boundary conditions, given that in their solutions,  $e_i^L \neq e_i^R$ .

In our setting, this difference is even more dramatic. Indeed, considering only the warp factor  $H$ , expanded as in (9.12), we compute both boundary conditions and get (up to higher powers of  $|y - y_0|$ , which vanish at  $y_0$ )

$$\text{Permissive : } a_1 = \frac{Q_{O_8}}{2}, \quad (9.15)$$

$$\text{Restrictive : } \frac{1}{|y - y_0|} + \frac{a_2}{a_1} = \frac{Q_{O_8}}{2a_1} \left( \frac{1}{|y - y_0|} - \frac{a_2}{a_1} \right) \iff a_1 = \frac{Q_{O_8}}{2}, a_2 = 0. \quad (9.16)$$

In other words, the restrictive boundary conditions do not allow for a correction in  $|y - y_0|^2$  in  $H$  when moving away from the source. This is in line with the fact that solutions of [247] do not satisfy those boundary conditions. This was made more explicit in [250] which indicates precisely  $|y - y_0|^2$  corrections in the various functions.

In the present context, given the complete expressions we have for the Green's function and warp factor, we could attempt, as mentioned above for  $d \geq 2$ , to determine the corrections away from the source for  $d = 1$ . Interestingly, for  $d = 1$ , the Fourier series (9.4) provides an exact expression of the Green's function. This allows us to find an alternative expression valid on one interval  $\sigma \in (-\frac{1}{2}, \frac{1}{2}]$ ,<sup>3</sup> by identifying the Fourier

---

<sup>3</sup>We thank D. Junghans for pointing to us the possibility of such an expression.

coefficients: we give it here in the last equality

$$(2\pi L)^{-1} G(\sigma) = \int_0^\infty dt \left( 1 - \theta_3(\sigma | 4\pi i t) \right) = - \sum_{n \in \mathbb{Z}^*} \frac{e^{2\pi i n \sigma}}{4\pi^2 n^2} = -\frac{1}{2} \left( \sigma^2 - |\sigma| + \frac{1}{6} \right), \quad (9.17)$$

where again, the first two expressions are periodic while the last one is only valid on one interval, and should be mirrored on other intervals. It is interesting that the last expression for  $G(\sigma)$  captures *all* corrections away from the source. This result is in agreement with the warp factor we already identified around Figure 3 in [170]: we obtained there the following complete warp factor

$$H(y) = \frac{Q_{O_8}}{2} (y_0 - |y|), \quad y \in (-y_0, y_0] \leftrightarrow H(y) = \frac{Q_{O_8}}{2} |y - y_0|, \quad y \in (0, 2y_0], \quad (9.18)$$

with  $y_0 = \pi L$ . In other words, the warp factor found for  $d = 1$  with our source configuration has *only* the behaviour close to the sources, without correction, contrary to the other dimensions  $d$  as mentioned above. In particular, the quadratic terms of (9.17) drop out by charge cancelation, the requirement of  $a_2 = 0$  is verified, and so are the restrictive boundary conditions.<sup>4</sup> This is also the case of standard warp factors for  $D_8/O_8$  in a (non-compact) Minkowski space-time, as mentioned in [249]. In that respect, the de Sitter solutions of [247] are certainly different.

While this choice of boundary conditions is connected to other interesting questions in [249], one point is particularly emphasized: the failure of the supergravity description close to the source. As mentioned already, considering short distances could involve string scale physics, and thus a break-down of the supergravity description. This is even more manifest here as  $e^\phi$  diverges close to the  $O_8$  since the warp factor vanishes, so one argues that the string coupling cannot be considered weak anymore. The supergravity equations that define the solutions, the warp factor and its expansion, may then be disputed. This brings us back to the idea of considering a string-length distance away from the source, as discussed around the prescription (9.8). We will come back to this idea in Section 10.1.2.

### 9.2.3 Gravitational waves and their spectrum

We are interested in 4d gravitational waves propagating on the background of Section 9.2.1, so we consider the fluctuations

$$\eta_{\mu\nu} \rightarrow \eta_{\mu\nu} + h_{\mu\nu}, \quad (9.19)$$

where  $h_{\mu\nu}$  depends a priori on all  $D$  coordinates. One then decomposes it as a Kaluza–Klein tower of 4d gravitational waves, each mode being generically labeled by  $N$

$$h_{\mu\nu} = \sum_N h_{\mu\nu}^N(x^\mu) \psi_N(y^m). \quad (9.20)$$

We could add a dependence of  $\psi_N$  on the other extra coordinates  $x^i$  but as shown in [170], those will not play any role, especially for toroidal directions. The modes  $h_{\mu\nu}^N$  are taken

<sup>4</sup>The fact our setting verifies the restrictive boundary conditions might be expected from [248]. There, it is argued that similar boundary conditions should be obtained whenever one works with the standard DBI + WZ action for sources. The latter holds for us, given our background is a standard type II Minkowski solution.

## Chapter 9. Kaluza–Klein gravitational waves in a warped toroidal background

---

transverse and traceless in 4d; this can be viewed as a consistent truncation [170, 246]. Provided the  $\psi_N$  are orthonormal eigenfunctions of a certain modified Laplacian operator, to be specified, with eigenvalues  $M_N^2$ , then each mode satisfies the Pauli-Fierz equation of a massive spin-2 field with mass  $M_N$  in Minkowski

$$\left(\eta^{\kappa\lambda}\partial_\kappa\partial_\lambda - M_N^2\right)h_{\mu\nu}^N = 0, \quad (9.21)$$

at linear order. This was shown in [245] to hold for any energy-momentum tensor, i.e. any matter content of the theory, thanks to having a maximally symmetric 4d background space-time. The generality of these equations, describing propagating 4d Kaluza–Klein gravitational waves on a warped Minkowski background, is thus interesting. A generalization of this setting was considered in [246] allowing fluctuations of the full  $D$ -dimensional metric, leading to additional 4d vector and scalar contributions with interesting effects. We refer to [170] for more details.

As shown in [170], on the background metric (9.1) with the transverse torus  $\mathbb{T}^d$ , the modified Laplacian operator and corresponding eigenmode equation boil down to

$$-\delta^{mn}\frac{\partial}{\partial\sigma^m}\frac{\partial}{\partial\sigma^n}\psi_N = (2\pi L M_N)^2 H \psi_N. \quad (9.22)$$

In absence of any source, the warp factor is given by its constant part,  $H = H_0$ . As explained at the end of Section 9.2.1, we then simply face a torus of radius  $\sqrt{H_0}L$ . The Kaluza–Klein spectrum in that case is the standard one: the masses are

$$\left(M_N^{(\text{st})}\right)^2 = \frac{N^2}{H_0 L^2}. \quad (9.23)$$

This is precisely what we recover from (9.22), writing  $\psi_N$  as a Fourier series on  $\mathbb{T}^d$ , with  $N = |\mathbf{n}|$ ,  $\mathbf{n} \in \mathbb{Z}^d$ . The variation of  $H$  beyond this average, due to the presence of  $D_p$  and  $O_p$  sources, makes the equation (9.22) much more complicated to solve. The main purpose of this work is to determine how much the spectrum deviates from the standard one (9.23) in presence of a (non-trivial) warp factor  $H$ . To that end, few techniques were introduced in [170], and they will be greatly improved in the following. Finally, let us recall that

$$d \geq 2, \quad \frac{L}{l_s} \gg 1 \quad \Rightarrow \quad M_N \approx M_N^{(\text{st})}, \quad (9.24)$$

while we stated below (9.8) the minimal value:  $L/l_s > 2$ . Deviations from the standard spectrum are thus expected close to this last bound.

# 10 The spectrum

## 10.1 Issues and method to determine the spectrum

We present here the method, both analytical and numerical, used to determine the Kaluza–Klein gravitational waves spectrum, defined in Section 9.2. The spectrum is governed by the eigenmode equation (9.22), while the reference for this spectrum is the standard one obtained in the absence of sources, i.e. with a trivial warp factor, given in (9.23). To determine the spectrum, we first need to overcome difficulties due to the negative region where  $H < 0$  (see Figure 9.2), responsible for tachyons. This is discussed in Sections 10.1.1 and 10.1.2. The numerical method is then presented in Section 10.1.3 and Appendix A.2.

Prior to determining the spectrum, we first have to fully specify the background, by indicating where we place our sources, i.e. give the vectors  $\sigma_i$  (or  $\mathbf{y}_i$ ). From now on, we consider the  $D_p$ -branes to be all at the origin in coordinates  $\sigma$  (or  $\mathbf{y}$ ). The orientifolds  $O_p$  are at the 2 fixed points of each circle of  $\mathbb{T}^d$ : those are at  $\sigma^m = 0$  or  $\frac{1}{2}$ . There are thus  $2^d$  distributed  $O_p$ . As specified in Section 9.2.1, we take an overall vanishing charge  $\sum_i Q_i = 0$ . Since the charge ratio (9.2) is given by a factor  $2^{4-d}$ , this always gives 16  $D_p$  at the origin. Note that one  $O_p$  also sits at the origin, making the total charge there slightly less negative. The positive charges, that give a negative  $H$ , are then at all the other positions of the  $O_p$ , as illustrated in Figure 9.2. This charge distribution exhibits certain discrete symmetries, which will be very helpful to the numerical resolution, as described at the end of Section 10.1.3. We now enter the details of the determination of the spectrum.

### 10.1.1 Negative region and tachyons

To determine the spectrum, we first improved the (numerical) method presented in [170], as detailed in Section 10.1.3. The resulting spectrum for  $d = 1, 2, 3$  is given in Appendix A.3. Doing so, we however noticed the systematic presence of tachyons at low  $L/l_s$ , i.e. eigenmodes with  $M_N^2 < 0$ . We understood that those are due to the negative region, meaning the region discussed in the Introduction and Section 9.2.1 where  $H < 0$ . This can be seen in several ways. First, it was noticed in [170] (see e.g. Figure 2 or Section 4.2) that low  $L/l_s$  make the variation of  $H$  stronger and the negative region larger, so

the impact of this region could then be more important. Secondly, the relation between tachyons and the negative region is most easily seen using the eigenmode equation (9.22), as follows

$$0 \leq \int_{-\frac{1}{2}}^{\frac{1}{2}} d^d \boldsymbol{\sigma} |\partial \psi_N|^2 = - \int_{-\frac{1}{2}}^{\frac{1}{2}} d^d \boldsymbol{\sigma} \psi_N^* \partial^2 \psi_N = (2\pi L M_N)^2 \int_{-\frac{1}{2}}^{\frac{1}{2}} d^d \boldsymbol{\sigma} H |\psi_N|^2 . \quad (10.1)$$

For a constant  $H$ , we deduce that  $H M_N^2 \geq 0$ . A negative constant  $H$  then leads to a tachyon. More generally, we infer that if the negative region is sufficiently large, as at low  $L/l_s$ , it may dominate the above integral, at least for some mode, and a tachyon can appear. Similarly, probing the negative region may require a small enough wavelength of the eigenmode, which may then lead to a negative integral (10.1), making the mode tachyonic. Small wavelengths correspond to Kaluza–Klein modes high in the tower. Those could then be truncated by our numerical approach, that only considers a finite number of modes. At low  $L/l_s$ , the negative region is larger, and such modes are more easily reached. This may explain why we only noticed tachyons at low  $L/l_s$ , while they may always exist as long as  $H < 0$  in some region. This interpretation seems confirmed in Appendix A.3. Finally, in Appendix A.1, we provide an analytical resolution of the eigenmode equation in the non-compact case, also corresponding to the behaviour close to a source: for an  $O_p$ , we conclude again on the presence of tachyons.

Neither these tachyons nor this negative region are however physical! As explained in the Introduction and Section 9.2.1, our supergravity description breaks down in the negative region and a proper description would require string theory. Our equations should not be trusted anymore in that region. Computing the spectrum, we should then find a way to fully ignore the effects of this region, in particular the tachyonic modes. To that end, we develop a procedure, presented in the following.

### 10.1.2 Restricting the domain and reformulating the eigenmode equation

We introduce a domain  $\mathcal{D}$  where the warp factor is non-negative, and solve the eigenmode equation on  $\mathcal{D}$  only. We recall that  $\sigma^m \in (-\frac{1}{2}, \frac{1}{2}]$  and that  $l_s/L < 1/2$ . We also recall that  $O_p$ , close to which  $H < 0$ , are placed precisely at  $\sigma^m = \frac{1}{2}$  as specified at the beginning of Section 10.1. We then define

$$\lambda = 1 - 2\frac{l_s}{L} , \quad \mathcal{D} = \left\{ \boldsymbol{\sigma}, |\sigma^m| \leq \frac{1}{2} - \frac{l_s}{L} = \frac{1}{2}\lambda \right\} . \quad (10.2)$$

The region of interest is thus reduced by a factor  $\lambda$ , as in Figure 9.2, and we introduce an appropriate coordinate to span it

$$\tau^m = \lambda^{-1} \sigma^m \quad \Rightarrow \quad \mathcal{D} = \left\{ \boldsymbol{\tau}, |\tau^m| \leq \frac{1}{2} \right\} . \quad (10.3)$$

This is designed to guarantee  $H \geq 0$  on  $\mathcal{D}$ , relative to prescription (9.8) that refers to a distance  $|\boldsymbol{\sigma} - \boldsymbol{\sigma}_j| = \frac{l_s}{L}$  from an  $O_p$  source  $j$ . This domain actually excludes a little more than needed by this prescription, as depicted for  $d = 2$  in Figure 10.1. We will then adjust the prescription.

The restricted domain  $\mathcal{D}$  leads us to slightly modify the prescription (9.8). We now consider points of  $\mathcal{D}$  which are the closest to the  $O_p$  sources (except the one at the origin,

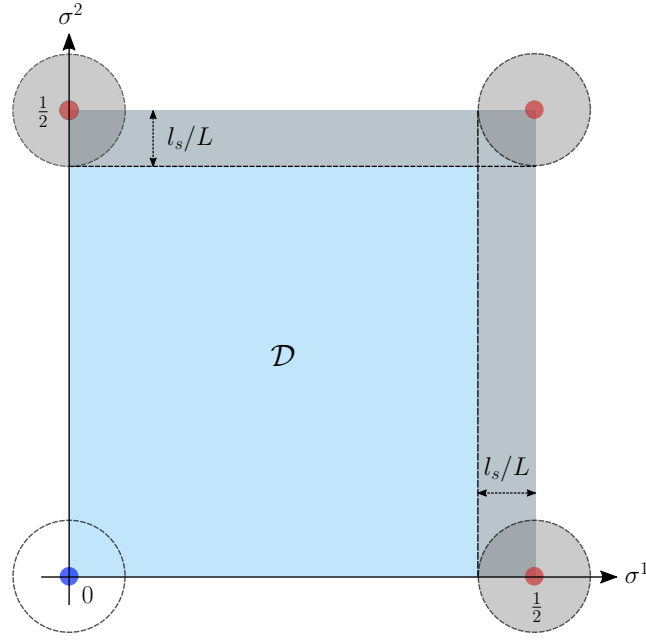


Figure 10.1: Regions in a quarter of  $\mathbb{T}^{d=2}$ , the rest of the torus being obtained by axis symmetry (as in Figure 9.1 and 9.4a). The  $O_p$  are placed at the four corners, and depicted by red and blue dots; the one at the origin (blue dot) is not problematic thanks to the 16 additional  $D_p$  present there which give an excess  $D_p$  charge. The restricted domain  $\mathcal{D}$  is light blue, while the excluded region is gray. The negative region corresponding to prescription (9.8) is darker gray and bounded by circles of radius  $l_s/L$  around the  $O_p$ . In general, these regions are actually not exactly circular as discussed in Section 9.2.2. We see that the excluded region is larger than what is a priori needed, leading to the adjusted prescription (10.4).

due to the additional  $D_p$ -branes there). In  $d = 2$ , as illustrated in Figure 10.1, these are the corners of the white rectangle. Those points are simply given by  $\sigma = \lambda\sigma_j$  for each source  $j$  located by  $\sigma_j$ . Indeed, the proportion  $\lambda$  is preserved thanks to the Intercept Theorem (or Thales's Theorem). We then need to compare the values of  $H$  at these various points, and take the most negative one. This gives the adjusted prescription

$$H_0 = \max_j \left\{ - \sum_i Q_i G(\lambda\sigma_j - \sigma_i) \right\}. \quad (10.4)$$

It would match the previous prescription (9.8) for a vector of norm  $|\sigma_j| = \frac{1}{2}$ : in that case one has for  $j = i$  that  $|\lambda\sigma_i - \sigma_i| = 2\frac{l_s}{L}|\sigma_i| = \frac{l_s}{L}$  as in (9.8). Some  $\sigma_j$  have however different norms. In any case, the adjusted prescription (10.4) guarantees that  $H \geq 0$  on  $\mathcal{D}$ . This gives appropriate boundary conditions to  $H$  to have a well-defined spectral problem on  $\mathcal{D}$ .

We then consider the warp factor restricted to  $\mathcal{D}$  only, and introduce some rescaling for convenience

$$\tilde{H}(\tau) = \lambda^2 \frac{1}{g_s} \left( \frac{L}{l_s} \right)^{d-2} H(\sigma)|_{\mathcal{D}}, \quad \tilde{H}_0 = \lambda^2 \frac{1}{g_s} \left( \frac{L}{l_s} \right)^{d-2} H_0. \quad (10.5)$$

The rescaling removes in the non-constant part of  $H$  all dependence on the physical parameters  $L$ ,  $l_s$  and  $g_s$ , except through the overall  $\lambda$ . We now solve the eigenmode equation (9.22) on  $\mathcal{D}$  only, considering now  $\psi_N(\boldsymbol{\tau})$  defined in that restricted domain. We rewrite that equation on  $\mathcal{D}$  as

$$-\delta^{mn} \frac{\partial}{\partial \tau^m} \frac{\partial}{\partial \tau^n} \psi_N(\boldsymbol{\tau}) = (2\pi \mu_N)^2 \tilde{H}(\boldsymbol{\tau}) \psi_N(\boldsymbol{\tau}) , \quad (10.6)$$

introducing as in [170] the convenient eigenvalues

$$\mu_N^2 = M_N^2 L^2 g_s \left( \frac{l_s}{L} \right)^{d-2} . \quad (10.7)$$

What will matter are not the actual eigenvalues, but their comparison to the standard spectrum (9.23) in the absence of sources. We now define the relevant ratio to the standard spectrum

$$f_N = \frac{M_N}{M_N^{(\text{st})}} = \frac{\mu_N}{\mu_N^{(\text{st})}} , \quad \text{where } \mu_N^{(\text{st})} = \frac{N}{\sqrt{\lambda^{-2} \tilde{H}_0}} . \quad (10.8)$$

In the following, we will refer to this ratio and its difference to 1 as the deviation, with respect to the standard spectrum.

To solve the eigenmode equation (10.6), we finally need a further rewriting. The warp factor and the eigenfunctions are now continuous functions defined on  $\mathcal{D}$  only. We can consider them as periodic on successive copies of  $\mathcal{D}$ , up to cuts at points at the boundaries. This allows us to develop them as Fourier series on  $\mathcal{D}$ . Equivalently, as square integrable functions on an interval, they can be developed on the basis of functions formed by integer Fourier modes. Writing them as Fourier series on  $\mathcal{D}$  corresponds to completely ignoring the negative region, and is again a way to provide appropriate boundary conditions for  $H$  and  $\psi_N$  to have a well-defined spectral problem. We now drop the  $N$ , considering only one eigenmode, and get

$$\tilde{H}(\boldsymbol{\tau}) = \sum_{\mathbf{m} \in \mathbb{Z}^d} d_{\mathbf{m}} e^{2i\pi \mathbf{m} \cdot \boldsymbol{\tau}} , \quad \psi(\boldsymbol{\tau}) = \sum_{\mathbf{m} \in \mathbb{Z}^d} c_{\mathbf{m}} e^{2i\pi \mathbf{m} \cdot \boldsymbol{\tau}} . \quad (10.9)$$

From (10.6) or (10.9), the zero mode with  $\mu_0 = 0$  is given by  $\psi_0$  being a constant (a continuous harmonic function on a compact space). From now on, we consider other eigenmodes and  $\mu \neq 0$ . For each of these modes, the eigenmode equation (10.6) becomes thanks to (10.9) the tower of equations

$$\frac{\mathbf{n}^2}{\mu^2} c_{\mathbf{n}} - \sum_{\mathbf{m} \in \mathbb{Z}^d} c_{\mathbf{m}} d_{\mathbf{n}-\mathbf{m}} = 0 , \quad \forall \mathbf{n} \in \mathbb{Z}^d . \quad (10.10)$$

The  $c_{\mathbf{n}}$  are the variables, together with the unknown  $\mu$ , while the coefficients  $d_{\mathbf{m}}$  are fixed by  $\tilde{H}$ . Let us determine the latter, before solving this reformulated eigenmode equation (10.10).

One obtains the  $d_{\mathbf{m}}$  as the following Fourier coefficients

$$d_{\mathbf{m}} = \lambda^2 \frac{1}{g_s} \left( \frac{L}{l_s} \right)^{d-2} \int_{-\frac{1}{2}}^{\frac{1}{2}} d^d \boldsymbol{\tau} e^{-2i\pi \mathbf{m} \cdot \boldsymbol{\tau}} H(\lambda \boldsymbol{\tau}) . \quad (10.11)$$

We further use the following Fourier series expression for  $H$

$$H(\boldsymbol{\sigma}) = H_0 - \frac{1}{(2\pi L)^{d-2}} \sum_{\mathbf{n} \in \mathbb{Z}^{d*}} e^{2\pi i \mathbf{n} \cdot \boldsymbol{\sigma}} \times \sum_i Q_i \frac{e^{-2\pi i \mathbf{n} \cdot \boldsymbol{\sigma}_i}}{4\pi^2 \mathbf{n}^2}, \quad (10.12)$$

based on the Green's function (9.4). We recall that this last Fourier series is not absolutely convergent and requires regularization. However, as argued in [170], we will truncate this infinite sum, thus avoiding this issue. We will also verify numerically in Section 10.1.3 the successful matching of the truncated Green's function and the proper expression (9.5). Using the various definitions and sources positions, we rewrite the above as

$$H(\boldsymbol{\sigma}) = g_s \left( \frac{l_s}{L} \right)^{d-2} \left( \lambda^{-2} \tilde{H}_0 + \sum_{\mathbf{n} \in \mathbb{Z}^{d*}} e^{2\pi i \mathbf{n} \cdot \boldsymbol{\sigma}} \times \frac{1}{4\pi^2 \mathbf{n}^2} (16 - 2^{4-d} \sum_{O_p} e^{-2\pi i \mathbf{n} \cdot \boldsymbol{\sigma}_i}) \right). \quad (10.13)$$

We deduce

$$\lambda^{-2} d_{\mathbf{m}} = \delta_{\mathbf{m}, \mathbf{0}} \lambda^{-2} \tilde{H}_0 + \sum_{\mathbf{n} \in \mathbb{Z}^{d*}} \frac{1}{4\pi^2 \mathbf{n}^2} (16 - 2^{4-d} \sum_{O_p} e^{-2\pi i \mathbf{n} \cdot \boldsymbol{\sigma}_i}) \prod_{q=1}^d \frac{\sin(\pi(\lambda \mathbf{n} - \mathbf{m})^q)}{\pi(\lambda \mathbf{n} - \mathbf{m})^q}, \quad (10.14)$$

where  $q$  labels the  $q$ -component of the  $d$ -vectors. We note that for  $\lambda \approx 1$ , i.e.  $L/l_s \gg 1$ , the last product boils down to  $\delta_{\mathbf{m}, \mathbf{n}}$ , reproducing the result of [170]. This is a consistency check since for  $\lambda \approx 1$ ,  $\mathcal{D}$  matches the full  $\mathbb{T}^d$ , considered here.

As a side remark, let us note that  $d_{\mathbf{0}}$  is not only  $\tilde{H}_0$ , contrary to  $H(\boldsymbol{\sigma})$ . This is because the average of the sum of Green's functions (or the varying part of  $H$ ) is not vanishing over the restricted domain. More precisely, one verifies that it is vanishing for  $\lambda \approx 1$  and  $\mathbf{m} = \mathbf{0}$  thanks to the cancellation of charges, but not otherwise. This is only an observation since we will not make use of this zero-mode  $d_{\mathbf{0}}$ , which is also the average of  $\tilde{H}$ . In particular, the deviation of the spectrum with respect to the case of a ‘‘constant warp factor’’ is computed with the standard spectrum (9.23), corresponding to the case without any source.

Having determined the  $d_{\mathbf{m}}$ , the problem now amounts to solving the tower of equations (10.10), to obtain the eigenvalues  $\mu$  and corresponding eigenfunctions in terms of their coefficients  $c_{\mathbf{n}}$ . More precisely, we are interested in the deviation  $f_N$  (10.8) between the eigenvalue for a (massive) state and the corresponding standard value, in the absence of sources. We now turn to the numerical method used to solve the tower of equations (10.10) and thus the eigenmode equation, determining this way the spectrum.

### 10.1.3 Numerical method to determine the spectrum

Determining the mass spectrum of Kaluza–Klein gravitational waves on our  $D_p/O_p$  warped toroidal background amounts to solving the eigenmode equation, decomposed into a tower of equations (10.10). To that end, we present in the following and in Appendix A.2 the numerical method used. Its starting point is similar to the one of [170], namely



having a vanishing determinant, but we improve it on many levels to be detailed, allowing us to reach a more precise spectrum, with more eigenmodes and in more dimensions ( $d = 1, \dots, 6$ , whereas we stopped at  $d = 3$  in [170]). That spectrum is given in Section 10.2.

To deal with the tower of equations (10.10), we start by imposing a truncation: we truncate the series (10.9) of the warp factor and the eigenfunction, keeping for each of them only a finite sample  $\Gamma$  of the Fourier modes in momentum space, depicted in Figure 10.3. This is done by retaining momenta whose norm is smaller than a value  $r$ . The size of the sample is denoted  $n = \dim \Gamma$ , and typically goes as  $r^d$ . As will be detailed, the larger  $r$  (and  $n$ ), the better the precision. We will be able to reach large  $n$ , and verify on that occasion that the truncated warp factor matches well its formal expression (9.3), (9.5), as depicted on Figure 10.2.

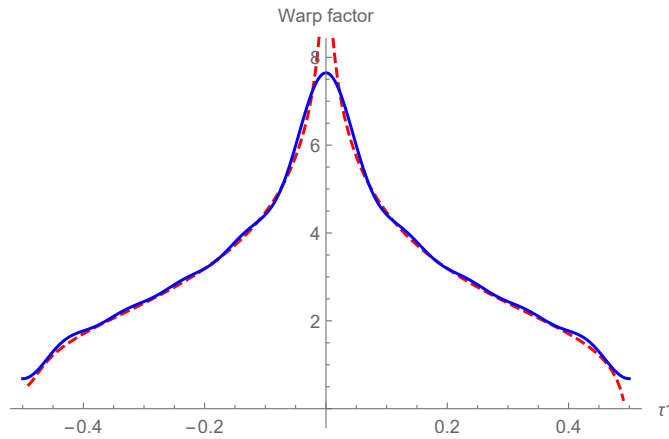


Figure 10.2: Comparison between the exact and the truncated warp factor. Here  $d = 2$  and the plots are along  $\tau^1$ , at fixed  $\tau^2 = 0$ . The red dashed line represents the exact  $\tilde{H}$ , while the blue line stands for the truncated  $\tilde{H}$ , with  $r = 10$  and  $n = 316$ .

We then establish a bijective map between the momenta  $\mathbf{m}$  kept in  $\Gamma$  and integers from 1 to  $n$  (see Appendix A.2 for more details). Improvements have been made w.r.t. [170] in establishing this sample and this map. The latter allows to write the coefficients  $c_{\mathbf{m}}$  as a  $n$ -dimensional vector  $\vec{c}$ . The tower of equations (10.10) becomes a finite system, written in matrix form as

$$\mathcal{O}(\mu) \cdot \vec{c} = 0 , \quad (10.15)$$

where  $\mathcal{O}(\mu)$  is an  $n \times n$  matrix, depending on the unknown  $\mu$  and the  $d_{\mathbf{m}}$  coefficients (10.14). Since  $\psi$  is not identically zero by construction, and its  $n$  first Fourier modes are assumed not to be all zero,  $\vec{c}$  is not a null vector. So (10.15) requires

$$\det \mathcal{O}(\mu) = 0 , \quad (10.16)$$

which can be further written as a polynomial equation. It can be solved numerically for a reasonable  $n$  (in our case not larger than  $\sim 80$ ), since this operation has complexity<sup>1</sup>

<sup>1</sup>We measured that the time  $t$  taken for such a computation obeys  $\log t = Cn + B_d$ , where the constant  $B_d$  is different from one dimension  $d$  to another, while the constant  $C$  seems to be the same for all  $d$ .

$\mathcal{O}(e^{Cn})$ . This does not allow for a high precision, especially for  $d > 3$  where such a  $n$  corresponds to a small radius  $r$  (for  $d = 4$  one has  $r \approx 2$ ), meaning that only the very first modes are not truncated. However, this first resolution still provides a good overview of the spectrum and its organization (degeneracy, approximate eigenvalues). In addition, for  $d = 1, 2$ , it already gives good estimates of the spectrum, detailed in Section 10.2. In particular, this reveals that the largest observed deviation occurs for the lightest (massive) mode. In addition, the deviation seems to grow with  $d$ ; this motivates us to access the spectrum for  $d \geq 3$  with a satisfactory accuracy. As this requires a larger and larger number of points  $n$ , we need yet another rewriting of the problem to be solved.

To reduce the number of variables and equations to solve, and thus be able to reach a higher precision, we can make use of the symmetries of the source distribution, specified at the beginning of Section 10.1. While the  $D_p$  are at the origin, the orientifold  $O_p$  are, for each circle of  $\mathbb{T}^d$ , at the 2 fixed points at  $\sigma^m = 0$  or  $\frac{1}{2}$ . Considering the  $O_p$  with mirrors (e.g. at  $\sigma^m = \pm\frac{1}{2}$ ), we see them placed for  $d = 2$  at the corners or on the edges of a square (see Figure 9.4a and 10.1), and generalizations thereof in higher dimensions  $d$ . This distribution is invariant under the exchange of the  $O_p$ : these permutations form the so-called hyperoctahedral group of degree  $d$ , that we denote  $G$ . For  $d = 2$ , one has  $G = D_4$  with  $\dim D_4 = 8$ . An interesting consequence is that for  $d \geq 2$ ,  $H$  and the lightest eigenmode  $\psi_1$  inherit this symmetry<sup>2</sup>. This gets translated in their Fourier coefficients, which are related to each other under transformations of  $G$

$$H(g \cdot \boldsymbol{\sigma}) = H(\boldsymbol{\sigma}) \iff d_{g \cdot \mathbf{n}} = d_{\mathbf{n}}, \quad \forall \mathbf{n} \in \mathbb{Z}^d, \quad \forall g \in G. \quad (10.17)$$

$$\psi_1(g \cdot \boldsymbol{\sigma}) = \psi_1(\boldsymbol{\sigma}) \iff c_{g \cdot \mathbf{n}} = c_{\mathbf{n}}, \quad \forall \mathbf{n} \in \mathbb{Z}^d, \quad \forall g \in G. \quad (10.18)$$

As noted previously, the highest deviation from the standard spectrum always occurs for the lightest mode, so we focus on the latter and its associated mass  $\mu_1$  in the following, and assume the property (10.18). This observation allows us to reduce drastically the number of independent Fourier coefficients to determine (for  $d = 6$ , this number is reduced by a factor  $\mathcal{O}(10^5)$ ), and correspondingly the number of independent equations (10.10). We reach this way higher  $r$  and  $n$ , i.e. larger samples, necessary to get a reasonable precision in high dimensions  $d$ . This last improvement w.r.t. [170] was crucial to get interesting results on the spectrum for  $d = 4, 5, 6$ . The details of this technical simplification are given in Appendix A.2. The upshot is that one can merely consider the points in the sample  $\Gamma$  that are not equivalent under the action of  $G$ , i.e. the points

$$\mathbf{m} \in \tilde{\Gamma} = \frac{\Gamma}{G}, \quad \tilde{n} = \dim \tilde{\Gamma} = \frac{\dim \Gamma}{2^d d!}. \quad (10.19)$$

For instance, for  $d = 2$ , one can consider the following representatives,

$$\tilde{\Gamma} = \{ \mathbf{m} \in \Gamma, m^1 \geq 0 \text{ and } 0 \leq m^2 \leq m^1 \}, \quad (10.20)$$

as illustrated on Figure 10.3.

<sup>2</sup>Let us note that for the special case  $d = 1$ , the lightest mass is rather associated to an odd mode. For  $d \geq 2$ , the higher modes can be odd under certain transformations of  $G$ , and even under others.

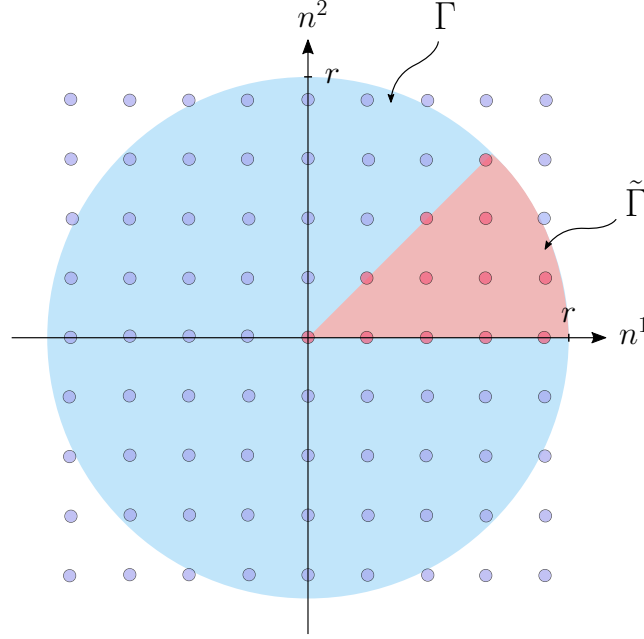


Figure 10.3: Example of the sample  $\Gamma$  (in blue) of size  $r$  for  $d = 2$ , and the smaller sample  $\tilde{\Gamma}$  (in red), sufficient to determine the spectrum. Here,  $n = 56$  and  $\tilde{n} = 12$ .

Eventually, one has  $\tilde{n}$  Fourier coefficients  $d_{\mathbf{m}}$  to compute, and  $\tilde{n}$  equations to solve

$$\frac{|\mathbf{n}|^2}{\mu_1^2} c_{\mathbf{n}} - \sum_{\mathbf{m} \in \Gamma} c_{R(\mathbf{m})} d_{R(\mathbf{n}-\mathbf{m})} = 0, \quad \forall \mathbf{n} \in \tilde{\Gamma}, \quad (10.21)$$

where  $R(\mathbf{m})$  denotes the representative of  $\mathbf{m}$  in  $\tilde{\Gamma}$ . We refer to Appendix A.2 for its explicit implementation, and for the derivation of (10.21).

As explained above, we start by solving the determinant equation (10.16). This provides a good overview of the spectrum, but also a good estimate of the lightest mass that we are interested in. In fact, we use this first value as a “seed” for our algorithm: we make use of minimization techniques that look for a solution to the system of equations (10.21) close to the seed, this time with more Fourier modes (i.e. larger  $r$  and  $n$ ). More specifically, we run a `FindMinimum` in Mathematica, where the quantity to be minimized is the sum of the squares of the left hand sides in (10.21) (see e.g. Appendix B of [1] for a more detailed description of this method, in a different context). The output provides a refined value for  $\mu_1$  and the deviation  $f_1$ . We then repeat the same step, and use the refined value as a new seed, and with a larger  $r$  (and  $n$ ). We repeat this procedure until we reach a satisfactory precision on  $\mu_1$  and  $f_1$ , i.e. when the latter converge towards fixed value, typically when the value does not vary of more than 1% with respect to the previous step. This method allows to reach very large  $n$ , at most  $n \sim 1.5 \cdot 10^6$  for  $d = 6$ . This is a significant improvement with respect to the first attempts made in [170], that reached at most  $n \sim 50$ . It also allows us to reach  $r \sim 10$  for every dimension  $d$ , and to rigorously compare the deviation obtained in each case.

Thanks to all these innovations, this method provides us with interesting, precise and

new results on the spectrum of Kaluza–Klein gravitational waves on this warped toroidal background. We now turn to those.

## 10.2 Spectrum

We present in this section the spectrum obtained for Kaluza–Klein gravitational waves on the warped toroidal background of Section 9.2.1. The  $D_p/O_p$  sources generating the warping are placed as specified at the beginning of Section 10.1. The numerical method used to determine this spectrum is presented in Section 10.1.3 and Appendix A.2. While based on initial ideas of [170], it got improved on many levels allowing us to present here more precise results as well as new results, especially regarding the higher dimensions  $d = 4, 5, 6$ . We also had to face the issue of the negative region, where  $H < 0$ , that leads to tachyons in the spectrum as discussed in Section 10.1.1, Appendix A.1 and A.3. Thanks to a restriction of the domain on which relevant functions are defined, we could overcome this issue, as described in Section 10.1.2. The spectrum obtained prior to this restriction is given for completeness in Appendix A.3 and exhibits (unphysical) tachyonic modes, while the resulting tachyon-free spectrum is given in the following.

When giving the spectrum, we display the eigenvalues  $\mu_N$  defined in (10.7), proportional to the Kaluza–Klein masses  $M_N$ . More importantly, we provide the value of  $f_N = M_N/M_N^{(\text{st})} = \mu_N/\mu_N^{(\text{st})}$  given in (10.8), the ratio to the standard mass or eigenvalue in absence of sources. The deviation  $1 - f_N$  evaluates the difference from a standard toroidal spectrum, and thus the impact of a non-trivial warp factor. As recalled in (9.24) and several occurrences in Section 10.1, the standard spectrum is recovered at  $L/l_s \gg 1$  (for  $d \geq 2$ ). This is verified in the tables below with  $f_N$  close to 1. We also recall that  $L/l_s > 2$ , so the largest deviations we will observe will happen at “low”  $L/l_s \approx 10$ . It is also for those values of  $L/l_s$  that reaching a satisfactory precision is the most difficult.

We start by giving in Tables 10.1, 10.2 and 10.3 the spectrum obtained for  $d = 1, 2, 3$  using simply the determinant method described in Section 10.1.3. We present the first modes of the tower, specifying for each dimension  $d$  the size  $n$  of the sample considered and the corresponding radius  $r$  (see Section 10.1.3). The corresponding precision is already good for  $d = 1, 2$ , but will be improved below for  $d = 3$ . The modes of the standard spectrum are labeled by an integer  $N$ : at each such level, the modes obey a certain degeneracy. This degeneracy gets partially lifted when moving away from that standard spectrum by lowering  $L/l_s$ . We distinguish the modes whose eigenfunction is symmetric ( $s$ ) or antisymmetric<sup>3</sup> ( $a$ ) under  $\sigma \rightarrow -\sigma$ , and indicate in parentheses for each of those their degeneracy, e.g.  $s(2)$ . The combinatorics explaining these degeneracies are discussed in Appendix A.3. The modes are ordered in the tables according to their mass at high  $L/l_s$ ; when lowering the latter, we note that this order can get modified.

<sup>3</sup>Antisymmetric modes would be projected out by orientifolds, since the metric should be symmetric under the involution. We keep them here for completeness.

$L/l_s$	$N$	1		2	
	$a/s$	$a$	$s$	$a$	$s$
10	$\mu_N$	1.369	1.593	2.846	3.081
	$f_N$	1.061	1.234	1.102	1.193
$10^2$	$\mu_N$	1.010	1.175	2.099	2.273
	$f_N$	0.9897	1.151	1.028	1.113
$10^3$	$\mu_N$	0.9829	1.143	2.043	2.211
	$f_N$	0.9809	1.141	1.019	1.103

Table 10.1: Spectrum of the first Kaluza–Klein modes for  $d = 1$ , with eigenvalue  $\mu_N$  and deviation  $f_N$  from the standard spectrum, according to the value of  $L/l_s$ . Sample specifications:  $r = 20$ ,  $n = 41$ .

$L/l_s$	$N$	1			$\sqrt{2}$		
	$a/s$	$s(1)$	$a(2)$	$s(1)$	$s(1)$	$a(2)$	$s(1)$
9	$\mu_N$	1.028	1.069	1.311	1.571	1.742	1.870
	$f_N$	0.9046	0.9407	1.154	0.9775	1.084	1.164
10	$\mu_N$	0.9916	1.034	1.269	1.517	1.679	1.794
	$f_N$	0.9115	0.9506	1.166	0.9863	1.092	1.166
$10^2$	$\mu_N$	0.6105	0.6492	0.7251	0.9288	0.9576	1.005
	$f_N$	0.9295	0.9884	1.104	1.000	1.031	1.082
$10^3$	$\mu_N$	0.4539	0.4735	0.4995	0.6719	0.6776	0.6925
	$f_N$	0.9519	0.9929	1.048	0.9964	1.005	1.027

Table 10.2: Spectrum of the first Kaluza–Klein modes for  $d = 2$ , with eigenvalue  $\mu_N$  and deviation  $f_N$  from the standard spectrum, according to the value of  $L/l_s$ . Sample specifications:  $r = 4.5$ ,  $n = 69$ .

$L/l_s$	$N$	1			$\sqrt{2}$				
		$a/s$	$s(1)$	$a(3)$	$s(2)$	$s(1)$	$a(3)$	$s(3)$	$a(3)$
7	$\mu_N$	0.8353	0.8553	1.124	1.513	1.234	1.487	1.620	1.645 ?
	$f_N$	0.7012	0.718	0.9437	0.898	0.7322	0.8825	0.9618	0.9763 ?
10	$\mu_N$	0.7356	0.8012	1.063	1.330	1.172	1.339	1.528	1.563 ?
	$f_N$	0.744	0.8103	1.075	0.9509	0.8378	0.9579	1.093	1.118 ?
$10^2$	$\mu_N$	0.2534	0.2615	0.2655	0.3593	0.3658	0.3700	0.3739	0.3771
	$f_N$	0.9859	1.017	1.033	0.9883	1.006	1.018	1.029	1.037
$10^3$	$\mu_N$	0.07941	0.07962	0.07972	0.1122	0.1125	0.1126	0.1127	0.1128
	$f_N$	0.9994	1.002	1.003	0.9986	1.001	1.002	1.003	1.004

Table 10.3: Spectrum of the first Kaluza–Klein modes for  $d = 3$ , with eigenvalue  $\mu_N$  and deviation  $f_N$  from the standard spectrum, according to the value of  $L/l_s$ . The question mark in the last entries indicates that the identification of the modes as being part of the same multiplet as those at higher  $L/l_s$  is not certain. Sample specifications:  $r = 2.6$ ,  $n = 81$ .

The spectrum for  $d = 3$  is illustrated in Figure 10.4 for the first two  $N$ . We see that the modes are degenerate to the standard spectrum values for large  $L/l_s$ , and the degeneracy gets lifted when lowering  $L/l_s$ , leading to the strongest deviations.

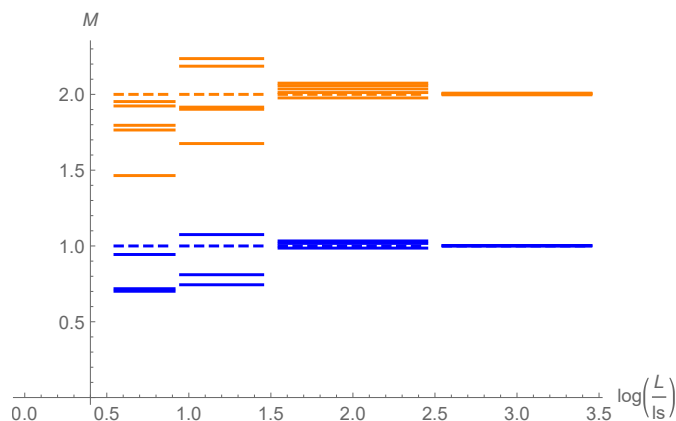


Figure 10.4: Mass spectrum for  $d = 3$  for the first two levels  $N$ , normalised to 1 and 2 for readability, in terms of  $\log \frac{L}{l_s}$ . We take for  $\frac{L}{l_s}$  the four values of Table 10.3. The standard spectrum is represented by the dashed lines, and the spectrum obtained here with non-trivial warp factor by plain lines.

The values obtained in Tables 10.1–10.3 should be compared to those of Appendix A.3 and to [170], where we did not restrict to the domain  $\mathcal{D}$  that excludes the negative region, and took a constant value of  $H_0$  instead of the prescribed one as here. The spectrum gets here corrected, and a crucial difference is the absence of tachyon for  $d = 2$  and  $d = 3$ , when probing the same low values of  $L/l_s$  as in Appendix A.3. Regarding the deviation  $f_N$ , which is the interesting physical effect of the warp factor, we reach at

best  $f_N \approx 0.70$ , i.e. 30%. For  $d \geq 2$ , the smallest  $f_N$  values are obtained for the lowest  $L/l_s$ , the lightest mode and the highest  $d$ . This motivates us in the following to further restrict the study to only the first mode with  $\mu_1$  and investigate all  $d$  up to 6. The more advanced numerical techniques presented in Section 10.1.3 will allow us to do so, while reaching a better precision thanks to a larger sample.

Before this, let us briefly comment on  $d = 1$ . This case is special, mostly because there is no divergence at the sources. As a consequence, one can find a finite constant  $H_0$  which makes  $H > 0$  everywhere, as done around Figure 3 in [170]. Here we still use the restricted domain and adjusted prescription (10.4) for consistency, leading to a variation of the spectrum in  $L/l_s$  (contrary to Appendix A.3 and [170]). Despite this variation, it is not true for  $d = 1$  that the spectrum matches the standard one at large  $L/l_s$  as discussed in [170]. So  $f_N$  does not particularly go to 1 in that limit. Another observed specificity of  $d = 1$  is that the first massive mode is antisymmetric, contrary to higher  $d$ .

We turn to studying the lightest massive mode, whose deviation is observed to be the strongest. We give in Tables 10.4-10.9 the values of  $\mu_1$  and  $1 - f_1$  for  $d = 1, \dots, 6$ . We note that  $1 - f_1$  is not always positive, which means that the deviation from the standard spectrum can either increase or decrease the mass. We also give the constant  $g_s^{-1}H_0$  obtained from the adjusted prescription (10.4). As mentioned above, its value for  $d = 1$  is special and varies strongly with  $L/l_s$ , but it is more regular for the other  $d$ . The precision reached is higher than above (in the sense of reducing the error), thanks to the additional steps described in Section 10.1.3 allowing us to use a larger sample. The results are however only obtained with two significant digits.

$L/l_s$	10	$10^2$	$10^3$	$10^4$
$g_s^{-1}H_0$	6.0	96	$10^3$	$10^4$
$\mu_1$	1.4	1.0	0.98	0.98
$1 - f_1$	-0.061	0.010	0.020	0.020

Table 10.4: First non-zero eigenvalue  $\mu_1$  and deviation  $f_1$  from the standard spectrum for  $d = 1$ , together with the constant  $g_s^{-1}H_0$  obtained from the adjusted prescription (10.4).

$L/l_s$	10	$10^2$	$10^3$	$10^4$
$g_s^{-1}H_0$	0.84	2.3	3.8	5.2
$\mu_1$	0.99	0.61	0.49	0.42
$1 - f_1$	0.091	0.071	0.054	0.041

Table 10.5: First non-zero eigenvalue  $\mu_1$  and deviation  $f_1$  from the standard spectrum for  $d = 2$ , together with the constant  $g_s^{-1}H_0$  obtained from the adjusted prescription (10.4).

$L/l_s$	10	$10^2$	$10^3$	$10^4$
$g_s^{-1}H_0$	0.1	0.15	0.16	0.16
$\mu_1$	0.65	0.25	0.079	0.025
$1 - f_1$	0.34	0.015	$6.4 \cdot 10^{-4}$	$5.6 \cdot 10^{-5}$

Table 10.6: First non-zero eigenvalue  $\mu_1$  and deviation  $f_1$  from the standard spectrum for  $d = 3$ , together with the constant  $g_s^{-1}H_0$  obtained from the adjusted prescription (10.4).

$L/l_s$	10	$10^2$	$10^3$	$10^4$
$g_s^{-1}H_0$	0.012	0.025	0.025	0.025
$\mu_1$	0.35	0.064	$6.3 \cdot 10^{-3}$	$6.3 \cdot 10^{-4}$
$1 - f_1$	0.62	-0.018	$-2.0 \cdot 10^{-3}$	$-2.0 \cdot 10^{-4}$

Table 10.7: First non-zero eigenvalue  $\mu_1$  and deviation  $f_1$  from the standard spectrum for  $d = 4$ , together with the constant  $g_s^{-1}H_0$  obtained from the adjusted prescription (10.4).

$L/l_s$	10	$10^2$	$10^3$	$10^4$
$g_s^{-1}H_0$	$3.9 \cdot 10^{-3}$	$6.3 \cdot 10^{-3}$	$6.3 \cdot 10^{-3}$	$6.3 \cdot 10^{-3}$
$\mu_1$	$< 0.17$	0.013	$4.0 \cdot 10^{-4}$	$1.3 \cdot 10^{-5}$
$1 - f_1$	$> 0.65$	-0.02	$-2.0 \cdot 10^{-3}$	$-2.0 \cdot 10^{-4}$

Table 10.8: First non-zero eigenvalue  $\mu_1$  and deviation  $f_1$  from the standard spectrum for  $d = 5$ , together with the constant  $g_s^{-1}H_0$  obtained from the adjusted prescription (10.4).



$L/l_s$	10	$10^2$	$10^3$	$10^4$
$g_s^{-1}H_0$	$1.6 \cdot 10^{-3}$	$2.0 \cdot 10^{-3}$	$2.0 \cdot 10^{-3}$	$2.0 \cdot 10^{-3}$
$\mu_1$	$< 0.078$	$2.3 \cdot 10^{-3}$	$2.2 \cdot 10^{-5}$	$2.2 \cdot 10^{-7}$
$1 - f_1$	$> 0.69$	-0.02	$-2.0 \cdot 10^{-3}$	$-2.0 \cdot 10^{-4}$

Table 10.9: First non-zero eigenvalue  $\mu_1$  and deviation  $f_1$  from the standard spectrum for  $d = 6$ , together with the constant  $g_s^{-1}H_0$  obtained from the adjusted prescription (10.4).

The largest deviation  $|1 - f_1|$  is obtained for the lowest  $L/l_s$  and highest dimension: it is of 69% for  $d = 6$ . This strong deviation is one of the main results of this analysis. We illustrate the evolution of the first non-zero mass in terms of the dimension in Figure 10.5, compared to the standard spectrum. We finally make side comments on the values of  $g_s^{-1}H_0$ : those match the ones obtained analytically in (9.9) at large  $L/l_s$  for  $d \geq 3$ , and slowly vary from there. This however does not hold for  $d = 2$ : the constant obtained by the prescription, while obeying the behaviour of (9.9) in  $L/l_s$ , seems to differ by a constant shift of approximately 0.6. This could correspond to the next order after the leading behaviour of (9.6).

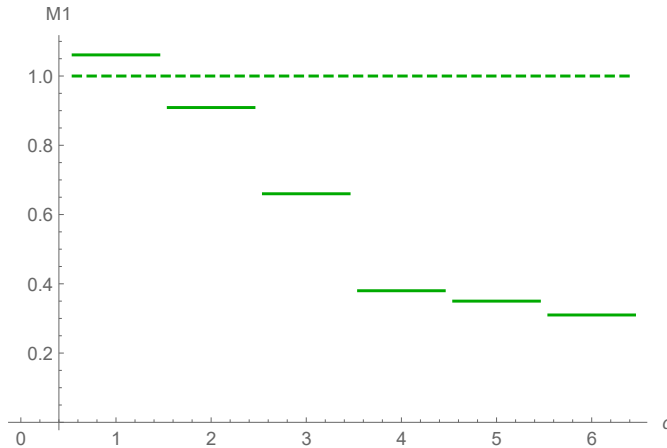


Figure 10.5: First non-zero mass  $M_1$  for  $d = 1, \dots, 6$  (plain lines), compared to that of the standard spectrum normalised to 1 (dashed line), for  $L/l_s = 10$ .

### 10.3 Summary and outlook

Kaluza–Klein gravitational waves, most likely of primordial origin, would provide a very specific signature of extra dimensions, in the form of a specific discrete spectrum. Motivated by this possibility, we determined in this work such a spectrum in the case where the extra dimensions include a warped torus  $\mathbb{T}^d$ .<sup>4</sup> While the Kaluza–Klein spectrum

<sup>4</sup>Considering other compact spaces would be very interesting, especially those appearing in different string compactifications. To that end, the Laplacian spectrum on e.g. a nilmanifold [122] or a Calabi–Yau

on a torus is well-known (we refer to it as the standard spectrum), we aimed here at measuring the effect of a non-trivial warp factor  $H$ , by evaluating the deviation of the resulting spectrum with respect to the standard one. We recall that a warp factor is a generic ingredient in BSM models as well as string compactifications, that captures the back-reaction of  $D_p$ -branes, as well as here orientifold  $O_p$ -planes. Characterising its impact on the spectrum is thus important. We considered the warp factor that would appear in common toroidal string compactifications, determined in [170], which differs from other options in the literature such as that of Randall-Sundrum models [243, 244], providing interesting novelties. We first tackled this problem in [170] and reviewed the relevant material in Section 9.2.1 and 9.2.3. New information on the profile of the Green’s function and the warp factor away from the sources is discussed in Section 9.2.2. We then made here important technical progress that eventually allowed a more precise and extended determination of the spectrum. The results are presented in Section 10.2. We first gave in Tables 10.1-10.3 the spectrum for the first massive Kaluza–Klein gravitational waves for  $d = 1, 2, 3$ , according to the ratio  $L/l_s$  of the radius of  $\mathbb{T}^d$  to the string (or fundamental) length. For large  $L/l_s$ , one recovers the standard spectrum, while for small ratios,  $2 < L/l_s < 10$ , the deviation is the most important. We illustrated these results, as well as the corresponding lift of degeneracies of the Kaluza–Klein modes, in Figure 10.4. We then focused on the lightest (massive) mode, for which the deviation is observed to be the highest, and we determined it for  $d = 1, \dots, 6$  in Tables 10.4-10.9 according to  $L/l_s$ . We illustrated the results in Figure 10.5: the highest deviation is obtained for  $d = 6$  at low  $L/l_s$ , and amounts to 69%. The Kaluza–Klein mass is thus significantly lowered because of the warp factor.

To reach these results, we had to overcome an important physical challenge: the negative region, depicted in Figure 9.2, where  $H < 0$ . As discussed in the introduction, the warp factor, and this negative region in particular, are currently at the center of many different investigations in string theory, and the present work may provide insights to these other related topics. We recalled there that  $H < 0$  close to orientifolds in the supergravity description. This is however unphysical, so this description is expected to break down, and be resolved by extra stringy physics. For this reason, the prescription of [170] was to place the “horizon” where  $H = 0$  at a string length from  $O_p$ . Thanks to the extra numerical precision gained here, we however realised that the negative region would generate tachyonic modes in the spectrum (see Appendix A.3). We argue in Section 10.1.1 and Appendix A.1 why this should happen in general. We excluded completely this negative, unphysical region from our analysis, and solved the eigenmode equation, that determines the spectrum, on a restricted domain  $\mathcal{D}$  where  $H \geq 0$ . We described this restriction in detail in Section 10.1.2 and illustrated the domain  $\mathcal{D}$  in Figure 10.1. This resolution, as well as several important numerical improvements presented in Section 10.1.3 and Appendix A.2, provided us with the tachyon-free, precise spectrum of Kaluza–Klein gravitational waves on a warped toroidal background described above. It would also be worth investigating richer compactifications, as initiated in [268] in the case of a Klebanov-Strassler warped throat. In addition, it would be interesting to link the Kaluza-Klein towers obtained in such constructions with existing Swampland conjectures, in the case of spin-2 fields.

---

manifold [267] would be useful.



APPENDICES PART IV



# A Details on the determination of the gravitational wave spectrum

This appendix provides additional details and supplementary material for Chapters 9 and 10.

## A.1 Tachyon in a non-compact case

In this section, we show analytically in a specific example the presence of tachyonic eigenmodes, due to the negative region close to an orientifold  $O_p$ , as discussed in Section 10.1.1; for completeness we also study the case of a  $D_p$ -brane. We consider the situation where the approximate behaviour (9.6) close to the source can be used, which also corresponds to the standard non-compact Green's function and warp factor. The differential problem to solve is the eigenvalue equation (9.22), which takes the form

$$\Delta\psi(\mathbf{r}) + \tilde{M}^2 H(\mathbf{r}) \psi(\mathbf{r}) = 0 , \quad (\text{A.1})$$

where  $H$  is the warp factor,  $\mathbf{r}$  parameterizes the position in the transverse torus  $\mathbb{T}^d$ , of Laplacian  $\Delta$ . We seek to determine the allowed eigenvalues  $\tilde{M}^2$ , especially their sign. We focus in the following on  $d = 3$  for simplicity.

### A.1.1 Orientifold source and negative region

Let us consider the problem in the vicinity of the origin,  $\mathbf{r} = \mathbf{0}$  where an orientifold  $O_6$  is located. The warp factor then takes the approximate form

$$H \simeq H_1 - \frac{C}{r} , \quad (\text{A.2})$$

where  $r = |\mathbf{r}|$ , and  $H_1, C$  are positive constants. We consider at first the problem in the region  $0 \leq r \leq C/H_1$ , where  $H$  is negative. We take the eigenfunction  $\psi$  to only depend on the radial coordinate  $r$ . The differential equation (A.1) then reduces to

$$\left[ r^2 \frac{d^2}{dr^2} + 2r \frac{d}{dr} + \lambda(Cr - H_1 r^2) \right] \psi(r) = 0 , \quad (\text{A.3})$$

where we have set  $\lambda = -\tilde{M}^2$ . By rescaling  $\lambda, r$ , we may henceforth set  $H_1 = C = 1$ , without loss of generality. Two linearly independent solutions

$$e^{-\sqrt{\lambda} r} {}_1F_1\left(1 - \frac{1}{2}\sqrt{\lambda}; 2; 2\sqrt{\lambda} r\right); \quad e^{-\sqrt{\lambda} r} U\left(1 - \frac{1}{2}\sqrt{\lambda}, 2, 2\sqrt{\lambda} r\right) , \quad (\text{A.4})$$

## Appendix A. Details on the determination of the gravitational wave spectrum

can be given in terms of the confluent hypergeometric functions of the first and second kind,  ${}_1F_1$ ,  $U$ , also known as Kummer's and Tricomi's function respectively. For  $-b \notin \mathbb{N}$  as here,  ${}_1F_1(a; b; z)$  is an entire function of both  $a, z \in \mathbb{C}$ . Tricomi's function can be defined in terms of  ${}_1F_1(a; b; z)$ .<sup>1</sup> For our purposes it suffices to note that  $U(a, 2, z)$  asymptotes  $\frac{1}{\Gamma(a)z}$ , as  $z \rightarrow 0$ .

The first of these solutions is real-valued for any  $\lambda \in \mathbb{R}$ , as can be seen from the defining series expansion of Kummer's function (equation (1) of p.248 of [269]); in particular,  $\lambda$  is allowed to be negative (despite the above notation  $\sqrt{\lambda}$ ). To obtain a discrete spectrum for  $\lambda$ , we may impose "separated" boundary conditions. As an example, we pick

$$\psi(0) = \psi(r_0) = 0, \quad (\text{A.5})$$

for some fixed radial distance  $r_0 > 0$ . The first boundary condition then implies  $\psi(r) \propto {}_1F_1$ , since  $U$  diverges at  $r = 0$ . For fixed  $r_0$ , the second boundary condition only has solutions for a discrete spectrum of values for  $\lambda$ . For example, let us consider  $r_0 = 1$ , which is the location of the "horizon" where the warp factor vanishes. Figure A.1 depicts  $f(\lambda) = e^{-\sqrt{\lambda} r_0} {}_1F_1(1 - \frac{1}{2}\sqrt{\lambda}; 2; 2\sqrt{\lambda} r_0)$  as a function of  $\lambda$ , for  $r_0 = 1$ . The spectrum of  $\lambda$  is then given by the zeros of the function  $f$ . We note that there are no zeros for negative  $\lambda$ , i.e. the spectrum of  $\tilde{M}^2$  is strictly negative.

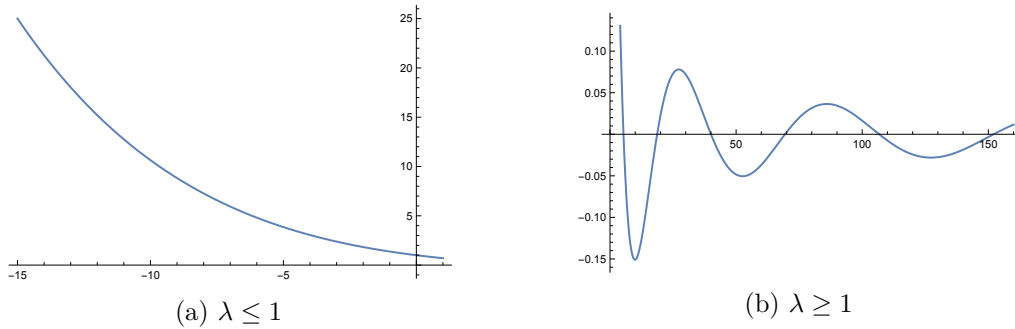


Figure A.1: Graph of  $f(\lambda) = e^{-\sqrt{\lambda}} {}_1F_1(1 - \frac{1}{2}\sqrt{\lambda}; 2; 2\sqrt{\lambda})$  as a function of  $\lambda$ . At  $\lambda = 0$  we have  $f = 1$ . For a better illustration, the graph is separated in two pieces, cutting at  $\lambda = 1$ , where the function is continuous. Importantly, all the zeros of  $f$  are located at positive  $\lambda$ .

These conclusions remain unchanged if we impose boundary conditions with  $0 < r_0 < 1$ , so that the warp factor is negative over the whole domain of definition  $[0, r_0]$  of the differential problem. However, the behaviour changes if we impose boundary conditions with  $r_0 > 1$ , in which case the warp factor does not have definite sign in the domain  $[0, r_0]$ : there are then zeros for both negative and positive  $\lambda$ . This means that the spectrum is not bounded, neither above nor below. We conclude that this example exhibits in any case tachyonic eigenmodes, i.e.  $\tilde{M}^2 < 0$ , as long we probe the region where  $H < 0$ .

<sup>1</sup>This can be seen e.g. in equation (7) of p.257 of [269]. That equation can be extended to all  $c \in \mathbb{Z}$  by continuity.

### A.1.2 $D_p$ -brane source

For completeness, let us now consider a warp factor corresponding to a  $D_6$ -brane source located at the origin

$$H \simeq H_1 + \frac{C}{r}, \quad (\text{A.6})$$

with  $H_1, C$  positive constants. The differential equation (A.1) then reduces to

$$\left[ r^2 \frac{d^2}{dr^2} + 2r \frac{d}{dr} - \lambda(H_1 r^2 + Cr) \right] \psi(r) = 0. \quad (\text{A.7})$$

As before, we may set  $H_1, C = 1$ , without loss of generality. Two linearly independent solutions are given by

$$e^{-\sqrt{\lambda}r} {}_1F_1\left(1 + \frac{1}{2}\sqrt{\lambda}; 2; 2\sqrt{\lambda}r\right); \quad e^{-\sqrt{\lambda}r} U\left(1 + \frac{1}{2}\sqrt{\lambda}; 2; 2\sqrt{\lambda}r\right). \quad (\text{A.8})$$

As before, it can be seen that the first solution is real-valued for any  $\lambda \in \mathbb{R}$ . To obtain a discrete spectrum for  $\lambda$ , we again impose the following ‘‘separated’’ boundary conditions

$$\psi(0) = \psi(r_0) = 0, \quad (\text{A.9})$$

for some fixed radial distance  $r_0 > 0$ , which we may choose to be  $r_0 = 1$  for simplicity. The first boundary condition implies  $\psi(r) \propto {}_1F_1$ . Figure A.2 depicts  $f(\lambda) = e^{-\sqrt{\lambda}r_0} {}_1F_1\left(1 + \frac{1}{2}\sqrt{\lambda}; 2; 2\sqrt{\lambda}r_0\right)$  as a function of  $\lambda$ , for  $r_0 = 1$ . The spectrum of  $\lambda$  is then given by the zeros of the function  $f$ . We note that this time, there are no zeros for positive  $\lambda$ , i.e. the spectrum of  $\tilde{M}^2$  is strictly positive.

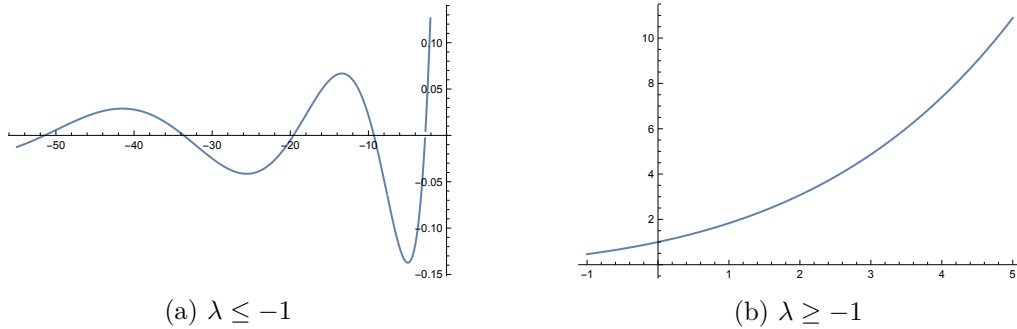


Figure A.2: Graph of  $f(\lambda) = e^{-\sqrt{\lambda}} {}_1F_1\left(1 + \frac{1}{2}\sqrt{\lambda}; 2; 2\sqrt{\lambda}\right)$  as a function of  $\lambda$ . At  $\lambda = 0$  we have  $f = 1$ . The graph is again cut in two, at  $\lambda = -1$  where there is no discontinuity. Importantly, all the zeros of  $f$  are located at negative  $\lambda$ .

In the  $D_p$ -brane case, these results are independent of the value of  $r_0$ . This is related to the fact that the warp factor is positive over the whole domain of definition  $[0, r_0]$  of the differential problem, for any value of  $r_0$ . We conclude on the absence of tachyonic eigenmodes in that case.



## A.2 Numerical details

### A.2.1 Making use of the symmetries

In this section, we come back to the numerical method used to determine the spectrum. Let us recall that we initially want to solve (10.10), that is a set of  $n$  equations. As mentioned in Section 10.1.3, one can use the symmetries of the problem to drastically reduce the size of the system, by merely working with the points  $\mathbf{m} \in \tilde{\Gamma}$  which are non-equivalent under the action of the symmetry group  $G$ . This is because in (10.10), the norm  $|\mathbf{n}|^2$  is naturally invariant under  $G$ , and the convolution product is also invariant whenever (10.17) and (10.18) are satisfied (i.e. when we consider the first Kaluza–Klein mode). Indeed,  $\forall g \in G$ , we have

$$\sum_{\mathbf{m} \in \mathbb{Z}^d} c_{\mathbf{m}} d_{\mathbf{n}-\mathbf{m}} = \sum_{\mathbf{m}' = g^{-1} \cdot \mathbf{m} \in \mathbb{Z}^d} c_{g \cdot \mathbf{m}'} d_{\mathbf{n}-g \cdot \mathbf{m}'} = \sum_{\mathbf{m}' \in \mathbb{Z}^d} c_{\mathbf{m}'} d_{g^{-1} \cdot \mathbf{n}-\mathbf{m}'}, \quad (\text{A.10})$$

so acting on  $\mathbf{n}$  in that sum also leaves it invariant. In this case, the system reduces to only  $\tilde{n}$  equations

$$\frac{|\mathbf{n}|^2}{\mu_1^2} c_{\mathbf{n}} - \sum_{\mathbf{m} \in \Gamma} c_{\mathbf{m}} d_{\mathbf{n}-\mathbf{m}} = 0, \quad \forall \mathbf{n} \in \tilde{\Gamma}. \quad (\text{A.11})$$

We also make use of (10.17) and (10.18) to only consider  $c_{\mathbf{m}}$  and  $d_{\mathbf{m}}$  for  $\mathbf{m} \in \tilde{\Gamma}$ , leaving us with only  $\tilde{n}$  unknowns  $c_{\mathbf{m}}$  (in addition to  $\mu_1$ ) and only  $\tilde{n}$  Fourier coefficients  $d_{\mathbf{m}}$  to compute. To that end, we need to choose a representative  $R(\mathbf{m}) \in \tilde{\Gamma}$  of the equivalence class  $[\mathbf{m}]$  defined by the relation  $\mathbf{m} \sim \mathbf{n} \Leftrightarrow \mathbf{m} = g \cdot \mathbf{n}$  (this amounts to define what we use as  $\tilde{\Gamma}$ ).

Let us note that, in  $d$  dimensions, the hyperoctahedral group  $G$  can be represented as the signed symmetric group of permutations of a set  $\{n^1, \dots, n^d\}$ . This provides a way to readily implement its action on points  $\mathbf{n} \in \Gamma$ : the orbit of one point is given by the set of possibilities of permuting its components and flipping their signs. Thus, it suffices to sort (say in decreasing order) the absolute value of the components of  $\mathbf{m}$  to pick a representative  $R(\mathbf{m})$ , as hinted around Figure 10.3. This algorithmic definition of the representative has the advantage to be simple to implement in a computer. For instance in Mathematica, one has

$$R[\mathbf{n}_] := \text{ReverseSort}[\text{Abs}[\mathbf{n}]]. \quad (\text{A.12})$$

With this at hand, one finally recovers (10.21), that is the set of equations to be solved.

### A.2.2 Bijective map

In order to manipulate the elements  $\mathbf{n}$  of  $\Gamma$  (or  $\tilde{\Gamma}$ ), it is useful to assign them a label, that is an integer index. This way, the coefficients  $d$  and  $c$  have an index which is an integer instead of a vector, and this allows to organize the equations and put them in an appropriate matrix form, as was done in (10.15). We thus need to introduce a one-to-one map,

$$F : \tilde{\Gamma} \longrightarrow \{1, 2, \dots, \tilde{n}\}. \quad (\text{A.13})$$

To implement such a map, one can do the following. Consider a vector  $\mathbf{n} \in \tilde{\Gamma}$  (for concreteness we focus on  $d = 2$ , but everything can be generalized trivially): following

the previous subsection, one can take its first entry  $n^1$  to be positive, so it goes from 0 to  $[r]$ , where  $[\cdot]$  denotes the integer part. Then for each of these possibilities,  $n^2$  can run from 0 to  $\max\{n^1, \sqrt{r^2 - (n^1)^2}\}$ . We then use this construction of  $\tilde{\Gamma}$  to label its elements: we start with the origin (indexed 1), then we increase  $n^1$ , there are now 2 possibilities for  $n^2$  (indexed 2 and 3 in order of increasing  $n^2$ ), then we increase  $n^1$  again, and so on.

In order to implement the inverse map  $F^{-1}$ , we construct a  $d$ -dimensional array  $[r] \times [r] \times \dots \times [r]$ , denoted  $\mathbf{F}$ . Whenever a point  $\mathbf{n}$  is added to  $\tilde{\Gamma}$  via the above algorithm, its label is added at the entry of  $\mathbf{F}$  that corresponds to the coordinates of  $\mathbf{n}$  (modulo a shift of 1 because indices start at 1 in Mathematica). Let us take an example: in  $d = 2$ , and say  $r = 3$ ,  $\mathbf{F}$  is  $3 \times 3$  matrix. The point  $(0, 0)$  is labeled 1, so the entry  $F_{11}$  takes the value 1. The next point  $(1, 0)$  is labeled 2, so  $F_{21}$  takes the value 2. The next point  $(1, 1)$  is labeled 3, so  $F_{22}$  takes the value 3, and so on. The advantage of this approach is that both  $F$  and its inverse  $F^{-1}$  are executed in constant time  $\mathcal{O}(1)$ .

### A.3 Tachyonic spectrum

In this section, we provide for completeness the Kaluza–Klein spectrum obtained for  $d = 1, 2, 3$  using the same method as in [170], namely the determinant method explained around (10.16) and a constant  $H_0$  given by (9.9). The spectrum is improved with respect to [170] in terms of precision and number of modes thanks to the bijective map described at the beginning of Section 10.1.3. We give in Tables A.1–A.3 the spectrum of the first modes of the tower, together with the sample specifications (see Section 10.1.3).

A crucial difference with the results of Section 10.2 is the presence here of tachyons for  $d \geq 2$ ,<sup>2</sup> as indicated in Tables A.2 and A.3. The resolution of the eigenmode equation is indeed performed here on the complete torus  $\mathbb{T}^d$ , including the negative region where  $H < 0$ . As discussed in Section 10.1.1 and Appendix A.1, this region is responsible for tachyonic modes in the spectrum. The solution proposed in Section 10.1.2 is then to solve the equation on a restricted domain  $\mathcal{D}$  that excludes the negative region. One can compare the resulting spectrum in Section 10.2 to the one here, at the same  $L/l_s$ , and note the absence of tachyon in Section 10.2.

Let us recall that we only consider a finite set of eigenmodes, because of the truncation made to solve the problem, as discussed in Section 10.1.3. When varying  $L/l_s$ , we can follow the evolution of the mass of each mode (or multiplet of modes with certain degeneracies). We note that the tachyons only become apparent to us at low  $L/l_s$ . In addition, they correspond to modes which were among most massive at higher  $L/l_s$ , and which disappear when lowering  $L/l_s$ . This is made manifest in Tables A.2 and A.3. As already mentioned in Section 10.1.1, we understand this phenomenon as follows: the eigenmodes need to have a small enough wavelength, i.e. a high enough mass, to probe the negative region. When  $L/l_s$  becomes small, the region becomes large and modes at high mass within our truncation then have the appropriate wavelength to become tachyonic, through the integral (10.1). In other words, tachyons may always be present in the spectrum, but for high  $L/l_s$ , they would lie outside our truncation. It would be

<sup>2</sup>Given that there is no divergence at the source for  $d = 1$ , one can find a constant  $H_0$  that makes  $H \geq 0$  everywhere, as done in [170], thus avoiding any tachyon in that case.

## Appendix A. Details on the determination of the gravitational wave spectrum

interesting to test further this interpretation.<sup>3</sup>

$N$	1		2	
$a/s$	$a$	$s$	$a$	$s$
$\mu_N$	0.9800	1.1400	2.037	2.205
$f_N$	0.9800	1.1400	1.018	1.102

Table A.1: Spectrum of the first Kaluza–Klein modes for  $d = 1$ , with eigenvalue  $\mu_N$  and deviation  $f_N$  from the standard spectrum, using the (improved) method of [170]. Sample specifications:  $r = 20$ ,  $n = 41$ .

$L/l_s$	$N$	1			$\sqrt{2}$			$2\sqrt{5}$
	$a/s$	$s(1)$	$a(2)$	$s(1)$	$s(1)$	$a(2)$	$s(1)$	Tachyon
9	$\mu_N$	0.7537	0.7944	0.9709	1.154	1.245	1.340	56.51 i
	$f_N$	0.8914	0.9395	1.148	0.9651	1.041	1.121	/
10	$\mu_N$	0.7378	0.7798	0.9435	1.131	1.213	1.305	10.54
	$f_N$	0.8932	0.9441	1.142	0.9681	1.039	1.117	2.852
$10^2$	$\mu_N$	0.5439	0.5749	0.6260	0.8192	0.8350	0.8692	2.920
	$f_N$	0.9312	0.9843	1.072	0.9918	1.011	1.052	1.118
$10^3$	$\mu_N$	0.4539	0.4735	0.4995	0.6719	0.6776	0.6925	2.247
	$f_N$	0.9519	0.9929	1.048	0.9964	1.005	1.027	1.054

Table A.2: Spectrum of the first Kaluza–Klein modes for  $d = 2$ , with eigenvalue  $\mu_N$  and deviation  $f_N$  from the standard spectrum, according to the value of  $L/l_s$ , using the (improved) method of [170]. Sample specifications:  $r = 4.5$ ,  $n = 69$ .

<sup>3</sup>An estimate of the wavelength is given by  $1/N = 1/|m|$ . The criterion for a tachyon to appear would then be that the wavelength is shorter or of the same order as the typical size of the negative region, i.e.  $1/N \lesssim 2l_s/L$ . We verify approximately in Tables A.2 and A.3 this inequality  $L/(2l_s) \lesssim N$  for the tachyonic mode. In addition, we also note that  $N \approx r$ , since the tachyon is among the highest modes of the truncation. Given a value of  $r$ , we deduce that a tachyon will appear for  $L/l_s \lesssim 2r$ .

$L/l_s$	$N$	1			$\sqrt{2}$					$\sqrt{6}$
	$a/s$	$s(1)$	$a(3)$	$s(2)$	$s(1)$	$a(3)$	$s(3)$	$a(3)$	$s(2)$	Tachyon
7	$\mu_N$	0.6681	0.7627	1.049	1.350	1.153	1.237	1.464	1.526	5.237 i
	$f_N$	0.7052	0.805	1.108	1.007	0.8607	0.9236	1.093	1.139	/
10	$\mu_N$	0.5899	0.6969	0.8729	1.118	1.027	1.028	1.205	1.275	3.019
	$f_N$	0.7442	0.8792	1.101	0.9971	0.916	0.9175	1.075	1.138	1.555
$10^2$	$\mu_N$	0.2433	0.2504	0.2538	0.3444	0.3507	0.3542	0.3575	0.3607	0.6231
	$f_N$	0.9704	0.9988	1.013	0.9714	0.9892	0.9991	1.008	1.017	1.015
$10^3$	$\mu_N$	0.07906	0.07927	0.07937	0.1117	0.1120	0.1121	0.1122	0.1123	0.1944
	$f_N$	0.9974	1.000	1.001	0.9966	0.9991	1.000	1.001	1.002	1.001

Table A.3: Spectrum of the first Kaluza–Klein modes for  $d = 3$ , with eigenvalue  $\mu_N$  and deviation  $f_N$  from the standard spectrum, according to the value of  $L/l_s$ , using the (improved) method of [170]. Sample specifications:  $r = 2.6$ ,  $n = 81$ .

We finally add a word on the degeneracies of each level. In the limit of large  $L/l_s$ , one recovers the standard Kaluza–Klein spectrum (9.23) on the torus  $\mathbb{T}^d$ . There, the eigenmodes are the Fourier modes, and the label  $N$  of each level is given by the norm of the vector  $\mathbf{m} \in \mathbb{Z}^d$  of the eigenmode. The spectrum is thus discrete and corresponds to points in  $\mathbb{Z}^d$  obtained when increasing the norm. Because of the symmetries of the lattice, the spectrum is degenerate; the degeneracy corresponds to the number of lattice points having the same norm. An illustration is provided in Figure 10.3. Knowing the exact degeneracy and the mass gap is actually a non-trivial question. It corresponds to a “generalized Gauss circle problem” in arbitrary dimension  $d$ . For  $d = 2$ , it is the problem of determining how many integer lattice points there are in a circle centered at the origin and with radius  $r$  as in Figure 10.3. In that case, the first levels are given by  $N = 1, \sqrt{2}, 2, \sqrt{5}, \dots$ , while the degeneracies are respectively given by  $\mathcal{D}_N = 4, 4, 4, 8, \dots$ . This knowledge is interesting to us, as it allows to classify the masses for the non-standard spectrum, for which the degeneracy is (partially) lifted: see Figure 10.4. Indeed, because of the different mass values, it is then unclear which one corresponds to a given level  $N$ . For  $d = 2$ , we now know that the first 4 masses correspond to  $N = 1$ , then the next 4 masses correspond to  $N = \sqrt{2}$ , etc.

It is easy to determine the degeneracy of levels due to vectors  $\mathbf{m} = (\pm 1, \dots, \pm 1, 0, \dots, 0)$ , i.e.  $k$  unit vectors (or their opposite) in  $d$  dimensions: those give  $N = \sqrt{k}$ . In that case, provided that no vector of a different kind contributes to that level, one gets the degeneracy

$$\mathcal{D}_{\sqrt{k}} = \binom{d}{k} \times 2^k, \quad 1 \leq k \leq d. \quad (\text{A.14})$$

This provides the first  $k$  levels for  $k \leq d \leq 3$ , and the first 3 levels for  $d \geq 4$ . We thus give the degeneracies of the first 3 levels in table A.4. They are useful to identify the eigenmodes in the spectra: the one given above or that of Section 10.2.

**Appendix A. Details on the determination of the gravitational wave spectrum**

---

		Level			
		1	2	3	
Dimension $d$	1	$N$	1	2	3
		$\mathcal{D}_N$	2	2	2
	2	$N$	1	$\sqrt{2}$	2
		$\mathcal{D}_N$	4	4	4
	3	$N$	1	$\sqrt{2}$	$\sqrt{3}$
		$\mathcal{D}_N$	6	12	8
	4	$N$	1	$\sqrt{2}$	$\sqrt{3}$
		$\mathcal{D}_N$	8	24	32
	5	$N$	1	$\sqrt{2}$	$\sqrt{3}$
		$\mathcal{D}_N$	10	40	80
	6	$N$	1	$\sqrt{2}$	$\sqrt{3}$
		$\mathcal{D}_N$	12	60	160

Table A.4: Label  $N$  and degeneracy  $\mathcal{D}_N$  of the first 3 Kaluza–Klein levels for each dimension  $d$ .

## B Cosmological solutions

In this appendix, we provide supplementary material related to the cosmological solutions presented in Chapter 8. For each type of compactification (Calabi-Yau, Einstein, Einstein-Kähler) we give the explicit ansatz for the fluxes and show how the equations of motion reduce to the form given in (7.13). Before working out each case in depth, let us display here for convenience the generic action and equations of motion, that we shall be using.

The ten-dimensional IIA action with Romans mass  $m$  reads

$$S = \frac{1}{2\kappa_{10}^2} \int d^{10}x \sqrt{g} \left( -R + \frac{1}{2}(\partial\phi)^2 + \frac{1}{2 \cdot 2!} e^{3\phi/2} F^2 + \frac{1}{2 \cdot 3!} e^{-\phi} H^2 + \frac{1}{2 \cdot 4!} e^{\phi/2} G^2 + \frac{1}{2} m^2 e^{5\phi/2} \right) + S_{CS} , \quad (\text{B.1})$$

where  $S_{CS}$  is the Chern-Simons term. The resulting equations of motion (EOM) read as follows:

- Einstein EOM's,

$$R_{MN} = \frac{1}{2} \partial_M \phi \partial_N \phi + \frac{1}{16} m^2 e^{5\phi/2} g_{MN} + \frac{1}{4} e^{3\phi/2} \left( 2F_{MN}^2 - \frac{1}{8} g_{MN} F^2 \right) + \frac{1}{12} e^{-\phi} \left( 3H_{MN}^2 - \frac{1}{4} g_{MN} H^2 \right) + \frac{1}{48} e^{\phi/2} \left( 4G_{MN}^2 - \frac{3}{8} g_{MN} G^2 \right) , \quad (\text{B.2})$$

where it is understood that  $\Phi_{MN}^2 := \Phi_{MM_2 \dots M_p} \Phi_N^{M_2 \dots M_p}$ , for any  $p$ -form  $\Phi$ .

- Dilaton EOM,

$$0 = -\nabla^2 \phi + \frac{3}{8} e^{3\phi/2} F^2 - \frac{1}{12} e^{-\phi} H^2 + \frac{1}{96} e^{\phi/2} G^2 + \frac{5}{4} m^2 e^{5\phi/2} . \quad (\text{B.3})$$

- Forms EOM's,

$$\begin{aligned} 0 &= d\star(e^{3\phi/2} F) + e^{\phi/2} H \wedge \star G \\ 0 &= d\star(e^{-\phi} H) + e^{\phi} F \wedge \star G - \frac{1}{2} G \wedge G + e^{3\phi/2} m \star F \\ 0 &= d\star(e^{\phi/2} G) - H \wedge G . \end{aligned} \quad (\text{B.4})$$

Additionally the forms obey the Bianchi identities,

$$dF = mH ; \quad dH = 0 ; \quad dG = H \wedge F . \quad (\text{B.5})$$

## B.1 Analytic solutions

### B.1.1 Compactification on Calabi-Yau manifolds

We follow the ansatz of the consistent truncation of [216], but we work directly with the 10d equations of motion. We will furthermore restrict to the case without fermion condensates.

The ansatz for the ten-dimensional two-form  $F$ , three-form  $H$  and four-form  $G$  reads

$$F = d\alpha ; \quad H = d\chi \wedge J + d\beta ; \quad G = \varphi \text{vol}_4 + J \wedge (d\gamma - \alpha \wedge d\chi) - \frac{1}{2} d\xi \wedge \text{Im}\Omega - \frac{1}{2} d\xi' \wedge \text{Re}\Omega , \quad (\text{B.6})$$

where  $\varphi, \chi, \xi, \xi'$  are 4d scalars,  $\alpha, \gamma$  are 4d one-forms, and  $\beta$  is a 4d two-form. We shall also introduce the 4d three-form  $h := d\beta$ . The ansatz for the ten-dimensional metric in 10d Einstein frame reads

$$ds_{10}^2 = e^{2A(x)} \left( e^{2B(x)} g_{\mu\nu} dx^\mu dx^\nu + g_{mn} dy^m dy^n \right) , \quad (\text{B.7})$$

where the scalars  $A, B$  only depend on the four-dimensional coordinates  $x^\mu$ , while  $y^m$  are the CY coordinates. The equations of motion are as follows,

$$0 = e^{-8A-2B} \nabla^\mu \left( e^{8A+2B} \partial_\mu A \right) - \frac{1}{32} e^{3\phi/2-2A-2B} d\alpha^2 + \frac{1}{8} e^{-\phi-4A} (\partial\chi)^2 - \frac{1}{48} e^{-\phi-4A-4B} h^2 \\ - \frac{1}{32} e^{\phi/2-6A-2B} (d\gamma - \alpha \wedge d\chi)^2 + \frac{1}{16} e^{\phi/2-6A} \left[ (\partial\xi)^2 + (\partial\xi')^2 \right] + \frac{3}{16} e^{\phi/2-6A-6B} \varphi^2 , \quad (\text{B.8})$$

coming from the internal  $(m, n)$ -components of the ten-dimensional Einstein equations. The external  $(\mu, \nu)$ -components give rise to

$$R_{\mu\nu}^{(4)} = g_{\mu\nu} \left( \nabla^2 A + \nabla^2 B + 8(\partial A)^2 + 2(\partial B)^2 + 10\partial A \cdot \partial B \right) \\ - 8\partial_\mu A \partial_\nu A - 2\partial_\mu B \partial_\nu B - 16\partial_{(\mu} A \partial_{\nu)} B + 8\nabla_\mu \partial_\nu A + 2\nabla_\mu \partial_\nu B \\ + \frac{3}{2} e^{-\phi-4A} \partial_\mu \chi \partial_\nu \chi + \frac{1}{2} e^{3\phi/2-2A-2B} d\alpha_{\mu\nu}^2 + \frac{1}{4} e^{\phi-4A-4B} h_{\mu\nu}^2 + \frac{1}{2} \partial_\mu \phi \partial_\nu \phi \\ + \frac{1}{2} e^{\phi/2-6A} (\partial_\mu \xi \partial_\nu \xi + \partial_\mu \xi' \partial_\nu \xi') + \frac{3}{2} e^{\phi/2-6A-2B} (d\gamma - \alpha \wedge d\chi)_{\mu\nu}^2 \\ + \frac{1}{16} g_{\mu\nu} \left( -\frac{1}{2} e^{3\phi/2-2A-2B} d\alpha^2 - \frac{1}{3} e^{\phi-4A-4B} h^2 - 3e^{\phi/2-6A} \left[ (\partial\xi)^2 + (\partial\xi')^2 \right] \right. \\ \left. - 6e^{-\phi-4A} (\partial\chi)^2 - 5e^{\phi/2-6A-6B} \varphi^2 - \frac{9}{2} e^{\phi/2-6A-2B} (d\gamma - \alpha \wedge d\chi)^2 \right) , \quad (\text{B.9})$$

while the mixed  $(\mu, m)$ -components are automatically satisfied. The dilaton equation reduces to

$$0 = e^{-10A-4B} \nabla^\mu \left( e^{8A+2B} \partial_\mu \phi \right) - \frac{1}{4} e^{\phi/2-8A-2B} \left[ (\partial\xi)^2 + (\partial\xi')^2 \right] - \frac{3}{8} e^{3\phi/2-4A-4B} d\alpha^2 \\ + \frac{3}{2} e^{-\phi-6A-2B} (\partial\chi)^2 + \frac{1}{12} e^{-\phi-6A-6B} h^2 + \frac{1}{4} e^{\phi/2-8A-8B} \varphi^2 - \frac{3}{8} e^{\phi/2-8A-4B} (d\gamma - \alpha \wedge d\chi)^2 . \quad (\text{B.10})$$

The  $F$ -form equation of motion reduces to the condition

$$d(e^{3\phi/2+6A} \star_4 d\alpha) = \varphi e^{\phi/2+2A-4B} d\beta - 3e^{\phi/2+2A} d\chi \wedge \star_4(d\gamma - \alpha \wedge d\chi) . \quad (\text{B.11})$$

The  $H$ -form equation gives rise to two equations,

$$d\left(e^{-\phi+4A+2B} \star_4 d\chi\right) = (d\gamma - \alpha \wedge d\chi) \wedge (d\gamma - \alpha \wedge d\chi) - e^{\phi/2+2A} d\alpha \wedge \star_4(d\gamma - \alpha \wedge d\chi) , \quad (\text{B.12})$$

and,

$$d\left(e^{-\phi+4A-2B} \star_4 d\beta\right) = -d\xi \wedge d\xi' + e^{\phi/2+2A-4B} \varphi d\alpha . \quad (\text{B.13})$$

The  $G$ -form equation reduces to

$$\begin{aligned} d\left(e^{\phi/2+2A+2B} \star_4 d\xi\right) &= h \wedge d\xi' \\ d\left(e^{\phi/2+2A+2B} \star_4 d\xi'\right) &= -h \wedge d\xi \\ d\left(e^{\phi/2+2A} \star_4 (d\gamma - \alpha \wedge d\chi)\right) &= 2d\chi \wedge d\gamma , \end{aligned} \quad (\text{B.14})$$

together with

$$0 = d\left(\varphi e^{\phi/2+2A-4B}\right) , \quad (\text{B.15})$$

which can be integrated to

$$\varphi = e^{-\phi/2-2A+4B} c_\varphi , \quad (\text{B.16})$$

for some constant  $c_\varphi$ .

• **Cosmological ansatz**

We will now make a cosmological ansatz for all fields, i.e. one that is (in general) only invariant under the isometries of the 3d spatial part of the metric. We assume that all scalars are functions of the time coordinate  $t$  alone. The one-forms are assumed to be of the form

$$\alpha = \alpha(t)dt ; \quad \gamma = \gamma(t)dt , \quad (\text{B.17})$$

for some scalars  $\alpha, \gamma$  which may be time-dependent in general. With some abuse of notation, we have denoted by the same letter the one-forms and the corresponding scalars. In the following all equations of motion will be expressed exclusively in terms of the scalars, so hopefully no confusion will occur. The three-form  $h$  is assumed to be of the form

$$h = c_h \sqrt{\gamma} dx^1 \wedge dx^2 \wedge dx^3 , \quad (\text{B.18})$$

where  $c_h$  is a constant. The unwarped 4d metric (A.2) is assumed to be of the form of eq. (7.2), while the 4d Einstein frame metric is thus given by (7.4).

Substituting the ansatz above into the form equations of motion (B.11)-(B.16), we obtain the following system: eq. (B.11) reduces to

$$c_\varphi c_h = 0 . \quad (\text{B.19})$$



## Appendix B. Cosmological solutions

Eq. (B.12) reduces to

$$\chi = c_\chi \int^t dt' e^{\phi(t')-4A(t')-2B(t')} + d_\chi , \quad (\text{B.20})$$

where  $c_\chi, d_\chi$  are constants. Eq. (B.13) is automatically satisfied. Eq. (B.14) reduces to

$$\begin{aligned} d_t \left( e^{\phi/2+2A+2B} d_t \xi \right) &= c_h d_t \xi' \\ d_t \left( e^{\phi/2+2A+2B} d_t \xi' \right) &= -c_h d_t \xi , \end{aligned} \quad (\text{B.21})$$

where  $d_t$  denotes the derivative with respect to  $t$ . Note that if eq. (B.21) is satisfied for some  $\xi, \xi' \neq 0$ , this implies

$$(d_t \xi)^2 + (d_t \xi')^2 = 2c_{\xi\xi'}^2 e^{-\phi-4A-4B} , \quad (\text{B.22})$$

for some arbitrary real constant  $c_{\xi\xi'}$ .

The system (B.21) can be integrated to give

$$\begin{aligned} e^{\phi/2+2A+2B} d_t \xi &= c_h \xi' + c_\xi \\ e^{\phi/2+2A+2B} d_t \xi' &= -c_h \xi + c_{\xi'} , \end{aligned} \quad (\text{B.23})$$

for some constants  $c_\xi, c_{\xi'}$ . Let us define a new time variable  $\nu$  by

$$\nu(t) := \int^t dt' e^{-[\phi(t')/2+2A(t')+2B(t')]} . \quad (\text{B.24})$$

If  $c_h \neq 0$ , the solution to (B.23) reads

$$\xi = \sin(c_h \nu + d_\xi) + \frac{c_{\xi'}}{c_h} ; \quad \xi' = \cos(c_h \nu + d_\xi) - \frac{c_\xi}{c_h} , \quad (\text{B.25})$$

where  $d_\xi$  is an arbitrary constant. If  $c_h = 0$ , the solution to (B.23) reads instead

$$\xi = c_\xi \nu + d_\xi ; \quad \xi' = c_{\xi'} \nu + d_{\xi'} , \quad (\text{B.26})$$

where  $d_\xi, d_{\xi'}$  are arbitrary constants. This then concludes the solution of all equations of motion for the forms.

### • Adapted time coordinate

In the following we will use the time variable  $\tau$  defined in (7.6). The internal Einstein and dilaton equations, (B.8), (B.10) reduce to

$$\begin{aligned} d_\tau^2 A &= \frac{3}{16} c_\varphi^2 e^{-\phi/2+6A+6B} - \frac{1}{8} c_h^2 e^{-\phi+12A} - \frac{1}{8} c_\chi^2 e^{\phi+4A} - \frac{1}{8} c_{\xi\xi'}^2 e^{-\phi/2+6A} \\ d_\tau^2 \phi &= \frac{1}{4} c_\varphi^2 e^{-\phi/2+6A+6B} + \frac{1}{2} c_h^2 e^{-\phi+12A} - \frac{3}{2} c_\chi^2 e^{\phi+4A} + \frac{1}{2} c_{\xi\xi'}^2 e^{-\phi/2+6A} . \end{aligned} \quad (\text{B.27})$$

The external Einstein equations (B.9) reduce to

$$\begin{aligned} -2k e^{16A+4B} - \frac{1}{2} c_\varphi^2 e^{-\phi/2+6A+6B} + \frac{1}{2} c_h^2 e^{-\phi+12A} + \frac{1}{2} c_\chi^2 e^{\phi+4A} + \frac{1}{2} c_{\xi\xi'}^2 e^{-\phi/2+6A} &= d_\tau^2 B \\ -12k e^{16A+4B} + c_\varphi^2 e^{-\phi/2+6A+6B} + c_h^2 e^{-\phi+12A} + 3c_\chi^2 e^{\phi+4A} + 2c_{\xi\xi'}^2 e^{-\phi/2+6A} &= 144(d_\tau A)^2 + 12(d_\tau B)^2 \\ &\quad + 96d_\tau A d_\tau B - (d_\tau \phi)^2 . \end{aligned} \quad (\text{B.28})$$

The second line above is a constraint, consistently propagated by the remaining equations of motion. Indeed the  $\tau$ -derivative of this equation is automatically satisfied by virtue of (B.27) and the first equation in (B.28).

• IIB solution

Although the main focus of the present work is on IIA supergravity, let us note that the minimal solution can be easily generalized to include a non-trivial axion  $C$ . The ten-dimensional Lagrangian,

$$\mathcal{L} = R - \frac{1}{2}(\partial\phi)^2 - \frac{1}{2}e^{2\phi}(\partial C)^2, \quad (\text{B.29})$$

together with the ansatz (A.2) for the metric, now lead to the following equations of motion: for the axio-dilaton we have

$$d_\tau C = c_a e^{-2\phi} \quad d_\tau^2 \phi = c_a^2 e^{-2\phi}, \quad (\text{B.30})$$

for some real constant  $c_a$ . The Einstein equations reduce to

$$d_\tau A = c_A \quad d_\tau B = c_B, \quad (\text{B.31})$$

for some real constants  $c_A, c_B$ , together with the constraint

$$12c_A^2 + c_B^2 + 8c_A c_B - \frac{1}{12}(d_\tau \phi)^2 - \frac{1}{12}c_a^2 e^{-2\phi} = 0. \quad (\text{B.32})$$

The solution for the axio-dilaton reads

$$C = \frac{c_\phi}{c_a} \tanh(c_\phi \tau + d_\phi) + d_a; \quad \phi = \frac{1}{2} \ln \frac{c_a^2}{c_\phi^2} + \ln[\cosh(c_\phi \tau + d_\phi)], \quad (\text{B.33})$$

for some constants  $d_a, d_\phi$ . Taking the above into account, (B.32) reduces to the constraint (8.5). It readily follows that, apart from the axio-dilaton, the IIB solution is identical to the minimal solution.

$k \neq 0$

As before, we will take

$$\varphi = h = 0; \quad \chi = d_\chi; \quad \xi = d_\xi; \quad \xi' = d_{\xi'}, \quad (\text{B.34})$$

which still solves the form equations (B.11)-(B.16) in the case of  $k \neq 0$ . Let us consider the remaining equations of motion. The internal Einstein and the dilaton equation give, cf. (B.27),

$$A = c_A \tau + d_A; \quad \phi = c_\phi \tau + d_\phi, \quad (\text{B.35})$$

for some constants  $d_A, d_\phi$ , exactly as for the minimal solution. From the first equation in (B.28), we obtain the solution for  $B$ ,

$$B = -4(c_A \tau + d_A) + \frac{1}{4}f(\tau), \quad (\text{B.36})$$

where,

$$f(\tau) = \begin{cases} \ln \left[ \frac{c_B^2}{4k} \operatorname{sech}^2(c_B \tau + d_B) \right] & , \quad k > 0 \\ \ln \left[ \frac{c_B^2}{4|k|} \operatorname{csch}^2(c_B \tau + d_B) \right] & , \quad k < 0 \end{cases}, \quad (\text{B.37})$$

for some constants  $c_B, d_B$ . Moreover, the second equation in (B.28) (the constraint) reduces to an algebraic condition,

$$c_\phi^2 + 48c_A^2 = 3c_B^2, \quad (\text{B.38})$$

for  $k$  of either sign. In particular this implies,  $r \leq |\frac{1}{4}|$ , cf. (8.6). In the following we consider the two cases in (B.37) in more detail.

## Appendix B. Cosmological solutions

---

- **Type I solution: closed universe**

Let us set  $k > 0$ . The 4d Einstein-frame metric reads

$$ds_{4E}^2 = \text{sech}^3(c_B \tau) \left( -d\tau^2 + \frac{4k}{c_B^2} \cosh^2(c_B \tau) d\Omega_k^2 \right), \quad (\text{B.39})$$

where we have set  $d_A, d_B = 0$  for simplicity. Since the sign of  $c_B$  can be absorbed in the definition of  $\tau$ , we may suppose  $c_B \geq 0$  without loss of generality; the inequality is saturated in case  $c_A, c_B, c_\phi$  all vanish. In terms of coordinates  $T_\pm \propto e^{\mp \frac{3}{2} c_B \tau}$  the metric asymptotically takes the form of (8.2), where  $a_\pm = \frac{1}{3}$ . For  $c_B \geq 0$ ,  $\tau \rightarrow \pm\infty$  corresponds to  $T_\pm \rightarrow 0$ , where a singularity is reached at finite proper time.

- **Type II solution: open universe**

Let us now set  $k < 0$ . The 4d Einstein-frame metric reads

$$ds_{4E}^2 = \text{csch}^3(c_B \tau) \left( -d\tau^2 + \frac{4|k|}{c_B^2} \sinh^2(c_B \tau) d\Omega_k^2 \right), \quad (\text{B.40})$$

where we have set  $d_A, d_B = 0$  for simplicity. Since the sign of  $c_B$  can be absorbed in the definition of  $\tau$ , we may suppose  $c_B \geq 0$  without loss of generality.

The  $\tau \rightarrow \pm\infty$  asymptotics of the warp factors are exactly the same as for  $k > 0$ . For  $\tau \rightarrow 0$ , on the other hand, the function  $f$  tends to  $f \rightarrow -\ln(4|k|\tau^2)$ , while the constraint imposes  $c_A, c_\phi = 0$ . Hence in the  $\tau \rightarrow 0$  limit the solution reads

$$A = d_A; \quad B = -4d_A - \frac{1}{4} \ln(4|k|\tau^2); \quad \phi = d_\phi, \quad (\text{B.41})$$

Note that comoving geodesics reach  $\tau = 0$  at infinite proper time. The metric becomes asymptotically that of a regular Milne universe,<sup>1</sup>

$$ds^2 = -dT^2 + |k| T^2 d\Omega_k^2, \quad (\text{B.42})$$

where we have defined  $T = 2(c_B^3 \tau)^{-\frac{1}{2}}$ . The warp factor of the internal space and the dilaton are constant.

### $\varphi \neq 0$

Let us now take

$$\varphi = e^{-\phi/2 - 2A + 4B} c_\varphi; \quad h = 0; \quad \chi = d_\chi; \quad \xi = d_\xi; \quad \xi' = d_{\xi'}, \quad (\text{B.43})$$

which still solves the form equations (B.11)-(B.16) in the case of  $\varphi \neq 0$ . Let us consider the remaining equations of motion. Eqs. (B.27) reduce to

$$d_\tau^2 A = \frac{3}{16} c_\varphi^2 e^{-\phi/2 + 6A + 6B}; \quad d_\tau^2 \phi = \frac{1}{4} c_\varphi^2 e^{-\phi/2 + 6A + 6B}, \quad (\text{B.44})$$

---

<sup>1</sup> Recall that the spatial 3d part of the metric is locally isometric to a hyperbolic space of scalar curvature  $6k$ , cf. (7.3). An explicit parametrization is given by,

$$d\Omega_k^2 = \frac{1}{|k|} (d\chi^2 + \sinh^2 \chi d\sigma^2),$$

with  $d\sigma^2$  the line element of the two-sphere.

while (B.28) reduce to the following two equations,

$$\begin{aligned} -\frac{1}{2}c_\phi^2 e^{-\phi/2+6A+6B} &= d_\tau^2 B \\ c_\phi^2 e^{-\phi/2+6A+6B} &= 144(d_\tau A)^2 + 12(d_\tau B)^2 + 96d_\tau A d_\tau B - (d_\tau \phi)^2 . \end{aligned} \quad (\text{B.45})$$

To obtain an analytic solution we proceed as follows. We define  $f := -\phi/2 + 6A + 6B$ , which by virtue of the equations of motion (B.44),(B.45) obeys,  $d_\tau^2 f = -2c_\phi^2 e^f$ . The solution to this equation reads

$$f = \ln \frac{c_\phi^2}{c_\phi^2} - 2 \ln [\cosh(c_\phi \tau + d_\phi)] , \quad (\text{B.46})$$

for some constants  $c_\phi, d_\phi$ . Plugging back into (B.44), and the first line of (B.45), we obtain the solution

$$\begin{aligned} A &= c_A \tau + d_A - \frac{3}{32} f \\ B &= c_B \tau + d_B + \frac{1}{4} f \\ \phi &= 12(c_A + c_B)\tau + 12(d_A + d_B) - \frac{1}{8} f , \end{aligned} \quad (\text{B.47})$$

for some constants  $c_A, c_B, d_A, d_B$ , and  $f$  as given in (B.46). Moreover, the second line of (B.45) imposes the constraint

$$c_\phi^2 = -12c_B(16c_A + 11c_B) , \quad (\text{B.48})$$

which implies  $r \leq -\frac{11}{16}$ . The 4d Einstein-frame metric reads

$$ds_{4E}^2 = e^{(24c_A+6c_B)\tau} \cosh^{\frac{3}{2}}(c_\phi \tau) \left( -d\tau^2 + e^{-(16c_A+4c_B)\tau} \text{sech}(c_\phi \tau) d\vec{x}^2 \right) , \quad (\text{B.49})$$

where we have set  $d_A, d_B, d_\phi = 0$  for simplicity.

Let us assume  $c_\phi \geq 0$ , without loss of generality, since the sign of  $c_\phi$  can be absorbed in the definition of  $\tau$ . In terms of coordinates  $T_\pm \propto e^{(12c_A+3c_B \pm \frac{3}{4}c_\phi)\tau}$ , the metric asymptotically takes the form of (8.2), where  $a_\pm = \frac{1}{3}$ .

If  $c_B > 0$ ,  $\tau = -\infty$  corresponds to  $T_- = \infty$  while  $\tau = \infty$  corresponds to  $T_+ = 0$ , where a singularity is reached at finite proper time. The situation is reversed for  $c_B < 0$ :  $\tau = -\infty$  corresponds to  $T_- = 0$ , where a singularity is reached at finite proper time, while  $\tau = \infty$  corresponds to  $T_+ = \infty$ . For a certain range of parameters, this model exhibits transient accelerated expansion, where  $\dot{S}(T), \ddot{S}(T) > 0$ , cf. Figure B.1.

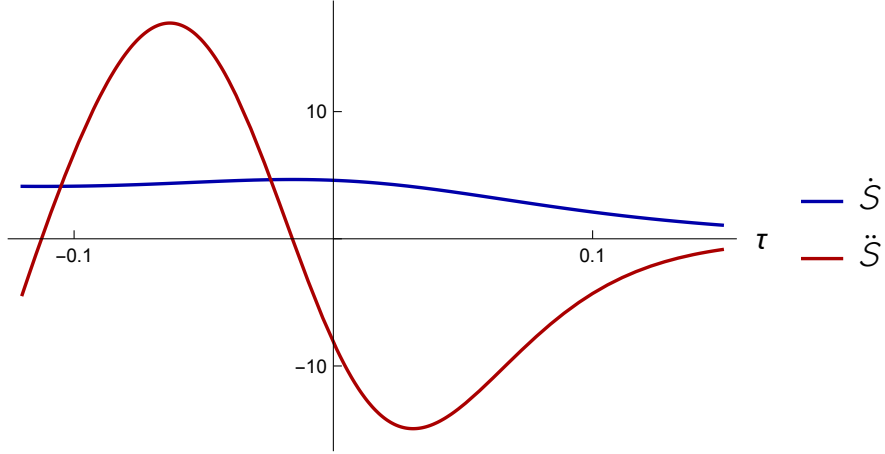


Figure B.1: Plot of  $\dot{S}(T), \ddot{S}(T)$  as a function of  $\tau$ , for  $c_B = -1, r = -1.4$ .

• **Critical solution:  $\varphi \neq 0, k < 0$**

Let us now consider  $k \neq 0$ . The equations of motion (B.27), (B.28) admit the following solution,

$$A = -\frac{3}{56} \ln |\tau| + d_A + 3d_\phi; \quad B = -\frac{2}{7} \ln |\tau| - 4d_A + 16d_\phi; \quad \phi = -\frac{1}{14} \ln |\tau| - 36d_A + 4d_\phi, \quad (\text{B.50})$$

for an arbitrary constant  $d_A$ , and  $k, d_\phi$  subject to the conditions

$$d_\phi = -\frac{1}{112} \ln\left(\frac{7}{2}c_\varphi^2\right); \quad k = -\frac{3}{4}c_\varphi^2 < 0. \quad (\text{B.51})$$

The 4d metric is that of a *singular* Milne universe *with angular defect*, cf. Footnote 1,

$$ds^2 = -dT^2 + \frac{7}{6}|k|T^2 d\Omega_k^2, \quad (\text{B.52})$$

where we set  $T \propto |\tau|^{-\frac{1}{2}}$  and  $d\Omega_k^2$  is the line element of a locally hyperbolic three-space. The warp factor of the internal space and the dilaton scale as  $e^A \propto T^{3/28}, e^\phi \propto T^{1/7}$  respectively.

• **Type II solution:  $\varphi \neq 0, k < 0$**

We will now construct a solution interpolating between future or past infinity  $\tau \rightarrow \pm\infty$ , and the above critical solution in the  $\tau \rightarrow 0$  limit. Let us use an ansatz of the form

$$A = c_A\tau + d_A + f(\tau); \quad B = c_B\tau + d_B + e_B f(\tau); \quad \phi = c_\phi\tau + d_\phi + e_\phi f(\tau), \quad (\text{B.53})$$

for some (non-linear) function  $f$  and constants  $c, d, e$ . Moreover we will require that the equations of motion (B.27) and the first line of (B.28) reduce to a single differential equation for  $f$ . These requirements impose the following condition on the spatial curvature,

$$k = -\frac{3}{4}c_\varphi^2, \quad (\text{B.54})$$

(open universe) and, after some redefinitions of the constants, lead to the solution,

$$\begin{aligned} A &= c_A \tau + d_A + 3g(\tau) \\ B &= -4(c_A \tau + d_A) + 16g(\tau) \\ \phi &= -36(c_A \tau + d_A) + 4g(\tau) , \end{aligned} \quad (\text{B.55})$$

where

$$g = \frac{1}{112} \ln \frac{2c_\phi^2}{7c_\varphi^2} - \frac{1}{112} \ln [\sinh^2(c_\phi \tau + d_\phi)] . \quad (\text{B.56})$$

The second line of the constraint then reduces to

$$c_\phi = \pm 28 \sqrt{\frac{3}{5}} c_A . \quad (\text{B.57})$$

The 4d Einstein metric reads

$$ds_{4E}^2 = \text{csch}^3(c_\phi \tau) \left( -d\tau^2 + \frac{7c_\varphi^2}{2c_\phi^2} \sinh^2(c_\phi \tau) d\Omega_k^2 \right) , \quad (\text{B.58})$$

where we have set  $d_A, d_\phi = 0$  for simplicity. The metric asymptotically takes the form (8.2), where  $a_\pm = \frac{1}{3}$ . On the other hand, for  $\tau \rightarrow 0$  we have

$$g \rightarrow -\frac{1}{112} \ln\left(\frac{7}{2}c_\varphi^2\right) - \frac{1}{56} \ln |\tau| . \quad (\text{B.59})$$

In this limit the solution (B.55) thus takes the form given in eqs. (B.50), (B.51). In other words, for  $\tau \rightarrow 0$  the solution asymptotes the critical solution. Comoving geodesics reach  $\tau = 0$  at infinite proper time.

## $\chi \neq 0$

Let us now take

$$d_t \chi = e^{\phi - 4A - 2B} c_\chi ; \quad \xi = d_\xi ; \quad \xi' = d_{\xi'} ; \quad \varphi = 0 ; \quad h = 0 , \quad (\text{B.60})$$

which still solves the form equations (B.11)-(B.16) in the case of  $\chi \neq 0$ . Let us consider the remaining equations of motion. Equations (B.27) and the first line of (B.28) are solved by

$$\begin{aligned} A &= c_A \tau + d_A + \frac{1}{16} f \\ B &= c_B \tau + d_B - \frac{1}{4} f \\ \phi &= -4(c_A \tau + d_A) + \frac{3}{4} f , \end{aligned} \quad (\text{B.61})$$

with

$$f := \ln \frac{c_\phi^2}{c_\chi^2} - 2 \ln [\cosh(c_\phi \tau + d_\phi)] , \quad (\text{B.62})$$

while the second line of (B.28) reduces to

$$3c_\phi^2 = 128c_A^2 + 96c_A c_B + 12c_B^2 . \quad (\text{B.63})$$

The constraint imposes in particular,  $r \leq -\frac{\sqrt{3}}{8}(1 + \sqrt{3})$  or  $r \geq \frac{\sqrt{3}}{8}(1 - \sqrt{3})$ .

The 4d Einstein metric reads

$$ds_{4E}^2 = -e^{(24c_A + 6c_B)\tau} d\tau^2 + e^{(8c_A + 2c_B)\tau} d\vec{x}^2 , \quad (\text{B.64})$$

where we have set  $d_A, d_B$ , and  $d_\phi = 0$  for simplicity. In terms of the coordinate  $T \propto e^{(12c_A + 3c_B)\tau}$ ,  $T \in [0, \infty)$ , the metric takes the form (8.2), with  $a_\pm = \frac{1}{3}$ .

## Appendix B. Cosmological solutions

---

### • Type I solution : $k > 0$

Let us now consider  $k \neq 0$ . Equations (B.27) can be solved to give

$$\begin{aligned} A &= c_A \tau + d_A + \frac{1}{16} g(\tau) \\ \phi &= -4(c_A \tau + d_A) + \frac{3}{4} g(\tau) , \end{aligned} \quad (\text{B.65})$$

for some constants  $c_A, d_A$ , where

$$g = \ln \frac{c_\phi^2}{c_\chi^2} - 2 \ln [\cosh(c_\phi \tau + d_\phi)] . \quad (\text{B.66})$$

Taking the above into account, the first of (B.28) can be solved for  $B$ ,

$$B = -4A + \frac{1}{4} f , \quad (\text{B.67})$$

where

$$f = \begin{cases} \ln \left[ \frac{c_B^2}{4k} \operatorname{sech}^2(c_B \tau + d_B) \right] & , \quad k > 0 \\ \ln \left[ \frac{c_B^2}{4|k|} \operatorname{csch}^2(c_B \tau + d_B) \right] & , \quad k < 0 \end{cases} , \quad (\text{B.68})$$

for some constants  $c_B, d_B$ . Plugging the solution into the second line of (B.28) we obtain the constraint

$$c_B^2 = \frac{64}{3} c_A^2 + c_\phi^2 , \quad (\text{B.69})$$

for either sign of  $k$ .

Let us first consider the case of a closed universe ( $k > 0$ ). The 4d metric reads, with  $d_A, d_B, d_\phi = 0$  for simplicity,

$$ds_4^2 = \operatorname{sech}^3(c_B \tau) \left( -d\tau^2 + \frac{4k}{c_B^2} \cosh^2(c_B \tau) d\Omega_k^2 \right) . \quad (\text{B.70})$$

### • Type II and critical solutions: $k < 0$

Let us now set  $k < 0$ . The 4d Einstein metric reads

$$ds_{4E}^2 = \operatorname{csch}^3(c_B \tau) \left( -d\tau^2 + \frac{4|k|}{c_B^2} \sinh^2(c_B \tau) d\Omega_k^2 \right) . \quad (\text{B.71})$$

### $\xi, \xi' \neq 0$

Let us assume that eq. (B.22) is satisfied for some arbitrary real constant  $c_{\xi\xi'}$ , and let us take

$$\chi = d_\chi ; \quad \varphi = 0 ; \quad h = 0 . \quad (\text{B.72})$$

This ansatz thus solves the form equations (B.11)-(B.16) in the case of  $\xi, \xi' \neq 0$ . Let us consider the remaining equations of motion. Equations (B.27) and the first of (B.28) are solved by

$$\begin{aligned} A &= c_A \tau + d_A + \frac{1}{8} f \\ B &= c_B \tau + d_B - \frac{1}{2} f \\ \phi &= 12(c_A \tau + d_A) - \frac{1}{2} f , \end{aligned} \quad (\text{B.73})$$

with

$$f := \ln \frac{2c_\phi^2}{c_{\xi\xi'}} - 2 \ln [\cosh(c_\phi\tau + d_{\xi\xi'})] , \quad (\text{B.74})$$

while the second line of (B.28) reduces to

$$c_\phi^2 = 24c_Ac_B + 3c_B^2 , \quad (\text{B.75})$$

which implies in particular,  $r \geq -\frac{1}{8}$ . The 4d Einstein metric reads

$$ds_{4E}^2 = -e^{(24c_A+6c_B)\tau} d\tau^2 + e^{(8c_A+2c_B)\tau} d\vec{x}^2 . \quad (\text{B.76})$$

• **Type I solution:  $k > 0$**

Let us now take  $k \neq 0$ . Equations (B.27) can be solved to give

$$\begin{aligned} A &= c_A\tau + d_A + \frac{1}{8}g(\tau) \\ \phi &= 12(c_A\tau + d_A) - \frac{1}{2}g(\tau) , \end{aligned} \quad (\text{B.77})$$

for some constants  $c_A, d_A$ , where

$$g := \ln \left[ \frac{2c_\phi^2}{c_{\xi\xi'}} \operatorname{sech}^2(c_\phi\tau + d_\phi) \right] , \quad (\text{B.78})$$

Moreover the first of (B.28) can be solved for  $B$ ,

$$B = -4A + \frac{1}{4}f , \quad (\text{B.79})$$

where

$$f = \begin{cases} \ln \left[ \frac{c_B^2}{4k} \operatorname{sech}^2(c_B\tau + d_B) \right] & , \quad k > 0 \\ \ln \left[ \frac{c_B^2}{4|k|} \operatorname{csch}^2(c_B\tau + d_B) \right] & , \quad k < 0 \end{cases} , \quad (\text{B.80})$$

for some constants  $c_B, d_B$ . Plugging the solution into the second line of (B.28) we obtain the constraint

$$3c_B^2 = 192c_A^2 + 4c_\phi^2 , \quad (\text{B.81})$$

for either sign of  $k$ , which imposes  $|r| \leq \frac{1}{8}$ . Let us first consider the case of closed universe ( $k > 0$ ). The 4d Einstein metric reads,

$$ds_{4E}^2 = \operatorname{sech}^3(c_B\tau) \left( -d\tau^2 + \frac{4k}{c_B^2} \cosh^2(c_B\tau) d\Omega_k^2 \right) , \quad (\text{B.82})$$

where we have set  $d_A, d_B, d_\phi = 0$  for simplicity.

• **Type II and critical solutions:  $k < 0$**

Let us now set  $k < 0$ . The 4d part of the Einstein metric reads

$$ds_{4E}^2 = \operatorname{csch}^3(c_B\tau) \left( -d\tau^2 + \frac{4|k|}{c_B^2} \sinh^2(c_B\tau) d\Omega_k^2 \right) . \quad (\text{B.83})$$



## Appendix B. Cosmological solutions

---

### $\chi, \xi, \xi' \neq 0$

Let us now take,

$$\chi = e^{\phi-4A-2B} c_\chi; \quad \varphi = 0; \quad h = 0. \quad (\text{B.84})$$

This ansatz thus solves the form equations (B.11)-(B.16) in the case of  $\chi, \xi, \xi' \neq 0$ . Let us consider the remaining equations of motion. Equations (B.27) and the first of (B.28) are solved by

$$\begin{aligned} A &= \frac{1}{8}f + \frac{1}{16}g \\ B &= c_B\tau + d_B - \frac{1}{2}f - \frac{1}{4}g \\ \phi &= -\frac{1}{2}f + \frac{3}{4}g, \end{aligned} \quad (\text{B.85})$$

with

$$f := \ln \left[ \frac{2c_A^2}{c_\xi^2 c_{\xi'}^2} \operatorname{sech}^2(c_A\tau + d_A) \right]; \quad g := \ln \left[ \frac{c_\phi^2}{c_\chi^2} \operatorname{sech}^2(c_\phi\tau + d_\phi) \right], \quad (\text{B.86})$$

while the second line of (B.28) reduces to

$$12c_B^2 = 4c_A^2 + 3c_\phi^2, \quad (\text{B.87})$$

which imposes  $|r| \leq \sqrt{3}$ . The 4d Einstein metric reads

$$ds_{4E}^2 = -e^{6c_B\tau} d\tau^2 + e^{2c_B\tau} d\vec{x}^2, \quad (\text{B.88})$$

where we have set  $d_A, d_B$ , and  $d_\phi = 0$  for simplicity.

#### • Type I solution: $k > 0$

Let us now assume that  $k > 0$ . Equations (B.27) are solved by

$$A = \frac{1}{8}f + \frac{1}{16}g; \quad \phi = -\frac{1}{2}f + \frac{3}{4}g, \quad (\text{B.89})$$

with,

$$f := \ln \left[ \frac{2c_A^2}{c_\xi^2 c_{\xi'}^2} \operatorname{sech}^2(c_A\tau + d_A) \right]; \quad g := \ln \left[ \frac{c_\phi^2}{c_\chi^2} \operatorname{sech}^2(c_\phi\tau + d_\phi) \right], \quad (\text{B.90})$$

Moreover the first equation of (B.27) can be combined with the first of (B.28) to solve for  $B$ ,

$$B = -4A + \frac{1}{4}h, \quad (\text{B.91})$$

where

$$h = \begin{cases} \ln \left[ \frac{c_B^2}{4k} \operatorname{sech}^2(c_B\tau + d_B) \right] & , \quad k > 0 \\ \ln \left[ \frac{c_B^2}{4|k|} \operatorname{csch}^2(c_B\tau + d_B) \right] & , \quad k < 0 \end{cases}, \quad (\text{B.92})$$

for some constants  $c_B, d_B$ . Plugging the solution into the second line of (B.28) we obtain the constraint

$$3c_B^2 = 4c_A^2 + 3c_\phi^2, \quad (\text{B.93})$$

which imposes  $|r| \leq \frac{\sqrt{3}}{2}$ . Let us first consider the case of a closed universe ( $k > 0$ ). The 4d Einstein metric reads

$$ds_{4E}^2 = \operatorname{sech}^3(c_B\tau) \left( -d\tau^2 + \frac{4k}{c_B^2} \cosh^2(c_B\tau) d\Omega_k^2 \right), \quad (\text{B.94})$$

where we have set  $d_A, d_B$ , and  $d_\phi = 0$  for simplicity.

• Type II and critical solutions:  $k < 0$

Let us now set  $k < 0$ . The 4d Einstein metric reads

$$ds_{4E}^2 = \text{csch}^3(c_B \tau) \left( -d\tau^2 + \frac{4|k|}{c_B^2} \sinh^2(c_B \tau) d\Omega_k^2 \right). \quad (\text{B.95})$$

$h, \chi, \xi, \xi' \neq 0$

Let us take

$$\chi = e^{\phi - 4A - 2B} c_\chi; \quad \varphi = 0. \quad (\text{B.96})$$

This ansatz thus solves the form equations (B.11)-(B.16) in the case of  $h, \chi, \xi, \xi' \neq 0$ . Let us consider the remaining equations of motion. Equations (B.27) are solved by

$$A = \frac{1}{8}f + \frac{1}{16}g; \quad \phi = -\frac{1}{2}f + \frac{3}{4}g, \quad (\text{B.97})$$

with

$$f := \ln \left[ \frac{2c_A^2 e^{c_A \tau + d_A}}{(c_{\xi\xi'}^2 + e^{c_A \tau + d_A})^2 + c_A^2 c_h^2} \right]; \quad g := \ln \left[ \frac{c_\phi^2}{c_\chi^2} \text{sech}^2(c_\phi \tau + d_\phi) \right], \quad (\text{B.98})$$

Moreover the first equation of (B.27) can be combined with the first of (B.28) to solve for  $B$ ,

$$B = -4A + \frac{1}{4}h, \quad (\text{B.99})$$

where,

$$h = \begin{cases} \ln \left[ \frac{c_B^2}{4k} \text{sech}^2(c_B \tau + d_B) \right] & , \quad k > 0 \\ \ln \left[ \frac{c_B^2}{4|k|} \text{csch}^2(c_B \tau + d_B) \right] & , \quad k < 0 \end{cases}, \quad (\text{B.100})$$

for some constants  $c_B, d_B$ . Plugging the solution into the second line of (B.28) we obtain the constraint

$$3c_B^2 = c_A^2 + 3c_\phi^2, \quad (\text{B.101})$$

for either sign of  $k$ . Let us first consider the case of a closed universe ( $k > 0$ ). The 4d Einstein metric reads

$$ds_{4E}^2 = \text{sech}^3(c_B \tau) \left( -d\tau^2 + \frac{4k}{c_B^2} \cosh^2(c_B \tau) d\Omega_k^2 \right), \quad (\text{B.102})$$

where we have set  $d_A, d_B, d_\phi = 0$  for simplicity.

• Type II and critical solutions:  $k < 0$

Let us now set  $k < 0$ . The 4d Einstein metric reads

$$ds_{4E}^2 = \text{csch}^3(c_B \tau) \left( -d\tau^2 + \frac{4|k|}{c_B^2} \sinh^2(c_B \tau) d\Omega_k^2 \right). \quad (\text{B.103})$$

## Appendix B. Cosmological solutions

### Compactification with background flux

The cosmological ansatz can be easily modified to accommodate a non-vanishing background flux for the three- and four-forms, as in [217],<sup>2</sup>

$$H = d\chi \wedge J + d\beta + \frac{1}{2}b_0 \text{Re}\Omega ; \quad G = \varphi \text{vol}_4 + J \wedge (d\gamma - \alpha \wedge d\chi) + \frac{1}{2}c_0 J \wedge J - \frac{1}{2}d\xi \wedge \text{Im}\Omega - \frac{1}{2}D\xi' \wedge \text{Re}\Omega , \quad (\text{B.104})$$

with background charges  $b_0, c_0 \in \mathbb{R}$ , where the covariant derivative is defined as:  $D\xi' = d\xi' + b_0\alpha$ . The internal  $(m, n)$ -components of the Einstein equations now read

$$0 = e^{-8A-2B} \nabla^\mu (e^{8A+2B} \partial_\mu A) + \frac{1}{8} e^{-\phi-4A} (\partial\chi)^2 - \frac{1}{48} e^{-\phi-4A-4B} h^2 \\ + \frac{1}{16} e^{\phi/2-6A} \left[ (\partial\xi)^2 + (D\xi')^2 \right] + \frac{3}{16} e^{\phi/2-6A-6B} \varphi^2 + 18 e^{-\phi-4A+2B} b_0^2 + \frac{7}{16} e^{\phi/2-6A+2B} c_0^2 . \quad (\text{B.105})$$

The external  $(\mu, \nu)$ -components read

$$R_{\mu\nu}^{(4)} = g_{\mu\nu} (\nabla^2 A + \nabla^2 B + 8(\partial A)^2 + 2(\partial B)^2 + 10\partial A \cdot \partial B) \\ - 8\partial_\mu A \partial_\nu A - 2\partial_\mu B \partial_\nu B - 16\partial_{(\mu} A \partial_{\nu)} B + 8\nabla_\mu \partial_\nu A + 2\nabla_\mu \partial_\nu B \\ + \frac{3}{2} e^{-\phi-4A} \partial_\mu \chi \partial_\nu \chi + \frac{1}{4} e^{\phi-4A-4B} h_{\mu\nu}^2 + \frac{1}{2} \partial_\mu \phi \partial_\nu \phi + \frac{1}{2} e^{\phi/2-6A} (\partial_\mu \xi \partial_\nu \xi + D_\mu \xi' D_\nu \xi') \\ + \frac{1}{16} g_{\mu\nu} \left( -\frac{1}{3} e^{\phi-4A-4B} h^2 - 3e^{\phi/2-6A} \left[ (\partial\xi)^2 + (D\xi')^2 \right] - 6e^{-\phi-4A} (\partial\chi)^2 \right. \\ \left. - 5e^{\phi/2-6A-6B} \varphi^2 - 288e^{-\phi-4A+2B} b_0^2 - 9c_0^2 e^{\phi/2-6A+2B} \right) , \quad (\text{B.106})$$

while the mixed  $(\mu, m)$ -components are automatically satisfied. The dilaton equation reads

$$0 = e^{-10A-4B} \nabla^\mu (e^{8A+2B} \partial_\mu \phi) - \frac{1}{4} e^{\phi/2-8A-2B} \left[ (\partial\xi)^2 + (D\xi')^2 \right] + \frac{3}{2} e^{-\phi-6A-2B} (\partial\chi)^2 \\ + \frac{1}{12} e^{-\phi-6A-6B} h^2 + \frac{1}{4} e^{\phi/2-8A-8B} \varphi^2 + 72e^{-\phi-6A} b_0^2 - \frac{3}{4} c_0^2 e^{\phi/2-8A} . \quad (\text{B.107})$$

The  $F$ -form equation of motion reduces to the condition

$$0 = \varphi d\beta - 12b_0 e^{6B} \star_4 D\xi' . \quad (\text{B.108})$$

The  $H$ -form equation reduces to

$$d \left( e^{-\phi+4A+2B} \star_4 d\chi \right) = c_0 \varphi \text{vol}_4 . \quad (\text{B.109})$$

The  $G$ -form equation of motion reduces to

$$d \left( e^{\phi/2+2A+2B} \star_4 d\xi \right) = h \wedge D\xi' + 12b_0 \varphi \text{vol}_4 \\ d \left( e^{\phi/2+2A+2B} \star_4 D\xi' \right) = -h \wedge d\xi \\ 0 = c_0 d\beta , \quad (\text{B.110})$$

<sup>2</sup>We have redefined:  $\xi \rightarrow c_0 + 4\omega\xi$  with respect to [217].

together with the constraint

$$0 = d \left( \varphi e^{\phi/2+2A-4B} + 3c_0\chi + 12b_0\xi \right) . \quad (\text{B.111})$$

The latter can be integrated to solve for  $\varphi$  in terms of the other fields,

$$\varphi = (C - 3c_0\chi - 12b_0\xi) e^{-2A+4B-\phi/2} , \quad (\text{B.112})$$

where  $C$  is an arbitrary constant.

• **Type I solution:  $b_0, c_0 \neq 0$**

If we want  $b_0, c_0 \neq 0$ , then we must set  $h, D\xi' = 0$ , as follows from (B.108), (B.110). It is then consistent to take  $\chi, \xi = \text{constant}$ , and  $\varphi = 0$ . This ansatz solves all form equations of motion. Let us consider the remaining equations of motion. Eq. (B.105) and the dilaton equation (B.107) reduce to

$$d_\tau^2 A = 18b_0^2 e^{-\phi+12A+6B} + \frac{7}{16}c_0^2 e^{\phi/2+10A+6B} ; \quad d_\tau^2 \phi = 72b_0^2 e^{-\phi+12A+6B} - \frac{3}{4}c_0^2 e^{\phi/2+10A+6B} . \quad (\text{B.113})$$

The external Einstein equations (B.106) now reduce to the following two equations,

$$\begin{aligned} -36b_0^2 e^{-\phi+12A+6B} - c_0^2 e^{\phi/2+10A+6B} &= d_\tau^2 B \\ +144b_0^2 e^{-\phi+12A+6B} + 3c_0^2 e^{\phi/2+10A+6B} &= 144(d_\tau A)^2 + 12(d_\tau B)^2 + 96d_\tau A d_\tau B - (d_\tau \phi)^2 . \end{aligned} \quad (\text{B.114})$$

The second line above is a constraint, consistently propagated by the remaining equations of motion. Indeed the  $\tau$ -derivative of this equation is automatically satisfied by virtue of (B.113).

Equations (B.113) and the first of (B.114) are solved by

$$\begin{aligned} A &= -\frac{9}{16}(c_B\tau + d_B) - \frac{1}{4}f - \frac{7}{32}g \\ B &= c_B\tau + d_B + \frac{1}{2}f + \frac{1}{2}g \\ \phi &= -\frac{3}{4}(c_B\tau + d_B) - f + \frac{3}{8}g , \end{aligned} \quad (\text{B.115})$$

with,

$$f := \ln \left[ \frac{c_A^2}{36b_0^2} \operatorname{sech}^2(c_A\tau + d_A) \right] ; \quad g := \ln \left[ \frac{c_\phi^2}{c_0^2} \operatorname{sech}^2(c_\phi\tau + d_\phi) \right] , \quad (\text{B.116})$$

while the second line of (B.114) reduces to

$$3c_B^2 = 4c_A^2 + 3c_\phi^2 , \quad (\text{B.117})$$

which imposes  $|r| \leq \frac{\sqrt{3}}{2}$ . The 4d Einstein metric reads

$$ds_{4E}^2 = -e^{-\frac{15}{2}c_B\tau} \cosh^6(c_A\tau) \cosh^{\frac{9}{2}}(c_\phi\tau) d\tau^2 + e^{-\frac{5}{2}c_B\tau} \cosh^2(c_A\tau) \cosh^{\frac{3}{2}}(c_\phi\tau) d\vec{x}^2 , \quad (\text{B.118})$$

where we have set  $d_A, d_B$  and  $d_\phi = 0$  for simplicity. In terms of the coordinates  $T_\pm = e^{(-\frac{15}{2}c_B \pm 3c_A \pm \frac{9}{4}c_\phi)\tau}$ , the metric asymptotically takes the form (8.2), where  $a_\pm = \frac{1}{3}$ .

## Appendix B. Cosmological solutions

For a certain range of parameters, this model exhibits transient accelerated expansion, where  $\dot{S}(T), \ddot{S}(T) > 0$ , cf. Figure B.2.

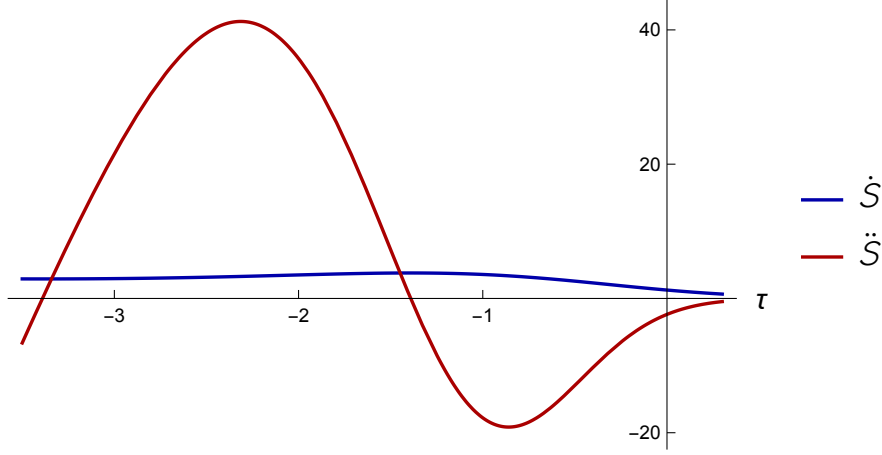


Figure B.2: Plot of  $\dot{S}(T), \ddot{S}(T)$  as a function of  $\tau$ , for  $c_B = -1, r = 0.67$ .

### B.1.2 Compactification on Einstein manifolds

We will now consider (massive) IIA backgrounds for which the internal 6d manifold is Einstein,

$$R_{mn} = \lambda g_{mn} , \quad (\text{B.119})$$

where  $R_{mn}$  is the Ricci tensor associated to  $g_{mn}$ , and  $\lambda \in \mathbb{R}$ . The 10d metric is as in (A.2). We assume the following form ansatz,

$$F = 0 ; \quad H = 0 ; \quad G = \varphi \text{vol}_4 , \quad (\text{B.120})$$

where  $\varphi$  is a 4d scalar.

The resulting equations of motion are as follows. The internal  $(m, n)$ -components of the Einstein equations read

$$e^{2B} \lambda = e^{-8A-2B} \nabla^\mu (e^{8A+2B} \partial_\mu A) + \frac{1}{16} m^2 e^{5\phi/2+2A+2B} + \frac{3}{16} e^{\phi/2-6A-6B} \varphi^2 , \quad (\text{B.121})$$

where  $m$  is the Romans' mass. The external  $(\mu, \nu)$ -components read

$$\begin{aligned} R_{\mu\nu}^{(4)} = & g_{\mu\nu} (\nabla^2 A + \nabla^2 B + 8(\partial A)^2 + 2(\partial B)^2 + 10\partial A \cdot \partial B) \\ & - 8\partial_\mu A \partial_\nu A - 2\partial_\mu B \partial_\nu B - 16\partial_{(\mu} A \partial_{\nu)} B + 8\nabla_\mu \partial_\nu A + 2\nabla_\mu \partial_\nu B + \frac{1}{2} \partial_\mu \phi \partial_\nu \phi \\ & + \frac{1}{16} g_{\mu\nu} (-5e^{\phi/2-6A-6B} \varphi^2 + m^2 e^{5\phi/2+2A+2B}) , \end{aligned} \quad (\text{B.122})$$

while the mixed  $(\mu, m)$ -components are automatically satisfied. The dilaton equation reads

$$0 = e^{-10A-4B} \nabla^\mu (e^{8A+2B} \partial_\mu \phi) - \frac{5}{4} m^2 e^{5\phi/2} + \frac{1}{4} e^{\phi/2-8A-8B} \varphi^2 . \quad (\text{B.123})$$

The  $F$ ,  $H$ -form equations are automatically satisfied, while the  $G$ -form equation of motion reduces to

$$\varphi = c_\varphi e^{-2A+4B-\phi/2}, \quad (\text{B.124})$$

where  $c_\varphi$  is an arbitrary constant.

As before, we will assume that the unwarped 4d metric is of the form (7.2) and moreover that  $A$ ,  $B$ ,  $\phi$  only depend on time. Eq. (B.121) and the dilaton equation (B.123) reduce to

$$\begin{aligned} d_\tau^2 A &= -\lambda e^{16A+6B} + \frac{1}{16} m^2 e^{5\phi/2+18A+6B} + \frac{3}{16} c_\varphi^2 e^{-\phi/2+6A+6B} \\ d_\tau^2 \phi &= -\frac{5}{4} m^2 e^{5\phi/2+18A+6B} + \frac{1}{4} c_\varphi^2 e^{-\phi/2+6A+6B}. \end{aligned} \quad (\text{B.125})$$

The external Einstein equations (B.122) reduce to the following two equations,

$$\begin{aligned} \lambda e^{16A+6B} - 2k e^{16A+4B} - \frac{1}{2} c_\varphi^2 e^{-\phi/2+6A+6B} &= d_\tau^2 B \\ -12\lambda e^{16A+6B} - 12k e^{16A+4B} + m^2 e^{5\phi/2+18A+6B} + c_\varphi^2 e^{-\phi/2+6A+6B} &= 144(d_\tau A)^2 + 12(d_\tau B)^2 \\ &\quad + 96d_\tau A d_\tau B - (d_\tau \phi)^2. \end{aligned} \quad (\text{B.126})$$

The second line above is the constraint, consistently propagated by the remaining equations of motion.

### $\lambda \neq 0$

For  $m$ ,  $k$ ,  $\varphi = 0$ , the system of equations in (B.125) and the first of (B.126) can be solved to give

$$\begin{aligned} A &= c_A \tau + d_A + \frac{1}{10} g(\tau) \\ B &= -\frac{8}{3} (c_A \tau + d_A) - \frac{1}{10} g(\tau) \\ \phi &= c_\phi \tau + d_\phi, \end{aligned} \quad (\text{B.127})$$

for some constants  $c_A$ ,  $d_A$ ,  $c_\phi$ ,  $d_\phi$ , where

$$g = \begin{cases} \ln \left[ \frac{c_B^2}{5\lambda} \operatorname{sech}^2(c_B \tau + d_B) \right] & , \quad \lambda > 0 \\ \ln \left[ \frac{c_B^2}{5|\lambda|} \operatorname{csch}^2(c_B \tau + d_B) \right] & , \quad \lambda < 0 \end{cases}, \quad (\text{B.128})$$

for some constants  $c_B$ ,  $d_B$ . Plugging the solution into the second line of (B.126) we obtain the constraint

$$\frac{12}{5} c_B^2 = c_\phi^2 + \frac{80}{3} c_A^2, \quad (\text{B.129})$$

for either sign of  $\lambda$ . The constraint imposes  $|r| \leq \frac{3}{10}$ .

#### • Type I solution: $\lambda > 0$

Let us first consider an internal space of positive curvature ( $\lambda > 0$ ). The 4d Einstein metric (A.2) reads

$$ds_{4E}^2 = -e^{8c_A \tau} \operatorname{sech}^{\frac{18}{5}}(c_B \tau) d\tau^2 + e^{\frac{8}{3}c_A \tau} \operatorname{sech}^{\frac{6}{5}}(c_B \tau) d\vec{x}^2, \quad (\text{B.130})$$

where we have set  $d_A$ , and  $d_\phi = 0$  for simplicity. To examine the asymptotic behavior of the metric it suffices to consider  $c_B \geq 0$  (the other cases are obtained by inverting the sign of  $\tau$ ). The metric asymptotically takes the form of (8.2), where  $a_\pm = \frac{1}{3}$ .

## Appendix B. Cosmological solutions

### • Type II and critical solutions: $\lambda < 0$

Let us now set  $\lambda < 0$ . The 4d Einstein metric reads

$$ds_{4E}^2 = -e^{8c_A\tau} \operatorname{csch}^{\frac{18}{5}}(c_B\tau) d\tau^2 + e^{\frac{8}{3}c_A\tau} \operatorname{csch}^{\frac{6}{5}}(c_B\tau) d\vec{x}^2, \quad (\text{B.131})$$

The  $\tau \rightarrow \infty$  asymptotics of the warp factors are the same as for  $\lambda > 0$ . For  $\tau \rightarrow 0$ , on the other hand, the function  $g$  in (B.128) tends to  $g \rightarrow -\ln(5|\lambda|\tau^2)$ . Moreover, the constraint imposes  $c_A, c_\phi = 0$ . Hence, in the  $\tau \rightarrow 0$  limit the solution reads

$$A = d_A - \frac{1}{10} \ln(5|\lambda|\tau^2); \quad B = -\frac{8}{3}d_A + \frac{1}{10} \ln(5|\lambda|\tau^2); \quad \phi = d_\phi. \quad (\text{B.132})$$

Asymptotically, at infinite proper time, the metric reaches the form

$$ds_{4E}^2 \rightarrow -dT^2 + T^{\frac{3}{2}} d\vec{x}^2, \quad (\text{B.133})$$

where we have defined  $T \propto \tau^{-\frac{4}{5}}$ . The warp factor of the internal space scales as  $e^A \propto T^{1/4}$ , while the dilaton is constant. This is also an exact solution of the theory in its own right. For a certain range of parameters, this model exhibits transient accelerated expansion, where  $\dot{S}(T), \ddot{S}(T) > 0$ , cf. Figure B.3.

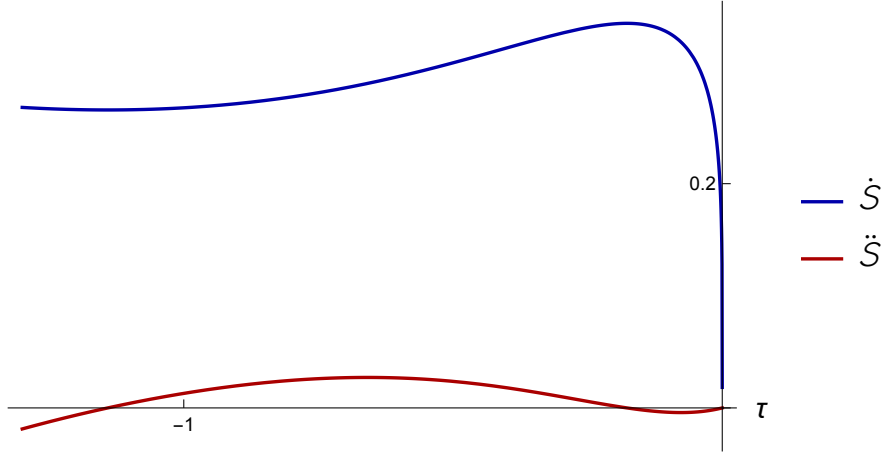


Figure B.3: Plot of  $\dot{S}(T), \ddot{S}(T)$  as a function of  $\tau$ , for  $c_B = -1, r = -0.26$ . In the  $\tau \rightarrow 0$  limit, we have  $\dot{S}(T), \ddot{S}(T) \rightarrow 0$ .

### Type I solution: $m \neq 0$

Setting  $k, \lambda, \varphi = 0$ , the system of equations in (B.125) and the first of (B.126) can be solved to give

$$\begin{aligned} A &= c_A\tau + d_A - \frac{1}{32}g(\tau) \\ B &= c_B\tau + d_B \\ \phi &= -\frac{12}{5}(3c_A + c_B)\tau - \frac{12}{5}(3d_A + d_B) + \frac{5}{8}g(\tau), \end{aligned} \quad (\text{B.134})$$

for some constants  $c_A, d_A, c_B$ , and  $d_B$  where

$$g = \ln \left[ \frac{c_\phi^2}{m^2} \operatorname{sech}^2(c_\phi\tau + d_\phi) \right], \quad (\text{B.135})$$

for some constant  $d_\phi$ . Plugging the solution into the second line of (B.126) we obtain the constraint

$$\frac{25}{12}c_\phi^2 = 192c_A^2 + 128c_Ac_B + 13c_B^2, \quad (\text{B.136})$$

which imposes  $r \leq -\frac{13}{24}$  or  $r \geq -\frac{1}{8}$ .

The 4d Einstein metric (A.2) reads

$$ds_{4E}^2 = -e^{(24c_A+6c_B)\tau} \cosh^{\frac{3}{2}}(c_\phi\tau) d\tau^2 + e^{(8c_A+2c_B)\tau} \cosh^{\frac{1}{2}}(c_\phi\tau) d\vec{x}^2, \quad (\text{B.137})$$

where we have set  $d_A, d_B$  and  $d_\phi = 0$  for simplicity. To examine the asymptotic behavior of the metric it suffices to consider  $c_\phi \geq 0$ . The metric asymptotically takes the form (8.2), where  $a_\pm = \frac{1}{3}$ . For a certain range of parameters, this model exhibits transient accelerated expansion, where  $\dot{S}(T), \ddot{S}(T) > 0$ , cf. Figure B.4.

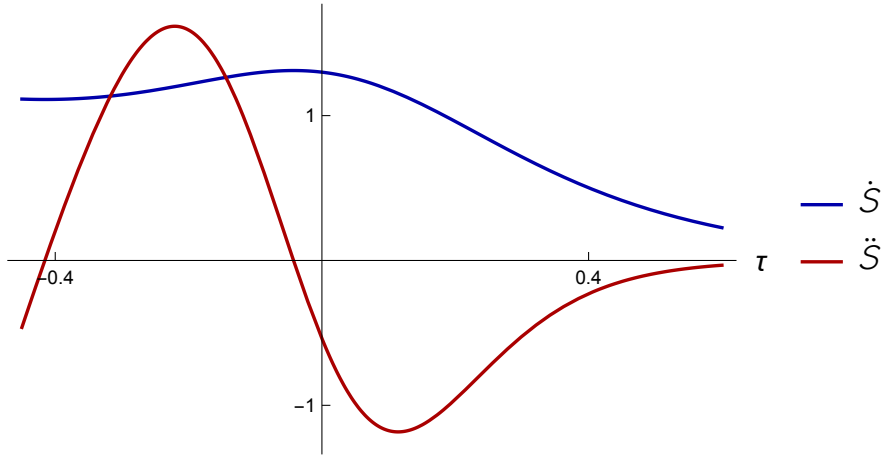


Figure B.4: Plot of  $\dot{S}(T), \ddot{S}(T)$  as a function of  $\tau$ , for  $c_B = 1, r = 0.075$ .

### $\lambda, k \neq 0$

Assuming  $B$  is constant (we may set  $B = 0$  for simplicity) and setting

$$k = \frac{1}{2}\lambda; \quad m, \varphi = 0, \quad (\text{B.138})$$

the system of equations in (B.125) and the first of (B.126) can be solved to give  $B = 0$ ,  $\phi = c_\phi\tau + d_\phi$ , for some constants  $c_\phi, d_\phi$ , and

$$A = \begin{cases} \frac{1}{16} \ln \left[ \frac{c_A^2}{8\lambda} \operatorname{sech}^2(c_A\tau + d_A) \right] & , \quad \lambda > 0 \\ \frac{1}{16} \ln \left[ \frac{c_A^2}{8|\lambda|} \operatorname{csch}^2(c_A\tau + d_A) \right] & , \quad \lambda < 0 \end{cases}, \quad (\text{B.139})$$

for some constants  $c_A, d_A$ . Plugging the solution into the second line of (B.126) we obtain the constraint

$$c_\phi^2 = \frac{9}{4}c_A^2, \quad (\text{B.140})$$

for either sign of  $\lambda$ .



## Appendix B. Cosmological solutions

---

- **Type I solution:  $\lambda > 0$**

Let us first consider the case  $\lambda > 0$ . The 4d Einstein metric reads

$$ds_{4E}^2 = \text{sech}^3(c_A \tau) \left( -d\tau^2 + \frac{16k}{c_A^2} \cosh^2(c_A \tau) d\Omega_k^2 \right), \quad (\text{B.141})$$

where we have set  $d_A$ , and  $d_\phi = 0$  for simplicity, and we took (B.138) into account. For  $\tau \rightarrow \pm\infty$  the metric asymptotically takes the form of a power-law expansion (8.2) for  $a_\pm = \frac{1}{3}$ .

- **Type II and critical solutions:  $\lambda < 0$**

Let us now set  $\lambda < 0$ . The 4d Einstein metric reads

$$ds_{4E}^2 = \text{csch}^3(c_A \tau) \left( -d\tau^2 + \frac{16|k|}{c_A^2} \sinh^2(c_A \tau) d\Omega_k^2 \right), \quad (\text{B.142})$$

where we took (B.138) into account. The  $\tau \rightarrow \infty$  asymptotics of the warp factors are the same as for  $\lambda > 0$ . For  $\tau \rightarrow 0$ , on the other hand, the function  $A$  in (B.139) tends to  $A \rightarrow -\frac{1}{16} \ln(8|\lambda|\tau^2)$ . Moreover, the constraint imposes  $c_\phi = 0$ . Hence, in the  $\tau \rightarrow 0$  limit, which is reached at infinite proper time, the solution reads

$$A = -\frac{1}{16} \ln(8|\lambda|\tau^2); \quad B = 0; \quad \phi = d_\phi. \quad (\text{B.143})$$

The metric asymptotes a singular Milne universe with angular defect,

$$ds^2 \rightarrow dT^2 + 4|k| T^2 d\Omega_k^2, \quad (\text{B.144})$$

where we have defined  $T \propto \tau^{-\frac{1}{2}}$ . The warp factor of the internal space scales as  $e^A \propto T^{1/4}$ , while the dilaton is constant. This is also an exact solution of the theory in its own right.

### Critical solution: $\lambda, m \neq 0$

Setting  $k, c_\phi = 0$ , the system of equations in (B.125), (B.126) admits the solution

$$A = -\frac{25}{128} \ln|\tau| + d_A; \quad B = \frac{3}{16} \ln|\tau| + d_B; \quad \phi = \frac{5}{32} \ln|\tau| + d_\phi, \quad (\text{B.145})$$

for arbitrary constants  $d_A, d_B, d_\phi$  subject to the conditions

$$9d_A + 3d_B + \frac{5}{4}d_\phi = -\frac{1}{2} \ln(8m^2); \quad \lambda = -\frac{3}{2}m^2 e^{2d_A + \frac{5}{2}d_\phi} < 0. \quad (\text{B.146})$$

The 4d Einstein metric takes the form

$$ds_{4E}^2 = -dT^2 + T^{\frac{38}{25}} d\vec{x}^2, \quad (\text{B.147})$$

where  $T \propto \tau^{-\frac{25}{32}}$ . The warp factor of the internal space and the dilaton scale as  $e^A \propto T^{1/4}$ ,  $e^\phi \propto T^{-1/5}$  respectively.

Type I solution:  $\varphi, m \neq 0$ 

Setting  $c_\varphi^2 = m^2$ , the system of equations in (B.125) and the first of (B.126) can be solved to give

$$\begin{aligned} A &= c_A \tau + d_A - \frac{1}{4}g(\tau) \\ B &= -\frac{4}{3}(c_A \tau + d_A) + \frac{1}{2}g(\tau) \\ \phi &= -4A, \end{aligned} \quad (\text{B.148})$$

for some constants  $c_A, d_A, c_B$ , and  $d_B$  where

$$g = \ln \left[ \frac{2c_\phi^2}{m^2} \operatorname{sech}^2(c_\phi \tau + d_\phi) \right], \quad (\text{B.149})$$

for some constant  $d_\phi$ . Plugging the solution into the second line of (B.126) we obtain the constraint

$$c_\phi = \pm \frac{4}{\sqrt{3}}c_A. \quad (\text{B.150})$$

The 4d Einstein metric reads

$$ds_{4E}^2 = -e^{16c_A \tau} \cosh^6(c_\phi \tau) d\tau^2 + e^{\frac{16}{3}c_A \tau} \cosh^2(c_\phi \tau) d\vec{x}^2, \quad (\text{B.151})$$

where we have set  $d_A$ , and  $d_\phi = 0$  for simplicity. The metric asymptotically takes the form (8.2), with  $a_\pm = \frac{1}{3}$ . For a certain range of parameters, this model exhibits transient accelerated expansion, where  $\dot{S}(T), \ddot{S}(T) > 0$ , cf. Figure B.5.

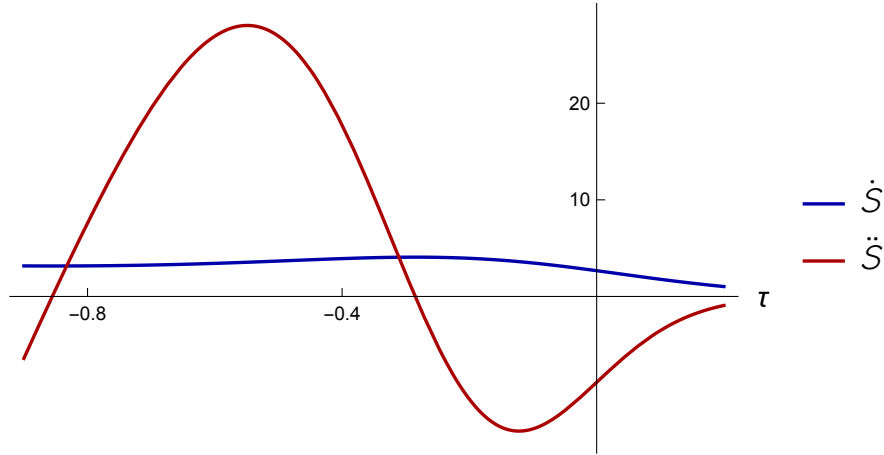


Figure B.5: Plot of  $\dot{S}(T), \ddot{S}(T)$  as a function of  $\tau$ , for  $c_A = 1$ .

 Type II and critical solution:  $k, m \neq 0$ 

Setting  $k = -\frac{3}{4}m^2$ , the system of equations in (B.125) and the first of (B.126) can be solved to give

$$\begin{aligned} A &= \frac{5}{12}(c_A \tau + d_A) - \frac{1}{112} \ln \left[ \frac{7m^2}{2c_\phi^2} \sinh^2(c_\phi \tau + d_\phi) \right] \\ B &= -\frac{35}{3}(c_A \tau + d_A) + 24A \\ \phi &= \frac{28}{3}(c_A \tau + d_A) - 20A, \end{aligned} \quad (\text{B.152})$$

## Appendix B. Cosmological solutions

---

for some constants  $c_A$ ,  $d_A$ ,  $c_\phi$  and  $d_\phi$ . Plugging the solution into the second line of (B.126) we obtain the constraint

$$c_\phi = \pm \frac{7}{\sqrt{15}} c_A . \quad (\text{B.153})$$

The scale factor reads

$$S^2 = \sqrt{\frac{2}{7}} \left| \frac{c_\phi}{m} \operatorname{csch}(c_\phi \tau + d_\phi) \right| . \quad (\text{B.154})$$

In the  $\tau \rightarrow 0$  limit, which is reached at infinite proper time, the solution reads

$$\begin{aligned} A &= \frac{5}{12} d_A - \frac{1}{112} \ln \left( \frac{7m^2}{2} \tau^2 \right) \\ B &= -\frac{35}{3} d_A + 24A \\ \phi &= \frac{28}{3} d_A - 20A . \end{aligned} \quad (\text{B.155})$$

The metric asymptotes a singular Milne universe with angular defect,

$$ds^2 = dT^2 + \frac{7}{6} |k| T^2 d\Omega_k^2 , \quad (\text{B.156})$$

where we have defined  $T \propto \tau^{-\frac{1}{2}}$ . This is also an exact solution of the theory in its own right.

### Critical solution: $k, \lambda, m \neq 0$

Setting  $c_\varphi = 0$ , equations (B.125), (B.126) admit the solution

$$A = -\frac{1}{8} \ln |\tau| + A_0 ; \quad B = B_0 ; \quad \phi = \frac{1}{10} \ln |\tau| + \phi_0 , \quad (\text{B.157})$$

for  $A_0, B_0, \phi_0$  arbitrary real constants and

$$k = -\frac{3}{50} e^{-16A_0 - 4B_0} ; \quad m^2 = \frac{2}{25} e^{-18A_0 - 6B_0 - 5\phi_0/2} ; \quad \lambda = -\frac{3}{25} e^{-16A_0 - 6B_0} . \quad (\text{B.158})$$

We thus obtain a singular Milne universe,

$$ds_{4E}^2 = dT^2 + \frac{25}{6} |k| T^2 d\Omega_k^2 . \quad (\text{B.159})$$

### Critical solution: $k, \varphi, m \neq 0$

Setting  $\lambda = 0$ , equations (B.125), (B.126) admit the solution

$$A = -\frac{1}{16} \ln |\tau| + A_0 ; \quad B = -\frac{1}{4} \ln |\tau| + B_0 ; \quad \phi = \frac{1}{4} \ln |\tau| + \phi_0 , \quad (\text{B.160})$$

for  $A_0, B_0, \phi_0$  arbitrary real constants and

$$k = -\frac{3}{16} e^{-16A_0 - 4B_0} ; \quad m^2 = \frac{1}{4} e^{-18A_0 - 6B_0 - 5\phi_0/2} ; \quad c_\varphi^2 = \frac{1}{4} e^{-6A_0 - 6B_0 + \phi_0/2} . \quad (\text{B.161})$$

We thus obtain a singular Milne universe,

$$ds_{4E}^2 = dT^2 + \frac{4}{3} |k| T^2 d\Omega_k^2 . \quad (\text{B.162})$$

**AdS solution:  $k, \lambda, m, \varphi \neq 0$** 

A different analytic solution is obtained by setting  $A, \phi = 0$ , and  $\lambda = m^2, c_\varphi = \pm\sqrt{5}m$ . Equations (B.125), (B.126) then reduce to

$$\begin{aligned} -\frac{3}{2}m^2 e^{6B} - 2ke^{4B} &= d_\tau^2 B \\ -\frac{1}{2}m^2 e^{6B} - ke^{4B} &= (d_\tau B)^2 . \end{aligned} \quad (\text{B.163})$$

Let us define a new time variable  $\sigma$  via

$$\frac{d\sigma}{d\tau} = e^{2B} , \quad (\text{B.164})$$

in terms of which the equations read

$$\begin{aligned} -\frac{1}{2}m^2 e^{2B} &= d_\sigma^2 B \\ -\frac{1}{2}m^2 e^{2B} - k &= (d_\sigma B)^2 . \end{aligned} \quad (\text{B.165})$$

These can be integrated to give

$$B = \frac{1}{2} \ln \left[ \frac{2c_B^2}{m^2} \operatorname{sech}^2(c_B \sigma + d_B) \right] ; \quad k = -c_B^2 , \quad (\text{B.166})$$

for some real constants  $c_B, d_B$ . The 4d Einstein metric reads

$$ds_{4E}^2 = \frac{2c_B^2}{m^2} \operatorname{sech}^2(c_B \sigma) (-d\sigma^2 + d\Omega_k^2) , \quad (\text{B.167})$$

where we set  $d_B = 0$  for simplicity. This is an  $\text{AdS}_4$  metric in conformal coordinates. To see this, we may define a new coordinate  $T$ , such that  $\cos T = \operatorname{sech}(c_B \sigma)$ , in terms of which the metric takes the well-known form,

$$ds_{4E}^2 = \frac{2}{m^2} (-dT^2 + |k| \cos^2 T d\Omega_k^2) . \quad (\text{B.168})$$

For  $T \in [-\frac{\pi}{2}, \frac{\pi}{2}]$ , this parameterizes  $\text{AdS}_4$  in global coordinates and hyperbolic slicing.

 **$\lambda, \varphi \neq 0$** 

Setting  $k, m = 0$ , the system of equations in (B.125) and the first of (B.126) can be solved to give

$$\begin{aligned} A &= -\frac{1}{48}(c_A \tau + d_A) + \frac{3}{16}f(\tau) + \frac{1}{10}g(\tau) \\ B &= \frac{1}{18}(c_A \tau + d_A) - \frac{1}{2}f(\tau) - \frac{1}{10}g(\tau) \\ \phi &= \frac{5}{12}(c_A \tau + d_A) + \frac{1}{4}f(\tau) , \end{aligned} \quad (\text{B.169})$$

for some constants  $c_A, d_A$ , where

$$f = -\frac{1}{2} \ln \left[ \frac{c_B^2}{c_\varphi^2} \operatorname{sech}^2(c_B \tau + d_B) \right] ; \quad g = \begin{cases} \ln \left[ \frac{c_\phi^2}{5\lambda} \operatorname{sech}^2(c_\phi \tau + d_\phi) \right] & , \quad \lambda > 0 \\ \ln \left[ \frac{c_\phi^2}{5|\lambda|} \operatorname{csch}^2(c_\phi \tau + d_\phi) \right] & , \quad \lambda < 0 \end{cases} , \quad (\text{B.170})$$

for some constants  $d_B, d_\phi$ . Plugging the solution into the second line of (B.126) we obtain the constraint

$$\frac{12}{5}c_\phi^2 = \frac{5}{27}c_A^2 + c_B^2 . \quad (\text{B.171})$$

for either sign of  $\lambda$ . The constraint allows any  $r \in \mathbb{R}$ .

## Appendix B. Cosmological solutions

### • Type I solution: $\lambda > 0$

Let us first consider the case  $\lambda > 0$ . The 4d Einstein metric (A.2) reads

$$ds_{4E}^2 = -e^{-\frac{1}{6}c_A\tau} \cosh^{\frac{3}{2}}(c_B\tau) \operatorname{sech}^{\frac{18}{5}}(c_\phi\tau) d\tau^2 + e^{-\frac{1}{18}c_A\tau} \cosh^{\frac{1}{2}}(c_B\tau) \operatorname{sech}^{\frac{6}{5}}(c_\phi\tau) d\vec{x}^2, \quad (\text{B.172})$$

where we have set  $d_A$ ,  $d_\phi$  and  $d_B = 0$  for simplicity. To examine the asymptotic behavior of the metric it suffices to consider  $c_\phi \geq 0$ . The metric asymptotically takes the form (8.2), with  $a_\pm = \frac{1}{3}$ .

### • Type II solution: $\lambda < 0$

Let us now set  $\lambda < 0$ . The 4d Einstein metric reads

$$ds_{4E}^2 = -e^{-\frac{1}{6}c_A\tau} \cosh^{\frac{3}{2}}(c_B\tau) \operatorname{csch}^{\frac{18}{5}}(c_\phi\tau) d\tau^2 + e^{-\frac{1}{18}c_A\tau} \cosh^{\frac{1}{2}}(c_B\tau) \operatorname{csch}^{\frac{6}{5}}(c_\phi\tau) d\vec{x}^2. \quad (\text{B.173})$$

The  $\tau \rightarrow \pm\infty$  asymptotics of the warp factors are the same as for  $\lambda > 0$ . For  $\tau \rightarrow 0$ , on the other hand, the function  $f$  in (B.170) tends to a constant, while  $g \rightarrow -\ln(5|\lambda|\tau^2)$ . Moreover, the constraint imposes  $c_A, c_B = 0$ . Hence, in the  $\tau \rightarrow 0$  limit, which is reached at infinite proper time, the solution reads

$$A = d_A - \frac{1}{10} \ln(5|\lambda|\tau^2); \quad B = -\frac{8}{3}d_A + \frac{1}{10} \ln(5|\lambda|\tau^2); \quad \phi = d_\phi. \quad (\text{B.174})$$

The metric takes the form

$$ds^2 \rightarrow -dT^2 + T^{\frac{3}{2}} d\vec{x}^2, \quad (\text{B.175})$$

where we have defined  $T \propto \tau^{-\frac{4}{5}}$ . This is *not* an exact solution of the theory, unless  $c_\phi = 0$ . In this case we recover precisely the critical solution with  $\lambda < 0$ . Hence the model interpolates between two metrics of the form (8.2), one with  $a = \frac{1}{3}$  for  $|\tau| \rightarrow \infty$ , and one with  $a = \frac{3}{4}$  for  $\tau \rightarrow 0$ . For a certain range of parameters, we can have transient accelerated expansion, where  $\dot{S}(T), \ddot{S}(T) > 0$ , cf. Figure B.6.

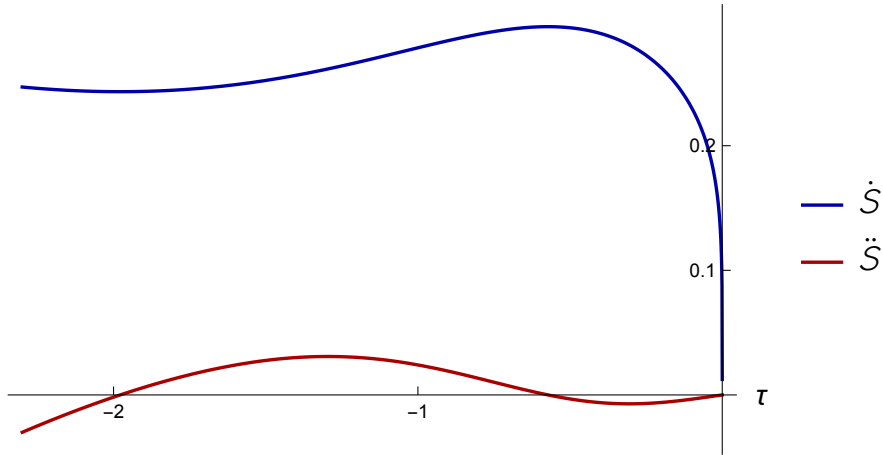


Figure B.6: Plot of  $\dot{S}(T), \ddot{S}(T)$  as a function of  $\tau$ , for  $c_A = 1$ . In the  $\tau \rightarrow 0$  limit, we have  $\dot{S}(T), \ddot{S}(T) \rightarrow 0$ .

## B.1.3 Compactification on Einstein-Kähler manifolds

We will now consider (massive) IIA backgrounds for which the internal 6d manifold is Einstein-Kähler,

$$R_{mn} = \lambda g_{mn} , \quad (\text{B.176})$$

where  $R_{mn}$  is the Ricci tensor associated to  $g_{mn}$ , and  $\lambda \in \mathbb{R}$ . In addition there is a real, closed Kähler two-form  $J$ ,  $dJ = 0$ .

Let us first consider the massless limit, and we take the form ansatz,

$$F = 0 ; \quad H = d\chi \wedge J + d\beta ; \quad G = \varphi \text{vol}_4 + J \wedge d\gamma + \frac{1}{2}c_0 J \wedge J . \quad (\text{B.177})$$

The internal  $(m, n)$ -components of the Einstein equations now read

$$\begin{aligned} e^{2B}\lambda &= e^{-8A-2B}\nabla^\mu (e^{8A+2B}\partial_\mu A) + \frac{1}{8}e^{-\phi-4A}(\partial\chi)^2 - \frac{1}{48}e^{-\phi-4A-4B}h^2 \\ &+ \frac{3}{16}e^{\phi/2-6A-6B}\varphi^2 + \frac{7}{16}e^{\phi/2-6A+2B}c_0^2 . \end{aligned} \quad (\text{B.178})$$

The external  $(\mu, \nu)$ -components read

$$\begin{aligned} R_{\mu\nu}^{(4)} &= g_{\mu\nu} (\nabla^2 A + \nabla^2 B + 8(\partial A)^2 + 2(\partial B)^2 + 10\partial A \cdot \partial B) \\ &- 8\partial_\mu A \partial_\nu A - 2\partial_\mu B \partial_\nu B - 16\partial_{(\mu} A \partial_{\nu)} B + 8\nabla_\mu \partial_\nu A + 2\nabla_\mu \partial_\nu B \\ &+ \frac{3}{2}e^{-\phi-4A}\partial_\mu \chi \partial_\nu \chi + \frac{1}{4}e^{\phi-4A-4B}h_{\mu\nu}^2 + \frac{1}{2}\partial_\mu \phi \partial_\nu \phi \\ &+ \frac{1}{16}g_{\mu\nu} \left( -\frac{1}{3}e^{\phi-4A-4B}h^2 - 6e^{-\phi-4A}(\partial\chi)^2 - 5e^{\phi/2-6A-6B}\varphi^2 - 9c_0^2 e^{\phi/2-6A+2B} \right) , \end{aligned} \quad (\text{B.179})$$

while the mixed  $(\mu, m)$ -components are automatically satisfied. The dilaton equation reads

$$\begin{aligned} 0 &= e^{-10A-4B}\nabla^\mu (e^{8A+2B}\partial_\mu \phi) + \frac{3}{2}e^{-\phi-6A-2B}(\partial\chi)^2 \\ &+ \frac{1}{12}e^{-\phi-6A-6B}h^2 + \frac{1}{4}e^{\phi/2-8A-8B}\varphi^2 - \frac{3}{4}c_0^2 e^{\phi/2-8A} . \end{aligned} \quad (\text{B.180})$$

The  $F$ -form equation of motion reduces to the condition

$$0 = \varphi h . \quad (\text{B.181})$$

The  $H$ -form equation reduces to

$$d \left( e^{-\phi+4A+2B} \star_4 d\chi \right) = c_0 \varphi \text{vol}_4 . \quad (\text{B.182})$$

The  $G$ -form equation of motion reduces to

$$0 = c_0 h , \quad (\text{B.183})$$

together with the constraint

$$0 = d \left( \varphi e^{\phi/2+2A-4B} + 3c_0 \chi \right) . \quad (\text{B.184})$$

The latter can be integrated to solve for  $\varphi$  in terms of the other fields,

$$\varphi = (C - 3c_0 \chi) e^{-2A+4B-\phi/2} , \quad (\text{B.185})$$

where  $C$  is an arbitrary constant.

## Appendix B. Cosmological solutions

### $c_0 = 0$

In this case, we set

$$\varphi = c_\varphi e^{-2A+4B-\phi/2} ; \quad d_t \chi = c_\chi e^{\phi-4A-2B} , \quad (\text{B.186})$$

and in addition we impose

$$c_\varphi c_h = 0 . \quad (\text{B.187})$$

All form equations are then satisfied. The internal Einstein and dilaton equations reduce to

$$\begin{aligned} d_\tau^2 A &= -\lambda e^{16A+6B} + \frac{3}{16} c_\varphi^2 e^{-\phi/2+6A+6B} - \frac{1}{8} c_h^2 e^{-\phi+12A} - \frac{1}{8} c_\chi^2 e^{\phi+4A} \\ d_\tau^2 \phi &= \frac{1}{4} c_\varphi^2 e^{-\phi/2+6A+6B} + \frac{1}{2} c_h^2 e^{-\phi+12A} - \frac{3}{2} c_\chi^2 e^{\phi+4A} , \end{aligned} \quad (\text{B.188})$$

The external Einstein equations reduce to

$$\begin{aligned} \lambda e^{16A+6B} - 2k e^{16A+4B} - \frac{1}{2} c_\varphi^2 e^{-\phi/2+6A+6B} + \frac{1}{2} c_h^2 e^{-\phi+12A} + \frac{1}{2} c_\chi^2 e^{\phi+4A} &= d_\tau^2 B \\ -12\lambda e^{16A+6B} - 12k e^{16A+4B} + c_\varphi^2 e^{-\phi/2+6A+6B} + c_h^2 e^{-\phi+12A} + 3c_\chi^2 e^{\phi+4A} &= \\ 144(d_\tau A)^2 + 12(d_\tau B)^2 + 96d_\tau A d_\tau B - (d_\tau \phi)^2 . & \end{aligned} \quad (\text{B.189})$$

#### • Critical solution: $h, \lambda \neq 0$

Setting  $k, c_\chi, c_\varphi = 0$ , equations (B.188), (B.189) admit the solution

$$A = -\frac{11}{64} \ln |\tau| + A_0 ; \quad B = \frac{1}{8} \ln |\tau| + B_0 ; \quad \phi = -\frac{1}{16} \ln |\tau| + \phi_0 , \quad (\text{B.190})$$

for  $A_0, B_0, \phi_0$  arbitrary real constants and

$$c_h^2 = \frac{1}{8} e^{-12A_0+\phi_0} ; \quad \lambda = -\frac{3}{16} e^{-16A_0-6B_0} . \quad (\text{B.191})$$

We thus obtain a power-law, flat universe expansion,

$$ds_{4E}^2 = dT^2 + T^{\frac{18}{11}} d\vec{x}^2 , \quad (\text{B.192})$$

where we have set  $T \propto |\tau|^{-\frac{11}{16}}$ . The warp factor of the internal space and the dilaton scale as  $e^A \propto T^{1/4}$ ,  $e^\phi \propto T^{1/11}$  respectively.

### $c_0 \neq 0$

In this case, we reinstate the Romans mass ( $m \neq 0$ ) and we set

$$\varphi = 0 ; \quad \chi = 0 ; \quad h = 0 . \quad (\text{B.193})$$

All form equations are then satisfied. The internal Einstein and dilaton equations reduce to

$$\begin{aligned} d_\tau^2 A &= -\lambda e^{16A+6B} + \frac{7}{16} c_0^2 e^{\phi/2+10A+6B} + \frac{1}{16} m^2 e^{5\phi/2+18A+6B} \\ d_\tau^2 \phi &= -\frac{3}{4} c_0^2 e^{\phi/2+10A+6B} - \frac{5}{4} m^2 e^{5\phi/2+18A+6B} . \end{aligned} \quad (\text{B.194})$$

The external Einstein equations reduce to

$$\begin{aligned} \lambda e^{16A+6B} - 2k e^{16A+4B} - c_0^2 e^{\phi/2+10A+6B} &= d_\tau^2 B \\ -12\lambda e^{16A+6B} - 12k e^{16A+4B} + 3c_0^2 e^{\phi/2+10A+6B} + m^2 e^{5\phi/2+18A+6B} &= 144(d_\tau A)^2 + 12(d_\tau B)^2 \\ &+ 96d_\tau A d_\tau B - (d_\tau \phi)^2 . \end{aligned} \quad (\text{B.195})$$

• **Critical solution:  $k, c_0 \neq 0$**

Setting  $m, \lambda = 0$ , equations (B.194), (B.195) admit the solution

$$A = -\frac{7}{104} \ln \tau + A_0 ; \quad B = -\frac{3}{13} \ln \tau + B_0 ; \quad \phi = \frac{3}{26} \ln \tau + \phi_0 , \quad (\text{B.196})$$

for  $A_0, B_0, \phi_0$  arbitrary real constants and

$$c_0^2 = \frac{2}{13} e^{-10A_0 - 6B_0 - \phi_0/2} ; \quad k = -\frac{5}{26} e^{-16A_0 - 4B_0} . \quad (\text{B.197})$$

We thus obtain a singular Milne universe,

$$ds_{4E}^2 = dT^2 + \frac{13}{10} |k| T^2 d\Omega_k^2 . \quad (\text{B.198})$$

**$c_f \neq 0$**

A different ansatz with non-vanishing two-form flux is also possible,

$$F = c_f J ; \quad H = 0 ; \quad G = \varphi \text{vol}_4 , \quad (\text{B.199})$$

where  $c_f$  is a constant. This automatically satisfies the Bianchi identities and the form equations of motion provided

$$\varphi = c_\varphi e^{-2A + 4B - \phi/2} , \quad (\text{B.200})$$

for some constant  $c_\varphi$ . The remaining equations of motion are as in (7.13), (7.14), with potential given by

$$U = \frac{1}{2} c_\varphi^2 e^{-\phi/2 + 6A + 6B} + \frac{3}{2} c_f^2 e^{3\phi/2 + 14A + 6B} - 6k e^{16A + 4B} - 6\lambda e^{16A + 6B} . \quad (\text{B.201})$$

• **Critical solution:  $k, c_f \neq 0$**

The equations of motion with potential (B.201) admit the solution

$$A = -\frac{5}{104} \ln \tau + A_0 ; \quad B = -\frac{4}{13} \ln \tau + B_0 ; \quad \phi = \frac{9}{26} \ln \tau + \phi_0 , \quad (\text{B.202})$$

for  $A_0, B_0, \phi_0$  arbitrary real constants and

$$c_f^2 = \frac{2}{13} e^{-14A_0 - 6B_0 - 3\phi_0/2} ; \quad k = -\frac{5}{26} e^{-16A_0 - 4B_0} . \quad (\text{B.203})$$

We thus obtain a Milne universe with angle defect,

$$ds_{4E}^2 = dT^2 + \frac{13}{10} |k| T^2 d\Omega_k^2 . \quad (\text{B.204})$$

## B.2 Two-flux dynamical systems

In this appendix, we provide some more details on the dynamical systems arising from compactifications with two species of fluxes turned on. For each of them, we give the system of equations together with the constraint, the equation defining the invariant plane  $\mathcal{P}$  (when it exists), the equation defining the acceleration region, the equation of state parameter  $w$ , as well as the list of critical points together with their stability analysis whenever it is relevant.



## Appendix B. Cosmological solutions

---

### B.2.1 Compactification on Calabi-Yau manifolds

$\varphi, \xi \neq 0$

System of equations,

$$\begin{aligned} x' &= \frac{3}{2} (x^2 - 2xz^2 + y^2 + 4z^2 - 1) \\ y' &= \frac{1}{2} (-\sqrt{3}x^2 - \sqrt{3}y^2 - 6yz^2 + \sqrt{3}) \\ z' &= -\frac{1}{2}z (9x + \sqrt{3}y + 6z^2 - 6) . \end{aligned} \quad (\text{B.205})$$

Constraint,

$$-2z^2 c_{\xi\xi}^2 e^{-6B} = c_{\varphi}^2 (x^2 + y^2 + z^2 - 1) . \quad (\text{B.206})$$

Invariant plane,

$$x + \sqrt{3}y = 2 . \quad (\text{B.207})$$

Acceleration condition,

$$z > \sqrt{\frac{2}{3}} . \quad (\text{B.208})$$

Equation of state parameter,

$$w = 1 - 2z^2 . \quad (\text{B.209})$$

Critical points:  $p_C$ .

$\varphi, k \neq 0$

System of equations,

$$\begin{aligned} x' &= 2x^3 + x(2y^2 - z^2 - 2) + \frac{9}{2}z^2 \\ y' &= y(2x^2 - z^2 - 2) + 2y^3 + \frac{\sqrt{3}}{2}z^2 \\ z' &= -\frac{1}{2}z (-4x^2 + 9x - 4y^2 + \sqrt{3}y + 2z^2 - 2) . \end{aligned} \quad (\text{B.210})$$

Constraint,

$$12kz^2 e^{10A-2B+\frac{\phi}{2}} = c_{\varphi}^2 (x^2 + y^2 + z^2 - 1) . \quad (\text{B.211})$$

Invariant plane,

$$x - 3\sqrt{3}y = 0 . \quad (\text{B.212})$$

Acceleration condition,

$$z^2 > 2(x^2 + y^2) , \quad (\text{B.213})$$

Equation of state parameter,

$$w = \frac{x^2 + y^2 - z^2}{x^2 + y^2 + z^2} . \quad (\text{B.214})$$

Critical points,

$$p_C , \quad p_0 , \quad p_1 = \left( \frac{3}{14}, \frac{1}{14\sqrt{3}}, \sqrt{\frac{2}{21}} \right) . \quad (\text{B.215})$$

The point  $p_1$  lies on the boundary of the acceleration region. The linearized system at  $p_1$  has one real and two complex eigenvalues:  $-2, -1 \pm i\sqrt{\frac{17}{7}}$ . It follows that  $p_1$  is a stable focus (resp. node) for trajectories within (resp. orthogonal to)  $\mathcal{P}$ . This model is qualitatively very similar to the one analyzed in detail in Section 8.2.2.

**$\chi, \xi \neq 0$**

System of equations,

$$\begin{aligned} x' &= \frac{1}{2} (3x^2 + 3y^2 + z^2 - 3) \\ y' &= -\frac{1}{2}\sqrt{3} (x^2 + y^2 + 3z^2 - 1) \\ z' &= z (x + \sqrt{3}y) . \end{aligned} \tag{B.216}$$

Constraint,

$$-\frac{2}{3}z^2 e^{2A-\frac{3\phi}{2}} c_{\xi\xi'}^2 = c_\chi^2 (x^2 + y^2 + z^2 - 1) . \tag{B.217}$$

The acceleration condition is impossible to satisfy, and  $w = 1$ .

Critical points:  $p_C$ .

**$\chi, h \neq 0$**

System of equations,

$$\begin{aligned} x' &= 3x^2 + 3y^2 + 2z^2 - 3 \\ y' &= -\sqrt{3} (x^2 + y^2 + 2z^2 - 1) \\ z' &= z (x + \sqrt{3}y) . \end{aligned} \tag{B.218}$$

Constraint,

$$-\frac{1}{3}z^2 c_h^2 e^{8A-2\phi} = c_\chi^2 (x^2 + y^2 + z^2 - 1) . \tag{B.219}$$

The acceleration condition is impossible to satisfy, and  $w = 1$ .

Critical points:  $p_C$ .

**$\chi, k \neq 0$**

System of equations,

$$\begin{aligned} x' &= 2x^3 + 2x (y^2 + z^2 - 1) - z^2 \\ y' &= 2y (x^2 + y^2 + z^2 - 1) - \sqrt{3}z^2 \\ z' &= z (2x^2 + x + 2y^2 + \sqrt{3}y + 2z^2 - 2) . \end{aligned} \tag{B.220}$$

Constraint,

$$4kz^2 e^{12A+4B-\phi} = c_\chi^2 (x^2 + y^2 + z^2 - 1) . \tag{B.221}$$

## Appendix B. Cosmological solutions

---

Invariant plane,

$$3x - \sqrt{3}y = 0 . \quad (\text{B.222})$$

Acceleration condition impossible to satisfy, and  $w = 1$ .

Critical points:  $p_C, p_0$ .

### $\xi, k \neq 0$

System of equations,

$$\begin{aligned} x' &= 2x(x^2 + y^2 + z^2 - 1) - \frac{3}{2}z^2 \\ y' &= 2y(x^2 + y^2 + z^2 - 1) + \frac{\sqrt{3}}{2}z^2 \\ z' &= \frac{1}{4}z(8(x^2 + y^2 + z^2 - 1) + 6x - 2\sqrt{3}y) . \end{aligned} \quad (\text{B.223})$$

Constraint,

$$6kz^2 e^{10A+4B+\frac{\phi}{2}} = c_{\xi\xi'}^2 (x^2 + y^2 + z^2 - 1) . \quad (\text{B.224})$$

Invariant plane,

$$x + \sqrt{3}y = 0 . \quad (\text{B.225})$$

Acceleration condition impossible to satisfy, and  $w = 1$ .

Critical points:  $p_C, p_0$ .

### $\xi, h \neq 0$

System of equations,

$$\begin{aligned} x' &= \frac{3}{2}(2x^2 + 2y^2 + z^2 - 2) \\ y' &= -\frac{1}{2}\sqrt{3}(2x^2 + 2y^2 + z^2 - 2) \\ z' &= \frac{1}{2}z(3x - \sqrt{3}y) . \end{aligned} \quad (\text{B.226})$$

Constraint,

$$-\frac{1}{2}z^2 c_h^2 e^{6A-\frac{\phi}{2}} = c_{\xi\xi'}^2 (x^2 + y^2 + z^2 - 1) . \quad (\text{B.227})$$

Acceleration condition impossible to satisfy, and  $w = 1$ .

Critical points:  $p_C$ .

### $h, k \neq 0$

System of equations,

$$\begin{aligned} x' &= 2x(x^2 + y^2 + z^2 - 1) - 3z^2 \\ y' &= 2y(x^2 + y^2 + z^2 - 1) + \sqrt{3}z^2 \\ z' &= z(2x^2 + 3x + 2y^2 - \sqrt{3}y + 2z^2 - 2) . \end{aligned} \quad (\text{B.228})$$

Constraint,

$$12kz^2 e^{4A+4B+\phi} = c_h^2 (x^2 + y^2 + z^2 - 1) . \quad (\text{B.229})$$

Invariant plane,

$$x + \sqrt{3}y = 0 . \quad (\text{B.230})$$

Acceleration condition impossible to satisfy, and  $w = 1$ .

Critical points:  $p_C, p_0$ .

**$c_0, b_0 \neq 0$**

System of equations,

$$\begin{aligned} x' &= \frac{1}{2} (6(x-1)(x^2+y^2-1) + z^2) \\ y' &= -(\sqrt{3}-3y)(x^2+y^2) - 3y + \frac{1}{2}\sqrt{3}(2-3z^2) \\ z' &= \frac{1}{2}z \left( x(6x-7) + y(6y+\sqrt{3}) \right) . \end{aligned} \quad (\text{B.231})$$

Constraint,

$$-72b_0^2 z^2 e^{2A-\frac{3\phi}{2}} = \frac{3}{2}c_0^2 (x^2 + y^2 + z^2 - 1) . \quad (\text{B.232})$$

Invariant plane,

$$9x + \sqrt{3}y = 10 . \quad (\text{B.233})$$

Acceleration condition,

$$3(x^2 + y^2) < 1 . \quad (\text{B.234})$$

Equation of state parameter,

$$w = -1 + 2(x^2 + y^2) . \quad (\text{B.235})$$

Critical points,

$$p_C , \quad p_1 = \left( 1, \frac{1}{\sqrt{3}}, 0 \right) , \quad (\text{B.236})$$

all outside the acceleration region. The point  $p_1$  lies in the region exterior to  $\mathcal{S}$ .

### B.2.2 Compactification on Einstein manifolds

**$\varphi, \lambda \neq 0$**

System of equations,

$$\begin{aligned} x' &= (3x-2)(x^2+y^2-1) + \frac{5}{2}z^2 \\ y' &= 3y(x^2+y^2-1) + \frac{\sqrt{3}}{2}z^2 \\ z' &= \frac{1}{2}z \left[ -9x + 6x^2 + y(6y-\sqrt{3}) \right] . \end{aligned} \quad (\text{B.237})$$

Constraint,

$$6\lambda z^2 e^{10A+\frac{\phi}{2}} = \frac{1}{2}c_\phi^2 (x^2 + y^2 + z^2 - 1) . \quad (\text{B.238})$$

## Appendix B. Cosmological solutions

---

Invariant plane,

$$3x - 5\sqrt{3}y - 2 = 0 . \quad (\text{B.239})$$

Acceleration condition,

$$\frac{1}{3} > x^2 + y^2 . \quad (\text{B.240})$$

Equation of state parameter,

$$w = -1 + 2(x^2 + y^2) . \quad (\text{B.241})$$

Critical points,

$$p_C , \quad p_1 = \left(\frac{2}{3}, 0, 0\right) , \quad (\text{B.242})$$

all outside of the acceleration region. In particular  $p_1$  lies on the invariant plane.

### $\varphi, m \neq 0$

System of equations,

$$\begin{aligned} x' &= \frac{3}{2}(-1 + 2x)(-1 + x^2 + y^2) + 3z^2 \\ y' &= \frac{1}{2} \left[ -6y + (5\sqrt{3} + 6y)(x^2 + y^2) + \sqrt{3}(-5 + 6z^2) \right] \\ z' &= \frac{1}{2}z \left[ -9x + 6x^2 + y(6y - \sqrt{3}) \right] . \end{aligned} \quad (\text{B.243})$$

Constraint,

$$-\frac{1}{2}m^2z^2e^{12A+3\phi} = \frac{1}{2}c_\phi^2(x^2 + y^2 + z^2 - 1) . \quad (\text{B.244})$$

Invariant plane,

$$3x - \sqrt{3}y - 4 = 0 . \quad (\text{B.245})$$

Acceleration condition,

$$\frac{1}{3} > x^2 + y^2 . \quad (\text{B.246})$$

Equation of state parameter,

$$w = -1 + 2(x^2 + y^2) . \quad (\text{B.247})$$

Critical points,

$$p_C , \quad p_1 = \left(\frac{1}{2}, -\frac{5}{2\sqrt{3}}, 0\right) , \quad (\text{B.248})$$

all outside the acceleration region. In particular  $p_1$  lies on the invariant plane and in the region exterior to  $\mathcal{S}$ .

### $\chi, \lambda \neq 0$

System of equations,

$$\begin{aligned} x' &= (3x - 2)(x^2 + y^2 - 1) + 3(x - 1)z^2 \\ y' &= -\sqrt{3}z^2 + 3y(x^2 + y^2 + z^2 - 1) \\ z' &= z \left[ x + \sqrt{3}y + 3(x^2 + y^2 + z^2 - 1) \right] . \end{aligned} \quad (\text{B.249})$$

Constraint,

$$6\lambda z^2 e^{12A+6B-\phi} = \frac{3}{2} c_\chi^2 (x^2 + y^2 + z^2 - 1) . \quad (\text{B.250})$$

Invariant plane,

$$3x - \sqrt{3}y - 2 = 0 . \quad (\text{B.251})$$

Acceleration condition,

$$\frac{1}{3} > x^2 + y^2 + z^2 , \quad (\text{B.252})$$

Equation of state parameter,

$$w = -1 + 2(x^2 + y^2 + z^2) . \quad (\text{B.253})$$

Critical points,

$$pc , \quad p_1 = \left(\frac{2}{3}, 0, 0\right) . \quad (\text{B.254})$$

The point  $p_1$  lies on the invariant plane, outside the acceleration region.

### **$h, \lambda \neq 0$**

System of equations,

$$\begin{aligned} x' &= (-2 + 3x)(-1 + x^2 + y^2) + (-5 + 3x)z^2 \\ y' &= \sqrt{3}z^2 + 3y(-1 + x^2 + y^2 + z^2) \\ z' &= z \left[ 3x - \sqrt{3}y + 3(x^2 + y^2 + z^2 - 1) \right] . \end{aligned} \quad (\text{B.255})$$

Constraint,

$$6\lambda z^2 e^{4A+6B+\phi} = \frac{1}{2} c_h^2 (x^2 + y^2 + z^2 - 1) . \quad (\text{B.256})$$

Invariant plane,

$$x + \sqrt{3}y - \frac{2}{3} = 0 . \quad (\text{B.257})$$

Acceleration condition,

$$\frac{1}{3} > x^2 + y^2 + z^2 . \quad (\text{B.258})$$

Equation of state parameter,

$$w = -1 + 2(x^2 + y^2 + z^2) . \quad (\text{B.259})$$

Critical points,

$$pc , \quad p_1 = \left(\frac{2}{3}, 0, 0\right) , \quad p_2 = \left(\frac{11}{18}, \frac{1}{18\sqrt{3}}, \frac{2}{9}\sqrt{\frac{2}{3}}\right) . \quad (\text{B.260})$$

The points  $p_1$  and  $p_2$  both lie on the invariant plane, in the region inside the invariant sphere  $\mathcal{S}$ , outside the acceleration region.

## Appendix B. Cosmological solutions

---

### $c_0, m \neq 0$

System of equations,

$$\begin{aligned} x' &= \frac{3}{2}(-1 + 2x)(-1 + x^2 + y^2) + 2z^2 \\ y' &= \frac{1}{2} \left[ -6y + (5\sqrt{3} + 6y)(x^2 + y^2) + \sqrt{3}(-5 + 4z^2) \right] \\ z' &= \frac{1}{2}z \left[ x(-7 + 6x) + y(\sqrt{3} + 6y) \right] . \end{aligned} \quad (\text{B.261})$$

Constraint,

$$-\frac{1}{2}m^2 z^2 e^{8A+2\phi} = \frac{3}{2}c_0^2 (x^2 + y^2 + z^2 - 1) . \quad (\text{B.262})$$

Invariant plane,

$$3x - \sqrt{3}y - 4 = 0 . \quad (\text{B.263})$$

Acceleration condition,

$$\frac{1}{3} > x^2 + y^2 . \quad (\text{B.264})$$

Equation of state parameter,

$$w = -1 + 2(x^2 + y^2) . \quad (\text{B.265})$$

Critical points,

$$p_C , \quad p_1 = \left( \frac{1}{2}, -\frac{5}{2\sqrt{3}}, 0 \right) , \quad (\text{B.266})$$

all outside the acceleration region. In particular  $p_1$  lies on the invariant plane and in the region exterior to  $\mathcal{S}$ .

### $c_0, k \neq 0$

System of equations,

$$\begin{aligned} x' &= 2x(-1 + x^2 + y^2) + \frac{1}{2}(7 - 2x)z^2 \\ y' &= -\frac{1}{2}(\sqrt{3} + 6y)z^2 + 2y(-1 + x^2 + y^2 + z^2) \\ z' &= \frac{1}{2}z \left[ 2 + x(-7 + 4x) + y(\sqrt{3} + 4y) - 2z^2 \right] . \end{aligned} \quad (\text{B.267})$$

Constraint,

$$6kz^2 e^{6A-2B-\frac{\phi}{2}} = \frac{3}{2}c_0^2 (x^2 + y^2 + z^2 - 1) . \quad (\text{B.268})$$

Invariant plane,

$$3x + 7\sqrt{3}y = 0 . \quad (\text{B.269})$$

Acceleration condition,

$$z^2 > 2(x^2 + y^2) . \quad (\text{B.270})$$

Equation of state parameter,

$$w = -\frac{1}{3} + \frac{4}{3}(x^2 + y^2) - \frac{2}{3}z^2 . \quad (\text{B.271})$$

Critical points,

$$p_C , \quad p_0 , \quad p_1 = \left( \frac{7}{26}, -\frac{\sqrt{3}}{26}, \sqrt{\frac{2}{13}} \right) . \quad (\text{B.272})$$

The point  $p_1$  lies in the region inside the invariant sphere  $\mathcal{S}$ . Both  $p_0$  and  $p_1$  lie on the boundary of the acceleration region and on the invariant plane. The linearized system at  $p_1$  has one real and two complex eigenvalues:  $-2, -1 \pm 3i\sqrt{\frac{3}{13}}$ . It follows that  $p_1$  is a stable focus (resp. node) for trajectories within (resp. orthogonal to)  $\mathcal{P}$ . This model is qualitatively very similar to the one analyzed in detail in Section 8.2.2.

**$c_0, \lambda \neq 0$**

System of equations,

$$\begin{aligned} x' &= (-2 + 3x)(-1 + x^2 + y^2) + \frac{3}{2}z^2 \\ y' &= 3y(-1 + x^2 + y^2) - \frac{\sqrt{3}}{2}z^2 \\ z' &= \frac{1}{2}z \left[ x(-7 + 6x) + y(\sqrt{3} + 6y) \right] . \end{aligned} \quad (\text{B.273})$$

Constraint,

$$6\lambda z^2 e^{6A - \frac{\phi}{2}} = \frac{3}{2}c_0^2 (x^2 + y^2 + z^2 - 1) . \quad (\text{B.274})$$

Invariant plane,

$$x + \sqrt{3}y - \frac{2}{3} = 0 . \quad (\text{B.275})$$

Acceleration condition,

$$\frac{1}{3} > x^2 + y^2 , \quad (\text{B.276})$$

with  $w = -1 + 2(x^2 + y^2)$ . Critical points,

$$p_C ; \quad p_1 = \left( \frac{2}{3}, 0, 0 \right) , \quad (\text{B.277})$$

all of them outside the acceleration region.  $p_1$  lies in the interior of  $\mathcal{S}$  and on the invariant plane.

**B.2.3 Compactification on Einstein-Kähler manifolds**

**$\varphi, c_f \neq 0$**

System of equations,

$$\begin{aligned} x' &= \frac{1}{2}(-5 + 6x)(-1 + x^2 + y^2) + 2z^2 \\ y' &= \frac{1}{2} \left[ -6y + 3(\sqrt{3} + 2y)(x^2 + y^2) + \sqrt{3}(-3 + 4z^2) \right] \\ z' &= \frac{1}{2}z \left[ -9x + 6x^2 + y(-\sqrt{3} + 6y) \right] . \end{aligned} \quad (\text{B.278})$$

Constraint,

$$-\frac{3}{2}c_f^2 z^2 e^{8A + 2\phi} = \frac{1}{2}c_\phi^2 (x^2 + y^2 + z^2 - 1) . \quad (\text{B.279})$$

Invariant plane,

$$3x - \sqrt{3}y - 4 = 0 . \quad (\text{B.280})$$

Acceleration condition,

$$\frac{1}{3} > x^2 + y^2 . \quad (\text{B.281})$$



## Appendix B. Cosmological solutions

---

Equation of state parameter,

$$w = -1 + 2(x^2 + y^2) . \quad (\text{B.282})$$

Critical points,

$$p_C , \quad p_1 = \left( \frac{5}{6}, -\frac{\sqrt{3}}{2}, 0 \right) , \quad (\text{B.283})$$

all outside the acceleration region. In particular  $p_1$  lies on the invariant plane and in the region exterior to  $\mathcal{S}$ .

### $k, c_f \neq 0$

System of equations,

$$\begin{aligned} x' &= 2x(x^2 + y^2 - 1) + \frac{1}{2}(5 - 2x)z^2 \\ y' &= 2y(x^2 + y^2 - 1) - yz^2 - \frac{3\sqrt{3}}{2}z^2 \\ z' &= \frac{1}{2}z \left( x(4x - 5) + 4y^2 + 3\sqrt{3}y - 2z^2 + 2 \right) . \end{aligned} \quad (\text{B.284})$$

Constraint,

$$6kz^2 e^{2A-2B-\frac{3\phi}{2}} = \frac{3}{2}c_f^2 (x^2 + y^2 + z^2 - 1) . \quad (\text{B.285})$$

Invariant plane,

$$9x + 5\sqrt{3}y = 0 . \quad (\text{B.286})$$

Acceleration condition,

$$z^2 > 2(x^2 + y^2) . \quad (\text{B.287})$$

Equation of state parameter,

$$w = \frac{x^2 + y^2 - z^2}{x^2 + y^2 + z^2} , \quad (\text{B.288})$$

Critical points,

$$p_C , \quad p_0 , \quad p_1 = \left( \frac{5}{26}, -\frac{3\sqrt{3}}{26}, \sqrt{\frac{10}{13}} \right) . \quad (\text{B.289})$$

The point  $p_1$  lies in the region inside of the invariant sphere  $\mathcal{S}$ . It lies on the boundary of the acceleration region, as well as on the invariant plane. The linearized system at  $p_1$  has one real and two complex eigenvalues:  $-2, -1 \pm 3i\sqrt{\frac{3}{13}}$ . It follows that  $p_1$  is a stable focus (resp. node) for trajectories within (resp. orthogonal to)  $\mathcal{P}$ . This model is qualitatively very similar to the one analyzed in detail in Section 8.2.2.

### $\lambda, c_f \neq 0$

System of equations,

$$\begin{aligned} x' &= \frac{1}{2} [(-5 + 6x)(-1 + x^2 + y^2) - z^2] \\ y' &= \frac{3}{2} [(\sqrt{3} + 2y)(x^2 + y^2 - 1) + \sqrt{3}z^2] \\ z' &= z [3(x^2 + y^2) - 2x] . \end{aligned} \quad (\text{B.290})$$

Constraint,

$$6\lambda (x^2 + y^2 + z^2 - 1) = \frac{3}{2}z^2 e^{\frac{3\phi}{2} - 2A} c_f^2 . \quad (\text{B.291})$$

Invariant plane,

$$9x + \sqrt{3}y - 6 = 0 . \quad (\text{B.292})$$

Acceleration condition,

$$\frac{1}{3} > x^2 + y^2 . \quad (\text{B.293})$$

Equation of state parameter,

$$w = -1 + 2(x^2 + y^2) . \quad (\text{B.294})$$

Critical points,

$$p_C , \quad p_1 = \left( \frac{2}{3}, 0, \frac{\sqrt{5}}{3} \right) , \quad p_2 = \left( \frac{9}{14}, \frac{\sqrt{3}}{14}, \frac{4\sqrt{2}}{7} \right) , \quad p_3 = \left( \frac{5}{6}, -\frac{\sqrt{3}}{2}, 0 \right) . \quad (\text{B.295})$$

The points  $p_2$  and  $p_3$  lie in the region exterior to  $\mathcal{S}$ , while  $p_1$  lies on the invariant sphere. The points  $p_1, p_2, p_3$  all lie on the invariant plane and outside the region of acceleration.



# C Minkowski and (anti-) de Sitter solutions

We list in this appendix the (anti-) dS and Minkowski solutions found in this work, and discussed in the first part of the thesis. They are first ordered according to their cosmological constant, in Appendices C.1, C.2 and C.3. In each of those, we follow the order of solution classes of Table 2.7. Solutions are labelled accordingly, as described there. While solutions have been found to a satisfactory precision level (see Section 2.2.2), we round them here to 5 significant digits for readability. The variables are expressed with the following symbols:  $T_{10}[I]$  for  $g_s T_{10}^I$ ,  $F_q[a_1, \dots, a_q]$  for  $g_s F_{q a_1 \dots a_q}$ ,  $H[a, b, c]$  for  $H_{abc}$ ,  $f[a, b, c]$  for  $f^a{}_{bc}$ . Only the non-zero variables are given. We also provide  $\mathcal{R}_4$  and  $\mathcal{R}_6$ . All values should be understood in units of  $2\pi l_s$ . Note though that as indicated at the end of Section 2.2.1, each solution can go through an overall rescaling of its values. The source sets are here labelled with a single index  $I$ , independently of the dimensionality  $p$ . We thus specify the internal directions wrapped by each set. The sets with  $O_p$  are the first ones, and their number can be read from the class name.

For each solution, we provide the stability data discussed in Section 3.2. We first give the mass spectrum, namely the mass matrix eigenvalues: masses<sup>2</sup>. For de Sitter solutions, we give an eigenvector  $\vec{v}$  in field space (in the  $(\rho, \tau, \sigma_I)$  basis) corresponding to the tachyonic direction. For (anti-) de Sitter solutions, we also compute the parameter  $\eta_V$ . We refer to [5] for more details. Algebras corresponding to the  $f^a{}_{bc}$  are identified in Section 3.1.4 for all solutions.

## C.1 De Sitter solutions

## Appendix C. Minkowski and (anti-) de Sitter solutions

---

### $s_{55}^+ 1$

$$I = 1: 12, \quad I = 2: 34, \quad I = 3: 56,$$

$$\begin{aligned} T_{10}[1] &\rightarrow 0.47704, T_{10}[2] \rightarrow 0.30751, T_{10}[3] \rightarrow -0.053848, F_1[5] \rightarrow 0.067964, F_1[6] \rightarrow -0.16337, \\ F_3[1, 3, 5] &\rightarrow 0.029423, F_3[1, 3, 6] \rightarrow 0.042531, F_3[1, 4, 5] \rightarrow 0.071507, F_3[1, 4, 6] \rightarrow 0.25908, \\ F_3[2, 3, 5] &\rightarrow -0.0029428, F_3[2, 3, 6] \rightarrow -0.011609, F_3[2, 4, 5] \rightarrow -0.026656, F_3[2, 4, 6] \rightarrow -0.056824, \\ H[1, 2, 5] &\rightarrow -0.089255, H[1, 2, 6] \rightarrow -0.020459, H[3, 4, 5] \rightarrow -0.10652, H[3, 4, 6] \rightarrow -0.0097439, \\ f[1, 3, 5] &\rightarrow -0.20034, f[1, 3, 6] \rightarrow -0.019633, f[1, 4, 5] \rightarrow 0.075638, f[1, 4, 6] \rightarrow -0.060835, \\ f[2, 3, 5] &\rightarrow 0.078361, f[2, 3, 6] \rightarrow -0.045623, f[2, 4, 5] \rightarrow -0.019626, f[2, 4, 6] \rightarrow 0.012723, \\ f[3, 1, 5] &\rightarrow 0.0062025, f[3, 1, 6] \rightarrow -0.013864, f[3, 2, 5] \rightarrow 0.042311, f[3, 2, 6] \rightarrow -0.061633, \\ f[4, 1, 5] &\rightarrow 0.016689, f[4, 1, 6] \rightarrow -0.051754, f[4, 2, 5] \rightarrow -0.16991, f[4, 2, 6] \rightarrow -0.037573, \\ f[5, 1, 3] &\rightarrow -0.0012195, f[5, 1, 4] \rightarrow 0.00029436, f[5, 2, 3] \rightarrow -0.046738, f[5, 2, 4] \rightarrow 0.011281, \\ f[6, 1, 3] &\rightarrow -0.00050733, f[6, 1, 4] \rightarrow 0.00012246, f[6, 2, 3] \rightarrow -0.019444, f[6, 2, 4] \rightarrow 0.0046932. \end{aligned}$$

$$\mathcal{R}_4 = 0.011482, \quad \mathcal{R}_6 = -0.062461, \quad \eta_V = -2.8544,$$

$$\text{masses}^2 = (0.086586, 0.048623, 0.044431, -0.0081936), \quad \vec{v} = (0.512, 0.83441, 0.15942, 0.12727).$$

### $s_{55}^+ 2$

$$\begin{aligned} T_{10}[1] &\rightarrow 0.46469, T_{10}[2] \rightarrow 0.4183, T_{10}[3] \rightarrow -0.13527, F_1[5] \rightarrow -0.054338, F_1[6] \rightarrow 0.09419, \\ F_3[1, 3, 5] &\rightarrow 0.19696, F_3[1, 3, 6] \rightarrow 0.029077, F_3[1, 4, 5] \rightarrow -0.14439, F_3[1, 4, 6] \rightarrow -0.018361, \\ F_3[2, 3, 5] &\rightarrow -0.14504, F_3[2, 3, 6] \rightarrow -0.023914, F_3[2, 4, 5] \rightarrow 0.1403, F_3[2, 4, 6] \rightarrow 0.01418, \\ H[1, 2, 5] &\rightarrow -0.0061166, H[1, 2, 6] \rightarrow 0.019678, H[3, 4, 5] \rightarrow 0.0072392, H[3, 4, 6] \rightarrow 0.029453, \\ f[1, 3, 5] &\rightarrow -0.043274, f[1, 3, 6] \rightarrow -0.12877, f[1, 4, 5] \rightarrow -0.0053473, f[1, 4, 6] \rightarrow -0.19337, \\ f[2, 3, 5] &\rightarrow 0.11672, f[2, 3, 6] \rightarrow 0.095978, f[2, 4, 5] \rightarrow 0.12856, f[2, 4, 6] \rightarrow 0.073781, \\ f[3, 1, 5] &\rightarrow -0.075441, f[3, 1, 6] \rightarrow 0.10485, f[3, 2, 5] \rightarrow -0.017193, f[3, 2, 6] \rightarrow 0.10796, \\ f[4, 1, 5] &\rightarrow 0.070637, f[4, 1, 6] \rightarrow -0.11098, f[4, 2, 5] \rightarrow 0.033071, f[4, 2, 6] \rightarrow -0.091882, \\ f[5, 1, 3] &\rightarrow -0.028108, f[5, 1, 4] \rightarrow -0.027949, f[5, 2, 3] \rightarrow 0.084778, f[5, 2, 4] \rightarrow 0.0843, \\ f[6, 1, 3] &\rightarrow -0.016215, f[6, 1, 4] \rightarrow -0.016124, f[6, 2, 3] \rightarrow 0.048908, f[6, 2, 4] \rightarrow 0.048633. \end{aligned}$$

$$\mathcal{R}_4 = 0.01048, \quad \mathcal{R}_6 = -0.072118, \quad \eta_V = -2.7030,$$

$$\text{masses}^2 = (0.12192, 0.054898, 0.02209, -0.0070818), \quad \vec{v} = (0.59801, 0.78544, 0.083651, 0.13587).$$

$s_{55}^+3$

$$\begin{aligned}
 T_{10}[1] &\rightarrow 0.72554, T_{10}[2] \rightarrow 0.56275, T_{10}[3] \rightarrow -0.11084, F_1[5] \rightarrow -0.046697, F_1[6] \rightarrow -0.14894, \\
 F_3[1, 3, 5] &\rightarrow -0.3778, F_3[1, 3, 6] \rightarrow -0.053076, F_3[1, 4, 5] \rightarrow 0.078924, F_3[1, 4, 6] \rightarrow -0.0016181, \\
 F_3[2, 3, 5] &\rightarrow 0.0067415, F_3[2, 3, 6] \rightarrow -0.015912, F_3[2, 4, 5] \rightarrow -0.0036507, F_3[2, 4, 6] \rightarrow -0.003343, \\
 H[1, 2, 5] &\rightarrow -0.011276, H[1, 2, 6] \rightarrow 0.046065, H[3, 4, 5] \rightarrow -0.028408, H[3, 4, 6] \rightarrow 0.039204, \\
 f[1, 3, 5] &\rightarrow 0.036555, f[1, 3, 6] \rightarrow 0.1166, f[1, 4, 5] \rightarrow -0.13275, f[1, 4, 6] \rightarrow 0.25613, \\
 f[2, 3, 5] &\rightarrow -0.0070935, f[2, 3, 6] \rightarrow -0.022625, f[2, 4, 5] \rightarrow -0.075855, f[2, 4, 6] \rightarrow -0.077621, \\
 f[3, 1, 5] &\rightarrow 0.055343, f[3, 1, 6] \rightarrow 0.077441, f[3, 2, 5] \rightarrow 0.08688, f[3, 2, 6] \rightarrow -0.23348, \\
 f[4, 1, 5] &\rightarrow -0.012378, f[4, 1, 6] \rightarrow -0.0034012, f[4, 2, 5] \rightarrow -0.06379, f[4, 2, 6] \rightarrow -0.017528, \\
 f[5, 1, 4] &\rightarrow -0.009863, f[5, 2, 4] \rightarrow -0.050828, f[6, 1, 4] \rightarrow 0.0030922, f[6, 2, 4] \rightarrow 0.015935.
 \end{aligned}$$

$$\mathcal{R}_4 = 0.019772, \mathcal{R}_6 = -0.1156, \eta_V = -2.9334,$$

$$\text{masses}^2 = (0.1202, 0.074661, 0.042293, -0.014499), \vec{v} = (0.5718, 0.79714, 0.1371, 0.13717).$$

$s_{55}^+4$

$$\begin{aligned}
 T_{10}[1] &\rightarrow 0.35972, T_{10}[2] \rightarrow 0.52854, T_{10}[3] \rightarrow -0.061607, F_1[5] \rightarrow -0.055616, F_1[6] \rightarrow -0.089616, \\
 F_3[1, 3, 5] &\rightarrow -0.2955, F_3[1, 3, 6] \rightarrow 0.14475, F_3[1, 4, 5] \rightarrow 0.053224, F_3[1, 4, 6] \rightarrow -0.01737, \\
 F_3[2, 3, 5] &\rightarrow 0.036808, F_3[2, 3, 6] \rightarrow -0.033252, F_3[2, 4, 5] \rightarrow -0.043811, F_3[2, 4, 6] \rightarrow 0.014833, \\
 H[1, 2, 5] &\rightarrow -0.0044838, H[1, 2, 6] \rightarrow 0.014822, H[3, 4, 5] \rightarrow 0.01242, H[3, 4, 6] \rightarrow 0.0093064, \\
 f[1, 3, 5] &\rightarrow 0.021656, f[1, 3, 6] \rightarrow 0.044792, f[1, 4, 5] \rightarrow -0.026067, f[1, 4, 6] \rightarrow 0.2064, \\
 f[2, 3, 5] &\rightarrow -0.018528, f[2, 3, 6] \rightarrow -0.033604, f[2, 4, 5] \rightarrow 0.05014, f[2, 4, 6] \rightarrow -0.013342, \\
 f[3, 1, 5] &\rightarrow -0.057579, f[3, 1, 6] \rightarrow 0.011876, f[3, 2, 5] \rightarrow -0.18459, f[3, 2, 6] \rightarrow -0.18172, \\
 f[4, 1, 5] &\rightarrow 0.0086028, f[4, 1, 6] \rightarrow 0.040689, f[4, 2, 5] \rightarrow 0.01433, f[4, 2, 6] \rightarrow 0.052753, \\
 f[5, 1, 3] &\rightarrow -0.00083758, f[5, 1, 4] \rightarrow -0.021022, f[5, 2, 3] \rightarrow -0.0009261, f[5, 2, 4] \rightarrow -0.023244, \\
 f[6, 1, 3] &\rightarrow 0.00051981, f[6, 1, 4] \rightarrow 0.013047, f[6, 2, 3] \rightarrow 0.00057474, f[6, 2, 4] \rightarrow 0.014425.
 \end{aligned}$$

$$\mathcal{R}_4 = 0.010644, \mathcal{R}_6 = -0.079291, \eta_V = -2.8966,$$

$$\text{masses}^2 = (0.081167, 0.046349, 0.018831, -0.0077075), \vec{v} = (0.59942, 0.77513, 0.12971, 0.15182).$$

## Appendix C. Minkowski and (anti-) de Sitter solutions

---

### $s_{55}^+ 5$

$$\begin{aligned}
& T_{10}[1] \rightarrow 0.5488, T_{10}[2] \rightarrow 0.49801, T_{10}[3] \rightarrow -0.09235, F_1[5] \rightarrow -0.1363, F_1[6] \rightarrow -0.035535, \\
& F_3[1, 3, 5] \rightarrow -0.058902, F_3[1, 3, 6] \rightarrow -0.32976, F_3[1, 4, 5] \rightarrow 0.011126, F_3[1, 4, 6] \rightarrow 0.1021, \\
& F_3[2, 3, 5] \rightarrow -0.0067774, F_3[2, 3, 6] \rightarrow 0.0038507, F_3[2, 4, 6] \rightarrow -0.005906, F_3[2, 4, 5] \rightarrow F_3[2, 4, 6], \\
& H[1, 2, 5] \rightarrow -0.041183, H[1, 2, 6] \rightarrow 0.015758, H[3, 4, 5] \rightarrow -0.034816, H[3, 4, 6] \rightarrow 0.018389, \\
& f[1, 3, 5] \rightarrow -0.12993, f[1, 3, 6] \rightarrow -0.033873, f[1, 4, 5] \rightarrow -0.20816, f[1, 4, 6] \rightarrow 0.095049, \\
& f[2, 3, 5] \rightarrow 0.025631, f[2, 3, 6] \rightarrow 0.0066821, f[2, 4, 6] \rightarrow 0.04532, f[3, 1, 5] \rightarrow -0.054525, \\
& f[3, 2, 5] \rightarrow 0.22297, f[3, 2, 6] \rightarrow -0.099548, f[4, 1, 5] \rightarrow 0.0012519, f[4, 1, 6] \rightarrow 0.018843, \\
& f[4, 2, 5] \rightarrow 0.006346, f[4, 2, 6] \rightarrow 0.095521, f[5, 1, 4] \rightarrow 0.0025089, f[5, 2, 4] \rightarrow 0.012718, \\
& f[6, 1, 4] \rightarrow -0.0096234, f[6, 2, 4] \rightarrow -0.048783, f[2, 4, 5] \rightarrow f[2, 4, 6], f[3, 1, 6] \rightarrow -f[2, 4, 6].
\end{aligned}$$

$$\mathcal{R}_4 = 0.016346, \mathcal{R}_6 = -0.094138, \eta_V = -2.9703,$$

$$\text{masses}^2 = (0.091114, 0.065509, 0.03436, -0.012138), \vec{v} = (0.56953, 0.79882, 0.14606, 0.12724).$$

### $s_{55}^+ 6$

$$\begin{aligned}
& T_{10}[1] \rightarrow 0.18633, T_{10}[2] \rightarrow 0.099822, T_{10}[3] \rightarrow -0.023249, F_1[5] \rightarrow -0.06428, F_1[6] \rightarrow -0.034831, \\
& F_3[1, 3, 5] \rightarrow 0.01078, F_3[1, 3, 6] \rightarrow -0.026777, F_3[1, 4, 5] \rightarrow -0.016182, F_3[1, 4, 6] \rightarrow 0.033328, \\
& F_3[2, 3, 5] \rightarrow -0.015359, F_3[2, 3, 6] \rightarrow 0.10935, F_3[2, 4, 5] \rightarrow -0.0041419, F_3[2, 4, 6] \rightarrow -0.14142, \\
& H[1, 2, 5] \rightarrow -0.024728, H[1, 2, 6] \rightarrow -0.0016963, H[3, 4, 5] \rightarrow -0.020168, H[3, 4, 6] \rightarrow 0.016339, \\
& f[1, 3, 5] \rightarrow -0.043546, f[1, 3, 6] \rightarrow -0.03002, f[1, 4, 5] \rightarrow -0.040593, f[1, 4, 6] \rightarrow -0.024861, \\
& f[2, 3, 5] \rightarrow 0.10185, f[2, 3, 6] \rightarrow -0.050296, f[2, 4, 5] \rightarrow 0.10301, f[2, 4, 6] \rightarrow 0.0087766, \\
& f[3, 1, 5] \rightarrow 0.03814, f[3, 1, 6] \rightarrow -0.032997, f[3, 2, 5] \rightarrow -0.005429, f[3, 2, 6] \rightarrow -0.022669, \\
& f[4, 1, 5] \rightarrow -0.09408, f[4, 1, 6] \rightarrow 0.0059857, f[4, 2, 5] \rightarrow 0.0090268, f[4, 2, 6] \rightarrow 0.025832, \\
& f[5, 1, 3] \rightarrow 0.0098816, f[5, 1, 4] \rightarrow 0.0044069, f[5, 2, 3] \rightarrow 0.0036326, f[5, 2, 4] \rightarrow 0.0016201, \\
& f[6, 1, 3] \rightarrow -0.018236, f[6, 1, 4] \rightarrow -0.008133, f[6, 2, 3] \rightarrow -0.006704, f[6, 2, 4] \rightarrow -0.0029898.
\end{aligned}$$

$$\mathcal{R}_4 = 0.004057, \mathcal{R}_6 = -0.025322, \eta_V = -2.9146,$$

$$\text{masses}^2 = (0.030262, 0.013323, 0.0092559, -0.0029562), \vec{v} = (0.56648, 0.80047, 0.14645, 0.12997).$$

$s_{55}^+ 7$

$$\begin{aligned}
 T_{10}[1] &\rightarrow 0.32241, T_{10}[2] \rightarrow 0.25405, T_{10}[3] \rightarrow -0.1001, F_1[5] \rightarrow 0.027908, F_1[6] \rightarrow 0.079651, \\
 F_3[1, 3, 5] &\rightarrow 0.057728, F_3[1, 3, 6] \rightarrow -0.0003245, F_3[1, 4, 5] \rightarrow -0.11383, F_3[1, 4, 6] \rightarrow 0.0043009, \\
 F_3[2, 3, 5] &\rightarrow 0.12422, F_3[2, 3, 6] \rightarrow 0.015909, F_3[2, 4, 5] \rightarrow -0.18375, F_3[2, 4, 6] \rightarrow -0.010172, \\
 H[1, 2, 5] &\rightarrow -0.0042465, H[1, 2, 6] \rightarrow -0.014838, H[3, 4, 5] \rightarrow 0.014738, H[3, 4, 6] \rightarrow -0.016011, \\
 f[1, 3, 5] &\rightarrow -0.0078082, f[1, 3, 6] \rightarrow -0.14573, f[1, 4, 5] \rightarrow 0.01363, f[1, 4, 6] \rightarrow -0.059324, \\
 f[2, 3, 5] &\rightarrow 0.14929, f[2, 3, 6] \rightarrow -0.10111, f[2, 4, 5] \rightarrow 0.11852, f[2, 4, 6] \rightarrow -0.081211, \\
 f[3, 1, 5] &\rightarrow -0.036299, f[3, 1, 6] \rightarrow -0.10329, f[3, 2, 5] \rightarrow 0.0019146, f[3, 2, 6] \rightarrow 0.028735, \\
 f[4, 1, 5] &\rightarrow 0.045777, f[4, 1, 6] \rightarrow 0.12971, f[4, 2, 5] \rightarrow 0.0092216, f[4, 2, 6] \rightarrow -0.044147, \\
 f[5, 1, 3] &\rightarrow 0.0014146, f[5, 1, 4] \rightarrow 0.0011256, f[5, 2, 3] \rightarrow 0.1058, f[5, 2, 4] \rightarrow 0.084183, \\
 f[6, 1, 3] &\rightarrow -0.00049565, f[6, 1, 4] \rightarrow -0.00039437, f[6, 2, 3] \rightarrow -0.037071, f[6, 2, 4] \rightarrow -0.029496.
 \end{aligned}$$

$$\mathcal{R}_4 = 0.0064113, \mathcal{R}_6 = -0.045751, \eta_V = -2.5101,$$

$$\text{masses}^2 = (0.09705, 0.033829, 0.014147, -0.0040233), \vec{v} = (0.61748, 0.7735, 0.071634, 0.12359).$$

$s_{55}^+ 8$

$$\begin{aligned}
 T_{10}[1] &\rightarrow 0.19717, T_{10}[2] \rightarrow 0.14783, T_{10}[3] \rightarrow -0.021473, F_1[5] \rightarrow -0.078205, F_1[6] \rightarrow 0.0049412, \\
 F_3[1, 3, 5] &\rightarrow -0.0099514, F_3[1, 3, 6] \rightarrow 0.011265, F_3[1, 4, 5] \rightarrow -0.053599, F_3[1, 4, 6] \rightarrow 0.17075, \\
 F_3[2, 3, 5] &\rightarrow 0.018747, F_3[2, 3, 6] \rightarrow -0.029133, F_3[2, 4, 5] \rightarrow -0.051305, F_3[2, 4, 6] \rightarrow 0.085993, \\
 H[1, 2, 5] &\rightarrow 0.015719, H[1, 2, 6] \rightarrow 0.0048415, H[3, 4, 5] \rightarrow 0.03184, H[3, 4, 6] \rightarrow 0.023596, \\
 f[1, 3, 5] &\rightarrow -0.12703, f[1, 3, 6] \rightarrow 0.028513, f[1, 4, 5] \rightarrow 0.012977, f[1, 4, 6] \rightarrow 0.014053, \\
 f[2, 3, 5] &\rightarrow -0.086914, f[2, 3, 6] \rightarrow -0.033169, f[2, 4, 5] \rightarrow -0.025341, f[2, 4, 6] \rightarrow -0.026465, \\
 f[3, 1, 5] &\rightarrow -0.011566, f[3, 1, 6] \rightarrow 0.00064098, f[3, 2, 5] \rightarrow -0.0058617, f[3, 2, 6] \rightarrow 0.00062058, \\
 f[4, 1, 5] &\rightarrow 0.046748, f[4, 1, 6] \rightarrow 0.031485, f[4, 2, 5] \rightarrow -0.077789, f[4, 2, 6] \rightarrow -0.091042, \\
 f[5, 1, 3] &\rightarrow 0.00041274, f[5, 1, 4] \rightarrow 0.00029964, f[5, 2, 3] \rightarrow -0.00115, f[5, 2, 4] \rightarrow -0.00083489, \\
 f[6, 1, 3] &\rightarrow 0.0065325, f[6, 1, 4] \rightarrow 0.0047425, f[6, 2, 3] \rightarrow -0.018202, f[6, 2, 4] \rightarrow -0.013214.
 \end{aligned}$$

$$\mathcal{R}_4 = 0.0042994, \mathcal{R}_6 = -0.030339, \eta_V = -2.7790,$$

$$\text{masses}^2 = (0.03168, 0.015949, 0.010753, -0.002987), \vec{v} = (0.57994, 0.78615, 0.14473, 0.15715).$$



## Appendix C. Minkowski and (anti-) de Sitter solutions

---

### $s_{55}^+9$

$$\begin{aligned}
&T_{10}[1] \rightarrow 0.35204, T_{10}[2] \rightarrow 0.32339, T_{10}[3] \rightarrow -0.12879, F_1[5] \rightarrow 0.05975, F_1[6] \rightarrow -0.058962, \\
&F_3[1, 3, 5] \rightarrow 0.11186, F_3[1, 3, 6] \rightarrow 0.059735, F_3[1, 4, 5] \rightarrow -0.21025, F_3[1, 4, 6] \rightarrow -0.094019, \\
&F_3[2, 3, 5] \rightarrow 0.042689, F_3[2, 3, 6] \rightarrow 0.030822, F_3[2, 4, 5] \rightarrow -0.060858, F_3[2, 4, 6] \rightarrow -0.043124, \\
&H[1, 2, 5] \rightarrow 0.0086458, H[1, 2, 6] \rightarrow -0.0086346, H[3, 4, 5] \rightarrow -0.0085054, H[3, 4, 6] \rightarrow -0.015009, \\
&f[1, 3, 5] \rightarrow -0.1416, f[1, 3, 6] \rightarrow -0.23025, f[1, 4, 5] \rightarrow -0.06172, f[1, 4, 6] \rightarrow -0.10511, \\
&f[2, 3, 5] \rightarrow 0.065963, f[2, 3, 6] \rightarrow -0.095767, f[2, 4, 5] \rightarrow 0.06644, f[2, 4, 6] \rightarrow -0.079327, \\
&f[3, 1, 5] \rightarrow 0.00092451, f[3, 1, 6] \rightarrow -0.011556, f[3, 2, 5] \rightarrow -0.061413, f[3, 2, 6] \rightarrow 0.061127, \\
&f[4, 1, 5] \rightarrow -0.0068416, f[4, 1, 6] \rightarrow 0.018309, f[4, 2, 5] \rightarrow 0.1371, f[4, 2, 6] \rightarrow -0.13586, \\
&f[5, 1, 3] \rightarrow -0.13707, f[5, 1, 4] \rightarrow -0.061505, f[5, 2, 3] \rightarrow 0.0067551, f[5, 2, 4] \rightarrow 0.0030311, \\
&f[6, 1, 3] \rightarrow -0.1389, f[6, 1, 4] \rightarrow -0.062327, f[6, 2, 3] \rightarrow 0.0068453, f[6, 2, 4] \rightarrow 0.0030716.
\end{aligned}$$

$$\mathcal{R}_4 = 0.0065997, \mathcal{R}_6 = -0.051929, \eta_V = -2.2494,$$

$$\text{masses}^2 = (0.15427, 0.045378, 0.015301, -0.0037113), \vec{v} = (0.6478, 0.75245, 0.047002, 0.10938).$$

### $s_{55}^+10$

$$\begin{aligned}
&T_{10}[1] \rightarrow 10, T_{10}[2] \rightarrow 10, T_{10}[3] \rightarrow -0.3259120382713294, F_1[5] \rightarrow 1, F_1[6] \rightarrow 1, \\
&F_3[1, 3, 5] \rightarrow -0.1349772714306872, F_3[1, 3, 6] \rightarrow -0.7456107008676475, \\
&F_3[1, 4, 5] \rightarrow 0.4757995474652397, F_3[1, 4, 6] \rightarrow -0.2227565010250167, \\
&F_3[2, 3, 5] \rightarrow -0.4614346028465642, F_3[2, 3, 6] \rightarrow 0.0426792857654753, \\
&F_3[2, 4, 5] \rightarrow 0.2860470205462396, F_3[2, 4, 6] \rightarrow -F_3[2, 4, 5], H[1, 2, 5] \rightarrow 0.9376250941912930, \\
&H[1, 2, 6] \rightarrow -0.2994901148924934, H[3, 4, 5] \rightarrow 0.6659796477910178, \\
&H[3, 4, 6] \rightarrow -0.7329190688589823, f[1, 3, 6] \rightarrow -0.1969129428812132, \\
&f[1, 4, 5] \rightarrow -0.2753236733652662, f[1, 4, 6] \rightarrow 0.3984487144549955, \\
&f[2, 4, 5] \rightarrow -0.0799090201373039, f[2, 4, 6] \rightarrow 0.3243522244088599, \\
&f[3, 1, 6] \rightarrow -0.2002924300421296, f[3, 2, 5] \rightarrow 0.4230701843222834, \\
&f[3, 2, 6] \rightarrow -0.0284354195594737, f[4, 2, 5] \rightarrow -0.1236377141499939, \\
&f[4, 2, 6] \rightarrow 0.5018478206399179, f[6, 2, 4] \rightarrow -0.0889546337076675, \\
&f[1, 3, 5] \rightarrow f[1, 3, 6], f[3, 1, 5] \rightarrow f[3, 1, 6], f[5, 2, 4] \rightarrow -f[6, 2, 4].
\end{aligned}$$

$$\mathcal{R}_4 = 0.05046560105547959, \mathcal{R}_6 = -0.7152057317272771, \eta_V = -2.0907955384379524,$$

$$\text{masses}^2 = (5.0863, 1.233, 0.57277, -0.026378), \vec{v} = (0.50049, 0.81331, 0.21722, 0.20212).$$

$s_{55}^+ 11$

$$\begin{aligned}
 T_{10}[1] &\rightarrow 0.72539, T_{10}[2] \rightarrow 0.57602, T_{10}[3] \rightarrow -0.11238, F_1[5] \rightarrow -0.046382, F_1[6] \rightarrow -0.14989, \\
 F_3[1, 3, 5] &\rightarrow -0.37962, F_3[1, 3, 6] \rightarrow -0.054102, F_3[1, 4, 5] \rightarrow 0.078715, F_3[1, 4, 6] \rightarrow -0.00035418, \\
 F_3[2, 3, 5] &\rightarrow 0.0058597, F_3[2, 3, 6] \rightarrow -0.014748, F_3[2, 4, 6] \rightarrow -0.0036669, F_3[2, 4, 5] \rightarrow F_3[2, 4, 6], \\
 H[1, 2, 5] &\rightarrow -0.011716, H[1, 2, 6] \rightarrow 0.045795, H[3, 4, 5] \rightarrow -0.02785, H[3, 4, 6] \rightarrow 0.039606, \\
 f[1, 3, 5] &\rightarrow 0.036064, f[1, 3, 6] \rightarrow 0.11655, f[1, 4, 5] \rightarrow -0.13436, f[1, 4, 6] \rightarrow 0.25498, \\
 f[2, 3, 5] &\rightarrow -0.0072143, f[2, 3, 6] \rightarrow -0.023314, f[2, 4, 5] \rightarrow -0.075938, f[2, 4, 6] \rightarrow -0.077789, \\
 f[3, 1, 5] &\rightarrow 0.056116, f[3, 2, 5] \rightarrow 0.086816, f[3, 2, 6] \rightarrow -0.23712, f[4, 1, 5] \rightarrow -0.012879, \\
 f[4, 1, 6] &\rightarrow -0.0033548, f[4, 2, 5] \rightarrow -0.064383, f[4, 2, 6] \rightarrow -0.016771, f[5, 1, 4] \rightarrow -0.010266, \\
 f[5, 2, 4] &\rightarrow -0.05132, f[6, 1, 4] \rightarrow 0.0031768, f[6, 2, 4] \rightarrow 0.015881, f[3, 1, 6] \rightarrow -f[2, 4, 6].
 \end{aligned}$$

$$\mathcal{R}_4 = 0.02004, \mathcal{R}_6 = -0.11684, \eta_V = -2.9354,$$

$$\text{masses}^2 = (0.12054, 0.076154, 0.042724, -0.014706), \vec{v} = (0.5719, 0.7971, 0.13641, 0.13769).$$

$s_{55}^+ 12$

$$\begin{aligned}
 T_{10}[1] &\rightarrow 7.7271771858613970, T_{10}[2] \rightarrow 2.2569215718539540, T_{10}[3] \rightarrow -0.1443613520399306, \\
 F_1[5] &\rightarrow 1, F_3[1, 3, 5] \rightarrow 0.4942839801759979, F_3[1, 3, 6] \rightarrow -0.2974725565593828, \\
 F_3[1, 4, 6] &\rightarrow -0.0819919421531531, F_3[2, 3, 5] \rightarrow 0.0065197489236415, \\
 F_3[2, 3, 6] &\rightarrow -0.2445092180276900, F_3[2, 4, 5] \rightarrow 0.2193161877900493, \\
 F_3[2, 4, 6] &\rightarrow 0.3644682080232862, H[1, 2, 5] \rightarrow -0.4230470081250839, \\
 H[1, 2, 6] &\rightarrow -0.2646546977657695, H[3, 4, 5] \rightarrow 0.2589549673229080, \\
 H[3, 4, 6] &\rightarrow -0.7901065711295830, f[1, 4, 5] \rightarrow -0.1277833635641377, \\
 f[1, 4, 6] &\rightarrow -0.5365645111668850, f[2, 3, 5] \rightarrow -0.4614839479014394, \\
 f[2, 4, 5] &\rightarrow -0.1062270206129369, f[2, 4, 6] \rightarrow -0.0551085436402409, \\
 f[3, 1, 5] &\rightarrow -0.0119865546470415, f[3, 2, 5] \rightarrow 0.2444904911694590, \\
 f[4, 1, 5] &\rightarrow -0.0650526285279246, f[4, 1, 6] \rightarrow -0.2731570906621740, \\
 f[6, 1, 4] &\rightarrow 0.0984021196994866, f[3, 1, 6] \rightarrow -f[2, 4, 6].
 \end{aligned}$$

$$\mathcal{R}_4 = 0.059663051023583824, \mathcal{R}_6 = -0.4094726936749863, \eta_V = -2.935420188208411,$$

$$\text{masses}^2 = (2.7155, 0.63285, 0.25637, -0.04109), \vec{v} = (0.46387, 0.85232, 0.19198, 0.1467).$$

## Appendix C. Minkowski and (anti-) de Sitter solutions

---

### $s_{55}^+ 13$

$$\begin{aligned}
T_{10}[1] &\rightarrow 10, T_{10}[2] \rightarrow 0.77399, T_{10}[3] \rightarrow -0.20221, F_1[5] \rightarrow 0.82894, F_3[1, 3, 5] \rightarrow 0.1905, \\
F_3[1, 3, 6] &\rightarrow 0.00375, F_3[1, 4, 6] \rightarrow -0.0039311, F_3[2, 3, 5] \rightarrow -0.46675, F_3[2, 3, 6] \rightarrow -0.57687, \\
F_3[2, 4, 5] &\rightarrow 0.0022733, F_3[2, 4, 6] \rightarrow 0.67087, H[1, 2, 5] \rightarrow 0.17259, H[1, 2, 6] \rightarrow -0.00071525, \\
H[3, 4, 5] &\rightarrow 0.0026425, H[3, 4, 6] \rightarrow -0.78712, f[1, 4, 6] \rightarrow -0.19142, f[2, 3, 5] \rightarrow -0.66446, \\
f[2, 4, 5] &\rightarrow -0.54418, f[2, 4, 6] \rightarrow 0.46713, f[3, 1, 5] \rightarrow -0.10243, f[3, 1, 6] \rightarrow 0.1473, \\
f[3, 2, 5] &\rightarrow -0.041972, f[4, 1, 6] \rightarrow -0.17985, f[6, 1, 4] \rightarrow 0.058422.
\end{aligned}$$

$$\mathcal{R}_4 = 0.037791, \mathcal{R}_6 = -0.5941, \eta_V = -2.9518,$$

$$\text{masses}^2 = (2.3792, 0.59264, 0.10413, -0.027888), \vec{v} = (0.41291, 0.87252, 0.22255, 0.13672).$$

### $s_{55}^+ 14$

$$\begin{aligned}
T_{10}[1] &\rightarrow 10, T_{10}[2] \rightarrow -0.0885069318066244, T_{10}[3] \rightarrow -0.7765198126057072, \\
F_1[5] &\rightarrow -0.2739820106484752, F_3[1, 3, 5] \rightarrow -0.5612239678297053, \\
F_3[1, 3, 6] &\rightarrow 0.7199875113561189, F_3[1, 4, 6] \rightarrow 0.0527969424771896, \\
F_3[2, 3, 5] &\rightarrow 0.6773312203822072, F_3[2, 3, 6] \rightarrow -0.3132864455247597, \\
F_3[2, 4, 6] &\rightarrow 0.1780541307257305, H[1, 2, 5] \rightarrow -0.0045785440625781, \\
H[3, 4, 6] &\rightarrow 0.2288818622936161, f[1, 4, 5] \rightarrow 0.8435712996340920, \\
f[1, 4, 6] &\rightarrow 0.6715419200224235, f[2, 3, 5] \rightarrow -0.2892985071257778, \\
f[2, 4, 5] &\rightarrow -0.0614203186917094, f[2, 4, 6] \rightarrow -0.8104719938914240, \\
f[3, 1, 5] &\rightarrow 0.0162126509210115, f[3, 2, 5] \rightarrow 0.0134334990107109, \\
f[6, 1, 4] &\rightarrow 0.4131042712391767.
\end{aligned}$$

$$\mathcal{R}_4 = 0.022658272206244612, \mathcal{R}_6 = -0.7577021085288538, \eta_V = -1.7067392663765713,$$

$$\text{masses}^2 = (1.9928, 0.24874, 0.02597, -0.0096679), \vec{v} = (0.11993, 0.95779, 0.06937, 0.25189).$$

$s_{55}^+ 14'$

$$\begin{aligned}
 T_{10}[1] &\rightarrow 10, T_{10}[2] \rightarrow -0.0885069318066244, T_{10}[3] \rightarrow -0.7765198126057072, \\
 F_1[5] &\rightarrow -0.2739820106484752, H[1, 2, 5] \rightarrow -0.0045785440625781, \\
 H[3, 4, 5] &\rightarrow -0.2875146945871226, H[3, 4, 6] \rightarrow 0.2288818622936161, \\
 F_3[1, 3, 5] &\rightarrow -2.7580681436956810, F_3[1, 3, 6] \rightarrow 1.0980873478564690, \\
 F_3[1, 4, 5] &\rightarrow -8.9169397596149600, F_3[1, 4, 6] \rightarrow 3.4691323044710350, \\
 F_3[2, 3, 5] &\rightarrow 1.0708724813659480, F_3[2, 3, 6] \rightarrow -0.3132864455247597, \\
 F_3[2, 4, 5] &\rightarrow 3.3175634705051610, F_3[2, 4, 6] \rightarrow -0.8579415960403540, \\
 f[1, 4, 6] &\rightarrow 0.6715419200224235, f[2, 3, 5] \rightarrow -0.2892985071257778, \\
 f[3, 2, 5] &\rightarrow 0.0134334990107109, f[6, 1, 4] \rightarrow 0.4131042712391767, \\
 g^{12} &\rightarrow 1.2068822060495703, g^{34} \rightarrow -3.3068641863224433, g^{56} \rightarrow 1.2561707236473398.
 \end{aligned}$$

$\mathcal{R}_4, \mathcal{R}_6, \eta_V$  unchanged.

$s_{55}^+ 15$

$$\begin{aligned}
 T_{10}[1] &\rightarrow 10, T_{10}[2] \rightarrow 0.4966295777593360, T_{10}[3] \rightarrow -0.1058505594207743, \\
 F_1[5] &\rightarrow 0.1394435290122775, F_3[1, 3, 6] \rightarrow 0.0034027792189916, \\
 F_3[1, 4, 6] &\rightarrow -0.0003267933126085, F_3[2, 3, 5] \rightarrow 0.0090828099128681, \\
 F_3[2, 3, 6] &\rightarrow -1.1496878282089060, F_3[2, 4, 5] \rightarrow -0.0048365319588065, \\
 F_3[2, 4, 6] &\rightarrow 0.6091051220227705, H[1, 2, 6] \rightarrow -0.0001845709594129, \\
 H[3, 4, 5] &\rightarrow -0.0010888652794866, f[2, 3, 5] \rightarrow -0.6020820458095239, \\
 f[2, 4, 5] &\rightarrow -1.1306855450590460, f[3, 1, 5] \rightarrow -0.0698547712340311, \\
 f[3, 1, 6] &\rightarrow -0.1916598129974718, f[3, 2, 5] \rightarrow -0.0588533218001099, \\
 f[4, 1, 6] &\rightarrow 0.1020574931847763, f[6, 1, 4] \rightarrow 0.0153448261959478.
 \end{aligned}$$

$$\mathcal{R}_4 = 0.019443278089360194, \mathcal{R}_6 = -0.8853409197705556, \eta_V = -2.9336294934114315,$$

$$\text{masses}^2 = (1.6415, 0.057392, 0.031507, -0.01426), \vec{v} = (0.60222, 0.77078, 0.17269, 0.11581).$$

## Appendix C. Minkowski and (anti-) de Sitter solutions

---

### $s_{55}^+ 15'$

$$\begin{aligned}
T_{10}[1] &\rightarrow 10, T_{10}[2] \rightarrow 0.4966295777593360, T_{10}[3] \rightarrow -0.1058505594207743, \\
F_1[5] &\rightarrow 0.1394435290122775, F_3[1, 3, 5] \rightarrow -0.0107806592596513, \\
F_3[1, 3, 6] &\rightarrow 1.3680017138866560, F_3[1, 4, 5] \rightarrow 0.0259862634523308, \\
F_3[1, 4, 6] &\rightarrow -3.2923433827652360, F_3[2, 3, 5] \rightarrow 0.0090828099128681, \\
F_3[2, 3, 6] &\rightarrow -1.1496878282089060, F_3[2, 4, 5] \rightarrow -0.0218936788185686, \\
F_3[2, 4, 6] &\rightarrow 2.7681720095568790, H[1, 2, 6] \rightarrow -0.0001845709594129, \\
H[3, 4, 5] &\rightarrow -0.0010888652794866, f[2, 3, 5] \rightarrow -0.6020820458095239, \\
f[3, 2, 5] &\rightarrow -0.0588533218001099, f[4, 1, 6] \rightarrow 0.1020574931847763, \\
f[6, 1, 4] &\rightarrow 0.0153448261959478, \\
g^{12} &\rightarrow 1.1869299658443528, g^{34} \rightarrow 1.8779592464658086.
\end{aligned}$$

$\mathcal{R}_4, \mathcal{R}_6, \eta_V$  unchanged.

### $s_{55}^+ 16$

$$\begin{aligned}
T_{10}[1] &\rightarrow 10, T_{10}[2] \rightarrow 1.0653924581926100, T_{10}[3] \rightarrow -0.2865487441401781, \\
F_1[5] &\rightarrow -0.3830798073971085, F_3[2, 3, 5] \rightarrow 0.5088261106821323, \\
F_3[2, 3, 6] &\rightarrow 1.0453549102326770, F_3[2, 4, 6] \rightarrow 0.3522836755847258, F_3[1, 3, 6] \rightarrow F_3[2, 4, 6], \\
H[1, 2, 5] &\rightarrow 0.0392319041342279, H[1, 2, 6] \rightarrow -0.0939555787571918, \\
H[3, 4, 5] &\rightarrow -0.0125416177756354, H[3, 4, 6] \rightarrow 0.2939059636978374, \\
f[2, 3, 5] &\rightarrow -0.3584729155627473, f[2, 4, 5] \rightarrow 0.9572822432446080, \\
f[2, 4, 6] &\rightarrow -0.5911827525101534, f[3, 1, 5] \rightarrow 0.2190447474382595, \\
f[3, 1, 6] &\rightarrow 0.1889887396788805, f[4, 1, 5] \rightarrow 0.1145962804793664, \\
f[6, 1, 4] &\rightarrow -0.0456860378765839, f[3, 2, 5] \rightarrow -f[4, 1, 5], f[1, 4, 5] \rightarrow -f[2, 3, 5].
\end{aligned}$$

$$\mathcal{R}_4 = 0.0498453380802234, \mathcal{R}_6 = -0.8996299138736688, \eta_V = -2.840382369328406,$$

$$\text{masses}^2 = (1.6235, 0.26174, 0.12567, -0.035395), \vec{v} = (0.48957, 0.83657, 0.20509, 0.13567).$$

$s_{55}^+17$

$$\begin{aligned}
 T_{10}[1] &\rightarrow 10, T_{10}[2] \rightarrow 1.1283773832265060, T_{10}[3] \rightarrow -0.3209376228220143, \\
 F_1[5] &\rightarrow 0.4281135811392881, F_3[2, 3, 5] \rightarrow 0.7295336312279515, \\
 F_3[2, 3, 6] &\rightarrow -0.9244213776567620, F_3[2, 4, 6] \rightarrow 0.2952514287937376, F_3[1, 3, 6] \rightarrow -F_3[2, 4, 6], \\
 H[1, 2, 5] &\rightarrow -0.1097182799067921, H[1, 2, 6] \rightarrow -0.1163339858329525, \\
 H[3, 4, 5] &\rightarrow -0.0405195014515629, H[3, 4, 6] \rightarrow -0.3150079434109206, \\
 f[2, 3, 5] &\rightarrow -0.3272913073142077, f[2, 4, 5] \rightarrow -0.8339260055526270, \\
 f[2, 4, 6] &\rightarrow -0.7780888837446737, f[3, 1, 6] \rightarrow -0.2873520591201465, \\
 f[4, 1, 5] &\rightarrow -0.1208702926537678, f[6, 1, 4] \rightarrow 0.0578627940639531, \\
 f[1, 4, 5] &\rightarrow f[2, 3, 5], f[3, 2, 5] \rightarrow f[4, 1, 5].
 \end{aligned}$$

$$\mathcal{R}_4 = 0.05683770674055544, \quad \mathcal{R}_6 = -0.8942359209665893, \quad \eta_V = -2.8748253009196407,$$

$$\text{masses}^2 = (1.6346, 0.33106, 0.14162, -0.04085), \quad \vec{v} = (0.48741, 0.84003, 0.20034, 0.12901).$$

$s_{55}^+18$

$$\begin{aligned}
 T_{10}[1] &\rightarrow 10, T_{10}[2] \rightarrow 5.0453, T_{10}[3] \rightarrow -1.7065, F_1[5] \rightarrow 0.14502, F_1[6] \rightarrow 1.1791, \\
 F_3[1, 3, 5] &\rightarrow -0.032396, F_3[1, 3, 6] \rightarrow -0.17114, F_3[1, 4, 5] \rightarrow -0.22672, F_3[1, 4, 6] \rightarrow 0.041315, \\
 F_3[2, 3, 5] &\rightarrow 0.55732, F_3[2, 3, 6] \rightarrow 0.038508, F_3[2, 4, 6] \rightarrow -0.62288, H[1, 2, 5] \rightarrow 0.69483, \\
 H[3, 4, 5] &\rightarrow 0.46484, H[3, 4, 6] \rightarrow -0.82698, f[1, 3, 5] \rightarrow -0.034063, f[1, 4, 5] \rightarrow 0.012660, \\
 f[1, 4, 6] &\rightarrow 0.15053, f[2, 3, 5] \rightarrow 1.5799, f[2, 4, 5] \rightarrow 0.27154, f[3, 2, 5] \rightarrow 0.12647, \\
 f[5, 2, 3] &\rightarrow 1.2374, f[5, 2, 4] \rightarrow 0.21267, f[6, 2, 3] \rightarrow -0.15219, f[6, 2, 4] \rightarrow -0.026158.
 \end{aligned}$$

$$\mathcal{R}_4 = 0.028430, \quad \mathcal{R}_6 = -0.44861, \quad \eta_V = 3.7926,$$

$$\text{masses}^2 = (4.4552, 3.6110, 0.29362, 0.026956), \quad \vec{v} = (0.49697, 0.84917, 0.046867, 0.17244).$$

## Appendix C. Minkowski and (anti-) de Sitter solutions

---

### $s_{55}^+19$

$$\begin{aligned}
T_{10}[1] &\rightarrow 10, T_{10}[2] \rightarrow 0.12358, T_{10}[3] \rightarrow -0.39675, F_1[5] \rightarrow 0.032992, F_1[6] \rightarrow 0.16433, \\
F_3[1, 3, 5] &\rightarrow -0.52888, F_3[1, 3, 6] \rightarrow 0.10898, F_3[1, 4, 5] \rightarrow 0.29728, F_3[1, 4, 6] \rightarrow -0.056703, \\
F_3[2, 3, 5] &\rightarrow 0.46336, F_3[2, 3, 6] \rightarrow -0.47205, F_3[2, 4, 5] \rightarrow -0.069697, F_3[2, 4, 6] \rightarrow 0.87424, \\
H[1, 2, 5] &\rightarrow 0.0018436, H[1, 2, 6] \rightarrow 0.010455, H[3, 4, 5] \rightarrow 0.15470, H[3, 4, 6] \rightarrow -0.029492, \\
f[1, 3, 5] &\rightarrow 0.058151, f[1, 3, 6] \rightarrow 0.32171, f[1, 4, 5] \rightarrow 0.11066, f[1, 4, 6] \rightarrow 0.56519, \\
f[2, 3, 5] &\rightarrow -0.92088, f[2, 3, 6] \rightarrow -0.059007, f[2, 4, 5] \rightarrow -0.48068, f[2, 4, 6] \rightarrow -0.41926, \\
f[3, 1, 5] &\rightarrow 0.0050094, f[3, 1, 6] \rightarrow -0.028443, f[3, 2, 5] \rightarrow 0.011003, f[3, 2, 6] \rightarrow -0.0028411, \\
f[4, 1, 5] &\rightarrow 0.0060442, f[4, 1, 6] \rightarrow 0.060379, f[4, 2, 5] \rightarrow -0.0063015, f[4, 2, 6] \rightarrow 0.0012974, \\
f[5, 1, 3] &\rightarrow -0.061155, f[5, 1, 4] \rightarrow -0.026674, f[5, 2, 3] \rightarrow -0.066026, f[5, 2, 4] \rightarrow -0.028799, \\
f[6, 1, 3] &\rightarrow 0.012278, f[6, 1, 4] \rightarrow 0.0053553, f[6, 2, 3] \rightarrow 0.013256, f[6, 2, 4] \rightarrow 0.0057819.
\end{aligned}$$

$$\mathcal{R}_4 = 0.0031779, \quad \mathcal{R}_6 = -0.44861, \quad \eta_V = -0.12141,$$

$$\text{masses}^2 = (1.7237, 0.060109, 0.0058657, -0.000096456), \quad \vec{v} = (0.35911, 0.91283, 0.19064, 0.037871).$$

### $s_{55}^+20$

$$\begin{aligned}
T_{10}[1] &\rightarrow 10, T_{10}[2] \rightarrow -0.19097, T_{10}[3] \rightarrow -1.1799, F_1[5] \rightarrow 0.15119, F_1[6] \rightarrow 0.17554, \\
F_3[1, 3, 5] &\rightarrow -0.23901, F_3[1, 3, 6] \rightarrow -0.64579, F_3[1, 4, 5] \rightarrow -0.017596, F_3[1, 4, 6] \rightarrow 0.19754, \\
F_3[2, 3, 5] &\rightarrow -0.16767, F_3[2, 3, 6] \rightarrow 0.88008, F_3[2, 4, 6] \rightarrow -0.22116, H[1, 2, 5] \rightarrow -0.0097969, \\
f[1, 4, 6] &\rightarrow 0.71835, f[2, 3, 5] \rightarrow 0.36455, f[2, 4, 5] \rightarrow 1.2126, f[3, 2, 5] \rightarrow -0.046623, \\
f[5, 2, 3] &\rightarrow 0.15822, f[5, 2, 4] \rightarrow 0.52631, f[6, 2, 3] \rightarrow -0.13627, f[6, 2, 4] \rightarrow -0.45329.
\end{aligned}$$

$$\mathcal{R}_4 = 0.019450, \quad \mathcal{R}_6 = -0.72144, \quad \eta_V = -1.3624,$$

$$\text{masses}^2 = (2.6116, 0.37159, 0.028935, -0.0066248), \quad \vec{v} = (0.10243, 0.94233, 0.030698, -0.31715).$$

### $s_{55}^+21$

$$\begin{aligned}
T_{10}[1] &\rightarrow 10, T_{10}[2] \rightarrow -0.13516, T_{10}[3] \rightarrow -0.67689, F_1[5] \rightarrow 0.25041, F_1[6] \rightarrow -0.18033, \\
F_3[1, 3, 5] &\rightarrow -0.41712, F_3[1, 3, 6] \rightarrow 0.57791, F_3[1, 4, 5] \rightarrow 0.0044424, F_3[1, 4, 6] \rightarrow 0.30091, \\
F_3[2, 3, 5] &\rightarrow 0.055123, F_3[2, 3, 6] \rightarrow 0.87210, F_3[2, 4, 6] \rightarrow 0.22542, H[1, 2, 5] \rightarrow 0.012410, \\
H[3, 4, 5] &\rightarrow -0.14114, H[3, 4, 6] \rightarrow -0.22801, f[1, 3, 5] \rightarrow -0.37658, f[1, 4, 5] \rightarrow 0.43325, \\
f[1, 4, 6] &\rightarrow 0.64505, f[2, 3, 5] \rightarrow -0.28801, f[2, 4, 5] \rightarrow 1.0164, f[3, 2, 5] \rightarrow 0.035108, \\
f[5, 2, 3] &\rightarrow -0.063291, f[5, 2, 4] \rightarrow 0.22337, f[6, 2, 3] \rightarrow -0.087890, f[6, 2, 4] \rightarrow 0.31018.
\end{aligned}$$

$$\mathcal{R}_4 = 0.023161, \quad \mathcal{R}_6 = -0.75279, \quad \eta_V = -1.7813,$$

$$\text{masses}^2 = (1.9567, 0.28341, 0.030287, -0.010314), \quad \vec{v} = (0.092869, 0.96324, 0.077710, -0.23978).$$

**$s_{55}^+ 22$**

$$\begin{aligned} T_{10}[1] &\rightarrow 10, T_{10}[2] \rightarrow 0.11698, T_{10}[3] \rightarrow -0.25961, F_1[5] \rightarrow 0.22288, \\ F_3[1, 3, 5] &\rightarrow 0.64570, F_3[1, 3, 6] \rightarrow 0.16612, F_3[1, 4, 6] \rightarrow 0.023090, F_3[2, 3, 5] \rightarrow -0.70283, \\ F_3[2, 3, 6] &\rightarrow 0.63805, F_3[2, 4, 6] \rightarrow -0.49421, H[1, 2, 5] \rightarrow -0.012009, H[3, 4, 6] \rightarrow -0.21608, \\ f[1, 4, 5] &\rightarrow 0.18908, f[1, 4, 6] \rightarrow -0.66397, f[2, 3, 5] \rightarrow 0.48234, f[2, 4, 5] \rightarrow 0.64579, \\ f[2, 4, 6] &\rightarrow 0.72271, f[3, 1, 5] \rightarrow 0.040164, f[3, 2, 5] \rightarrow 0.036900, f[6, 1, 4] \rightarrow -0.067815. \end{aligned}$$

$$\mathcal{R}_4 = 0.0028407, \quad \mathcal{R}_6 = -0.80087, \quad \eta_V = -1.0525,$$

$$\text{masses}^2 = (1.6969, 0.099699, 0.0037153, -0.00074744), \quad \vec{v} = (0.34472, 0.91135, 0.21299, 0.072416).$$

**$s_{55}^+ 23$**

$$\begin{aligned} T_{10}[1] &\rightarrow 10, T_{10}[2] \rightarrow 0.84108, T_{10}[3] \rightarrow -1.7713, F_1[5] \rightarrow 0.28275, \\ F_3[1, 3, 5] &\rightarrow 0.76288, F_3[1, 3, 6] \rightarrow 0.34090, F_3[1, 4, 6] \rightarrow 0.18689, F_3[2, 3, 5] \rightarrow 0.23849, \\ F_3[2, 3, 6] &\rightarrow 0.70671, F_3[2, 4, 6] \rightarrow 0.32182, H[1, 2, 5] \rightarrow 0.047753, H[3, 4, 6] \rightarrow -0.19749, \\ f[1, 4, 5] &\rightarrow 0.15989, f[1, 4, 6] \rightarrow -1.0319, f[2, 3, 5] \rightarrow -0.35628, f[2, 4, 5] \rightarrow 0.81719, \\ f[2, 4, 6] &\rightarrow -0.32259, f[3, 1, 5] \rightarrow 0.078001, f[3, 2, 5] \rightarrow -0.24951, f[6, 1, 4] \rightarrow -0.41774. \end{aligned}$$

$$\mathcal{R}_4 = 0.038665, \quad \mathcal{R}_6 = -0.77384, \quad \eta_V = -1.2253,$$

$$\text{masses}^2 = (2.1222, 0.21211, 0.072030, -0.011844), \quad \vec{v} = (0.59221, 0.79571, 0.10757, 0.067508).$$

**$s_{55}^+ 24$**

$$\begin{aligned} T_{10}[1] &\rightarrow 10, T_{10}[2] \rightarrow 0.19660, T_{10}[3] \rightarrow -0.44890, F_1[5] \rightarrow 0.23918, \\ F_3[1, 3, 5] &\rightarrow 0.70008, F_3[1, 3, 6] \rightarrow -0.072124, F_3[1, 4, 6] \rightarrow 0.044829, F_3[2, 3, 5] \rightarrow 0.60939, \\ F_3[2, 3, 6] &\rightarrow 0.68494, F_3[2, 4, 6] \rightarrow 0.47273, H[1, 2, 5] \rightarrow 0.019075, H[3, 4, 6] \rightarrow -0.22522, \\ f[1, 4, 5] &\rightarrow -0.11312, f[1, 4, 6] \rightarrow -0.73817, f[2, 3, 5] \rightarrow -0.45730, f[2, 4, 5] \rightarrow 0.70098, \\ f[2, 4, 6] &\rightarrow -0.64254, f[3, 1, 5] \rightarrow 0.054422, f[3, 2, 5] \rightarrow -0.062521, f[6, 1, 4] \rightarrow -0.10923. \end{aligned}$$

$$\mathcal{R}_4 = 0.0061178, \quad \mathcal{R}_6 = -0.79288, \quad \eta_V = -0.95955,$$

$$\text{masses}^2 = (1.7245, 0.11797, 0.0082620, -0.0014676), \quad \vec{v} = (0.38671, 0.89718, 0.19939, 0.075995).$$



## Appendix C. Minkowski and (anti-) de Sitter solutions

---

### $s_{55}^+ 25$

$$\begin{aligned}
 T_{10}[1] &\rightarrow 10, T_{10}[2] \rightarrow 0.28255, T_{10}[3] \rightarrow -0.66015, F_1[5] \rightarrow 0.24822, \\
 F_3[1, 3, 5] &\rightarrow 0.73650, F_3[1, 3, 6] \rightarrow 0.0099987, F_3[1, 4, 6] \rightarrow 0.070509, F_3[2, 3, 5] \rightarrow 0.52642, \\
 F_3[2, 3, 6] &\rightarrow 0.71248, F_3[2, 4, 6] \rightarrow 0.44686, H[1, 2, 5] \rightarrow 0.025515, H[3, 4, 6] \rightarrow -0.22535, \\
 f[1, 4, 5] &\rightarrow -0.051498, f[1, 4, 6] \rightarrow -0.80098, f[2, 3, 5] \rightarrow -0.43118, f[2, 4, 5] \rightarrow 0.74004, \\
 f[2, 4, 6] &\rightarrow -0.57251, f[3, 1, 5] \rightarrow 0.064822, f[3, 2, 5] \rightarrow -0.090691, f[6, 1, 4] \rightarrow -0.15442.
 \end{aligned}$$

$$\mathcal{R}_4 = 0.010180, \quad \mathcal{R}_6 = -0.78633, \quad \eta_V = -0.90691,$$

$$\text{masses}^2 = (1.7623, 0.13189, 0.014432, -0.0023081), \quad \vec{v} = (0.43152, 0.87989, 0.18312, 0.077785).$$

### $s_{55}^+ 26$

$$\begin{aligned}
 T_{10}[1] &\rightarrow 10, T_{10}[2] \rightarrow 0.60749, T_{10}[3] \rightarrow -1.3921, F_1[5] \rightarrow 0.26812, \\
 F_3[1, 3, 5] &\rightarrow -0.77550, F_3[1, 3, 6] \rightarrow -0.23680, F_3[1, 4, 6] \rightarrow -0.15385, F_3[2, 3, 5] \rightarrow -0.31347, \\
 F_3[2, 3, 6] &\rightarrow -0.72645, F_3[2, 4, 6] \rightarrow -0.36053, H[1, 2, 5] \rightarrow 0.041294, H[3, 4, 6] \rightarrow -0.20803, \\
 f[1, 4, 5] &\rightarrow -0.10180, f[1, 4, 6] \rightarrow 0.96159, f[2, 3, 5] \rightarrow 0.36993, f[2, 4, 5] \rightarrow -0.80647, \\
 f[2, 4, 6] &\rightarrow 0.38869, f[3, 1, 5] \rightarrow -0.077154, f[3, 2, 5] \rightarrow 0.19087, f[6, 1, 4] \rightarrow 0.31938.
 \end{aligned}$$

$$\mathcal{R}_4 = 0.026903, \quad \mathcal{R}_6 = -0.77236, \quad \eta_V = -1.0438,$$

$$\text{masses}^2 = (1.9625, 0.17832, 0.045753, -0.0070202), \quad \vec{v} = (0.55137, 0.82094, 0.12983, 0.072063).$$

### $s_{55}^+ 27$

$$\begin{aligned}
 T_{10}[1] &\rightarrow 10, T_{10}[2] \rightarrow 0.69681, T_{10}[3] \rightarrow -1.5499, F_1[5] \rightarrow -0.27379, \\
 F_3[1, 3, 5] &\rightarrow 0.77212, F_3[1, 3, 6] \rightarrow -0.28080, F_3[1, 4, 6] \rightarrow 0.16865, F_3[2, 3, 5] \rightarrow -0.27968, \\
 F_3[2, 3, 6] &\rightarrow 0.71969, F_3[2, 4, 6] \rightarrow -0.34410, H[1, 2, 5] \rightarrow 0.044110, H[3, 4, 6] \rightarrow 0.20379, \\
 f[1, 4, 5] &\rightarrow -0.12773, f[1, 4, 6] \rightarrow -0.99090, f[2, 3, 5] \rightarrow 0.36320, f[2, 4, 5] \rightarrow 0.81222, \\
 f[2, 4, 6] &\rightarrow 0.35892, f[3, 1, 5] \rightarrow 0.077686, f[3, 2, 5] \rightarrow 0.21447, f[6, 1, 4] \rightarrow -0.35893.
 \end{aligned}$$

$$\mathcal{R}_4 = 0.031484, \quad \mathcal{R}_6 = -0.77199, \quad \eta_V = -1.1172,$$

$$\text{masses}^2 = (2.0231, 0.19153, 0.055590, -0.0087933), \quad \vec{v} = (0.56984, 0.80991, 0.12007, 0.070019).$$

$s_{55}^+ 28$

$$\begin{aligned}
 T_{10}[1] &= 2.2601, T_{10}[2] = 5.167, T_{10}[3] = -0.46062, F_1[5] = 1, F_3[1, 3, 5] = -0.16181, \\
 F_3[1, 3, 6] &= -0.0038892, F_3[1, 4, 6] = 0.16022, F_3[2, 3, 5] = -0.0001645, F_3[2, 3, 6] = -0.1408, \\
 F_3[2, 4, 5] &= -0.13582, F_3[2, 4, 6] = -0.0045142, H[1, 2, 5] = 0.057659, H[1, 2, 6] = 0.84321, \\
 H[3, 4, 5] &= -0.38, H[3, 4, 6] = 0.26525, f[1, 4, 5] = -0.052068, f[1, 4, 6] = -0.68811, \\
 f[2, 3, 5] &= -0.062695, f[2, 4, 5] = 0.00011416, f[2, 4, 6] = 0.00020752, f[3, 1, 5] = -0.00002051, \\
 f[3, 2, 5] &= -0.015941, f[4, 1, 5] = -0.0099985, f[4, 1, 6] = -0.13214, f[6, 1, 4] = -0.54525, \\
 f[3, 1, 6] &= -0.00020752,
 \end{aligned}$$

$$\mathcal{R}_4 = 0.070923, \quad \mathcal{R}_6 = -0.18693, \quad \eta_V = -3.2374,$$

$$\text{masses}^2 = (2.6997, 0.83912, 0.17195, -0.057401), \quad \vec{v} = (0.39746, 0.91322, 0.04005, 0.080317).$$

$s_{66}^+ 1$

$$I = 1: 123, \quad I = 2: 145, \quad I = 3: 256, \quad I = 4: 346,$$

$$\begin{aligned}
 T_{10}[1] &= 10, T_{10}[2] = 8.6452, T_{10}[3] = -0.8438, T_{10}[4] = -0.8438, \\
 F_0 &= 1.2685, F_2[1, 6] = -0.053287, F_2[2, 4] = 0.18526, F_2[2, 5] = -0.44051, \\
 F_2[3, 4] &= 0.44051, F_2[3, 5] = 0.18526, F_4[1, 2, 4, 6] = 0.20229, F_4[1, 2, 5, 6] = 0.080552, \\
 F_4[1, 3, 4, 6] &= -0.080552, F_4[1, 3, 5, 6] = 0.20229, H[1, 2, 5] = -0.095031, H[1, 3, 4] = -0.095031, \\
 H[2, 3, 6] &= -0.69318, H[4, 5, 6] = -0.79175, f[1, 2, 3] = -0.48293, f[1, 4, 5] = 0.50315, \\
 f[2, 4, 6] &= -0.38643, f[2, 5, 6] = -0.15388, f[3, 4, 6] = 0.15388, f[3, 5, 6] = -0.38643, \\
 f[4, 2, 6] &= -0.37091, f[4, 3, 6] = 0.14769, f[5, 2, 6] = -0.14769, f[5, 3, 6] = -0.37091,
 \end{aligned}$$

$$\mathcal{R}_4 = 0.25915, \quad \mathcal{R}_6 = -0.90769, \quad \eta_V = -3.617,$$

$$\text{masses}^2 = (5.5537, 1.1135, 0.91621, 0.39899, -0.23434), \quad \vec{v} = (0.21153, 0.95997, 0.13038, 0.1293, 0).$$

$s_{6666}^+ 1$

$$I = 1: 123, \quad I = 2: 145, \quad I = 3: 256, \quad I = 4: 346,$$

$$\begin{aligned}
 T_{10}[1] &= 10, T_{10}[2] = -0.64856, T_{10}[3] = -0.28674, T_{10}[4] = -0.62522, \\
 F_0 &= -0.5871, F_2[1, 6] = 0.56149, F_2[2, 4] = 0.49009, F_2[3, 5] = -0.551, \\
 H[1, 2, 5] &= 0.24103, H[1, 3, 4] = 0.098649, H[2, 3, 6] = -0.25101, H[4, 5, 6] = 0.45935, \\
 f[1, 2, 3] &= 0.11063, f[1, 4, 5] = -0.71643, f[2, 1, 3] = -0.028654, f[2, 5, 6] = -0.73726, \\
 f[3, 1, 2] &= 0.10166, f[3, 4, 6] = -0.71741, f[4, 1, 5] = 0.10447, f[4, 3, 6] = 0.11384, \\
 f[5, 1, 4] &= -0.027882, f[5, 2, 6] = 0.11078, f[6, 2, 5] = -0.10152, f[6, 3, 4] = -0.027844,
 \end{aligned}$$

## Appendix C. Minkowski and (anti-) de Sitter solutions

---

$$\mathcal{R}_4 = 0.0019, \quad \mathcal{R}_6 = -0.4338, \quad \eta_V = -18.445,$$

$$\text{masses}^2 = (2.6542, 0.51278, 0.11832, 0.025737, -0.0087616),$$

$$\vec{v} = (-0.21114, -0.97063, -0.10494, -0.0044338, 0.047676).$$

### $s_{6666}^+ 2$

$$I = 1: 123, \quad I = 2: 145, \quad I = 3: 256, \quad I = 4: 346,$$

$$T_{10}[1] = 0.28747, T_{10}[2] = 10, T_{10}[3] = -0.27065, T_{10}[4] = -0.29230,$$

$$F_0 = 0.59808, F_2[1, 6] = 0.72514, F_2[2, 4] = 0.48711, F_2[3, 5] = 0.50209,$$

$$H[1, 2, 5] = -0.026084, H[1, 3, 4] = -0.12392, H[2, 3, 6] = -0.55827, H[4, 5, 6] = -0.074278,$$

$$f[1, 2, 3] = -0.79263, f[1, 4, 5] = 0.048506, f[2, 1, 3] = 0.032869, f[2, 5, 6] = -0.032187,$$

$$f[3, 1, 2] = -0.023594, f[3, 4, 6] = 0.032142, f[4, 1, 5] = 0.023626, f[4, 3, 6] = 0.52596,$$

$$f[5, 1, 4] = -0.032823, f[5, 2, 6] = -0.52523, f[6, 2, 5] = 0.035605, f[6, 3, 4] = -0.049535,$$

$$\mathcal{R}_4 = 0.016318, \quad \mathcal{R}_6 = -0.54431, \quad \eta_V = -2.6435,$$

$$\text{masses}^2 = (2.6325, 0.25768, 0.021208, 0.011834, -0.010784),$$

$$\vec{v} = (-0.11873, -0.95004, -0.14484, -0.23405, -0.087002).$$

### $s_{6666}^+ 3$

$$I = 1: 123, \quad I = 2: 145, \quad I = 3: 256, \quad I = 4: 346,$$

$$T_{10}[1] = 10, T_{10}[2] = -0.022254, T_{10}[3] = -0.56181, T_{10}[4] = -0.022254,$$

$$F_0 = 0.27366, F_2[1, 6] = 0.15807, F_2[2, 4] = -0.88473, F_2[3, 5] = -0.66851,$$

$$F_4[1, 2, 4, 6] = -0.040498, F_4[2, 3, 4, 5] = 0.064472, H[1, 2, 5] = -0.011617, H[1, 3, 4] = -0.13984,$$

$$H[2, 3, 6] = 0.011617, H[4, 5, 6] = -0.19831, f[1, 4, 5] = -0.50423, f[2, 1, 3] = 0.25402,$$

$$f[2, 5, 6] = 0.85671, f[3, 4, 6] = -0.80274, f[5, 1, 4] = -0.23802, f[6, 3, 4] = -0.14951,$$

$$\mathcal{R}_4 = 0.0066281, \quad \mathcal{R}_6 = -0.64803, \quad \eta_V = -2.3772,$$

$$\text{masses}^2 = (2.1906, 0.2362, 0.036109, 0.003449, -0.0039391),$$

$$\vec{v} = (-0.10262, -0.93062, -0.25695, 0, -0.23957).$$

$s_{6666}^+$ 4

$$I = 1: 123, \quad I = 2: 145, \quad I = 3: 256, \quad I = 4: 346,$$

$$T_{10}[1] = 10, T_{10}[2] = -0.11433, T_{10}[3] = -0.68982, T_{10}[4] = -0.11433,$$

$$F_0 = 0.68725, F_2[1, 6] = -0.49234, F_2[2, 4] = -0.48960, F_2[3, 5] = 0.55498,$$

$$F_4[1, 2, 4, 6] = 0.023125, F_4[2, 3, 4, 5] = -0.024432, H[1, 2, 5] = -0.023765, H[1, 3, 4] = -0.32922,$$

$$H[2, 3, 6] = 0.023765, H[4, 5, 6] = -0.55765, f[1, 4, 5] = 0.73078, f[2, 1, 3] = 0.1262,$$

$$f[2, 5, 6] = 0.52498, f[3, 4, 6] = 0.77209, f[5, 1, 4] = 0.18561, f[6, 3, 4] = 0.17568,$$

$$\mathcal{R}_4 = 0.033794, \quad \mathcal{R}_6 = -0.47223, \quad \eta_V = -3.6231,$$

$$\text{masses}^2 = (2.876, 0.62526, 0.047899, 0.017462, -0.03061), \quad \vec{v} = (0.17002, 0.96611, 0.16803, 0, 0.097448).$$

$m_{46}^+$ 1

$$I = 1: 4, \quad I = 2: 123, \quad I = 3: 156,$$

$$T_{10}[1] = 0.055518, T_{10}[2] = 0.91544, T_{10}[3] = -0.012619, F_2[1, 5] = 0.068521,$$

$$F_2[1, 6] = -0.12113, F_2[2, 5] = 0.029417, F_2[2, 6] = -0.27374, F_2[3, 5] = -0.024587,$$

$$F_2[3, 6] = 0.20380, F_4[1, 2, 4, 5] = -0.012313, F_4[1, 2, 4, 6] = 0.0020369, F_4[1, 3, 4, 5] = 0.0086934,$$

$$F_4[1, 3, 4, 6] = 0.0013222, H[1, 2, 5] = 0.020813, H[1, 2, 6] = -0.040268, H[1, 3, 5] = 0.025725,$$

$$H[1, 3, 6] = -0.054176, H[2, 3, 5] = -0.030633, H[2, 3, 6] = 0.021713, f[1, 4, 5] = 0.12212,$$

$$f[1, 4, 6] = 0.022477, f[2, 4, 5] = 0.26303, f[2, 4, 6] = 0.048411, f[3, 4, 5] = -0.19690,$$

$$f[3, 4, 6] = -0.036239, f[4, 2, 5] = -0.01635, f[4, 2, 6] = -0.0030093, f[4, 3, 5] = -0.040938,$$

$$f[4, 3, 6] = -0.0075347, f[5, 2, 4] = 0.0044539, f[5, 3, 4] = 0.011152, f[6, 2, 4] = 0.0025194,$$

$$f[6, 3, 4] = 0.0063081,$$

$$\mathcal{R}_4 = 0.0025394, \quad \mathcal{R}_6 = -0.069048, \quad \eta_V = -3.6764,$$

$$\text{masses}^2 = (0.23781, 0.043113, 0.0095625, 0.0042868, -0.002334),$$

$$\vec{v} = (-0.49298, -0.86049, -0.048158, -0.11911, -0.0044811).$$

## Appendix C. Minkowski and (anti-) de Sitter solutions

---

### $m_{46}^+ 2$

$$I = 1: 4, \quad I = 2: 123, \quad I = 3: 156,$$

$$T_{10}[1] = 0.021786, T_{10}[2] = 0.21625, T_{10}[3] = -0.0050741, F_2[1, 5] = 0.05579,$$

$$F_2[2, 5] = -0.053314, F_2[2, 6] = 0.036657, F_2[3, 5] = -0.13111, F_2[3, 6] = 0.094822,$$

$$F_4[1, 2, 4, 6] = 0.0014442, F_4[1, 3, 4, 5] = 0.004467, F_4[1, 3, 4, 6] = 0.00090447, H[1, 2, 5] = 0.045867,$$

$$H[1, 2, 6] = -0.0071595, H[1, 3, 5] = -0.020177, H[2, 3, 5] = -0.015322, H[2, 3, 6] = -0.0021738,$$

$$f[1, 4, 5] = 0.022176, f[1, 4, 6] = 0.036871, f[2, 4, 5] = -0.031927, f[2, 4, 6] = -0.053084,$$

$$f[3, 4, 5] = -0.079393, f[3, 4, 6] = -0.132, f[4, 2, 5] = -0.013161, f[4, 2, 6] = -0.021882,$$

$$f[6, 2, 4] = 0.0076445,$$

$$\mathcal{R}_4 = 0.0010218, \quad \mathcal{R}_6 = -0.016884, \quad \eta_V = -3.7145,$$

$$\text{masses}^2 = (0.05838, 0.0064771, 0.0036211, 0.0016224, -0.0009489),$$

$$\vec{v} = (-0.49448, -0.85989, -0.046114, -0.1178, -0.008685).$$

### $m_{46}^+ 3$

$$I = 1: 4, \quad I = 2: 123, \quad I = 3: 156,$$

$$T_{10}[1] = 0.52281, T_{10}[2] = 0.065807, T_{10}[3] = -0.029745, F_2[1, 5] = -0.078038,$$

$$F_2[1, 6] = -0.033188, F_2[2, 5] = -0.092832, F_2[2, 6] = 0.25624, F_2[3, 5] = 0.012313,$$

$$F_2[3, 6] = 0.093103, F_4[1, 2, 4, 5] = 0.03363, F_4[1, 2, 4, 6] = 0.052371, F_4[1, 3, 4, 5] = -0.046776,$$

$$F_4[1, 3, 4, 6] = -0.10158, H[1, 2, 5] = 0.097704, H[1, 2, 6] = -0.010041, H[1, 3, 5] = -0.23018,$$

$$H[1, 3, 6] = -0.12995, H[2, 3, 5] = -0.036589, H[2, 3, 6] = 0.052514, f[1, 4, 5] = -0.0063799,$$

$$f[1, 4, 6] = 0.0030219, f[2, 4, 5] = -0.043334, f[2, 4, 6] = 0.020526, f[3, 4, 5] = -0.0065711,$$

$$f[3, 4, 6] = 0.0031125, f[4, 2, 5] = -0.11424, f[4, 2, 6] = 0.054112, f[4, 3, 5] = -0.070979,$$

$$f[4, 3, 6] = 0.03362, f[5, 2, 4] = 0.018851, f[5, 3, 4] = 0.011712, f[6, 2, 4] = -0.044327,$$

$$f[6, 3, 4] = -0.02754,$$

$$\mathcal{R}_4 = 0.0030452, \quad \mathcal{R}_6 = -0.016095, \quad \eta_V = -2.2769,$$

$$\text{masses}^2 = (0.16326, 0.049326, 0.014903, 0.0022091, -0.0017334),$$

$$\vec{v} = (-0.5219, -0.81615, -0.17652, -0.16336, -0.06057).$$

$m_{46}^+4$

$$I = 1: 4, \quad I = 2: 123, \quad I = 3: 156, \quad I = 4: 256, \quad I = 5: 356,$$

$$T_{10}[1] = 10, T_{10}[2] = 5.5434, T_{10}[3] = -0.28263, T_{10}[4] = -0.34668, T_{10}[5] = -3.0483,$$

$$F_2[1, 5] = -0.0046132, F_2[1, 6] = -0.86711, F_2[2, 5] = -0.0071933, F_2[2, 6] = 0.62328,$$

$$F_2[3, 5] = 0.28752, F_2[3, 6] = -0.56401, F_4[1, 2, 4, 5] = 0.069428, F_4[1, 2, 4, 6] = -0.073577,$$

$$F_4[1, 3, 4, 5] = 0.41804, F_4[1, 3, 4, 6] = -0.47935, F_4[2, 3, 4, 5] = -0.23603, F_4[2, 3, 4, 6] = 0.20559,$$

$$H[1, 2, 5] = -0.42143, H[1, 2, 6] = 0.16444, H[1, 3, 5] = -0.36009, H[1, 3, 6] = 0.40252,$$

$$H[2, 3, 5] = -0.68041, H[2, 3, 6] = 0.45725, f[1, 4, 5] = 0.47613, f[1, 4, 6] = 0.26763,$$

$$f[2, 4, 5] = -0.343, f[2, 4, 6] = -0.1928, f[3, 4, 5] = 0.22756, f[3, 4, 6] = 0.12791,$$

$$f[4, 1, 5] = -0.5254, f[4, 1, 6] = -0.29533, f[4, 2, 5] = -1.1177, f[4, 2, 6] = -0.62827,$$

$$f[4, 3, 5] = 0.17583, f[4, 3, 6] = 0.098834, f[5, 1, 4] = 0.35275, f[5, 2, 4] = 0.75044,$$

$$f[5, 3, 4] = -0.11805, f[6, 1, 4] = 0.17608, f[6, 2, 4] = 0.37458, f[6, 3, 4] = -0.058926,$$

$$\mathcal{R}_4 = 0.21259, \quad \mathcal{R}_6 = -0.76168, \quad \eta_V = -2.8266,$$

$$\text{masses}^2 = (5.1417, 2.5653, 1.2597, 0.92638, 0.34999, -0.15023),$$

$$\vec{v} = (0.476, 0.87352, -0.049169, 0.04948, -0.037752, -0.064036).$$

$m_{46}^+5$

$$I = 1: 4, \quad I = 2: 123, \quad I = 3: 156, \quad I = 4: 256, \quad I = 5: 356,$$

$$T_{10}[1] = 10, T_{10}[2] = 0.089559, T_{10}[3] = -0.0014549, T_{10}[4] = -0.12442, T_{10}[5] = -0.020044,$$

$$F_2[1, 5] = -0.054582, F_2[1, 6] = -0.87864, F_2[2, 5] = 0.18170, F_2[2, 6] = -0.0428,$$

$$F_2[3, 5] = -1.0043, F_2[3, 6] = 0.31220, F_4[1, 2, 4, 6] = -0.038841, F_4[1, 3, 4, 5] = 0.0031155,$$

$$F_4[1, 3, 4, 6] = -0.0062571, F_4[2, 3, 4, 5] = 0.26643, H[1, 2, 5] = 0.36510, H[1, 2, 6] = 0.99268,$$

$$H[1, 3, 5] = 0.052376, H[1, 3, 6] = 0.17775, H[2, 3, 5] = -0.87116, H[2, 3, 6] = 0.10088,$$

$$f[1, 4, 5] = -0.0024863, f[1, 4, 6] = 0.032591, f[2, 4, 5] = -0.00018986, f[2, 4, 6] = 0.0024887,$$

$$f[3, 4, 5] = 0.0012693, f[3, 4, 6] = -0.016639, f[4, 1, 5] = -0.023942, f[4, 1, 6] = 0.31384,$$

$$f[4, 2, 5] = 0.00036106, f[4, 2, 6] = -0.0047329, f[4, 3, 5] = -0.00050343, f[4, 3, 6] = 0.0065991,$$

$$f[5, 1, 4] = -0.013785, f[5, 2, 4] = 0.00020788, f[5, 3, 4] = -0.00028985, f[6, 1, 4] = -0.095571,$$

$$f[6, 2, 4] = 0.0014413, f[6, 3, 4] = -0.0020096,$$

$$\mathcal{R}_4 = 0.0035366, \quad \mathcal{R}_6 = -0.038434, \quad \eta_V = -0.36462,$$

$$\text{masses}^2 = (3.9077, 1.8356, 0.20839, 0.07304, 0.00126, -0.00032237),$$

## Appendix C. Minkowski and (anti-) de Sitter solutions

---

$$\vec{v} = (-0.51698, -0.8149, -0.17672, -0.19284, 0.00063048, -0.015972).$$

### $m_{46}^+$ 6

$$I = 1: 4, I = 2: 123, I = 3: 156, I = 4: 256, I = 5: 356,$$

$$T_{10}[1] = 10, T_{10}[2] = -0.056703, T_{10}[3] = -0.000039105, T_{10}[4] = -0.17140, T_{10}[5] = -0.89612,$$

$$F_2[1, 5] = 0.17355, F_2[1, 6] = -0.16826, F_2[2, 5] = 0.78091, F_2[2, 6] = 0.43765,$$

$$F_2[3, 5] = -0.093708, F_2[3, 6] = -0.016276, F_4[1, 2, 4, 5] = 0.0097804, F_4[1, 2, 4, 6] = -0.0010561,$$

$$F_4[1, 3, 4, 5] = 0.051354, F_4[1, 3, 4, 6] = -0.0055164, F_4[2, 3, 4, 5] = 0.97045, F_4[2, 3, 4, 6] = 0.021534,$$

$$H[1, 2, 5] = -0.038322, H[1, 2, 6] = 0.080497, H[1, 3, 5] = -0.66493, H[1, 3, 6] = 0.67871,$$

$$H[2, 3, 5] = -0.17221, H[2, 3, 6] = -0.27621, f[1, 4, 6] = 0.0028299, f[2, 4, 6] = -f[6, 2, 4],$$

$$f[3, 4, 6] = 0.00062974, f[4, 1, 6] = 1.1245, f[4, 2, 6] = -0.050407, f[4, 3, 6] = 0.0095924,$$

$$f[5, 1, 4] = 0.29524, f[5, 2, 4] = -0.013235, f[5, 3, 4] = 0.0025187, f[6, 1, 4] = -0.24375,$$

$$f[6, 2, 4] = 0.010927, f[6, 3, 4] = -0.0020793,$$

$$\mathcal{R}_4 = 0.025555, \quad \mathcal{R}_6 = -0.43692, \quad \eta_V = -3.0124,$$

$$\text{masses}^2 = (3.9604, 2.0538, 0.31293, 0.080416, 0.013095, -0.019246),$$

$$\vec{v} = (0.39122, 0.81467, -0.25082, -0.27852, -0.1723, -0.11441).$$

### $m_{46}^+$ 7

$$I = 1: 4, I = 2: 123, I = 3: 156, I = 4: 256, I = 5: 356,$$

$$T_{10}[1] = 10, T_{10}[2] = 1.231, T_{10}[4] = -0.41407, T_{10}[5] = -0.22002,$$

$$F_2[1, 5] = -0.86747, F_2[1, 6] = 0.80575, F_2[2, 5] = -0.33502, F_2[2, 6] = -0.080621,$$

$$F_2[3, 5] = 0.29941, F_2[3, 6] = -0.12093, F_4[1, 2, 4, 5] = -0.0059089, F_4[1, 2, 4, 6] = 0.0071751,$$

$$F_4[1, 3, 4, 5] = -0.0031397, F_4[1, 3, 4, 6] = 0.0038126, F_4[2, 3, 4, 5] = -0.63918,$$

$$F_4[2, 3, 4, 6] = 0.0013336, H[1, 2, 5] = -0.16391, H[1, 2, 6] = -0.28872, H[1, 3, 6] = -0.31351,$$

$$H[2, 3, 5] = 0.88184, H[2, 3, 6] = 0.72621, f[1, 4, 6] = -0.19050, f[3, 4, 6] = 0.035408,$$

$$f[4, 1, 6] = -0.70120, f[5, 1, 4] = -0.13255, f[6, 1, 4] = 0.16096,$$

$$\mathcal{R}_4 = 0.051861, \quad \mathcal{R}_6 = -0.33773, \quad \eta_V = -2.0672,$$

$$\text{masses}^2 = (4.2779, 1.3549, 0.2529, 0.2332, 0.03157, -0.026802),$$

$$\vec{v} = (0.52897, 0.82878, 0.12912, 0.1256, -0.023729, 0.017464).$$

$m_{46}^+ 8$

$$I = 1: 4, \quad I = 2: 123, \quad I = 3: 156, \quad I = 4: 256, \quad I = 5: 356,$$

$$T_{10}[1] = 10, T_{10}[2] = 1.1329, T_{10}[3] = -0.047213, T_{10}[4] = -0.36849, T_{10}[5] = -0.34388,$$

$$F_2[1, 5] = 1.16, F_2[1, 6] = 0.35495, F_2[2, 5] = 0.058393, F_2[2, 6] = -0.10173,$$

$$F_2[3, 5] = -0.20905, F_2[3, 6] = -0.017627, F_4[1, 3, 4, 5] = 0.047094, F_4[1, 3, 4, 6] = 0.072761,$$

$$F_4[2, 3, 4, 5] = 0.36756, F_4[2, 3, 4, 6] = 0.56788, H[1, 2, 6] = 0.20821, H[1, 3, 5] = 0.081993,$$

$$H[1, 3, 6] = 0.047365, H[2, 3, 5] = 0.18002, H[2, 3, 6] = -1.167, f[1, 4, 5] = -0.14323,$$

$$f[1, 4, 6] = 0.092704, f[2, 4, 5] = -0.013694, f[2, 4, 6] = 0.0088635, f[3, 4, 5] = 0.02839,$$

$$f[3, 4, 6] = -0.018375, f[4, 1, 5] = -0.64444, f[4, 1, 6] = 0.41710, f[4, 2, 5] = 0.082569,$$

$$f[4, 2, 6] = -0.053442, f[5, 1, 4] = 0.24838, f[5, 2, 4] = -0.031823, f[6, 1, 4] = 0.040763,$$

$$f[6, 2, 4] = -0.0052227,$$

$$\mathcal{R}_4 = 0.058901, \quad \mathcal{R}_6 = -0.36229, \quad \eta_V = -2.3554,$$

$$\text{masses}^2 = (4.5142, 1.4638, 0.12601, 0.072419, 0.019515, -0.034684),$$

$$\vec{v} = (-0.59793, -0.79614, -0.032498, -0.0074837, 0.076122, -0.04174).$$

$m_{46}^+ 9$

$$I = 1: 4, \quad I = 2: 123, \quad I = 3: 156,$$

$$T_{10}[1] = 2.3582, T_{10}[2] = 0.48564, T_{10}[3] = -0.14556, F_2[1, 5] = -0.20255,$$

$$F_2[1, 6] = -0.039083, F_2[2, 5] = -0.0014989, F_2[2, 6] = 0.0077682, F_2[3, 5] = 0.0015074,$$

$$F_2[3, 6] = -0.62275, F_4[1, 2, 4, 5] = -0.16121, F_4[1, 2, 4, 6] = -0.19422, F_4[1, 3, 4, 5] = -0.05474,$$

$$F_4[1, 3, 4, 6] = -0.059983, H[1, 2, 5] = -0.58038, H[1, 2, 6] = -0.11199, H[2, 3, 5] = -0.071827,$$

$$H[2, 3, 6] = 0.13254, f[1, 4, 5] = -0.014297, f[1, 4, 6] = 0.011866, f[3, 4, 5] = 0.11639,$$

$$f[3, 4, 6] = -0.096608, f[4, 2, 5] = -0.073867, f[4, 2, 6] = 0.061309, f[4, 3, 5] = 0.22131,$$

$$f[4, 3, 6] = -0.18369, f[5, 2, 4] = 0.0066995, f[5, 3, 4] = -0.020072, f[6, 2, 4] = -0.03472,$$

$$f[6, 3, 4] = 0.10402,$$

$$\mathcal{R}_4 = 0.01948, \quad \mathcal{R}_6 = -0.093534, \quad \eta_V = -2.6418,$$

$$\text{masses}^2 = (0.73377, 0.22015, 0.084047, 0.020082, -0.012866),$$

$$\vec{v} = (0.5243, 0.81491, 0.16459, 0.17724, 0.050354).$$



## Appendix C. Minkowski and (anti-) de Sitter solutions

---

### $m_{46}^+ 10$

$$I = 1: 4, \quad I = 2: 123, \quad I = 3: 156,$$

$$T_{10}[1] = 1.0414, T_{10}[2] = -0.024954, T_{10}[3] = -0.18988, F_2[1, 5] = -0.054017,$$

$$F_2[1, 6] = 0.049286, F_2[2, 5] = 0.11254, F_2[2, 6] = -0.063389, F_2[3, 5] = -0.20671,$$

$$F_2[3, 6] = 0.064899, F_4[1, 2, 4, 5] = 0.16296, F_4[1, 2, 4, 6] = 0.035464, F_4[1, 3, 4, 5] = -0.27918,$$

$$F_4[1, 3, 4, 6] = -0.028805, H[1, 2, 5] = 0.20416, H[1, 2, 6] = 0.14499, H[1, 3, 5] = 0.18054,$$

$$H[1, 3, 6] = 0.0063486, H[2, 3, 5] = 0.049823, H[2, 3, 6] = 0.028726, f[1, 4, 5] = 0.0002223,$$

$$f[1, 4, 6] = 0.0026105, f[2, 4, 5] = -0.00084459, f[2, 4, 6] = -0.0099182, f[3, 4, 5] = 0.00090002,$$

$$f[3, 4, 6] = 0.010569, f[4, 2, 5] = 0.035286, f[4, 2, 6] = 0.41437, f[4, 3, 5] = 0.018223,$$

$$f[4, 3, 6] = 0.21399, f[5, 2, 4] = -0.17188, f[5, 3, 4] = -0.088762, f[6, 2, 4] = -0.18838,$$

$$f[6, 3, 4] = -0.097283,$$

$$\mathcal{R}_4 = 0.0020327, \quad \mathcal{R}_6 = -0.041506, \quad \eta_V = -1.2539,$$

$$\text{masses}^2 = (0.47078, 0.1756, 0.042927, 0.0029872, -0.0006372),$$

$$\vec{v} = (-0.31927, -0.90628, -0.14898, 0.19575, -0.12736).$$

### $m_{55}^+ 1$

$$I = 1: 12, \quad I = 2: 34, \quad I = 3: 56, \quad I = 4: 2456, \quad I = 5: 2356, \quad I = 6: 1456, \quad I = 7: 1356,$$

$$T_{10}[1] = 1, T_{10}[2] = 0.40965, T_{10}[3] = -3.1313 \cdot 10^{-6}, T_{10}[4] = -0.053217, T_{10}[5] = -0.0092735,$$

$$T_{10}[6] = -0.00016486, T_{10}[7] = -0.043252, F_1[5] = -0.22187, F_1[6] = -0.078553,$$

$$F_3[1, 3, 5] = -0.15921, F_3[1, 3, 6] = -0.15796, F_3[1, 4, 5] = -0.20668, F_3[1, 4, 6] = -0.063676,$$

$$F_3[2, 3, 5] = 0.029101, F_3[2, 3, 6] = 0.0063373, F_3[2, 4, 5] = 0.15168, F_3[2, 4, 6] = 0.18072,$$

$$H[1, 2, 5] = 0.1014, H[1, 2, 6] = -0.047922, H[3, 4, 5] = 0.16404, H[3, 4, 6] = -0.12833,$$

$$f[1, 3, 5] = -0.13246, f[1, 3, 6] = 0.2164, f[1, 4, 5] = 0.14238, f[1, 4, 6] = -0.094809,$$

$$f[2, 3, 5] = 0.14693, f[2, 3, 6] = -0.069881, f[2, 4, 5] = -0.039316, f[2, 4, 6] = -0.097488,$$

$$f[3, 1, 5] = -0.068956, f[3, 1, 6] = 0.12569, f[3, 2, 5] = -0.093779, f[3, 2, 6] = 0.056352,$$

$$f[4, 1, 5] = -0.10651, f[4, 1, 6] = 0.08305, f[4, 2, 5] = -0.042607, f[4, 2, 6] = -0.061736,$$

$$f[5, 1, 3] = -0.027059, f[5, 1, 4] = 0.008422, f[5, 2, 3] = -0.0048102, f[5, 2, 4] = -0.017341,$$

$$f[6, 1, 3] = -0.0082548, f[6, 1, 4] = -0.0090315, f[6, 2, 3] = 0.013849, f[6, 2, 4] = -0.019847,$$

$$\mathcal{R}_4 = 0.012683, \quad \mathcal{R}_6 = -0.095557, \quad \eta_V = -2.5435,$$

$$\text{masses}^2 = (0.25785, 0.19856, 0.13284, 0.061518, 0.054618, -0.0080648),$$

$$\vec{v} = (0.47634, 0.83174, 0.19612, 0.20396, 0.0040682, 0.034975).$$

### $m_{55}^+ 2$

$$I = 1: 12, I = 2: 34, I = 4: 2456, I = 6: 1456, I = 7: 1356,$$

$$T_{10}[1] = 1, T_{10}[2] = 0.52948, T_{10}[4] = -0.10152, T_{10}[6] = -0.046308, T_{10}[7] = -0.037988,$$

$$F_1[5] = 0.1755, F_1[6] = 0.091816, F_3[1, 3, 5] = -0.15299, F_3[1, 3, 6] = -0.057731,$$

$$F_3[1, 4, 5] = 0.20799, F_3[1, 4, 6] = -0.046086, F_3[2, 3, 5] = -0.19793, F_3[2, 3, 6] = -0.15965,$$

$$F_3[2, 4, 5] = 0.16758, F_3[2, 4, 6] = -0.040334, H[1, 2, 5] = -0.032156, H[1, 2, 6] = 0.1053$$

$$, H[3, 4, 5] = -0.051015, H[3, 4, 6] = 0.14757, f[1, 3, 5] = -0.031329, f[1, 3, 6] = -0.17231,$$

$$f[1, 4, 5] = 0.085189, f[1, 4, 6] = -0.10795, f[2, 3, 5] = -0.00037676, f[2, 3, 6] = -0.12381,$$

$$f[2, 4, 5] = 0.18707, f[2, 4, 6] = -0.1351, f[3, 1, 5] = -0.034965, f[3, 1, 6] = -0.19981,$$

$$f[3, 2, 5] = -0.0015592, f[3, 2, 6] = 0.1123, f[4, 1, 5] = -0.046789, f[4, 1, 6] = 0.05653,$$

$$f[4, 2, 5] = 0.079254, f[4, 2, 6] = -0.05598, f[5, 1, 3] = 0.031953, f[5, 1, 4] = -0.018806,$$

$$f[5, 2, 3] = -0.011485, f[5, 2, 4] = 0.041502, f[6, 1, 3] = 0.077132, f[6, 1, 4] = 0.035947,$$

$$f[6, 2, 3] = -0.04109, f[6, 2, 4] = -0.027612,$$

$$\mathcal{R}_4 = 0.025958, \quad \mathcal{R}_6 = -0.12355, \quad \eta_V = -2.6059,$$

$$\text{masses}^2 = (0.26217, 0.16278, 0.12817, 0.066834, 0.06477, -0.016911),$$

$$\vec{v} = (0.45995, 0.86092, 0.1783, 0.12363, 0.011867, 0.0073728).$$

### $m_{55}^+ 3$

$$I = 1: 12, I = 2: 34, I = 4: 2456, I = 6: 1456, I = 7: 1356,$$

$$T_{10}[1] = 1, T_{10}[2] = 0.39649, T_{10}[4] = -0.13597, T_{10}[6] = -0.0044617, T_{10}[7] = -0.0016095,$$

$$F_1[5] = 0.059917, F_1[6] = 0.02568, F_3[1, 3, 5] = 0.00041564, F_3[1, 3, 6] = 0.00015725,$$

$$F_3[1, 4, 5] = -0.037163, F_3[1, 4, 6] = 0.23926, F_3[2, 3, 5] = 0.10469, F_3[2, 3, 6] = -0.075765,$$

$$F_3[2, 4, 5] = 0.25509, F_3[2, 4, 6] = -0.22331, H[1, 2, 5] = 0.018151, H[1, 2, 6] = 0.012143,$$

$$H[3, 4, 5] = -0.024397, H[3, 4, 6] = 0.02125, f[1, 3, 5] = 0.34509, f[1, 3, 6] = 0.21035,$$

$$f[1, 4, 5] = -0.0017562, f[1, 4, 6] = -0.00080959, f[2, 3, 6] = -0.27667, f[2, 4, 5] = -0.053521,$$

$$f[2, 4, 6] = 0.075134, f[3, 1, 5] = 0.055747, f[3, 1, 6] = 0.033981, f[3, 2, 6] = -0.00027177,$$

$$f[4, 1, 5] = 0.15453, f[4, 1, 6] = 0.071239, f[4, 2, 5] = 0.028637, f[4, 2, 6] = -0.040202,$$

$$f[5, 1, 3] = 0.20748, f[5, 1, 4] = 0.0034883, f[5, 2, 3] = -0.0293, f[5, 2, 4] = 0.011216,$$

$$f[6, 1, 3] = 0.17777, f[6, 1, 4] = -0.0081389, f[6, 2, 3] = 0.046644, f[6, 2, 4] = -0.018335,$$

## Appendix C. Minkowski and (anti-) de Sitter solutions

---

$$\begin{aligned}\mathcal{R}_4 &= 0.020481, \quad \mathcal{R}_6 = -0.12722, \quad \eta_V = -2.7126, \\ \text{masses}^2 &= (0.43621, 0.3025, 0.07476, 0.029728, 0.017301, -0.01389), \\ \vec{v} &= (0.55604, 0.81549, 0.098113, 0.096111, 0.07969, 0.024069).\end{aligned}$$

### $m_{554}^+$

$$\begin{aligned}I = 1: 12, \quad I = 2: 34, \quad I = 3: 56, \quad I = 4: 2456, \quad I = 5: 2356, \quad I = 6: 1456, \quad I = 7: 1356, \\ T_{10}[1] = 1, T_{10}[2] = 0.79176, T_{10}[3] = -0.026181, T_{10}[4] = -0.11482, T_{10}[5] = -0.058768, \\ T_{10}[6] = -0.07157, T_{10}[7] = -0.036564, F_1[5] = 0.049133, F_1[6] = -0.3157, \\ F_3[1, 3, 5] = 0.0023854, F_3[1, 3, 6] = 0.13983, F_3[1, 4, 5] = -0.0018503, F_3[1, 4, 6] = -0.10956, \\ F_3[2, 3, 5] = 0.0093444, F_3[2, 3, 6] = 0.30172, F_3[2, 4, 5] = 0.0078262, F_3[2, 4, 6] = -0.024632, \\ H[1, 2, 5] = 0.23093, H[1, 2, 6] = -0.053949, H[3, 4, 5] = 0.21663, H[3, 4, 6] = 0.022755, \\ f[1, 3, 5] = -0.058367, f[1, 3, 6] = 0.011708, f[1, 4, 5] = -0.13198, f[1, 4, 6] = -0.065907, \\ f[2, 3, 5] = -0.042264, f[2, 3, 6] = -0.037247, f[2, 4, 5] = -0.23808, f[2, 4, 6] = -0.077091, \\ f[3, 1, 5] = -0.15019, f[3, 1, 6] = 0.1257, f[3, 2, 5] = 0.037172, f[3, 2, 6] = -0.099223, \\ f[4, 1, 5] = -0.020208, f[4, 1, 6] = -0.052354, f[4, 2, 5] = -0.097708, f[4, 2, 6] = -0.0082088, \\ f[5, 1, 3] = 0.015919, f[5, 1, 4] = -0.0081269, f[5, 2, 3] = -0.0099126, f[5, 2, 4] = 0.005096, \\ f[6, 1, 3] = -0.042985, f[6, 1, 4] = 0.022004, f[6, 2, 3] = 0.026795, f[6, 2, 4] = -0.013684, \\ \mathcal{R}_4 &= 0.033613, \quad \mathcal{R}_6 = -0.11129, \quad \eta_V = -3.3574, \\ \text{masses}^2 &= (0.32162, 0.2238, 0.097703, 0.080953, 0.04155, -0.028213), \\ \vec{v} &= (0.42536, 0.89622, 0.095324, 0.069018, -0.01847, -0.040805).\end{aligned}$$

### $m_{55771}^+$

$$\begin{aligned}I = 1: 12, \quad I = 2: 34, \quad I = 3: 1356, \quad I = 4: 2456, \\ T_{10}[1] = 1, T_{10}[2] = -0.07936, T_{10}[3] = 0.40065, T_{10}[4] = -0.40663, F_1[5] = 0.26286, \\ F_1[6] = -0.053736, F_3[1, 4, 5] = -0.25386, F_3[2, 3, 5] = 0.044692, F_3[1, 4, 6] = 0.091146, \\ F_3[2, 3, 6] = -0.0632, H[1, 2, 5] = -0.016356, H[3, 4, 5] = 0.25937, H[1, 2, 6] = -0.041749, \\ H[3, 4, 6] = 0.038482, f[5, 1, 3] = 0.25208, f[5, 2, 4] = -0.17534, f[6, 1, 3] = 0.28717, \\ f[6, 2, 4] = 0.074302, f[1, 3, 5] = 0.2044, f[1, 3, 6] = 0.48235, f[2, 4, 5] = 0.063944, \\ f[2, 4, 6] = -0.05613, f[3, 1, 5] = -0.0062549, f[3, 1, 6] = -0.01476, f[4, 2, 5] = 0.0024215, \\ f[4, 2, 6] = -0.0021256, \\ \mathcal{R}_4 &= 0.0019652, \quad \mathcal{R}_6 = -0.042929, \quad \eta_V = -4.7535,\end{aligned}$$

$$\text{masses}^2 = (0.4787, 0.24925, 0.029271, 0.014598, -0.0023354),$$

$$\vec{v} = (0.12012, -0.95576, -0.028666, 0.25498, -0.079111).$$

### $m_{5577}^+ 2$

$$I = 1: 12, I = 2: 34, I = 3: 1356, I = 4: 2456,$$

$$T_{10}[1] = 0.39149, T_{10}[2] = -0.037084, T_{10}[3] = -0.071447, T_{10}[4] = 0.65108, F_1[5] = -0.084985,$$

$$F_1[6] = -0.31118, F_3[1, 4, 5] = -0.0059985, F_3[2, 3, 5] = -0.01598, F_3[1, 4, 6] = -0.093141,$$

$$F_3[2, 3, 6] = -0.032537, H[1, 2, 5] = -0.034905, H[3, 4, 5] = 0.11369, H[1, 2, 6] = 0.0038944,$$

$$H[3, 4, 6] = -0.0010591, f[5, 1, 3] = 0.073946, f[5, 2, 4] = -0.0016865, f[6, 1, 3] = 0.24134,$$

$$f[6, 2, 4] = -0.02824, f[1, 3, 5] = -0.25493, f[1, 3, 6] = 0.015225, f[2, 4, 5] = 0.15877,$$

$$f[2, 4, 6] = -0.048646, f[3, 1, 5] = 0.18839, f[3, 1, 6] = -0.011251, f[4, 2, 5] = 0.01366,$$

$$f[4, 2, 6] = -0.0041853,$$

$$\mathcal{R}_4 = 0.017441, \quad \mathcal{R}_6 = -0.076121, \quad \eta_V = -3.5034,$$

$$\text{masses}^2 = (0.26179, 0.13316, 0.014967, 0.0080815, -0.015276),$$

$$\vec{v} = (0.37062, 0.92139, -0.027258, -0.078704, -0.082072).$$

### $m_{5577}^+ 3$

$$I = 1: 12, I = 2: 34, I = 3: 1356, I = 4: 2456,$$

$$T_{10}[1] = 0.10391, T_{10}[2] = 0.16488, T_{10}[3] = -0.016864, T_{10}[4] = -0.016864, F_1[5] = -0.025133,$$

$$F_1[6] = -0.16238, F_3[1, 4, 5] = -0.021515, F_3[2, 3, 5] = -0.01636, F_3[1, 4, 6] = 0.074891,$$

$$F_3[2, 3, 6] = -0.051884, H[1, 2, 5] = 0.1121, H[3, 4, 5] = 0.076829, H[1, 2, 6] = -0.069412,$$

$$H[3, 4, 6] = 0.058085, f[6, 1, 3] = -0.012982, f[6, 2, 4] = -0.012982, f[1, 3, 5] = 0.055126,$$

$$f[2, 4, 5] = 0.041919, f[3, 1, 5] = 0.050093, f[4, 2, 5] = 0.065875,$$

$$\mathcal{R}_4 = 0.0045531, \quad \mathcal{R}_6 = -0.011514, \quad \eta_V = -3.2722,$$

$$\text{masses}^2 = (0.070903, 0.014266, 0.0087496, 0.0024451, -0.0037247),$$

$$\vec{v} = (0.4319, 0.88855, 0.1044, 0.1142, 0).$$

## Appendix C. Minkowski and (anti-) de Sitter solutions

---

### $m_{5577}^+4$

$$I = 1: 12, \quad I = 2: 34, \quad I = 3: 1356, \quad I = 4: 2456,$$

$$T_{10}[1] = 0.45199, T_{10}[2] = 0.29433, T_{10}[3] = -0.043543, T_{10}[4] = -0.043543, F_1[5] = 0.051509,$$

$$F_1[6] = 0.26368, F_3[1, 4, 5] = -0.030379, F_3[2, 3, 5] = -0.052113, F_3[1, 4, 6] = -0.072095,$$

$$F_3[2, 3, 6] = 0.14403, H[1, 2, 5] = -0.13471, H[3, 4, 5] = -0.17112, H[1, 2, 6] = -0.094273,$$

$$H[3, 4, 6] = 0.12252, f[6, 1, 3] = 0.020642, f[6, 2, 4] = 0.020642, f[1, 3, 5] = -0.074879,$$

$$f[2, 4, 5] = -0.12845, f[3, 1, 5] = -0.098833, f[4, 2, 5] = -0.057615,$$

$$\mathcal{R}_4 = 0.011738, \quad \mathcal{R}_6 = -0.032824, \quad \eta_V = -3.1779,$$

$$\text{masses}^2 = (0.18893, 0.041491, 0.024343, 0.006295, -0.0093255),$$

$$\vec{v} = (0.43789, 0.88332, 0.12479, 0.11147, 0).$$

### $m_{5577}^+5$

$$I = 1: 12, \quad I = 2: 34, \quad I = 3: 1356, \quad I = 4: 2456,$$

$$T_{10}[1] = -0.064412, T_{10}[2] = 0.4785, T_{10}[3] = -0.007451, T_{10}[4] = -0.007451, F_1[5] = 0.15359,$$

$$F_1[6] = 0.18186, F_3[1, 4, 5] = 0.0023579, F_3[2, 3, 5] = -0.0023524, F_3[1, 4, 6] = -0.067459,$$

$$F_3[2, 3, 6] = -0.063327, H[1, 2, 5] = -0.12592, H[3, 4, 5] = 0.11951, H[1, 2, 6] = 0.13358,$$

$$H[3, 4, 6] = -0.092897, f[6, 1, 3] = 0.0051214, f[6, 2, 4] = 0.0051214, f[1, 3, 5] = -0.19341,$$

$$f[2, 4, 5] = 0.19295, f[3, 1, 5] = 0.27746, f[4, 2, 5] = -0.27812,$$

$$\mathcal{R}_4 = 0.0019152, \quad \mathcal{R}_6 = -0.0071851, \quad \eta_V = -4.7957,$$

$$\text{masses}^2 = (0.26356, 0.13546, 0.0012618, 0.00098383, -0.0022962),$$

$$\vec{v} = (0.35331, 0.93501, -0.027321, 0.013431, 0).$$

### $m_{5577}^+6$

$$I = 1: 12, \quad I = 2: 34, \quad I = 3: 1356, \quad I = 4: 2456,$$

$$T_{10}[1] = 0.67182, T_{10}[2] = -0.094833, T_{10}[3] = -0.009195, T_{10}[4] = T_{10}[3], F_1[5] = -0.18732,$$

$$F_1[6] = -0.21629, F_3[1, 4, 6] = -0.069422, F_3[2, 3, 6] = F_3[1, 4, 6], H[1, 2, 5] = -0.14442,$$

$$H[3, 4, 5] = 0.14945, H[1, 2, 6] = 0.11761, H[3, 4, 6] = -0.15745, f[1, 3, 5] = -0.36121,$$

$$f[2, 4, 5] = -f[1, 3, 5], f[3, 1, 5] = 0.26982, f[4, 2, 5] = -f[3, 1, 5], f[6, 1, 3] = -0.0053141,$$

$$f[6, 2, 4] = f[6, 1, 3],$$

$$\mathcal{R}_4 = 0.0023552, \quad \mathcal{R}_6 = -0.0083805, \quad \eta_V = -4.9129,$$

$$\text{masses}^2 = (0.45272, 0.19968, 0.0014455, 0.0012059, -0.0028928),$$

$$\vec{v} = (0.35065, 0.93594, 0.0020433, -0.032402, 0).$$

$m_{5577}^+$ 7

$$I = 1: 12, I = 2: 34, I = 3: 1356, I = 4: 2456,$$

$$T_{10}[1] = 1, T_{10}[2] = 0.96829, T_{10}[4] = -0.28566, T_{10}[3] = -0.13815, F_1[5] = -0.30382,$$

$$F_1[6] = -0.33842, F_3[1, 4, 5] = 0.048987, F_3[1, 4, 6] = 0.05421, F_3[2, 3, 5] = -0.12112,$$

$$F_3[2, 3, 6] = -0.10184, H[1, 2, 5] = -0.024807, H[1, 2, 6] = -0.3069, H[3, 4, 5] = 0.29781,$$

$$H[3, 4, 6] = -0.1961, f[1, 3, 5] = 0.049702, f[1, 3, 6] = -0.030596, f[2, 4, 5] = -0.020729,$$

$$f[2, 4, 6] = -0.034844, f[3, 1, 5] = 0.4302, f[3, 1, 6] = -0.26482, f[4, 2, 5] = -0.022984,$$

$$f[4, 2, 6] = -0.038634, f[5, 1, 3] = -0.34838, f[5, 2, 4] = -0.020232, f[6, 1, 3] = 0.20726,$$

$$f[6, 2, 4] = -0.032866,$$

$$\mathcal{R}_4 = 0.037858, \quad \mathcal{R}_6 = -0.064418, \quad \eta_V = -3.421,$$

$$\text{masses}^2 = (0.62528, 0.47689, 0.057455, 0.026924, -0.032378),$$

$$\vec{v} = (0.39299, 0.91772, 0.03649, 0.021945, -0.039089).$$

$m_{5577}^+$ 8

$$I = 1: 12, I = 2: 34, I = 3: 1356, I = 4: 2456,$$

$$T_{10}[1] = 1, f[2, 4, 5] = 0, T_{10}[2] = 0.38463, T_{10}[4] = -0.075911, T_{10}[3] = -0.070294,$$

$$F_1[5] = -0.40134, F_1[6] = -0.1518, F_3[1, 4, 5] = 0.069139, F_3[1, 4, 6] = 0.025857,$$

$$F_3[2, 3, 5] = -0.050848, F_3[2, 3, 6] = -0.025092, H[1, 2, 5] = -0.10906, H[1, 2, 6] = -0.1663,$$

$$H[3, 4, 5] = 0.16742, H[3, 4, 6] = -0.33927, f[1, 3, 5] = 0.030643, f[1, 3, 6] = -0.062096,$$

$$f[2, 4, 6] = 0, f[3, 1, 5] = 0.10625, f[3, 1, 6] = -0.2153, f[4, 2, 5] = -0.027693,$$

$$f[4, 2, 6] = -0.014767, f[5, 1, 3] = -0.081342, f[5, 2, 4] = -0.01845, f[6, 1, 3] = 0.15255,$$

$$f[6, 2, 4] = -0.0091045,$$

$$\mathcal{R}_4 = 0.019711, \quad \mathcal{R}_6 = -0.034616, \quad \eta_V = -3.5611,$$

$$\text{masses}^2 = (0.509, 0.1253, 0.029292, 0.013056, -0.017548),$$

$$\vec{v} = (0.39247, 0.91709, 0.056825, 0.033463, -0.023711).$$

## Appendix C. Minkowski and (anti-) de Sitter solutions

---

### $m_{5577}^+9$

$$I = 1: 12, I = 2: 34, I = 3: 1356, I = 4: 2456,$$

$$T_{10}[1] = 1, T_{10}[2] = 0.35086, T_{10}[4] = -0.000037783, T_{10}[3] = -0.090423, F_1[5] = 0.17143,$$

$$F_1[6] = 0.17787, F_3[1, 4, 5] = 0.35651, F_3[1, 4, 6] = 0.11205, F_3[2, 3, 5] = -0.025709,$$

$$F_3[2, 3, 6] = -0.015791, H[1, 2, 5] = -0.00038072, H[1, 2, 6] = 0.16276, H[3, 4, 5] = -0.095935,$$

$$H[3, 4, 6] = 0.15619, f[1, 3, 5] = 0.17737, f[1, 3, 6] = -0.28878, f[3, 1, 5] = 0.027193,$$

$$f[3, 1, 6] = -0.044273, f[4, 2, 5] = -0.11253, f[4, 2, 6] = -0.11655, f[5, 1, 3] = -0.014749,$$

$$f[5, 2, 4] = 0.04027, f[6, 1, 3] = 0.014241, f[6, 2, 4] = 0.024734,$$

$$\mathcal{R}_4 = 0.012244, \quad \mathcal{R}_6 = -0.089117, \quad \eta_V = -2.9333,$$

$$\text{masses}^2 = (0.19582, 0.089391, 0.046288, 0.0069341, -0.0089789),$$

$$\vec{v} = (0.45671, 0.85731, 0.20184, 0.1253, -0.00083919).$$

### $m_{5577}^+10$

$$I = 1: 12, I = 2: 34, I = 3: 1356, I = 4: 2456,$$

$$T_{10}[1] = 1, T_{10}[2] = 0.22554, T_{10}[4] = -0.0017644, T_{10}[3] = -0.05895, F_1[5] = 0.018004,$$

$$F_1[6] = 0.22278, F_3[1, 4, 5] = 0.13535, F_3[1, 4, 6] = -0.34611, F_3[2, 3, 5] = -0.003407,$$

$$F_3[2, 3, 6] = 0.01705, H[1, 2, 5] = -0.093626, H[1, 2, 6] = -0.086751, H[3, 4, 5] = -0.17802,$$

$$H[3, 4, 6] = -0.035572, f[1, 3, 5] = -0.34208, f[1, 3, 6] = -0.068354, f[3, 1, 5] = -0.033679,$$

$$f[3, 1, 6] = -0.0067298, f[4, 2, 5] = 0, f[4, 2, 6] = -0.13075, f[5, 1, 3] = 0.01225,$$

$$f[5, 2, 4] = -0.0067179, f[6, 2, 4] = 0.033619,$$

$$\mathcal{R}_4 = 0.008297, \quad \mathcal{R}_6 = -0.082007, \quad \eta_V = -2.9003,$$

$$\text{masses}^2 = (0.18601, 0.074824, 0.031424, 0.0045174, -0.0060158),$$

$$\vec{v} = (0.4472, 0.85893, 0.21089, 0.1333, -0.0034951).$$

$m_{5577}^+ 11$

$$I = 1: 12, I = 2: 34, I = 3: 1356, I = 4: 2456,$$

$$\begin{aligned} T_{10}[1] &= 1, T_{10}[2] = 0.22558, T_{10}[4] = -0.03301, T_{10}[3] = -0.047252, F_1[5] = 0.07129, \\ F_1[6] &= 0.40424, F_3[1, 4, 5] = -0.019431, F_3[1, 4, 6] = -0.10771, F_3[2, 3, 5] = 0.0026386, \\ F_3[2, 3, 6] &= 0.022276, H[1, 2, 5] = -0.060697, H[1, 2, 6] = 0.13547, H[3, 4, 5] = -0.37583, \\ H[3, 4, 6] &= 0.044517, f[1, 3, 5] = -0.10513, f[1, 3, 6] = 0.012452, f[3, 1, 5] = -0.11979, \\ f[3, 1, 6] &= 0.014189, f[4, 2, 6] = 0.035884, f[5, 1, 3] = 0.057879, f[5, 2, 4] = 0.0016953, \\ f[6, 2, 4] &= 0.014312, \end{aligned}$$

$$\mathcal{R}_4 = 0.013256, \quad \mathcal{R}_6 = -0.027736, \quad \eta_V = -3.4806,$$

$$\text{masses}^2 = (0.47349, 0.044026, 0.019742, 0.0073066, -0.011535),$$

$$\vec{v} = (0.40291, 0.90746, 0.098306, 0.066818, -0.007421).$$

$m_{5577}^+ 12$

$$I = 1: 12, I = 2: 34, I = 3: 1356, I = 4: 2456,$$

$$\begin{aligned} T_{10}[1] &= 1, T_{10}[2] = -0.020994, T_{10}[3] = -0.44158, T_{10}[4] = 0.35501, F_1[5] = -0.28314, \\ F_1[6] &= 0.020063, F_3[1, 4, 5] = -0.096704, F_3[1, 4, 6] = 0.01269, F_3[2, 3, 5] = -0.14117, \\ F_3[2, 3, 6] &= 0.16128, H[1, 2, 5] = 0.0073583, H[1, 2, 6] = 0.0098314, H[3, 4, 5] = 0.16407, \\ H[3, 4, 6] &= -0.21909, f[1, 3, 5] = -0.083967, f[1, 3, 6] = 0.062978, f[2, 4, 5] = -0.28112, \\ f[2, 4, 6] &= -0.40774, f[3, 1, 5] = 0.0024625, f[3, 1, 6] = -0.001847, f[5, 1, 3] = 0.14943, \\ f[5, 2, 4] &= -0.21529, f[6, 1, 3] = -0.10302, f[6, 2, 4] = -0.28704, f[4, 2, 5] = -0.0028201, \\ f[4, 2, 6] &= -0.0040902, \end{aligned}$$

$$\mathcal{R}_4 = 0.016322, \quad \mathcal{R}_6 = -0.05496, \quad \eta_V = -2.8966,$$

$$\text{masses}^2 = (0.44749, 0.25896, 0.026744, 0.010937, -0.011819),$$

$$\vec{v} = (0.19862, 0.96945, 0.0087219, -0.14259, -0.01742).$$



$m_{5577}^{*+}1$

$$\begin{aligned}
 I = 1: 12, \quad I = 2: 34, \quad I = 3: 1456, \quad I = 4: 2356, \\
 T_{10}[1] = 1, T_{10}[2] = -0.14921, T_{10}[3] = -0.010785, T_{10}[4] = T_{10}[3], F_1[5] = 0.23733, \\
 F_1[6] = 0.26419, F_3[1, 3, 6] = -0.071529, F_3[2, 4, 6] = -F_3[1, 3, 6], H[1, 2, 5] = 0.17952, \\
 H[1, 2, 6] = -0.15497, H[3, 4, 5] = -0.18274, H[3, 4, 6] = 0.19088, f[1, 4, 5] = 0.5109, \\
 f[2, 3, 5] = f[1, 4, 5], f[3, 2, 5] = -0.41478, f[4, 1, 5] = f[3, 2, 5], f[6, 1, 4] = -0.0051027, \\
 f[6, 2, 3] = f[6, 1, 4],
 \end{aligned}$$

$$\mathcal{R}_4 = 0.0027482, \quad \mathcal{R}_6 = -0.0092648, \quad \eta_V = -5.0483,$$

$$\text{masses}^2 = (0.93309, 0.31193, 0.00155, 0.0014002, -0.0034685),$$

$$\vec{v} = (0.34756, 0.93684, -0.011322, -0.037404, 0).$$

## C.2 Minkowski solutions

$s_{555}^01$

$$\begin{aligned}
 I = 1: 12, \quad I = 2: 34, \quad I = 3: 56, \\
 T_{10}[1] = 0.0053035, T_{10}[2] = -0.036698, T_{10}[3] = 0.23829, F_3[1, 3, 5] = 0.079466, \\
 F_3[1, 3, 6] = -0.10085, F_3[1, 4, 5] = 0.083997, F_3[1, 4, 6] = -0.029797, F_3[2, 3, 5] = 0.052531, \\
 F_3[2, 3, 6] = 0.047731, F_3[2, 4, 5] = -0.069737, F_3[2, 4, 6] = -0.01231, f[1, 3, 5] = 0.003039, \\
 f[1, 3, 6] = 0.0013338, f[1, 4, 5] = 0.0048401, f[1, 4, 6] = 0.0089686, f[2, 3, 5] = -0.0020841, \\
 f[2, 3, 6] = 0.0024116, f[2, 4, 5] = 0.00016488, f[2, 4, 6] = -0.0057166, f[3, 1, 5] = 0.030623, \\
 f[3, 1, 6] = 0.032105, f[3, 2, 5] = 0.020769, f[3, 2, 6] = 0.0031838, f[4, 1, 5] = 0.023694, \\
 f[4, 1, 6] = 0.032186, f[4, 2, 5] = 0.0093169, f[4, 2, 6] = 0.020989, f[5, 1, 3] = -0.073303, \\
 f[5, 1, 4] = -0.091413, f[5, 2, 3] = -0.11303, f[5, 2, 4] = 0.045887, f[6, 1, 3] = -0.0028902, \\
 f[6, 1, 4] = -0.07716, f[6, 2, 3] = 0.060108, f[6, 2, 4] = -0.11056,
 \end{aligned}$$

$$\mathcal{R}_4 = 0, \quad \mathcal{R}_6 = -0.017241,$$

$$\text{masses}^2 = (0.052928, 0.0021215, 0.00005291, 0).$$

$s_{555}^0 2$

$$I = 1: 12, I = 2: 34, I = 3: 56,$$

$$\begin{aligned} T_{10}[1] &= 1, T_{10}[2] = -0.01029, T_{10}[3] = 0.40819, F_3[1, 3, 6] = 0.25963, F_3[1, 4, 6] = 0.1769, \\ F_3[2, 3, 6] &= 0.31373, F_3[2, 4, 6] = -0.18935, f[1, 3, 5] = 0.25151, f[1, 4, 5] = 0.19442, \\ f[2, 3, 5] &= 0.15194, f[2, 4, 5] = -0.64202, f[3, 1, 5] = 0.13744, f[3, 2, 5] = -0.076135, \\ f[4, 1, 5] &= -0.19357, f[4, 2, 5] = 0.55299, f[6, 1, 3] = 0.084844, f[6, 1, 4] = -0.071486, \\ f[6, 2, 3] &= -0.0021672, f[6, 2, 4] = 0.23605, \end{aligned}$$

$$\mathcal{R}_4 = 0, \quad \mathcal{R}_6 = -0.11649,$$

$$\text{masses}^2 = (0.83127, 0.07301, 0.068032, 0).$$

$s_{555}^0 3$

$$I = 1: 12, I = 2: 34, I = 3: 56,$$

$$\begin{aligned} T_{10}[1] &= 1, T_{10}[2] = 0.45016, T_{10}[3] = 0.2758, F_3[1, 3, 6] = -0.15407, F_3[1, 4, 6] = 0.44154, \\ F_3[2, 3, 6] &= 0.21176, F_3[2, 4, 6] = 0.15532, f[1, 3, 5] = 0.40512, f[1, 4, 5] = 0.010458, \\ f[2, 3, 5] &= 0.12269, f[2, 4, 5] = 0.15527, f[3, 1, 5] = -0.0096352, f[3, 2, 5] = -0.24852, \\ f[4, 1, 5] &= -0.22339, f[6, 1, 3] = -0.1286, f[6, 2, 3] = -0.10094, f[6, 2, 4] = -0.13871, \end{aligned}$$

$$\mathcal{R}_4 = 0, \quad \mathcal{R}_6 = -0.14383,$$

$$\text{masses}^2 = (0.2163, 0.098852, 0.045967, 0).$$

$s_{555}^0 4$

$$I = 1: 12, I = 2: 34, I = 3: 56,$$

$$\begin{aligned} T_{10}[1] &= 1, T_{10}[2] = -0.11111, T_{10}[3] = 0.46692, F_3[1, 3, 6] = -0.11301, F_3[1, 4, 6] = 0.34733, \\ F_3[2, 3, 6] &= 0.30083, F_3[2, 4, 6] = -0.045329, f[1, 3, 5] = 0.2766, f[1, 4, 5] = -0.17052, \\ f[2, 3, 5] &= -0.27582, f[2, 4, 5] = -0.25716, f[3, 2, 5] = 0.21512, f[4, 1, 5] = 0.12779, \\ f[6, 1, 3] &= -0.12305, f[6, 2, 3] = -0.14059, f[6, 2, 4] = -0.20715, \end{aligned}$$

$$\mathcal{R}_4 = 0, \quad \mathcal{R}_6 = -0.11298,$$

$$\text{masses}^2 = (0.27831, 0.077819, 0.032095, 0).$$

## Appendix C. Minkowski and (anti-) de Sitter solutions

---

### $m_{46}^0 1$

$$I = 1: 4, \quad I = 2: 123, \quad I = 3: 156,$$

$$\begin{aligned} T_{10}[1] &= 2.1676, T_{10}[2] = 0.0094995, T_{10}[3] = -1, F_2[2, 5] = 0.019929, F_2[2, 6] = 0.33076, \\ F_2[3, 5] &= 0.010943, F_2[3, 6] = 0.099361, F_4[1, 2, 4, 5] = -0.13174, F_4[1, 2, 4, 6] = 0.38654, \\ F_4[1, 3, 4, 5] &= -0.049892, F_4[1, 3, 4, 6] = 0.054594, H[1, 2, 5] = 0.063142, H[1, 2, 6] = 0.09965, \\ H[1, 3, 5] &= -0.30783, H[1, 3, 6] = -0.39066, f[2, 4, 5] = -0.0037153, f[2, 4, 6] = 0.0017274, \\ f[3, 4, 5] &= -0.00089793, f[3, 4, 6] = 0.00041749, f[4, 2, 5] = 0.087441, f[4, 2, 6] = -0.040656, \\ f[4, 3, 5] &= -1.0193, f[4, 3, 6] = 0.47393, f[5, 2, 4] = -0.073129, f[5, 3, 4] = 0.85247, \\ f[6, 2, 4] &= 0.040618, f[6, 3, 4] = -0.47349, \end{aligned}$$

$$\mathcal{R}_4 = 0, \quad \mathcal{R}_6 = -0.015368,$$

$$\text{masses}^2 = (3.3631, 0.45394, 0.067729, 9.1638 \cdot 10^{-6}, 0).$$

### $m_{46}^0 2$

$$I = 1: 4, \quad I = 2: 123, \quad I = 3: 156,$$

$$\begin{aligned} T_{10}[1] &= 0.13033, T_{10}[2] = 0.59346, T_{10}[3] = -0.25891, F_2[2, 5] = -0.11038, F_2[2, 6] = -0.23729, \\ F_2[3, 5] &= -0.0057951, F_2[3, 6] = -0.073035, H[1, 2, 5] = -0.11108, H[1, 2, 6] = 0.071214, \\ H[1, 3, 5] &= 0.033558, H[1, 3, 6] = -0.086773, f[2, 4, 5] = 0.26228, f[2, 4, 6] = -0.40397, \\ f[3, 4, 5] &= -0.30188, f[5, 2, 4] = 0.18217, f[5, 3, 4] = -0.20391, f[6, 2, 4] = -0.31933, \\ f[6, 3, 4] &= 0.15688, \end{aligned}$$

$$\mathcal{R}_4 = 0, \quad \mathcal{R}_6 = -0.023897,$$

$$\text{masses}^2 = (0.52608, 0.077079, 0.021226, 0, 0).$$

### $m_{466}^0 1$

$$I = 1: 4, \quad I = 2: 123, \quad I = 3: 156,$$

$$\begin{aligned} T_{10}[1] &= 0.15998, T_{10}[2] = -0.17570, T_{10}[3] = 0.54357, F_2[2, 5] = 0.23575, \\ F_2[2, 6] &= -0.058553, F_2[3, 5] = -0.07524, F_2[3, 6] = 0.14100, H[1, 2, 5] = 0.076732, \\ H[1, 2, 6] &= 0.13386, H[1, 3, 5] = -0.064786, H[1, 3, 6] = 0.063202, f[2, 4, 5] = -0.05151, \\ f[2, 4, 6] &= 0.01468, f[3, 4, 5] = 0.24009, f[3, 4, 6] = -0.11041, f[5, 2, 4] = 0.098223, \\ f[5, 3, 4] &= 0.33923, f[6, 2, 4] = 0.14162, f[6, 3, 4] = -0.17514, \end{aligned}$$

$$\mathcal{R}_4 = 0, \quad \mathcal{R}_6 = -0.026276,$$

$$\text{masses}^2 = (0.26972, 0.074729, 0.020261, 0, 0).$$

$m_{466}^0 2$

$$I = 1: 4, \quad I = 2: 123, \quad I = 3: 156,$$

$$\begin{aligned} T_{10}[1] &= 0.00089705, T_{10}[2] = -0.12343, T_{10}[3] = 0.67703, F_2[2, 6] = -0.073204, \\ F_2[3, 5] &= 0.095626, F_2[3, 6] = -0.25448, H[1, 2, 5] = -0.0019212, H[1, 2, 6] = 0.0099455, \\ H[1, 3, 5] &= 0.0087639, H[1, 3, 6] = 0.000016316, f[2, 4, 5] = -0.11340, f[2, 4, 6] = 0.12143, \\ f[3, 4, 5] &= 0.001685, f[3, 4, 6] = -0.10207, f[5, 2, 4] = -0.09093, f[5, 3, 4] = 0.17684, \\ f[6, 2, 4] &= 0.33283, f[6, 3, 4] = -0.04542, \end{aligned}$$

$$\mathcal{R}_4 = 0, \quad \mathcal{R}_6 = -0.039542,$$

$$\text{masses}^2 = (0.23513, 0.03448, 0.00023868, 0, 0).$$

$m_{466}^0 3$

$$I = 1: 4, \quad I = 2: 123, \quad I = 3: 156,$$

$$\begin{aligned} T_{10}[1] &= 0.038745, T_{10}[2] = -0.0089326, T_{10}[3] = 0.015046, F_2[2, 6] = 0.090971, \\ F_2[3, 5] &= 0.016576, F_2[3, 6] = 0.0084743, H[1, 2, 6] = 0.0093718, H[1, 3, 5] = -0.086888, \\ H[1, 3, 6] &= -0.010563, f[2, 4, 5] = 0.0067077, f[2, 4, 6] = 0.029515, f[3, 4, 5] = 0.10123, \\ f[3, 4, 6] &= 0.011584, f[5, 2, 4] = -0.0087884, f[5, 3, 4] = 0.10755, f[6, 2, 4] = 0.048721, \\ f[6, 3, 4] &= 0.026565, \end{aligned}$$

$$\mathcal{R}_4 = 0, \quad \mathcal{R}_6 = -0.00043667,$$

$$\text{masses}^2 = (0.026127, 0.015642, 0.00062489, 0, 0).$$

$m_{466}^0 4$

$$I = 1: 4, \quad I = 2: 123, \quad I = 3: 156,$$

$$\begin{aligned} T_{10}[1] &= 0.036472, T_{10}[2] = 0.56902, T_{10}[3] = -0.054643, F_2[2, 5] = 0.18885, \\ F_2[2, 6] &= 0.11872, F_2[3, 5] = -0.16477, F_2[3, 6] = -0.062198, H[1, 2, 5] = 0.049683, \\ H[1, 2, 6] &= -0.011537, H[1, 3, 5] = 0.0051745, H[1, 3, 6] = 0.068309, f[2, 4, 5] = -0.052342, \\ f[2, 4, 6] &= 0.22423, f[3, 4, 5] = 0.14330, f[3, 4, 6] = -0.14454, f[6, 2, 4] = 0.012182, \\ f[6, 3, 4] &= -0.072132, \end{aligned}$$

$$\mathcal{R}_4 = 0, \quad \mathcal{R}_6 = -0.036741,$$

$$\text{masses}^2 = (0.17069, 0.012707, 0.0044701, 0, 0).$$

## Appendix C. Minkowski and (anti-) de Sitter solutions

---

### $m_{466}^0 5$

$$I = 1: 4, \quad I = 2: 123, \quad I = 3: 156,$$

$$T_{10}[1] = 0.65414, T_{10}[2] = 0.55886, T_{10}[3] = -0.070139, F_2[2, 5] = -0.31326,$$

$$F_2[2, 6] = -0.19336, F_2[3, 5] = 0.20421, F_2[3, 6] = -0.15304, H[1, 2, 5] = -0.20324,$$

$$H[1, 2, 6] = -0.014823, H[1, 3, 5] = 0.016713, H[1, 3, 6] = -0.29836, f[2, 4, 5] = 0.043513,$$

$$f[2, 4, 6] = -0.23363, f[3, 4, 5] = -0.16787, f[3, 4, 6] = 0.11717, f[5, 3, 4] = -0.028836,$$

$$f[6, 2, 4] = -0.015351, f[6, 3, 4] = 0.086384,$$

$$\mathcal{R}_4 = 0, \quad \mathcal{R}_6 = -0.034908,$$

$$\text{masses}^2 = (0.32049, 0.11059, 0.0073101, 0, 0).$$

### $m_{466}^0 6$

$$I = 1: 4, \quad I = 2: 123, \quad I = 3: 156,$$

$$T_{10}[1] = 0.1391, T_{10}[2] = 0.21921, T_{10}[3] = 0.6068, F_2[2, 5] = 0.17163,$$

$$F_2[2, 6] = 0.030109, F_2[3, 5] = 0.032577, F_2[3, 6] = -0.33822, H[1, 2, 5] = -0.083254,$$

$$H[1, 2, 6] = 0.098809, H[1, 3, 5] = 0.099749, H[1, 3, 6] = 0.034276, f[2, 4, 6] = -0.048187,$$

$$f[3, 4, 5] = 0.11704, f[5, 2, 4] = -0.037857, f[5, 3, 4] = -0.023053, f[6, 2, 4] = 0.26141,$$

$$f[6, 3, 4] = 0.033041,$$

$$\mathcal{R}_4 = 0, \quad \mathcal{R}_6 = -0.059001,$$

$$\text{masses}^2 = (0.21201, 0.035651, 0.013395, 0, 0).$$

## C.3 Anti-de Sitter solutions

$s_{55}^- 1$

$$I = 1: 12, \quad I = 2: 34,$$

$$\begin{aligned} T_{10}[1] &= 0.65385, T_{10}[2] = 0.067793, F_1[5] = 0.011227, F_1[6] = -0.070069, F_3[1, 3, 5] = 0.16616, \\ F_3[1, 3, 6] &= 0.17837, F_3[1, 4, 5] = 0.11969, F_3[1, 4, 6] = -0.2383, F_3[2, 3, 5] = -0.075801, \\ F_3[2, 3, 6] &= -0.077512, F_3[2, 4, 5] = -0.0060063, F_3[2, 4, 6] = -0.079968, H[1, 2, 5] = 0.064459, \\ H[1, 2, 6] &= 0.0056405, H[3, 4, 5] = 0.069322, H[3, 4, 6] = -0.17184, F_5[1, 2, 3, 4, 5] = -0.008645, \\ F_5[1, 2, 3, 4, 6] &= -0.0013851, f[1, 3, 5] = -0.27755, f[1, 3, 6] = -0.0073778, f[1, 4, 5] = -0.25336, \\ f[1, 4, 6] &= -0.039444, f[2, 3, 5] = 0.054799, f[2, 3, 6] = 0.057591, f[2, 4, 5] = 0.059283, \\ f[2, 4, 6] &= 0.0022988, f[3, 1, 5] = 0.0028896, f[3, 1, 6] = -0.0044766, f[3, 2, 5] = 0.0019835, \\ f[3, 2, 6] &= -0.020978, f[4, 1, 5] = 0.016741, f[4, 1, 6] = 0.0075944, f[4, 2, 5] = -0.014713, \\ f[4, 2, 6] &= 0.020748, f[5, 1, 3] = -0.14682, f[5, 1, 4] = -0.13679, f[5, 2, 3] = 0.093115, \\ f[5, 2, 4] &= 0.086751, f[6, 1, 3] = -0.023524, f[6, 1, 4] = -0.021917, f[6, 2, 3] = 0.014919, \\ f[6, 2, 4] &= 0.0139, \end{aligned}$$

$$\mathcal{R}_4 = -0.033561, \quad \mathcal{R}_6 = -0.0073162, \quad \eta_V = 0.7785,$$

$$\text{masses}^2 = (0.19854, 0.060726, 0.04147, -0.0065318).$$

$s_{55}^- 2$

$$I = 1: 12, \quad I = 2: 34,$$

$$\begin{aligned} T_{10}[1] &= 0.28653, T_{10}[2] = 0.19465, F_3[1, 3, 5] = 0.030441, F_3[1, 3, 6] = -0.18245, \\ F_3[1, 4, 5] &= 0.1287, F_3[1, 4, 6] = -0.047985, F_3[2, 3, 5] = 0.09543, F_3[2, 3, 6] = -0.049685, \\ F_3[2, 4, 5] &= 0.16944, F_3[2, 4, 6] = 0.045125, H[1, 2, 5] = 0.013663, H[1, 2, 6] = -0.086069, \\ H[3, 4, 5] &= -0.087243, H[3, 4, 6] = 0.0012479, f[1, 3, 6] = -0.15281, f[1, 4, 6] = 0.13141, \\ f[2, 3, 6] &= -0.095775, f[2, 4, 6] = 0.082363, f[3, 1, 5] = 0.067638, f[3, 1, 6] = 0.011932, \\ f[3, 2, 5] &= -0.10792, f[3, 2, 6] = -0.019038, f[4, 1, 5] = 0.078652, f[4, 1, 6] = 0.013875, \\ f[4, 2, 5] &= -0.12549, f[4, 2, 6] = -0.022138, f[5, 1, 3] = -0.02027, f[5, 1, 4] = -0.061815, \\ f[5, 2, 3] &= 0.057795, f[5, 2, 4] = 0.076739, f[6, 1, 3] = -0.09923, f[6, 1, 4] = 0.085335, \\ f[6, 2, 3] &= 0.014035, f[6, 2, 4] = -0.012069, \end{aligned}$$

$$\mathcal{R}_4 = -0.015208, \quad \mathcal{R}_6 = -0.017287, \quad \eta_V = -4,$$

$$\text{masses}^2 = (0.070021, 0.044657, 0.027383, 0.015208).$$

## Appendix C. Minkowski and (anti-) de Sitter solutions

---

### $s_{55}^-3$

$$I = 1: 12, \quad I = 2: 34,$$

$$\begin{aligned} T_{10}[1] &= 0.39238, T_{10}[2] = 0.5567, F_3[1, 3, 5] = 0.091642, F_3[1, 3, 6] = 0.19088, \\ F_3[1, 4, 5] &= -0.21033, F_3[1, 4, 6] = 0.23536, F_3[2, 3, 5] = -0.010403, F_3[2, 3, 6] = -0.0046634, \\ F_3[2, 4, 5] &= -0.20495, F_3[2, 4, 6] = -0.091878, H[1, 2, 5] = 0.0040374, H[1, 2, 6] = -0.16052, \\ H[3, 4, 5] &= -0.10526, H[3, 4, 6] = 0.00052599, f[1, 3, 6] = 0.31796, f[1, 4, 6] = -0.016139, \\ f[3, 2, 5] &= 0.018778, f[3, 2, 6] = 0.00052518, f[4, 2, 5] = 0.36995, f[4, 2, 6] = 0.010347, \\ f[5, 1, 3] &= -0.0057443, f[5, 1, 4] = 0.00029156, f[5, 2, 3] = 0.08266, f[5, 2, 4] = -0.2441, \\ f[6, 1, 3] &= 0.20538, f[6, 1, 4] = -0.010425, f[6, 2, 3] = -0.092728, f[6, 2, 4] = 0.0047066, \end{aligned}$$

$$\mathcal{R}_4 = -0.036862, \quad \mathcal{R}_6 = -0.023797, \quad \eta_V = -3.8495,$$

$$\text{masses}^2 = (0.20393, 0.11596, 0.074406, 0.035475).$$

### $s_{55}^-4$

$$I = 1: 12, \quad I = 2: 34,$$

$$\begin{aligned} T_{10}[1] &= 0.14258, T_{10}[2] = 0.58135, F_3[1, 3, 5] = 0.075163, F_3[1, 3, 6] = -0.1116, \\ F_3[1, 4, 5] &= -0.11823, F_3[1, 4, 6] = -0.2689, F_3[2, 4, 5] = -0.19084, F_3[2, 4, 6] = 0.065352, \\ H[1, 2, 5] &= -0.0073236, H[1, 2, 6] = -0.15603, H[3, 4, 5] = 0.0029354, H[3, 4, 6] = 0.0040146, \\ f[1, 3, 6] &= 0.20098, f[4, 2, 5] = -0.35082, f[4, 2, 6] = 0.021637, f[5, 1, 3] = 0.0088588, \\ f[5, 2, 3] &= -0.11714, f[5, 2, 4] = 0.18033, f[6, 1, 3] = 0.14363, f[6, 2, 3] = -0.027522, \end{aligned}$$

$$\mathcal{R}_4 = -0.024424, \quad \mathcal{R}_6 = -0.023691, \quad \eta_V = -2.4901,$$

$$\text{masses}^2 = (0.15904, 0.067206, 0.039032, 0.015205).$$

$m_{46}^-1$

$$I = 1: 4, \quad I = 2: 123, \quad I = 3: 156,$$

$$T_{10}[1] = 1.1971, T_{10}[2] = 0.072312, T_{10}[3] = -0.062975, F_2[1, 5] = -0.041978,$$

$$F_2[1, 6] = 0.14026, F_2[2, 5] = 0.066399, F_2[2, 6] = 0.21752, F_2[3, 5] = 0.011368,$$

$$F_2[3, 6] = -0.011895, F_4[1, 2, 4, 5] = -0.11379, F_4[1, 2, 4, 6] = -0.19903, F_4[1, 3, 4, 5] = -0.28462,$$

$$F_4[1, 3, 4, 6] = 0.28620, H[1, 2, 5] = -0.079033, H[1, 2, 6] = -0.10719, H[1, 3, 5] = -0.072608,$$

$$H[1, 3, 6] = 0.077682, H[2, 3, 5] = 0.21997, H[2, 3, 6] = -0.13693, f[1, 4, 5] = -0.042794,$$

$$f[1, 4, 6] = -0.025141, f[2, 4, 5] = -0.019349, f[2, 4, 6] = -0.011367, f[3, 4, 5] = -0.0097687,$$

$$f[3, 4, 6] = -0.005739, f[4, 2, 5] = 0.37334, f[4, 2, 6] = 0.21933, f[4, 3, 5] = 0.16584,$$

$$f[4, 3, 6] = 0.097433, f[5, 2, 4] = -0.17777, f[5, 3, 4] = -0.078969, f[6, 2, 4] = -0.053204,$$

$$f[6, 3, 4] = -0.023634,$$

$$\mathcal{R}_4 = -0.048164, \quad \mathcal{R}_6 = -0.02412, \quad \eta_V = 1.2531,$$

$$\text{masses}^2 = (0.49918, 0.13392, 0.060085, 0.054407, -0.015089).$$

$m_{46}^-2$

$$I = 1: 4, \quad I = 2: 123, \quad I = 3: 156,$$

$$T_{10}[1] = 0.7165, T_{10}[2] = 0.0763, T_{10}[3] = -0.10534, F_2[1, 6] = 0.24176,$$

$$F_2[2, 5] = 0.037154, F_2[2, 6] = -0.000011568, F_2[3, 5] = -0.042859, F_2[3, 6] = 0.0067886,$$

$$F_4[1, 2, 4, 5] = -0.13513, F_4[1, 2, 4, 6] = -0.17510, F_4[1, 3, 4, 5] = -0.13777, F_4[1, 3, 4, 6] = 0.16894,$$

$$H[1, 2, 5] = 0.0036697, H[1, 2, 6] = 0.004547, H[1, 3, 5] = 0.0038034, H[1, 3, 6] = -0.0037413,$$

$$H[2, 3, 5] = 0.19615, H[2, 3, 6] = 0.19189, f[1, 4, 5] = -0.045081, f[1, 4, 6] = 0.010927,$$

$$f[2, 4, 5] = -0.00053083, f[2, 4, 6] = 0.00012866, f[3, 4, 5] = -0.0010236, f[3, 4, 6] = 0.0002481,$$

$$f[4, 2, 5] = 0.27295, f[4, 2, 6] = -0.066157, f[4, 3, 5] = 0.28289, f[4, 3, 6] = -0.068567,$$

$$f[5, 2, 4] = -0.18495, f[5, 3, 4] = -0.19169,$$

$$\mathcal{R}_4 = -0.019002, \quad \mathcal{R}_6 = -0.012892, \quad \eta_V = 1.5483,$$

$$\text{masses}^2 = (0.38901, 0.18817, 0.031941, 0.013066, -0.0073556).$$



## Appendix C. Minkowski and (anti-) de Sitter solutions

---

### $m_{46}^-3$

$$I = 1: 4, \quad I = 2: 123, \quad I = 3: 156,$$

$$T_{10}[1] = 5.9022, T_{10}[2] = 0.67951, T_{10}[3] = -0.88782, F_2[1, 5] = 0.32655,$$

$$F_2[1, 6] = 0.61787, F_2[2, 5] = -0.060571, F_2[2, 6] = 0.032012, F_2[3, 5] = 0.13077,$$

$$F_2[3, 6] = -0.069114, F_4[1, 2, 4, 5] = -0.30798, F_4[1, 2, 4, 6] = 0.49291, F_4[1, 3, 4, 5] = -0.50027,$$

$$F_4[1, 3, 4, 6] = -0.44836, H[2, 3, 5] = 0.75352, H[2, 3, 6] = 0.23160, f[1, 4, 5] = -0.10747,$$

$$f[1, 4, 6] = 0.093925, f[4, 2, 5] = -0.79910, f[4, 2, 6] = 0.69839, f[4, 3, 5] = -0.37013,$$

$$f[4, 3, 6] = 0.32348, f[5, 2, 4] = 0.62420, f[5, 3, 4] = 0.28912, f[6, 2, 4] = -0.32990,$$

$$f[6, 3, 4] = -0.15280,$$

$$\mathcal{R}_4 = -0.1534, \quad \mathcal{R}_6 = -0.11122, \quad \eta_V = 1.5537,$$

$$\text{masses}^2 = (3.2576, 1.5711, 0.26172, 0.109, -0.059584).$$

### $m_{46}^-4$

$$I = 1: 4, \quad I = 2: 123, \quad I = 3: 156,$$

$$T_{10}[1] = 0.072202, T_{10}[2] = 1.0613, T_{10}[3] = -0.090953, F_2[1, 6] = 0.35610,$$

$$F_2[3, 5] = 0.075768, F_4[1, 2, 4, 5] = -0.20253, H[1, 3, 5] = -0.046817, H[1, 3, 6] = 0.016544,$$

$$H[2, 3, 5] = 0.040552, H[2, 3, 6] = 0.0087218, f[1, 4, 5] = -0.42575, f[1, 4, 6] = -0.059404,$$

$$f[2, 4, 5] = 0.11424, f[2, 4, 6] = -0.21770, f[5, 1, 4] = -0.19798, f[5, 2, 4] = 0.17149,$$

$$f[6, 3, 4] = -0.042125,$$

$$\mathcal{R}_4 = -0.020509, \quad \mathcal{R}_6 = -0.053926, \quad \eta_V = 1.3004,$$

$$\text{masses}^2 = (0.4783, 0.10213, 0.034824, 0.030265, -0.0066676).$$

### $m_{46}^-5$

$$I = 1: 4, \quad I = 2: 123, \quad I = 3: 156,$$

$$T_{10}[1] = 0.05707, T_{10}[2] = 1.3103, T_{10}[3] = -0.091524, F_2[1, 5] = -0.28057,$$

$$F_2[1, 6] = -0.092774, F_2[2, 5] = 0.26093, F_2[2, 6] = 0.086279, F_2[3, 5] = 0.019,$$

$$F_2[3, 6] = -0.057461, F_4[1, 2, 4, 5] = -0.061201, F_4[1, 2, 4, 6] = 0.18509, H[1, 3, 6] = 0.043744,$$

$$f[1, 4, 6] = -0.40037, f[2, 4, 5] = -0.25405, f[2, 4, 6] = 0.20285, f[5, 1, 4] = 0.07293,$$

$$f[5, 3, 4] = -0.04517, f[6, 1, 4] = -0.22056, f[6, 3, 4] = -0.014936,$$

$$\mathcal{R}_4 = -0.019001, \quad \mathcal{R}_6 = -0.072802, \quad \eta_V = 1.2548,$$

$$\text{masses}^2 = (0.4181, 0.16632, 0.043898, 0.028584, -0.0059604).$$

# Bibliography

- [1] D. Andriot, P. Marconnet, and T. Wrase, *New de Sitter solutions of 10d type IIB supergravity*, *JHEP* **08** (2020) 076, [[arXiv:2005.12930](#)].
- [2] D. Andriot, P. Marconnet, and T. Wrase, *Intricacies of classical de Sitter string backgrounds*, *Phys. Lett. B* **812** (2021) 136015, [[arXiv:2006.01848](#)].
- [3] D. Andriot, P. Marconnet, and D. Tsimpis, *Warp factor and the gravitational wave spectrum*, *JCAP* **07** (2021) 040, [[arXiv:2103.09240](#)].
- [4] D. Andriot, L. Horer, and P. Marconnet, *Charting the landscape of (anti-) de Sitter and Minkowski solutions of 10d supergravities*, *JHEP* **06** (2022) 131, [[arXiv:2201.04152](#)].
- [5] D. Andriot, L. Horer, and P. Marconnet, *Exploring the landscape of (anti-) de Sitter and Minkowski solutions: group manifolds, stability and scale separation*, *JHEP* **08** (2022) 109, [[arXiv:2204.05327](#)]. [Erratum: *JHEP* 09, 184 (2022)].
- [6] D. Andriot, P. Marconnet, M. Rajaguru, and T. Wrase, *Automated consistent truncations and stability of flux compactifications*, *JHEP* **12** (2022) 026, [[arXiv:2209.08015](#)]. [Addendum: *JHEP* 04, 044 (2023)].
- [7] P. Marconnet and D. Tsimpis, *Universal accelerating cosmologies from 10d supergravity*, *JHEP* **01** (2023) 033, [[arXiv:2210.10813](#)].
- [8] **WMAP** Collaboration, D. N. Spergel et al., *First year Wilkinson Microwave Anisotropy Probe (WMAP) observations: Determination of cosmological parameters*, *Astrophys. J. Suppl.* **148** (2003) 175–194, [[astro-ph/0302209](#)].
- [9] **WMAP** Collaboration, D. N. Spergel et al., *Wilkinson Microwave Anisotropy Probe (WMAP) three year results: implications for cosmology*, *Astrophys. J. Suppl.* **170** (2007) 377, [[astro-ph/0603449](#)].
- [10] **WMAP** Collaboration, E. Komatsu et al., *Five-Year Wilkinson Microwave Anisotropy Probe (WMAP) Observations: Cosmological Interpretation*, *Astrophys. J. Suppl.* **180** (2009) 330–376, [[arXiv:0803.0547](#)].
- [11] **Planck** Collaboration, P. A. R. Ade et al., *Planck 2013 results. XVI. Cosmological parameters*, *Astron. Astrophys.* **571** (2014) A16, [[arXiv:1303.5076](#)].

## Bibliography

---

- [12] **Planck** Collaboration, P. A. R. Ade et al., *Planck 2013 results. XXII. Constraints on inflation*, *Astron. Astrophys.* **571** (2014) A22, [[arXiv:1303.5082](#)].
- [13] **Planck** Collaboration, P. A. R. Ade et al., *Planck 2013 Results. XXIV. Constraints on primordial non-Gaussianity*, *Astron. Astrophys.* **571** (2014) A24, [[arXiv:1303.5084](#)].
- [14] **Supernova Cosmology Project** Collaboration, S. Perlmutter et al., *Measurements of  $\Omega$  and  $\Lambda$  from 42 high redshift supernovae*, *Astrophys. J.* **517** (1999) 565–586, [[astro-ph/9812133](#)].
- [15] **Supernova Search Team** Collaboration, A. G. Riess et al., *Observational evidence from supernovae for an accelerating universe and a cosmological constant*, *Astron. J.* **116** (1998) 1009–1038, [[astro-ph/9805201](#)].
- [16] **SDSS** Collaboration, K. N. Abazajian et al., *The Seventh Data Release of the Sloan Digital Sky Survey*, *Astrophys. J. Suppl.* **182** (2009) 543–558, [[arXiv:0812.0649](#)].
- [17] V. F. Mukhanov and G. V. Chibisov, *Quantum Fluctuations and a Nonsingular Universe*, *JETP Lett.* **33** (1981) 532–535.
- [18] G. V. Chibisov and V. F. Mukhanov, *Galaxy formation and phonons*, *Mon. Not. Roy. Astron. Soc.* **200** (1982) 535–550.
- [19] A. H. Guth and S. Y. Pi, *Fluctuations in the New Inflationary Universe*, *Phys. Rev. Lett.* **49** (1982) 1110–1113.
- [20] S. W. Hawking, *The Development of Irregularities in a Single Bubble Inflationary Universe*, *Phys. Lett. B* **115** (1982) 295.
- [21] A. A. Starobinsky, *Dynamics of Phase Transition in the New Inflationary Universe Scenario and Generation of Perturbations*, *Phys. Lett. B* **117** (1982) 175–178.
- [22] J. M. Bardeen, P. J. Steinhardt, and M. S. Turner, *Spontaneous Creation of Almost Scale - Free Density Perturbations in an Inflationary Universe*, *Phys. Rev. D* **28** (1983) 679.
- [23] A. H. Guth, *Inflationary universe: A possible solution to the horizon and flatness problems*, *Phys. Rev. D* **23** (Jan, 1981) 347–356.
- [24] A. D. Linde, *A New Inflationary Universe Scenario: A Possible Solution of the Horizon, Flatness, Homogeneity, Isotropy and Primordial Monopole Problems*, *Phys. Lett. B* **108** (1982) 389–393.
- [25] A. Albrecht and P. J. Steinhardt, *Cosmology for Grand Unified Theories with Radiatively Induced Symmetry Breaking*, *Phys. Rev. Lett.* **48** (1982) 1220–1223.
- [26] P. J. Steinhardt and M. S. Turner, *A Prescription for Successful New Inflation*, *Phys. Rev. D* **29** (1984) 2162–2171.

- [27] E. J. Copeland, A. R. Liddle, D. H. Lyth, E. D. Stewart, and D. Wands, *False vacuum inflation with Einstein gravity*, *Phys. Rev. D* **49** (1994) 6410–6433, [[astro-ph/9401011](#)].
- [28] D. Baumann and L. McAllister, *Inflation and String Theory*. Cambridge Monographs on Mathematical Physics. Cambridge University Press, 5, 2015.
- [29] T. Kaluza, *Zum Unitätsproblem der Physik*, *Sitzungsber. Preuss. Akad. Wiss. Berlin (Math. Phys. )* **1921** (1921) 966–972, [[arXiv:1803.08616](#)].
- [30] O. Klein, *Quantum Theory and Five-Dimensional Theory of Relativity*. (In German and English), *Z. Phys.* **37** (1926) 895–906.
- [31] G. Gibbons, *Aspects of supergravity theories, GIFT Seminar 1984:0123 (QCD161:G2:1984)* (1984).
- [32] G. W. Gibbons, *Thoughts on tachyon cosmology*, *Class. Quant. Grav.* **20** (2003) S321–S346, [[hep-th/0301117](#)].
- [33] J. M. Maldacena and C. Nunez, *Supergravity description of field theories on curved manifolds and a no go theorem*, *Int. J. Mod. Phys. A* **16** (2001) 822–855, [[hep-th/0007018](#)].
- [34] U. H. Danielsson and T. Van Riet, *What if string theory has no de Sitter vacua?*, *Int. J. Mod. Phys. D* **27** (2018), no. 12 1830007, [[arXiv:1804.01120](#)].
- [35] T. Van Riet and G. Zoccarato, *Beginners lectures on flux compactifications and related Swampland topics*, [arXiv:2305.01722](#).
- [36] D. Andriot and J. Blåbäck, *Refining the boundaries of the classical de Sitter landscape*, *JHEP* **03** (2017) 102, [[arXiv:1609.00385](#)]. [Erratum: *JHEP* **03**, 083 (2018)].
- [37] J. Shelton, W. Taylor, and B. Wecht, *Nongeometric flux compactifications*, *JHEP* **10** (2005) 085, [[hep-th/0508133](#)].
- [38] M. P. Hertzberg, S. Kachru, W. Taylor, and M. Tegmark, *Inflationary Constraints on Type IIA String Theory*, *JHEP* **12** (2007) 095, [[arXiv:0711.2512](#)].
- [39] B. de Carlos, A. Guarino, and J. M. Moreno, *Flux moduli stabilisation, Supergravity algebras and no-go theorems*, *JHEP* **01** (2010) 012, [[arXiv:0907.5580](#)].
- [40] B. de Carlos, A. Guarino, and J. M. Moreno, *Complete classification of Minkowski vacua in generalised flux models*, *JHEP* **02** (2010) 076, [[arXiv:0911.2876](#)].
- [41] S. Kachru, R. Kallosh, A. D. Linde, and S. P. Trivedi, *De Sitter vacua in string theory*, *Phys. Rev. D* **68** (2003) 046005, [[hep-th/0301240](#)].
- [42] V. Balasubramanian, P. Berglund, J. P. Conlon, and F. Quevedo, *Systematics of moduli stabilisation in Calabi-Yau flux compactifications*, *JHEP* **03** (2005) 007, [[hep-th/0502058](#)].

## Bibliography

---

- [43] S. B. Giddings, S. Kachru, and J. Polchinski, *Hierarchies from fluxes in string compactifications*, *Phys. Rev. D* **66** (2002) 106006, [[hep-th/0105097](#)].
- [44] I. R. Klebanov and M. J. Strassler, *Supergravity and a confining gauge theory: Duality cascades and chi SB resolution of naked singularities*, *JHEP* **08** (2000) 052, [[hep-th/0007191](#)].
- [45] S. Sethi, *Supersymmetry Breaking by Fluxes*, *JHEP* **10** (2018) 022, [[arXiv:1709.03554](#)].
- [46] I. Bena, J. Blåbäck, M. Graña, and S. Lüst, *The tadpole problem*, *JHEP* **11** (2021) 223, [[arXiv:2010.10519](#)].
- [47] M. Demirtas, M. Kim, L. McAllister, J. Moritz, and A. Rios-Tascon, *Small cosmological constants in string theory*, *JHEP* **12** (2021) 136, [[arXiv:2107.09064](#)].
- [48] M. Demirtas, M. Kim, L. McAllister, and J. Moritz, *Vacua with Small Flux Superpotential*, *Phys. Rev. Lett.* **124** (2020), no. 21 211603, [[arXiv:1912.10047](#)].
- [49] M. Demirtas, M. Kim, L. McAllister, J. Moritz, and A. Rios-Tascon, *Exponentially Small Cosmological Constant in String Theory*, *Phys. Rev. Lett.* **128** (2022), no. 1 011602, [[arXiv:2107.09065](#)].
- [50] R. Álvarez-García, R. Blumenhagen, M. Brinkmann, and L. Schlechter, *Small Flux Superpotentials for Type IIB Flux Vacua Close to a Conifold*, *Fortsch. Phys.* **68** (2020) 2000088, [[arXiv:2009.03325](#)].
- [51] J. Moritz, A. Retolaza, and A. Westphal, *Toward de Sitter space from ten dimensions*, *Phys. Rev. D* **97** (2018), no. 4 046010, [[arXiv:1707.08678](#)].
- [52] F. F. Gautason, V. Van Hemelryck, and T. Van Riet, *The Tension between 10D Supergravity and dS Uplifts*, *Fortsch. Phys.* **67** (2019), no. 1-2 1800091, [[arXiv:1810.08518](#)].
- [53] D. Junghans, *LVS de Sitter vacua are probably in the swampland*, *Nucl. Phys. B* **990** (2023) 116179, [[arXiv:2201.03572](#)].
- [54] G. W. Gibbons and C. M. Hull, *De Sitter space from warped supergravity solutions*, [hep-th/0111072](#).
- [55] I. P. Neupane, *De Sitter brane-world, localization of gravity, and the cosmological constant*, *Phys. Rev. D* **83** (2011) 086004, [[arXiv:1011.6357](#)].
- [56] M. Minamitsuji and K. Uzawa, *Warped de Sitter compactifications*, *JHEP* **01** (2012) 142, [[arXiv:1103.5326](#)].
- [57] E. Silverstein, *(A)dS backgrounds from asymmetric orientifolds*, *Clay Mat. Proc.* **1** (2002) 179, [[hep-th/0106209](#)].
- [58] A. Maloney, E. Silverstein, and A. Strominger, *De Sitter space in noncritical string theory*, in *Workshop on Conference on the Future of Theoretical Physics and Cosmology in Honor of Steven Hawking's 60th Birthday*, pp. 570–591, 5, 2002. [[hep-th/0205316](#)].

- [59] S. Harribey and D. Tsimpis, *One-loop bosonic string and De Sitter space*, *Nucl. Phys. B* **948** (2019) 114768, [[arXiv:1810.02236](#)].
- [60] D. Lüst, E. Palti, and C. Vafa, *AdS and the Swampland*, *Phys. Lett. B* **797** (2019) 134867, [[arXiv:1906.05225](#)].
- [61] D. Andriot, *On the de Sitter swampland criterion*, *Phys. Lett. B* **785** (2018) 570–573, [[arXiv:1806.10999](#)].
- [62] S. K. Garg and C. Krishnan, *Bounds on Slow Roll and the de Sitter Swampland*, *JHEP* **11** (2019) 075, [[arXiv:1807.05193](#)].
- [63] H. Ooguri, E. Palti, G. Shiu, and C. Vafa, *Distance and de Sitter Conjectures on the Swampland*, *Phys. Lett. B* **788** (2019) 180–184, [[arXiv:1810.05506](#)].
- [64] D. Andriot and C. Roupec, *Further refining the de Sitter swampland conjecture*, *Fortsch. Phys.* **67** (2019), no. 1-2 1800105, [[arXiv:1811.08889](#)].
- [65] D. Andriot, *Tachyonic de Sitter Solutions of 10d Type II Supergravities*, *Fortsch. Phys.* **69** (2021), no. 7 2100063, [[arXiv:2101.06251](#)].
- [66] B. S. Acharya, *Supersymmetry, Ricci Flat Manifolds and the String Landscape*, *JHEP* **08** (2020) 128, [[arXiv:1906.06886](#)].
- [67] B. S. Acharya, G. Aldazabal, E. Andrés, A. Font, K. Narain, and I. G. Zadeh, *Stringy Tachyonic Instabilities of Non-Supersymmetric Ricci Flat Backgrounds*, *JHEP* **04** (2021) 026, [[arXiv:2010.02933](#)].
- [68] H. Ooguri and C. Vafa, *Non-supersymmetric AdS and the Swampland*, *Adv. Theor. Math. Phys.* **21** (2017) 1787–1801, [[arXiv:1610.01533](#)].
- [69] N. Cribiori, D. Junghans, V. Van Hemelryck, T. Van Riet, and T. Wrase, *Scale-separated AdS<sub>4</sub> vacua of IIA orientifolds and M-theory*, *Phys. Rev. D* **104** (2021), no. 12 126014, [[arXiv:2107.00019](#)].
- [70] D. Andriot, *Open problems on classical de Sitter solutions*, *Fortsch. Phys.* **67** (2019), no. 7 1900026, [[arXiv:1902.10093](#)].
- [71] D. Andriot, E. Goi, R. Minasian, and M. Petrini, *Supersymmetry breaking branes on solvmanifolds and de Sitter vacua in string theory*, *JHEP* **05** (2011) 028, [[arXiv:1003.3774](#)].
- [72] D. Andriot and A. Betz,  *$\beta$ -supergravity: a ten-dimensional theory with non-geometric fluxes, and its geometric framework*, *JHEP* **12** (2013) 083, [[arXiv:1306.4381](#)].
- [73] D. Andriot, *On classical de Sitter and Minkowski solutions with intersecting branes*, *JHEP* **03** (2018) 054, [[arXiv:1710.08886](#)].
- [74] U. H. Danielsson, S. S. Haque, P. Koerber, G. Shiu, T. Van Riet, and T. Wrase, *De Sitter hunting in a classical landscape*, *Fortsch. Phys.* **59** (2011) 897–933, [[arXiv:1103.4858](#)].



## Bibliography

---

- [75] C. Caviezel, T. Wrase, and M. Zagermann, *Moduli Stabilization and Cosmology of Type IIB on  $SU(2)$ -Structure Orientifolds*, *JHEP* **04** (2010) 011, [[arXiv:0912.3287](#)].
- [76] D. Andriot, *New supersymmetric vacua on solvmanifolds*, *JHEP* **02** (2016) 112, [[arXiv:1507.00014](#)].
- [77] D. Andriot, *New constraints on classical de Sitter: flirting with the swampland*, *Fortsch. Phys.* **67** (2019), no. 1-2 1800103, [[arXiv:1807.09698](#)].
- [78] D. Andriot, N. Cribiori, and D. Erkiner, *The web of swampland conjectures and the TCC bound*, *JHEP* **07** (2020) 162, [[arXiv:2004.00030](#)].
- [79] G. Obied, H. Ooguri, L. Spodyneiko, and C. Vafa, *De Sitter Space and the Swampland*, [arXiv:1806.08362](#).
- [80] A. Bedroya and C. Vafa, *Trans-Planckian Censorship and the Swampland*, *JHEP* **09** (2020) 123, [[arXiv:1909.11063](#)].
- [81] T. Rudelius, *Dimensional reduction and (Anti) de Sitter bounds*, *JHEP* **08** (2021) 041, [[arXiv:2101.11617](#)].
- [82] D. Andriot, J. Blåbäck, and T. Van Riet, *Minkowski flux vacua of type II supergravities*, *Phys. Rev. Lett.* **118** (2017), no. 1 011603, [[arXiv:1609.00729](#)]. [Erratum: *Phys.Rev.Lett.* 120, 169901 (2018)].
- [83] M. Grana, R. Minasian, M. Petrini, and A. Tomasiello, *A Scan for new  $N=1$  vacua on twisted tori*, *JHEP* **05** (2007) 031, [[hep-th/0609124](#)].
- [84] P. G. Camara, A. Font, and L. E. Ibanez, *Fluxes, moduli fixing and MSSM-like vacua in a simple IIA orientifold*, *JHEP* **09** (2005) 013, [[hep-th/0506066](#)].
- [85] F. Marchesano and J. Quirant, *A Landscape of AdS Flux Vacua*, *JHEP* **12** (2019) 110, [[arXiv:1908.11386](#)].
- [86] O. DeWolfe, A. Giriyavets, S. Kachru, and W. Taylor, *Type IIA moduli stabilization*, *JHEP* **07** (2005) 066, [[hep-th/0505160](#)].
- [87] C. Caviezel, P. Koerber, S. Kors, D. Lust, D. Tsimpis, and M. Zagermann, *The Effective theory of type IIA  $AdS(4)$  compactifications on nilmanifolds and cosets*, *Class. Quant. Grav.* **26** (2009) 025014, [[arXiv:0806.3458](#)].
- [88] M. Petrini, G. Solard, and T. Van Riet, *AdS vacua with scale separation from IIB supergravity*, *JHEP* **11** (2013) 010, [[arXiv:1308.1265](#)].
- [89] C. Caviezel, P. Koerber, S. Kors, D. Lust, T. Wrase, and M. Zagermann, *On the Cosmology of Type IIA Compactifications on  $SU(3)$ -structure Manifolds*, *JHEP* **04** (2009) 010, [[arXiv:0812.3551](#)].
- [90] R. Flauger, S. Paban, D. Robbins, and T. Wrase, *Searching for slow-roll moduli inflation in massive type IIA supergravity with metric fluxes*, *Phys. Rev. D* **79** (2009) 086011, [[arXiv:0812.3886](#)].

- 
- [91] U. H. Danielsson, P. Koerber, and T. Van Riet, *Universal de Sitter solutions at tree-level*, *JHEP* **05** (2010) 090, [[arXiv:1003.3590](#)].
- [92] C. Roupec and T. Wrase, *de Sitter Extrema and the Swampland*, *Fortsch. Phys.* **67** (2019), no. 1-2 1800082, [[arXiv:1807.09538](#)].
- [93] P. Koerber, *Lectures on Generalized Complex Geometry for Physicists*, *Fortsch. Phys.* **59** (2011) 169–242, [[arXiv:1006.1536](#)].
- [94] P. Fre, M. Trigiante, and A. Van Proeyen, *Stable de Sitter vacua from  $N=2$  supergravity*, *Class. Quant. Grav.* **19** (2002) 4167–4194, [[hep-th/0205119](#)].
- [95] M. de Roo, D. B. Westra, and S. Panda, *De Sitter solutions in  $N=4$  matter coupled supergravity*, *JHEP* **02** (2003) 003, [[hep-th/0212216](#)].
- [96] O. Ogetbil, *Stable de Sitter Vacua in 4 Dimensional Supergravity Originating from 5 Dimensions*, *Phys. Rev. D* **78** (2008) 105001, [[arXiv:0809.0544](#)].
- [97] D. Roest and J. Rosseel, *De Sitter in Extended Supergravity*, *Phys. Lett. B* **685** (2010) 201–207, [[arXiv:0912.4440](#)].
- [98] G. Dall’Agata and G. Inverso, *de Sitter vacua in  $N = 8$  supergravity and slow-roll conditions*, *Phys. Lett. B* **718** (2013) 1132–1136, [[arXiv:1211.3414](#)].
- [99] N. Cribiori, G. Dall’agata, and F. Farakos, *Weak gravity versus de Sitter*, *JHEP* **04** (2021) 046, [[arXiv:2011.06597](#)].
- [100] G. Dibitetto, A. Guarino, and D. Roest, *Charting the landscape of  $N=4$  flux compactifications*, *JHEP* **03** (2011) 137, [[arXiv:1102.0239](#)].
- [101] E. Plauschinn, *Moduli Stabilization with Non-Geometric Fluxes — Comments on Tadpole Contributions and de-Sitter Vacua*, *Fortsch. Phys.* **69** (2021), no. 3 2100003, [[arXiv:2011.08227](#)].
- [102] G. Dall’Agata, M. Emelin, F. Farakos, and M. Morittu, *The unbearable lightness of charged gravitini*, *JHEP* **10** (2021) 076, [[arXiv:2108.04254](#)].
- [103] G. J. Loges and G. Shiu, *Breeding Realistic D-Brane Models*, *Fortsch. Phys.* **70** (2022), no. 5 2200038, [[arXiv:2112.08391](#)].
- [104] W. He, T. Li, and R. Sun, *The complete search for the supersymmetric Pati-Salam models from intersecting D6-branes*, *JHEP* **08** (2022) 044, [[arXiv:2112.09632](#)].
- [105] C. Bock, *On low-dimensional solvmanifolds*, 2009.
- [106] L. Snobl and P. Winternitz, *Classification and identification of Lie algebras*, vol. 33. American Mathematical Society and Centre de Recherches Mathématiques Montréal, 2014.
- [107] C. Bock, *On low-dimensional solvmanifolds*, 2009.
- [108] U. H. Danielsson, G. Shiu, T. Van Riet, and T. Wrase, *A note on obstinate tachyons in classical dS solutions*, *JHEP* **03** (2013) 138, [[arXiv:1212.5178](#)].



## Bibliography

---

- [109] D. Junghans, *Tachyons in Classical de Sitter Vacua*, *JHEP* **06** (2016) 132, [[arXiv:1603.08939](#)].
- [110] L. Andrianopoli, R. D’Auria, S. Ferrara, and M. A. Lledo, *Gauged extended supergravity without cosmological constant: No scale structure and supersymmetry breaking*, *Mod. Phys. Lett. A* **18** (2003) 1001–1012, [[hep-th/0212141](#)].
- [111] G. Dall’Agata and F. Zwirner, *New Class of  $N = 1$  No-Scale Supergravity Models*, *Phys. Rev. Lett.* **111** (2013), no. 25 251601, [[arXiv:1308.5685](#)].
- [112] J. Blåbäck, U. Danielsson, G. Dibitetto, and S. Giri, *Constructing stable de Sitter in M-theory from higher curvature corrections*, *JHEP* **09** (2019) 042, [[arXiv:1902.04053](#)].
- [113] G. Dibitetto, J. J. Fernández-Melgarejo, and M. Nozawa, *6D (1,1) Gauged Supergravities from Orientifold Compactifications*, *JHEP* **05** (2020) 015, [[arXiv:1912.04142](#)].
- [114] G. Dall’Agata and F. Zwirner, *Quantum corrections to broken  $N = 8$  supergravity*, *JHEP* **09** (2012) 078, [[arXiv:1205.4711](#)].
- [115] A. Micu, E. Palti, and G. Tasinato, *Towards Minkowski Vacua in Type II String Compactifications*, *JHEP* **03** (2007) 104, [[hep-th/0701173](#)].
- [116] M. Ihl, D. Robbins, and T. Wrase, *Toroidal orientifolds in IIA with general NS-NS fluxes*, *JHEP* **08** (2007) 043, [[arXiv:0705.3410](#)].
- [117] L. Covi, M. Gomez-Reino, C. Gross, J. Louis, G. A. Palma, and C. A. Scrucca, *de Sitter vacua in no-scale supergravities and Calabi-Yau string models*, *JHEP* **06** (2008) 057, [[arXiv:0804.1073](#)].
- [118] R. Kallosh, A. Linde, B. Vercnocke, and T. Wrase, *Analytic Classes of Metastable de Sitter Vacua*, *JHEP* **10** (2014) 011, [[arXiv:1406.4866](#)].
- [119] D. Junghans and M. Zagermann, *A Universal Tachyon in Nearly No-scale de Sitter Compactifications*, *JHEP* **07** (2018) 078, [[arXiv:1612.06847](#)].
- [120] J. Bardzell, E. Gonzalo, M. Rajaguru, D. Smith, and T. Wrase, *Type IIB flux compactifications with  $h^{1,1} = 0$* , *JHEP* **06** (2022) 166, [[arXiv:2203.15818](#)].
- [121] D. Andriot, G. Cacciapaglia, A. Deandrea, N. Deutschmann, and D. Tsimpis, *Towards Kaluza-Klein Dark Matter on Nilmanifolds*, *JHEP* **06** (2016) 169, [[arXiv:1603.02289](#)].
- [122] D. Andriot and D. Tsimpis, *Laplacian spectrum on a nilmanifold, truncations and effective theories*, *JHEP* **09** (2018) 096, [[arXiv:1806.05156](#)].
- [123] J. P. Conlon, S. Ning, and F. Revello, *Exploring the holographic Swampland*, *JHEP* **04** (2022) 117, [[arXiv:2110.06245](#)].
- [124] F. Apers, M. Montero, T. Van Riet, and T. Wrase, *Comments on classical AdS flux vacua with scale separation*, *JHEP* **05** (2022) 167, [[arXiv:2202.00682](#)].

- 
- [125] F. Apers, J. P. Conlon, S. Ning, and F. Revello, *Integer conformal dimensions for type IIA flux vacua*, *Phys. Rev. D* **105** (2022), no. 10 106029, [[arXiv:2202.09330](#)].
- [126] J. Quirant, *Noninteger conformal dimensions for type IIA flux vacua*, *Phys. Rev. D* **106** (2022), no. 6 066017, [[arXiv:2204.00014](#)].
- [127] B. S. Acharya, F. Benini, and R. Valandro, *Fixing moduli in exact type IIA flux vacua*, *JHEP* **02** (2007) 018, [[hep-th/0607223](#)].
- [128] A. Ashmore, C. Strickland-Constable, D. Tennyson, and D. Waldram, *Generalising  $G_2$  geometry: involutivity, moment maps and moduli*, *JHEP* **01** (2021) 158, [[arXiv:1910.04795](#)].
- [129] A. Ashmore, C. Strickland-Constable, D. Tennyson, and D. Waldram, *Heterotic backgrounds via generalised geometry: moment maps and moduli*, *JHEP* **11** (2020) 071, [[arXiv:1912.09981](#)].
- [130] S. Gurrieri, J. Louis, A. Micu, and D. Waldram, *Mirror symmetry in generalized Calabi-Yau compactifications*, *Nucl. Phys. B* **654** (2003) 61–113, [[hep-th/0211102](#)].
- [131] R. D’Auria, S. Ferrara, M. Trigiante, and S. Vaula, *Gauging the Heisenberg algebra of special quaternionic manifolds*, *Phys. Lett. B* **610** (2005) 147–151, [[hep-th/0410290](#)].
- [132] T. House and E. Palti, *Effective action of (massive) IIA on manifolds with  $SU(3)$  structure*, *Phys. Rev. D* **72** (2005) 026004, [[hep-th/0505177](#)].
- [133] M. Grana, J. Louis, and D. Waldram, *Hitchin functionals in  $N=2$  supergravity*, *JHEP* **01** (2006) 008, [[hep-th/0505264](#)].
- [134] I. Benmachiche and T. W. Grimm, *Generalized  $N=1$  orientifold compactifications and the Hitchin functionals*, *Nucl. Phys. B* **748** (2006) 200–252, [[hep-th/0602241](#)].
- [135] J. Louis and A. Micu, *Heterotic-Type IIA duality with fluxes*, *JHEP* **03** (2007) 026, [[hep-th/0608171](#)].
- [136] A.-K. Kashani-Poor and R. Minasian, *Towards reduction of type II theories on  $SU(3)$  structure manifolds*, *JHEP* **03** (2007) 109, [[hep-th/0611106](#)].
- [137] M. Grana, J. Louis, and D. Waldram,  *$SU(3) \times SU(3)$  compactification and mirror duals of magnetic fluxes*, *JHEP* **04** (2007) 101, [[hep-th/0612237](#)].
- [138] A.-K. Kashani-Poor, *Nearly Kaehler Reduction*, *JHEP* **11** (2007) 026, [[arXiv:0709.4482](#)].
- [139] D. Cassani and A.-K. Kashani-Poor, *Exploiting  $N=2$  in consistent coset reductions of type IIA*, *Nucl. Phys. B* **817** (2009) 25–57, [[arXiv:0901.4251](#)].
- [140] H. Samtleben, *Lectures on Gauged Supergravity and Flux Compactifications*, *Class. Quant. Grav.* **25** (2008) 214002, [[arXiv:0808.4076](#)].

## Bibliography

---

- [141] M. Trigiante, *Gauged Supergravities*, *Phys. Rept.* **680** (2017) 1–175, [[arXiv:1609.09745](#)].
- [142] L. Andrianopoli, M. A. Lledo, and M. Trigiante, *The Scherk-Schwarz mechanism as a flux compactification with internal torsion*, *JHEP* **05** (2005) 051, [[hep-th/0502083](#)].
- [143] G. Villadoro and F. Zwirner,  *$N=1$  effective potential from dual type-IIA  $D6/O6$  orientifolds with general fluxes*, *JHEP* **06** (2005) 047, [[hep-th/0503169](#)].
- [144] G. Dall’Agata, G. Villadoro, and F. Zwirner, *Type-IIA flux compactifications and  $N=4$  gauged supergravities*, *JHEP* **08** (2009) 018, [[arXiv:0906.0370](#)].
- [145] J. Polchinski, *String Theory*, vol. 2 of *Cambridge Monographs on Mathematical Physics*. Cambridge University Press, 1998.
- [146] D. Cassani, *String theory compactifications with fluxes, and generalized geometry*. PhD thesis, Paris U., VI-VII, 2009.
- [147] E. Bergshoeff, M. de Roo, M. B. Green, G. Papadopoulos, and P. K. Townsend, *Duality of type II 7 branes and 8 branes*, *Nucl. Phys. B* **470** (1996) 113–135, [[hep-th/9601150](#)].
- [148] L. McAllister, E. Silverstein, A. Westphal, and T. Wrase, *The Powers of Monodromy*, *JHEP* **09** (2014) 123, [[arXiv:1405.3652](#)].
- [149] D. Andriot and L. Horer, *(Quasi-) de Sitter solutions across dimensions and the TCC bound*, *JHEP* **01** (2023) 020, [[arXiv:2208.14462](#)].
- [150] P. Koerber and D. Tsimpis, *Supersymmetric sources, integrability and generalized-structure compactifications*, *JHEP* **08** (2007) 082, [[arXiv:0706.1244](#)].
- [151] P. Svrcek, *Cosmological Constant and Axions in String Theory*, [hep-th/0607086](#).
- [152] D. Junghans, *Weakly Coupled de Sitter Vacua with Fluxes and the Swampland*, *JHEP* **03** (2019) 150, [[arXiv:1811.06990](#)].
- [153] A. Banlaki, A. Chowdhury, C. Roupec, and T. Wrase, *Scaling limits of  $dS$  vacua and the swampland*, *JHEP* **03** (2019) 065, [[arXiv:1811.07880](#)].
- [154] T. W. Grimm, C. Li, and I. Valenzuela, *Asymptotic Flux Compactifications and the Swampland*, *JHEP* **06** (2020) 009, [[arXiv:1910.09549](#)]. [Erratum: *JHEP* 01, 007 (2021)].
- [155] M. Graña, R. Minasian, H. Triendl, and T. Van Riet, *Quantization problem in Scherk-Schwarz compactifications*, *Phys. Rev. D* **88** (2013), no. 8 085018, [[arXiv:1305.0785](#)].
- [156] R. Blumenhagen, M. Brinkmann, and A. Makridou, *Quantum Log-Corrections to Swampland Conjectures*, *JHEP* **02** (2020) 064, [[arXiv:1910.10185](#)].

- 
- [157] F. Apruzzi, G. Bruno De Luca, A. Gnecci, G. Lo Monaco, and A. Tomasiello, *On  $AdS_7$  stability*, *JHEP* **07** (2020) 033, [[arXiv:1912.13491](#)].
- [158] D. Lüst and D. Tsimpis,  *$AdS_2$  type-IIA solutions and scale separation*, *JHEP* **07** (2020) 060, [[arXiv:2004.07582](#)].
- [159] F. Farakos, G. Tringas, and T. Van Riet, *No-scale and scale-separated flux vacua from IIA on  $G_2$  orientifolds*, *Eur. Phys. J. C* **80** (2020), no. 7 659, [[arXiv:2005.05246](#)].
- [160] M. Emelin, *Effective Theories as Truncated Trans-Series and Scale Separated Compactifications*, *JHEP* **11** (2020) 144, [[arXiv:2005.11421](#)].
- [161] D. Tsimpis, *Supersymmetric  $AdS$  vacua and separation of scales*, *JHEP* **08** (2012) 142, [[arXiv:1206.5900](#)].
- [162] F. F. Gautason, M. Schillo, T. Van Riet, and M. Williams, *Remarks on scale separation in flux vacua*, *JHEP* **03** (2016) 061, [[arXiv:1512.00457](#)].
- [163] A. Font, A. Herráez, and L. E. Ibáñez, *On scale separation in type II  $AdS$  flux vacua*, *JHEP* **03** (2020) 013, [[arXiv:1912.03317](#)].
- [164] G. Buratti, J. Calderon, A. Mininno, and A. M. Uranga, *Discrete Symmetries, Weak Coupling Conjecture and Scale Separation in  $AdS$  Vacua*, *JHEP* **06** (2020) 083, [[arXiv:2003.09740](#)].
- [165] D. Junghans, *O-Plane Backreaction and Scale Separation in Type IIA Flux Vacua*, *Fortsch. Phys.* **68** (2020), no. 6 2000040, [[arXiv:2003.06274](#)].
- [166] F. Marchesano, E. Palti, J. Quirant, and A. Tomasiello, *On supersymmetric  $AdS_4$  orientifold vacua*, *JHEP* **08** (2020) 087, [[arXiv:2003.13578](#)].
- [167] D. Lust and D. Tsimpis, *Supersymmetric  $AdS(4)$  compactifications of IIA supergravity*, *JHEP* **02** (2005) 027, [[hep-th/0412250](#)].
- [168] B. S. Acharya, F. Benini, and R. Valandro, *Warped models in string theory*, [hep-th/0612192](#).
- [169] S. L. Parameswaran and I. Zavala, *Prospects for Primordial Gravitational Waves in String Inflation*, *Int. J. Mod. Phys. D* **25** (2016), no. 12 1644011, [[arXiv:1606.02537](#)].
- [170] D. Andriot and D. Tsimpis, *Gravitational waves in warped compactifications*, *JHEP* **06** (2020) 100, [[arXiv:1911.01444](#)].
- [171] J. Blåbäck, U. H. Danielsson, D. Junghans, T. Van Riet, T. Wrase, and M. Zagermann, *Smeared versus localised sources in flux compactifications*, *JHEP* **12** (2010) 043, [[arXiv:1009.1877](#)].
- [172] D. Junghans, *Backreaction of Localised Sources in String Compactifications*. PhD thesis, Leibniz U., Hannover, 2013. [arXiv:1309.5990](#).

## Bibliography

---

- [173] S. Baines and T. Van Riet, *Smearing orientifolds in flux compactifications can be OK*, *Class. Quant. Grav.* **37** (2020), no. 19 195015, [[arXiv:2005.09501](#)].
- [174] H. Lu and C. N. Pope, *Interacting intersections*, *Int. J. Mod. Phys. A* **13** (1998) 4425–4443, [[hep-th/9710155](#)].
- [175] D. Youm, *Partially localized intersecting BPS branes*, *Nucl. Phys. B* **556** (1999) 222–246, [[hep-th/9902208](#)].
- [176] M. Cvetič, H. Lu, C. N. Pope, and J. F. Vazquez-Poritz, *AdS in warped space-times*, *Phys. Rev. D* **62** (2000) 122003, [[hep-th/0005246](#)].
- [177] D. J. Smith, *Intersecting brane solutions in string and M theory*, *Class. Quant. Grav.* **20** (2003) R233, [[hep-th/0210157](#)].
- [178] B. Assel, C. Bachas, J. Estes, and J. Gomis, *Holographic Duals of D=3 N=4 Superconformal Field Theories*, *JHEP* **08** (2011) 087, [[arXiv:1106.4253](#)].
- [179] B. Assel, C. Bachas, J. Estes, and J. Gomis, *IIB Duals of D=3 N=4 Circular Quivers*, *JHEP* **12** (2012) 044, [[arXiv:1210.2590](#)].
- [180] A. Rota and A. Tomasiello, *AdS<sub>4</sub> compactifications of AdS<sub>7</sub> solutions in type II supergravity*, *JHEP* **07** (2015) 076, [[arXiv:1502.06622](#)].
- [181] P. K. Townsend and M. N. R. Wohlfarth, *Accelerating cosmologies from compactification*, *Phys. Rev. Lett.* **91** (2003) 061302, [[hep-th/0303097](#)].
- [182] N. Ohta, *Accelerating cosmologies from S-branes*, *Phys. Rev. Lett.* **91** (2003) 061303, [[hep-th/0303238](#)].
- [183] N. Ohta, *A Study of accelerating cosmologies from superstring / M theories*, *Prog. Theor. Phys.* **110** (2003) 269–283, [[hep-th/0304172](#)].
- [184] N. Ohta, *Accelerating cosmologies and inflation from M/superstring theories*, *Int. J. Mod. Phys. A* **20** (2005) 1–40, [[hep-th/0411230](#)].
- [185] S. Roy, *Accelerating cosmologies from M / string theory compactifications*, *Phys. Lett. B* **567** (2003) 322–329, [[hep-th/0304084](#)].
- [186] M. Gutperle, R. Kallosh, and A. D. Linde, *M / string theory, S-branes and accelerating universe*, *JCAP* **07** (2003) 001, [[hep-th/0304225](#)].
- [187] R. Emparan and J. Garriga, *A Note on accelerating cosmologies from compactifications and S branes*, *JHEP* **05** (2003) 028, [[hep-th/0304124](#)].
- [188] P. K. Townsend, *Cosmic acceleration and M theory*, in *14th International Congress on Mathematical Physics*, pp. 655–662, 8, 2003. [[hep-th/0308149](#)].
- [189] J. G. Russo and P. K. Townsend, *Late-time Cosmic Acceleration from Compactification*, *Class. Quant. Grav.* **36** (2019), no. 9 095008, [[arXiv:1811.03660](#)].

- 
- [190] J. G. Russo and P. K. Townsend, *Time-dependent compactification to de Sitter space: a no-go theorem*, *JHEP* **06** (2019) 097, [[arXiv:1904.11967](#)].
- [191] H. Bernardo, S. Brahma, and M. M. Faruk, *The inheritance of energy conditions: Revisiting no-go theorems in string compactifications*, [arXiv:2208.09341](#).
- [192] H. Bernardo, S. Brahma, K. Dasgupta, M. M. Faruk, and R. Tatar, *Four-Dimensional Null Energy Condition as a Swampland Conjecture*, *Phys. Rev. Lett.* **127** (2021), no. 18 181301, [[arXiv:2107.06900](#)].
- [193] C.-M. Chen, P.-M. Ho, I. P. Neupane, N. Ohta, and J. E. Wang, *Hyperbolic space cosmologies*, *JHEP* **10** (2003) 058, [[hep-th/0306291](#)].
- [194] L. Andersson and J. M. Heinzle, *Eternal acceleration from M-theory*, *Adv. Theor. Math. Phys.* **11** (2007), no. 3 371–398, [[hep-th/0602102](#)].
- [195] M. N. R. Wohlfarth, *Inflationary cosmologies from compactification?*, *Phys. Rev. D* **69** (2004) 066002, [[hep-th/0307179](#)].
- [196] J. Halliwell, *Scalar Fields in Cosmology with an Exponential Potential*, *Phys. Lett. B* **185** (1987) 341.
- [197] A. Collinucci, M. Nielsen, and T. Van Riet, *Scalar cosmology with multi-exponential potentials*, *Class. Quant. Grav.* **22** (2005) 1269–1288, [[hep-th/0407047](#)].
- [198] E. Bergshoeff, W. Chemissany, A. Ploegh, M. Trigiante, and T. Van Riet, *Generating Geodesic Flows and Supergravity Solutions*, *Nucl. Phys. B* **812** (2009) 343–401, [[arXiv:0806.2310](#)].
- [199] E. Bergshoeff, W. Chemissany, A. Ploegh, and T. Van Riet, *Geodesic flows in cosmology*, *J. Phys. Conf. Ser.* **110** (2008) 102002.
- [200] P. K. Townsend and M. N. R. Wohlfarth, *Cosmology as geodesic motion*, *Class. Quant. Grav.* **21** (2004) 5375, [[hep-th/0404241](#)].
- [201] F. Catino, C. A. Scrucca, and P. Smyth, *Simple metastable de Sitter vacua in N=2 gauged supergravity*, *JHEP* **04** (2013) 056, [[arXiv:1302.1754](#)].
- [202] M. de Roo, D. B. Westra, and S. Panda, *Gauging CSO groups in N=4 Supergravity*, *JHEP* **09** (2006) 011, [[hep-th/0606282](#)].
- [203] A. Kleinschmidt and H. Nicolai, *E(10) cosmology*, *JHEP* **01** (2006) 137, [[hep-th/0511290](#)].
- [204] J. Blåbäck, A. Borghese, and S. S. Haque, *Power-law cosmologies in minimal and maximal gauged supergravity*, *JHEP* **06** (2013) 107, [[arXiv:1303.3258](#)].
- [205] J. J. Heckman, C. Lawrie, L. Lin, and G. Zoccarato, *F-theory and Dark Energy*, *Fortsch. Phys.* **67** (2019), no. 10 1900057, [[arXiv:1811.01959](#)].



## Bibliography

---

- [206] J. J. Heckman, C. Lawrie, L. Lin, J. Sakstein, and G. Zoccarato, *Pixelated Dark Energy*, *Fortsch. Phys.* **67** (2019), no. 11 1900071, [[arXiv:1901.10489](#)].
- [207] A. Hebecker, T. Skrzypek, and M. Wittner, *The F-term Problem and other Challenges of Stringy Quintessence*, *JHEP* **11** (2019) 134, [[arXiv:1909.08625](#)].
- [208] J. Calderón-Infante, I. Ruiz, and I. Valenzuela, *Asymptotic Accelerated Expansion in String Theory and the Swampland*, [arXiv:2209.11821](#).
- [209] R. Gregory, *Nonsingular global string compactifications*, *Phys. Rev. Lett.* **84** (2000) 2564–2567, [[hep-th/9911015](#)].
- [210] A. Chodos, E. Poppitz, and D. Tsimpis, *Nonsingular deformations of singular compactifications, the cosmological constant, and the hierarchy problem*, *Class. Quant. Grav.* **17** (2000) 3865–3880, [[hep-th/0006093](#)].
- [211] L. Jarv, T. Mohaupt, and F. Saueressig, *Quintessence cosmologies with a double exponential potential*, *JCAP* **08** (2004) 016, [[hep-th/0403063](#)].
- [212] J. Sonner and P. K. Townsend, *Recurrent acceleration in dilaton-axion cosmology*, *Phys. Rev. D* **74** (2006) 103508, [[hep-th/0608068](#)].
- [213] J. Sonner and P. K. Townsend, *Axion-Dilaton Domain Walls and Fake Supergravity*, *Class. Quant. Grav.* **24** (2007) 3479–3514, [[hep-th/0703276](#)].
- [214] J. G. Russo and P. K. Townsend, *A dilaton-axion model for string cosmology*, *JHEP* **06** (2022) 001, [[arXiv:2203.09398](#)].
- [215] G. D’Amico and N. Kaloper, *Rollercoaster cosmology*, *JCAP* **08** (2021) 058, [[arXiv:2011.09489](#)].
- [216] R. Terrisse and D. Tsimpis, *Consistent truncation and de Sitter space from gravitational instantons*, *JHEP* **07** (2019) 034, [[arXiv:1903.10504](#)].
- [217] D. Tsimpis, *Consistent truncation on Calabi-Yau and Nearly-Kähler manifolds*, *PoS CORFU2019* (2020) 122, [[arXiv:2002.09359](#)].
- [218] **LIGO Scientific, Virgo** Collaboration, R. Abbott et al., *GWTC-2: Compact Binary Coalescences Observed by LIGO and Virgo During the First Half of the Third Observing Run*, *Phys. Rev. X* **11** (2021) 021053, [[arXiv:2010.14527](#)].
- [219] **LIGO Scientific, Virgo** Collaboration, R. Abbott et al., *Population Properties of Compact Objects from the Second LIGO-Virgo Gravitational-Wave Transient Catalog*, *Astrophys. J. Lett.* **913** (2021), no. 1 L7, [[arXiv:2010.14533](#)].
- [220] **NANOGrav** Collaboration, Z. Arzoumanian et al., *The NANOGrav 12.5 yr Data Set: Search for an Isotropic Stochastic Gravitational-wave Background*, *Astrophys. J. Lett.* **905** (2020), no. 2 L34, [[arXiv:2009.04496](#)].
- [221] **LIGO Scientific, Virgo** Collaboration, R. Abbott et al., *Tests of general relativity with binary black holes from the second LIGO-Virgo gravitational-wave transient catalog*, *Phys. Rev. D* **103** (2021), no. 12 122002, [[arXiv:2010.14529](#)].

- 
- [222] E. Barausse et al., *Prospects for Fundamental Physics with LISA*, *Gen. Rel. Grav.* **52** (2020), no. 8 81, [[arXiv:2001.09793](#)].
- [223] S. E. Perkins, N. Yunes, and E. Berti, *Probing Fundamental Physics with Gravitational Waves: The Next Generation*, *Phys. Rev. D* **103** (2021), no. 4 044024, [[arXiv:2010.09010](#)].
- [224] H. S. Chia, *Probing Particle Physics with Gravitational Waves*. PhD thesis, Amsterdam U., 2020. [arXiv:2012.09167](#).
- [225] G. Calcagni, *Quantum gravity and gravitational-wave astronomy*, [arXiv:2012.08251](#).
- [226] A. Kuntz, R. Penco, and F. Piazza, *Extreme Mass Ratio Inspirals with Scalar Hair*, *JCAP* **08** (2020) 023, [[arXiv:2004.10772](#)].
- [227] L. K. Wong, *Evolution of diffuse scalar clouds around binary black holes*, *Phys. Rev. D* **101** (2020), no. 12 124049, [[arXiv:2004.03570](#)].
- [228] M. Khodadi, A. Allahyari, S. Vagnozzi, and D. F. Mota, *Black holes with scalar hair in light of the Event Horizon Telescope*, *JCAP* **09** (2020) 026, [[arXiv:2005.05992](#)].
- [229] M. Gorghetto, E. Hardy, and H. Nicolaescu, *Observing invisible axions with gravitational waves*, *JCAP* **06** (2021) 034, [[arXiv:2101.11007](#)].
- [230] A. Addazi, M. Bianchi, M. Firrotta, and A. Marcianò, *String Memories ... Lost and Regained*, *Nucl. Phys. B* **965** (2021) 115356, [[arXiv:2008.02206](#)].
- [231] V. M. Mehta, M. Demirtas, C. Long, D. J. E. Marsh, L. McAllister, and M. J. Stott, *Superradiance Exclusions in the Landscape of Type IIB String Theory*, [arXiv:2011.08693](#).
- [232] **LIGO Scientific, Virgo, KAGRA** Collaboration, R. Abbott et al., *Constraints on Cosmic Strings Using Data from the Third Advanced LIGO–Virgo Observing Run*, *Phys. Rev. Lett.* **126** (2021), no. 24 241102, [[arXiv:2101.12248](#)].
- [233] V. M. Mehta, M. Demirtas, C. Long, D. J. E. Marsh, L. McAllister, and M. J. Stott, *Superradiance in string theory*, *JCAP* **07** (2021) 033, [[arXiv:2103.06812](#)].
- [234] D. Hooper, G. Krnjaic, J. March-Russell, S. D. McDermott, and R. Petrossian-Byrne, *Hot Gravitons and Gravitational Waves From Kerr Black Holes in the Early Universe*, [arXiv:2004.00618](#).
- [235] C. Caprini et al., *Science with the space-based interferometer eLISA. II: Gravitational waves from cosmological phase transitions*, *JCAP* **04** (2016) 001, [[arXiv:1512.06239](#)].
- [236] C. Caprini and D. G. Figueroa, *Cosmological Backgrounds of Gravitational Waves*, *Class. Quant. Grav.* **35** (2018), no. 16 163001, [[arXiv:1801.04268](#)].



## Bibliography

---

- [237] C. Caprini et al., *Detecting gravitational waves from cosmological phase transitions with LISA: an update*, *JCAP* **03** (2020) 024, [[arXiv:1910.13125](#)].
- [238] A. Eichhorn, J. Lumma, J. M. Pawłowski, M. Reichert, and M. Yamada, *Universal gravitational-wave signatures from heavy new physics in the electroweak sector*, *JCAP* **05** (2021) 006, [[arXiv:2010.00017](#)].
- [239] T. Kite, A. Ravenni, S. P. Patil, and J. Chluba, *Bridging the gap: spectral distortions meet gravitational waves*, *Mon. Not. Roy. Astron. Soc.* **505** (2021), no. 3 4396–4405, [[arXiv:2010.00040](#)].
- [240] Y. Du, S. Tahura, D. Vaman, and K. Yagi, *Probing Compactified Extra Dimensions with Gravitational Waves*, *Phys. Rev. D* **103** (2021), no. 4 044031, [[arXiv:2004.03051](#)].
- [241] E. Megias, G. Nardini, and M. Quiros, *Gravitational Imprints from Heavy Kaluza-Klein Resonances*, *Phys. Rev. D* **102** (2020), no. 5 055004, [[arXiv:2005.04127](#)].
- [242] D. Dalmazi and R. R. L. d. Santos, *The dimensional reduction of linearized spin-2 theories invariant under transverse diffeomorphisms*, *Eur. Phys. J. C* **81** (2021), no. 6 547, [[arXiv:2010.12051](#)].
- [243] L. Randall and R. Sundrum, *A Large mass hierarchy from a small extra dimension*, *Phys. Rev. Lett.* **83** (1999) 3370–3373, [[hep-ph/9905221](#)].
- [244] L. Randall and R. Sundrum, *An Alternative to compactification*, *Phys. Rev. Lett.* **83** (1999) 4690–4693, [[hep-th/9906064](#)].
- [245] C. Bachas and J. Estes, *Spin-2 spectrum of defect theories*, *JHEP* **06** (2011) 005, [[arXiv:1103.2800](#)].
- [246] D. Andriot and G. Lucena Gómez, *Signatures of extra dimensions in gravitational waves*, *JCAP* **06** (2017) 048, [[arXiv:1704.07392](#)]. [Erratum: *JCAP* **05**, E01 (2019)].
- [247] C. Córdova, G. B. De Luca, and A. Tomasiello, *Classical de Sitter Solutions of 10-Dimensional Supergravity*, *Phys. Rev. Lett.* **122** (2019), no. 9 091601, [[arXiv:1812.04147](#)].
- [248] N. Cribiori and D. Junghans, *No classical (anti-)de Sitter solutions with O8-planes*, *Phys. Lett. B* **793** (2019) 54–58, [[arXiv:1902.08209](#)].
- [249] C. Córdova, G. B. De Luca, and A. Tomasiello, *New de Sitter Solutions in Ten Dimensions and Orientifold Singularities*, *JHEP* **08** (2020) 093, [[arXiv:1911.04498](#)].
- [250] N. Kim, *Towards an explicit construction of de Sitter solutions in classical supergravity*, *JHEP* **10** (2020) 057, [[arXiv:2004.05885](#)].
- [251] I. Bena, G. B. De Luca, M. Graña, and G. Lo Monaco, *Oh, wait, O8 de Sitter may be unstable!*, *JHEP* **03** (2021) 168, [[arXiv:2010.05936](#)].

- [252] R. Blumenhagen, D. Kläwer, and L. Schlechter, *Swampland Variations on a Theme by KKLT*, *JHEP* **05** (2019) 152, [[arXiv:1902.07724](#)].
- [253] K. Dimmitt, G. Larios, P. Ntokos, and O. Varela, *Universal properties of Kaluza-Klein gravitons*, *JHEP* **03** (2020) 039, [[arXiv:1911.12202](#)].
- [254] E. Malek and H. Samtleben, *Kaluza-Klein Spectrometry for Supergravity*, *Phys. Rev. Lett.* **124** (2020), no. 10 101601, [[arXiv:1911.12640](#)].
- [255] M. Cesaro, G. Larios, and O. Varela, *A Cubic Deformation of ABJM: The Squashed, Stretched, Warped, and Perturbed Gets Invaded*, *JHEP* **10** (2020) 041, [[arXiv:2007.05172](#)].
- [256] E. Malek and H. Samtleben, *Kaluza-Klein Spectrometry from Exceptional Field Theory*, *Phys. Rev. D* **102** (2020), no. 10 106016, [[arXiv:2009.03347](#)].
- [257] J.-M. Richard, R. Terrisse, and D. Tsimpis, *On the spin-2 Kaluza-Klein spectrum of  $\text{AdS}_4 \times S^2(\mathcal{B}_4)$* , *JHEP* **12** (2014) 144, [[arXiv:1410.4669](#)].
- [258] X. Gao, A. Hebecker, and D. Junghans, *Control issues of KKLT*, *Fortsch. Phys.* **68** (2020) 2000089, [[arXiv:2009.03914](#)].
- [259] F. Carta and J. Moritz, *Resolving spacetime singularities in flux compactifications & KKLT*, *JHEP* **08** (2021) 093, [[arXiv:2101.05281](#)].
- [260] F. Carta, J. Moritz, and A. Westphal, *Gaugino condensation and small uplifts in KKLT*, *JHEP* **08** (2019) 141, [[arXiv:1902.01412](#)].
- [261] R. Courant and D. Hilbert, *Methods of Mathematical Physics*, vol. 1. Wiley, 1989.
- [262] S. Shandera, B. Shlaer, H. Stoica, and S. H. H. Tye, *Interbrane interactions in compact spaces and brane inflation*, *JCAP* **02** (2004) 013, [[hep-th/0311207](#)].
- [263] S. B. Giddings and A. Maharana, *Dynamics of warped compactifications and the shape of the warped landscape*, *Phys. Rev. D* **73** (2006) 126003, [[hep-th/0507158](#)].
- [264] G. Shiu, G. Torroba, B. Underwood, and M. R. Douglas, *Dynamics of Warped Flux Compactifications*, *JHEP* **06** (2008) 024, [[arXiv:0803.3068](#)].
- [265] M. R. Douglas and G. Torroba, *Kinetic terms in warped compactifications*, *JHEP* **05** (2009) 013, [[arXiv:0805.3700](#)].
- [266] A. R. Frey, G. Torroba, B. Underwood, and M. R. Douglas, *The Universal Kähler Modulus in Warped Compactifications*, *JHEP* **01** (2009) 036, [[arXiv:0810.5768](#)].
- [267] A. Ashmore, *Eigenvalues and eigenforms on Calabi-Yau threefolds*, [[arXiv:2011.13929](#)].
- [268] B. Valeixo Bento, D. Chakraborty, S. Parameswaran, and I. Zavala, *Gravity at the tip of the throat*, *JHEP* **09** (2022) 208, [[arXiv:2204.02086](#)].
- [269] H. Bateman, *Higher Transcendental Functions*, vol. 1. McGraw-Hill, 1953.